

Development of Novel Technologies for Parallel Synthesis of Glycans and Glycopeptides for Microarray Generation

Inaugural-Dissertation
Doctor rerum naturalium (Dr. rer. nat.)

Submitted to the Department of Biology, Chemistry, Pharmacy
of Freie Universität Berlin

by

Alexandra Tsouka

From Naoussa Imathias, Greece

December 2022

This work was performed between January 2019 and December 2022 under the supervision of Prof. Dr. Peter H. Seeberger in the Department of Biomolecular Systems, at Max Planck Institute of Colloids and Interfaces, and the Department of Biology, Chemistry and Pharmacy, Freie Universität Berlin.

1st reviewer: Prof. Dr. Peter H. Seeberger

2nd reviewer: Prof. Dr. Rainer Haag

Date of oral defense: 4th of May 2023

Acknowledgements

This work/achievement would not have been possible without the support of many people.

First and foremost, I would like to express my gratitude to Prof. Dr. Seeberger and Dr. Felix Löffler for giving me the opportunity to perform research and be part of the Max Plank Institute of Colloids and Interfaces the past years. I would like to thank both for their supervision, suggestions, encouragement and support throughout my postgraduate studies. I thank Prof. Dr. Reiner Haag for his recommendations and for kindly agreeing to supervise this work.

My deepest gratitude is also extended to Dr. Marco Mende, Dr. Kim Lemaihoang for the invaluable assistance, and the excellent collaboration we had the past years even remotely. I would like to thank Dr. José Angél Danglad-Flores, Dr. Eric Sletten, and Dr. Manuel Garcia Ricardo for their advices and help in automation and peptide chemistry. I am thankful to Dr. Martina Delbianco and the other group leaders of the Biomolecular Systems Department for their valuable input, as well as all the collaborators I was blessed to work with, within different projects. I would also like to convey thanks to Dorothee Böhme, Eva Settels, Olaf Niemeyer, and Klaus Bienert who were particularly considerate and offered invaluable assistance. Moreover, I thank all my friends and colleagues within the Biomolecular Systems Department since I have been blessed with a friendly and helpful group. Special thanks go to Jasmin Heidepriem and Dr. Marco Mende for all the fun inside and outside the lab. To all the current and former members of the SAT group and my students Niki Katsimani and Kassandra Hoetzel for the fruitful discussions and their help. To CD, Grigori, Jasmin, Marco and Sandra for their friendship inside and outside the lab.

I also wish to express my love and gratitude to my family and friends. To my Berlin-gang Andrew, Anna-Maria, Elef, the alumni Brian and Ilgin for being by my side all these years here in Berlin. To my friends that became officially family the past years Eleanna, Marianna, and Xristina in Greece for supporting me every step of the way with their visits, calls and messages. To my beloved cousins Konstantinos, Maria, and Eleni that are like siblings to me and of course to my parents for their constant love, support, and company through difficult times.

Lastly, I would like to thank Prof. Dr. Alexandros Koumbis since I would not be pursuing a PhD or even getting more involved with chemistry if I had not joined his lab for my bachelor thesis.

Herewith I certify that I have prepared and written my thesis independently and that I have not used any sources and aids other than those indicated by me. The work from others has been clarified and acknowledged within the text. I also declare that I have not submitted the dissertation in this or any other form to any other institution as a dissertation.

Alexandra Tsouka

Date & Signature: May 2023

List of Publications and Scientific Conferences

List of Publications and Patents

EP18213784.4: Löffler, F. F.; Mende, M.; Eickelmann, S.; **Tsouka, A.**; Heidepriem, J.; Seeberger, P. H.; Paris, G.; Method and device for producing saccharides and saccharide arrays. Filed December 18, **2018**.

Paris, G.; Heidepriem, J.; **Tsouka, A.**; Mende, M.; Eickelmann, S.; Löffler, F. F.; Automated laser-assisted synthesis of microarrays for infectious disease research. In: *Microfluidics, BioMEMS, and Medical Microsystems XVII*, Vol. 10875, 108750C (Eds. Gray, B. L.; Becker, H.). SPIE BiOS, 2019, San Francisco, CA, USA, February 02, 2019 - February 07, **2019**.

Mende, M.; Bordoni, V.; **Tsouka, A.**; Löffler, F. F.; Delbianco, M.; Seeberger, P. H.; Multivalent glycan arrays, *Faraday Discuss.*, **2019**, 219, 9–32.

Eickelmann, S.; **Tsouka, A.**; Heidepriem, J.; Paris, G.; Zhang, J.; Molinari, V.; Mende, M.; Löffler, F. F.; A low-cost laser-based nano-3D polymer printer for rapid surface patterning and chemical synthesis of peptide and glycan microarrays, *Advanced Mater. Technol.*, **2019**, 4 (11), 1900503.

Paris, G.; Klinkusch, A.; Heidepriem, J.; **Tsouka, A.**; Zhang, J.; Mende, M.; Mattes, D.; Mager, D.; Riegler, H.; Eickelmann, S.; Loeffler, F.F.; Laser-induced forward transfer of soft material nanolayers with millisecond pulses shows contact-based material deposition., *Applied Surface Science*, **2020**, 508, 144973.

Mende, M.*; **Tsouka, A.***; Heidepriem, J.; Paris, G.; Mattes, D. S.; Eickelmann, S.; Bordoni, V.; Wawrzinek, R.; Fuchsberger, F. F.; Seeberger, P. H.; Rademacher C.; Delbianco M.; Mallagaray A.; Loeffler F. F.; On-Chip Neo-Glycopeptide Synthesis for Multivalent Glycan Presentation, *Chem.Eur.J.*, **2020**, 26, 9954 –9963.

Ilic, I. K.; **Tsouka, A.**; Perovic, M.; Hwang, J.; Heil, T.; Loeffler, F. F.; Oschatz, M.; Antonietti, M.; Liedel, C.; Sustainable Cathodes for Lithium-Ion Energy Storage Devices Based on Tannic Acid—Toward Ecofriendly Energy Storage, *Adv. Sustainable Syst.*, **2020**, 2000206

Tsouka, A.; Hoetzel, K.; Mende, M.; Heidepriem, J.; Paris, G.; Eickelmann, S.; Seeberger P. H.; Lepenies, B.; and Loeffler, F. F.; Probing Multivalent Carbohydrate-Protein Interactions with On-Chip Synthesized Glycopeptides Using Different Functionalized Surfaces, *Front. Chem.*, **2021**, 9:766932.

Paris, G.; Heidepriem, J.; **Tsouka, A.**; Liu, Y.; Mattes, D. S.; Pinzón Martín. S.; Dallabernardina, P.; Mende, M.; Lindner, C.; Wawrzinek, R.; Rademacher, C.; Seeberger, P.H.; Breitling, F.; Bischoff, F. R.; Wolf, T.; and Loeffler, F.F.; Automated Laser-Transfer Synthesis of High-Density Microarrays for Infectious Disease Screening, *Adv. Mater.* **2022**, 2200359.

Tsouka, A.*; Dallabernardina, P.*; Mende, M.; Sletten E. T.; Lechnitz, S.; Bienert, K.; Le Mai Hoang, K.; Seeberger, P. H.; and Loeffler, F. F.; VaporSPOT: Parallel Synthesis of Oligosaccharides on Membranes; *J. Am. Chem. Soc.* **2022**, *144*, 19832–19837.

Tsouka, A.; Mende, M.; Paris, G.; Heidepriem, J.; Dallabernardina P.; Bienert K.; Seeberger, P. H.; and Loeffler, F. F.; *In-situ* chemical synthesis of glycan microarrays via sugarLIFT; *in preparation*

*These authors contributed equally.

Scientific Conferences and Symposia Presentations:

Laser-assisted chemical synthesis of microarrays for disease research, XXth European Carbohydrate Symposium 2019, Leiden, Netherlands (**poster**).

Novel Methods for Glycan Synthesis, Ringberg Conference 2019, Ringberg Castle, Rottach-Egern, Germany (**talk**)

Laser-Assisted Chemical Synthesis of Neoglycopeptides for Multivalency Studies, 5th International Symposium of the Collaborative Research Center 765 “Multivalency in Chemistry and Biology” 2019, Berlin, Germany (**poster**).

On-Chip Neo-Glycopeptide Synthesis for Multivalent Glycan Presentation, RSC Carbohydrate ECR Webinar 3, July 2020 (**talk**)

Parallel Synthesis of Glycans on Membranes *via* Aerosol Activator Depositio, 21st European Carbohydrate Symposium, Paris, France (**talk** accepted in 2021, postponed for 2023)

Table of content

Acknowledgements	i
List of Publications and Scientific Conferences	iii
List of Abbreviation.....	viii
Summary	xi
Zusammenfassung.....	xiii
1. Introduction	1
1.1. Carbohydrates in nature - role and complexity	1
1.2. Carbohydrate binding proteins.....	2
1.3. Types of glycan-lectin interactions.....	6
1.3.1. Monovalent interaction	6
1.3.2. Multivalent interactions	6
1.4. Glycan microarrays.....	8
1.4.1. Access to glycan collections for microarray fabrication	10
1.4.2. Printing methods of glycans	15
1.4.3. Immobilization of glycans	17
1.4.4. Multivalent glycan arrays.....	20
1.4.5. Detection of binding mode.....	22
1.5. Solid phase synthesis of biomolecules	23
1.5.1. Solid phase peptide synthesis.....	24
1.5.2. Solid-phase glycans synthesis - AGA.....	30
1.6. Aim of this thesis.....	31
2. SugarLIFT: <i>in-situ</i> chemical synthesis of glycan microarrays.....	34
2.1. Introduction	35
2.2. Results and Discussion	37
2.2.1. General characteristics of the sugarLIFT process.....	37
2.2.2. Optimization of the sugarLIFT process.....	39

2.2.3.	Validation of the synthesized structures	47
2.2.4.	Synthesis of building blocks library.....	49
2.2.5.	Parallel oligosaccharide synthesis <i>via</i> sugarLIFT.....	52
2.2.6.	Evaluation of fluorescence signal for reference building block.....	54
2.3.	Conclusions	56
2.4.	Outlook	57
2.5.	Experimental Section.....	58
2.5.1.	Syntheses of linkers and building blocks.....	62
2.5.2.	Functionalization of acceptor glass slides	84
2.5.3.	SugarLIFT process	87
2.5.4.	Glycosylation in solution	92
2.5.5.	Parallel oligosaccharide synthesis <i>via</i> sugarLIFT.....	92
3.	On-chip neo-glycopeptide synthesis for multivalency studies.....	95
3.1.	Introduction	96
3.2.	Results and Discussion	97
3.2.1.	Method development for neo-glycopeptide synthesis	97
3.2.2.	Concept validation and evaluation of glycan-lectin interaction	100
3.2.3.	Neo-glycopeptide synthesis on different surfaces	104
3.2.4.	Glycan-lectin evaluation on differently functionalized surfaces	106
3.2.5.	Synthesis of heteromultivalent neo-glycopeptides	114
3.3.	Conclusions	115
3.4.	Outlook	116
3.5.	Experimental Section.....	118
3.5.1.	Synthesis of sugar azides.....	122
3.5.2.	Donor and acceptor slide preparation	133
3.5.3.	Parameter optimization for tetrapeptides synthesis.....	136
3.5.4.	CuAAC reaction.....	139
3.5.5.	Modules of synthesis	140

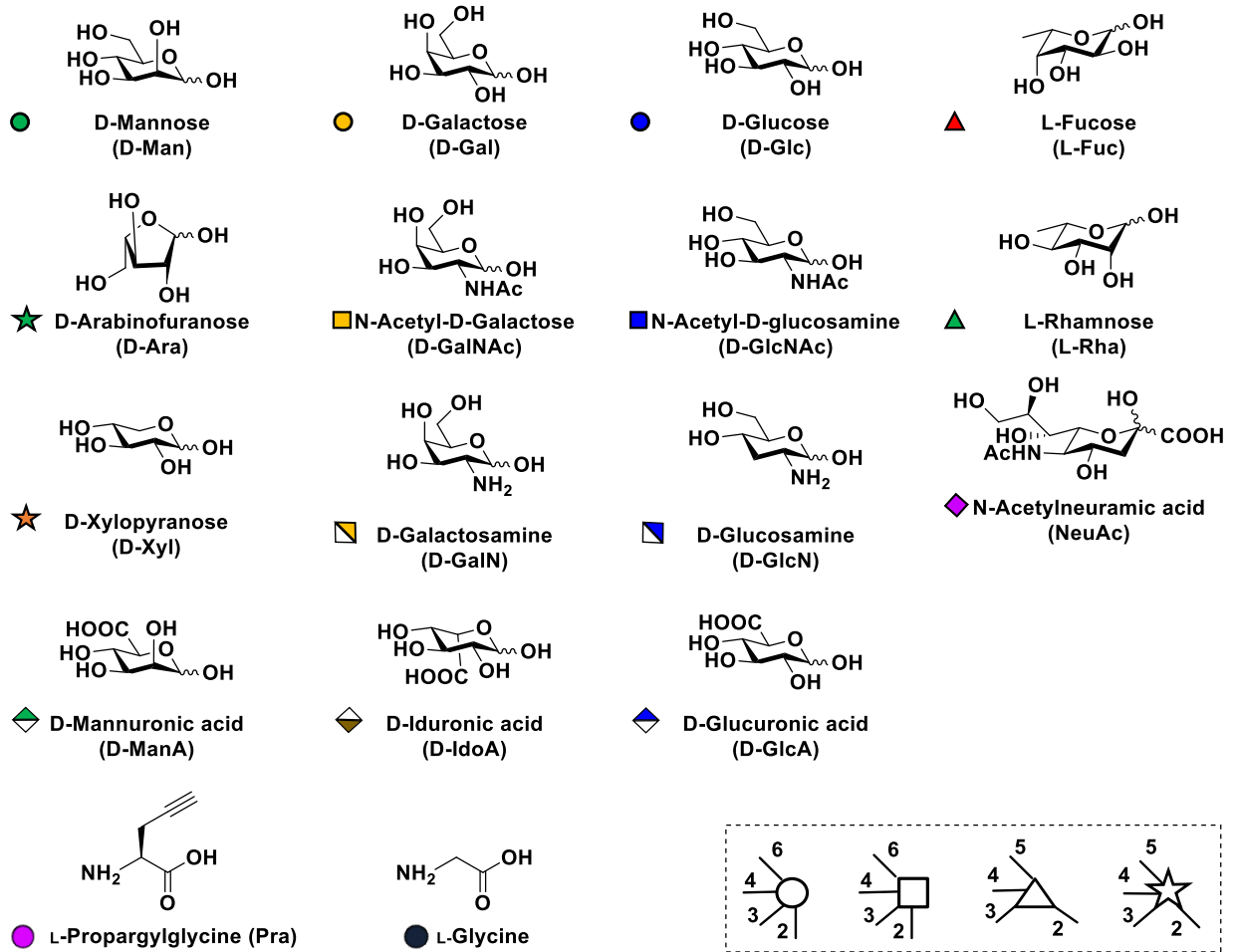
3.5.6.	Positioning of the acceptor slide before cLIFT process.....	141
3.5.7.	Contact angle measurements.....	143
3.5.8.	Calculation of the spatial distances of sugar moieties.....	144
4.	VaporSPOT: Parallel Synthesis of Oligosaccharides on Membranes	150
4.1.	Introduction	151
4.2.	Results and Discussion	152
4.2.1.	Development of VaporSPOT method and initial screening	152
4.2.2.	Oligosaccharide synthesis.....	155
4.2.3.	Parallel synthesis.....	159
4.3.	Conclusions	162
4.4.	Outlook	163
4.5.	Experimental Section.....	164
4.5.1.	Syntheses of linkers and building blocks.....	166
4.5.2.	Functionalization of cellulose membrane	174
4.5.3.	VaporSPOT glycosylation.....	177
4.5.4.	Oligosaccharide syntheses.....	182
4.5.5.	Parallel synthesis.....	192
5.	Conclusion and Perspectives.....	196
6.	References.....	200
7.	Appendix.....	214

List of Abbreviation

AA	Amino acid
Ac	Acetyl-
Ac ₂ O	Acetic anhydride
AGA	Automated glycan assembly
AMS	Automated multiplicative synthesis
Arg	Arginine
Asn	Asparagine
Asp	Aspartic acid
BA-LIFT	Blister-actuated laser-induced forward transfer
BB	Building block
Bn	Benzyl
Boc	tert-Butyloxycarbonyl
BPB	Bromophenol blue
Bz	Benzoyl
calcd	Calculated
Cbz	Benzyloxycarbonyl
cLIFT	Combinatorial LIFT
CMPI	2-Chloro-1-methylpyridinium iodide
Con A	Concanavalin A lectin
CRD	Carbohydrate recognition domain
CuAAC	Copper-catalyzed azide-alkyne cycloaddition
DABCO	1,4-diazabicyclo[2.2.2]octane
DBA	Dolichos biflorus agglutinin
DBU	1,8-Diazabicyclo[5.4.0]undec-7-ene
DCC	<i>N,N'</i> -Dicyclohexylcarbodiimide
DCM	Dichloromethane
DDQ	2,3-Dichloro-5,6-dicyano-p-benzoquinone
DIC	<i>N,N'</i> -Diisopropylcarbodiimide
DIPEA	<i>N,N'</i> -Diisopropylethylamine
DMF	Dimethylformamide
DRL-LIFT	Dynamic release layer LIFT
EA	Ethyl acetate
EDC	1-Ethyl-3-(3-dimethylaminopropyl)carbodiimide
EtOH	Ethanol
ESI	Electron spray ionization
Fmoc	9-Fluorenylmethyloxycarbonyl
Gal	Galactose
GalN	Galactosamine
GalNAc	<i>N</i> -Acetyl galactosamine
GBP	Glycan binding protein
Glc	Glucose
GlcN	Glucosamine
GlcNAc	<i>N</i> -Acetyl glucosamine
HA	Human influenza hemmagglutinin
HOBt	1-Hydroxybenzotriazol
HPLC	High performance liquid chromatography

Leu	Leucine
Lev	Levulinoyl
LG	Leaving group
LIFT	Laser-induced forward transfer
LiGA	Liquid glycan array
MALDI	Matrix-assisted laser desorption-ionization
Man	Mannose
MAPLE-DW	Matrix assisted pulsed laser evaporation-direct write
MeCN	Acetonitrile
MeOH	Methanol
MGL	Macrophage galactose-type lectin
Mincle	Macrophage inducible C-type lectin
MS	Mass spectrometry
Nap	2-Naphthylmethyl
NBS	<i>N</i> -Bromosuccinimide
NHS	<i>N</i> -Hydroxysuccinimide
NIS	<i>N</i> -Iodosuccinimide
NP-HPLC	Normal phase HPLC
NMR	Nuclear magnetic resonance
PEG	Poly(ethylene glycol)
PfOH	Pentafluorophenol
PG	Protecting group
Ph	Phenyl-
PMB	<i>p</i> -methoxybenzyl ether
PNP	<i>p</i> -nitrophenol
PNA	Peanut agglutinin
PS	Polystyrene
PTFE	Polytetrafluoroethylene
RCA-I	Ricinus communis agglutinin I
RP-HPLC	Reverse-phase HPLC
RRV	Relative reactivity values
SBA	Soybean agglutinin
SPR	Surface plasmon resonance
SPPS	Solid phase peptide synthesis
TBS	<i>tert</i> -Butyldimethylsilyl
TFA	Trifluoroacetic acid
THF	Tetrahydrofuran
TLC	Thin layer chromatography
TMS	Trimethylsilyl
tPG	Temporary PG
Tyr	Tyrosine
WGA	Wheat germ agglutinin

Symbols



Summary

Carbohydrates are ubiquitous biopolymers mediating fundamental biological processes such as cell–cell interaction, immune response, and host–pathogen interactions. They can selectively interact with each other (carbohydrate–carbohydrate interactions), with glycan binding proteins (carbohydrate–protein interactions), and pathogens. In order to study these interactions, glycan microarray technology has been developed, becoming nowadays a primary analytical tool. Glycan arrays enable high-throughput screening of these interactions in a fast manner, to identify new drug candidates, biomarkers, or vaccine candidates.

The main strategy to generate glycan arrays is the immobilization of pure and structurally defined oligosaccharides and glycomimetics on solid surfaces. The required oligosaccharides can either be isolated from natural sources or synthesized enzymatically and/or chemically. Automated chemical synthesis of oligosaccharides has become a streamline process, revolutionizing and simplifying the synthesis of linear and branched natural and unnatural glycan collections. In contrast to other common biopolymers, there is no method available for parallel oligosaccharide synthesis. In this work, different cost- and time-efficient approaches have been developed for parallel synthesis of oligosaccharides and glycopeptides on solid supports.

The first approach uses the combinatorial laser-induced forward transfer (cLIFT) as a printing technology for the *in-situ* chemical synthesis of glycan microarrays under the conditions required in carbohydrate chemistry. This so-called sugarLIFT method was developed and optimized, allowing the synthesis of glycan structures on defined positions of a surface, using a library of different glycosyl donors. Detection of the synthesized structures was achieved with their corresponding fluorescently labelled binding proteins (*Chapter 2*).

In addition, cLIFT was combined with copper-catalyzed azide–alkyne cycloaddition (CuAAC) to generate glycopeptides on-chip for multivalency studies. Specifically, 16 different peptide scaffolds were synthesized directly on-chip and a variety of glycosyl azides were attached to these scaffolds with various degrees of flexibility and orientation. Differently functionalized surfaces were employed to study the importance of surface functionalization for a variety of glycan–protein interactions. In the future, this approach may be utilized to generate large and much more complex multivalent glycomimetics, to investigate the binding mechanisms that nature has implemented to intricate biological processes (*Chapter 3*).

The last approach uses the basic principles of SPOT-synthesis, allowing the parallel synthesis of oligosaccharides under chemical vapor glycosylation conditions. The developed VaporSPOT method uses differently functionalized cellulose membranes as the solid phase synthesis support, for flexible and straightforward cleavage, purification, and characterization of the produced oligosaccharides. This approach is a first step towards the development of parallelized and automated glycan synthesis platforms (*Chapter 4*).

Zusammenfassung

Kohlenhydrate sind ubiquitäre Biopolymeren, die fundamentale biologische Prozesse wie Zell-Zell-Interaktionen, Immunreaktionen und Interaktionen zwischen Wirt und Erreger vermitteln. Sie können selektiv untereinander (Kohlenhydrat-Kohlenhydrat-Wechselwirkungen) wechselwirken, mit Glykan-bindenden Proteinen (Kohlenhydrat-Protein-Wechselwirkungen) und mit Pathogenen wechselwirken. Um diese Interaktionen zu untersuchen, wurde die Glykan-Microarray-Technologie entwickelt, die heute zu einem wichtigen Analyseinstrument geworden ist. Glykan-Arrays ermöglichen ein schnelles Hochdurchsatzscreening dieser Wechselwirkungen, um neue Arzneimittelkandidaten, Biomarker oder Impfstoffkandidaten zu identifizieren.

Die wichtigste Strategie zur Herstellung von Glykan-Arrays ist die Immobilisierung von reinen und strukturell definierten Oligosacchariden und Glykomimetika auf planaren Oberflächen. Die benötigten Oligosaccharide können entweder aus natürlichen Quellen isoliert oder enzymatisch und/oder chemisch synthetisiert werden. Die automatisierte chemische Synthese von Oligosacchariden hat sich zu einem Standardverfahren entwickelt, das die Synthese von linearen und verzweigten natürlichen und unnatürlichen Glykanen revolutioniert und erheblich vereinfacht hat. Im Gegensatz zu anderen gängigen Biopolymeren gibt es jedoch bisher keine Methode zur parallelen Oligosaccharidsynthese. In dieser Arbeit wurden verschiedene kosten- und zeiteffiziente Ansätze für die parallele Festphasensynthese von Oligosacchariden und Glykopeptiden entwickelt.

Der erste Ansatz nutzt den kombinatorischen Laser-induzierten Vorwärtstransfer (cLIFT) als Drucktechnologie für die chemische *In-situ*-Synthese von Glykan-Microarrays zusammen mit den in der Kohlenhydratchemie erforderlichen spezifischen Bedingungen. Dafür wurde die so genannte sugarLIFT-Methode entwickelt und optimiert, welche die Synthese von Glykanen auf definierten Positionen einer Oberfläche mit verschiedenen Glykosyl-donoren ermöglicht. Die synthetisierten Strukturen wurden anschließend mit den entsprechenden fluoreszenzmarkierten Bindungsproteinen detektiert (*Kapitel 2*).

Darüber hinaus wurde cLIFT mit der Kupfer-katalysierten Azid-Alkin-Cycloaddition (CuAAC) kombiniert, um Glykopeptide im Microarray-Format für Multivalenzstudien zu erzeugen. Konkret wurden 16 verschiedene Peptidgerüste direkt auf dem Microarray synthetisiert und verschiedene Glykosylazide mit unterschiedlichen Flexibilitätsgraden und Ausrichtungen an diese Gerüste gebunden. Zusätzlich wurden unterschiedlich funktionalisierte Oberflächen verwendet, um den Einfluss der Oberflächenfunktionalisierung auf eine Vielzahl von Glykan-

Protein-Wechselwirkungen zu untersuchen. In Zukunft könnte dieser Ansatz zur Erzeugung großer und sehr viel komplexerer multivalenter Glykomimetika genutzt werden, um jene Bindungsmechanismen zu untersuchen, die die Natur für komplexe biologische Prozesse eingerichtet hat (*Kapitel 3*).

Im letzten Ansatz wurden die Grundprinzipien der SPOT-Synthese genutzt, um die parallele Synthese von Oligosacchariden mittels chemischer Dampf-Glykosylierung zu ermöglichen. Diese sogenannte VaporSPOT-Methode verwendet unterschiedlich funktionalisierte Zellulosemembranen als Träger für die Festphasensynthese und erlaubt eine unkomplizierte Abspaltung, Aufreinigung und Charakterisierung der erzeugten Oligosaccharide. Dieser Ansatz ist ein erster Schritt zur Entwicklung von parallelisierten und automatisierten Glykansynthese-Plattformen (*Kapitel 4*).

1. Introduction

1.1. Carbohydrates in nature - role and complexity

Three types of biopolymers exist in nature: oligonucleotides, oligopeptides, and oligosaccharides mediating essential functions in organisms. Their participation in life-sustaining processes, as storage materials, structural components and primary metabolites of animals, plants and bacteria, as well as in life-threatening processes, (e.g., cardiovascular diseases, cancer and sepsis), urge their study. Additionally, their involvement in biological and chemical functions, such as immune defense, cell growth, adhesion, fertilization, metastasis, host interaction and cell-signaling, led scientists to investigate their structural characteristics on a cellular and molecular level.^[1,2] Carbohydrates, also named glycans, form a thick dense layer on the surface of all mammalian cells, the so-called glycocalyx. This glycocalyx consists of proteoglycans, glycolipids and glycoproteins with a thickness of ~100 nm (Figure 1.1). It is believed that the number of glycans comprising the glycocalyx to be around 100.000–500.000 different structures, serving as a protecting layer towards receptors from other cells, antibodies, viruses and pathogens.^[3] In addition, their selective recognition by carbohydrate/glycan binding proteins (GBPs), triggered their thorough investigation. However, their exact function is still not fully understood compared to the working mechanisms of proteins and nucleic acids. This is due to their high structural complexity, diversity (linkage type, branching, stereochemistry), and post-glycosylation modifications such as, methylation, acetylation, phosphorylation and epimerization.^[4,5] Furthermore the isolation, purification and characterization of carbohydrates remains a bottleneck, despite the large collection of glycans that can be already obtained.

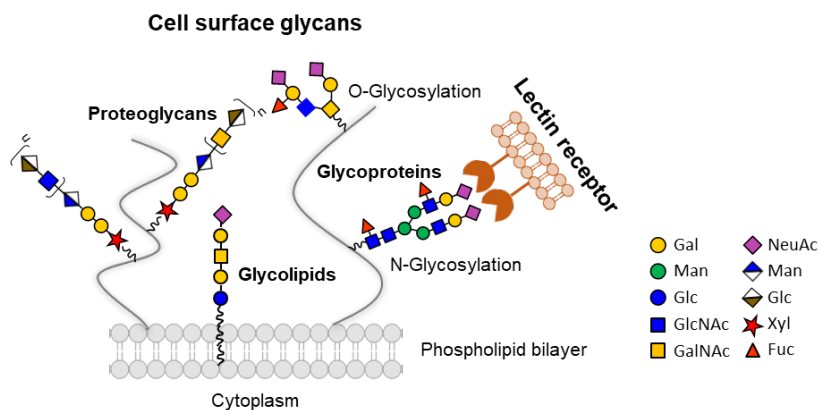


Figure 1.1: Example of glycans coating the surface of mammalian cells (modified^[6])

Additionally, the number of building blocks (BBs) required for their chemical synthesis compared to other biopolymers (Figure 1.2) makes their synthesis intricate. Their monomeric units, from which they arise, are called monosaccharides. Unlike other biopolymers that are linear, oligosaccharides are branched molecules, where each hydroxy group has the ability to serve as a branching point for chain elongation. In addition, the formation of the glycosidic bond that connects two monosaccharides can either have an α - or β - orientation (Figure 1.2), generating a new stereogenic center. This stereochemistry and complexity that nature developed plays a fundamental role in the interaction of GBPs as well as in their biological function.

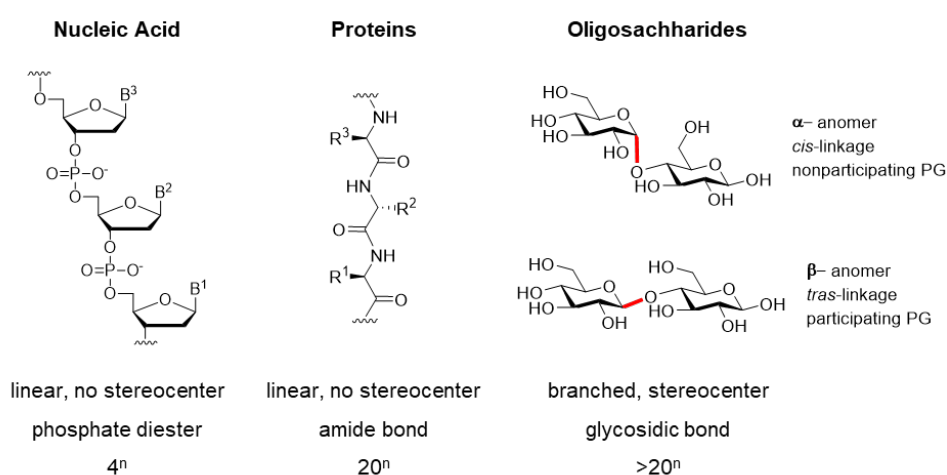


Figure 1.2: Complexity of typical biopolymers. Structural characteristics, bond type and number of building blocks required for the construction of an n-mer (modified^[7]).

1.2. Carbohydrate binding proteins

GBP can be classified into two major categories, lectins and sulfated glycosaminoglycan binding proteins.^[2] While enzymes are sometimes also considered as part of GBPs, they will be neglected here, to restrict it to the scope of this thesis. Lectins are GBPs, which are highly specific towards certain sugar moieties, playing a crucial role in multiple biological processes, while sulfated glycosaminoglycan binding proteins only recognize sulfated glycosaminoglycans (GAGs) selectively. Lectins, have widely been used since 1950s, to study different physiological mechanisms of glycoproteins and glycolipids at the molecular level.^[8] Their simple isolation from plants, animals and microorganisms, and their selectivity and specificity towards glycans, made them important tools for different purification, characterization and labeling techniques, with great value in diagnostics.^[9,10] Single interactions between glycans and their GBPs have relatively weak affinities in solution (millimolar scale) due to their small binding pocket (*Section 1.3*). To overcome this problem,

nature enabled lectins to develop and assemble into more complex structures, containing more than one binding pocket. This enhanced binding strength towards different monomeric units, bonds, atoms or even complex oligosaccharide structures, is called multivalency (*Section 1.3.2*), enabling higher affinities/avidities (nanomolar scale).^[11]

Classification of lectins

Lectins can be classified based on their a) monosaccharide recognition pattern, b) structural differences, and c) folding mechanism. They show higher affinities towards monosaccharide BBs such as: mannose (Man), fucose (Fuc), galactose (Gal), *N*-acetyl-galactosamine (GalNac), *N*-acetyl-glucosamine (GlcAc), and *N*-acetyl-neuraminic acid (NeuAc, sialic acid), since these units are typical constituents of the eukaryotic cell surfaces. Lectins can be isolated from plants, animals and pathogens. Plant and animal lectins can be classified into many structurally different categories,^[12] while pathogen lectins can be also found in viruses and bacteria.^[2] In this work, different plant and animal lectins were used as a detection technique (*Chapter 2*), as well as the binding mechanism of some lectins was investigated towards different glycan structures (*Chapter 3*). Thus, their basic characteristics will be further discussed for these two categories.

From the family of plant lectins, the so-called legume lectins^[13], are the most well-known and commonly used carbohydrate binding proteins. They found great use in biochemistry, molecular biology and physiology. Concanavalin A (ConA) was the first isolated plant lectin, derived from jack-beans. It is by far the most studied plant lectin until today, with a molecular weight of 104-112 kDa (250 amino acids). ConA primarily recognizes structures with terminal α -mannosides, α -glucosides, and secondarily β -glucosides. It is a pH and temperature dependent protein, having a homotetrameric form at natural pH (pH 7.4). Each binding site is ~ 72 Å apart, while the binding ability of each subunit is metal dependent, binding Ca and Mn cations.^[14] Similarly, more than a hundred other plant lectins have been isolated and structurally and mechanistically studied in the last decades, such as: Ricinus communis agglutinin I (RCA-I),^[15] Peanut agglutinin (PNA),^[16,17] Dolichos biflorus agglutinin (DBA),^[18] Soybean Agglutinin (SBA),^[19–21] and Wheat germ agglutinin (WGA).^[22] (Table 1.1).

Table 1.1: Structural characteristics and binding ability of important plant lectins.

Plant lectin	Ligand	Binding sites	
		primary	secondary
ConA	α -Man > α -Glc >> β -Glc	4	-
RCA-I	β -Gal	2 ^[a]	-
PNA	Gal- β -(1,3)-GalNAc- α -Thr/Ser	4	-
SBA	terminal GalNAc	4	-
DBA	α -GalNAc	4	-
WGA	terminal GlcNAc; Neu5Ac	4	4

^[a] RCA-I is a tetramer with only two Gal-specific subunits

The naturally most abundant animal lectins are the C- and the S-type lectins. Specifically, C-type lectins are transmembrane or soluble extracellular proteins, activating the defense or the immune response of the cell against pathogens. Despite their subdivision into three categories, all C-type lectins form a main core of 110-130 amino acids (AAs) and a carbohydrate recognition domain (CRD) of 120 AAs. For those using the Ca ion binding site to enhance their binding strength,^[23] Ca cations act as a bridge between the free hydroxyl groups of the glycans and the amino acid side chains of the lectin. Lectins with multiple subunits and up to eight binding sites in each subunit have been discovered. Langerin (CD207), as an example, is a type II transmembrane C-type lectin, isolated from Langerhans cells of 40 kDa molecular weight (328 AAs in total including the CRD). It contains a glutamic acid-proline-asparagine (EPN) recognition domain, binding diverse carbohydrate structures, such as high- mannose and fucose structures (e.g., blood group antigens), glycosamino glycans (GAGs, *N*-linked oligosaccharides, including heparin and heparan sulfate), and β -glucans.^[24–26] It has been proven that Langerin is a homo-trimer with the primary CRD to be 42 Å apart.^[27] Other mammalian lectins of structural and biological interest are the macrophage galactose type C-type lectin (MGL), and the macrophage-inducible C-type lectin (Mincle)^[9,28–30] (Table 1.2). Additional animal lectins that have been extensively studied, are the S-type lectins, I-type lectins, and P-type lectins^[2] that will not be further discussed in this work.

Table 1.2: Structural characteristics and binding ability of important C-type lectins.

C-type lectin	Ligand	CRDs
Langerin	Man structures; β -glucans; Fuc-blood group antigens	trimer
MGL	O-linked GalNAc; <i>N</i> -linked GalNAc >> Gal	trimer
Mincle	Man structures; glycolipids	monomer; dimer

Glycan-lectins recognition mechanism

Non-covalent interactions are the recognition forces between lectins and carbohydrates. Hydrogen bonds, π -stacking and electrostatic interactions, are involved in the interactions between the hydroxyl groups of the sugar moieties and the AAs of the lectins. In plant lectins, a hydrogen bond network is formed between the carbohydrate hydroxy groups and the acidic side chains of the peptide backbone, (-OH as acceptors with aspartic acid (Asp) and glutamic acid (Glu)) and the amines (-NH) of the peptide backbone (-OH as donors). Electrostatic (-CH- π) interactions are developed between the pyranose ring and the aromatic AAs of the lectins like phenylalanine (Phe), tyrosine (Tyr), and tryptophan (Trp).^[31]

Specifically, in α -Man-ConA recognition, the hydrogen bond network and the recognition is achieved between the O-3, O-4, O-5, O-6 of the mannose moiety with the asparagine (Asn) 14, leucine (Leu) 99, tyrosine (Tyr) 100, aspartic acid (Asp) 208 and arginine (Arg) 228, forming the binding pocket. Bidentate bonds are formed between the O-4 and O-6 with the Asp 208, as well as with O-5 and O-6 with the amine of the backbone of Leu 99 and Tyr 100 respectively. The other two hydroxy groups of the anomeric position, C-1 and the C-2 do not participate in the binding mode. One water molecule is also involved in the binding mechanism giving stability through interaction with the Ca cation. Additionally, the Ca cation interacts with Tyr 12, Asp14, Asp 19, Asp10 and Asp 208. Similarly, the crystal structure analysis showed that the Mn cation is also coordinated with Asp19 and Asp10 (Figure 1.3).^[14]

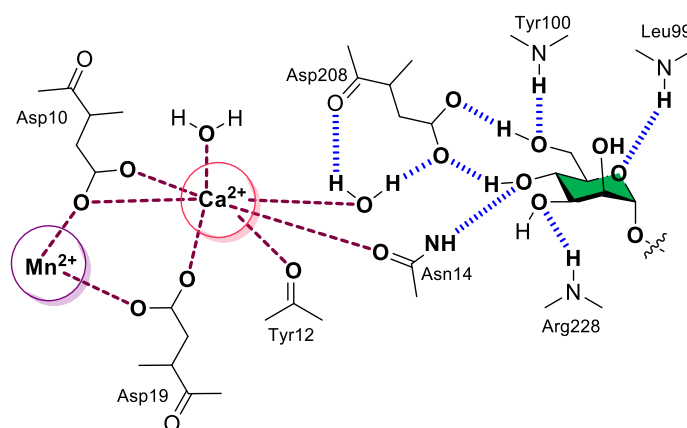


Figure 1.3: Schematic representation of non-covalent interactions of α -mannose-ConA binding. Hydrogen bond network is represented in blue and metal-ligand coordination in magenta (modified^[14]).

C-type animal lectins, can also be classified in two categories based on their carbohydrate recognition pattern. Lectins can have two different tripeptide sequences responsible for carbohydrate recognition in their CRD. Lectins with glutamic acid-proline-

asparagine motif (Glu-Pro-Asn, EPN motif, positions 185-187 in CRD), like Langerin, recognize Man, Glc, Fuc, and GlcNAc moieties, coordinating the Ca cation in the vicinal equatorial hydroxy groups, (3-OH and 4-OH). On the contrary, lectins with glutamine-proline-aspartic acid (Gln-Pro-Asp, QPD motif, positions 185-187 in CRD), like MGL^[32], recognize Gal and GalNAc moieties, *via* Ca cation coordination in the vicinal hydroxy groups with opposite stereochemistry (equatorial 3-OH and axial 4-OH).^[33] In both cases stabilization is achieved *via* a hydrogen bond network between the side chains of the mentioned AA moieties and the corresponding hydroxy groups.

1.3. Types of glycan-lectin interactions

1.3.1. Monovalent interaction

Lectins, as mentioned in the previous sections, can have more than one binding/recognition sites towards their binding partners. The simultaneous recognition of multiple ligands by a single lectin is called multivalency, enhancing the binding strength. Individual interactions (Figure 1.4A) between protein-glycan,^[34] protein-small molecule^[35] and protein-antibody^[36] are relatively weak (Table 1.3), while the multivalent interactions are stronger, enabling much higher affinities.

Table 1.3: Monovalent protein-ligand interactions sorted from the weakest to the strongest.

Protein	Ligand	Dissociation Constant (K_d)
ConA	Mannan	$\approx 2.9 \mu\text{M}$
anti-HA	HA	$\approx 0.38 \text{ nM}$
Streptavidin	Biotin	$\approx 1.00 \text{ fM}$

Key factors for strong multivalent interactions are the type(s) and number of available binding sugar moieties, their accessibility, and relative distance. Thus, several multivalent binding modes have been investigated and identified in the last decades.^[11,37,38]

1.3.2. Multivalent interactions

Chelating effect

The first method that can be implemented to enhance the binding mode is chelation. This can be applied for proteins having more than one binding sides. The available binding sites have the ability to bind simultaneously one chelating ligand. A chelating ligand is a molecule

that has as many required binding moieties as the available binding sites of the acceptor. In this specific case, the energy loss, transitional and rotational, is required only once, leading to $\approx 10^3$ - 10^6 enhanced binding (Figure 1.4B).^[39] The chelating effect strongly depends on the nature, the flexibility and the distance of the linker connecting the ligands together since it needs to match with the exact distance of the binding pockets of the lectin.^[40,41]

Clustering Effect – Statistical / Proximity effect

Another approach to enhance the binding mode is the clustering of a multivalent molecule around the receptor, having only one binding site and vice versa. In this recognition mode, fast binding exchange between a single receptor and a multivalent molecule is observed (Figure 1.4C), resulting in an increased affinity. However, aggregation is one of the main disadvantages of this phenomenon observed in carbohydrate-lectin interactions.^[39,42] The same effect contains clustering of multiple binding sites of a receptor around a multivalent molecule. This effect is observed in solution or on surfaces, depending on the concentration of the lectin and the concentration of the multivalent sugar molecules. Soluble clusters and aggregates are the mainly observed “side-effects”.^[43]

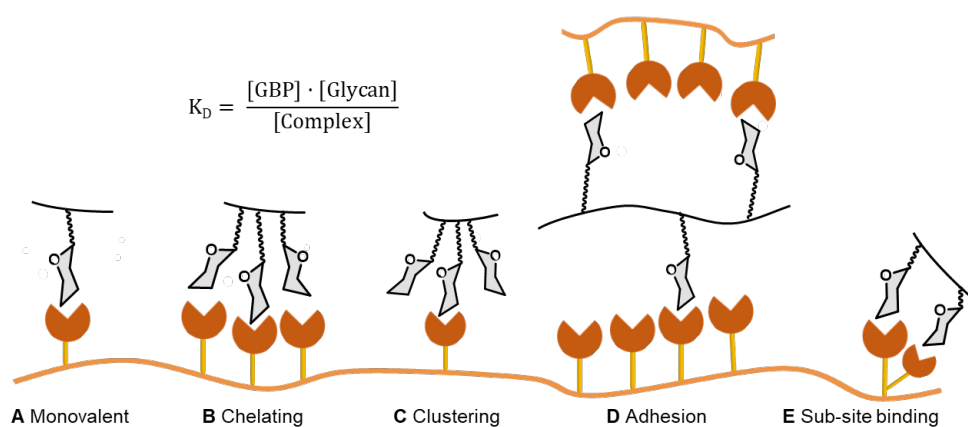


Figure 1.4: Schematic representation of most common interactions: A) monovalent interaction, weakest interaction between monovalent ligand and one binding site. Multivalent interactions are identified as B) chelating, simultaneous recognition of a multivalent ligand by an oligomeric receptor; C) clustering, one binding site is surrounded by a multivalent ligand; D) steric stabilization effect, simultaneous recognition of a multivalent ligand from opposite sides; E) subsite binding, recognition of multivalent ligand from an extended binding site.

Steric stabilization effect – Adhesion

In this effect, multivalent receptors are used with multivalent molecules having the desired ligands in favored and disfavored positions. Although the competition for binding in the receptor is higher, stabilization of the ligands is observed due to steric hindrance. Different

scaffolds have been used in the past years to investigate these phenomena (Figure 1.4D).^[44,45]

Sub-site binding

Some lectins can simultaneously recognize multivalent ligands from their extended binding sites. It is reported in the literature that ConA has the ability, apart from the main binding sugar on the ligand to interact with additional sugar moieties of the ligand, involving ConA-disaccharide and trisaccharide binding.^[14,46] The resulting enhanced binding is called sub-site binding (Figure 1.4E).

In summary, non-chelating effects give lower binding affinities compared to chelating and clustering effects. Thus, multiple oligosaccharide structures have been either isolated from natural sources or synthesized chemically to mimic nature.^[45] One of the main methods widely used to investigate and understand glycan-GBP interactions is the microarray technology that will be explained in the following *Section*.

1.4. Glycan microarrays

This chapter has been partly modified from: Mende, M.; Bordoni, V.; **Tsouka, A.**; Löffler, F. F.; Delbianco, M.; Seeberger, P. H.; Multivalent glycan arrays, *Faraday Discuss.*, **2019**, 219, 9–32. DOI: 10.1039/c9fd00080a.

Microarrays are miniaturized tools containing collections of different biomolecules placed in defined positions on a solid support. They have been widely used for the analysis of different biomolecules in molecular biology and biomedical research, since they allow for high-throughput screening of potential binding partners. Using microarrays, quantitative and qualitative data can be acquired, for example for gene expression or diagnostics. A microarray assay involves an initial chip incubation with diluted patient serum, an additional incubation with secondary fluorescently labeled reagents, such as antibodies, a visualization of the binding recognition *via* high resolution fluorescence scan and, finally, the analysis of the obtained result. There is a variety of commercially available microarrays such as protein and peptide,^[47,48] carbohydrate,^[6] DNA,^[49,50] and cell array.^[51]

Glycan microarrays are considered versatile screening tools for the investigation of glycan-GBP interaction studies. This method has been widely used to understand and identify the role of glycans in many biological processes. For the preparation of microarrays, glycans have either been isolated or/and synthesized (*see Chapter 1.4.1*), printed (*see*

Chapter 1.4.2), and immobilized on the microarray (see Chapter 1.4.3) with a highly dense and spatially defined pattern. Since 2002, the development of different robotics and high-resolution screening technologies has led to the immobilization of thousands of glycans on microscope glass slides, allowing rapid simultaneous screening of multiple glycan-GBP interactions.^[52,53] As “arrays”, different forms have been used lately e.g., silica plates,^[53] beads,^[54,55] microplates,^[56] cells,^[57] M13 bacteriophages (LiGA)^[58] and DNA coded solid supports.^[59] (Figure 1.5).

There are only few reported methods in the literature so far for the *in-situ* generation of glycan microarrays. In 2008, Mrksich *et al.*,^[60] introduced for the first time the *in-situ* chemical synthesis on chip. They synthesized 24 different disaccharides, which were subsequently enzymatically modified for a label-free bio-assay, demonstrating the importance and the to develop *in-situ* methodologies for glycan microarray preparation, analogous to the well-established DNA and peptide microarray techniques.^[61] Recently, Heo *et al.*,^[62] reported their sequential enzymatic on-chip glycosylation strategy for the synthesis of several Globo H oligosaccharides. All structures were characterized, purified and subsequently re-immobilized on the microarray since a pH-dependent DNA i-motif was used. Additional screening of the formed structures in the array format was achieved after fluorescent staining with their corresponding fluorescently labeled lectins. Despite the importance and the urgent need for on-chip paralleled glycan synthesis, most methods are still in a very early stage of development. However, different methodologies for contact and non-contact printing of compounds have evolved using different glycan concentration and surface functionalization,^[6,63] and immobilization techniques, using different functional groups. In these following *Sections*, the methods to generate glycan microarrays will be explained in detail.

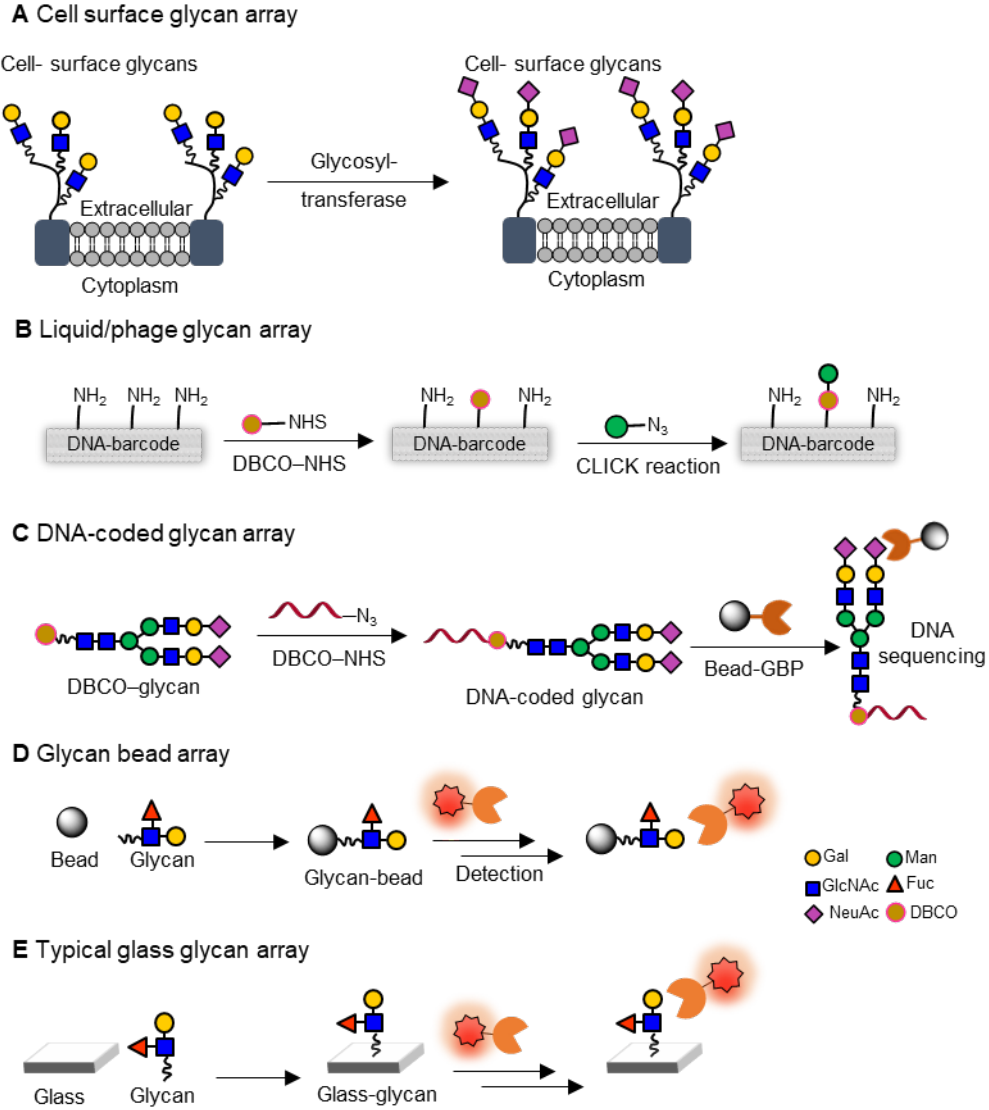


Figure 1.5: Types of glycan microarrays: A) cell surface glycan arrays; B) Liquid/phage glycan arrays (LiGA); C) DNA-coded glycan array (DBCO: dibenzocyclooctyne); D) multiplex glycan bead array; E) most commonly used glass glycan arrays (modified^[64]).

1.4.1. Access to glycan collections for microarray fabrication

There are two different ways to access different oligosaccharide structures: isolation from natural sources and/or biological/chemical synthesis. Oligosaccharides can be synthesized by enzymatic, chemo-enzymatic, and chemical strategies with stereo- and regio-control. In the last decades, different automated platforms have been established for enzymatic and chemical oligosaccharide synthesis, allowing the synthesis of complex and biologically valuable structures.

Natural isolation of glycans

In general, natural glycans exist in organisms and can be obtained from animal/plant tissues, and pathogens. After being treated with enzymatic and chemical means, a large variety of oligosaccharides (*N*-glycans, *O*-glycans, and glycosphingolipid-derived glycans from glycoproteins and glycosphingolipids respectively) can be delivered into aqueous solution. Nevertheless, the released oligosaccharides require an extensive and laborious purification since they are in a heterogeneous form. Additional labelling is required for their separation and characterization by tandem analytical techniques (HPLC, MS-MS).^[65–67] Lastly, for their immobilization on the microarray, further functionalization is required at their anomeric position with respective functional groups. Typical derivatization of naturally isolated oligosaccharides involves reductive amination (with amine linkers) forming ring-opened glycoconjugates, reactions with hydrazide, and *N*-substituted *N*-hydroxylamine linkers, leading to closed-form glycan moieties, eventually allowing their immobilization.

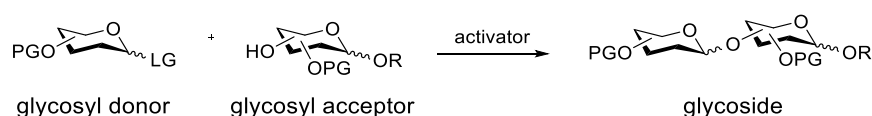
Enzymatic synthesis of glycans

Enzymatic synthesis of carbohydrates is stereo- and regioselective, relying on enzyme specificity.^[68] Synthesis is performed without tedious protecting group control, giving access to natural and unnatural analogues. Their use is highly recommended for poorly reactive monosaccharides (e.g., sialic acid) and for challenging linkages. The reactions are considered to be environmentally friendly, since they are performed in aqueous media under temperature and pH control in presence of the required metal ions, with no toxic byproduct generation.^[69]

However, the availability of glycosyltransferases (enzymes responsible to establish glycosidic bonds) to cover all the existing synthetic needs is limited.^[70] The difficulty to produce synthetic enzymes *in vitro* is one of the main reasons and only recently some progress was shown.^[71] To overcome the ineffectiveness of enzymes towards minor modifications for complex glycan synthesis, chemoenzymatic approaches have been developed, combining the flexibility of the chemical synthesis with the high regio- and stereoselectivity of enzyme-catalyzed reactions.^[72] Recently, multiple automated platforms for enzymatic and chemoenzymatic synthesis have been introduced with promising results using HPLC-based techniques and peptide synthesizers for glycan generation.^[73–77]

Basic characteristics of chemical glycosidic bond formation

A chemical glycosylation reaction is considered a fundamental and complex process, widely studied for the last hundred years.^[78] It is defined as a reaction between two monosaccharides in the presence of an activator/promoting agent. During glycosylations, one sugar moiety acts as the glycosyl donor (electrophile) bearing the glycosyl carbon in the anomeric position to form the glycosidic linkage, while the other sugar moiety serves as the glycosyl acceptor (nucleophile), bearing one deprotected hydroxy group in the position where the glycosidic linkage is needed to be formed (Scheme 1.1).



Scheme 1.1: Chemical glycosylation reaction.

The challenges of a chemical glycosylation reaction are the stereo-selectivity (selective formation either of α - or β - anomer), and the regioselectivity (type of glycosidic bond formation) (Figure 1.6).^[79]

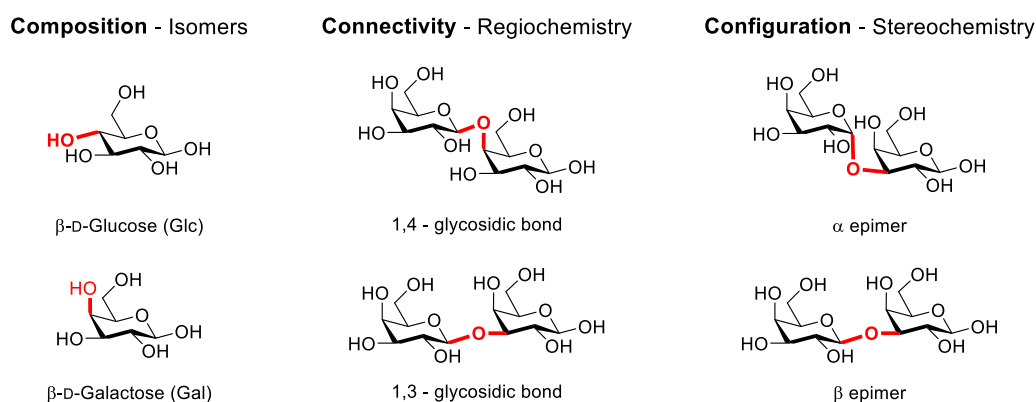
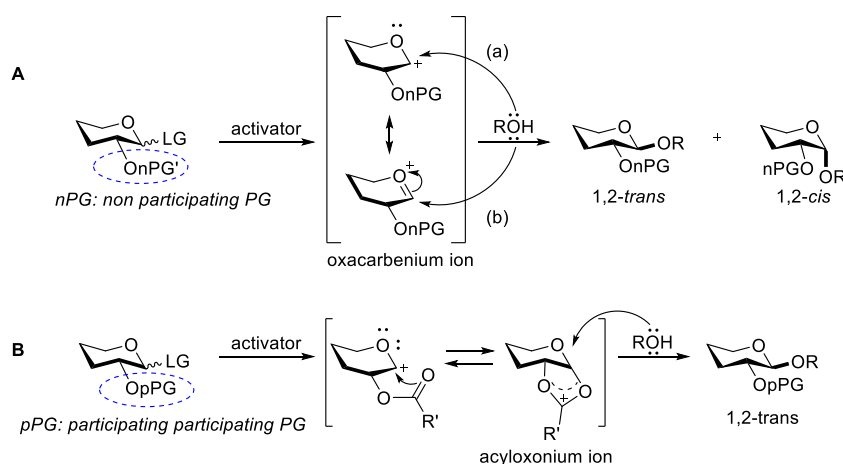


Figure 1.6: Types of structural differences between glycans. Monosaccharide building blocks are stereoisomers and differ only in the stereochemistry of one -OH group (position of C4 for galactose and glucose). The difference in the position of the glycosidic bond defines the regionchemistry of the molecule, while the type of the glycosidic linkage the stereochemistry (modified^[80]).

Multiple factors influence the glycosylation outcome, such as reactivity and structure of the monosaccharide BB, conformational constrains, protecting groups,^[81–83] temperature,^[84,85] solvent,^[86] activation agents/promoters and other additives.^[85,87,88] However, there is no clear rule to direct the desired glycosyl linkage since multiple mechanisms are engaged within the progress of the reaction delivering a mixture of α - and β - anomers. A glycosylation reaction proceeds through nucleophilic attack from the glycosyl

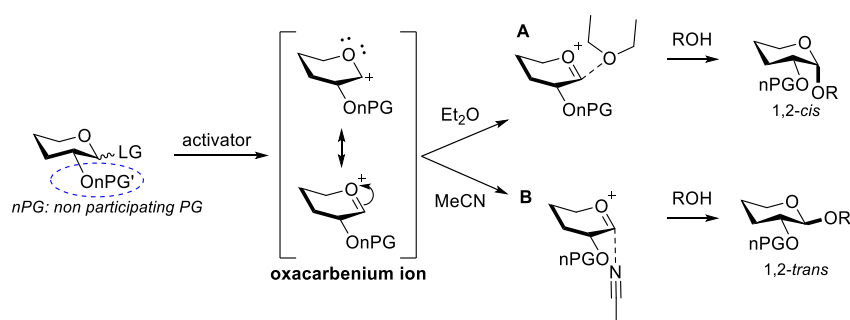
acceptor to the anomeric center of the glycosyl donor (C-1). Prior to the nucleophilic attack the glycosyl donor forms an oxacarbenium ion intermediate *via* addition of an electrophilic promoter which activates the leaving group on the anomeric carbon of the donor. The oxocarbenium is stabilized by the lone pairs of the O-5, forming a highly electrophilic intermediate. Two possible mechanistic pathways can be followed: nucleophilic attack from the top, and from the bottom face, giving a mixture of 1,2-*trans* (β -anomer) and 1,2-*cis* (α -anomer) products respectively (Scheme 1.2A). In presence of a neighboring participating protecting group (acyl moiety, participating protecting group: pPG) in the C-2, the oxocarbenium is converted to an acyloxonium ion intermediate. This favors the formation of the stereochemically controlled 1,2-*trans* product (β -anomer), since the nucleophilic attack can only proceed from the top face (Scheme 1.2B).



Scheme 1.2: Mechanism of glycosylation reaction in presence of: A) non-participating protecting group in C-2, oxacarbenium pathway; B) participating protecting group in C-2, acyloxonium formation.

As apparent from the previous mechanistic explanation, the formation of the 1,2-*cis* product cannot be as selective as the 1,2-*trans* glycosides (anchimeric assistance by participating protecting groups). Thus, different synthetic strategies should be considered. The challenging 1,2-*cis* linkage can only be achieved in absence of a neighboring protecting group in the C-2 position. Although the thermodynamically controlled α -product is favored by the anomeric effect,^[89] the solvent effects and various electronic and steric factors^[90] could play a crucial role to obtain the desired α : β ratio of the glycosylation reaction. Specifically, solvents that participate in glycosylation reactions can influence the outcome. Ethers (e.g., diethyl ether, tetrahydrofuran, 1,3-dioxane) and nitrile solvents (e.g., acetonitrile, MeCN) drive the reaction toward α - and β -selectivity respectively. In particular, diethyl ether adopts an equatorial conformation (Scheme 1.3A) while the nitrilium cation that is formed *in-situ* in

the presence of MeCN prefers the axial coordination allowing the nucleophilic attack to take place from one face only (Scheme 1.3B).^[91,92]



Scheme 1.3: Solvent participation in glycosylation mechanism for stereochemical control. A) Etheral solvents for α -selectivity; B) nitrile solvents for β -selectivity, *via* nitrilium cation formation.

Nowadays, chemical synthesis of carbohydrates is considered the most powerful tool for the preparation of natural and unnatural complex analogues in high purity. Chemical synthesis can be performed in solution or in solid phase systems and is already automated. In the following *Sections* the methods to obtain synthetic carbohydrates will be explained.

Manual synthesis

The one-pot strategy is one of the main batch synthesis approaches used nowadays. It allows multiple sequential transformations to be carried out without isolation and purification of the formed intermediates in one reaction vessel, reducing the production of chemical waste. It can be subdivided into: a) reactivity-based approach, which relies in the “armed-disarmed” donor-acceptor relation,^[93] orthogonal protection approach, based on the different reactivities of the anomeric leaving groups, and c) preactivation-based approach, where the donor is preactivated and then coupled with an acceptor. In the last 20 years, these one-pot strategies gave access to complex oligosaccharide structures with biological importance,^[94] like the 92mer mycobacterial arabinogalactan.^[95] Additionally, the development of the programmable one-pot synthesis, the “OptiMer” data base and the “Auto-CHO” software gave access to the relative reactivity values (RRVs) of different BBs, allowing better design of synthetic procedures and more efficient assembly.^[96,97] Lastly, the development of the automated multiplicative synthesis (AMS), relying on the preactivation-based approach of one-pot synthesis gave access to multiple linear and branched structures with up to 15 residues, when working in dual-mode. The transformation of this AMS system to a light-induced activation system with a photo-activator (Umemoto’s reagent as activator) resulted in the automated synthesis of multiple bioactive oligosaccharides in high overall

yield (>59%), allowing the synthesis of structurally challenging biopolymers with pharmaceutical and material interest in gram scale with up to ~1000 units.^[98]

Automated synthesis

Different automated platforms have been developed for the assembly of oligosaccharides to overcome the challenges of the traditional synthesis. The first attempt for the development of an automated technology dates back to 1971.^[99] Over the past years, multiple efforts resulted in the development of three main technologies, revolutionizing the synthesis of oligosaccharides: electrochemical assembly, assisted synthesis, and solid-phase synthesis.^[100] However, electrochemical synthesis,^[101] fluororous tagged-assisted solution,^[102] and HPLC-assisted chemical synthesis,^[103–105] have certain limitations, only giving access to a small hexasaccharide libraries of compounds.

A game changer was the development of the solid-phase automated glycan assembly (AGA) (*Section 1.5.2*),^[106] which uses a modified peptide synthesizer. Within the last 10 years, AGA has been fully automated and commercialized.^[107] Up to date, many processes have been modified and optimized,^[108–110] achieving the synthesis of long and highly branched polysaccharides of up to 100mers with biological and structural interest.^[111–118] Oligosaccharides obtained from AGA can be used for multiple applications such as glycan microarray generation for infectious disease research, vaccine development, as well as for conformational and structural studies that can lead to tailor-made carbohydrate based materials, glycan-peptide hybrids, and in general, to the production of bio-inspired materials with different properties.^[7,119–123]

1.4.2. Printing methods of glycans

After the successful isolation and/or synthesis of the desired glycan structures, glycans can be printed in the microarray format. Two different methodologies have been developed for contact and non-contact deposition of the desired material on functionalized solid supports with high accuracy and reproducibility.

Contact technologies include pin printing and microstamping, allowing the deposition of desired materials with high precision (Figure 1.7A). Pin printing setups contain a robotically controlled pin printing head with multiple printing pins for nanoliter droplet deposition of the desired biomolecules. The pins are soaked with a specific volume of the prepared solutions from a microtiter plate. Once the amount is captured inside the pin, the robot head slightly

touches the solid support with the pin to deposit the biomolecule on the microarray. Alternatively, microstamping is used as a printing method. In this case, the solution is not deposited as a droplet, but is stamped on the surface *via* a stamp. The stamp is soaked in the solution either by a spray-on or by a robotic feature-feature ink method and the substance is stamped to the substrate. Microstamping is mainly used for single or a few biomolecules. It is much more difficult to be applied for the transfer of multiple components as in pin printing. Extensive cleaning, dust free conditions and refilling is required for both methods.^[124]

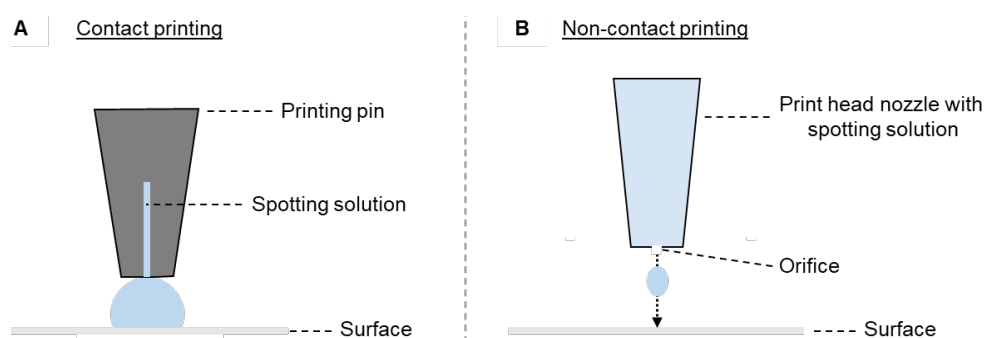


Figure 1.7: Schematic representation of A) contact- and, B) non-contact printing of glycan microarrays (modified^[125]).

In non-contact deposition, printing is achieved by ejection of the biomolecules as droplets or jets on the solid support from a reservoir through an orifice (Figure 1.7B). The distance between the orifice and the solid support is kept in a precise distance (1-5 mm) for accurate and reproducible deposition of the material. This method relies on the inkjet printing technology, using each biomolecule solution as an “ink”. Three different methods can be applied for successful ejection of the ink: piezo, valve-jet, and thermal inkjet. The non-contact approach ensures no surface damage and longer printing runs compared to the contact printing technologies. However, challenging remains the clogging of the printing head nozzle due to accumulation of the ink material. Other artifacts can result in failed spot delivery and low solubility of the biomolecule.^[124]

The development of the combinatorial laser-induced forward transfer (cLIFT) overcomes all the mentioned contamination, solubility and clogging issues.^[126] This method currently allows for flexible, precise and rapid deposition of amino acids for high density peptide and peptoid microarray generation. However, while this method has been optimized and already automated, it is restricted to amino acid printing so far (see *Section 1.5*).^[127,128]

Dip-pen nanolithography using the principles of atomic force microscopy,^[129] and dip-pen lithography coupled with microfluidics and photochemistry,^[130] have also been applied

for the preparation of glycan microarrays. After the successful printing onto the solid support, different immobilization approaches have been investigated for covalent and non-covalent attachment of the glycan moieties.

1.4.3. Immobilization of glycans

Multiple methods have been investigated for efficient immobilization of glycans on the solid support. However, many practical issues need to be considered prior to microarray generation, such as glycan structure in a free or modified form, as well as microarray surface functionalization. The immobilization strategies are: a) non-covalent immobilization, and b) covalent, while both categories are subdivided to site-nonspecific and site-specific (Figure 1.8).

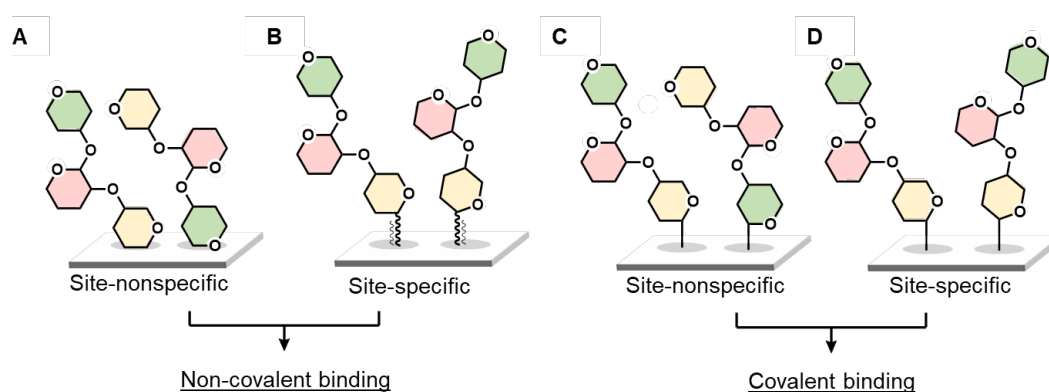


Figure 1.8: Immobilization strategies for glycan microarrays. A) Non-covalent, non-specific; B) non-covalent site-specific; C) covalent, site non-specific; and D) covalent, site-specific glycan attachment (modified^[125]).

Non-covalent immobilization

Non-covalent immobilization relies on electrostatic and hydrophobic interactions between the glycan structures and the solid support. The used glycans can either be free or functionalized, while the solid support can either be functionalized or non-functionalized.

The most effortless way to attach a glycan on a solid support is the site non-covalent, site-nonspecific immobilization (Figure 1.8A). Unmodified long polysaccharides are randomly bound onto the surface due to the large contact area between the sugars and the solid support. This method is restricted to polysaccharides and cannot be applied for small-size structures due to the weak attachment. Moreover, this non-specific binding makes the biomolecular recognition less precise, carrying constant risk of compound loss during the washing steps. A characteristic example of non-covalent electrostatic interaction is the

efficient attachment and analysis of the binding mode of heparin on poly-lysine glass slides.^[131]

The other non-covalent way to attach a sugar moiety on a solid support is the non-covalent site-specific immobilization. In this mode, high reproducibility is achieved *via* chemical modification of the sugar structure at the reducing end, allowing specific attachment of the glycan on the solid support (Figure 1.8B). Glycoconjugates like glycolipids, fluoros tagged-glycans, biotinylated-glycans, and oligonucleotide-conjugated glycans can be easily immobilized, while DNA hybridization (DNA i-motifs) can also be used for the preparation of glycan microarrays, through complementary oligonucleotide attachment.^[53,62,132–135]

Covalent immobilization

The covalent attachment of sugar molecules onto the microarray format is preferred, since it overcomes the problems of the non-covalent immobilization. Covalently immobilized structures can be found on the solid support with well-defined structures and orientation resulting in accurate binding recognition. Similar to the non-covalent immobilization strategy, covalent glycan attachment is divided into site non-specific and site-specific. For both, the glass slides are coated with a silane or thin polymer film and are additionally functionalized with the corresponding functional groups to perform coupling reactions.

The least demanding way to immobilize glycans covalently on a solid support is to use unmodified glycans and functionalized glass slides (Figure 1.8C). With this approach, random binding of the sugar moiety is achieved resulting in inaccurate binding modes. The glass slides used for covalent, site non-specific immobilization, are functionalized with photo-reactive protecting groups^[136,137] or boronic acid.^[138]

Covalent and site-specific immobilization is the most extensively studied and precise method for glycan microarray fabrication (Figure 1.8D). Single carbohydrates or oligosaccharides with functional groups on the anomeric position (*Section 1.4*) can selectively react with the available functional groups of the solid support, forming a covalent bond. These coupling reactions make the attachment of the sugar moieties highly selective, increasing the quality and precision of the derived binding mode. Chemical modification is required on the solid support or/and the anomeric position of the glycans. The distance between the sugar moieties and the solid support plays a crucial role on the binding mode of the protein as well as on the accessibility of the attached glycan.^[139,140] Hydrophilic poly(ethylene glycol)-based (PEG) linkers on the anomeric position of the glycans are preferred in comparison with their corresponding hydrophobic analogues. However, the

synthesis and the proper functionalization of the targeted oligosaccharides remains a bottleneck requiring multiple synthetic steps to obtain a single compound.

Thiol-maleimide chemistry for the covalent attachment of glycans on solid supports has widely been used, since it is fast under mild conditions and with high selectivity. Glycans are either functionalized with a maleimide group and then attached to functionalized thiol solid support^[140] or thiol-linked sugars are attached to maleimide-coated surfaces^[141] (Figure 1.9A). It is essential to mention that the thiol functionalization requires delicate handling and no air exposure due to their ability to undergo oxidation under ambient conditions.

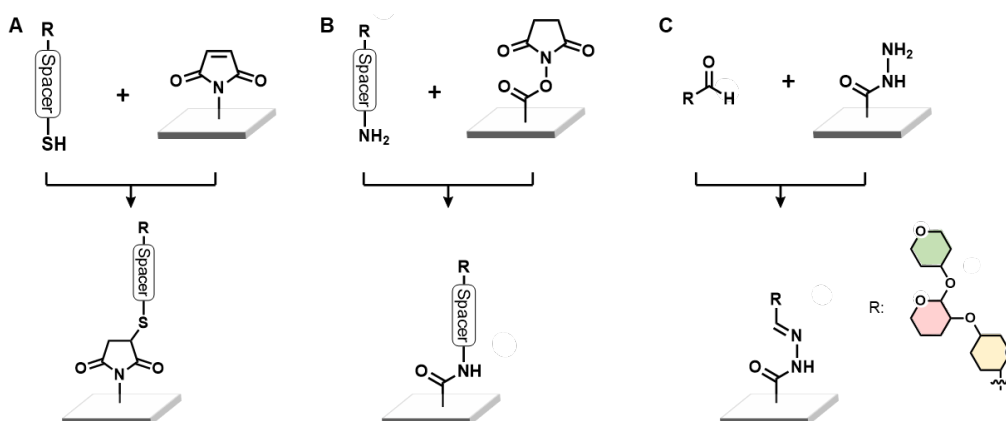


Figure 1.9: Commonly used method for site-specific covalent bond attachment. A) Thiol-maleimide; B) amide-NHS-ester; and C) free reducing end and hydrazine immobilization (modified^[125]).

Today, the amine-based chemistry is the most frequently applied method. Amine functionalized glycans can react with *N*-hydroxysuccinimide (NHS) esters and cyanuric chloride-coated surfaces *via* nucleophilic aromatic substitution^[142] (Figure 1.9B). The coupling with NHS-esters can take place in basic pH (~8.5) yielding a very stable and selective amide bond.^[143,144] NHS-functionalized slides are commercially available and the synthesis of amine-functionalized glycans is simple, well established and can be performed in a fully automated fashion.^[7]

Hydrazide-functionalized surfaces are also used for covalent site-specific immobilization (Figure 1.9C). However, with this modification, free and unmodified reducing carbohydrates have to be used.^[145] The high nucleophilic character of the functional groups on the solid support ensure fast and stable bond formation between the reducing end of the glycans and the microarray. Similarly, amine-functionalized slides and aldehyde sugar moieties have been coupled successfully on the solid support by Schiff base formation.^[146]

Different ligation reactions have also been applied on epoxy-functionalized slides (Figure 1.10). Epoxides can form stable covalent bonds with multiple nucleophiles such as thiol-, amine- and hydrazide- conjugated oligosaccharides.^[63]

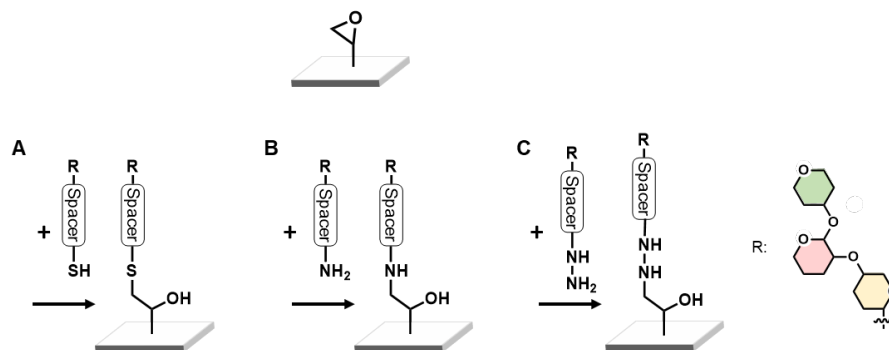


Figure 1.10: Possible coupling reactions of epoxide functionalized slides with corresponding functionalized sugar moieties. A) Thiol-; B) amine-; and C) hydrazine-functionalization of sugars (modified^[125]).

Cycloaddition reactions have also been used for the preparation of glycan microarrays such as Diels-Alder and azide-based reactions (Figure 1.11).^[147,148] Copper-catalyzed azide-alkyne cycloaddition (CuAAC) reaction^[149] and Staudinger ligation^[150] have also been applied for the immobilization of azide moieties on alkyne- and phosphane-coated surfaces, respectively.

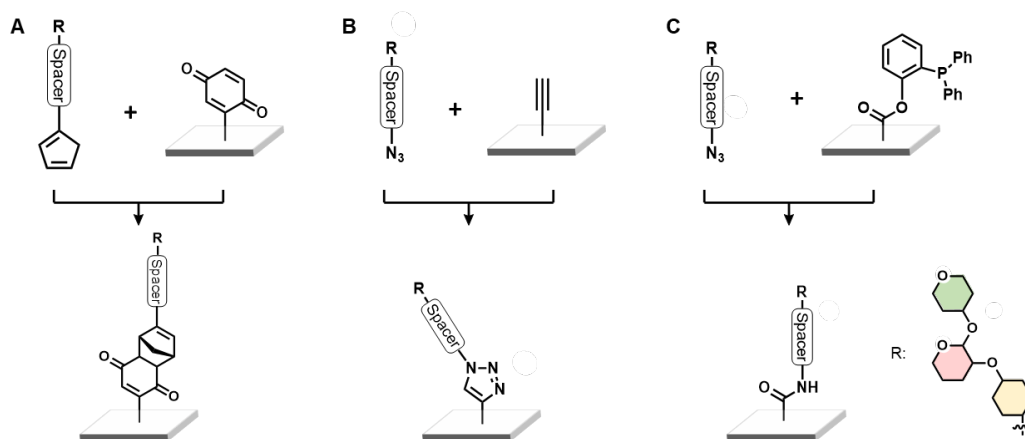


Figure 1.11: Possible cycloaddition coupling reactions: A) Diels-Alder reaction; B) copper-catalyzed azide-alkyne cycloaddition (CuAAC); and C) Staudinger ligation (modified^[125]).

1.4.4. Multivalent glycan arrays

As mentioned in *Section 1.3*, multivalency is one of the most important mechanisms that nature has developed to increase the binding strength with different proteins. Typically, on the microarray, monovalent glycans are printed in an uncontrolled manner, and multivalency is neglected since the spatial distribution and orientation of the sugar moieties

cannot be identified. The obtained avidity depends on the density and the spatial orientation between the spotted structures and can either be enhanced or restrained (Figure 1.12). Thus, in the last decades, multiple studies have been focused on identifying the optimal presentation, concentration, orientation, flexibility and density needed on the microarray for multivalent interaction. The density of pre-synthesized structures or natural glycoconjugates can be regulated by variations in the concentration of the printed solution and printing process.^[151]

A plethora of different scaffolds have been used to synthesize multivalent glycoconjugates with different sizes and shapes to mimic the natural presentation.^[45,152,153] Multivalent glycan microarrays, containing multivalent structures such as neoglycoproteins/neoglycopeptides,^[52,154] glycodendrimers,^[155] DNA-linked glycans,^[156] glycoclusters^[157] and glycopolymers^[158–160] have extensively been studied with diverse glycan densities.

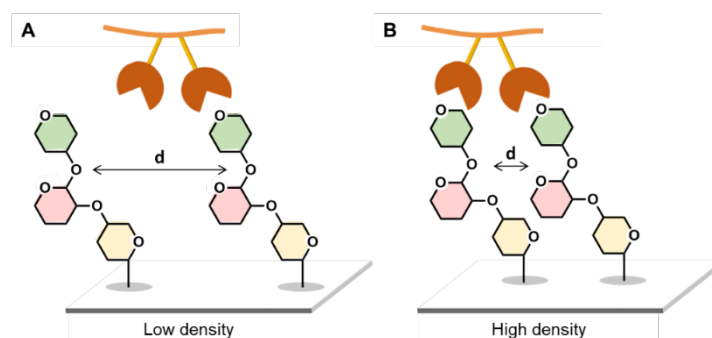


Figure 1.12: Schematic representation of glycan microarrays. A) Low density glycan immobilization; B) high density of glycan immobilization (modified^[125]).

Synthetic and natural glycoprotein and glycopeptide multivalent microarrays showed that the multivalent recognition of the protein is density dependent. The binding ability is decreased by increasing the distance between the spotted compounds and by decreasing the number of sugar moieties on the multivalent structures. Additionally, by altering the spacing between the sugar moieties on the multivalent ligands decreased binding was observed. Thus, the spacing, orientation and density, of ligands must be adequate to the respective binding sides of the receptor.^[161–163]

Recently, biocompatible unnatural dendritic glycomimetics have also been synthesized on arrays, offering a highly defined structure and density. Particularly, Pieters *et al.*,^[164,165] synthesized a multivalent glycan microarray using five different glycans with mono- to octavalent presentation. Screening of the multivalent character with the corresponding binding lectin showed that lectin recognition with closely located binding sites resulted in

stronger multivalent interactions. This strong interaction was observed due to the chelating effect, while for lectins, where the binding sites were relatively further away, no major multivalent binding was observed by increasing the valency. Glycodendrimers have been even synthesized stepwise on the solid support, by dendrimer attachment followed by mono-, oligo-, and polysaccharide installation with different valencies and concentrations.^[166,167] The binding profiles of different lectins were identified due to specific recognitions between sugar moieties and structures *via* enhanced binding due to clustering and statistical effects. Interestingly, a microarray containing different dendron spacers with azido mannose, galactose, glucose and α -1.2-dimannose was prepared to study in which degree density and concentration of the used solutions can affect the binding mode.^[168] Different concentrations used for the attachments of the dendrons, showed linear surface density increase by increasing the concentration of the dendron solution, as well as structure dependent spatial immobilization. Attachment of the azido sugar moieties was also performed in different concentrations, concluding that monovalent and divalent representations can give the same binding mode due to saturation and crosslinking of the used lectins in high concentrations.

1.4.5. Detection of binding mode

A variety of methods to detect binding modes between glycans-GBP have been developed. The binding mode can be identified either directly, using fluorescently labeled GBPs, or indirectly. Indirect methods include detection *via* secondary fluorescently labeled components (e.g., antibodies) that bind the GBP or by fluorescently labelled reagents that bind a tag (e.g. biotin- streptavidin recognition, His-tag) on the GBP. Visualization of the result in all cases can be achieved *via* a high-resolution fluorescence scanner (Figure 1.13). Despite the versatility of this approach, there are important limitations. Different parameters need to be taken into consideration such as the spotting technology, the coupling efficiency during immobilization, the nature, presentation, and density of the immobilized compound (monovalent or multivalent), and the fluorescence detection method.^[169,170] Fluctuations on the spotted material and inconsistencies during coupling can lead to low glycan density and, as a result, to the loss of signal and misleading results. Moreover, modification on the GBP during the labeling process may lead to reduced activity or can influence the selectivity of the GBP.^[171] Indirect labelling unfortunately cannot completely mitigate this problem, due to the limited availability of secondary fluorescently labelled reagents, and fluorophore degradation due to light sensitivity.^[63]

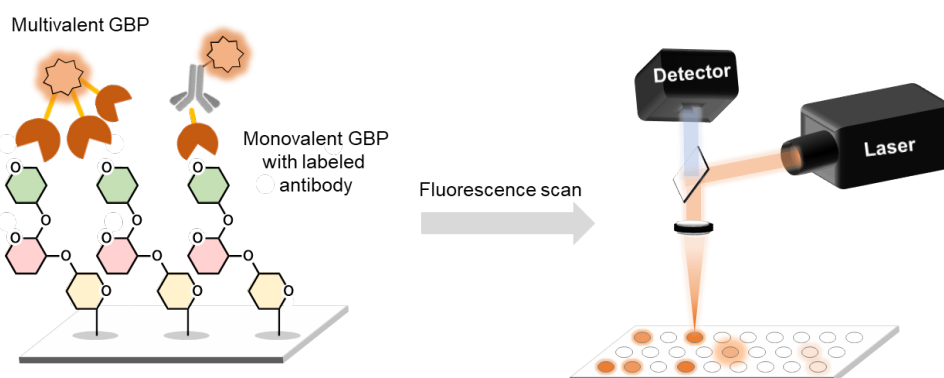


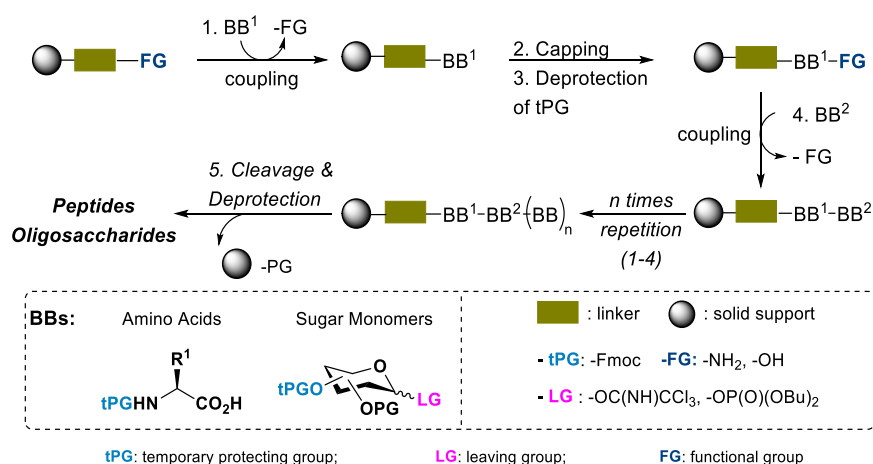
Figure 1.13: Direct and indirect detection of binding (modified^[125]).

Other common methodologies to study the binding mode (not applied in this work) involve mass spectrometry techniques (MS), surface plasmon resonance (SPR) imaging, and other techniques that will not be further mentioned.^[125]

1.5. Solid phase synthesis of biomolecules

Solid-phase synthesis was initially introduced in early 1960s by Merrifield^[172] for the assembly of AAs, in a miniaturized and cost efficient manner to overcome solution phase problems. Since the introduction, it has been extensively applied for the generation of complex peptides, oligosaccharides and oligonucleotides.^[173–175] It is a stepwise synthesis approach, growing molecules on an insoluble solid support, where respective BBs are sequentially attached. The synthesis starts with the preparation of the solid support with a linker bearing the desired functionalization. In the initial loading step, the functional group of the solid support forms a covalent bond with the first monomer. Prior to deprotection of the temporary protecting group of the coupled monomer, capping to minimize deletion sequences is required. Upon deprotection, the second monomer can be loaded, and the same steps can be repeated until the assembly of the desired biopolymer is completed. Finally, the formed biopolymer is cleaved off from the solid support and isolated for further purification and characterization (Scheme 1.4).

Solid-phase synthesis allows miniaturization and rapid synthesis of biomolecules in one vessel, minimizing the need for purification and characterization steps to only one (after cleavage from the solid support). Additionally, the excess of reagents used to force completion of the performed reactions can easily be removed after every reaction without influencing the synthesis, reducing solubility and precipitation issues. The solid phase synthesis of biomolecules is well established and has already been parallelized for peptides and nucleotides.^[61]



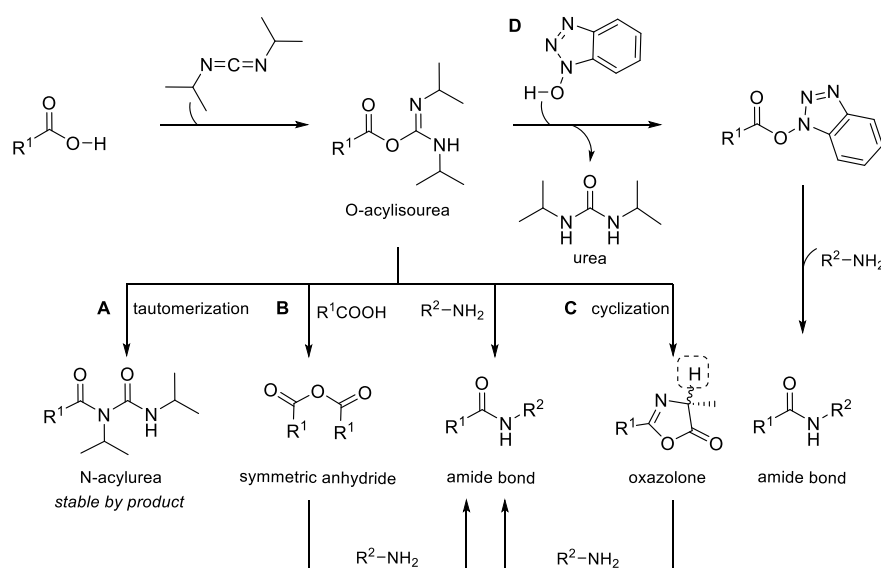
Scheme 1.4: General representation of solid phase synthesis of biomolecules, such as peptides and oligosaccharides.

1.5.1. Solid phase peptide synthesis

For peptides, the synthesis on the solid support starts from the C-terminus to the N-terminus, with consecutive amide bond formation. The functional groups in the side chain of each AA should be protected with a permanent protecting group that will be removed, simultaneously during cleavage from the solid support after completion of the synthesis. The temporary protecting groups, used for the N-terminus during synthesis are a) *tert*-butoxycarbonyl (Boc) group in combination with benzyl based side chain protecting groups and b) 9-fluorenylmethoxycarbonyl (Fmoc) group with acid labile groups for side chain protection. However, the Fmoc strategy has dominated over the Boc-approach, since the orthogonal Fmoc group can be easily removed under basic conditions (e.g., piperidine, DBU) and is stable during synthesis. Cleavage from the solid support in this approach is commonly achieved under acidic conditions (e.g., TFA). In addition, Fmoc can be used for the synthesis of acid-sensitive peptides and it is relatively safer than the Boc synthesis, where special equipment is needed. Finally, during deprotection of the Fmoc protecting group, the dibenzofulvene-piperidine adduct is formed that can be detected with a UV spectrometer, making Fmoc a great candidate to monitor the efficiency of AA coupling during synthesis.^[176]

During synthesis, a very important step is the appropriate activation of the C-terminus. Conversion of the α -carboxy group into a highly reactive moiety is necessary, to achieve fast and quantitative amide bond formation. Numerous reagents have been investigated and are commercially available, such as carbodiimides, phosphoniums, uroniums and others.^[177] One important class of inexpensive activating agents used in this work are the carbodiimides. During activation with carbodiimides, such as

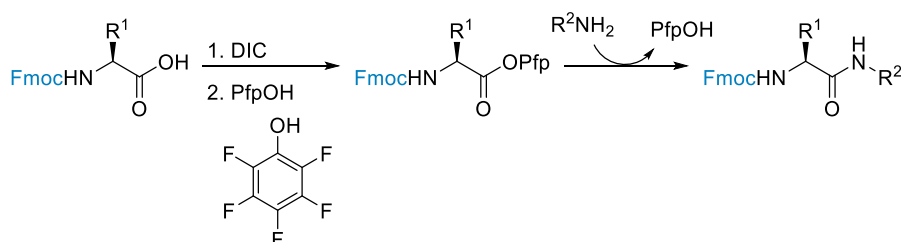
dicyclohexycarbodiimide (DCC), diisopropylcarbodiimide (DIC), 1-ethyl-3-(3-dimethylamino) carbodiimide hydrochloride salt (EDC), *O*-acylisourea is generated (Scheme 1.5). The former *O*-acylisourea intermediate is one of the most reactive intermediates for the amide bond formation in presence of an amine. Unfortunately, multiple side reactions can occur in a fast manner. Rapid rearrangement of the *O*-acylisourea (most commonly formed by-product) leads to the formation of the corresponding stable and inert *N*-acylurea, which consumes the carboxylic acid and terminates the reaction (Scheme 1.5A). Excess of carboxylic acid after the formation of the *O*-acylisourea can lead to the formation of a symmetric anhydride that can react with the second AA for the formation of the amide bond (Scheme 1.5B). *O*-acylisourea can also cyclize to the corresponding oxazolone intermediate, leading to higher chances of racemization (Scheme 1.5C).^[178] To overcome these problems and to suppress the formation of the *N*-acylurea and the oxazolone intermediate, *N*-hydroxy derivatives (e.g., HOBt, HOAt) are added. The newly formed active ester (Scheme 1.5D) is less reactive and the coupling efficiency with the corresponding amine is increased by reducing side reactions. The most commonly used carbodiimide-additive combination is DIC-HOBt. DIC is preferred over DCC, since the formed urea byproduct is soluble and therefore can be easily removed *via* filtration during synthesis.



Scheme 1.5: Peptide bond formation with carbodiimides and carbodiimide-*N*-hydroxy triazole additives as activating agents, such as DIC-HOBt (modified^[178]).

Other additives that can be used with carbodiimides to form active species, are pentafluorophenol (PfpOH), *p*-nitrophenol (PNP), and *N*-hydroxysuccinimide (NHS) (Scheme 1.6). The corresponding leaving group, reduce the risk and the degree of racemization during couplings. These activated AAs are stable and sufficiently reactive

during coupling in solid-phase peptide synthesis (SPPS), with minimum side reactions. They are already commercially available and can be easily synthesized *in-situ*.^[178]



Scheme 1.6: Peptide bond formation with DIC-PfpOH activation.

The solid support used for the assembly of peptides plays a crucial role in solid phase synthesis. The mechanical properties, the stability towards synthesis and cleavage, wettability/swelling in different solvents are important parameters to be considered. The first solid support used by Merrifield was a cross linked polystyrene (PS)-divinylbenzene polymer, carrying chloromethyl functional groups for further AA coupling.^[174] Through the years, various solid supports have been used to synthesize chemically miniaturized peptide libraries in a cost- and time-efficient way (resin beads, pins, tea bags, cellulose membranes, and glass chips).^[61,176,179] The development of parallel and automated array platforms enabled the development of the SPOT-synthesis^[180] approach and the combinatorial laser-induced forward transfer (cLIFT)^[126] for *in-situ* high-throughput synthesis of hundreds of sequences on the solid support. The automated manner of both methods gives access to multiple compounds and facilitates the combination with setups for biological screenings.^[181]

SPOT-synthesis

Frank *et al.* introduced the SPOT-synthesis in 1992,^[180] for parallel generation of peptides using membranes as the solid support. SPOT relies on the standard Merrifield SPPS, employing successive cycles of AA coupling, capping, deprotection of temporary protecting groups and final cleavage with side-chain deprotection of the desired sequence after completion of the entire process (Figure 1.14). In SPOT synthesis, cellulose membranes are used as solid supports, which are inexpensive, flexible, hydrophilic, and compatible with a variety of solvents. However, other modified membranes have also been investigated, e.g., nitrocellulose, polytetrafluoroethylene (PTFE/Teflon), acrylate-coated PTFE, and polystyrene-grafted PTFE.^[182,183] The AAs and the coupling reagents, dispersed in solvents with low volatility, are spotted on defined positions on the surface of the membrane, and the membrane is able to absorb the material, forming a small reactor. The droplets of the used reagents and reactants are spotted with ~1-3 mm diameter distance to

avoid diffusion between the synthesized sequences. Diffusion, spot size and droplet volume problems can be solved by using Teflon patterned membranes.^[182] The efficiency of every coupling and capping steps can be detected *via* bromophenol blue staining (staining of free amino groups). In addition, manual synthesis with premade kits can give access to 96 spots (5 spots/cm²), while semi-automated and automated platforms (inkjet printing, *Section 1.4.2*) allow the synthesis of 15 spots/cm² on a membrane piece.^[184–186] With this, multiple natural and unnatural peptide structures (e.g., linear, cyclic), branched molecules, small-molecule, and glycopeptide libraries have been successfully synthesized.^[187–191]

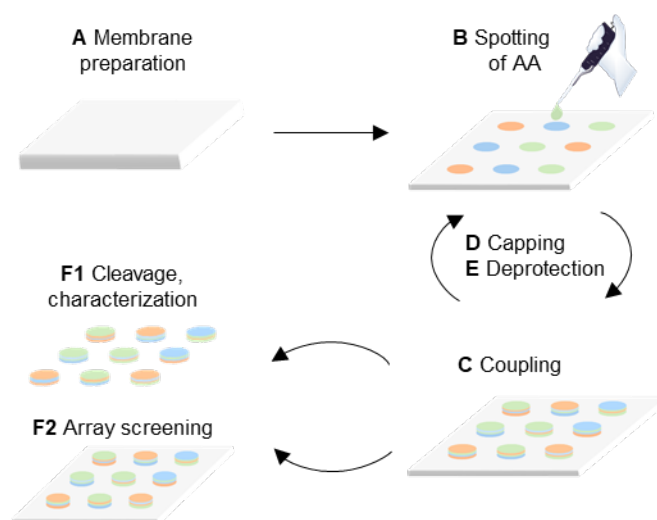


Figure 1.14: Illustration of SPOT synthesis. A) Preparation of membrane as solid support; B) spotting of activated amino acids; C) coupling of transferred amino acids; D) capping of unreacted group; E) deprotection to unmask the nucleophiles for the next spotting and coupling cycle. The synthesized sequences can either F1) be cleaved from solid support for further characterization or F2) can be subjected for membrane-bound peptide assay.

Combinatorial laser-induced forward transfer

Laser printing was first introduced in the late 1960s^[192] but the term laser-induced forward transfer (LIFT) was only used in the 1980s.^[193] This LIFT only revolved around the transfer of inorganic material from a donor onto a receiving substrate (acceptor) via laser irradiation. Since then, besides organic and inorganic compounds also biomolecules have been successfully transferred by bringing donor and acceptor in close proximity or in contact. Moreover, a range of transfer mechanisms was observed due to the different chemical and physical properties of the transfer materials (solids, liquids and pastes) and acceptor surfaces (silicon-based, polymer-based and paper substrates).

For metal transfer (e.g., copper) onto a silicon surface, the laser irradiation induces material melting, followed by vaporization and finally ejection of the molten material onto the

receiving substrate (Figure 1.15A). For transfer of liquid materials, such as biomolecules (proteins, DNA, and cells) in solution, liquid donor films with larger micrometer thickness are prepared. After laser irradiation tiny fractions of liquids are removed and transferred onto the substrate (similar to ink printing described in *Section 1.4.2*), where the material is deposited as a droplet, followed by evaporation of the solvent (Figure 1.15B). Photo-labile materials (enzymes, proteins, antibodies, cells and bacteria) have also been transferred *via* LIFT. The material is mixed with an absorbing matrix, forming organo-aqueous gels. During this so called matrix-assisted pulsed laser evaporation-direct method (MAPLE-DW),^[194] laser irradiation promotes vaporization and consequently transfer of the desired material (Figure 1.15C). A LIFT variation containing a dynamic release layer (DRL) has been developed. With this method, a donor with a sacrificial pre-coated layer is used that absorbs the majority of laser irradiation and upon vaporization the material is deposited onto the acceptor. Blister-actuated LIFT (BA-LIFT) could be considered as an extension of the DRL method. Transfer of liquid and sensitive materials (ink printing method) can be achieved by using polymer layers as absorbing irradiation materials (e.g., polyimide) before the immobilization of the desired material (Figure 1.15E). BA-LIFT seems to be similar to the DRL-LIFT. However, the transfer mechanism is quite different. Prior to laser irradiation, a blister formation is observed in between the solid support (e.g., glass slide) and the absorbing polymer layer. Laser irradiation promotes the expansion of the trapped gas (blister) leading to a deformation of the absorbing layer and subsequently deposition of the “ink” on the substrate.^[194]

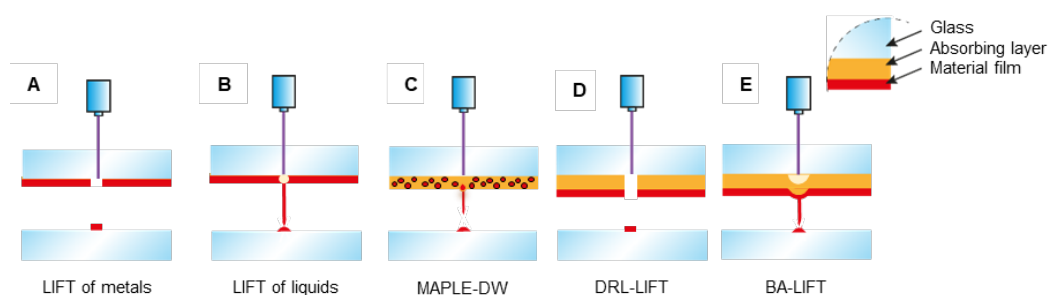


Figure 1.15: Illustration of the different LIFT mechanisms: A) LIFT of metals, melting and transfer of material; B) LIFT transfer of liquids; C) matrix-assisted pulsed laser evaporation-direct write, MAPLE-DW, matrix vaporization and transfer of material; D) sacrificial dynamic release layer, DRL-LIFT, absorption of laser irradiation within the sacrificial layer, vaporization and solid transfer; E) blister-actuated, BA-LIFT, absorption of laser radiation by a polymer layer and transfer of desired material.

In 2016, Loeffler *et al.*^[126] introduced cLIFT for the *in-situ* generation of high-density peptide libraries on a solid support. This laser-based printing methodology enabled homogeneous spot patterns on a solid support (acceptor slide), in which each spot contained immobilized Fmoc protected AAs. Each donor slide for the generation of the spot pattern,

consisted of a matrix-embedded AA that was spin-coated on top of an absorbing layer (e.g., polyimide Kapton foil) (Figure 1.16A), while the acceptor slide was functionalized with the needed functional group (mainly free amino groups). The used donor slides were easily exchangeable and reusable allowing transfer of a nanometer thin polymer spots (Figure 1.15B). Every spot was formed through a contact-based process between donor and acceptor slides. During laser irradiation, the absorber of the donor slide was absorbing energy and a bell-shape expansion was observed. Subsequently, as soon as the laser irradiation was stopped the absorber relaxed while a matrix-AA spot was retained on the acceptor surface (Figure 1.16B).^[195,196]

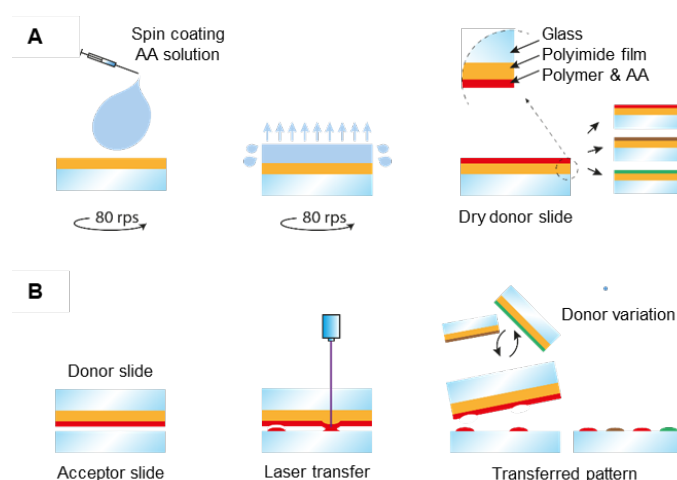


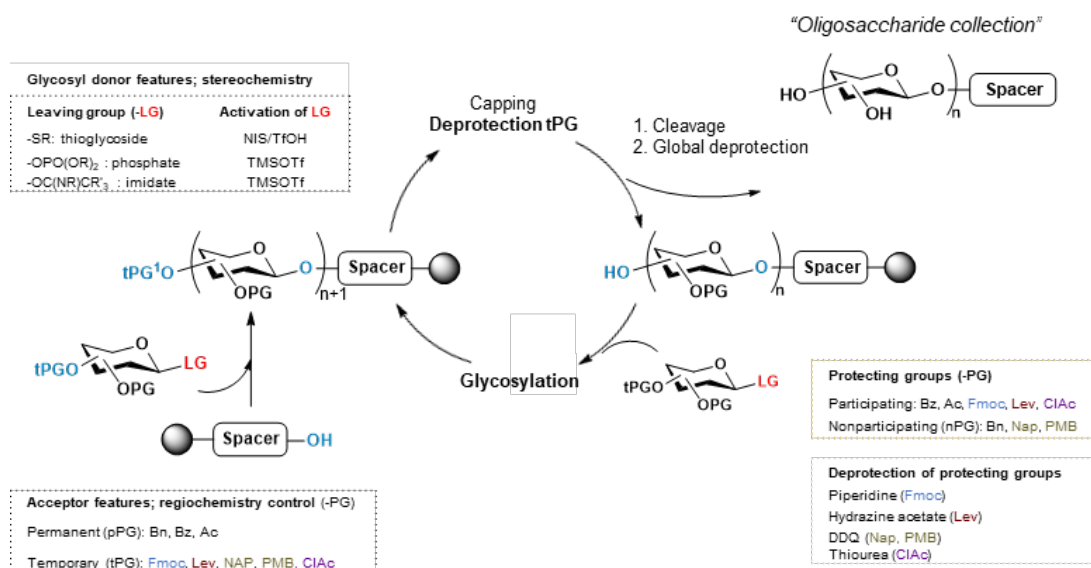
Figure 1.16: Illustration of the cLIFT process. A) Preparation of donor slides containing activated amino acids *via* spin coating; B) Transfer of activated amino acid and polymer matrix using cLIFT technology (modified ^[197]).

From a chemical point of view, the method relied on the basic principle of SPPS. Coupling of the transferred material is achieved under heat, and upon completion, washing, capping, and deprotection steps of the temporary protecting group are performed prior to the subsequent layer coupling. The initial report of the method was only capable to synthesize 64 peptide sequences with 9 residues.^[126,127] Automation of this process^[128] led to the synthesis of 5200-5500 different sequences with up to ~20 residues (including all natural occurring AAs and a spot density of up to 10000 spots/cm²). Using this laser printing methodology, different peptide and peptoid arrays of biological interest have been generated.^[128,198] The method was used within the field of materials science,^[199,200] with studies focused on the relationship between used inert polymer structure and acceptor nature in regards to the obtained spot morphology.^[201]

1.5.2. Solid-phase glycans synthesis - AGA

One of the most powerful solid phase synthesis methods for oligosaccharide assembly is the automated glycan assembly (AGA).^[106] The synthesis cycle relies on the standard methodology of solid phase synthesis (Scheme 1.7). Similar to the peptide synthesis approach, the selection of the solid support and the linker plays a significant role on the reaction conditions. Solid supports need to be resistant under the conditions used throughout the entire synthesis, and cost efficient. Many linkers with different characteristics have been synthesized for faster and more efficient cleavage of the bound compound. Currently, the most commonly used linker in AGA, is a photocleavable linker, showing stability under all basic and acidic conditions during glycosylation reactions, and high compatibility towards a wide range of protecting groups, such as carbonates, ethers and esters.^[202] Nowadays, thioglycosides are the main class of BBs used in AGA.^[84,113,203] They show high bench stability for a long period of time and are commercially available.^[110] Activation during glycosylation reactions can be achieved using NIS/TfOH at a range of temperatures and with reduced formation of side products. Glycosyl trichloroacetimidates,^[106] and glycosyl phosphates^[116,204] are also used in the synthesizer as an alternative to increase the reactivity of the less reactive glycosyl donors (Scheme 1.7). To achieve the desired stereocontrol during oligosaccharide assembly, the selection of the protecting groups on the glycosyl donor is important. To selectively obtain the 1.2-*trans* linkage, a participating protecting group is needed at the C2 hydroxy group, while for 1.2-*cis* linkage, a non-participating protecting group should be installed in the C2 position, giving a mixture of stereoisomers. For more efficient formation of such challenging bonds, remote participation strategies, solvent effect, and temperature control should be taken into consideration.^[91] For regioselective control during glycosylations, the protecting groups on the acceptor should be chosen wisely. Permanent protecting groups are installed in all hydroxy groups that are not participating in the oligosaccharide assembly. Temporary protecting groups are introduced, where a glycosidic linkage is involved, and orthogonal temporary protecting groups for branching. Permanent protecting groups, mainly used in carbohydrate chemistry, are benzyl ethers (Bn) as non-participating PG and benzoyl esters (Bz) as participating PG. These can be easily removed by hydrogenation and methanolysis, respectively. Acetyl esters (Ac) are used when remote participation strategies need to be implemented and they can be easily removed by methanolysis. As orthogonal/temporary PGs, 9-fluorenylmethyloxycarbonyl (Fmoc), levulinoyl ester (Lev), 2-naphthylmethyl ether (Nap), *p*-methoxybenzyl ether (PMB) and chloroacetate ester (ClAc) are used, since orthogonal deprotection of these groups can be

achieved after treatment with piperidine or triethylamine, hydrazine acetate, 2,3-dichloro-5,6-dicyano-1,4-benzoquinone (DDQ), and thiourea, respectively (Scheme 1.7).^[7,109]



Scheme 1.7: General representation and key points for successful assembly of oligosaccharides in AGA. Commonly used leaving groups: R = Et, Tol, Ph, for thioglycosides; R = Bu, for phosphates; R = Ph, R' = F or R = H, R' = Cl, for imidates, Fmoc is a temporary protecting group, while Lev, NAP, PMB, CIAC are orthogonal temporary protecting groups (modified^[7]).

Despite the diverse collections of natural and unnatural analogues that can be obtained from AGA for multiple applications, it still requires extensive preparation for design and synthesis of BBs, as well as a long time for the assembly of a single oligosaccharide. Thus, there is a pivotal need for cost- and time-efficient strategies for parallel synthesis of oligosaccharides, analogous to the well-established parallel oligopeptide and oligonucleotide synthesis technologies described above.

1.6. Aim of this thesis

Microarray technology is considered as one of the most prominent research tools for high-throughput screening of potential binding partners. There is a variety of commercially available microarrays available, synthesized either *in-situ* or *via* immobilization of the pre-synthesized compounds. Despite the rapid development of methodologies for *in-situ* and high-throughput synthesis of peptide and DNA arrays, for glycan microarrays, there is no well-established method for their chemical *in-situ* generation. The glycans needed for the preparation of glycan microarrays are either isolated from natural sources and/or pre-synthesized individually (e.g., solution or solid phase). In that respect, for the synthesis of oligosaccharides, there is not yet a methodology for their parallel synthesis.

Thus, aim of this thesis was to develop methodologies for parallel glycan and neo-glycopeptide synthesis directly on the array that will allow simultaneous generation of compounds on defined areas for biological screenings. These strategies will use the principles of solid phase synthesis, and will rely on the BB flexibility. Cost- and time-efficient methodologies will give access to multiple structures concomitantly, to study their behavior towards corresponding binding partners. In this regard, two different methodologies were developed, based on the previously introduced concepts, making them compatible with carbohydrate chemistry requirements. The first method, uses the cLIFT technology as a printing method for deposition of AA and monosaccharide BBs onto the microarray for *in-situ* high-throughput synthesis, while the second makes use of the SPOT-synthesis approach for parallel synthesis of glycans on membranes.

The first approach using the cLIFT technology was divided into two sections: A) *in-situ* chemical synthesis of glycan microarrays, and B) on-chip synthesis of glycopeptides for multivalency studies. In both cases, detection of the synthesized structures can be achieved with their corresponding fluorescently labelled partners, e.g., lectins.

The focus of the first part (*Chapter 2*) was set to develop a new methodology, sugarLIFT that will allow parallel glycosylation reactions of different glycosyl donors directly on the microarray. Therefore, cLIFT was combined with an vapor glycosylation approach.^[205] cLIFT allows spatial deposition of the desired materials on acceptor-glass slides, while the vapor activation of the glycosyl donors leads to parallel glycosylation reactions in the same pattern. Upon optimization, the application of this method to different glycosyl donors in a parallel fashion was envisioned to investigate the versatility of this methodology.

In the second part (*Chapter 3*), the goal was the synthesis of well-defined neo-glycopeptides directly on differently functionalized glass slides to manufacture microarrays with different multivalent characteristics. For the generation of the peptide scaffolds, cLIFT was used as a printing technique and combined with CuAAC to conjugate the monosaccharide ligands to the scaffolds. Thus, surface dependent binding and the importance of spacing, density, and orientation of glycopeptides were investigated in regards to the binding recognition. Visualization of the resulting neo-glycomimetics was achieved with a wide range of lectins in a high-throughput manner to explore the importance of the surface accessibility and wettability for glycan-GBP interactions.

Finally, the third project focused on devising a method, based on the SPOT-synthesis, for parallel oligosaccharide synthesis on a solid support (*Chapter 4*). Modification

of the classical SPOT synthesis to make it compatible with carbohydrate chemistry was required, as well as the use of a vapor deposition method for the deposition of the activator solution, to activate the spotted glycosyl donors on the solid support. A new method for parallel oligosaccharide synthesis was developed that is ideal for microarray production, giving access to oligosaccharide collections.

2. SugarLIFT: *in-situ* chemical synthesis of glycan microarrays

This chapter has been modified in part from the following articles:

Tsouka, A.; Mende, M.; Paris, G.; Heidepriem, J.; Dallabernardina P.; Bienert K.; Seeberger, P. H.; and Loeffler, F. F.; *In-situ* chemical synthesis of glycan microarrays via sugarLIFT, *in preparation*.

Tsouka, A.*; Dallabernardina, P.*; Mende, M.; Sletten E. T.; Lechnitz, S.; Bienert, K.; Le Mai Hoang, K.; Seeberger, P. H.; and Loeffler, F. F.; VaporSPOT: Parallel Synthesis of Oligosaccharides on Membranes; *J. Am. Chem. Soc.* **2022**, *144*, 19832–19837.

DOI: 10.1021/jacs.2c07285.

*These authors contributed equally.

Specific contribution

I developed the methodology and synthesized all building blocks (if not otherwise stated within the chapter), linkers and final structures on the acceptor slides. I validated the formation of the desired structures by performing glycosylation reactions in solution and under vapor. For glycosylation reactions in solution, I synthesized a photocleavable linker with input from Dr. Kim Le Mai Hoang. I optimized the conditions for the successful functionalization of the custom-built setup. Dr. Marco Mende performed initial experiments and tested different commercially available glass slides are compatible for chemical glycosylation reactions as well as their stability upon conditions used in carbohydrate chemistry. Dr. Grigori Paris designed and developed the automated cLIFT system and contributed with physics and engineering input. Finally, cLIFT (laser transfer) of different glycosyl donors was performed with the help of Jasmin Heidepriem using the automated cLIFT system. Dr. Pietro Dallabernardina developed the *in-situ* MALDI-ToF detection process. Klaus Bienert and Tobias Schmidt designed and constructed the home-built setup.

2.1. Introduction

Oligosaccharides, like proteins and DNA, are the most abundant biopolymers on earth mediating key functions in organisms.^[2] The understanding of the role that carbohydrates play in essential life processes is still limited compared to proteins and nucleic acids.^[206] The structural complexity and diversity of oligosaccharides present a bottleneck for their investigation. The development of microarray technology enabled parallel mechanistic and functional studies in genomics and proteomics. The *in-situ* chemical synthesis of nucleic acids and peptides in the array format has revolutionized microarray production, meanwhile being fully automated.^[61,181] However, these approaches are not compatible with glycan microarray synthesis, due to the complex synthesis conditions, involving low temperatures and harsh chemicals.

Various literature examples for the immobilization of pre-synthesized oligosaccharides on microarray surfaces have been illustrated (*Section 1.4.2*).^[125] One of the chemically most versatile methodologies used for microarray fabrication is based on the synthesis of C5-amino-linked glycan collections, using the automated glycan assembly (AGA), followed by covalent attachment of the free amine on *N*-hydroxysuccinimide (*NHS*) esters slides.^[207] AGA has given access to different biologically and structurally interesting carbohydrate families of different lengths, substitution patterns and complexity. Ink-jet printing of the synthesized structures on a solid support, allows for high-throughput screening of carbohydrate-binding macromolecules, such as proteins, viruses, bacteria, yeast or even mammalian cells.^[7,116,120,208,209] Despite the automation of this technology, chemical synthesis of glycans gives only a single oligosaccharides at a time. Thus, there is a pivotal need to develop parallel on-chip glycan methodologies, analogous to those for other biomolecules, such as peptides. Until today, there are only few reported methods in the literature for on-chip generation of glycan microarrays. Particularly, in 2008, Mrksich *et al.*,^[60] introduced the manual on-chip chemical synthesis of carbohydrates for the first time. The used gold surface was functionalized with a phenol-terminated disulfide, to serve as the nucleophile for the attachment of the first carbohydrate building block. Using trichloroacetimidate donors, ~20 different disaccharides were obtained for subsequent enzymatic modification, while all synthesized structures were detected on-chip *via* SAMDI-ToF mass spectrometry. Furthermore, on-chip enzymatic synthesis has been used for microarray generation. Despite different on-chip enzymatic approaches, all of them deliver qualitative and not quantitative data.^[210,211] In 2021, Heo *et al.*,^[62] reported the *in-situ* sequential enzymatic on-chip glycosylation strategy for the synthesis of several Globo H related oligosaccharides. The

synthesis was performed on a pH-dependent i-motif DNA linker, allowing controlled immobilization, isolation, and purification of the synthesized glycan moieties in each step. Despite the advantages and the importance of these methods, all of them remain in a proof-of-principle state, facing on-chip limitations of low throughput and limited availability of glycosyl transferases.

Herein, the sugarLIFT method (Figure 2.1) was developed for *in-situ* chemical synthesis of glycan microarrays. In the first part of this work (*Section 2.2.1*), the general design and the modules of this method are demonstrated. The sugarLIFT process uses the advantages of the combinatorial laser-induced forward transfer (cLIFT),^[126] allowing the deposition of different glycosyl donors on defined areas with high spatial resolution. Controlled glycosylation conditions (temperature and inert conditions) are ensured by a brand-new constructed glycosylation setup. Technical and chemical protocol modifications and optimizations to make the setup/method functional are reported in the second part of this work (*Section 2.2.2*). For screening and characterization of the synthesized structures, deprotection of the glycans and staining with fluorescent binding partners (e.g., lectins) was performed. Furthermore, validation of the synthesized structures by MALDI-ToF was achieved, using a modified solid support (*Section 2.2.3*). Finally, a library of glycosyl donors (*Section 2.2.4*) was generated and employed for the parallel synthesis of glycan microarrays using the optimized conditions in the sugarLIFT process (*Section 2.2.5*). With this I was able to synthesize two different disaccharides in parallel, using different glycosyl donors, as well as one trisaccharide, using a disaccharide building block. The validation of these synthesized glycans was achieved *via* staining with fluorescently labeled plant lectins, showing the versatility and the importance of the newly developed method. The fluorescence signal between two glycosylation cycles for the reference building block was evaluated (*Section 2.2.6*).

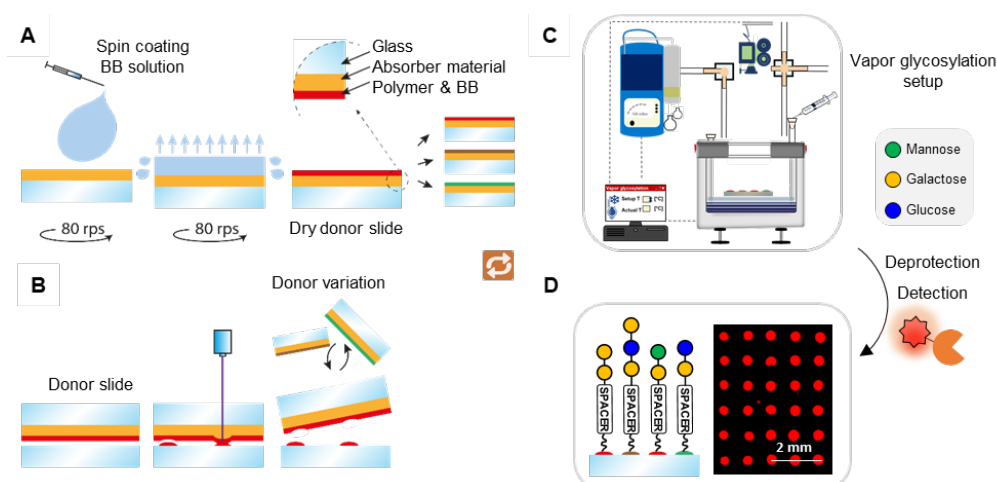


Figure 2.1: Schematic representation of sugarLIFT process. A) Preparation of glycosyl donor slides *via* spin coating; B) Transfer of the glycosyl donors and polymer matrix (polystyrene or styrene acrylic copolymer) using cLIFT technology; C) Vapor glycosylation; D) Deprotection and staining with fluorescently labeled lectins. BB: building block

2.2. Results and Discussion

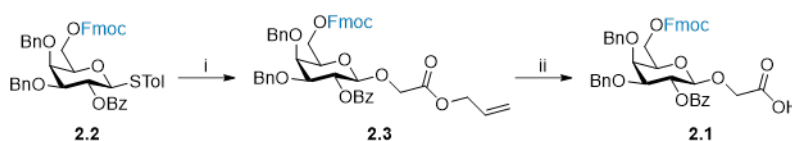
2.2.1. General characteristics of the sugarLIFT process

The sugarLIFT synthesis begins with the functionalization of a commercially available 3D amino glass slide^I, with the galactopyranoside BB **2.1** (Scheme 2.1), bearing an Fmoc-protecting group on the C-6 position. Linker **2.1** was synthesized using the commercially available thioglycoside **2.2**^{II}. Glycosylation reaction of thioglycoside **2.2** with allyl 2-hydroxyacetate^[212], promoted by *N*-iodosuccinimide (NIS) and a catalytic amount of triflic acid (TfOH) afforded derivative **2.3** in 57% yield. Allyl-deprotection in presence of tetrakis (triphenyl-phosphine) palladium(0) [Pd(PPh₃)₄], afforded the targeted galactosyl linker **2.1** in 76% yield (Scheme 2.1A). Attachment of the galactopyranoside linker **2.1** on the amine acceptor glass slide was achieved forming an amide bond, while the unreacted free amino groups were acetylated resulting in the acceptor glass slide **2.4** (Scheme 2.1B). After Fmoc-deprotection, the free hydroxyl group on the C6-position of the galactopyranoside linker was used as the nucleophile for the first glycosylation. An acidic wash to remove any residual base was required (Scheme 2.1B) before the transfer the desired glycosyl donors *via* cLIFT on defined areas/spots of the acceptor slide (Figure 2.1B).

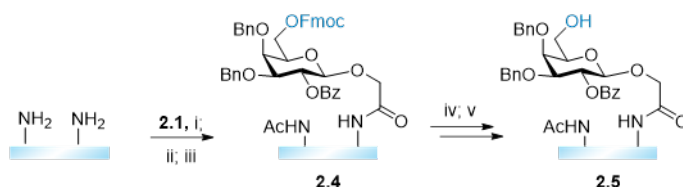
^I PolyAn PolyAn GmbH, Berlin, Germany

^{II} Purchased from GlycoUniverse GmbH & Co. KGaA, Potsdam, Germany.

A Synthesis of galactopyrannoside linker **2.1**



B Functionalization of acceptor slide



Scheme 2.1: Synthesis of the glycosyl acceptor **2.1** and functionalization of the acceptor glass slides **2.5**. A) Reagents and conditions used for the synthesis of **2.1**: i) allyl 2-hydroxyacetate^[212,213], NIS, TfOH, anhydr. DCM, $-20\text{ }^{\circ}\text{C}$, 1.5 h, 57% ; ii) Pd(PPh₃)₄, AcOH, THF, rt, overnight, 76%; B) Reagents and conditions: i) attachment of linker **2.1**, DIC, HOBT, anhydr. DMF, rt, overnight; ii) 10% Ac₂O, 20% DIPEA in DMF (v/v), rt, 30 min (×2); ii) 10% Ac₂O, 2% MsOH in DCM (v/v), rt, 30 min (×2); iv) 20% piperidine in DMF(v/v), rt, 20 min; v) acidic wash using 0.5% TMSOTf in DCM (v/v), rt, 1 min.

Freshly prepared donor slides were simultaneously prepared, containing the desired glycosyl donors embedded in polymer matrix (Figure 2.1A). For the laser transfer, the acceptor glass slide **2.5** was placed inside the laser synthesizer and different donor slides were placed, one by one, on the top of the acceptor slide and laser processed, generating a pattern (Figure 2.1B). After the printing step, the acceptor glass slide carrying the glycosyl donor patterns in unreacted form, was placed onto the metal surface inside the custom-built instrument for glycosylation (Figure 2.1C). The glycosylation chamber was evacuated (100 mbars) while being cooled to $-5\text{ }^{\circ}\text{C}$. Activation of the glycosyl donors was achieved by injection and condensation of the activator solution (10% TMSOTf in dichloromethane, DCM) into the chamber. Then, the temperature was slowly increased ($7\text{ }^{\circ}\text{C}/\text{min}$) to room temperature and maintained for 30 min. After completion, the residual condensate was removed under high vacuum and the glass slide was transferred to a Petri dish for wash using dichloromethane, and dimethylformamide. To achieve higher coupling, repetition of the patterning and coupling process was required (*Section 2.2.4*). Deprotection of the ester and carbonyl protecting groups on the sugar moieties was achieved on-chip using a sodium methoxide solution overnight in a glass bowl chamber (see *Experimental section*), followed by detection of the deprotected oligosaccharides *via* direct staining with their corresponding fluorescently labelled plant lectins (Figure 2.1D).

2.2.2. Optimization of the sugarLIFT process

The cLIFT method was established for peptide microarray generation, following the Fmoc-based SPPS of Merrifield^[172] on amino-functionalized glass slides. However, these conditions are incompatible with the principles of chemical carbohydrate synthesis. Thus, a glycosylation chamber had to be designed, ensuring temperature and inert controlled conditions (Figure 2.2). The inert chamber was mainly made of PTFE, stainless steel and glass. The bottom steel plate was connected to four piezoelectric elements located at the bottom of the chamber, to control the temperature and vapor condensation. Whereas the lid was made of steel, containing a glass window and two heating resistors to prevent undesired condensation on the lid, the rest by PTFE. The temperature profile was regulated by a computer system with an automated control software^{III}.

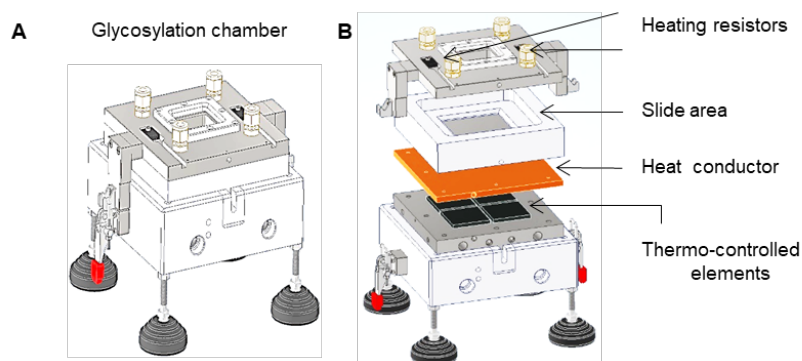


Figure 2.2: Glycosylation chamber for *in-situ* chemical vapor glycosylation: A) Experimental glycosylation chamber; B) compartments of the glycosylation chamber.

To develop the sugarLIFT method, a thorough investigation of chemical and technical parameters was required (Figure 2.3). Chemical optimizations included the optimum functionalization of the acceptor glass solid support, the concentration of the donor slides (BB & polymer), the chemical glycosylation conditions to ensure a sufficient glycosylation outcome, the deprotection of the permanent protecting groups, and the lectin concentration for the screening of the synthesized structures. In addition, technical modifications and optimizations were necessary to ensure successful and reproducible glycosylation results, while maintaining the laser transferred pattern, preventing diffusion or blurring.

^{III} Designed by Klaus Bienert

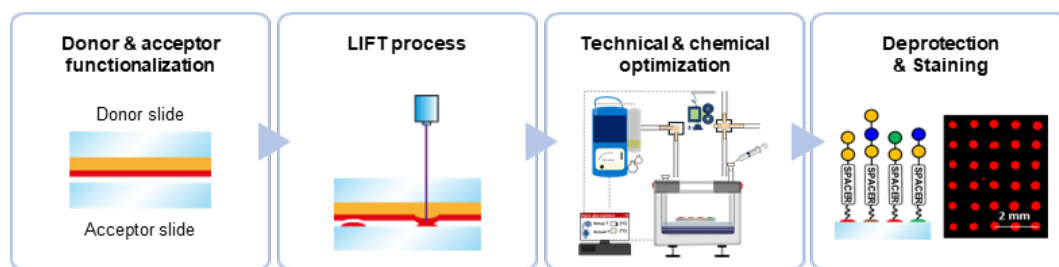
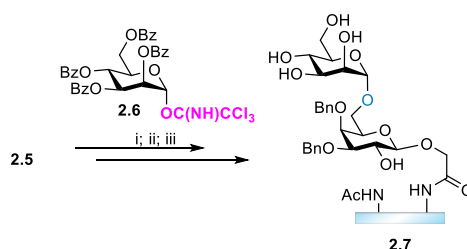


Figure 2.3: Identification of the key parameters required for the development and optimization of sugarLIFT.

For the initial development of the methodology, the perbenzoylated trichloroacetimidate Man donor **2.6** was synthesized^[214] as a reference BB. Man **2.6** was selected, since after laser transfer, glycosylation and deprotection of the permanent benzyl ester protecting groups, dimer **2.7** (Scheme 2.2) can selectively be detected *via* fluorescently labelled ConA. Benzyl ester groups were chosen for the protection of the free hydroxyl groups due to their higher stability during glycosylation reactions in contrast to acetyl groups. A trichloroacetimidate leaving group was installed on the anomeric position, since it can be obtained in high yields and stereoselectivity, requiring only catalytic amount of Lewis acid for its activation during glycosylation reactions.



Scheme 2.2: Reference reaction for the optimization of the sugarLIFT process. Reagents and conditions used for the synthesis of **2.7**: i) cLIFT of glycosyl donor **2.6**; ii) glycosylation; iii) deprotection of the ester protecting groups using NaOMe in MeOH.

LIFT process

For the laser transfer (LIFT) process, a gradient lasing pattern was implemented and no repeating coupling cycles were performed to study the efficiency, the precision, and the reproducibility of this method.

Development of the vapor glycosylation setup

Initial studies were focused on a) testing and identifying the compartments required to conserve the laser transferred pattern during/after glycosylation, and b) the optimal chemical glycosylation conditions needed for successful glycosylation.

The first idea was to use a vapor glycosylation setup (Figure 2.4, derived from the setup in *Chapter 4*). Therefore, a vapor generator vessel for delivery and condensation of the activator solution inside the glycosylation chamber was installed. The glycosylation setup contained eight different compartments: a vapor generator vessel, a thermocontrolled tube, a vapor flow regulator/controller, a syringe for activator solution delivery inside the vapor generator vessel, two valves for flow control and adjustment of the activator solution inside the glycosylation chamber, and a camera.

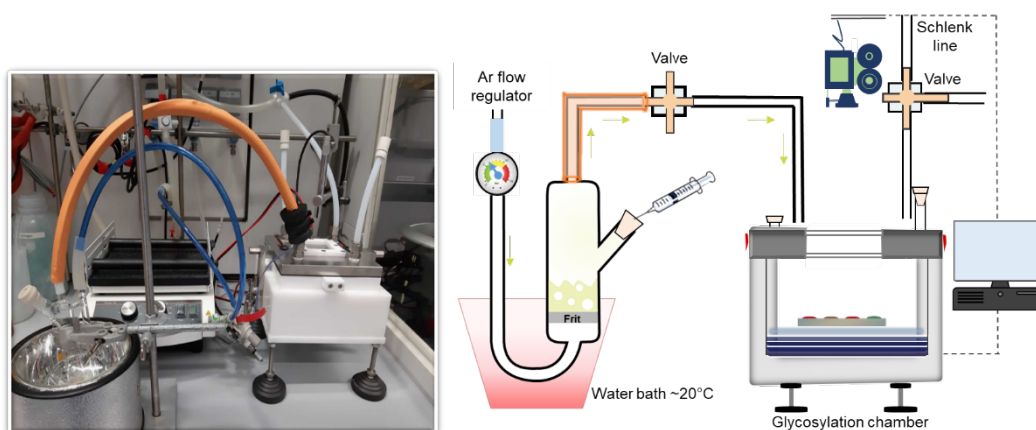


Figure 2.4: Vapor glycosylation setup for the *in-situ* chemical glycosylation on glass slides.

Using this complex setup in numerous test rounds, it was found that many different parameters needed to be controlled simultaneously, giving large reproducibility problems. To overcome this, the setup was transformed to an injection-based low-pressure glycosylation setup. The vapor generator vessel was removed and the glycosylation chamber was connected directly to the Schlenk line for vapor generation under high vacuum. The conservation of the transferred pattern during the vapor glycosylation was one of the most tedious encountered issues. The glycosylation approach under high vacuum (~ 3 mbar) and the highly concentrated activator solution ($\sim 20\%$ TMSOTf in DCM), resulted in shrinking/aggregation and migration of the finally stained pattern. At that point, it was assumed that a relationship between the transferred pattern, the applied vacuum, and the concentration of the activator solution exists. Therefore, it was considered that the installation of a vacuum pump would be beneficial for the optimization and the maintenance of the transferred laser pattern (Figure 2.5). The simplified glycosylation setup consisted of: the glycosylation chamber connected to the vacuum pump, two valves, a syringe for activator solution delivery into the chamber, a camera to visualize the progress of the reaction, and a control software, regulating the applied conditions.

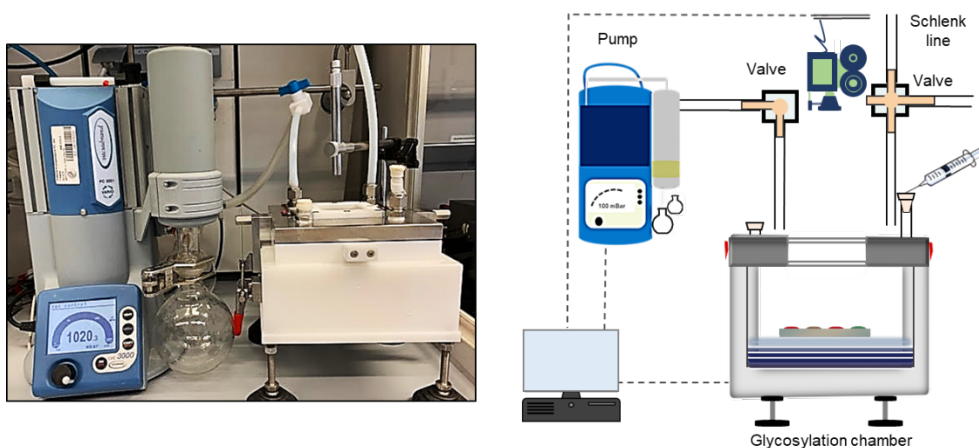


Figure 2.5: Optimized and simplified injection-based low-pressure glycosylation setup for *in-situ* generation of glycan microarrays.

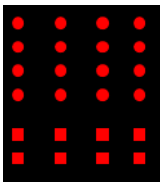
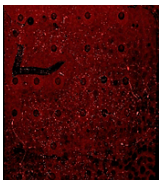
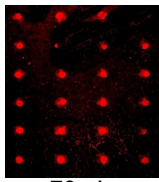

Different vacuum values were evaluated under the same glycosylation conditions. During this process, vacuum was applied inside the system and the custom-built instrument (Figure 2.5) was cooled to $-5\text{ }^{\circ}\text{C}$. Activation of the glycosyl donor was achieved by injection of a 20% TMSOTf in DCM (30 μL) solution and the applied temperature ($-5\text{ }^{\circ}\text{C}$) was maintained for 30 min. After completion, the remaining condensate was removed from the glycosylation chamber under high vacuum and the temperature was increased to room temperature. Each slide was washed, deprotected overnight with NaOMe, and stained with ConA to visualize the result. From these experiments (Table 2.1), under high vacuum (*Entry 1*), migration and shrinking of the transferred pattern was observed, while under low vacuum (*Entry 3*) no successful glycosylation was detected. The condensate distribution of the activator solution, under low vacuum was insufficient to initiate the glycosylation on the glass slide. At 100 mbar vacuum (*Entry 2*), the transferred laser pattern was relatively consistent, and as a result was chosen for further optimizations.

Table 2.1: Vacuum/pressure optimizations of the glycosylation chamber. Reagents and conditions: Donor slide preparation, 25 mg of **2.6** embedded in 25 mg matrix in 500 μL DCM; activator solution, 20% TMSOTf in DCM (v/v), injection, 30.0 μL ; deprotection of $-\text{Bz}$ groups, NaOMe in MeOH; ConA staining, 100 $\mu\text{g}/\text{mL}$.

Expected pattern	Entry	Vacuum [mbar]	Fluorescence signal
		1	50
	2	100	Promising
	3	200	—
	50 mbar	100 mbar	200 mbar

As the next parameter, the amount of activator solution inside the chamber was optimized. Different syringes and amounts were tested for an even/homogenous distribution of the activator solution inside the chamber. The most precise one was a Hamilton syringe with a maximum volume of 100 μL , which became the standard for the setup. Three different injection amounts were tested (Table 2.2). The use of 60 μL (*Entry 1*) led to reverse staining results, which was not further investigated. The injection of 70 μL (*Entry 2*) showed potential to give the optimum stability of the transferred pattern, while 100 μL (*Entry 3*), resulted in high background noise with no distinguishable pattern. Thus, further chemical optimization of the glycosylation reaction was achieved using 100 mbar of vacuum/pressure inside the glycosylation chamber, and 70 μL of activator solution.

Table 2.2: Activator solution tested for injection-based low-pressure vapor generation. Reagents and conditions: Donor slide preparation, 25 mg of **2.6** embedded in 25 mg matrix in 500 μL DCM; activator solution, 20% TMSOTf in DCM(v/v); vacuum, 100 mbar; deprotection of -Bz groups, NaOMe in MeOH; ConA staining: 100 $\mu\text{g}/\text{mL}$.

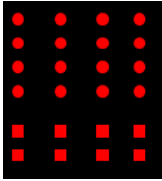
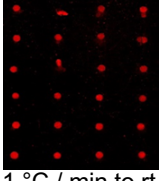
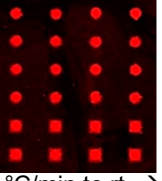
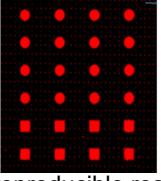
	Entry	Injection [μL]	Fluorescence signal
Expected pattern	1	60	—
	2	70	Promising
	3	100	Diffusion of glycosyl donor
			
	60 μL	70 μL	100 μL

Chemical optimization of glycosylation reactions

After optimizing the injection amount and the applied vacuum, the optimization of the glycosylation reaction was the next goal. The stereochemistry of a glycosidic bond can be affected by multiple factors during glycosylation, such as temperature, leaving group of the glycosyl donor, and concentration of the used Lewis acid. Thus, the temperature effect and the concentration of the activator solution were further studied. Parameters that needed to be taken into consideration were: a) the influence of the temperature during the progress of the glycosylation, and b) the temperature needed for the activation of the used glycosyl donor. Two different approaches were tested (Table 2.3). A slow temperature increase (*Entry 1*) led to shrinking of the transferred pattern, while a more rapid temperature increase (*Entry 2*) after the injection of the activator solution led to a significant increase in the

fluorescence signal and pattern stability. The temperature after the injection of the activator solution is connected to the homogeneity and the stability of the finally obtained pattern.

Table 2.3: Temperature effect on pattern conservation and glycosylation outcome. Reagents and conditions: Donor slide preparation, 25 mg of **2.6** embedded in 25 mg matrix in 500 μ L DCM; activator solution, 20% TMSOTf in DCM; vacuum, 100 mbar; injection: 70 μ L; deprotection of -Bz groups, NaOMe in MeOH; ConA staining, 100 μ g/mL.

Expected pattern	Entry	Temperature [°C]	Fluorescent signal
		1	1 °C /min to rt
	2	~7 °C/min to rt	Pattern conservation
	 1 °C / min to rt	 ~7 °C/min to rt	 → reproducible result

Finally, the concentration of the activator solution and the amount of the glycosyl donor used for the donor slide preparation were investigated. As mentioned, glycosyl trichloroacetimidates only require catalytic amounts of activator for their activation. Despite the intense fluorescence signal obtained using 20% TMSOTf in DCM (Figure 2.6A), there was a need to reduce the amount of the used Lewis acid to potential minimize side reactions and ensure that sufficient activation of the glycosyl donor. Five different concentrations were screened 5%, 10%, 15% and 20% of activator in DCM (Figure 2.6A). Using 5% TMSOTf in DCM, no successful glycosylation was observed (Figure 2.6, *Entry 5*), while when using 10% and 15%, similar glycosylation outcomes were obtained in terms of fluorescence intensity (Figure 2.6A, *Entry 2* and 3). Concluding, 10% were sufficient for the activation of the used glycosyl donor.

Moreover, using 25 mg of BB per sugarLIFT donor slide would be cost-inefficient. Therefore, different BB concentrations on donor slides were investigated (Figure 2.6B). The reduction of the glycosyl donor **2.6** to 5 mg using the same amount of polymer matrix gave a comparable glycosylation outcome and homogeneous spot morphologies (*Entries 1* and 2). Reducing both, the amount of glycosyl donor and polymer matrix, resulted in slightly different fluorescence intensities (*Entries 3* and 4). However, concerns arose in regards to the thickness of the transferred spots and the stability of the transferred glycosyl donor. Therefore, to avoid potential decomposition of the transferred BB, due to the heat generated from the laser transfer process, it was concluded that only the amount of BB should be reduced to 5 mg maintaining the amount of polymer matrix at 25 mg/donor slide.

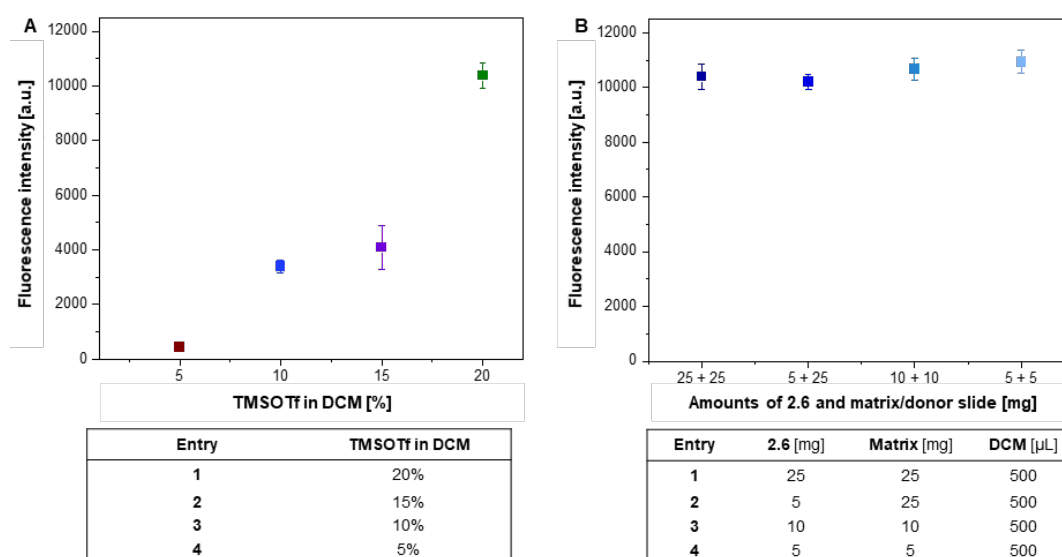


Figure 2.6: Concentration experiments for optimization of the activator solution and the amount of glycosyl donor: A) Activator solutions and fluorescence intensities of the stained dimers. Reagents and conditions: Donor slide preparation, 25 mg of **2.6** embedded in 25 mg matrix in 500 μ L DCM; vacuum, 100 mbar; injection: 70 μ L; temperature, 1 $^{\circ}$ C/min to rt, deprotection of –Bz groups, NaOMe in MeOH; ConA staining, 100 μ g/mL. B) Glycosyl donor concentrations tested for the preparation for each individual donor slide and fluorescence intensities of the formed dimers. Reagents and conditions: Activator solution, 10% TMSOTf in DCM (v/v); vacuum, 100 mbar; injection: 70 μ L; temperature, 1 $^{\circ}$ C/min to rt, deprotection of –Bz groups, NaOMe in MeOH; ConA staining, 100 μ g/mL.

Deprotection of ester protecting groups and staining

For the screening of the synthesized structures, the deprotection of the benzyl ester groups with NaOMe and K_2CO_3 in methanol was investigated. Treatment of the slides with K_2CO_3 resulted in scratches on the functionalized glass surface, due to low solubility of K_2CO_3 in methanol. Although successful deprotection was observed with both solutions, NaOMe was preferred over K_2CO_3 . Validation of the synthesized dimer **2.7** was achieved after selective staining of the α -Man with fluorescently labeled Concanavalin A (ConA) lectin (red channel, 635 nm). The concentration of the used lectin to screen the result was dependent on the glycosylation efficiency and it was eventually reduced to 20 μ g/mL. All further investigation were performed using the mentioned optimized conditions (Figure 2.7).

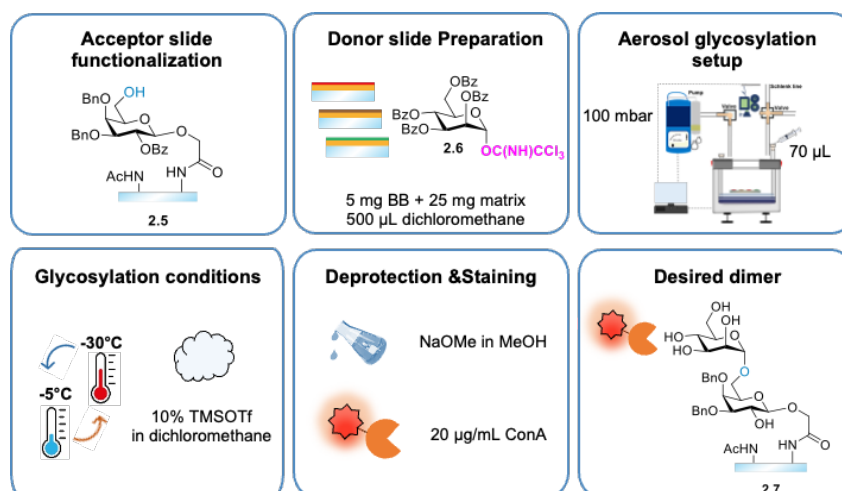


Figure 2.7: Optimized sugarLIFT parameters.

Empirical detection of sugarLIFT process

Throughout the optimization process, an empirical fluorescence based approach that uses a microarray fluorescence scanner was opted, to follow the sugarLIFT process. With this approach, different parameters were simultaneously detected such as the successful functionalization of the acceptor glass slide **2.5**, the deposition of the reference glycosyl donor **2.6** *via* cLIFT, and the maintenance of the transferred pattern after the glycosylation reaction. Initially, it was observed that functionalized acceptor slide **2.5** was giving a bright green fluorescence signal when exposed to a wavelength of $\lambda = 530$ nm (Figure 2.8A), while unfunctionalized slides were not. Encouraged by this, it was assumed that all changes on the solid support might be detectable by fluorescence. Thus, after cLIFT transfer the patterned glass slide, was placed into the fluorescence scanner for detection (under the same conditions, Figure 2.8B), verifying the successful deposition of BB **2.6** on desired areas. Then, the slide was placed for vapor glycosylation and upon completion, prior to the washing step, detection of the fluorescence signal was attained revealing the maintenance of the transferred pattern (Figure 2.8C). Finally, the attained result was detected after successful deprotection and lectin staining with ConA (Figure 2.8D), showing successful synthesis of the desired disaccharide **2.7**. This approach was used as a supplementary method to monitor the changes on each step while optimizing sugarLIFT process.

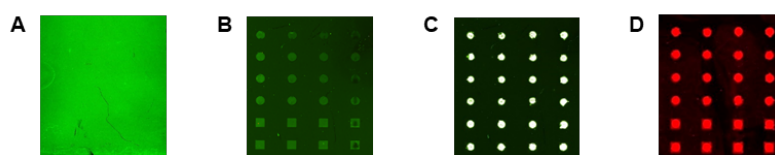
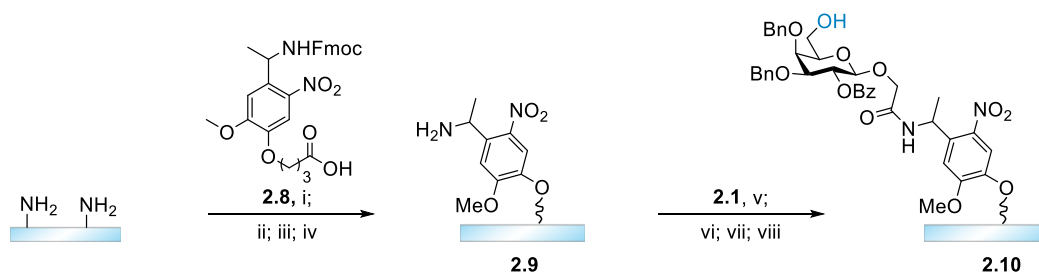


Figure 2.8: Empirical detection of sugarLIFT *via* fluorescence scan. Fluorescence scan of A) functionalized glass slide **2.5**; B) acceptor glass slide after laser transfer; C) glass slide after vapor glycosylation, without wash; D) staining result of dimer **2.7** with ConA after successful deprotection with NaOMe in MeOH. Scanning parameters: Wavelengths 635 nm and 532 nm, PMT gain 600, power 33%, pixel size 5 μm .

2.2.3. Validation of the synthesized structures

Encouraged by the reproducible synthesis and detection of dimer **2.7** patterns *via* ConA, next goal was the validation of the synthesized structure using mass spectrometry (MS). To accomplish this, commercial photocleavable linker **2.8** (Scheme 2.3) was covalently attached to the slide. Then, galactopyranoside **2.1** was connected via amide coupling. Subsequent Fmoc removal at the C-6 position of the galactopyranoside was performed to form the acceptor slide **2.10**. Glass slide **2.10** was placed for glycosylation under inert conditions in a glass chamber (see *Experimental Section 2.5.4*) with mannose BB **2.6**.



Scheme 2.3: Functionalization of acceptor slide **2.10**. Reagents and conditions : i) Attachment of photo-linker **2.8**, DIC, HOBt, anhydr. DMF, rt, overnight; ii) 10% Ac_2O , 20% DIPEA in DMF:DCM (v/v), rt, 30 min ($\times 2$); iii) 10% Ac_2O , 2% MsOH in DCM (v/v), rt, 30 min ($\times 2$); iv) 20% piperidine in DMF (v/v), v) attachment of linker **2.1**, DIC, HOBt, anhydr. DMF, rt, overnight; vi) 10% Ac_2O , 20% DIPEA in DMF:DCM (v/v), rt, 30 min ($\times 2$); vii) 10% Ac_2O , 2% MsOH in DCM (v/v), rt, 30 min ($\times 2$).

Successful detection of disaccharide **2.11** was achieved after cleavage under UV-light irradiation (365 nm) and analysis by MALDI-ToF mass spectrometry (Figure 2.9). Apart from the desired dimer **2.11**, also the mass corresponding to a trimer was detected. It is hypothesized that during the glycosylation reaction the high Lewis acid concentration resulted in cleavage of a benzyl group and the corresponding nucleophile was glycosylated. An exemplary structure of a trimer is reported to justify the observed mass (Figure 2.9).

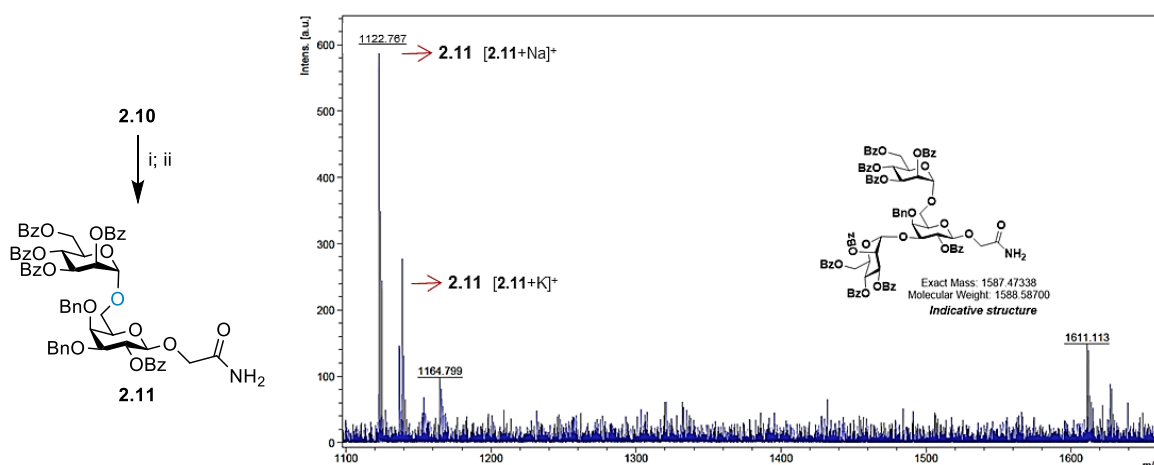
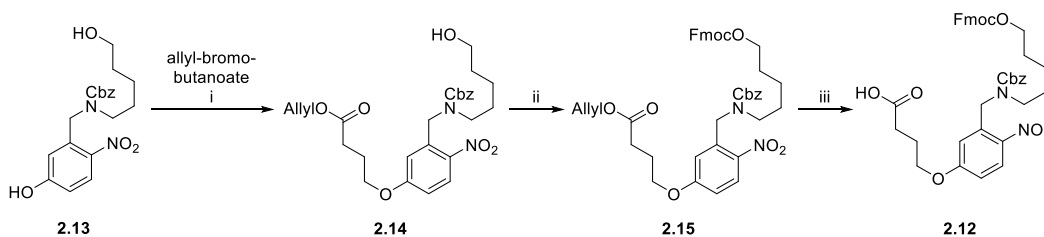


Figure 2.9: Glycosylation reaction in solution under inert conditions on functionalized-acceptor glass **2.11**. Disaccharide **2.11** characterized by MALDI. Reagents and conditions: i) **2.6**, TMSOTf, DCM, -15°C to rt, 30 min; ii) cleavage under UV-light (365 nm), 30 min prior to MALDI detection.

Furthermore, for direct glycosylation without prior attachment of a sugar moiety on the solid support, the photocleavable linker **2.12** was synthesized. Synthesis of the photocleavable linker **2.12** was performed in three steps using precursor **2.13** bearing a Cbz-protected C5-amino-linker.^[202] Derivative **2.12** was synthesized after nucleophilic substitution reaction between precursor **2.13** and allyl-bromobutanoate^[215] with potassium carbonate (K_2CO_3), in 95% yield. Fmoc-protection of the free hydroxyl group of **2.15** with FmocCl and pyridine, yielded derivative **2.16**, which was subjected for allyl group cleavage employing $\text{Pd}(\text{PPh}_3)_4$, and acetic acid to provide the targeted photocleavable linker **2.12** in 83% yield (Scheme 2.4).



Scheme 2.4: Synthesis of photocleavable linker **2.12**. Reagents and conditions: i) **2.13**, allyl-bromobutanoate, K_2CO_3 , DMF, 24 h, 60°C , 95%; ii) **2.14**, FmocCl, pyridine, anhydr. DCM, overnight, rt, 99%; iii) **2.15**, $\text{Pd}(\text{PPh}_3)_4$, CH_3COOH , anhydr. THF, 4 h, rt, 83%.

Photocleavable linker **2.12** was covalently attached to the amino-functionalized glass slide, as previously reported in the formation of acceptor slide **2.16** (see *Experimental Section 2.5.2*). Then, the acceptor was glycosylated upon transfer of glycosyl donor **2.6** over the entire acceptor slide, followed by vapor activation. The optimized glycosylation conditions were applied and monitored by direct MALDI-ToF MS for the detection of synthesized monosaccharide **2.17** (Figure 2.10). Additionally, monosaccharide **2.17** was detected after glycosylation in solution, cleavage under UV-light (365 nm) and MALDI-ToF mass

spectrometry (see *Experimental Section 2.2.3*). Further characterization of both compounds **2.11** and **2.17** was not possible due to inefficient photocleavage from the solid support.

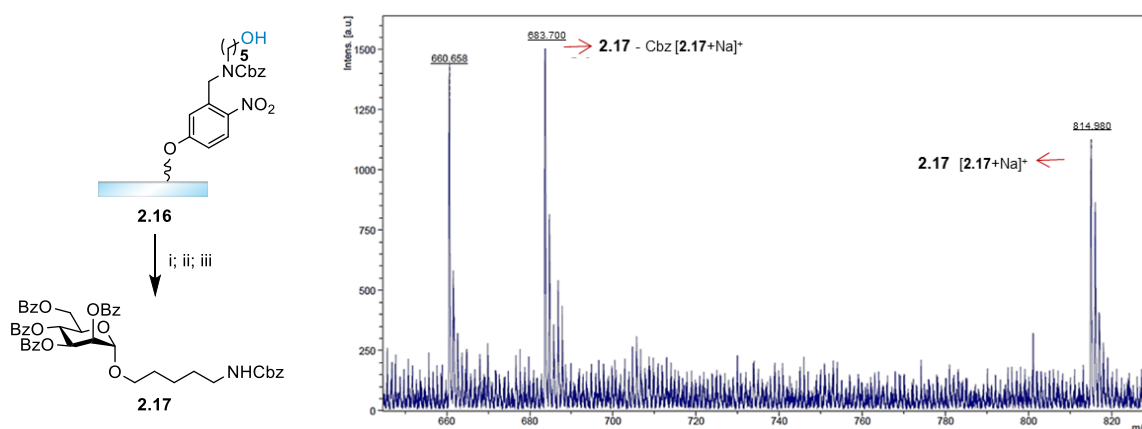


Figure 2.10: SugarLIFT synthesis of monosaccharide **2.17** using the optimized conditions on a functionalized-acceptor slide **2.16**. Monosaccharide **2.17** was detected by *in-situ* MALDI. Reagents and conditions: i) **2.6** transferred *via* laser transfer on the glass solid support; ii) vapor glycosylation reaction, 10% TMSOTf in DCM, -5 °C to rt, 30 min; iii) direct detection *via in-situ* MALDI.

2.2.4. Synthesis of building blocks library

For further validation and evaluation of the method, investigations were focused on the versatility of the vapor glycosylation. Thus, simultaneous glycosylation reactions of different glycosyl donors on the same solid support were investigated. Nine additional BBs **2.18-2.26** (Figure 2.11) were synthesized following either already established protocols (**2.6**, **2.22-2.24**, **2.26**)^[103,214,216–218] or prepared from commercially available precursors (**2.18-2.21**, **2.25**). The synthesized BBs contained permanent protecting groups (Bz and Bn), as well as temporary protecting groups (Fmoc and Lev) to identify candidates for chain elongation with good glycosylation efficiency.

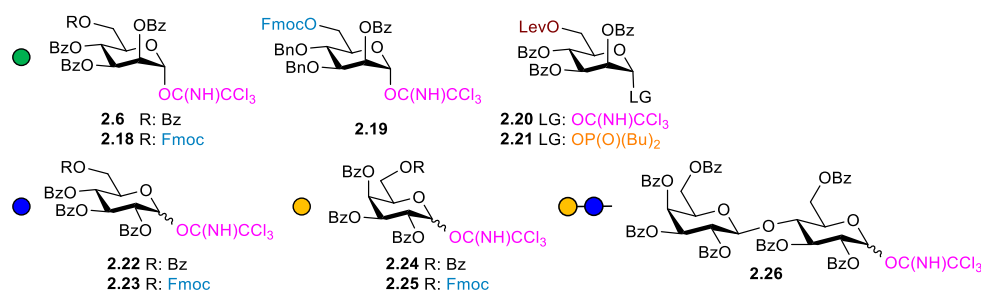


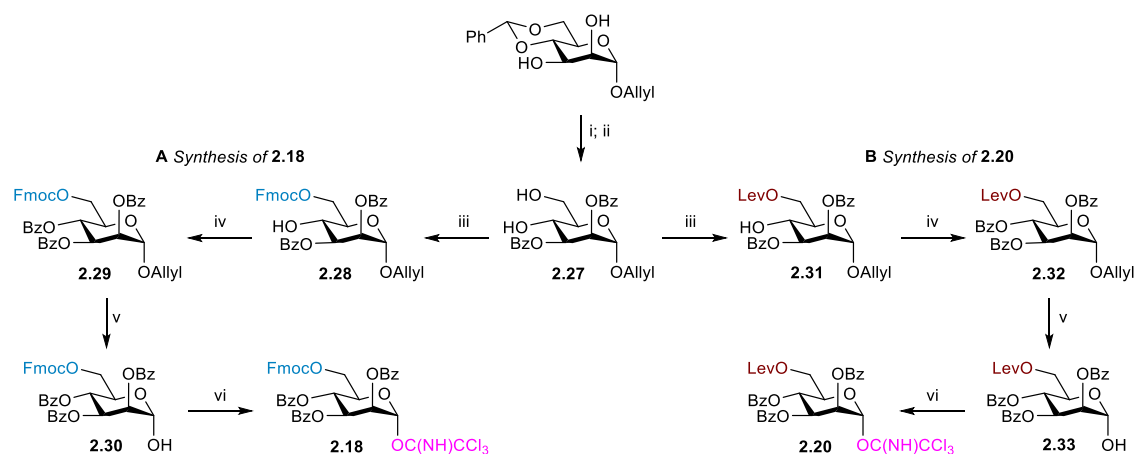
Figure 2.11: Synthesized building blocks for parallel synthesis using sugarLIFT.

Synthesis of **2.18** and **2.20** started from the same commercially available benzylidene acetal (Scheme 2.5). Diol **2.27** was synthesized through benzylation of the benzylidene acetal

using benzoyl chloride (BzCl) in pyridine, followed by benzylidene cleavage with trifluoroacetic acid (TFA) and catalytic amounts of water in 84% yield over two steps.

To construct mannopyranoside **2.18**, diol **2.27** was treated with 9-fluorenylmethoxycarbonyl chloride (FmocCl) in presence of pyridine at -20 °C to afford selectively the C-6 Fmoc-protected derivative **2.28** in 78% yield. Through benzylation, the tribenzoylated derivative, **2.29** was obtained in 89% yield, which was subjected for allyl deprotection with palladium chloride (89%). The desired mannopyranoside building block **2.18** was afforded after treatment of **2.30** with trichloroacetonitrile (CCl₃CN) and catalytic amount of sodium hydride (NaH) in 97% yield (Scheme 2.5A).

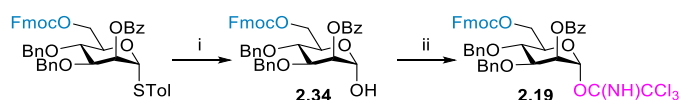
Similarly, treatment of diol **2.27** with levulinic acid (LevOH) in the presence of 2-chloro-1-methylpyridinium iodide (CMPI) and 1, 4-diazabicyclo[2.2.2]octane (DABCO) led to selective protection of the primary hydroxyl group in 67% yield^{IV}. Derivative **2.31** was again benzylation to obtain the tribenzoylated derivative **2.32**. Removal of the allyl group with palladium chloride afforded **2.33**, followed by imidate-formation with trichloroacetonitrile (CCl₃CN) and catalytic amount of 1,8-diazabicyclo[5.4.0]undec-7-ene (DBU) to obtain the targeted trichloroacetimidate mannopyranoside **2.20** in 43% yield (Scheme 2.5B).



Scheme 2.5: Synthetic route to **2.18** and **2.20** using the same benzylidene acetal as starting material. Reagents and conditions: i) BzCl, pyridine, 0 °C to rt, overnight; ii) TFA, water, DCM, rt, 3 h, 84% over two steps; A) iii) FmocCl, pyridine, anhydr. DCM, -20 °C, 30 min, 78%; iv) BzCl, pyridine, 0 °C to rt, 3 h, 89%; v) PdCl₂, MeOH/DCM, rt, 4 h, 98%; vii) CCl₃CN, NaH, anhydr. DCM, rt, overnight, 97%; B) iii) LevOH, CMPI, DABCO, DCM, -15 °C, 67%; iv) BzCl, pyridine, 0 °C to rt, overnight; v) PdCl₂, MeOH/DCM, rt, 4 h, 74%; vii) CCl₃CN, DBU, anhydr. DCM, rt, 2 h, 43%.

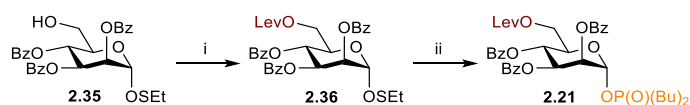
^{IV} reaction performed by Dr. Pietro Dallabernardina

Imidate **2.19** was obtained in two steps starting from a corresponding commercially available mannosyl- thioglycoside (Scheme 2.6). Hydrolysis of the anomeric position with *N*-bromosuccinimide (NBS) afforded derivative **2.34** in 88% yield which was subjected to form the targeted imidate **2.19** with trichloroacetonitrile (CCl₃CN) and sodium hydride (NaH) in 81% yield.



Scheme 2.6: Synthetic route to **2.19**. Reagents and conditions: i) NBS, acetone/water, rt, overnight, 88%; ii) CCl₃CN, NaH, anhydr. DCM, rt, overnight, 81%.

Phosphate mannopyranoside **2.21** was synthesized over two steps from thioglycoside **2.35** (Scheme 2.7). Therefore, thioglycoside **2.35**^V was synthesized as reported in the literature^[204], which was then subjected for Lev-protection using LeOH, *N,N'*-diisopropylcarbodiimide (DIC), and 4-(dimethyl-amino)pyridine (DMAP), affording derivative **2.36** in 93% yield. Glycosylation reaction of derivative **2.36** with dibutyl hydrogen phosphate promoted by *N*-iodosuccinimide (NIS) and a catalytic amount of triflic acid (TfOH) afforded the desired mannosyl phosphate **2.21** in 79% yield.



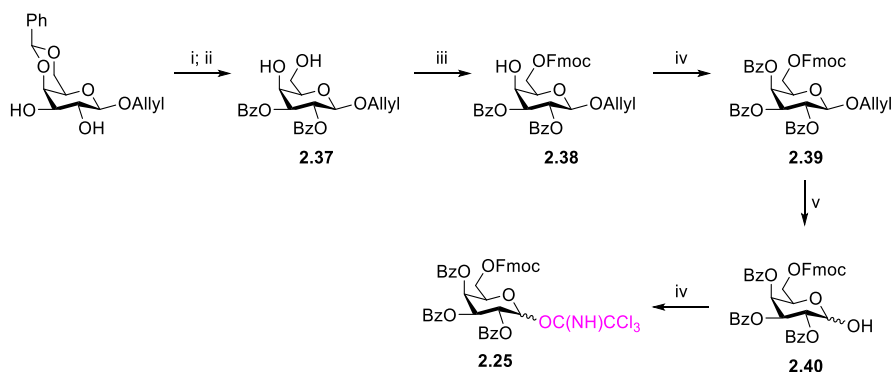
Scheme 2.7: Synthetic route to **2.21** from thioglycoside **2.35**. Reagents and conditions: i) LeOH, DIC, DMAP, 0 °C to rt, overnight, 93%; ii) HOP(O)(OBu)₂, NIS, TfOH, DCM, 0 °C, 79%.

Synthesis of galactopyranoside building blocks

Galactopyranoside **2.25** was synthesized in a similar fashion to mannopyranoside **2.18**, starting from the corresponding commercially available galactosyl benzylidene acetal (Scheme 2.8). Diol **2.37** was synthesized through benzylation of the benzylidene acetal using benzoyl chloride (BzCl) and 4-dimethylaminopyridine (DMAP) in pyridine, followed by benzylidene cleavage with trifluoroacetic acid (TFA) and catalytic amount of water in 62% yield over two steps. Selective protection of the primary hydroxyl group on the C-6 position was performed with FmocCl (50%) and the tribenzoylated derivative **2.39** was formed after treatment with BzCl and pyridine in 94% yield. Allyl deprotection with PdCl₂ delivered

^V thioglycoside **2.35** was obtained from the carbohydrate database of *Biomolecular Systems, MPIKG* (synthesized by Oliviana Calin).

derivative **2.40** which was transformed to the targeted imidate **2.25** using trichloroacetonitrile (CCl_3CN) and sodium hydride (NaH) in 45% yield.



Scheme 2.8: Synthetic route to **2.25**. Reagents and conditions: i) BzCl , DMAP, pyridine, 0 to 50 °C, overnight; ii) TFA, water, DCM, rt; 3 h, 62% over two steps; iii) FmocCl, pyridine, anhydr. DCM, -20 °C, 30 min, 50%; iv) BzCl , pyridine, 0 °C to rt, 2 h, 94%; v) PdCl_2 , MeOH/DCM, rt, 5 h, 68%; vii) CCl_3CN , NaH, anhydr. DCM, rt, overnight, 45%.

2.2.5. Parallel oligosaccharide synthesis *via* sugarLIFT

Synthesis of oligosaccharides

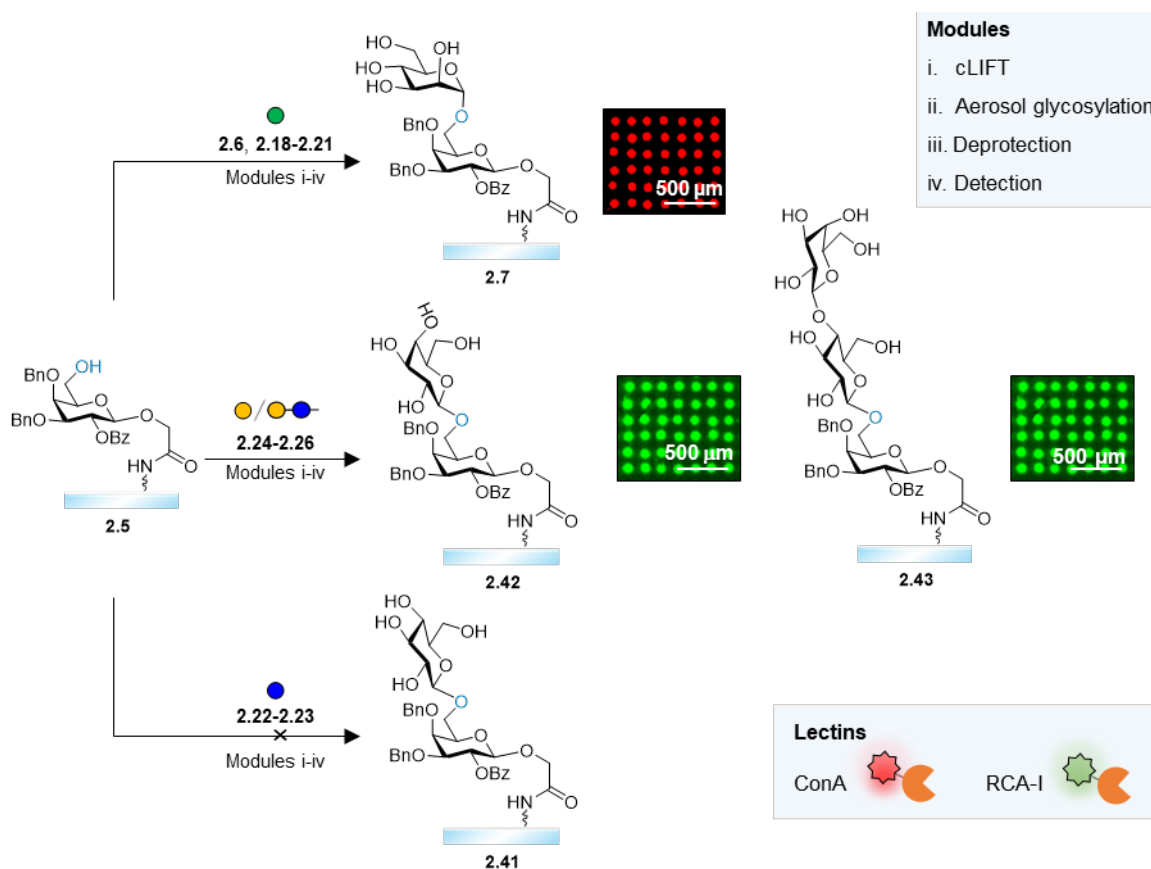
For the parallel synthesis, ten different donor slides were prepared, bearing the synthesized building blocks **2.6**, **2.18-2.26**, and transferred on substrate **2.5** with a gradient pattern, varying the lasing power and duration with our automated system^[128] for higher precision. The used lasing parameters were in the range of 110–190 mW and 21-25 ms, with a spot density of 100 spots/cm². The perbenzoylated imidate **2.6** was used as a positive control/reference and **2.19** as a negative control, bearing on the C-3 and C-4 positions the permanent benzyl (Bn) ether protecting groups. The used building blocks were mainly carrying ester and carbonyl protecting groups (-Bz, -Fmoc, -Lev), that can be easily removed under the same basic NaOMe conditions for subsequent lectin recognition.

A single simultaneous vapor glycosylation on the functionalized glass slide with mannopyranosides **2.6**, **2.18-2.21**, followed by deprotection and ConA staining, showed successful synthesis of the α -D-mannopyranosyl-1,6- β -D-galactopyranoside **2.7**. Promising candidates were identified for chain elongation, while double glycosylation was acquired for building blocks **2.18** and **2.21** for successful staining. Imidate **2.20** was identified as a good candidate from the first glycosylation cycle and double glycosylation was not required. However, mannopyranoside **2.19** unexpectedly also gave a positive fluorescence signal (Table 2.4), leading to the consideration that the used 10% TMSOTf in DCM solution might be too acidic, which could lead to acidic cleavage of the benzyl ether groups. This indicates

that further optimizations of the activator solution should be performed in the future (Scheme 2.9).

Despite the successful glycosylation observed for the synthesized mannopyranosides, no successful glycosylation was observed with glucopyranosyl imidates **2.22** and **2.23**. For these two building blocks, single and double glycosylation cycles were implemented (Table 2.5). However, after vapor glycosylation, acceptor glass slide **2.41** was subjected to deprotection and no positive ConA staining could be observed (Scheme 2.9).

For the terminal galactopyranoside building blocks **2.24-2.26**, after single glycosylation and Ricinus communis agglutinin-I (RCA-I) staining, no successful staining of the galactopyranoside dimer **2.42** and the trisaccharide **2.43** was detected. Repetition of the glycosylation cycle with a freshly prepared donor slide, deprotection and staining of the formed structures with the same lectin showed that all building blocks can be successfully generated (Table 2.5). This observation demonstrates that the method can also be compatible with more complex glycosyl donors in the future (Scheme 2.9).



Scheme 2.9: Parallel sugarLIFT synthesis of disaccharides **2.7**, **2.42** and trisaccharide **2.43**, synthesized from mannosyl **2.6**, **2.18-2.21**, galactosyl **2.24-2.25**, and lactosyl donor **2.26**, respectively. Disaccharide **2.41** was not obtained after glycosylation with **2.22-2.23**. Screening of the synthesized structures achieved with their corresponding fluorescently labeled plant lectins (ConA staining represented with red and RCA-I staining with green). Reagents and conditions: i) cLIFT, laser power 110–190 mW duration time 21-25 ms; ii) vapor

glycosylation, 10% TMSOTf in DCM, vacuum 100 mbar, -5 °C to rt, 30 min; iii) NaOMe in MeOH, rt, overnight; iv) ConA (20 µg/mL) and RCA-I (10 µg/mL) staining; Scanning parameters: 635 nm excitation, PMT gain 600, pixel size 5 µm for ConA and 532 nm excitation, PMT gain 400, pixel size 5 µm for RCA-I.

Table 2.4: Fluorescence scan images of α -D-mannopyranosyl-1,6- β -D-galactopyranosides **2.7** of donors **2.18-2.21**, after deprotection and incubation with fluorescently labeled ConA. Staining was performed in HEPES-buffer (50 mM HEPES, 100 mM NaCl, 1 mM CaCl₂, 1 mM MnCl₂, 10 % blocking buffer and 0.05 % Tween-20, pH 7.5) at 20 µg/mL ConA concentration. Scanning parameters: wavelength 635 nm, PMT gain 600, laser power 33%, pixel size 5 µm. Spot pitch is 1000 µm.

Building block	2.6	2.18	2.19	2.20	2.21
1 st Glycosylation					
2 nd Glycosylation				Not performed	

Table 2.5: Fluorescence scan images of oligosaccharides **2.42** and **2.43** obtained from donors **2.24-2.26** bearing a terminal galactose moiety, after deprotection and incubation with fluorescently labeled RCA-I. Staining was performed in HEPES-buffer (50 mM HEPES, 100 mM NaCl, 1 mM CaCl₂, 1 mM MnCl₂, 10 % blocking buffer and 0.05 % Tween-20, pH 7.5) at 10 µg/mL RCA-I concentration. Scanning parameters: Wavelength 532 nm, PMT gain 500, laser power 33 %, pixel size 5 µm. Spot pitch is 1000 µm.

Building block	2.24	2.25	2.26	2.22	2.23
1 st Glycosylation					
2 nd Glycosylation					

2.2.6. Evaluation of fluorescence signal for reference building block

Single glycosylation with the optimized conditions gave homogeneously glycosylated spots or areas in defined positions. However, the minimization of the activator used for the preparation of the activator solution caused a reduction of the fluorescence intensity. Therefore, the transfer of the desired pattern and the glycosylation reaction were repeated after the completion of the first glycosylation cycle. For this experiment and for the parallel

synthesis, the automated cLIFT system^[128] was used to assure precision during the sugarLIFT process. The size of the spots and the fluorescence intensities between the two glycosylations (Figure 2.12A), were increased. The fluorescence intensity after the second glycosylation was higher than the intensities obtained from single glycosylations (Figure 2.12B). However, the increase in the spot size indicated that future investigations should be focused on optimizing the conditions for the sugarLIFT process. Additionally, analysis of the fluorescence results showed that the fluorescence intensities were increasing for both glycosylations in combination with the lasing power increase (Figure 2.12C), while the lasing duration was irrelevant with the obtained result (Figure 2.12D). Finally, major observations from these experiments were that the position of the slide inside the glycosylation chamber in regard to the injection site as well as the position of the transferred pattern on the acreage of the slides have a great influence on the spot size. A decrease in the spot size was observed for all lasing powers (Figure 2.12E) from the top to the bottom of the acceptor slide. Future investigations should be focused on how to control the spot size in regard to the position of the slide inside the setup as well as to probe different injection techniques to more quickly generate a homogeneous activator atmosphere.

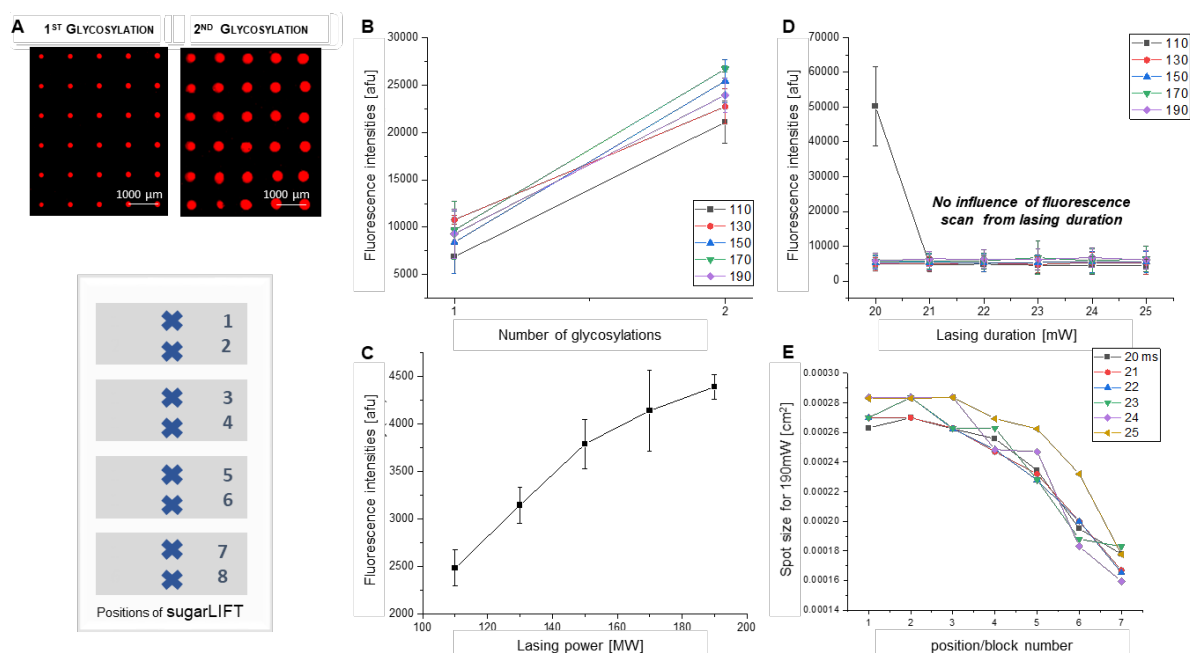


Figure 2.12: Observations after analyzing the fluorescence intensities of dimer 2.7 obtained with the optimized conditions for reference donor 2.6: A) fluorescence staining between first and second glycosylation with increased spot size, and positions of transferred pattern during sugarLIFT; B) fluorescence difference between first and second glycosylation; C) increased fluorescence intensities by increasing the lasing power during sugarLIFT; D) no difference in the fluorescence intensities by increasing the lasing duration; E) changes of the spot size depending on the position of the pattern on the acreage of the acceptor slide.

2.3. Conclusions

In conclusion, the sugarLIFT method has been developed for *in-situ* chemical parallel synthesis of oligosaccharides on a glass solid support, under inert and temperature-controlled conditions. A custom-built vapor condensation glycosylation setup was designed and optimized to ensure control of the applied glycosylation conditions, maintaining the laser transferred pattern, generated by cLIFT.

All optimizations were performed using the perbenzoylated mannose imidate **2.6** and the functionalized solid support **2.5**. Detection of the formed disaccharide was achieved after deprotection of the permanent benzyl ester protecting groups of the terminal mannose moiety with fluorescently labelled ConA, while mass detection of the formed disaccharide **2.7** was achieved using the functionalized acceptor slide **2.10**, bearing the photocleavable linker **2.8**. In addition, further validation of the optimized conditions was achieved *via* synthesizing photocleavable linker **2.12** for direct glycosylation on the solid support **2.16**, and *in-situ* MALDI detection of the formed monosaccharide **2.17**. The deprotection conditions of the benzoyl ester protecting groups were investigated using NaOMe and K₂CO₃ in methanol for successful lectin staining of the resulting disaccharide **2.7**, after successful glycosylation.

Different glycosyl donors (Man, Glc, and Gal) were synthesized bearing different permanent and temporary protecting groups on the C-6 position, as well as leaving groups on the anomeric position, to find the best candidates for future chain elongation. All synthesized donors were subjected to sugarLIFT glycosylation in parallel on the solid support **2.5** under the same optimized glycosylation conditions for lectin screening. Single cLIFT transfer, vapor glycosylation, deprotection and ConA detection of the terminal mannopyranosides showed successful formation of disaccharide **2.7**, while no signal was detected after ConA staining for terminal glucopyranosides **2.41**. Similarly, no staining was detected after single vapor glycosylation, deprotection and RCA-I staining of structures with terminal galactopyranosides. However, repetition of patterning and coupling process with freshly prepared glycosyl donor slides yielded the desired oligosaccharides **2.42**, and **2.43** in good fluorescence signal.

This result indicates that the sugarLIFT method offers a first step for parallel and direct glycosylation of glycosyl donors in the microarray format, minimizing costs and time needed for the on-chip synthesis of different oligosaccharides.

2.4. Outlook

The sugarLIFT method is still in an early stage of development showing limitations. Additional optimizations should be focused on the concentration of the activator solution, to bypass the possible acidic cleavage of the benzyl ether protecting groups. Then, the glycosylation efficiency with imidate **2.19** should be further studied to justify the obtained positive signal.

Moreover, the current method could be modified to be applicable for self-assembled monolayers with matrix-assisted laser desorption-ionization mass spectrometry (SAMDI ToF MS, by *Mrksich et al.*)^[60] for faster screening and validation of the sugarLIFT chemical conditions.

Future investigations, should be also focused on the deprotection of the benzyl ether (Bn) groups that still remain a bottleneck (Figure 2.13A). Heterogeneous catalytic hydrogenation with Pd/C or Pd(OH)₂/C cannot be performed on the glass solid support **2.5**, since heterogeneous catalytic systems not only resulted in scratches on the glass support **2.44**, but are also incompatible with solid phase synthesis, since the staining was unsuccessful. Alternatively, deprotection of Bn groups could be facilitated by single electron oxidants, such as 2,3-dichloro-5,6-dicyano-1,4-benzoquinone (DDQ) as a stoichiometric or catalytic photo-oxidant.^[219] Moreover, benzyl ether protecting groups can be replaced either with *p*-methoxybenzyl (PMB) or with 2-naphthylmethyl (NAP) ether protecting groups, that can be also cleaved with DDQ, in both cases forming a stabilized intermediate due to resonance.

By performing simple modifications on the protecting groups of the synthesized glycosyl donors, the process could be improved, allowing access to more complex structures. The selective deprotection, such as the Lev group on the microarray should be explored, to use more complex donors (**2.46**, **2.47**), bearing different orthogonal protecting groups (Fmoc, Lev, and chloroacetate ester (-ClAc)) as reported in the literature^[109] (Figure 2.13B).

Furthermore, optimization of the patterning parameters should further improve the microarray spot density, enabling smaller spot sizes, especially upon repetitive glycosylation cycles.

Finally, the use of the automated synthesizer^[128] and the newly developed hematite absorber for donor generation^[220] may drastically accelerate the screening of glycan-glycan binding protein interactions.

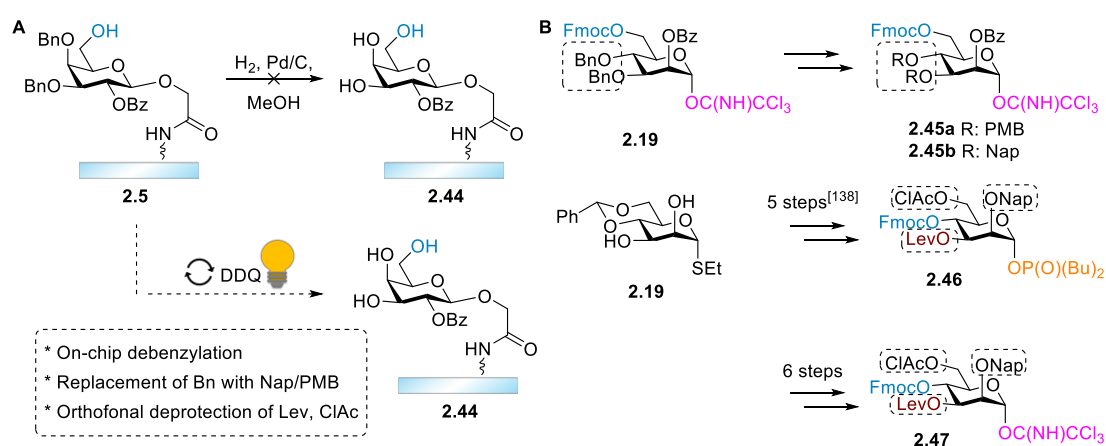


Figure 2.13: Deprotection of Bn groups on chip and additional building blocks that could be synthesized bearing orthogonal protecting groups.

2.5. Experimental Section

General remarks

All applied solvents, deuterated solvents (99.5 atom% D), and chemicals were purchased from common suppliers such as Sigma-Aldrich, Alfa Aesar, Tokio Chemical Industry (TCI), Thermo Fischer Scientific, Acros Organics, Iris Biotech, Merck, and used without further purification. All starting materials such and all starting glycopyranoside building blocks used for the synthesis of the targeted compounds were purchased from GlycoUniverse GmbH & Co KGaA, apart from the lactose starting material purchased from Tokyo Chemical Industry (TCI). If not mentioned otherwise, saturated aqueous solutions of inorganic salts were used. Thin layer chromatography (TLC) using silica gel coated aluminum plates (MACHEREY-NAGEL, pre-coated TLC sheets ALUGRAM® Xtra SIL G/UV254 or Merck, pre-coated TLC sheets 60 F254) was applied to monitor reactions until completion. Compounds were visualized by UV light ($\lambda = 254$ nm) or stained with Seebach (phosphomolybdic acid hydrate, cerium (IV) sulfate tetrahydrate, sulfuric acid and water). Flash column chromatography was carried out by using MACHEREY-NAGEL silica gel 60 (0.040 × 0.063 mm) and quartz sand. The spectra were recorded on Varian 400-MR (400 MHz) or Bruker Ascend 400 (400 MHz) spectrometer. Chemical shifts δ are reported in ppm and are adjusted to internal standards of the residual proton signal of the deuterated solvent ($CDCl_3$: 7.26 ppm for 1H and 77.0 ppm for ^{13}C). The spectra were measured at room temperature. Having symmetrical signals, the center of the signal is given and for multiplets the area. The following characterization was used: s: singlet, d: doublet, t: triplet, q: quartet, m: multiplet or combinations like dd: doublet of doublet or dt: doublet of triplet and m: multiplet. Coupling constants (J) are given in Hz.

The spectra were evaluated according to 1st order. For ¹H NMR spectra, the correlation of the signals was done according to the multiplicities. IR spectra were recorded on a FT-IR spectrometer from Perkin-Elmer. High-resolution mass spectrometry (HRMS) was conducted on a Waters Xevo G2-XS QToF device using ESI (electrospray ionization). Low-resolution mass spectrometry (LRMS) were obtained using an HPLC-System Series 1100 coupled with ESI-single quadrupole from Agilent. The abbreviation [M+Na]⁺ refers to the product–sodium adduct. ESI mass spectra were run on IonSpec Ultima instruments and MALDI-ToF autoflexTM (Bruker) instrument. UV-cleavage of the photolabile linker was performed in a Vilber Lourmat black light (VL.208.BL) lamp emitting 365 nm UV light with fractions of visible light (wavelength [nm]: 365, filter size [mm]: 230 × 60, power [W]: 2 × 8). A Molecular Devices microarray scanner, GenePix 4000B, San Jose, USA, was used for the analysis of all arrays. The detection wavelength was $\lambda = 523$ nm, with PMT gain 500 for Rhodamine RCA-I, and $\lambda = 635$ nm, with PMT gain 600, for CF[®]633 ConA. The laser power was 33% for every measurement and the pixel size was 5 μ m for high-resolution scans.

Laser transfer parameters

For process optimization: A laser scanning system with 488 nm wavelength and 120 mW maximum output power was used^[197,221], with a laser focus diameter of ~20 μ m. A laser power of 80 mW with a pulse duration range of 20-27.5 ms was applied for the optimization experiments.

For sugarLIFT vapor glycosylation: A laser scanning system with 488 nm wavelength and 120 mW maximum output power was used^[197,221], with a laser focus diameter of ~20 μ m. A laser power of 80 mW with a pulse duration range of 20 ms was applied.

For parallel synthesis: For the array synthesis, a spot pitch of 1 mm was used. A laser scanning system with 405 nm wavelength and 210 mW maximum output power with a laser focus diameter of 50 μ m was used.^[128] The automated transfer of the donor slides to the acceptors, placed in the slide holder with a robot with 20 μ m precision. A laser gradient from 110 to 190 mW was applied with a pulse duration range of 20-25 ms.

Laser transfer system for method optimization

The laser system consists of a 200 mW TOPTICA iBeam smart 488-S laser with a wavelength of 488 nm (TOPTICA Photonics, AG, Gräfelfing/Bayern, Germany), which is passed through a 1:10 beam expander and a Racoon 11 laser scanning system (ARGES GmbH, Wackersdorf/Bayern, Germany), equipped with an f-Theta lens (S4LFT5110/322, Sill Optics GmbH, Wendelstein/Bayern, Germany). High quality laser transfer with reproducible

results at various positions is achieved with scanning the laser beam in a 66 mm × 66 mm plane. The acceptor slide in the lasing areas was aligned with three mechanical springs and a vacuum mechanism.^[197]

Laser transfer system for parallel synthesis

The lasing system consists of a 405 nm wavelength diode laser with a Gaussian beam profile and a maximum of 300 mW power (iBeam smart 405-S, TOPTICA Photonics AG), lead through a laser scanning system (intelliSCAN III 10, SCANLAB), linked to an f-theta- lens (JENar 170-355-140, JENOPTIK Optical Systems GmbH). The measured maximum power in the lasing area is 210 mW. Transport of donor slides between the slide holder and the lasing area is achieved with a KUKA AGILUS six KR 3 R540 robot (KUKA AG), with 20 µm precision. A robot tool, a gripper (with four 2 mm diameter rubber suction cups) is incorporated connected to a pneumatics system that initiates and releases vacuum for transportation. Within the lasing area, simple pressure is produced to ensure mechanical alignment, controlled by the pneumatics system. A strong vacuum (-80 kPa) suction is applied to keep the acceptor slide in place during the process.^[128]

pH measurements

The pH was determined using a FiveEasy pH/mV meter F20, equipped with a plastic pH electrode LE438 from Mettler Toledo.

Fluorescence scan

Molecular Devices microarray scanner, GenePix 4000B, San Jose, USA, was used for the screening of the obtained oligosaccharides. The detection wavelength was $\lambda = 523$ nm (for Rhodamine RCA-I), with PMT gain of 500 respectively, and $\lambda = 635$ nm (for CF[®]633 ConA), with PMT gain 600. The laser power was 33% for every measurement and the pixel size was 5 µm for high-resolution scans.

Plant lectin assay

Before lectin staining, acceptor slides were incubated with a blocking buffer for 30 min (Rockland, USA; blocking buffer for fluorescent western blotting MB-070). Fluorescently labeled plant lectins, concanavalin A (ConA; CF[®]633 ConA, Biotium, Inc., USA) was diluted to 20 µg/mL in lectin buffer (50 mM HEPES, 100 mM NaCl, 1 mM CaCl₂, 1 mM MnCl₂, 10% blocking buffer, 0.05% Tween 20, pH 7.5), and Ricinus communis agglutinin I, (RCA-I, Rhodamine labeled, Lectin kit 1, Vector laboratories, USA) was diluted to 10 µg/mL in lectin buffer and incubated for 1 h at room temperature. Subsequently, each stained well was

washed with PBS-T buffer (3 ×3 min). Then, the acceptor slide was rinsed with Tris buffer (1 mM Tris-HCl buffer, pH=7.4) to remove all the remaining salt residues, and dried by a jet of air. Fluorescence scanning was used to detect the lectin binding on the corresponding sugar moieties.

MALDI-ToF mass spectrometry

Mass spectra were obtained from a MALDI-ToF autoflex™ (Bruker) instrument. For *in situ*/direct MALDI, the slide was placed on a MTP-TLC adapter obtained from Bruker. On the edges between the slide and the adapter small pieces of (~1 cm²) of aluminum (3M, aluminum foil tape 425, silver, 75 mm×55 m, 0.12 mm) and copper foil tape (True Components, 20 m×50 mm) were placed to increase the conductivity.

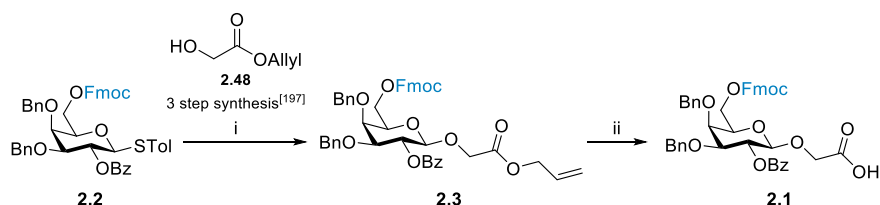
Preparation of stock solutions

- **Donor slide preparation:** Building block (5 mg) and inert polymer matrix (SLEC, 25 mg) were dissolved in 500 µL of anhydr. dichloromethane (DCM) in a vial. The final mixture was shaken for 2 min and afterwards the solution was spin-coated on top of the polyimide foil of the microscope glass slide, forming a thin layer of the transferred material.
- **Fmoc-deprotection:** A solution of 20% piperidine in dimethylformamide (DMF) (v/v) was prepared.
- **Acidic capping:** A solution of 10% acetic anhydride (Ac₂O) and 2% methanesulfonic acid (MsOH) in anhydr. DCM (v/v) was used.
- **Basic capping A:** A solution containing 10% Ac₂O and 20% *N,N*-diisopropylethylamine (DIPEA) in DMF (v/v) was prepared.
- **Basic capping B:** A solution containing 10% Ac₂O and 20% *N,N*-diisopropylethylamine (DIPEA) in DMF:DCM (1:1 v/v) was prepared.
- **Basic capping C:** A solution containing 60% Ac₂O and 40% pyridine (v/v) was prepared.
- **Acidic wash:** A solution of 0.5% trimethylsilyl trifluoromethanesulfonate (TMSOTf) in dichloromethane (DCM) was prepared (0.05 mL TMSOTf in 9.95 mL DCM).
- **Activator solution:** A solution of 10% TMSOTf in DCM was prepared.
- **Pyridine solution:** A solution of 10% pyridine in DMF (v/v).

- **Basic wash:** 10% of pyridine was added in anhydrous DMF (v/v).
- **Methanolysis solution:** A solution of 0.5 mL of sodium methoxide (NaOMe, 0.5 M) solution in 5 mL of methanol (MeOH) was prepared.

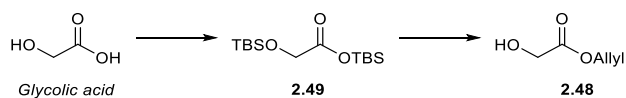
2.5.1. Syntheses of linkers and building blocks

Synthesis of base-labile linker (2.1)

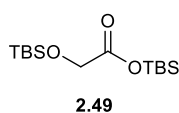


Allyl 2-hydroxyacetate **2.48** synthesized in 3 steps from glycolic acid, according to literature procedure.^[212,213]

Allyl 2-hydroxyacetate (2.48)



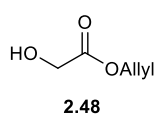
tert-Butyldimethylsilyl (tert-butyldimethylsilyloxy) acetate (2.49)



Glycolic acid (4.19 g, 55.0 mmol, 1.00 equiv.) and *tert*-butyldimethylsilyl chloride (TBSCl) (17.7 g, 117 mmol, 2.10 equiv.) were stirred in anhydr. DMF (10.0 mL). Imidazole (15.6 g, 230 mmol, 4.10 equiv.) was added to the mixture and stirred under inert conditions over weekend. The mixture was poured into water (250 mL). The water phase was washed with diethyl ether (3 × 100 mL). The organic phases were combined, washed with aqueous NaHCO₃ solution (250 mL), dried over MgSO₄, and concentrated under vacuum. ¹H NMR (400 MHz, CDCl₃): δ = 4.14 (s, 2H, Si-CH₂-CO-), 0.92 (s, 9H, 3 -CH₃), 0.91 (s, 9H, 3 -CH₃), 0.27 (s, 6H, 2 -CH₃), 0.09 (s, 6H, 2 -CH₃) ppm.

*The crude product was used without further characterization.

Allyl 2-hydroxyacetate (2.48)

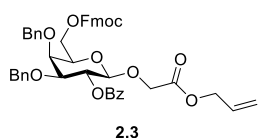


2.49 (4.62 g, 15.1 mmol, 1.00 equiv.) was dissolved in anhydr. DCM (35.0 mL) and cooled down to 0 °C. Oxalyl chloride (1.56 mL, 18.2 mmol, 1.20 equiv.) added dropwise under inert conditions, and then nine drops of dimethylformamide. After stirring the solution at 0 °C for 1 h the mixture warmed up at room

temperature and stirred for additionally 1 h. The reaction was quenched by allyl alcohol (5.50 mL) and was stirred for additional 2 h at room temperature. Then, the solvents were removed under reduced pressure and the crude product was purified by flash column chromatography using a mixture of hexane/ethyl acetate (2:1) as eluent. The product was obtained as a colorless oil in 52% yield (0.90 g, 7.83 mmol). ¹H NMR (400 MHz, CDCl₃): δ = 5.93 (ddt, 1H, *J* = 17.2, 10.4, 5.9 Hz, 1H, CH₂=CH-, allyl), 5.40 – 5.25 (m, 2H, -CH₂=CH-, allyl), 4.70 (dt, *J* = 5.9, 1.4 Hz, 2H -CH₂CH=CH₂), 4.19 (s, 2H, -CH₂-OH), 2.34 (s, 1H, -OH) ppm; ¹³C NMR (101 MHz, CDCl₃): δ = 173.0, 131.3, 119.3, 77.4, 77.0, 76.7, 66.1, 60.5 ppm.

*Experimental data agree with the literature.^[213]

Acetic acid 2-((2-O-benzoyl-3,4-di-O-benzyl-6-O-(9-fluorenylmethoxycarbonyl)-β-D-galactopyranosyl)oxy)-2-propen-1-yl ester (2.3)

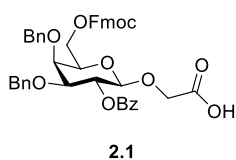


4-Methylphenyl-2-O-benzoyl-3,4-di-O-benzyl-6-O-(9-fluorenylmethoxy-carbonyl)-1-thio-β-D-galactopyranoside (2.2) (3.00 g, 3.80 mmol, 1.30 equiv.) was dissolved in 176 mL of anhydr.

DCM under argon atmosphere in the presence of 4 Å molecular sieves (powder) and allyl 2-hydroxyacetate **2.47** (0.29 μL, 2.90 mmol, 1.00 equiv.) was added. The mixture was stirred for 1 h at rt. The mixture was cooled down to -20 °C and NIS (0.78 g, 3.47 mmol, 1.20 equiv.) and TfOH (50.0 μL, 0.30 mmol, 0.10 equiv.) were added consecutively. The reaction was stirred for 1.5 h at -20 °C and then quenched by addition of a 1:1 mixture of NaHCO₃ and Na₂S₂O₄ solution. The solution was filtered through a pad of Celite[®] and the organic layer was washed with water (100 mL) and saturated aqueous NaCl solution (100 mL). The organic layer was dried over Na₂SO₄ and the solvent was removed under reduced pressure. The crude product was purified by flash column chromatography using a mixture of hexane/ethyl acetate (3:1) as eluent. The product was obtained as a white foam in 57% yield (1.30 g, 1.66 mmol). ¹H NMR (400 MHz, CDCl₃): δ = 8.10 – 8.05 (m, 2H, -Ar), 7.80 – 7.76 (m, 2H, -Ar), 7.63 – 7.55 (m, 3H, -Ar), 7.49 – 7.39 (m, 4H, -Ar), 7.37 – 7.27 (m, 8H, -Ar), 7.23 – 7.15 (m, 5H, -Ar), 5.83 – 5.65 (m, 2H, *H*-2, -CH=CH₂, allyl), 5.21 (dd, *J* = 17.2, 1.5 Hz, 2H, -CH=CH₂, allyl), 5.02 (d, *J* = 11.6 Hz, 1H, -Bn), 4.77 (d, *J* = 7.8 Hz, 1H, *H*-1), 4.68 (dd, *J* = 12.0, 8.9 Hz, 2H, -Bn), 4.61 – 4.15 (m, 10H, -OCH₂-, -COO-CH₂-, *Hb*-6, *Ha*-6, -CH-), 3.93 (dd, *J* = 2.8, 1.2 Hz, 1H, *H*-4), 3.71 (ddd, *J* = 7.8, 5.4, 1.9 Hz, 2H, *H*-2, *H*-3) ppm.; ¹³C NMR (101 MHz, CDCl₃): δ = 169.4, 165.6, 154.9, 143.3, 143.3, 141.4, 137.9, 137.5, 133.1, 131.6, 130.2, 130.1, 128.6, 128.5, 128.4, 128.1, 128.0, 127.9, 127.8, 127.3,

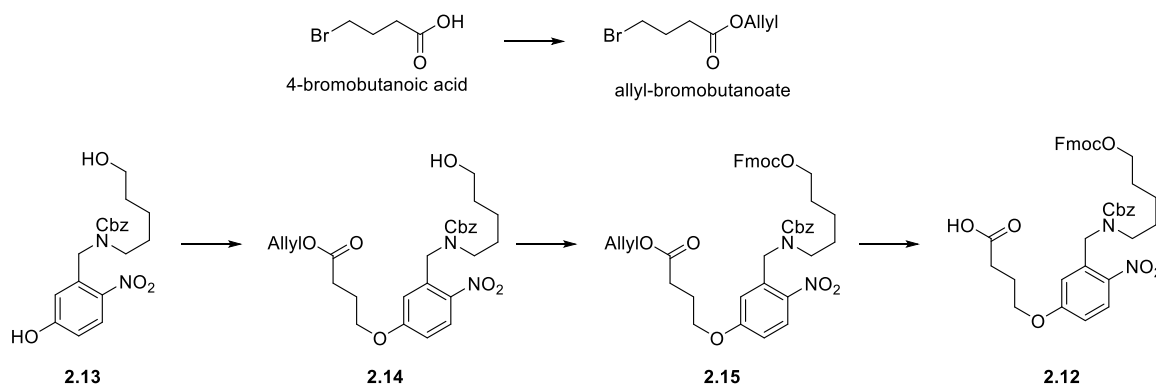
125.2, 120.2, 118.9, 100.0, 79.6, 74.5, 72.5, 72.3, 72.0, 71.3, 70.1, 66.6, 65.5, 64.0, 46.8 ppm.

2-((2-O-Benzoyl-3,4-di-O-benzyl-6-O-(9-fluorenylmethoxycarbonyl)- β -D-galactopyranosyl)oxy)-acetic acid (2.1)

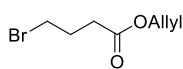


Galactoside **2.3** (1.30 g, 1.66 mmol, 1.00 equiv.) was dissolved in 40.0 mL of anhydr. tetrahydrofuran under argon atmosphere and tetrakis(triphenyl-phosphine)palladium(0) (0.21 g, 0.18 mmol, 0.11 equiv.) and acetic acid (7.40 mL) were added consecutively. The solution was stirred overnight at room temperature and then diluted with DCM (100 mL). Then, the mixture was washed with 0.5 M aqueous HCl solution (100 mL), the organic layer was dried over Na₂SO₄ and the solvent was removed under reduced pressure. The crude product was purified by flash column chromatography using a mixture of hexane/ethyl acetate (1.5:2) containing 0.5% of acetic acid as eluent. The product was obtained as a yellow foam in 76% yield (0.95 g, 1.27 mmol). ¹H NMR (400 MHz, CDCl₃): δ = 8.04 – 7.99 (m, 2H, -Ar), 7.78 (m, 2H, -Ar), 7.60 (m, 3H, -Ar), 7.50 – 7.39 (m, 5H, -Ar), 7.37 – 7.28 (m, 7H, -Ar), 5.68 (dd, *J* = 10.0, 7.8 Hz, 1H, *H*-2), 5.02 (d, *J* = 11.6 Hz, 1H, -CHH-, *Bn*) 4.74 – 4.56 (m, 4H, -CHH-, -CH₂-, *Bn*, *H*-1), 4.48 – 4.29 (m, 5H, OCH₂-COOH, -CH₂-, Fmoc, *Ha*-6), 4.25 (t, *J* = 5.2 Hz, 1H, -CH- Fmoc), 4.17 (dd, *J* = 11.2, 5.4 Hz, 1H, *Hb*-6), 3.95 (dd, *J* = 2.8, 1.2 Hz, 1H, *H*-4), 3.78 – 3.69 (m, 2H, *H*-3, *H*-5) ppm; ¹³C NMR (101 MHz, CDCl₃) δ = 170.7, 165.8, 154.8, 143.3, 143.2, 141.4, 141.4, 137.6, 137.3, 133.5, 130.0, 129.6, 128.6, 128.6, 128.5, 128.2, 128.1, 128.1, 127.9, 127.3, 125.2, 125.2, 120.2, 101.1, 79.3, 74.6, 72.9, 72.48, 71.9, 71.5, 70.1, 66.4, 65.6, 46.7 ppm; IR (neat) ν_{\max} : 2992, 1747, 1452, 1265, 1096, 1028 cm⁻¹; ESI-HRMS: *m/z* [M+Na]⁺ calcd. for C₄₄H₄₀O₁₁ Na: 767.2492; found 767.2473.

Synthesis of photocleavable linker (2.12)



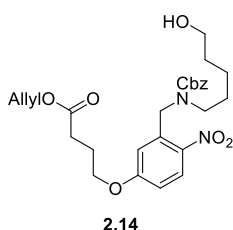
Allyl-bromobutanoate



A solution of allyl alcohol (0.41 mL, 5.98 mmol, 1.00 equiv.), 4-bromobutanoic acid (1.00 g, 5.98 mmol, 1.00 equiv.), and DMAP (92.0 mg, 0.75 mmol, 0.25 equiv.) in anhydr. DCM (60 mL) was stirred at 0 °C under argon atmosphere for 30 min. Then *N,N'*-diisopropylcarbodiimide (DIC) (1.70 mL, 10.8 mmol, 1.80 equiv) was added dropwise. The reaction mixture was slowly left to warm up to room temperature overnight. Then, the reaction mixture was filtrated to remove the formed solid. The residue was diluted in cold hexane, and then filtered on a pad of silica gel. The pad of silica gel was washed with hexane/ethyl acetate (4.5:1) and the solvents were removed under reduced pressure giving the desired compound as a yellow oil in 79% yield (971 mg, 4.69 mmol). ¹H NMR (400 MHz, CDCl₃): δ = 5.91 (m, 1H, -CH=CH₂), 5.32 (dd, *J* = 17.2 Hz, 1H, -CH=CH₂), 5.24 (dd, *J* = 10.4 Hz, 1H, -CH=CH₂), 4.59 (dt, *J* = 5.8, 1.4 Hz, 2H, -O-CH₂-), 3.47 (t, *J* = 6.4 Hz, 2H, Br-CH₂-), 2.53 (t, *J* = 7.2 Hz, 2H, -CO-CH₂-), 2.13 – 2.21 (m, 2H, -CH₂-) ppm; ¹³C NMR (101 MHz, CDCl₃): δ = 172.1, 131.9, 118.3, 65.2, 32.6, 32.3, 27.6 ppm.

The analytical data agree with the literature.^[215]

7-(3-(((5-Hydroxypentyl)amino)methyl)-4-nitrophenoxy)hept-1-en-4-one (2.14)

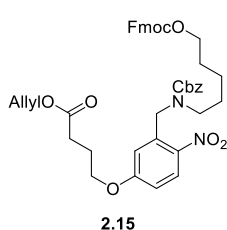


N-(((5-Hydroxy-2-nitrophenyl)methyl)-*N*-(5-hydroxypentyl) phenylmethyl ester carbamic acid^[202] **2.13** (2.37 g, 4.70 mmol, 1.00 equiv.) and potassium carbonate (K₂CO₃) (1.62 g, 11.7 mmol, 2.50 equiv.) were dissolved in DMF (30 mL) at 60 °C. After 1 h, allyl 4-bromobutanoate (384 mg, 1.86 mmol, 1.00 equiv.) was added dropwise and the solution stirred for 24 h. The reaction mixture was quenched with water and stirred for additional 15 min to reach rt. The resulted mixture was diluted in DCM and washed with water. The aqueous phase was washed with DCM three times. The combined organic phases were washed with NaCl-solution and dried over Na₂SO₄. The residue was purified by flash column chromatography using a mixture of hexane/ethyl acetate (1:1) to afford the desired compound as a yellow oil in 95% yield (2.28 g, 4.44 mmol). ¹H NMR (400 MHz, CDCl₃): δ = 8.15 (m, 1H, -Ar), 7.44 – 7.33 (m, 3H, -Ar), 7.20 – 7.11 (m, 1H, -Ar), 6.88 – 6.59 (m, 3H, -Ar), 5.92 (ddt, *J* = 17.3, 10.4, 5.8 Hz, 1H, -CH₂-CH=CH₂, Allyl), 5.33 (dd, *J* = 17.1, 1.6 Hz, 1H, -CH=CHH, Allyl), 5.25 (dd, *J* = 10.4, 1.3 Hz, 1H, -CH=CHH, Allyl), 5.15 (d, *J* = 4.2 Hz, 2H, -CH₂-Ar, Cbz), 4.89 (d, *J* = 4.4 Hz, 2H, Ar-CH₂-N-), 4.60 (dd, *J* = 5.8, 1.4 Hz, 2H, -CH₂-CH=CH₂), 3.94 (m, 2H, -CH₂-CH₂-O), 3.65 – 3.53 (m, 2H, -CH₂-OH), 3.31 (m, 2H, -NCbz-CH₂-), 2.54 (m, 2H, -CO-CH₂-CH₂-), 2.10 (m, 2H, -CO-CH₂-CH₂-), 1.71 – 1.43 (m, 4H, -CH₂-

CH₂-CH₂-), 1.40 – 1.26 (m, 2H, -CH₂-CH₂-CH₂-) ppm; ¹³C NMR (101 MHz, CDCl₃): δ = 172.5, 163.2, 156.3, 140.9, 137.7, 136.4, 131.9, 128.5, 128.3, 128.0, 127.9, 118.4, 113.5, 113.0, 112.5, 67.4, 67.1, 65.3, 62.6, 60.3, 48.7, 48.1, 32.2, 30.3, 27.6, 24.1, 22.8 ppm; ESI-LRMS: m/z [M+Na]⁺ calcd. for C₂₇H₃₄N₂O₈ Na: 537.2207 found 537.2.

* The compound was used without further characterization.

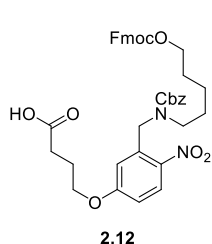
Allyl-4-(3-(((5-(((9-fluorenylmethoxycarbonyl) pentyl) ((benzyloxy) carbonyl) amino) methyl)-4-nitrophenoxy) butanoate (2.15)



7-(3-(((5-Hydroxypentyl)amino)methyl)-4-nitrophenoxy)hept-1-en-4-one **2.14** (2.28 g, 4.43 mmol, 1.00 equiv.) was dissolved in anhydr. DCM (50 mL) and pyridine (2.50 mL, 10.0 mmol, 7.00 equiv.) and FmocCl (2.30 mg, 8.86 mmol, 2.00 equiv.) were added consecutively. The solution was stirred overnight at rt, and then the solvent was removed under reduced pressure. Residual pyridine was coevaporated with toluene. The crude product was purified by flash column chromatography using a mixture of hexane/ethyl acetate (2:1) as eluent. The product was obtained as a yellow oil in 99% yield (3.22 g, 4.37 mmol). ¹H NMR (400 MHz, CDCl₃): δ = 8.17 (m, 1H, -Ar), 7.76 (dt, *J* = 7.6, 0.9 Hz, 2H, -Ar), 7.66 – 7.58 (m, 2H, -Ar), 7.45 – 7.28 (m, 8H, -Ar), 7.18 (m, 1H, -Ar), 6.82 (dd, *J* = 9.1, 2.7 Hz, 1H, -Ar), 6.76 – 6.62 (m, 1H, -Ar), 6.00 – 5.83 (m, 1H, -CH=CH₂, Allyl), 5.37 – 5.24 (m, 2H, -, -CH=CH₂, Allyl), 5.10 (d, *J* = 4.2 Hz, 2H, -CH₂-, Cbz), 4.90 (d, *J* = 4.5 Hz, 2H, Ar-CH₂-N-), 4.60 (dd *J* = 5.8, 1.4 Hz, 2H, -CH₂-CH=CH₂), 4.40 (d, *J* = 7.6 Hz, 2H, -CH₂-OFmoc), 4.26 (t, *J* = 7.4 Hz, 1H; -CH-; Fmoc), 4.20 – 4.07 (m, 2H, -CH₂-, Fmoc), 3.94 (dt, *J* = 34.5, 6.0 Hz, 1H, -CH₂-CH₂-O-Ar), 3.32 (m, 2H, -NCbz-CH₂-CH₂-), 2.54 (m, 2H, -CO-CH₂-CH₂-), 2.10 (, 2H, -CO- CH₂-CH₂-), 1.77 – 1.64 (m, 4H, -CH₂-CH₂-CH₂-), 1.46 – 1.29 (m, 2H, -CH₂-CH₂-); ¹³C NMR (101 MHz, CDCl₃): δ = 172.6, 155.3, 143.5, 141.4, 132.1, 128.5, 127.9, 127.2, 125.3, 120.1, 118.6, 113.7, 113.2, 112.6, 69.8, 68.0, 67.6, 67.4, 65.4, 60.5, 53.5, 48.8, 48.2, 46.8, 30.5, 28.1, 24.3, 23.1 ppm; ESI-LRMS: m/z [M+Na]⁺ calcd. for C₄₂H₃₄N₂O₈ Na: 759.28 found 759.2.

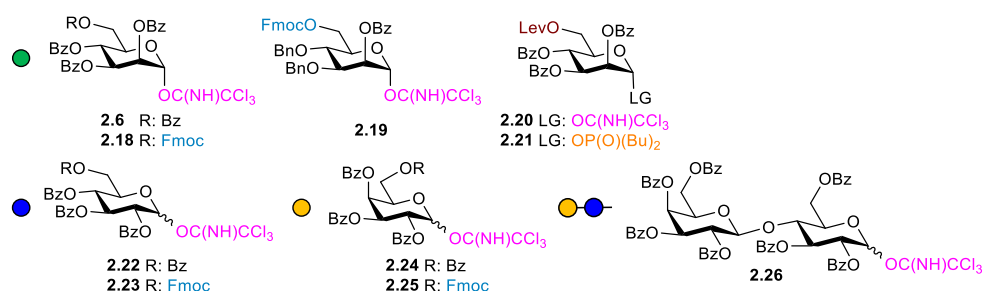
*The compound was used without further characterization.

4-(3-(((5-(((9-Fluorenylmethoxycarbonyl)-pentyl) ((benzyloxy) carbonyl) amino) methyl)-4-nitrophenoxy) butanoic acid (2.12)



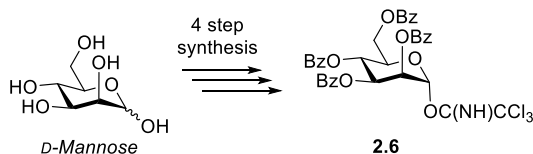
Allyl-4-(3-(((5-(((9H-fluoren-9yl) methoxy) carbonyl) oxy) pentyl) ((benzyloxy) carbonyl) amino) methyl)-4-nitrophenoxy) butanoate **2.15** (3.22 g, 4.38 mmol, 1.00 equiv.) was dissolved in anhydr. tetrahydrofuran (THF) (138 mL) under argon atmosphere and Pd(PPh₃)₄ (557 mg, 0.48 mmol, 0.11 equiv.) and acetic acid (20.4 mL) were added consecutively. The solution was stirred for 4 h at rt, and then, diluted with DCM (200 mL). Then the mixture was washed with 0.5 M aqueous HCl solution (200 mL), the organic layer was dried over Na₂SO₄ and the solvent was removed under reduced pressure. The crude product was purified by flash column chromatography using a mixture of hexane/ethyl acetate (1:1 with 0.5% of acetic acid) as eluent. The product was obtained as a yellow oil in 83% yield (2.53 g, 3.63 mmol). ¹H NMR (400 MHz, CDCl₃): δ = 8.17 (m, 1H, -Ar), 7.76 (dd, *J* = 7.6, 1.0 Hz, 2H, -Ar), 7.63 – 7.59 (m, 2H, -Ar), 7.43 – 7.28 (m, 8H, -Ar), 7.21 – 7.13 (m, 1H, -Ar), 6.84 – 6.63 (m, 2H, -Ar), 5.16 (d, *J* = 44.7 Hz, 2H, -CH₂-, Cbz), 4.91 (d, *J* = 2.4 Hz, 2H, Ar-CH₂-N-), 4.40 (d, *J* = 7.4 Hz, 2H, -CH₂-OFmoc), 4.25 (t, *J* = 7.4 Hz, 1H, -CH-, Fmoc), 4.20 – 4.07 (m, 2H, -CH₂-OFmoc), 3.94 (dt, *J* = 42.4, 6.0 Hz, 2H, -O-CH₂-CH₂-CH₂-COOH), 3.40 – 3.26 (m, 2H, -NCbz-CH₂-CH₂-), 2.59 – 2.52 (m, 2H, -CH₂-CH₂-COOH), 2.14 – 2.05 (m, 2H, -CH₂-CH₂-CH₂-), 1.76 – 1.56 (m, 4H, CH₂-CH₂-CH₂-), 1.45 – 1.3 (m, 2H, -CH₂-CH₂-CH₂-) ppm; ¹³C NMR (101 MHz, CDCl₃): δ = 178.2, 177.1, 163.3, 156.5, 155.4, 143.5, 141.4, 141.1, 140.8, 137.8, 137.3, 136.5, 128.7, 128.5, 128.4, 128.3, 128.2, 128.1, 128.0, 127.2, 125.3, 120.1, 113.7, 112.9, 112.9, 112.6, 69.8, 68.1, 67.7, 67.4, 67.2, 49.1, 48.9, 48.2, 47.7, 46.8, 30.3, 30.2, 28.4, 28.1, 27.6, 24.1, 24.1, 23.1, 20.8 ppm; IR (neat) ν_{max}: 2951, 1743, 1707, 1580, 1514, 1258, 744 cm⁻¹; UV/Vis (DMF): λ_{max}(ε) = 268; 300 nm; ESI-HRMS: *m/z* [M+Na]⁺ calcd. for C₃₉H₄₀N₂O₁₀ Na: 719.2575 found 719.2585.

Building block syntheses



Building blocks **2.6**, **2.22-2.24** and **2.26** were synthesized as reported, and their analytical data agree with the literature.^[214,216,217]

2,3,4,6-Tetra-O-benzoyl- α -D-mannopyranosyl trichloroacetimidate (**2.6**)

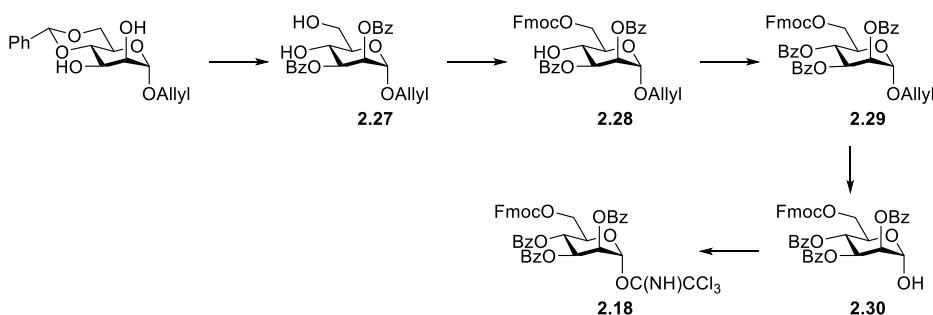


2.6 was prepared according to previously established procedures.^[214]

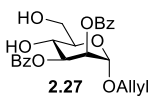
2,3,4,6-tetra-O-benzoyl-D-mannopyranose (3.22 g, 5.40 mmol, 1.00 equiv.) was dissolved in 40 mL of anhydr. DCM under argon atmosphere and trichloroacetonitrile (5.41 mL, 53.9 mmol, 10.0 equiv.) and DBU (0.20 μ L, 1.35 mmol, 0.25 equiv.) were added consecutively. The solution was stirred for 3 h at room temperature. The solvent was removed under reduced pressure. The crude product was purified by flash column chromatography using a mixture of hexane/ethyl acetate (4:1) as eluent. The product was obtained as a white foam in 90% yield (3.61 g, 4.87 mmol). ^1H NMR (400 MHz, CDCl_3): δ = 8.84 (s, 1H, C(NH)CCl₃), 8.10 – 7.31 (m, 21H, -Ar), 6.58 (d, J = 1.9 Hz, 1H, 1H, *H*-1), 6.24 (t, J = 10.1 Hz, 1H, *H*-4), 5.97 (dd, J = 10.0, 3.3 Hz, 1H, *H*-3) 5.94 (dd, J = 3.4, 1.9 Hz, 1H, *H*-2), 4.73 (dd, J = 12.3, 2.4 Hz, 1H, *H*-6b), 4.65 – 4.57 (m, 1H, *H*-5), 4.52 (dd, J = 12.3, 4.1 Hz, 1H, *H*b-6) ppm; ^{13}C NMR (101 MHz, CDCl_3): δ = 166.1, 165.6, 165.4, 165.2, 159.9, 133.8, 133.7, 133.5, 133.2, 130.0, 130.0, 129.8, 129.0, 128.9, 128.8, 128.6, 128.5, 128.5, 94.7, 90.7, 71.6, 69.9, 68.9, 66.1, 62.4 ppm.

* The analytical data agree with the literature.^[214]

Synthesis of 2,3,4-O-Tri-benzoyl-6-O-(9-fluorenylmethoxycarbonyl)- α -D-mannopyranosyl trichloroacetimidate (**2.18**)

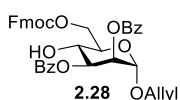


Allyl 2,3-di-O-benzoyl- α -D-mannopyranoside (2.27)



Allyl 4,6-O-benzylidene- α -D-mannopyranoside (5.00 g, 16.2 mmol, 1.00 equiv.) was dissolved in pyridine (50 mL) and the solution was cooled to 0 °C. Benzoyl chloride (BzCl) (4.90 mL, 42.2 mmol, 2.60 equiv.) was added dropwise to the solution and left to react overnight at room temperature. After completion, the mixture was poured into iced water; the precipitate was filtered off and washed with water. The solid was dissolved in DCM (100 mL) and washed with HCl (1 M, 100 mL), NaHCO₃ solution (100 mL), and water (100 mL). The organic layer was dried over Na₂SO₄ and the solvent was removed under reduced pressure. The crude product was used without any further purification. Trifluoroacetic acid (TFA) (9.17 mL, 119 mmol, 7.50 equiv.) and water (1.23 mL, 68.3 mmol, 4.30 equiv.) were added to a solution of the crude product (8.20 g, 15.9 mmol, 1.00 equiv.) in DCM (215 mL). The mixture was stirred for 3 h, diluted with DCM (200 mL), washed with 10% (w/v) NaHCO₃ solution until neutral pH and 10% (w/v) NaCl solution. The organic layer was dried over Na₂SO₄, filtered, and concentrated. The crude product was purified by flash column chromatography using a mixture of hexane/ethyl acetate (1:2) as eluent. The desired product was obtained as a white foam in 84% yield over two steps (5.70 g, 13.28 mmol). ¹H NMR (400 MHz, CDCl₃): δ = 8.10 – 8.05 (m, 2H, -Ar), 7.97 – 7.88 (m, 2H, -Ar), 7.64 – 7.57 (m, 1H, -Ar), 7.55 – 7.46 (m, 3H, -Ar), 7.38 – 7.33 (m, 2H, -Ar), 6.01 – 5.85 (m, 1H, CH₂=CH-) 5.61 (m, 2H, H-2, H-3), 5.36 (dd, *J* = 17.3, 1.6 Hz, 1H, CHH=CH-), 5.26 (dd, *J* = 10.4, 1.3 Hz, 1H, CHH=CH-), 5.05 (d, *J* = 1.6 Hz, 1H, H-1), 4.40 – 4.20 (m, 2H, H-4, H-6a), 4.14 – 4.06 (m, 1H, H-6b), 3.98 (d, *J* = 3.8 Hz, 2H, -CH₂-CH=), 3.90 (dt, *J* = 9.6, 3.7 Hz, 1H, H-5), 2.77 (s, 1H, -OH) ppm; ¹³C NMR (101 MHz, CDCl₃): δ = 166.9, 165.5, 133.5, 133.4, 133.1, 129.8, 129.8, 129.4, 129.2, 128.6, 128.4, 118.2, 96.7, 73.2, 72.4, 70.6, 66.9, 62.3 ppm; IR (neat) ν_{max} : 3468, 2964, 2345, 1726, 1601, 1452, 1277, 1114, 1071 cm⁻¹; ESI-HRMS: *m/z* [M+Na]⁺ calcd. for C₂₃H₂₄O₈Na: 451.1363 found 451.1369.

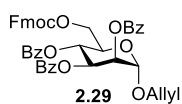
Allyl 2,3-di-O-benzoyl-6-O-(9-fluorenylmethoxycarbonyl)- α -D-mannopyranoside (2.28)



To a stirred suspension of **2.27** (4.00 g, 9.34 mmol, 1.00 equiv.) in anhydr. DCM (20 mL) and pyridine (3.77 mL, 46.7 mmol, 5.00 equiv.), at -20 °C fluorenylmethoxycarbonyl chloride (FmocCl) (2.90 g, 11.2 mmol, 1.20 equiv.) was added and the reaction mixture was stirred for 30 min. Upon completion, all volatiles were removed under reduced pressure. The residue was purified by flash column chromatography using a mixture of hexane/ethyl acetate (4:1) as eluent. The product was obtained as a white solid in 78% yield (4.74 g, 7.28 mmol). ¹H NMR (400 MHz, CDCl₃): δ =

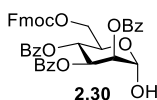
8.13 – 8.06 (m, 2H, -Ar), 7.96 – 7.89 (m, 2H, -Ar), 7.78 (m, 2H, -Ar), 7.64 (m, 2H, -Ar), 7.59 – 7.50 (m, 2H, -Ar), 7.44 – 7.28 (m, 8H, -Ar), 6.04 – 5.87 (m, 1H, CH₂=CH-, Allyl), 5.64 – 5.59 (m, 2H, H-2, H-3), 5.36 (dd, *J* = 17.2, 1.6 Hz, 1H, CHH=CH-, Allyl), 5.27 (dd, *J* = 10.4, 1.3 Hz, 1H, CHH=CH-, Allyl), 5.09 (d, *J* = 1.4 Hz, 1H, H-1), 4.69 – 4.54 (m, 2H, H-6a, H-6b), 4.48 – 4.43 (m, 2H, -CH₂-CH-, Fmoc), 4.33 – 4.23 (m, 3H, H-4, -OCHH-CH=CH₂, Allyl, -CH₂-CH-, Fmoc), 4.17 – 4.04 (m, 2H, -OCHH-CH=CH₂, Allyl, H-5), 2.85 (d, *J* = 4.9 Hz, 1H, -OH) ppm; ¹³C NMR (101 MHz, CDCl₃): δ = 167.1, 165.5, 155.6, 143.4, 143.4, 141.4, 133.6, 133.6, 133.2, 130.0, 129.9, 129.5, 129.2, 128.7, 128.5, 128.0, 127.3, 125.3, 120.2, 118.5, 96.8, 73.1, 71.1, 70.6, 70.3, 68.8, 66.8, 66.7, 46.8 ppm; IR (neat) *v*_{max}: 3528, 2983, 2928, 1725, 1601, 1386, 1281, 1256, 1154 cm⁻¹; ESI-HRMS: *m/z* [M+Na]⁺ calcd. for C₃₈H₃₄O₁₀Na: 673.2044 found 673.2070.

Allyl 2,3,4-tri-O-benzoyl-6-O-(9-fluorenylmethoxycarbonyl)-α-D-mannopyranoside (2.29)



2.28 (2.30 g, 3.53 mmol, 1.00 equiv.) was dissolved in pyridine (23 mL) and the solution was cooled to 0 °C. BzCl (1.40 mL, 12.2 mmol, 4.00 equiv.) was added dropwise to the solution and the mixture was left for 3 h at rt. Then, the mixture was concentrated under vacuum to remove pyridine. The residue was diluted and extracted with ethyl acetate (50 mL), washed with water (50 mL), NaHCO₃ solution (50 mL), and NaCl solution. The combined organic layers were dried over Na₂SO₄ and concentrated under reduced pressure. The crude product was purified by flash column chromatography using a mixture of hexane/ethyl acetate (4:1) as eluent. The product was obtained as a white solid in 89% yield (2.38 g, 3.15 mmol). ¹H NMR (400 MHz, CDCl₃): δ = 8.15 – 8.09 (m, 2H, -Ar), 8.01 – 7.95 (m, 2H, -Ar), 7.86 – 7.82 (m, 2H, -Ar), 7.82 – 7.74 (m, 2H, -Ar), 7.63 – 7.35 (m, 12H, -Ar), 7.33 – 7.28 (m, 3H, -Ar), 6.05 – 5.96 (m, 1H, -CH₂=CH-), 5.96 – 5.91 (m, 1H, H-3), 5.71 (t, *J* = 2.3 Hz, 1H, H-2), 5.44 – 5.26 (m, 2H, CH₂=CH-), 5.17 (d, *J* = 1.8 Hz, 1H, H-1), 4.53 – 4.09 (m, 7H, H-4, H-5, H-6a, H-6b, -CH₂-CH=, -CH-Fmoc) ppm; ¹³C NMR (101 MHz, CDCl₃): δ = 165.7, 165.6, 165.5, 155.1, 143.5, 143.3, 141.3, 141.3, 133.7, 133.6, 133.3, 133.1, 130.0, 129.9, 129.8, 129.3, 129.1, 129.0, 128.7, 128.6, 128.4, 128.0, 128.0, 127.3, 127.3, 125.4, 125.3, 120.1, 120.1, 118.7, 96.7, 70.5, 70.3, 70.0, 69.1, 68.9, 67.2, 66.5, 46.7 ppm; IR (neat) *v*_{max}: 3068, 2919, 1729, 1452, 1259, 1108, 1070, 1027 cm⁻¹; ESI-HRMS: *m/z* [M+Na]⁺ calcd. for C₄₅H₃₈O₁₁: 777.2306 found 777.2349.

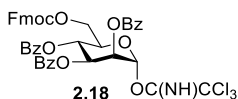
2,3,4-Tri-O-benzoyl-6-O-(9-fluorenylmethoxycarbonyl)- α -D-mannopyranoside (3.30)



The mixture of **2.29** (2.22 g, 2.95 mmol, 1.00 equiv.) and PdCl₂ (260 mg, 1.47 mmol, 0.50 equiv.) in MeOH/DCM (1:1, 14 mL) was stirred for 4 h at rt.

The reaction mixture was filtered through Celite[®] and concentrated under vacuum. The residue was purified by flash column chromatography using a mixture of hexane/ethyl acetate (2:1) as eluent. The product was obtained as a white solid in 98% yield (2.08 g, 2.91 mmol). ¹H NMR (400 MHz, CDCl₃): δ = 8.16 – 8.09 (m, 2H, -Ar), 8.01 – 7.94 (m, 2H, -Ar), 7.86 – 7.82 (m, 2H, -Ar), 7.77 (d, *J* = 7.6 Hz, 2H, -Ar), 7.64 – 7.37 (m, 12H, -Ar), 7.32 – 7.27 (m, 3H, -Ar), 6.00 (dd, *J* = 10.0, 3.1 Hz, 1H, *H*-3), 5.98 – 5.91 (m, 1H, *H*-4), 5.73 (dd, *J* = 3.1, 1.9 Hz, 1H, *H*-2), 5.55 (dd, *J* = 4.1, 1.9 Hz, 1H, *H*-1), 4.62 (dt, *J* = 9.1, 4.3 Hz, 1H, *H*-5), 4.51 – 4.39 (m, 3H, *H*-6a, -CH₂-CH- Fmoc), 4.35 (dd, *J* = 10.4, 7.4 Hz, 1H, *H*-6b), 4.24 (t, *J* = 7.4 Hz, 1H, -CH- Fmoc), 2.11 (d, *J* = 4.1 Hz, 1H, -OH) ppm; ¹³C NMR (101 MHz, CDCl₃): δ = 165.7, 165.6, 165.6, 155.1, 143.5, 143.3, 141.3, 133.7, 133.6, 133.3, 130.0, 130.0, 129.9, 129.9, 129.8, 129.3, 129.1, 129.0, 128.9, 128.9, 128.7, 128.6, 128.4, 128.0, 128.0, 127.3, 127.3, 125.4, 125.3, 120.1, 120.1, 70.7, 70.2, 69.5, 69.0, 68.9, 67.1, 66.6, 46.8 ppm; IR (neat) ν_{\max} : 3438, 2982, 1730, 1603, 1452, 1263, 1109, 1070, 1027 cm⁻¹; ESI-HRMS: *m/z* [M+Na]⁺ calcd. for C₄₂H₃₄O₁₁ Na: 737.1993 found 737.2000.

2,3,4-O-Tri-benzoyl-6-O-(9-fluorenylmethoxycarbonyl)- α -D-mannopyranosyl trichloroacetimidate (2.18)

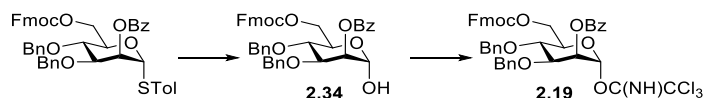


To a stirred solution of **2.30** (1.00 g, 1.40 mmol, 1.00 equiv.) and trichloroacetonitrile (2.81 mL, 28.0 mmol, 20.00 equiv.) in anhydr. DCM (13 mL), NaH (60% dispersion in oil, 16.8 mg, 0.70 mmol, 0.50 equiv.)

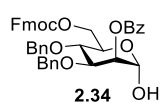
was added at room temperature under argon atmosphere and the reaction left to react overnight. Upon completion, solvent (in presence of silica to quench the remaining NaH) was evaporated and the residue was purified by flash column chromatography using a mixture of hexane/ethyl acetate (3:1) to afford the desired compound as a white solid in 97% yield (1.17 g, 1.37 mmol). ¹H NMR (400 MHz, CDCl₃): δ = 8.87 (s, 1H, =NH), 8.17 – 8.12 (m, 2H, -Ar), 8.01 – 7.96 (m, 2H, -Ar), 7.86 – 7.80 (m, 2H, -Ar), 7.79 – 7.74 (m, 2H, -Ar), 7.63 – 7.36 (m, 11H, -Ar), 7.30 – 7.27 (m, 4H, -Ar), 6.59 (d, *J* = 2.0 Hz, 1H, *H*-1), 6.09 (t, *J* = 10.0 Hz, 1H, *H*-4), 5.97 (dd, *J* = 10.0, 3.3 Hz, 1H, *H*-3), 5.93 (dd, *J* = 3.3, 2.0 Hz, 1H, *H*-2), 4.58 (dt, *J* = 10.0, 3.9 Hz, 1H, *H*-5), 4.51 – 4.39 (m, 3H, *H*-6a, -CH₂-CH-, Fmoc), 4.35 (dd, *J* = 10.4, 7.4 Hz, 1H, *H*-6b), 4.24 (t, *J* = 7.4 Hz, 1H, -CH₂-CH-, Fmoc) ppm; ¹³C NMR (101 MHz, CDCl₃): δ = 165.5, 165.3, 159.9, 155.0, 143.5, 143.3, 141.3, 141.3, 133.9, 133.8, 133.5,

130.1, 130.0, 129.8, 128.9, 128.8, 128.8, 128.8, 128.7, 128.6, 128.6, 128.5, 128.0, 128.0, 127.3, 127.3, 125.5, 125.3, 120.1, 120.1, 94.5, 90.6, 71.4, 70.4, 69.7, 68.8, 66.3, 66.0, 46.7 ppm; IR (neat) ν_{max} : 3372, 2256, 1733, 1694, 1603, 1452, 1260, 1093, 1070 cm^{-1} ; ESI-HRMS: m/z $[M+Na]^+$ calcd. for $C_{44}H_{34}Cl_3NO_{11}Na$: 880.1090 found 880.1144.

Synthesis of 2-O-benzoyl-3,4-di-O-benzyl-6-O-(9-fluorenylmethoxycarbonyl)- α -D-mannopyranosyl trichloroacetimidate (2.19)

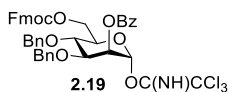


2-O-Benzoyl-3,4-di-O-benzyl-6-O-(9-fluorenylmethoxycarbonyl)- α -D-mannopyranoside (2.34)



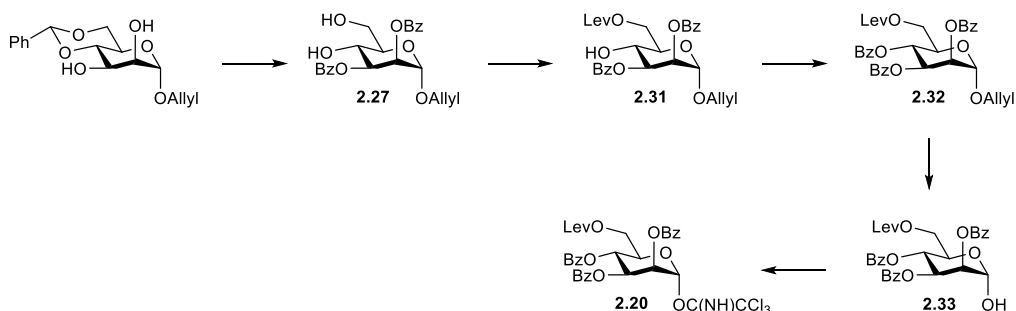
N-Bromosuccinimide (NBS) (1.60 g, 8.99 mmol, 2.00 equiv.) was added to a stirred solution of 2-O-benzoyl-3,4-di-O-benzyl-6-O-(9-fluorenylmethoxycarbonyl)- α -D-mannopyranosyl thioglycoside (4.41 g, 16.1 mmol, 1.00 equiv.) in acetone/water (9:1, 40 mL). The reaction was stirred overnight at rt. Additional amount of NBS (2.00 g, 11.2 mmol, 2.50 equiv.) was added. After 1 h, the reaction mixture was diluted with water (50 mL) and extracted with DCM (50 mL) three times. The combined organic phase was washed with NaHCO_3 solution (100 mL), dried over Na_2SO_4 and concentrated under reduced pressure. The crude compound was purified by flash column chromatography using a mixture of hexane/ethyl acetate (3:1) to afford the desired compound as a white foam in 88% yield (2.68 g, 3.90 mmol). ^1H NMR (400 MHz, CDCl_3): δ = 8.13 – 7.27 (m, 23H, -Ar), 5.67 (dd, J = 3.1, 2.0 Hz, 1H, H -2), 5.38 (dd, J = 3.9, 1.9 Hz, 1H, H -1), 4.94 (d, J = 10.9 Hz, 1H, -CHH-, Bn), 4.82 (d, J = 11.3 Hz, 1H, -C HH-, Bn), 4.65 – 4.56 (m, 2H, -CHH-, Bn, -CHH-, -Bn), 4.52 (dd, J = 11.5, 2.2 Hz, 1H, H -6a), 4.45 – 4.36 (m, 3H, - CH_2 -CH- Fmoc, H -6b), 4.26 (t, J = 7.4 Hz, 1H, -CH-, Fmoc), 4.20 (ddt, J = 10.3, 7.1, 2.6 Hz, 2H, H -3, H -4), 3.95 (t, J = 9.6 Hz, 1H, H -5), 3.14 (brs, 1H, -OH) ppm; ^{13}C NMR (101 MHz, CDCl_3): δ = 165.6, 155.2, 143.4, 143.3, 141.2, 137.9, 137.7, 133.3, 129.9, 129.7, 128.5, 128.4, 128.4, 128.2, 128.1, 127.9, 127.8, 127.7, 127.2, 125.2, 125.2, 120.1, 92.6, 75.2, 73.8, 71.5, 70.0, 69.9, 68.9, 67.0, 46.7 ppm; IR (neat) ν_{max} : 2932, 1750, 1726, 1452, 1257, 1099 cm^{-1} ; ESI-HRMS: m/z $[M+Na]^+$ calcd. for $C_{42}H_{38}O_9Na$: 709.2407 found 709.2425.

2-O-Benzoyl-3,4-di-O-benzyl-6-O-(9-fluorenylmethoxycarbonyl)- α -D-mannopyranosyl trichloroacetimidate (2.19)

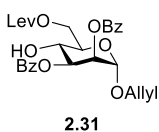


To a stirred solution of **2.34** (2.68 g, 3.90 mmol, 1.00 equiv.) in DCM (40 mL), trichloroacetonitrile (3.91 mL, 39.0 mmol, 10.00 equiv.) was added and NaH (60% dispersion in oil) (47.0 mg, 1.20 mmol, 0.30 equiv.) were added. After 4 h, additional amount of NaH (10.0 mg, 0.25 mmol, 0.06 equiv.) was added. Upon completion, the solvent was evaporated (in presence of silica to quench the remaining NaH) and the residue was purified by flash column chromatography using a mixture of hexane/ethyl acetate (3:1) to afford the desired compound as a white foam in 81% yield (2.64 g, 3.18 mmol). ^1H NMR (400 MHz, CDCl_3): δ = 8.73 (s, 1H, =NH), 8.21 – 7.20 (m, 23H, -Ar), 6.41 (d, J = 2.1 Hz, 1H, H -1), 5.78 (t, J = 2.2 Hz, 1H, H -2), 4.95 (d, J = 10.8 Hz, 1H, -CHH-, Bn), 4.85 (d, J = 11.3 Hz, 1H, -CHH- Bn), 4.66 (d, J = 3.4 Hz, 1H, -CHH-, Bn), 4.63 (d, J = 4.0 Hz, 1H, -CHH-, Bn), 4.54 – 4.41 (m, 2H, H -6a, H -6b), 4.38 (dd, J = 7.7, 1.5 Hz, 2H, - CH_2 -CH-, Fmoc), 4.26 (t, J = 7.5 Hz, 1H, -CH- Fmoc), 4.19 (m, 1H, H -3), 4.12 (m, 2H, H -4, H -5) ppm; ^{13}C NMR (101 MHz, CDCl_3): δ = 165.4, 160.0, 155.1, 155.0, 143.5, 143.4, 141.3, 137.7, 137.4, 133.6, 130.1, 129.5, 128.8, 128.7, 128.6, 128.6, 128.6, 128.5, 128.1, 128.0, 127.3, 127.3, 125.3, 125.3, 120.2, 120.2, 120.1, 95.1, 95.1, 90.7, 75.6, 73.1, 73.0, 72.5, 72.4, 71.9, 70.2, 67.4, 66.2, 46.8 ppm; IR (neat) ν_{max} : 3333, 2930, 1729, 1676, 1452, 3334, 3033, 1750, 1729, 1677, 1452, 1261, 1164, 1094 cm^{-1} ; ESI-HRMS: m/z $[\text{M}+\text{Na}]^+$ calcd. for $\text{C}_{44}\text{H}_{38}\text{Cl}_3\text{NO}_9\text{Na}$: 852.1504, found 852.1543.

Synthesis of 2,3,4-O-tri-benzoyl-6-O-levulinoyl- α -D-mannopyranosyl trichloroacetimidate (2.20)



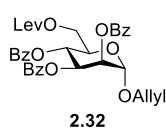
Allyl 2,3-di-O-benzoyl-6-O-levulinoyl- α -D-mannopyranoside (2.31)



2.27 (5.40 g, 12.6 mmol, 1.00 equiv) was dissolved in DCM (90 mL), levulinic acid (2.19 g, 18.9 mmol, 1.50 equiv.) and 2-chloro-1-methylpyridinium iodide (8.05 g, 31.5 mmol, 2.50 equiv.) were added. The reaction was stirred for 15

min and then cooled to -15 °C. At this temperature 1,4-diazabicyclo[2.2.2]octane (DABCO) (4.95 g, 44.1 mmol, 3.50 equiv) was added. The reaction mixture was stirred for 40 min, filtered over a plug of Celite[®] and concentrated. The crude product was purified by flash column chromatography using a mixture of hexane/ethyl acetate (4:1) as eluent. The product was obtained as a white solid in 67% yield (4.41 g, 8.38 mmol). ¹H NMR (400 MHz, CDCl₃): δ = 8.12 – 8.06 (m, 2H, -Ar), 7.95 – 7.90 (m, 2H, -Ar), 7.64 – 7.57 (m, 1H, -Ar), 7.54 – 7.44 (m, 2H, -Ar), 7.37 – 7.31 (m, 2H, -Ar), 5.94 (m, 1H, CH₂=CH-, Allyl), 5.64 – 5.56 (m, 2H, H-2, H-3), 5.36 (dd, *J* = 17.2, 1.6 Hz, 1H, CHH=CH-, Allyl), 5.26 (dd, *J* = 10.4, 1.3 Hz, 1H, CHH=CH-, Allyl), 5.06 (d, *J* = 1.6 Hz, 1H, H-1), 4.63 (dd, *J* = 12.1, 4.3 Hz, 1H, H-6a), 4.39 (dd, *J* = 12.1, 2.3 Hz, 1H, H-6b), 4.30 – 4.24 (m, 1H, -OCHH-CH=CH₂, Allyl), 4.20 (d, *J* = 9.6 Hz, 1H, H-4), 4.09 (m, 1H, -OCHH-CH=CH₂, Allyl), 4.02 (ddd, *J* = 9.8, 4.3, 2.3 Hz, 1H, H-5), 2.87 – 2.54 (m, 4H, -CH₂-CH₂-, Lev), 2.18 (s, 3H, -CO-CH₃, Lev) ppm; ¹³C NMR (101 MHz, CDCl₃): δ = 206.7, 173.3, 166.7, 165.5, 133.6, 133.4, 133.3, 133.2, 130.0, 129.9, 129.7, 129.6, 129.4, 128.6, 128.4, 118.4, 96.8, 72.6, 71.1, 70.7, 68.7, 66.4, 63.5, 38.0, 29.9, 27.9 ppm; ESI-LRMS: *m/z* [M+Na]⁺ calcd. for C₂₈H₃₀O₁₀Na: 549.1 found 549.0.

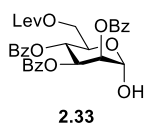
Allyl 2,3,4-tri-*O*-benzoyl-6-*O*-levulinoyl- α -D-mannopyranoside (2.32)



2.31 (4.41 g, 3.38 mmol, 1.00 equiv.) was dissolved in pyridine (50 mL) and the solution was cooled to 0 °C. BzCl (2.92 mL, 25.1 mmol, 3.00 equiv.) was added dropwise to the solution and the mixture was left for 3 h at rt. Then, the mixture was concentrated under vacuum to remove pyridine. The residue was diluted and extracted with ethyl acetate (50 mL), washed with water (50 mL), NaHCO₃ solution (50 mL), and NaCl solution. The combined organic layers were dried over Na₂SO₄ and concentrated under reduced pressure. The crude product was purified by flash column chromatography using a mixture of hexane/ethyl acetate (4:1) as eluent. The product was obtained as a white solid in 99% yield (5.23 g, 8.29 mmol). ¹H NMR (400 MHz, CDCl₃): δ = 8.15 – 8.05 (m, 2H, -Ar), 7.99 – 7.92 (m, 2H, -Ar), 7.86 – 7.79 (m, 2H, -Ar), 7.67 – 7.57 (m, 1H, -Ar), 7.56 – 7.34 (m, 6H, -Ar), 7.29 – 7.23 (m, 1H, -Ar), 6.07 – 5.87 (m, 1H, -CH₂=CH-), 5.72 – 5.66 (m, 1H, H-3), 5.46 – 5.36 (m, 1H, CHH=CH-, -Allyl), 5.35 – 5.27 (m, 1H, CHH=CH-, -Allyl), 5.14 (d, *J* = 1.8 Hz, 1H, H-1), 4.41 – 4.27 (m, 4H, H-5, H-6a, H-6b, -CHH-CH=, Allyl), 4.16 (m, 1H, -CHH-CH=, Allyl), 2.84 – 2.60 (m, 4H, -CH₂-CH₂-, Lev), 2.16 (s, 3H, -CO-CH₃, Lev) ppm; ¹³C NMR (101 MHz, CDCl₃): δ = 206.4, 172.5, 165.6, 165.5, 133.7, 133.7, 133.6, 133.3, 133.1, 130.3, 130.0, 129.9, 129.8, 129.4, 129.2, 129.0, 128.7, 128.6, 128.5, 128.4, 118.6, 96.7, 70.6, 70.0, 69.0, 68.9, 67.1, 63.1, 38.0, 29.9, 27.9 ppm; IR (neat) ν_{max} : 1726, 1603,

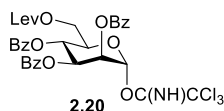
1452, 1418, 1278, 1261, 1178, 1096 cm^{-1} ; ESI-HRMS: m/z $[\text{M}+\text{Na}]^+$ calcd. for $\text{C}_{35}\text{H}_{34}\text{O}_{11}\text{Na}$: 653.1993 found 653.1998.

2,3,4-Tri-O-benzoyl-6-O-levulinoyl- α -D-mannopyranoside (2.33)



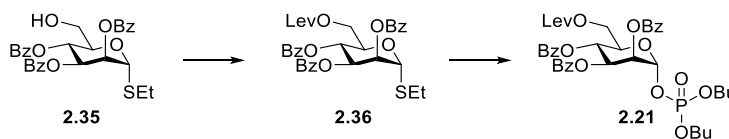
To a mixture of **2.32** (2.01 g, 3.19 mmol, 1.00 equiv.) and PdCl_2 (0.28 mg, 1.59 mmol, 0.50 equiv.) in MeOH/DCM (1:1, 17 mL) was stirred for 4 h at rt. The reaction mixture was filtered through Celite[®] and concentrated under vacuum. The residue was purified by flash column chromatography using a mixture of hexane/ethylacetate (1:1) as eluent. The product was obtained as a white solid in 74% yield (1.38 g, 2.35 mmol). ^1H NMR (400 MHz, CDCl_3): δ = 8.13 – 7.35 (m, 15H, -Ar), 5.98 (dd, J = 10.0, 3.3 Hz, 1H, H -3), 5.87 – 5.80 (m, 1H, H -4), 5.72 (dd, J = 3.4, 1.8 Hz, 1H, H -2), 5.50 (d, J = 1.9 Hz, 1H, H -1), 4.58 (m, 1H, H -5), 4.42 (dd, J = 11.9, 2.5 Hz, 1H, H -6a), 4.28 (dd, J = 11.9, 6.7 Hz, 1H, H -6b), 3.98 (s, 1H, -OH), 2.85 – 2.72 (m, 2H, $-\text{CH}_2-$, Lev), 2.60 (m, 2H, $-\text{CH}_2-$, Lev), 2.19 (s, 3H, $-\text{CO}-\text{CH}_3$, Lev) ppm; ^{13}C NMR (101 MHz, CDCl_3): δ = 207.9, 172.4, 165.8, 165.6, 165.5, 133.8, 133.7, 133.6, 133.3, 133.3, 130.1, 130.0, 129.9, 129.9, 129.8, 129.4, 129.2, 129.0, 128.8, 128.7, 128.7, 128.6, 128.6, 128.4, 128.4, 128.4, 92.5, 70.9, 69.7, 68.4, 67.5, 63.3, 38.4, 30.02, 28.19 ppm; IR (neat) ν_{max} : 3436, 1727, 1452, 1264, 1111, 1070 cm^{-1} ; ESI-HRMS: m/z $[\text{M}+\text{Na}]^+$ calcd. for $\text{C}_{32}\text{H}_{30}\text{O}_{11}\text{Na}$: 613.1680 found 613.1766.

2,3,4-O-Tri-benzoyl-6-O-levulinoyl- α -D-mannopyranosyl trichloroacetimidate (2.20)



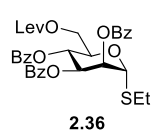
2.33 (100 mg, 0.17 mmol, 1.00 equiv) was dissolved in 2 mL of anhydrous DCM under argon atmosphere and trichloroacetonitrile (0.17 mL, 1.70 mmol, 10.0 equiv.) and DBU (10 μL , 0.04 mmol, 0.25 equiv.) were added consecutively. The solution was stirred for 2 h at room temperature. The solvent was removed under reduced pressure. The crude mixture was purified by flash chromatography using hexane/ethyl acetate (3:1) as eluent. The product was obtained as yellowish foam in 43% yield (54 mg, 0.07 mmol). ^1H NMR (400 MHz, CDCl_3): δ = 8.88 (s, 1H, =NH), 8.15 – 7.27 (m, 15H, -Ar), 6.58 – 6.53 (m, 1H, H -1), 6.04 (t, J = 10.0 Hz, 1H, H -4), 5.97 – 5.87 (m, 2H, H -2, H -3), 4.50 (m, 1H, H -5), 4.36 (d, J = 3.7 Hz, 2H, H -6a, H -6b), 2.84 – 2.71 (m, 2H, $-\text{CH}_2-$, Lev), 2.68 – 2.58 (m, 2H, $-\text{CH}_2-$, Lev), 2.16 (s, 3H, $-\text{CO}-\text{CH}_3$, Lev) ppm; ^{13}C NMR (101 MHz, CDCl_3): δ = 206.4, 172.4, 165.5, 165.2, 160.0, 134.0, 133.7, 133.5, 130.1, 130.0, 129.8, 128.8, 128.6, 128.5, 94.6, 90.7, 71.4, 69.7, 68.8, 66.2, 62.6, 38.0, 29.9, 27.9 ppm; IR (neat) ν_{max} : 3007, 2920, 1710, 1421, 1360, 1221, 1039 cm^{-1} ; ESI-HRMS: m/z $[\text{M}+\text{Na}]^+$ calcd. for $\text{C}_{34}\text{H}_{30}\text{Cl}_3\text{NO}_{11}\text{Na}$: 756.0776 found 756.1059.

Synthesis of dibutoxyphosphoryloxy 2,3,4-O-tri-benzoyl-6-O-levulinoyl- α -D-mannopyranosyl phosphate (2.21)



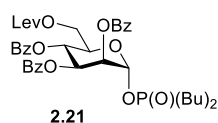
Ethyl 2,3,4-tri-O-benzoyl-1-thio- α -D-mannosylpyranoside **2.35** was synthesized as reported in the literature^[204]

Ethyl 2,3,4-tri-O-benzoyl-6-O-Levulinoyl-1-thio- α -D-mannosylpyranoside (2.36)



2.35 (0.44 g, 0.82 mmol, 1.00 equiv.) was dissolved in 22 mL of anhydr. DCM under argon atmosphere and cooled down to 0 °C. *N,N*-diisopropylcarbodiimide (DIC) (0.24 mL, 1.56 mmol, 1.90 equiv.), 4-(dimethylamino)pyridine (DMAP) (0.11 g, 0.90 mmol, 1.10 equiv.) and levulinic acid (0.13 g, 1.15 mmol, 1.40 equiv.), were added and the reaction was protected with aluminum foil from the light. The mixture was allowed to warm slowly overnight to room temperature. The reaction was quenched by adding NaHCO₃ solution (50 mL). The aqueous phase washed with ethyl acetate (2 × 50 mL) and the combined organic layer dried over MgSO₄ and the solvent was removed under reduced pressure. The crude product was purified by flash chromatography using a mixture of hexane/ethyl acetate (2:1) as eluent. The product was obtained as a white foam in 93% yield (0.49 g, 0.77 mmol). ¹H NMR (400 MHz, CDCl₃): δ = 8.10 – 7.32 (m, 14H, -Ar), 7.25 – 7.22 (m, 1H, -Ar), 5.98 (d, *J* = 3.2 Hz, 1H, *H*-2), 5.80 (t, *J* = 10.0 Hz, 1H, *H*-4), 5.62 (dd, *J* = 10.1, 3.4 Hz, 1H, *H*-3), 5.07 (d, *J* = 1.1 Hz, 1H, *H*-1), 4.43 – 4.30 (m, 2H, *H*-6a, *H*-6b), 4.04 (ddd, *J* = 9.4, 5.5, 3.4 Hz, 1H, *H*-5), 2.87 – 2.70 (m, 4H, -CH₂-, Lev, -CH₂-CH₃, SEt), 2.58 (m, 2H, -CH₂-, Lev), 2.17 (s, 3H, -CO-CH₃, Lev), 1.34 (t, *J* = 7.4 Hz, 3H, -CH₂-CH₃, SEt) ppm; ¹³C NMR (101 MHz, CDCl₃): δ = 206.5, 172.5, 130.2, 129.9, 129.3, 128.9, 128.7, 128.6, 128.4, 83.0, 76.6, 72.7, 71.4, 67.1, 63.6, 38.0, 29.9, 27.9, 26.0, 15.1 ppm; ESI-LRMS: *m/z* [M+Na]⁺ calcd. for C₃₄H₃₄O₁₁SNa: 673.1 found 673.0.

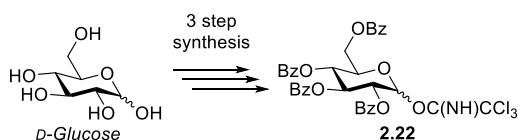
Dibutoxyphosphoryloxy 2,3,4-tri-O-benzoyl-6-O-levulinoyl- α -D-mannopyranosyl phosphate (2.21)



Dibutyl hydrogen phosphate (0.17 mL, 0.87 mmol, 2.00 equiv.) was added to a round-bottom flask containing activated 4Å molecular sieves anhydrous DCM (5.00 mL) and left stirring for 1.5 h. The molecular sieves were allowed to settle and the supernatant (5.00 mL) was added to a solution of the donor

2.36 (275 mg, 0.43 mmol, 1.00 equiv.) in anhydrous DCM (3.00 mL). The mixture was cooled down to 0 °C, and *N*-iodosuccinimide (NIS) (120 mg, 0.42 mmol, 1.23 equiv.) and triflic acid (10.0 μ L, 0.13 mmol, 0.30 equiv.) were added. The reaction was stirred for 1h and then quenched with NaHCO₃ (1.00 mL). The organic layer was washed with Na₂S₂O₃ (5.00 mL) and water (5.00 mL), dried with Na₂SO₄, filtered and the solvent was removed under reduced pressure. The crude product was purified by flash column chromatography using a mixture of hexane/ethyl acetate (2:1.5). The product was obtained as a yellow/orange oil in 79% yield (266 mg, 0.34 mmol). ¹H NMR (400 MHz, CDCl₃): δ = 8.12 – 7.28 (m, 15H, -Ar), 5.99 (t, *J* = 10.1 Hz, 1H, *H*-4), 5.92 – 5.85 (m, 2H, *H*-1, *H*-2), 5.75 (t, *J* = 2.6 Hz, 1H, *H*-3), 4.52 (dt, *J* = 10.0, 3.4 Hz, 1H, *H*-5), 4.37 (dd, *J* = 12.3, 4.2 Hz, 1H, *H*-6a), 4.30 (dd, *J* = 12.3, 2.8 Hz, 1H, *H*-6b), 4.20 (m, 4H, 2-OCH₂-, Bu), 2.83 – 2.68 (m, 2H, -CH₂-, Lev), 2.64 (m, 2H, -CH₂-, Lev), 2.16 (s, 3H, -CO-CH₃, Lev), 1.75 (p, *J* = 6.8 Hz, 4H, -CH₂-, Bu), 1.47 (h, *J* = 7.4 Hz, 4H, -CH₂-, Bu), 0.97 (t, *J* = 7.4 Hz, 6H, 2-CH₃, Bu) ppm; ¹³C NMR (101 MHz, CDCl₃) δ 206.3, 172.3, 165.3, 165.0, 133.8, 133.6, 133.3, 129.9, 129.8, 129.7, 128.9, 128.8, 128.7, 128.5, 128.3, 94.8, 70.3, 69.7, 69.6, 69.1, 68.4, 68.4, 68.3, 68.3, 66.0, 62.4, 37.8, 32.3, 32.3, 32.2, 32.2, 29.8, 27.7, 18.6, 13.6 ppm; IR (neat) ν_{\max} : 1733, 1453, 1262, 1095, 1027 cm⁻¹; ESI-HRMS: *m/z* [M+Na]⁺ calcd. for C₄₀H₄₇O₁₄PNa: 805.2595 found 805.2606.

Synthesis of 2,3,4,6-tetra-*O*-benzoyl-*D*-glucopyranosyl trichloroacetimidate (**2.22**)



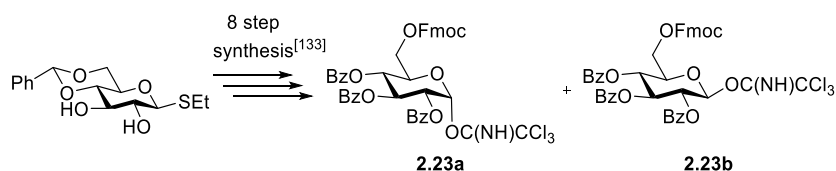
2.22 was prepared according to previously established procedures. ^[218]

Perbenzoylated *D*-glucose (1.71 g, 2.44 mmol, 1.00 equiv.) was dissolved in 22 mL of anhydr. DMF under inert atmosphere and hydrazine acetate (247 mg, 2.68 mmol, 1.10 equiv.) was added. The solution was stirred for 1h at room temperature, after which the solution was diluted with DCM and then washed with NaHCO₃ solution (50 mL). The aqueous phase was washed with DCM (2 × 40 mL). The organic layers were combined, dried over MgSO₄ and the solvent was removed under reduced pressure. The crude product was re-dissolved in 32 mL of anhydr. DCM under argon atmosphere and trichloroacetonitrile (2.50 mL, 24.4 mmol, 10.0 equiv.) and DBU (90 μ L, 0.61 mmol, 0.25 equiv.) were added consecutively. The solution was stirred for 2h at room temperature. The solvent was removed under reduced pressure. The crude product was purified by flash column chromatography using a mixture of hexane/ethyl acetate (3:1) as eluent. The product was obtained as yellow

solid in 59% yield (1.06 g, 1.43 mmol). ^1H NMR (400 MHz, CDCl_3): δ = 8.63 (s, 1H, $\text{C}(\text{NH})\text{CCl}_3$), 8.06 – 8.01 (m, 2H, -Ar), 7.95 (m, 4H, -Ar), 7.89 – 7.85 (m, 2H, -Ar), 7.59 – 7.28 (m, 12H, -Ar), 6.83 (d, J = 3.7 Hz, 1H, H -1), 6.27 (t, J = 10.0 Hz, 1H; H -3), 5.82 (t, J = 9.9 Hz, 1H; H -4), 5.62 (dd, J = 10.2, 3.7 Hz, 1H; H -2), 4.69 – 4.59 (m, 2H; H -6a, H -5), 4.52 – 4.44 (m, 1H, H -6b) ppm; ^{13}C NMR (101 MHz, CDCl_3): δ = 166.2, 165.7, 165.5, 165.3, 160.6, 133.7, 133.4, 133.3, 130.0, 129.9, 129.8, 129.6, 128.9, 128.7, 128.6, 128.5, 128.5, 128.5, 93.2, 90.8, 70.8, 70.2, 68.7, 62.5 ppm.

* The analytical data agree with the literature.^[218]

Synthesis of 2,3,4-tri-*O*-benzoyl-6-*O*-(9-fluorenylmethoxycarbonyl)-*D*-glucopyranosyl trichloroacetimidate (**2.23**)



2.23a and **2.23b** were prepared according to previously established procedures.^[103]

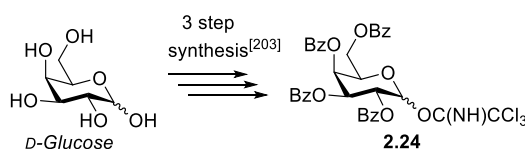
To a stirred solution of 2,3,4-tri-*O*-benzoyl-6-*O*-(9-fluorenylmethoxycarbonyl)-*D*-galactose (850 mg, 1.19 mmol, 1.00 equiv.) in anhydr. DCM, trichloroacetonitrile (2.38 mL, 23.8 mmol, 20.0 equiv.) and NaH (60% dispersion in oil, 14.3 mg, 0.60 mmol, 0.50 equiv.) were added at room temperature under argon atmosphere and the reaction was left to react overnight. Upon completion, the solvent was evaporated (in presence of silica to quench the remaining NaH) and the residue was purified by flash column chromatography using a mixture of hexane/ethyl acetate (3:1) to afford the desired α -anomer as a white foam in 55% yield (556 mg, 0.65 mmol) and the β -anomer as a yellowish foam in 20% yield (203 mg, 0.24 mmol).

Assignments for β -anomer **2.23b** (20%): ^1H NMR (400 MHz, CDCl_3): δ = 8.70 (s, 1H, $\text{C}(\text{NH})\text{CCl}_3$), 7.99 – 7.29 (m, 23H, -Ar), 6.23 (d, J = 7.7 Hz, 1H, H -1), 5.97 (dd, J = 9.1 Hz, 1H, H -3), 5.86 – 5.72 (m, 2H, H -2, H -4), 4.48 (t, J = 4.3 Hz, 2H, H -6a, H -6b), 4.40 – 4.29 (m, 3H H -5, - CH_2 - Fmoc), 4.24 (t, J = 7.5 Hz, 1H, - CH - Fmoc) ppm; ^{13}C -NMR (101 MHz, CDCl_3): δ = 165.6, 165.1, 164.8, 160.9, 154.7, 143.4, 143.2, 141.2, 141.2, 133.6, 133.4, 129.9, 129.8, 129.8, 128.9, 128.6, 128.5, 128.4, 128.4, 127.9, 127.2, 125.3, 125.3, 120.0, 95.7, 90.2, 72.9, 72.5, 70.6, 70.3, 68.8, 65.8, 46.64 ppm.

Assignments for α -anomer **2.23a** (55%): ^1H NMR (400 MHz, CDCl_3): δ = 8.57 (s, 1H, $\text{C}(\text{NH})\text{CCl}_3$), 7.94 – 7.22 (m, 23H, -Ar), 6.78 (d, J = 3.6 Hz, 1H, H -1), 6.27 (t, J = 9.9 Hz, 1H, H -3), 5.77 (t, J = 10.0 Hz, 1H, H -4), 5.56 (dd, J = 10.2, 3.7 Hz, 1H, H -2), 4.50 (dt, J = 10.2, 3.8 Hz, 1H, H -5), 4.39 – 4.16 (m, 6H, H -6a, H -6b, $-\text{CH}_2-$ Fmoc, $-\text{CH}-$ Fmoc), 4.27 – 4.17 (m, 2H) ppm; ^{13}C -NMR (101 MHz, CDCl_3): δ = 165.6, 165.4, 165.2, 160.5, 154.8, 143.4, 143.2, 141.2, 141.2, 133.6, 133.6, 133.3, 129.9, 129.9, 129.7, 128.8, 128.5, 128.4, 128.4, 127.9, 127.2, 125.4, 125.3, 120.0, 93.0, 90.6, 70.5, 70.4, 70.3, 70.0, 69.3, 68.4, 65.4, 46.6 ppm; ESI-LRMS: m/z $[\text{M}+\text{Na}]^+$ calcd. for $\text{C}_{44}\text{H}_{34}\text{Cl}_3\text{NO}_{11}\text{Na}$: 880.1 found 880.0.

The analytical data agree with the literature.^[103]

Synthesis of 2,3,4,6-tetra-*O*-benzoyl-D-galactopyranosyl trichloroacetimidate (**2.24**)



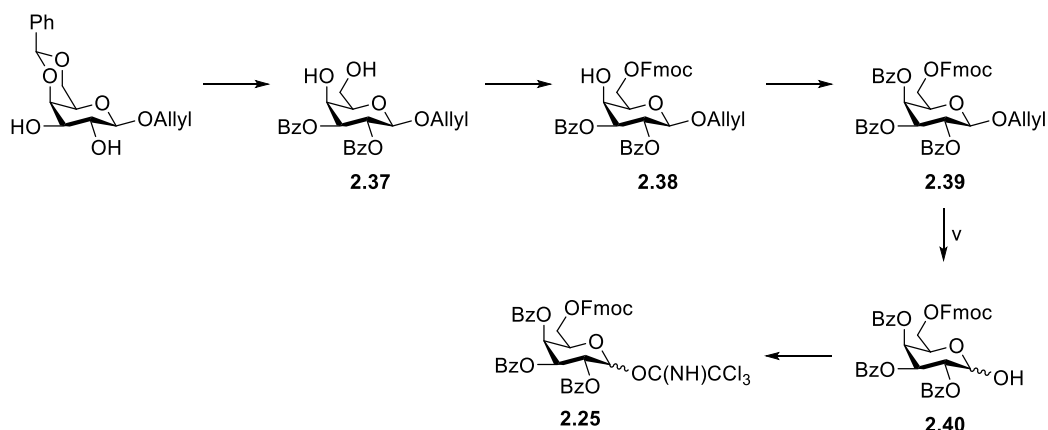
2.24 was prepared according to previously established procedures.^[217]

Perbenzoylated D-galactose (1.90 g, 2.70 mmol, 1.00 equiv.) was dissolved in 24 mL of anhydr. DMF under inert atmosphere and hydrazine acetate (274 mg, 2.97 mmol, 1.10 equiv.) was added. The solution was stirred for 1h at room temperature, after which the solution was diluted with DCM and then washed with NaHCO_3 solution (50 mL). The aqua phase was washed with DCM (2×40 mL). The organic layers were combined, dried over MgSO_4 and the solvent was removed under reduced pressure. The crude product was redissolved in 35 mL of anhydr. DCM under argon atmosphere and trichloroacetonitrile (2.71 mL, 27.0 mmol, 10.0 equiv.) and DBU (100 μL , 0.68 mmol, 0.25 equiv.) were added consecutively. The solution was stirred for 2 h at room temperature. The solvent was removed under reduced pressure. The crude product was purified by flash column chromatography using a mixture of hexane/ethyl acetate (3:1.5) as eluent. The product was obtained as white solid in 75% yield (1.50 g, 2.02 mmol). ^1H NMR (400 MHz, CDCl_3): δ = 8.63 (s, 1H, $\text{C}(\text{NH})\text{CCl}_3$), 8.13 – 8.05 (m, 2H, -Ar), 8.04 – 7.92 (m, 4H, -Ar), 7.89 – 7.75 (m, 2H, -Ar), 7.68 – 7.26 (m, 12H, -Ar), 6.91 (d, J = 3.7 Hz, 1H, H -1), 6.16 (dd, J = 3.4, 1.3 Hz, 1H, H -4), 6.08 (dd, J = 10.6, 3.3 Hz, 1H, H -3), 5.96 (dd, J = 10.7, 3.6 Hz, 1H, H -2), 4.86 (t, J = 6.4 Hz, 1H, H -5), 4.62 (dd, J = 11.4, 6.9 Hz, 1H, H -6a), 4.43 (dd, J = 11.4, 6.0 Hz, 1H, H -6b) ppm; ^{13}C -NMR (101 MHz, CDCl_3): δ = 166.0, 165.7, 165.6, 165.5, 160.7, 133.8, 133.7,

133.5, 133.4, 130.1, 129.9, 129.8, 129.4, 129.0, 128.9, 128.8, 128.7, 128.5, 128.5, 128.4, 93.8, 90.8, 69.8, 68.6, 68.4, 67.9, 62.3 ppm

* The analytical data agree with the literature.^[217]

Synthesis of 2,3,4-O-tri-benzoyl-6-O-(9-fluorenylmethoxycarbonyl)-D-galactopyranosyl trichloroacetimidate (2.25)

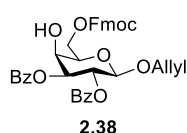


Allyl 2,3-di-O-benzoyl-β-D-galactopyranoside (2.37)

Allyl 4,6-O-benzylidene-β-D-galactopyranoside (3.00 g, 9.73 mmol, 1.00 equiv.) was dissolved in pyridine (30 mL) and the solution was cooled to 0 °C. BzCl (2.91 mL, 25.3 mmol, 2.60 equiv.) was added dropwise to the solution and left to react overnight at rt. Then, 4-dimethylaminopyridine (DMAP) (590 mg, 4.86 mmol, 0.50 equiv.) was added and the mixture was heated up to 50 °C until completion). After completion, the mixture was poured into iced water; the precipitate was filtered off and washed with water. The solid was dissolved in DCM (100 mL) and washed with water (100 mL). Then, the organic layer was washed with hydrochloric acid (1 M, 100 mL), NaHCO₃ solution (100 mL), and water (100 mL). The organic layer was dried over Na₂SO₄ and the solvent was removed under reduced pressure. The crude product was used without any further purification. TFA (4.47 mL, 58.1 mmol, 7.50 equiv.) and water (0.60 mL, 33.3 mmol, 4.30 equiv.) were added to a solution of the crude (4.00 g, 7.74 mmol, 1.00 equiv.) in DCM (105 mL). The mixture was stirred for 3 h, diluted with DCM, washed with 10% (w/v) aqueous NaHCO₃ solution until neutral pH; and 10% (w/v) aqueous NaCl solution. The organic layer was dried over Na₂SO₄, filtered, and concentrated. The residue was purified by flash column chromatography using a mixture of hexane/ethyl acetate (1:2) as eluent. The product was obtained as a white solid in 62% yield over two steps (2.04 g, 4.76 mmol). ¹H NMR (400 MHz, CDCl₃): δ = 7.98 (ddd, *J* = 8.5, 3.3, 1.4 Hz, 4H, -Ar), 7.62 –

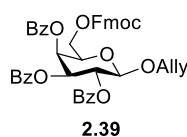
7.32 (m, 6H, -Ar), 5.86 – 5.73 (m, 2H, H-2, -CH₂-CH=CH₂ Allyl), 5.30 (dd, *J* = 10.3, 3.1 Hz, 1H, H-3), 5.25 (dd, *J* = 17.3, 1.7 Hz, 1H, -CH₂-CH=CHH Allyl), 5.13 (dd, *J* = 10.5, 1.5 Hz, 1H, -CH₂-CH=CHH Allyl), 4.77 (d, *J* = 8.0 Hz, 1H, H-1), 4.38 (m, 2H, H-4, -CHH-CH=CH₂ Allyl), 4.18 (m, 1H, -CHH-CH=CH₂ Allyl), 4.14 – 4.02 (m, 1H, H-6a), 3.95 (dd, *J* = 11.8, 4.4 Hz, 1H, H-6b), 3.78 (m, 1H, H-5); ¹³C NMR (101 MHz, CDCl₃): δ = 166.0, 165.5, 133.7, 133.6, 133.2, 130.0, 129.8, 129.6, 129.1, 128.6, 128.4, 117.8, 100.5, 74.4, 74.2, 70.2, 69.6, 68.6, 62.8 ppm; IR (neat) *v*_{max}: 3478, 1723, 1603, 1452, 1316, 1279, 1179, 1111, 1071, 1029 cm⁻¹; ESI-HRMS: *m/z* [M+Na]⁺ calcd. for C₂₃H₂₄O₈Na: 451.1363 found 451.1360.

Allyl 2,3-di-O-benzoyl-6-O-(9-fluorenylmethoxycarbonyl)-β-D-galactopyranoside (2.38)



To a stirred suspension of **2.37** (1.30 g, 2.94 mmol, 1.00 equiv.) in anhydr. DCM (51 mL), pyridine (1.18 mL, 14.7 mmol, 5.00 equiv.) was added and the solution was stirred for 15 min at room temperature. Then, the mixture was cooled to 0 °C and FmocCl (910 mg, 3.52 mmol, 1.20 equiv.) was added. After complete conversion (2 h), the solvent was removed and the residue was purified by flash column chromatography using a mixture of hexane/ethyl acetate (4:1 and 1% toluene) to yield the titled compound as a yellowish solid in 50% yield (962 mg, 1.48 mmol). ¹H NMR (400 MHz, CDCl₃): δ = 7.99 (m, 4H, -Ar), 7.78 (ddt, *J* = 7.6, 2.1, 0.9 Hz, 2H, -Ar), 7.62 (ddt, *J* = 7.6, 1.8, 0.9 Hz, 2H, -Ar), 7.56 – 7.44 (m, 2H, -Ar), 7.43 – 7.30 (m, 8H, -Ar), 5.86 – 5.72 (m, 2H, -CH₂-CH=CH₂ Allyl, H-2), 5.33 (dd, *J* = 10.3, 3.2 Hz, 1H, H-3), 5.24 (dd, *J* = 17.3, 1.7 Hz, 1H, -CH₂-CH=CHH Allyl), 5.13 (dd, *J* = 10.4, 1.4 Hz, 1H, -CH₂-CH=CHH Allyl), 4.75 (d, *J* = 7.9 Hz, 1H, H-1), 4.53 – 4.42 (m, 4H, H-6a, H-6b, -CH₂-CH- Fmoc), 4.37 (ddt, *J* = 13.2, 4.9, 1.6 Hz, 1H, -CHH-CH=CH₂ Allyl), 4.33 – 4.23 (m, 2H, H-4, H-5), 4.17 (ddt, *J* = 13.2, 6.3, 1.4 Hz, 1H, -CHH-CH=CH₂), 3.96 (t, *J* = 6.3 Hz, 1H, -CH- Fmoc), 2.32 (s, 1H, -OH) ppm; ¹³C NMR (101 MHz, CDCl₃): δ = 165.8, 165.3, 155.0, 143.2, 143.2, 141.3, 133.6, 133.4, 133.2, 129.9, 129.7, 129.4, 128.9, 128.5, 128.3, 127.9, 127.2, 125.1, 125.1, 120.1, 117.8, 100.0, 74.0, 72.0, 70.1, 69.9, 69.4, 67.2, 65.7, 46.7 ppm; IR (neat) *v*_{max}: 2354, 1728, 1451, 1263, 1110 cm⁻¹; ESI-HRMS: *m/z* [M+Na]⁺ calcd. for C₃₈H₃₄O₁₀Na: 673.2044 found 673.2068

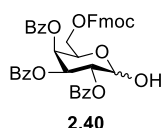
Allyl 2,3,4-tri-O-benzoyl-6-O-(9-fluorenylmethoxycarbonyl)-β-D-galactopyranoside (2.39)



2.38 (960 mg, 1.47 mmol, 1.00 equiv.) was dissolved in pyridine (10 mL) and the solution was cooled to 0 °C. BzCl (0.68 mL, 5.90 mmol, 4.00 equiv.) was added dropwise to the solution and the mixture was stirred for 2 h at room temperature. Then, the mixture was quenched with iced water. The precipitate was

filtered off and washed with water (50 mL). The precipitate was dissolved in DCM and washed with water (50 mL). Then, the organic layer was washed with hydrochloric acid (1 M, 50 mL), NaHCO₃ solution (50 mL), and water (50 mL). The organic layer was dried over Na₂SO₄ and the solvent was removed under reduced pressure. The crude product was purified by flash column chromatography using a mixture of hexane/ethyl acetate (3:1) as eluent. The product was obtained as a white foam in 94% yield (1.05 g, 1.39 mmol). ¹H NMR (400 MHz, CDCl₃): δ = 8.12 – 7.27 (m, 23H, -Ar), 5.92 (dd, *J* = 3.5, 1.2 Hz, 1H, *H*-4), 5.86 – 5.75 (m, 2H, -CH₂-CH=CH₂ Allyl, *H*-2), 5.57 (dd, *J* = 10.4, 3.4 Hz, 1H, *H*-3), 5.27 (dd, *J* = 17.2, 1.6 Hz, 1H, -CH₂-CH=CHH Allyl), 5.16 (dd, *J* = 10.5, 1.4 Hz, 1H, -CH₂-CH=CHH Allyl), 4.85 (d, *J* = 8.0 Hz, 1H, *H*-1), 4.47 – 4.38 (m, 4H, *H*-6a, -CH₂-CH- Fmoc, -CHH-CH=CH₂ Allyl), 4.36 (m, 1H, *H*-6b), 4.28 – 4.18 (m, 3H, -CHH-CH=CH₂ Allyl, *H*-5, -CH- Fmoc) ppm; ¹³C NMR (101 MHz, CDCl₃): δ = 165.7, 165.6, 165.3, 154.8, 143.3, 143.3, 141.4, 133.7, 133.4, 133.4, 133.4, 130.2, 129.9, 129.8, 129.4, 129.0, 128.8, 128.7, 128.6, 128.5, 128.4, 128.0, 127.3, 127.3, 125.3, 125.2, 120.2, 118.1, 100.3, 71.8, 71.4, 70.4, 70.3, 69.7, 68.2, 65.7, 46.7 ppm; IR (neat) ν_{max}: 3068, 2982, 2928, 1726, 1603, 1452, 1251, 1177, 1069, 1027 cm⁻¹; ESI-HRMS: *m/z* [M+Na]⁺ calcd. for C₄₅H₃₈O₁₁Na: 777.2306 found 777.2333.

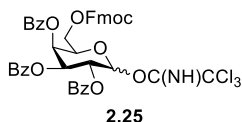
2,3,4-Tri-*O*-benzoyl-6-*O*-(9-fluorenylmethoxycarbonyl)-β-*D*-galactopyranoside (**2.40**)



A mixture of **2.39** (980 mg, 1.30 mmol, 1.00 equiv.) and PdCl₂ (115 mg, 0.65 mmol, 0.50 equiv.) in MeOH/DCM (1:1 = 7 mL) was stirred for 5 h at room temperature. The reaction mixture was filtered through Celite® and concentrated under reduced pressure. The residue was purified by flash column chromatography using a mixture of hexane/ethyl acetate (2:1) as eluent. The product was obtained as a white solid in 68% yield (635 mg, 0.89 mmol). The crude product was used without any further purification. α-anomer; ¹H NMR (400 MHz, CDCl₃): δ = 8.11 – 7.28 (m, 23H, -Ar), 6.03 (dd, *J* = 10.6, 3.4 Hz, 1H, *H*-3), 5.99 (dd, *J* = 3.5, 1.3 Hz, 1H; *H*-4), 5.84 (t, *J* = 3.6 Hz, 1H; *H*-1), 5.70 (dd, *J* = 10.7, 3.7, Hz, 1H; *H*-2), 4.76 (t, 1H; *J* = 6.0 Hz, -CH- Fmoc), 4.46 – 4.30 (m, 4H, *H*-6a, *H*-6b, -CH₂- Fmoc), 4.27 – 4.21 (m, 1H, *H*-5), 2.97 (dd, *J* = 3.7, 1.3 Hz, 1H, -OH) ppm; ¹³C NMR (101 MHz, CDCl₃): δ = 165.6, 154.9, 143.3, 141.4, 133.7, 133.6, 133.3, 130.1, 129.9, 129.8, 129.1, 128.8, 128.6, 128.4, 128.0, 127.3, 125.3, 120.2, 91.1, 70.2, 69.4, 68.0, 67.1, 66.2, 60.5, 46.7 ppm. ESI-LRMS: *m/z* [M+Na]⁺ calcd. for C₄₂H₃₄O₁₁Na: 737.1993 found 737.2000

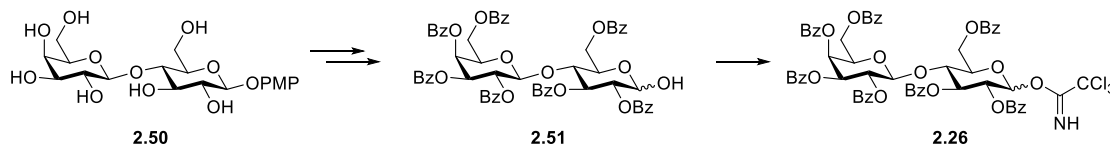
* The analytical data agree with the literature^[222]

2,3,4-*O*-Tri-benzoyl-6-*O*-(9-fluorenylmethoxycarbonyl)-*D*-galactopyranosyl trichloroacetimidate (**2.25**)

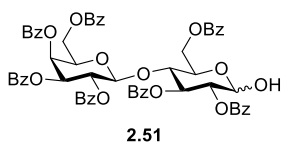


To a stirred solution of **2.40** (400 mg, 0.56 mmol, 1.00 equiv.) in trichloroacetonitrile (1.12 mL, 11.2 mmol, 20.0 equiv.) anhydr. DCM (5 mL), NaH (60 % dispersion in oil, 6.70 mg, 0.28 mmol, 0.50 equiv.) was added at room temperature under argon atmosphere and the reaction was left to react overnight. Upon completion, solvent (in presence of silica to quench the remaining NaH) was evaporated and the residue was purified by flash column chromatography using a mixture of hexane/ethyl acetate (3:1) to afford the desired compound as a white solid in 45% yield (208 mg, 0.24 mmol). ^1H NMR (400 MHz, CDCl_3): δ = 8.63 (s, 1H, =NH), 8.16 – 7.33 (m, 23H, -Ar), 6.91 (d, J = 3.6 Hz, 1H, H -1), 6.13 – 6.01 (m, 2H, H -4, H -3), 5.95 (dd, J = 10.6, 3.6 Hz, 1H, H -2), 4.81 (t, J = 6.2 Hz, 1H, H -5), 4.45 – 4.30 (m, 4H, - CH_2 -CH- Fmoc, H -6a, H -6b), 4.22 (t, J = 7.6 Hz, 1H, - CH - Fmoc) ppm; ^{13}C NMR (101 MHz, CDCl_3): δ = 165.5, 165.5, 165.4, 160.5, 154.6, 143.2, 141.2, 141.2, 133.7, 133.5, 133.3, 129.9, 129.8, 129.7, 128.8, 128.7, 128.6, 128.4, 128.3, 127.8, 127.2, 127.1, 125.2, 120.0, 93.6, 70.2, 69.5, 68.3, 68.2, 67.7, 65.2, 46.5 ppm; IR (neat) ν_{max} : 3341, 3068, 2959, 2927, 1729, 1677, 1603, 1452, 1259, 1094, 1069, 1026 cm^{-1} ; ESI-HRMS: m/z $[\text{M}+\text{Na}]^+$ calcd. for $\text{C}_{44}\text{H}_{34}\text{Cl}_3\text{NO}_{11}\text{Na}$: 880.1090 found 880.1104.

Synthesis of 2,3,4,6-tetra-*O*-benzoyl- β -*D*-galactopyranosyl-(1 \rightarrow 4)-2,3,6-tri-*O*-benzoyl- β -*D*-glucopyranosyl trichloroacetimidate (**2.26**)



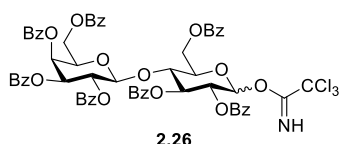
2,3,4,6-Tetra-*O*-benzoyl- β -*D*-galactopyranosyl-(1 \rightarrow 4)-2,3,6-tri-*O*-benzoyl- β -*D*-glucopyranoside (**2.51**)



4-Methoxyphenyl β -*D* galactopyranosyl-(1 \rightarrow 4)- β -*D*-glucopyranoside **2.50** (300 mg, 0.67 mmol, 1.00 equiv.) was dissolved in pyridine (12 mL) and the solution was cooled down to 0 $^{\circ}\text{C}$. BzCl (0.70 mL, 6.09 mmol, 9.10 equiv.) was added dropwise to the solution and then DMAP (81.7 mg, 0.67 mmol, 1.00 equiv.) was added. The solution was left overnight at rt. Then, the mixture was poured into acid water, the precipitate was filtered off and washed with water. The solid was dissolved in DCM and washed with hydrochloric acid, NaHCO_3 solution (10 mL) and

then water. The organic layer was dried over Na₂SO₄ and the solvent was removed under reduced pressure. The crude product was dissolved in acetonitrile: water (15 mL; 4:1) and ceric ammonium nitrate (CAN) (780 mg, 1.42 mmol, 2.50 equiv.) was added. The mixture was stirred at room temperature for 1 h. Then diluted with ethyl acetate (10 mL), and washed with water (10 mL), NaHCO₃ solution (10 mL), and NaCl solution (10 mL). The organic layer was dried over Na₂SO₄ and the solvent was removed under reduced pressure. The residue was purified by flash column chromatography using a mixture of hexane/ethyl acetate (2:1) as eluent. Crude reaction was then utilized for next reaction

2,3,4,6-Tetra-O-benzoyl-β-D-galactopyranosyl-(1→4)-2,3,6-tri-O-benzoyl-β-D-glucopyranosyl trichloroacetimidate (**2.26**)



2.51 was dissolved in anhydr. DCM (13 mL) under argon atmosphere and cooled down to 0 °C. Trichloroacetonitrile (0.59 mL, 5.86 mmol, 12.00 equiv.) and DBU (20 μL, 0.15 mmol, 0.30 equiv.) were added consecutively and the solution was stirred for 2 h at 0 °C. The solvent was removed under reduced pressure. The crude product was purified by flash column chromatography using a mixture of hexane/ethyl acetate (3:1.5) as eluent. The product was obtained as a white foam in 58% yield over three steps (472 mg, 0.39 mmol). ¹H NMR (400 MHz, CDCl₃): δ = 8.55 (s, 1H, C(NH)CCl₃), 8.05 – 7.86 (m, 12H, -Ar), 7.75 – 7.70 (m, 2H, -Ar), 7.66 – 7.55 (m, 3H, -Ar), 8.05 – 7.86 (m, 15H, -Ar), 7.25 – 7.17 (m, 3H, -Ar), 6.70 (d, *J* = 3.8 Hz, 1H), 6.16 (m, 1H), 5.78 – 5.69 (m, 2H), 5.55 (dd, *J* = 10.2, 3.8 Hz, 1H), 5.41 – 5.33 (m, 1H), 4.92 (d, *J* = 7.9 Hz, 1H), 4.60 – 4.48 (m, 2H), 4.36 – 4.27 (m, 2H), 3.92 – 3.63 (m, 3H) ppm; ¹³C NMR (101 MHz, CDCl₃): δ = 165.7, 165.52, 165.5, 165.4, 165.2, 165.17, 164.8, 160.7, 133.7, 133.6, 133.5, 133.4, 130.1, 130.0, 129.8, 129.8, 129.80, 129.7, 129.4, 129.4, 128.8, 128.7, 128.7, 128.6, 128.6, 128.6, 128.4, 128.4, 101.1, 93.16, 90.77, 76.8, 76.4, 75.2, 74.0, 71.8, 71.5, 71.4, 70.0, 67.5, 62.1, 60.5 ppm.

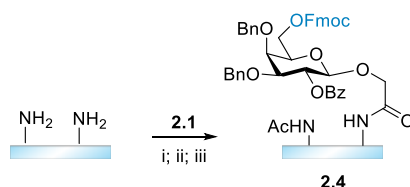
* The analytical data agree with the literature.^[216]

2.5.2. Functionalization of acceptor glass slides

D1. For fluorescent binding assay

Galactopyranoside linker (**2.1**) (19.0 mg, 25.0 μmol, 1.00 equiv.) was dissolved in 250 μL of anhydr. DMF in a vial. *N,N'*-diisopropylcarbodiimide (DIC) (12.0 μL, 75.0 μmol, 3.00 equiv.) and hydroxybenzotriazole (HOBt) (3.50 mg, 25.0 μmol, 1.00 equiv.) were added consecutively and the vial was shaken for a few seconds. The resulting solution was pipetted

on the free amino glass slide and another slide was placed on top of the first one (sandwich functionalization method). The slides were left overnight in a petri dish to react. Then, slides were washed with DMF (3 × 3 min), MeOH (1 × 2 min), and DCM (1 × 3 min), and dried by a jet of air to obtain the Gal-6-OFmoc-functionalized slides. The remaining unreacted free NH₂-groups on the acceptor slide were subjected to acetylation for 30 min using initially, the basic capping A solution. The same process was repeated with a freshly prepared capping solution for another 30 min at room temperature (300 rpm), and then the slide was washed with DMF (3 × 1 min), and DCM (3 × 1 min). The slide was subjected for addition acetylation with the acidic capping solution for 30 min, and the same process was repeated with a freshly prepared capping solution for another 30 min at room temperature (300 rpm). Slide was washed with DCM (3 × 1 min) and dried by a jet of air to obtain the capped Gal-6-OFmoc-functionalized glass slides **2.4**.



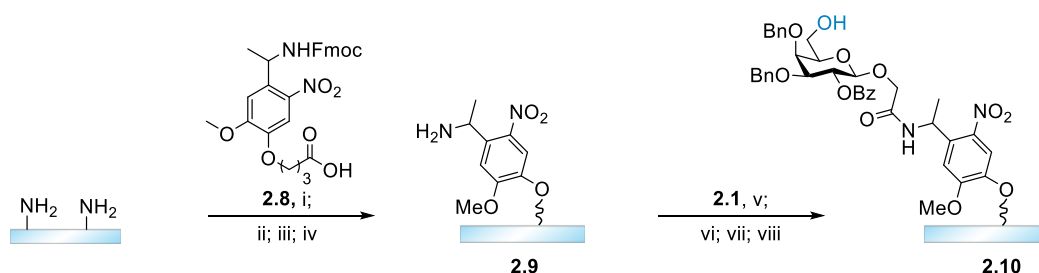
Experimental Figure 2.1: i) Attachment of linker **2.1**, DIC, HOBt, anhydr. DMF, rt, overnight; ii) 10% Ac₂O, 20% DIPEA in DMF, rt, 30 min (×2); ii) 10% Ac₂O, 2% MsOH, 88% DCM, rt, 30 min (×2).

D2. For MALDI analysis

D2.1. Glycosylation in solution

Fmoc-Photo-linker **2.8** (26.0 mg, 50.0 μmol, 1.00 equiv.) was dissolved in 250 μL of anhydrous DMF in a vial. DIC (23.2 μL, 150 μmol, 3.00 equiv.) and HOBt (6.76 mg, 50.0 μmol, 1.00 equiv) were added consecutively and the vial was shaken for a few seconds. The resulting solution was pipetted on the amino glass slide and another slide was placed on top (sandwich functionalization method). The slides were left overnight to react in a petri dish. Then, the slides were washed consecutively with DMF (3 × 3 min), MeOH (1 × 2 min), and DCM (1 × 1 min), and dried by a jet of air. The remaining unreacted free NH₂ groups on the slide were subjected for basic acetylation using the basic capping solution B (see Preparation of Solutions) for 30 min. The same process was repeated with a freshly prepared capping solution for another 30 min at room temperature (300 rpm). The slide was washed with DMF (3 × 1 min), and DCM (3 × 1 min) and subjected for additional acetylation with the acidic capping solution for 30 min. The same process was repeated with a freshly prepared capping solution for another 30 min at room temperature (300 rpm). Slide was washed with

DCM (3 × 1 min) and dried by a jet of air. Deprotection of the Fmoc group was achieved followed by attachment of galactopyrannoside **2.1**, and capping using the basic capping solution B and acidic solution (see Preparation of Solutions). The resulted Fmoc-protected glass slide was then subjected for the first sugarLIFT module, Fmoc-deprotection and acidic wash to form glass slide **2.10**.

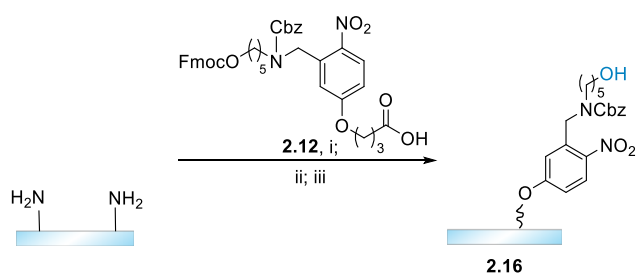


Experimental Figure 2.2: i) Attachment of photo-linker **2.8**, DIC, HOBt, anhydr. DMF, rt, overnight; ii) 10% Ac₂O, 20% DIPEA in 35% DMF and 35% DCM (v/v), rt, 30 min (×2); iii) 10% Ac₂O, 2% MsOH, 88% DCM, rt, 30 min (×2), iv) 20% piperidine in DMF ; v) attachment of linker **2.1**, DIC, HOBt, anhydr. DMF, rt, overnight; vi) 10% Ac₂O, 20% DIPEA in 35% DMF and 35% DCM (v/v), rt, 30 min (×2); vii) 10% Ac₂O, 2% MsOH, 88% DCM, rt, 30 min (×2).

D2.2. sugarLIFT and injection-based vapor glycosylation

Attachment of photocleavable linker **2.9**

Photocleavable linker **2.9** (17.5 mg, 25.0 μmol, 1.00 equiv.) was dissolved in 250 μL of anhydr. DMF in a vial, DIC (12.0 μL, 75.0 μmol, 3.00 equiv.) and HOBt (3.50 mg, 25.0 μmol, 1.00 equiv.) were added consecutively and the vial was shaken for 5 min. The resulting solution was pipetted on the free amino slide and left overnight in a petri dish to react. Then, the slide washed consecutively with DMF (3 × 5 min), MeOH (1 × 2 min), DCM (1 × 1 min) and dried by a jet of air. Then the resulted slide was subjected for basic and acidic capping as reported previously using basic capping solution A and acidic solution (see Preparation of Solutions) yielding the desired Fmoc-protected glass slide, which was then subjected for the first sugarLIFT module, Fmoc-deprotection and acidic wash to form glass slide **2.16**.



Experimental Figure 2.3: Reactions and conditions used: i) Attachment of photo-linker **2.12**, DIC, HOBT, anhydr. DMF, rt, overnight; ii) 10% Ac₂O, 20% DIPEA in DMF (v/v), rt, 30 min (×2); iii) 10% Ac₂O, 2% MsOH in DCM (v/v), rt, 30 min (×2).

2.5.3. SugarLIFT process

Custom-built setup

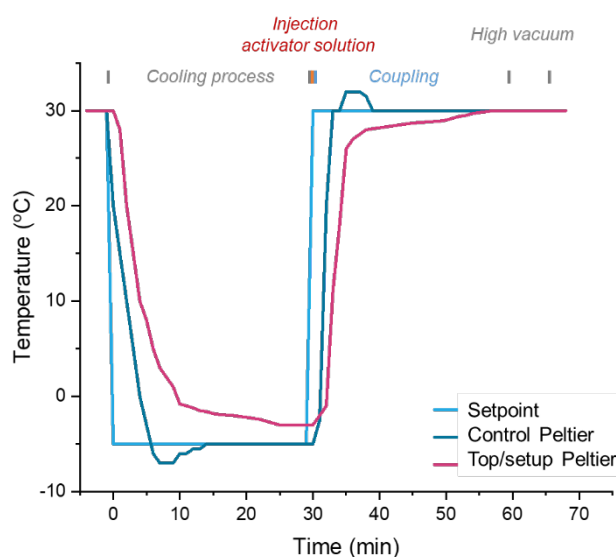
The optimized vapor glycosylation setup consisted of six components: a glycosylation chamber; a Hamilton syringe; a vacuum pump (PC 3001, VARIO[®], Vacuubrand GmbH & Co KG, Wertheim, Germany); two valves; a camera to visualize the deposition of the activator solution, and a computer system for temperature of the glycosylation chamber. As mentioned in the previous sections, no technical and mechanical changes were performed regarding the function of the glycosylation chamber. The temperature is ensured inside and on top (lid) of the chamber by a software installed on a computer. The two valves provide control over the atmosphere inside the setup. The left one is responsible for the applied vacuum from the vacuum pump and the right one for the atmosphere inside the setup after the completion of the glycosylation reaction (air, high vacuum and argon from the Schlenk line). The vapor of the activator solution is formed after injection of the desired amount *via* a Hamilton syringe. The progress of the entire process is visualized through a window in the lid by a camera placed on top of the glycosylation chamber, which is connected with the control software.

Technical characteristics

- Control Software: Multi Control 8Ch: This software (by Klaus Bienert) was used for control of the temperature inside and on top of the glycosylation chamber (thermoelectric cooling elements inside the chamber and the heaters in the steel lid). Additionally, it controls the heated tube of the first generation-setup for vapor generation of the activator solution. Furthermore, the temperature of the cooling water system can also be monitored.
- Multi Camera Viewer: Visualization of the reaction and the vapor deposition is achieved by this USB camera.

- Control Box Compartments: USB 6008 (in the control box), 1 × Analog Out: Control of power supply unit Manson HCS - 3402 (0.32V, 0.20A) for the Peltier elements, 1 × Analogue Out: Control of power supply unit Manson HCS - 3402 (0.32V, 0.20A) for pipe heater, 1 × Digital Out: Control of Peltier switchover, 1 × Digital Out: Control of lid heating 1x CBox for measuring all temperatures (in the control box), Water temperature, Peltier temperature, lid temperature, 1 × Control box for lid heating (separate box) 1x Manson HCS - 3402 power supply unit (0.32V, 0.20A) for the Peltier elements
- Reaction chamber: 4 × Peltier element PE-127-14-11 15.7V, 8.5A, 82 Watt for temperature control of the chamber, 2 × heating resistors 6.2 Ohm 100 Watt for lid heating USB camera

Temperature profile and regulation system



Experimental Figure 2.4: Temperature profile inside the reaction chamber during one coupling cycle (cooling rate is slower than the heating rate, 7°C/min).

The glycosylation chamber, as mentioned in the previous section, consists of four Peltier elements, allowing absolute control of the temperature during the entire process. These thermoelectric cooling elements are located in the bottom of the chamber, while on top a steel lid closes the reaction chamber. The typical temperature range during a glycosylation cycle was adjusted from -5 °C to 30 °C. The typical temperature of -5 °C was programmed and could be compared with the actual Peltier

element and steel plate temperature (setpoint, Control Peltier, Top/setup Peltier temperature, Experimental Figure 2.4, light blue). The temperature of the lid was kept stable throughout the entire process at 40 °C (not shown). The cooling process before initiating the glycosylation requires about 30 min to reach about -3 °C, with a cooling rate inside the chamber (red curve, Experimental Figure 2.4) ~4-5 °C/min during the first 10 min of the process and then ~0.5 °C/min. After the cooling process, the reaction starts by injecting the desired amount of the activator solution into the glycosylation chamber (-5 °C set point, Top/setup Peltier -3 °C). Then, the set temperature was increased from -5 °C to 30 °C and the reaction continues for 30 min under these conditions. The heating rate of the top Peltier

was ~ 7 °C/min. After 30 min, the setup was subjected to high vacuum for 5 min, at 30 °C to remove the remaining solvent and activator from the glycosylation chamber. Experimental Figure 2.4 depicts the temperature profile of every step inside the glycosylation chamber.

Modules of *in-situ* synthesis via sugarLIFT

Module A: Acceptor slide preparation for synthesis (71 min)

All syntheses were performed on 3D-Amino glass slides, (according to vendor 1 – 5 nmol/cm²). The slides were functionalized as described. Then, the slides were initially placed into a petri dish, and swollen for 30 min in DMF on a shaker at room temperature prior to the synthesis (300 rpm). Then, each slide was washed with DMF (3 × 3 min), deprotected using Fmoc-deprotection solution, and washed with DMF (3 × 3 min), MeOH (1 × 2 min), and DCM (1 × 3 min).

Module B: Acidic wash prior to glycosylation (58 min)

The acidic wash solution was added to the petri dish under room temperature and stirred for 1 min (300 rpm). The acidic solution was removed, the slide washed with anhydr. DCM (1 × 3 min), DMF (1 × 1 min), DCM (1 × 1 min) and dried by a jet of air.

Module C: Donor slide preparation

Donor slides bearing the desired glycosyl donor (5 mg), inert polymer matrix (25 mg) in anhydrous DMF (500 μ L) were prepared. The solution was spin coated onto the polyimide coated microscope glasses (80 rps) using a positive displacement pipette.

Module D: cLIFT of BB (s)

For process optimization: A laser scanning system with 488 nm wavelength and 120 mW maximum output power was used,^[197,221] with a laser focus diameter of ~ 20 μ m. A laser power of 100 mW with a pulse duration range of 20-27.5 ms was applied for the optimization experiments, while for the MALDI-ToF mass spectrometry analysis a lasing power of 100 mW and pulse duration of 20 ms was used.

For parallel synthesis: For the array synthesis, a spot pitch of 1 mm was used. A laser scanning system with 405 nm wavelength and 210 mW maximum output power was used (~ 50 μ m laser focus diameter).^[128] The automated transfer of the donor slides to the

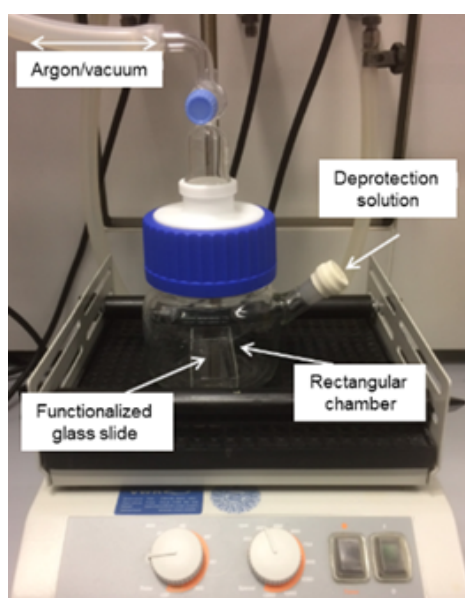
acceptors, were placed in the slide holder by a robot with 20 μm precision. A laser gradient from 110 to 190 mW was applied with a pulse duration range of 20-25 ms.

Module E: Vapor glycosylation (72 min)

The slide was placed inside the glycosylation chamber and the temperature adjusted to $-5\text{ }^{\circ}\text{C}$, while the pressure was set to 100 mbar. For the next 30 min, the glycosylation chamber was kept under these setting to reach the final conditions. After the set temperature was reached, the valve connecting the glycosylation chamber with the vacuum pump was closed and the reaction was initiated by injecting 70 μL of activator solution into the glycosylation chamber with a Hamilton syringe. The solvent and activator were deposited in the chamber, condensing on the cooled surface, while the temperature was slowly increased to room temperature ($7\text{ }^{\circ}\text{C}/\text{min}$ to $30\text{ }^{\circ}\text{C}$). After 30 min, the setup was subjected to high vacuum for 5 min to remove the residual solvent and activator from the glycosylation chamber. Finally, the slide was washed with DCM (1×3 min), DMF (1×1 min), DCM (1×3 min), dried by a jet of air. Modules C, D and E were repeated one more time to ensure high conversion.

Post-Synthesis manipulation

Module F1: Deprotection and plant lectin detection assay



Experimental Figure 2.5: Custom-made setup for the deprotection of the benzyl ester groups on the synthesized oligosaccharides.

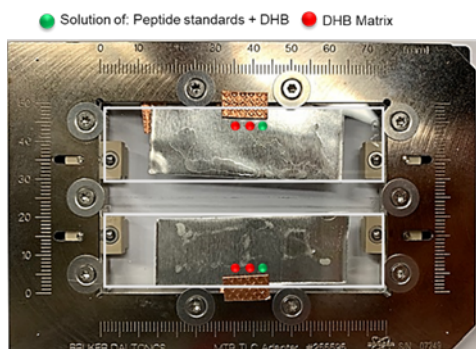
After completion of synthesis, the microarray was subjected to deprotection using Zemplén deprotection conditions. The slide was placed inside the rectangular chamber of the glass bowl chamber and 5 mL of the deprotection solution was added under inert atmosphere at room temperature (Experimental Figure 2.5) and left to react overnight on a shaker (150 rpm). Then, the solution was removed, and the slide was washed consecutively with MeOH (10 mL, 3×3 min), and water (10 mL, 3×3 min) and dried by a jet of air. Before lectin staining, acceptor slides were incubated with a blocking buffer for 30 min (Rockland, USA; blocking buffer for fluorescent western blotting MB-070). Fluorescently labeled plant lectins, concanavalin A (ConA; CF[®]633 ConA, Biotium, Inc., USA) was diluted to 20 $\mu\text{g}/\text{mL}$ in lectin

buffer (50 mM HEPES, 100 mM NaCl, 1 mM CaCl₂, 1 mM MnCl₂, 10% blocking buffer, 0.05% Tween 20, pH 7.5), and ricinus communis agglutinin I, (RCA-I, Rhodamine labeled, Lectin kit 1, Vector laboratories, USA) was diluted to 10 µg/mL in lectin buffer and incubated for 1h at room temperature. Subsequently, each stained well was washed with PBS-T (3 × 3 min). Then, the acceptor slide was rinsed with Tris buffer (1 mM Tris-HCl buffer, pH=7.4) to remove all remaining salt residues, and dried by a jet of air. Fluorescence scanning was used to detect the lectin binding on the corresponding sugar moieties.

Module F2: MALDI-detection (A)

After completion of the synthesis, the oligosaccharide bound to a photo labile linker on a glass slide was subjected to cleavage under a UV-lamp (365 nm, 2×8 W). The distance between the lamp and the glass slide was approximately 4 cm, and the glass slide was irradiated for 30 min. Then, on top of the slide, 3 mL of MeOH and 3 mL of DCM were pipetted in total, each time 500-700 µL of solvent alternately, and everything collected together in a vial. The solvents were removed under reduced pressure resulting in the obtained oligosaccharide.

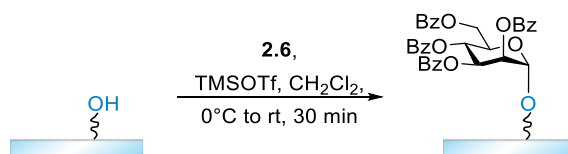
Module F2: in-situ MALDI-detection (B)



Experimental Figure 2.6: TLC MALDI-plate for in-situ MALDI bearing the glass slides and the need stickers to make the substrate conductive enough for ionization.

After completion of the synthesis, the glass slide bearing the synthesized oligosaccharide was placed on the MTP-TLC MALDI adapter as shown in Experimental Figure 2.6. Since the glass slides are not conductive, self-adhesive copper and aluminum foil tapes were placed between the MALDI plate and the glass slides, to promote ion acceleration and be able to (more) correctly detect the synthesized structures. 2,5-Dihydroxybenzoic acid (DHB) matrix was spotted on top of the glass slide close to the conductive copper sticker, while as positive control, a solution containing the peptide standard in DHB was used. DHB matrix was spotted on defined areas to ionize the cleaved components, after *in-situ* cleavage of the synthesized structures bound on a photo labile linker. The MALDI laser source cleaves the synthesized structures and due to the conductivity of the TLC-MALDI adapter from the metal tape, detection of the formed structures could be achieved.

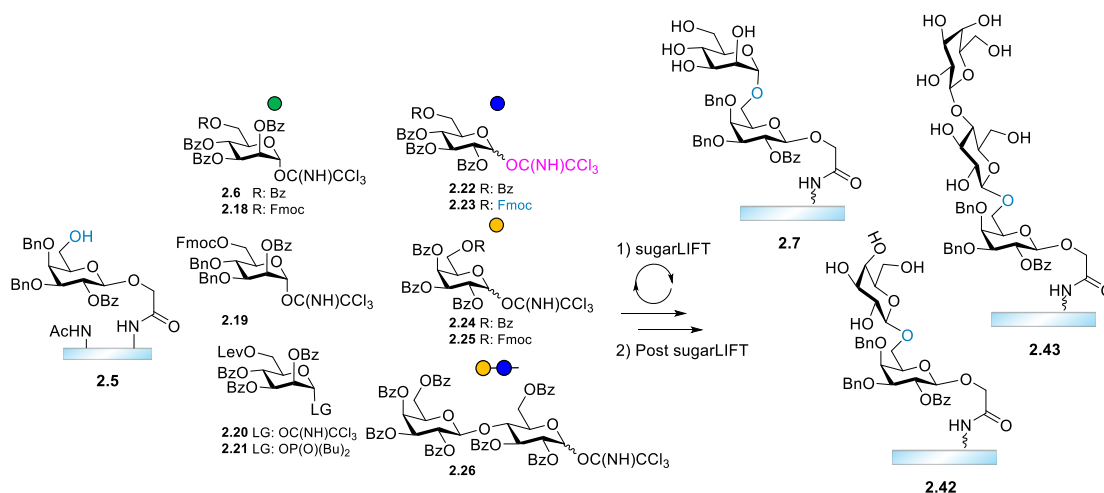
2.5.4. Glycosylation in solution



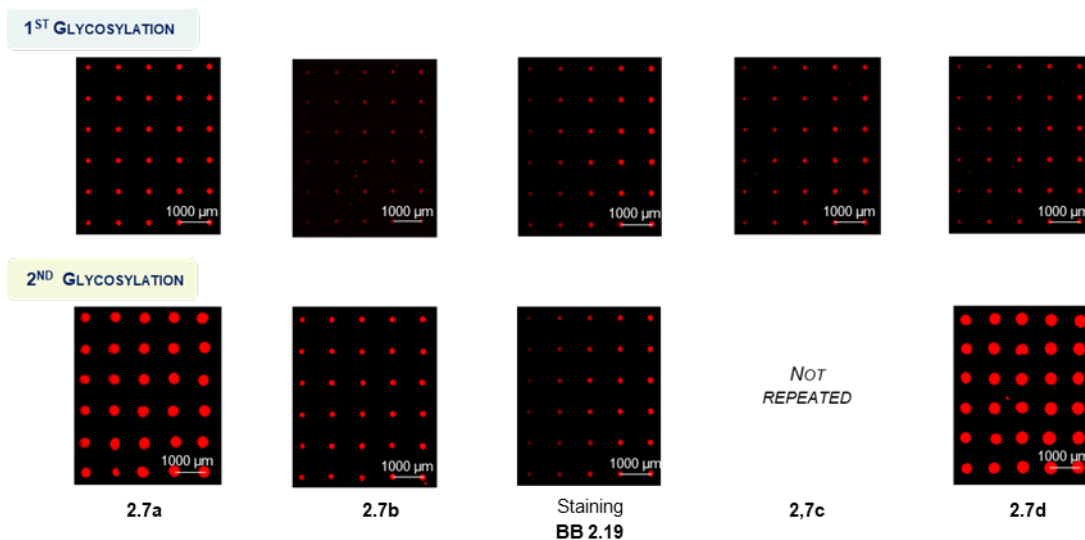
Functionalized-acceptor slide (**2.10/2.16**) was placed inside the small rectangular chamber of the glass bowl chamber under inert conditions (Experimental Figure 2.5). Glycosyl donor **2.6** (30.0 mg, 0.04 mmol, 1.00 equiv.) and DCM (4 mL) were added and the chamber was cooled down to 0 °C and shaken (300 rpm). After 10 min, 1 mL of the activator solution (0.4 equiv./mL, 0.01 mmol) was added in the reaction and the temperature was increased to room temperature. After 30 min, the reaction mixture was removed from the glass chamber with a glass pipette and the slide was washed consecutively with DCM (1 × 1 min), DMF (1 × 1 min), DCM (3 × 1 min) and dried by a jet of air. The slide was placed inside a Petri dish and 10 mL of the pyridine solution was added to remove any residual of activator for 1 min, and then washed with 10 mL of DMF, DCM and DMF (1 × 1 min each). Basic capping solution A was added for 2 min, and the same process was repeated two times with a freshly prepared solution for 30 min (300 rpm). The slide was washed with DMF (1 × 1 min) and DCM (3 × 1 min), followed by another capping cycle with the acidic capping solution (1 × 2 min, and 2 × 30 min) as mentioned above. After completion the slide was washed with DCM (3 × 1 min) and dried by a jet of air.

UV-cleavage and MALDI-ToF as well as direct/*in-situ* MALDI were performed as explained above

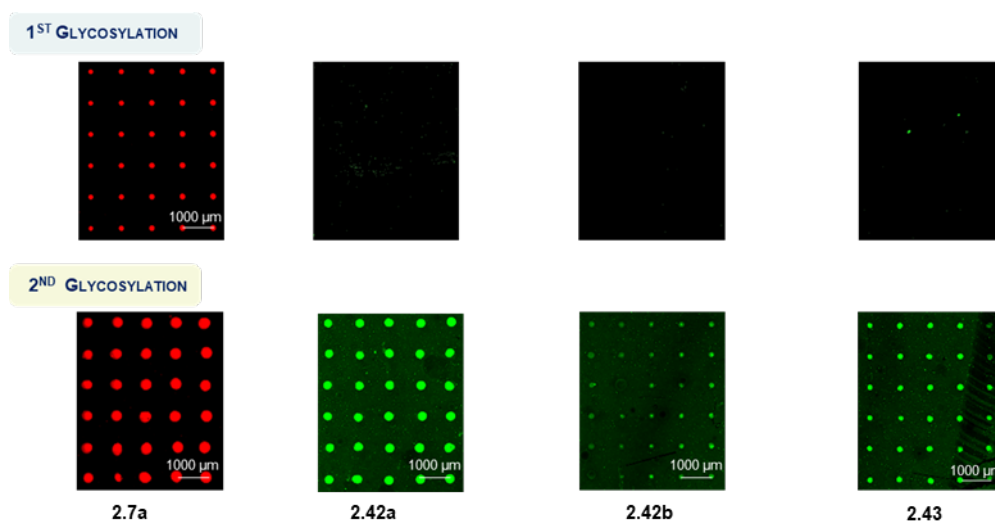
2.5.5. Parallel oligosaccharide synthesis via sugarLIFT



Action	BB	Modules	Notes	Result
sugarLIFT		A, B	2.4 swell, in a petri dish (2 slides)	
	2.6			2.7a Difference between 1 st and 2 nd glycosylations were analysed
	2.18			2.7b needs to be further investigated
	2.19			
	2.20	C, D; E; C; D; E	8 different slides prepared for each BB	2.7c
	2.21		2.6, 2.14-2.17 transferred in one slide (1)	2.7d
	2.22		2.6, 2.18-2.20 transferred in one slide (2)	-
	2.23		Activator solution, 70 µL	-
	2.24			2.42a
				2.42b
			2.43	
Post sugarLIFT	F1		2.6, 2.14-2.17 ConA & 2.18-2.20 RCA-I	



Experimental Figure 2.7: Fluorescence scan images of α -D-mannopyranosyl-1,6- β -D-galactopyranosides **2.7** of donors **2.18-2.21**, after deprotection and incubation with fluorescently labeled ConA. Staining was performed in HEPES-buffer (50 mM HEPES, 100 mM NaCl, 1 mM CaCl₂, 1 mM MnCl₂, 10 % blocking buffer and 0.05 % Tween-20, pH 7.5) at 20 µg/mL ConA concentration. Scanning parameters: wavelength 635 nm, PMT gain 600, laser power 33%, pixel size 5 µm. Spot pitch is 1000 µm.



Experimental Figure 2.8: Fluorescence scan images of oligosaccharides **2.42** and **2.43** obtained from donors **2.24-2.26** bearing a terminal galactose moiety, after deprotection and incubation with fluorescently labeled RCA-I. Staining was performed in HEPES-buffer (50 mM HEPES, 100 mM NaCl, 1 mM CaCl₂, 1 mM MnCl₂, 10 % blocking buffer and 0.05 % Tween-20, pH 7.5) at 10 µg/mL RCA-I concentration. Scanning parameters: Wavelength 532 nm, PMT gain 500, laser power 33 %, pixel size 5 µm. Spot pitch is 1000 µm.

3. On-chip neo-glycopeptide synthesis for multivalency studies

This chapter has been modified in part from the following articles:

Mende, M.*; **Tsouka, A.***; Heidepriem, J.; Paris, G.; Mattes, D. S.; Eickelmann, S.; Bordoni, V.; Wawrzinek, R.; Fuchsberger, F. F.; Seeberger, P. H.; Rademacher C.; Delbianco M.; Mallagaray A.; Loeffler F. F.; On-Chip Neo-Glycopeptide Synthesis for Multivalent Glycan Presentation, *Chem.Eur.J.*, **2020**, 26, 9954 –9963. DOI: 10.1002/chem.202001291.

Tsouka, A.; Hoetzel, K.; Mende, M.; Heidepriem, J.; Paris, G.; Eickelmann, S.; Seeberger P. H.; Lepenies, B.; and Loeffler, F. F.; Probing Multivalent Carbohydrate-Protein Interactions with On-Chip Synthesized Glycopeptides Using Different Functionalized Surfaces, *Front. Chem.*, **2021**, 9:766932. DOI: 10.3389/fchem.2021.766932.

*These authors contributed equally.

Specific contribution

Section 3.2.1 and 3.2.2: I performed all the preliminary experiments *via* cLIFT and Dr. Marco Mende synthesized the azide monomers. Other sugar azides used in this chapter were provided by Dr. Martina Delbianco, Dr. Vittorio Bordoni, Dr. Robert Wawrzinek, Dr. Christoph Rademacher and Dr. Alvaro Mallagaray. The generation of the final glycomimetics, the $K_{D,surf}$ experiments and the evaluation of the obtained results were performed in collaboration with Dr. Marco Mende. The plotting of the $K_{D,surf}$ was conducted by Dr. Felix Loeffler. The fluorescently labelled hLangerin was provided by Dr. Felix Fuchsberger and Dr. Christoph Rademacher.

Section 3.2.3- 3.2.5: I performed the synthesis and characterization of the used azides. Together with the student research assistant Kassandra Hoetzel (supervised by me), we performed the synthesis, characterization and evaluation of the formed glycopeptides. The optimization of the process and the new conditions were investigated in collaboration with Dr. Grigori Paris and Jasmin Heidepriem. Dr. Bernd Lepenies provided the C-type lectins. The hydrophobicity of the used surfaces was measured by Dr. Stephan Eickelmann.

Sections 3.2.2., 3.5.1., 3.5.6., 3.5.8. have been removed for copyright reasons in the online version. For more information about this section please check this link:

<https://doi.org/10.1002/chem.202001291>

Mende, M.*; **Tsouka, A.***; Heidepriem, J.; Paris, G.; Mattes, D. S.; Eickelmann, S.; Bordoni, V.; Wawrzinek, R.; Fuchsberger, F. F.; Seeberger, P. H.; Rademacher C.; Delbianco M.; Mallagaray A.; Loeffler F. F.; On-Chip Neo-Glycopeptide Synthesis for Multivalent Glycan Presentation, *Chem.Eur.J.*, **2020**, 26, 9954 –9963.

3.1. Introduction

Glycan arrays are considered versatile tools for high-throughput screening of glycan-protein interactions existing in biological processes such as protein folding, cell-cell interaction, cell-adhesion, and signaling. Immobilization of glycans on solid support by high-precision robotics can be achieved in multiple ways (see *Section 1.4*),^[55,125,207,223,224] becoming nowadays a dominant methodology for detection of novel interactions in immunological and biomedical research,^[225,226] as well as drug discovery.^[225,227,228] Individual interactions between glycans and their GBPs are relatively weak. The recognition process that nature has evolved to enhance the binding strength is called multivalency (see *Section 1.3.2*). Despite the importance of multivalency, it is often neglected on the solid support, since the density and the spacing between sugar moieties is difficult to be determined. Various studies have been focused on the optimum glycan presentation, concentration, flexibility, orientation, and density in the array format (see *Section 1.4.4*).^[41,125,160,161,163,168] Thus, a plethora of multivalent glycan scaffolds have been investigated with diverse size and shape to mimic the natural recognition.^[45,152,153]

The application of this approach in the microarray format remains challenging. Conjugation of natural glycoproteins,^[154] and glycomimetics^[52,149,155–157,159] in the microarray format with multivalent presentation require extensive synthetic work prior to the printing onto glass slides. Unfortunately, printing of these compounds on the microarray ties in with solubility and density fluctuations of the material, printing and humidity inconsistencies during coupling, and the microarray surface functionalization (linker) effect, resulting in insufficient coupling and/or poor morphology of the spotted material.^[169,170]

To overcome these shortcomings, a flexible strategy to manufacture multivalent glycomimetics directly on-chip was utilized, enabling defined spacing and glycan orientation. In the first part of this chapter (*Section 3.2.1*), the required methodology was developed combining cLIFT^[126] with CuAAC, building a variety of neo-glycopeptides on functionalized glass slides. A sugar azide library was generated, with and without flexible linkers between the anomeric position and the azide moieties. A variety of plant (ConA, RCA-I, PNA, SBA, DBA, WGA) and animal C-type (hLangerin, mLangerin, mMinCLE, and mMGL-1) lectins were chosen to investigate their binding. In the second part (*Section 3.2.2*), as proof of concept, an array was generated and different sugar azides were conjugated and probed with their corresponding fluorescently labeled lectins. On the same array, the surface dissociation constant ($K_{D,surf}$) of mannose-ConA was additionally evaluated. Furthermore, the synthesis conditions for the peptide backbone were optimized and applied on different commercially

available arrays (hydrophobic and hydrophilic functionalization), to probe previously inaccessible glycan interactions (Sections 0 and 3.2.4) (Figure 3.1). Finally, a microarray bearing homo- and heteromultivalent GlcNAc and Man glycopeptides was generated and probed with WGA and ConA (Sections 3.2.5).

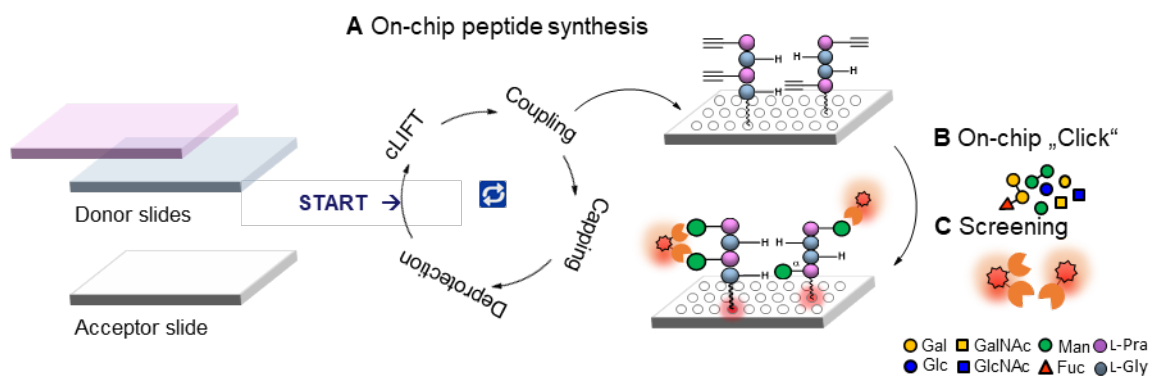


Figure 3.1: Overview on the research aims described in this chapter.

3.2. Results and Discussion

3.2.1. Method development for neo-glycopeptide synthesis

For a flexible, cost-efficient, and rapid *in-situ* generation of peptide scaffolds onto the array format, cLIFT was chosen as the printing methodology.^[126,127] Prior to synthesis the precise positioning of the acceptor slide in the laser area, was investigated (*Experimental Section 3.5.6*). After verifying that the positioning mechanism of the cLIFT gives reproducible results, the next goal was to synthesize the desired peptide scaffolds on defined positions. For the synthesis of the peptide scaffolds, two derivatives, Fmoc-Gly-OPfp (**3.1**) and Fmoc-Pra-OPfp (**3.2**), were chosen and sixteen possible variants of peptide tetramers were synthesized based on already known conditions^[126] (Figure 3.2). The commercially available 3D amine functionalized glass slides, Fmoc-NH- β -Ala-PEGMA-co-MMA¹, were used as acceptor slides for the peptide generation with prior functionalization with a PEG-based spacer (PPP-spacer).^[229] Pre-patterning of all acceptor slides was carried out with two glycines, to further increase the distance between the tetrapeptides and the solid support and, thereby, the accessibility of the glycopeptides. After Fmoc deprotection of the N-terminus, the free amino groups were used for peptide synthesis (conventional synthesis from C-terminus to N-terminus, e.g., N-GBGB-C, 1VII). Coupling and laser transfer of each amino acid layer was repeated three times to achieve high coupling efficiency and prevent deletion sequences while growing the chains. Coupling of the amino acids was conducted in an oven under inert

nitrogen conditions at $\sim 95\text{ }^{\circ}\text{C}$, resulting in three sets of quadruplicate spots on one array ($n=12$ spots; binding intensity was calculated as the mean of the 12 spot replica) (Figure 3.2B).

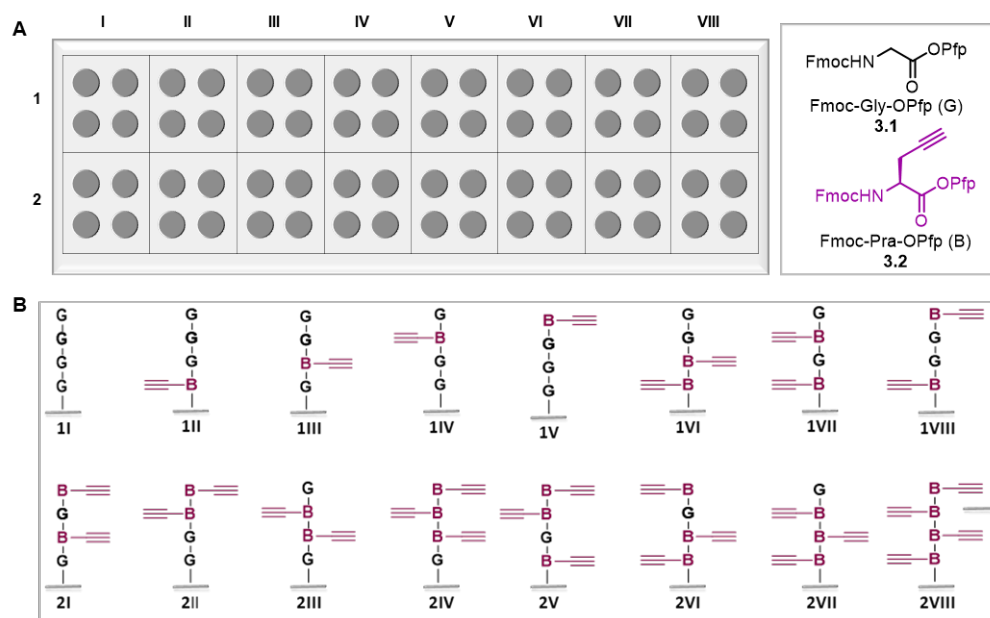


Figure 3.2: Overview of the synthesized peptide tetramers: A) Illustration of the acceptor slide with the tetrapeptide spot pattern created by cLIFT. Sixteen different tetrapeptides (1I-1VIII and 2I-2VIII) were synthesized using the two amino acids Fmoc-Gly-OPfp **3.1** (=G), and Fmoc-Pra-OPfp **3.2** (=B). Each dashed square represents one sequence as quadruplicate spots; B) Structures of the peptides according to the position of the squares.

Quality control of the three synthesized arrays was carried out *via* CuAAC on the peptide scaffolds using TAMRA azide dye (**3.3**), analyzing the fluorescence intensity (Figure 3.3). For peptides containing one Pra (i.e., one dye molecule per scaffold), highly similar staining intensities were observed. This showed that the synthesis yield was comparable. Interestingly, for all other sequences with more than one Pra, less intensity was attained. This can likely be attributed to the FRET mechanism,^[230] causing self-quenching of multiple adjacent dye molecules.

¹ Purchased from PEPperPRINT GmbH, Heidelberg, Germany.

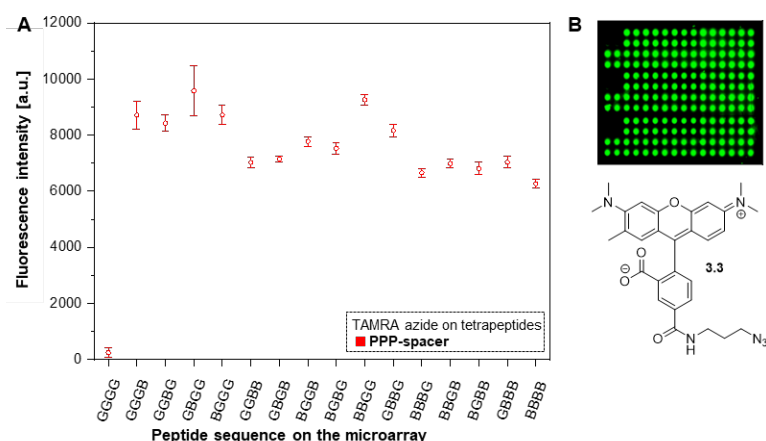


Figure 3.3: Overview of the coupling efficiency of the synthesized peptides containing TAMRA azide dye **3.3**: A) Fluorescence staining intensities, and B) fluorescence scan image attained using TAMRA-azide **3.3**.

Prior to on-chip synthesis, a collection of sugar azides was generated and their specific plant (ConA, RCA-I, PNA, DBA, SBA, and WGA)^{II} and C-type binding lectins (human-derived, hLangerin, and mouse-derived, mLangerin, mMincle, and mMGL-1)^{III} were chosen. The sugar azides **3.4–3.14** and **3.16** were synthesized from their corresponding unmodified monomer building blocks, while **3.15** and **3.17** were acquired^{IV} (Figure 3.4).^[26,231–235] For each sugar azides, CuAAC was performed on an individual array and the theoretical spacing in a scaffold was approximated^V (see *Experimental Section 3.5.8*).

^{II} ConA purchased from *Biotium Inc., Fremont, CA*, and other plant lectins from *Vector laboratories Burlingame, USA*.

^{III} hLangerin provided by Dr. Felix Fuchsberger and Prof. Dr. Christoph Rademacher and mC-type lectins by Prof. Dr. Bernd Lepenies.

^{IV} **3.5** synthesized by Dr. Marco Mende, **3.9–3.10** provided by Dr. Vittorio Bordoni and Dr. Martina Delbianco, **3.11** by Dr. Robert Wawrzinek and Prof. Dr. Christoph Rademacher, and **3.12** by Dr. Alvaro Mallagaray. **3.15** and **3.17** purchased from *Conju-Probe*.

^V Calculations of the spatial distances performed for **3.4–3.12** by Dr. Marco Mende.

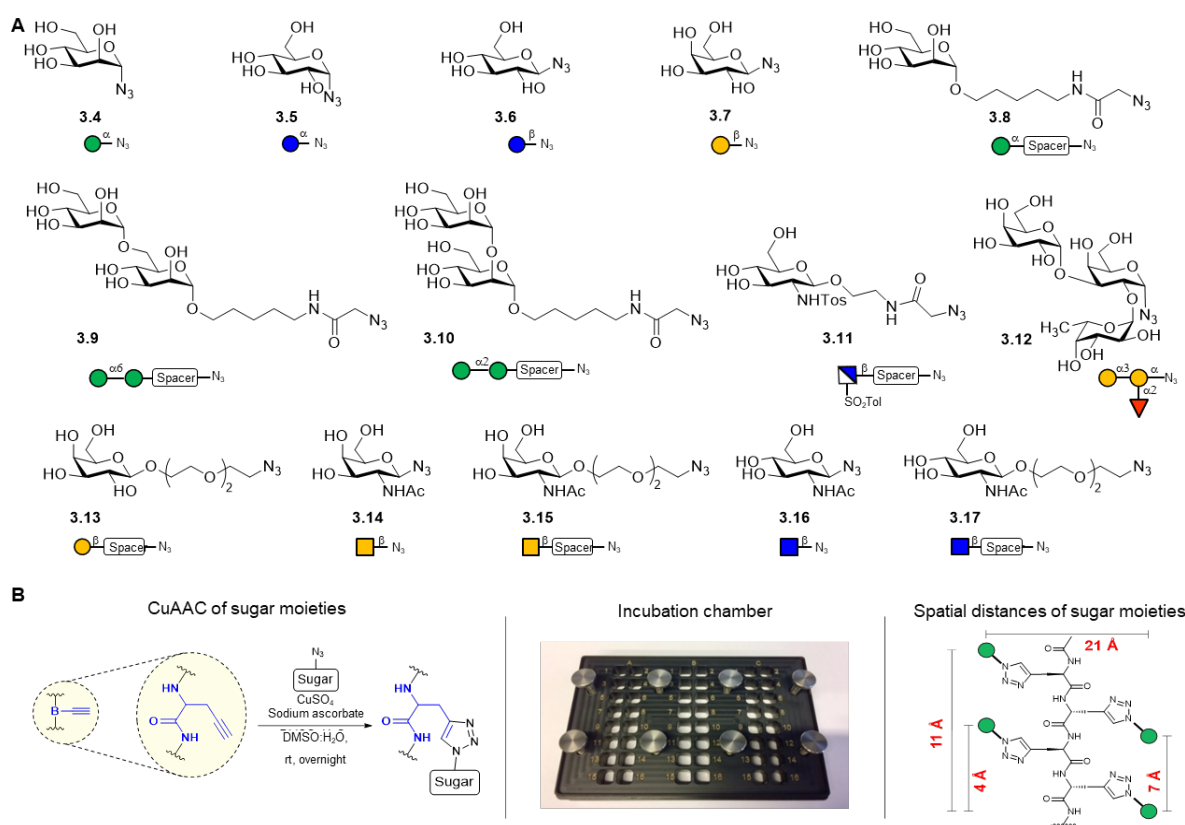


Figure 3.4: General reaction conditions for neo-glycopeptide formation: A) collection of sugar azides **3.4-3.12** were applied for neo-glycopeptides synthesis for concept validation (*Section 3.2.2*) and sugar azides **3.13-3.17** for the generation of glycopeptides on different surfaces (*Section 2.2.4*); B) General reaction using CuAAC in the 16 well chamber with the corresponding sugar azide and theoretical spacing estimates in a simplified scaffold.

3.2.2. Concept validation and evaluation of glycan-lectin interaction

Section has been removed for copyright reasons in the online version. For more information about this section please check this link: <https://doi.org/10.1002/chem.202001291>

Mende, M.*; **Tsouka, A.***; Heidepriem, J.; Paris, G.; Mattes, D. S.; Eickelmann, S.; Bordoni, V.; Wawrzinek, R.; Fuchsberger, F. F.; Seeberger, P. H.; Rademacher C.; Delbianco M.; Mallagaray A.; Loeffler F. F.; On-Chip Neo-Glycopeptide Synthesis for Multivalent Glycan Presentation, *Chem.Eur.J.*, **2020**, 26, 9954 –9963.

3.2.3. Neo-glycopeptide synthesis on different surfaces

To overcome the issues with the protein resistant PEPperPRINT glass slides, the importance of the surface functionalization was studied, to determine in which degree the functionalization influences the glycan-lectin interactions. Specifically, amine functionalized glass slides from PEPperPRINT were used as already reported with a PEG-based spacer^[229] (PPP-spacer, as reported in *Section 3.2.2.*), while 3D-amino glass slides from PolyAn were either used with or without spacer (PolyAn-spacer vs PolyAN). Before the synthesis, the (water) contact angle of the different surfaces was experimentally determined^{VII} (*Experimental Section 3.5.6*). PEPperPRINT slides are more hydrophobic than PolyAn slides, maintaining their slightly hydrophobic character even after the attachment of a PEG-spacer. For successful glycopeptide synthesis (Figure 3.2), the coupling time was reduced to 10 min to ensure better coupling efficiency and the amino acid concentration per slide generation was kept constant for both amino acids (pre-activated and non-activated, *Experimental Section 3.5.3*).^[128]

As described in *Section 3.2.1*, tetrapeptide scaffolds were synthesized *in-situ* on-chip, and prior to CuAAC of the sugar moieties, quality control of the three synthesized arrays was carried out (Figure 3.8) as described. On the PEPperPRINT slides, a rather constant

^{VI} PolyAn PolyAn GmbH, Berlin, Germany

^{VII} Experiments performed by Dr. Stephan Eickelmann

fluorescence intensity was observed (as reported in *Section 3.2.1*), while the self-quenching trend of multiple adjacent dye molecules was reduced.

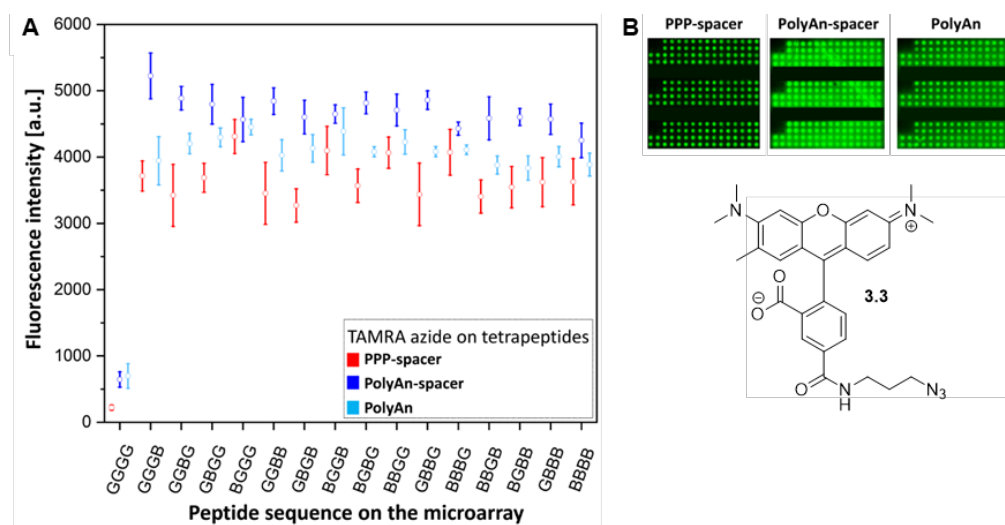


Figure 3.8: Overview of the coupling efficiency of the synthesized peptides containing TAMRA azide dye **3.3**: A) Fluorescence staining intensities, and B) fluorescence scan image obtained.

The new conditions for the preparation of the donor slides and the reduced oven coupling time seemed to give better microarray quality (due to generally stronger binding of lectins). The further the Pra was away from the solid support, the higher was the fluorescence intensity. Similar results were also detected for the two PolyAn slides. On the PolyAn slide with spacer, higher staining intensities were observed, probably due to the larger distance between the solid support and the attached dye molecules, making the peptide scaffold more accessible for the dye. Additionally, lower intensities were detected for scaffolds with more molecules of Pra, resulting in higher quenching than in monovalent and bivalent systems. On the PolyAn slides without spacer, a linear increase in binding was detected, depending on the position of Pra within the monovalent scaffolds. In comparison to PEPperPRINT surfaces, both PolyAn slides show higher intensities.

To compare same binding interactions on different functionalized surfaces, sugar azides **3.4-3.7**, and **3.13-3.17** were implemented and probed with their corresponding fluorescently labelled plant lectins (ConA, RCA-I, PNA, DBA, SBA, and WGA) and mouse-derived C-type lectins (mLangerin, mMincl, and mMGL-1). In particular, glycopeptides carrying Man azide **3.4** were incubated with ConA, mLangerin and mMincl, while mMincl was implemented also for sugar azides **3.5-3.6**. Gal azides **3.7** and **3.13**, were probed with fluorescently labeled RCA-I, PNA and mMGL-1, GalNAc azides **3.14-3.15** were incubated with DBA and SBA, and scaffolds with β -GlcNAc **3.16** and **3.17** were probed with WGA. The plain peptides served, once again, as negative controls for each used lectin.

3.2.4. Glycan-lectin evaluation on differently functionalized surfaces

As a general observation, it was noted that protein binding was surface dependent. In the case of multivalent glycan-lectin interactions, similar intensity trends were observed for all used lectins on the microarrays (except for WGA), with an increase in binding by increasing the number of sugars on the peptide backbone. Structures with only one attached sugar moiety, *e.g.*, BGGG, GGBG, GBGG, GGGB, showed structure dependent binding, with higher intensity for the N-terminal Pra on all used slides. This could be explained by the higher distance between the sugar and the surface, making it more accessible for the lectin. In terms of slide functionalization, for all detected interactions, the fluorescence intensities were higher on the PEPperPRINT slides (apart from WGA and DBA), while no binding was observed between the C-type animal lectins and their corresponding sugars. Between the two differently functionalized PolyAn slides, some structure and lectin dependent binding differences were detected. Additionally, comparing the more hydrophilic PolyAn to the hydrophobic PEPperPRINT slides, generally similar interactions were discovered with no remarkable differences on multivalent sugar orientation, density, and spacing.

Evaluation of Concanavalin A binders: On PEPperPRINT-spacer, the binding of ConA to α -Man 3.4 increased exponentially with linear increase in the number of sugar moieties. Although, the obtained intensities were one order of magnitude higher than the ones reported in *Section 3.2.2*, the binding trend of ConA did not show any differences. However, the binding ability of ConA on PolyAn slides bearing the spacer decreased by a factor of 2 compared to the intensities observed on the PEPperPRINT slides with the same functionalization (Figure 3.9A). The reduced laser power for the transfer of the amino acids (25% less power on PolyAn), potentially resulted in a lower amount of amino acid transfer, and in a smaller number of available peptide structures to attach the sugar azides. Consequently, fewer ConA lectins were bound. In addition, PolyAn surfaces are known to be less protein resistant in comparison to the PEPperPRINT surfaces^[229]. Although, on the PolyAn slides with spacer, the hydrophilicity was higher than on the PolyAn slides without a spacer, it was observed that the prior functionalization had no significant effect. Legume lectin binding depends on hydrophobic interactions (see *Section 1.2*), which can explain the lower binding intensity on the PolyAn-spacer slides in comparison to the PolyAn without functionalization, leading to diminished binding of ConA. The general binding profile of ConA was the same regardless of the slide functionalization.

Evaluation of Soybean agglutinin binders: According to literature, SBA^[13,19–21] is a GalNAc-/Gal-specific tetrameric legume lectin. For these studies, β -Gal **3.7** and **3.13**, β -GalNAc **3.14** and **3.15** were implemented. In the case of sugar azides **3.7**, **3.13**, and **3.14**, no binding was identified on all surfaces. As mentioned in literature, binding between the SBA tetramers and the terminal β -Gal involves cross-linking of the sugar to symmetry-related neighboring molecules, potentially explaining the unsuccessful staining. Notably, increased multivalent binding of β -GalNAc **3.15** was pointed out (Figure 3.9B). The enhanced flexibility between the anomeric position and the azide moiety given from the spacer allows the SBA to bind to the more flexible β -GalNAc **3.15**, but not to the β -GalNAc **3.14**. The successful binding can be explained by sugar participation in a hydrogen bond network between the acetate group of the sugar moieties and the side chain of asparagine 88 (Asp 88) of the lectin, as well as between the triazole ring and the same Asp 88 of the lectin.^[20,21] The fluorescence intensities of SBA on PEPperPRINT slides followed the same binding trend as ConA, but the binding to the tetravalent vs. the monovalent structures only increased about 6-fold. Despite the fact that ConA and SBA differ in their sugar specificity, both lectins have similar binding site orientation and ligand recognition mechanism.^[19] Finally, on the PolyAn slide surfaces, SBA seems to prevent a multivalent effect (i.e., only linear intensity increase), for this specific lectin concentration.

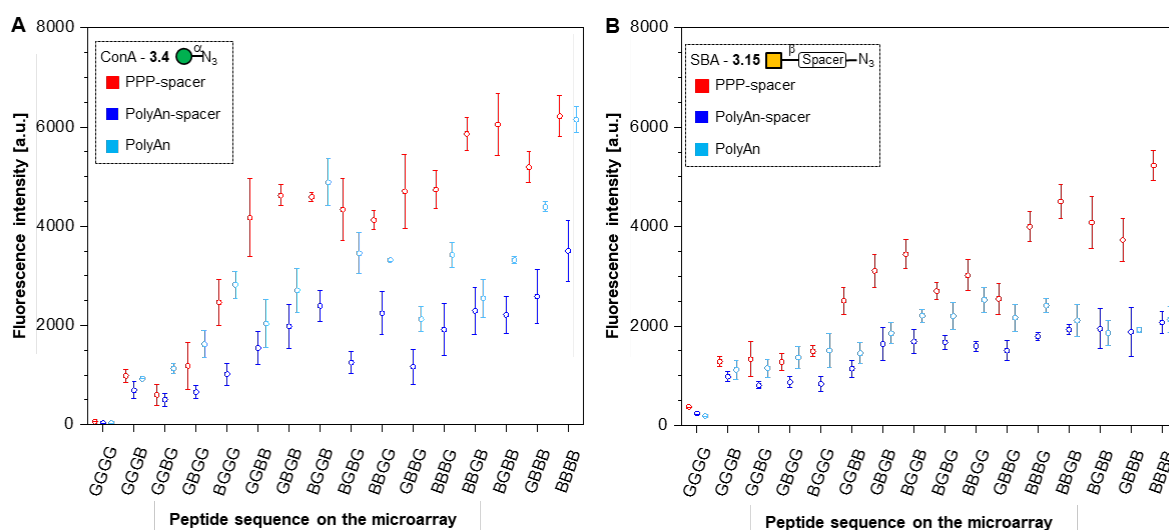


Figure 3.9: Fluorescence staining intensities of respective sugar azides with their corresponding lectins: A) α -Man **3.4** with ConA at a concentration of 100 μ g/mL; and B) β -GalNAc **3.15** with SBA at a concentration of 10 μ g/ml, on PEPperPRINT slides with spacer (PPP-spacer; red), and on PolyAn functionalized slides with (dark blue) and without PEG-spacer (light blue).

Evaluation of Peanut agglutinin binders: For the PNA binding assay, β -Gal **3.7** and **3.13** were used. No binding was obtained for PNA on the PEPperPRINT-spacer slide for both sugar azides, whereas on PolyAn surfaces with and without spacer, a very weak interaction

was identified. For better understanding, staining was repeated with higher lectin concentration (100 $\mu\text{g}/\text{mL}$), resulting in insufficient binding on the PEPperPRINT surface, and a visible but weak fluorescence for both PolyAn slides (Figure 3.10) on the hydrophobic peptide backbone. According to literature, the structure of this non-glycosylated lectin has

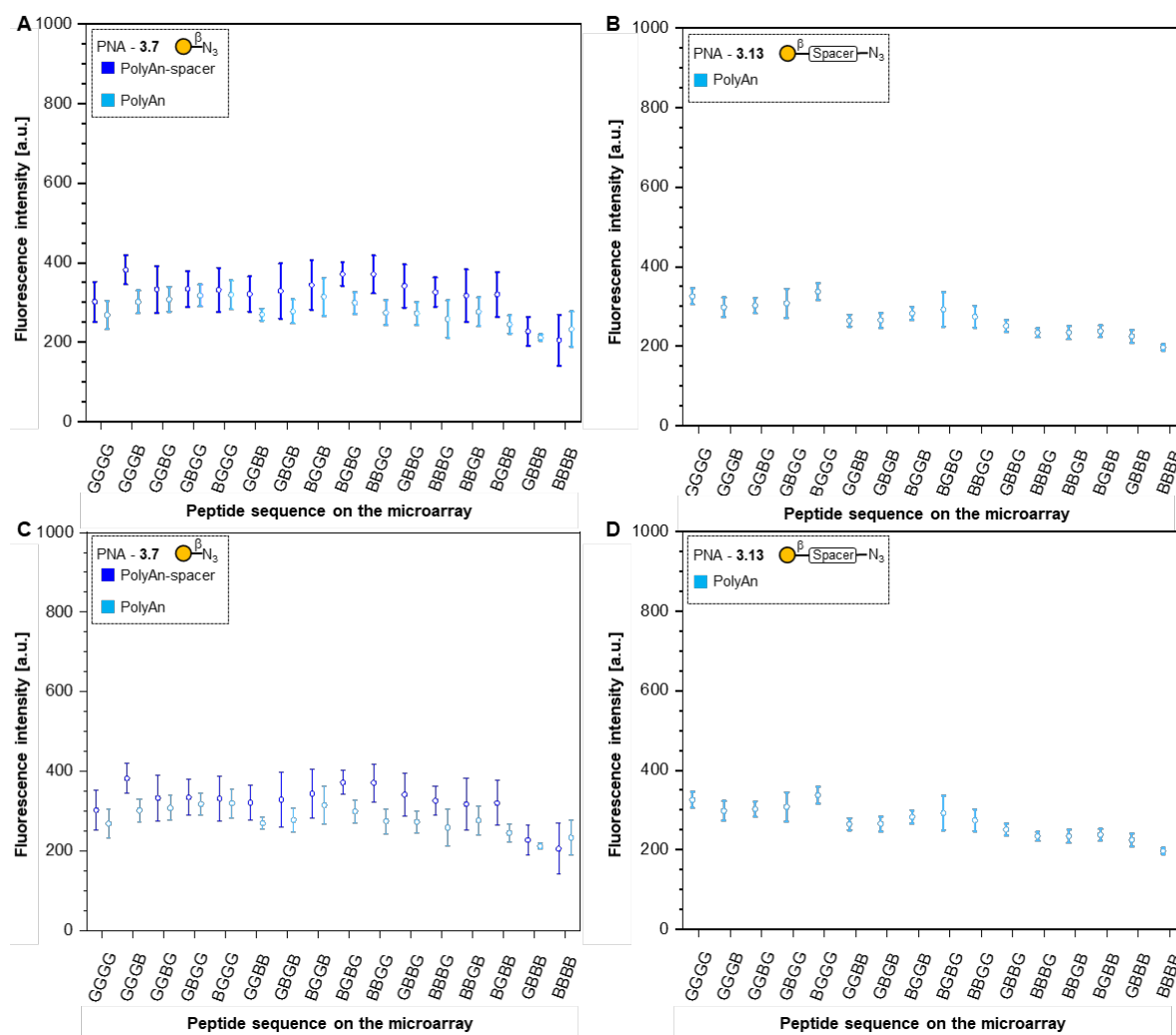


Figure 3.10: Fluorescence staining intensities of respective β -Gal 3.7 and 3.13 with PNA (Rhodamine labeled, 10 $\mu\text{g}/\text{mL}$ and 100 $\mu\text{g}/\text{mL}$ lectin concentration): A) β -Gal 3.7 with 10 $\mu\text{g}/\text{mL}$ lectin concentration; B) β -Gal 3.13 with 10 $\mu\text{g}/\text{mL}$ lectin concentration; C) β -Gal 3.7 with 100 $\mu\text{g}/\text{mL}$ lectin concentration; and D) β -Gal 3.13 with 100 $\mu\text{g}/\text{mL}$ lectin concentration, on PEPperPRINT slides with spacer (PPP-spacer), and on PolyAn functionalized slides with (PolyAn-spacer) and without PEG-spacer (PolyAn).

been extensively studied, in regards to the distance between the carbohydrate recognition domains (CRDs) and the ligand recognition mechanism.^[16,17] In case of the β -Gal 3.7, the azide in the anomeric position might disturb the formation of all seven hydrogen bonds required for successful recognition, while the hydrophobicity of the PEPperPRINT surface could diminish the lectin binding. Thus, no binding was detected for β -Gal 3.13, despite the accessibility and flexibility given to the sugar moieties with the PEG-spacer. The distances

between the sugar moieties and the peptide backbone, as well as the length of peptide backbone were too small/short and as a result no cross-linked multivalent mode could be detected.

Evaluation of *Ricinus communis* agglutinin I binders: In contrast to PNA, RCA-I bound to both, β -Gal **3.7** (Figure 3.11A) and **3.13** (Figure 3.11B). In the case of the less flexible β -Gal **3.7**, RCA-I revealed similar binding trends on all used substrates. The highest binding was achieved for the tetravalent sugar display, while in the monovalent scaffolds, the fluorescence intensity was increased linearly with the position of the Pra in the peptide tetramer. Higher fluorescence signals were obtained for Pra located further from the solid support (strongest binding for BGGG). A similar behavior was observed for the divalent and the trivalent scaffolds. Strongest binding on the divalent system was attained for the structures having two terminal sugar azides (BBGG), and three terminal sugar azides (BBBG) for the trivalent system, whereas less intensity was observed on the scaffolds with an intermediated glycine (BBGB, BGBB). Based on these findings, it was assumed that the binding mechanism between RCA-I and the β -Gal **3.7** relies on the statistical/proximity effect. A chelating binding mechanism (*Section 1.3.2*) seems to be less likely because the Pra in the peptide scaffold are at maximum 11 Å apart. The CRDs of RCA-I display a distance of ≈ 100 Å.^[15]

For the more flexible β -Gal **3.13**, the binding intensities of RCA-I were already at least 4-folds higher for the monovalent structures in comparison to the β -Gal **3.7**. The hydrophilic spacer increased the flexibility of the sugar moiety and as a result the distance of the triazole ring. This interspace allowed higher lectin-sugar accessibility, resulting in a much more pronounced multivalent recognition with the tetravalent structures reaching a maximum (i.e., saturation) intensity at the tested lectin concentration. The same binding trend was detected on all used slides, with 2- to 3-fold lower general intensity on both PolyAn slides. Comparing both PolyAn slides, stronger binding was detected on the more hydrophilic PolyAn slide without spacer, while the intensities were again higher on PEPperPRINT slides.

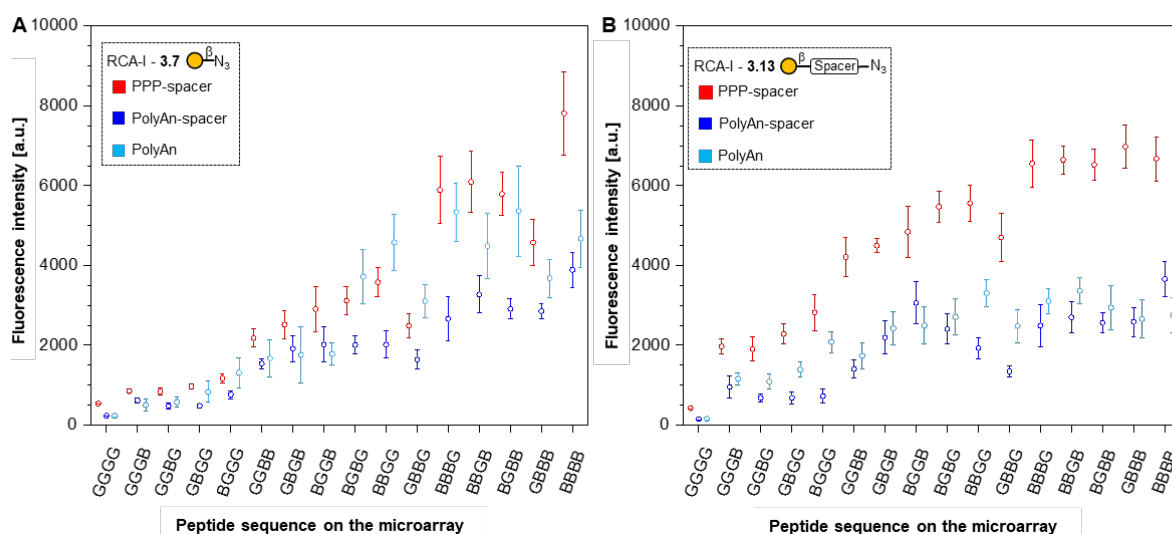


Figure 3.11: Fluorescence staining intensities of respective A) β -Gal 3.7, and B) β -Gal 3.13 with RCA-I at a concentration of 10 μ g/mL, on PEPperPRINT slides with spacer (PPP-spacer; red), and on PolyAn functionalized slides with (dark blue) and without spacer (light blue).

Evaluation of *Dolichos biflorus* agglutinin binders: DBA is a glycoprotein with specificity towards terminal non-reducing GalNAc structures, showing unique high specificity toward α -GalNAc moieties.^[18] Herein, the binding behavior of DBA was tested towards the β -GalNAc 3.14 and the flexible β -GalNAc 3.15, to determine whether binding on beta residues can be achieved *via* changes on the anomeric center and the hydrophobicity of the solid support. On PEPperPRINT slides, no interaction was detected, while on PolyAn surfaces, a weak interaction with the peptide backbone (GGGG) for both sugar azides was identified. For better understanding, the staining intensities of the plain peptides and the formed glycopeptides were compared. From these experiments, it was noticed that the further apart the sugar moiety was from the peptide scaffold, the better the binding between lectin and glycopeptides. The fluorescence was rather constant in the plain peptide and not as high as for the screened glycopeptides. Less binding was detected on the hydrophilic surfaces, resulting in weak lectin binding (Figure 3.12).

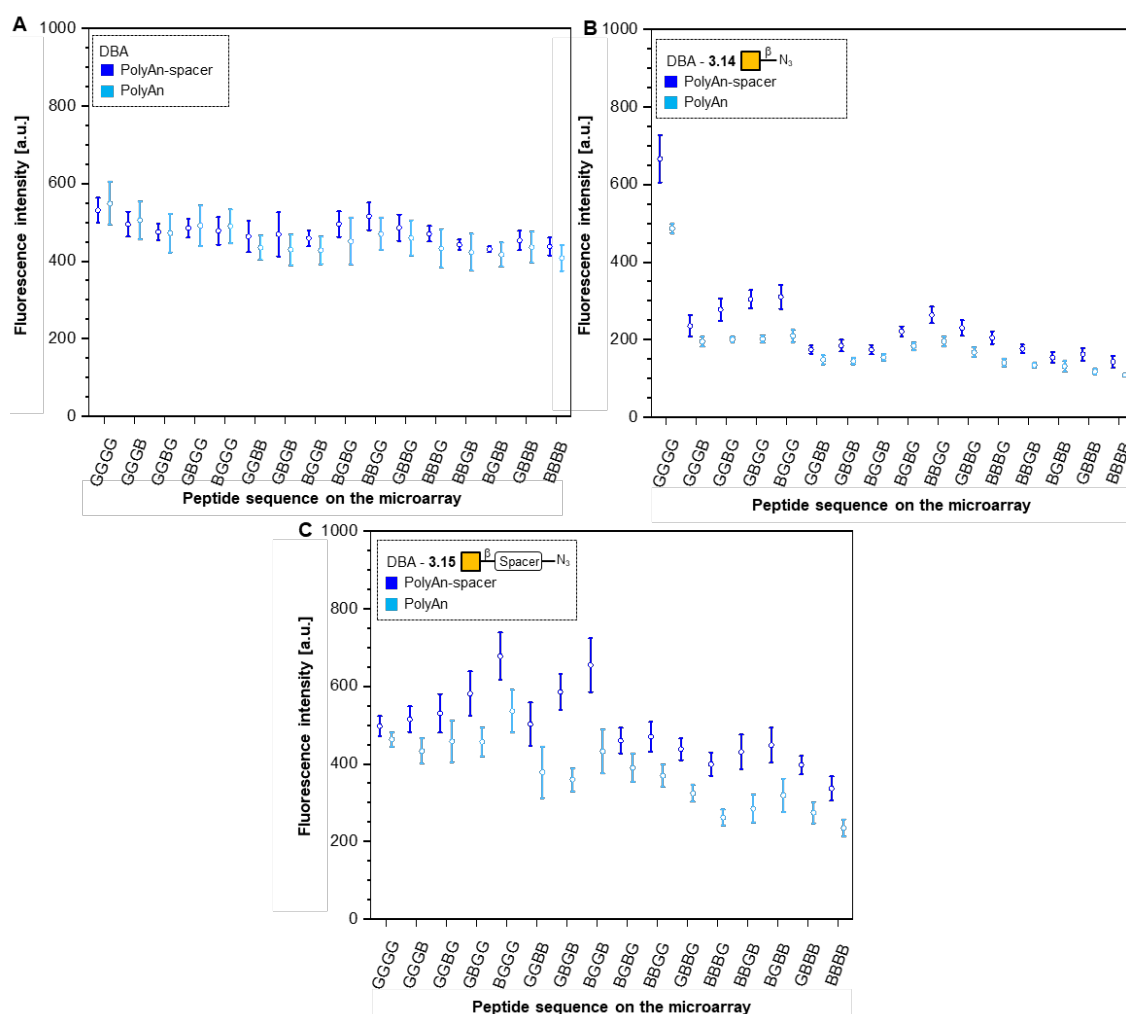


Figure 3.12: Fluorescence staining intensities of (A) plain peptide scaffolds, (B) GalNAc **3.14**, and (C) GalNAc **3.15**, with DBA (Rhodamine labeled, 10 $\mu\text{g/mL}$ concentration) on PolyAn functionalized slides with (PolyAn-spacer) and without (PolyAn) PEG-spacer.

Evaluation of Wheat germ agglutinin binders: In contrast to the already used lectins, WGA has a homodimeric structure, binding selectively to GlcNAc and Neu5Ac residues.^[15] Thus, the binding behavior of WGA was tested towards the β -GlcNAc **3.16** and **3.17**. Stronger binding of WGA was detected on structures bearing the more flexible **3.17** than the **3.16**. Two different lectin concentration were implemented for the glycopeptides formed with both sugar azides, since incubation with the standard lectin concentration (10 $\mu\text{g/mL}$) led to high saturation of WGA. Specifically, saturation was attained on the tri- and tetravalent tetrapeptide scaffolds on the hydrophilic PolyAn microarrays, whereas it was better controlled on the hydrophobic PEPperPRINT slides.

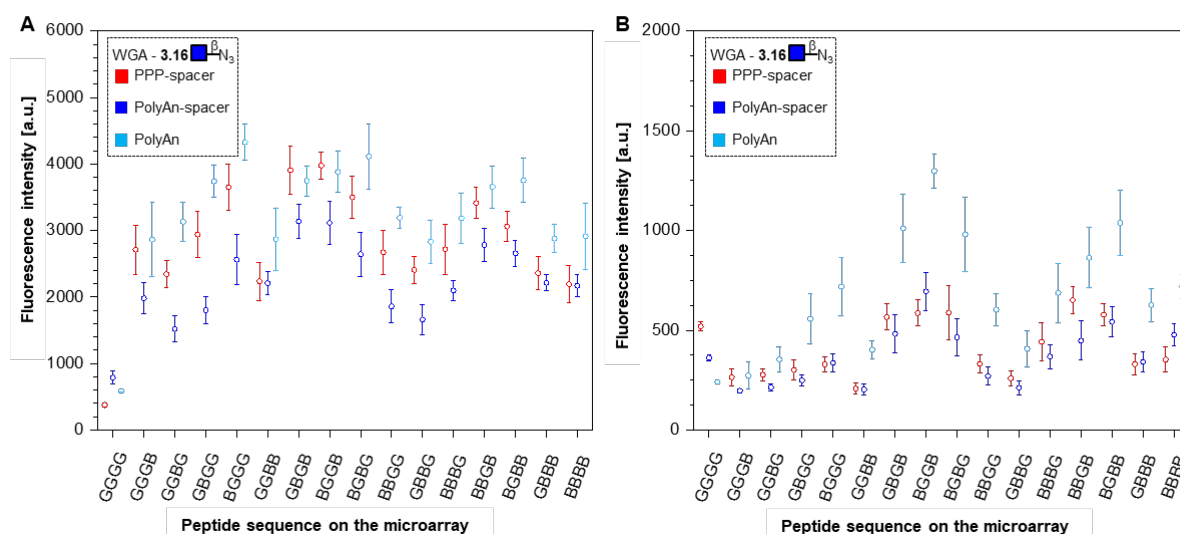


Figure 3.13 : Fluorescence staining intensities of respective sugar azides **3.16** with WGA: A) at a concentration of 10 $\mu\text{g/ml}$, and B) at a concentration of 0.2 $\mu\text{g/mL}$ on PEPperPRINT slides with PEG-spacer (PPP-spacer; red), and on PolyAn functionalized slides with (dark blue) and without PEG-spacer (light blue).

Despite this effect, for the β -GlcNAc **3.16** (Figure 3.13A), the binding trend of WGA was the same on all used slides. On the monovalent structures, increased fluorescence intensities were detected for scaffolds with terminal Pra (BGGG, GGGB). Additionally, remarkable was the spacing impact between the solid support and the sugar moieties. In the divalent systems, scaffolds with two neighboring Pra (GGBB, BBGG, GBBG) showed less binding intensities, whereas structures with non-neighboring Pra (GBGB, BGGB, BGBG) stronger binding. The theoretical spacing of the scaffolds with two adjacent Pra was calculated to be ≈ 2.1 nm, while in the non-adjacent ≈ 0.7 nm and ≈ 2.3 nm, respectively. Binding on the trivalent system indicated that the intermediate Gly (BBGB, BGBB) increases the binding strength, in comparison to the structures with terminal glycine (GBBB, BBBG). To control the saturation, the concentration of WGA was decreased 50-fold (0.2 $\mu\text{g/mL}$) (Figure 3.13B) with the intensities to be 2.5-fold lower, but with no significant change on the recognition pattern. For the monovalent scaffolds, linear increase of fluorescence was obtained with the position of the Pra in the peptide tetramer (GGGB > GGBG > GBGG > BGGG), which was inverse to most other lectins. On the bi-, tri- and tetravalent system, the same binding mode was attained as previously explained. Thus, it can be concluded that a surface and concentration dependent binding for WGA was detected due to chelating effect.

For glycopeptides bearing the β -GlcNAc **3.17** on PEPperPRINT slides, the intensities attained at high lectin concentration for the mono- and divalent structures were already reaching a plateau/saturation (Figure 3.14A), whereas at low concentration, the total intensity was reduced (Figure 3.14B). Yet, a somewhat decreased intensity for trivalent structures was apparent, which was considered as a density or spacing related effect. Notably, for

WGA, the monovalent structure GGGB had a stronger binding (sugar closer to the surface), while for all other lectins the opposite trend was detected (BGGG, sugar furthest away from the surface, stronger binding). In contrary, on the PolyAn surface with spacer, WGA showed a generally higher intensity in the assay with high concentration. For the low concentration, the same PolyAn surface showed a lower intensity, but still the same trend.

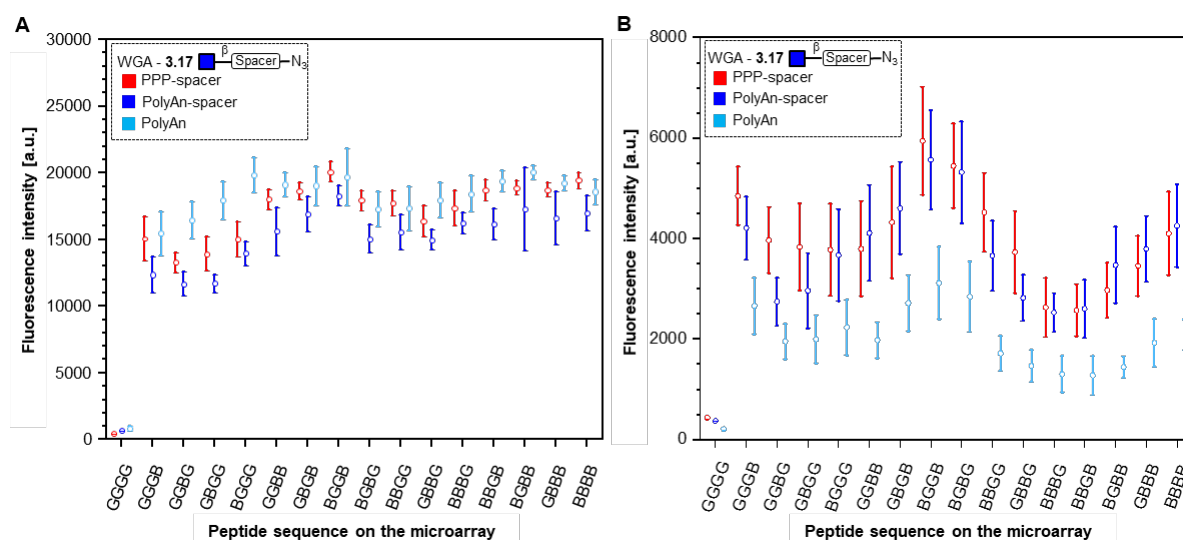





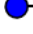







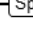


Figure 3.14: Fluorescence staining intensities of respective sugar β -GlcNAc **3.17** with WGA: A) at a concentration of 10 $\mu\text{g/ml}$, and B) at a concentration of 0.2 $\mu\text{g/mL}$ on PEPperPRINT slides with PEG-spacer (PPP-spacer; red), and on PolyAn functionalized slides with (dark blue) and without PEG-spacer (light blue).

Binding assay of C-type lectins: For the binding assay of the mouse-derived C-type lectins (mLangerin, mMincle, and mMGL-1), all synthesized sugar monomers **3.4-3.7**, **3.14**, **3.15** and the more flexible β -Gal **3.13** were used. Thus, structures containing the α -Man **3.4** were incubated with mLangerin and mMincle. Glycopeptides with β -Gal **3.7**, β -Gal-PEG3 **3.13**, and β -GalNAc **3.14** were incubated with mMGL-1, and structures containing α - and β -Glc **3.5-3.6** incubated with mMincle. Since all used lectins were fused with human Fc antibody fragment,^[238] secondary antibody staining to screen the result was required using the goat polyclonal anti-human IgG Fc DyLight™ 650. Regardless the multiple lectin concentrations, buffers, and anti-human IgG concentrations (1:1000 and 1:500, secondary antibody staining) screened, it was not possible to detect any binding (Table 3.1).

Table 3.1: Glycan-Glycan binding protein assays with C-type lectins. No binding is represented (×).

Entry	Lectin	Conc. [$\mu\text{g}/\text{mL}$]	Specificity [term. sugar]	Buffer	Results
1	mLangerin	10	 N_3	A	×
2	mLangerin	10	 N_3	A	×
3	mMincle	10	 N_3	A	×
4	mMincle	10	 N_3	A	×
5	mMincle	10	 N_3	A	×
6	mMGL-1	10	 N_3	A	×
7	mMGL-1	10	 N_3	A	×
8	mLangerin	30	 N_3	A	×
9	mLangerin	60	 N_3	B	×
10	mMGL-1	10	 N_3	B	×
11	mMGL-1	10	 N_3	B	×
12	mMGL-1	10	 Spacer N_3	B	×
13	mMGL-1	60	 N_3	B	×
11	mMGL-1	60	 N_3	B	×

- Buffer A: 50 mM HEPES, 100 mM NaCl, 1 mM CaCl_2 , 1 mM MnCl_2 , 10% blocking buffer, 0.05% Tween 20, pH 7.5.
- Buffer B: 10 mM HEPES, 1 mM MgCl_2 , 1 mM CaCl_2 , 0.01% Tween 20, 2% BSA, pH 7.42.

3.2.5. Synthesis of heteromultivalent neo-glycopeptides

In all previously described *Sections*, the synthesized structures were displaying only one sugar azide type. However, the inherent heterogeneity of glycans in biological systems makes the synthesis and the investigation of heteromultivalent glyco-oligomers a promising target. Interestingly, Ponader *et al.*,^[239] showed that heteromultivalent structures bearing Man, Gal and Glc sugar moieties, have higher affinities towards ConA than the homomultivalent analogues.^[239] Regardless of ConA, the presence of non-binders (e.g., Gal moieties) on the synthesized ligands promoted a steric shielding, yielding higher affinities and it was considered that non-binders suppress the clustering of the receptors on the multivalent ligand. Inspired by this work, a sequential synthesis protocol for PolyAn slides was developed (capping between each step and, de-acetylation with NaOMe before the binding assays), which should be further optimized and investigated (Figure 3.15). As proof of concept, hetero-structures bearing Man and GlcNAc moieties were synthesized. Homo-Man and homo-GalNAc structures were stained with ConA (red spots Figure 3.15D) and WGA (green spots Figure 3.15D) respectively, serving as positive controls, while the peptide back bone served as negative control. As additional negative controls, homo-Man and homo-

GalNAc structures were also stained with WGA and ConA respectively (no binding detected). The synthesized hetero-structures were stained with both lectins showing lectin intercalation despite the position of the respective sugar that should be further investigated (yellow spots Figure 3.15D). This concept validation, showed the prospects and urged further evaluation of the binding mode with different lectins and sugar combinations. Characterization and evaluation of the binding mode should also be considered. For this experiment, stepwise synthesis was achieved by implementing the already reported conditions (pattern and parameters of the first two layers of Figure 3.2), resulting in different fluorescence intensities due to variable number and positions of sugar moieties.

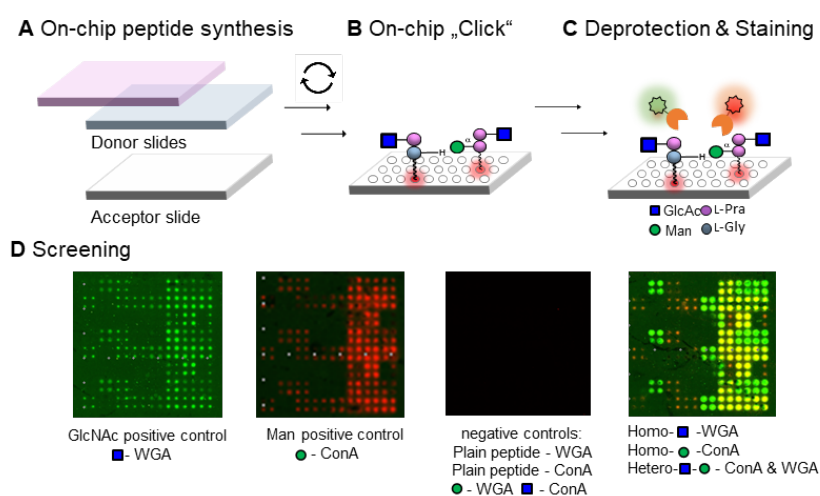


Figure 3.15: General overview of protocol for heteromultivalent glycomimetics synthesis. Suggested modules for on-chip hetero-structure synthesis: A) cLIFT transfer and coupling of the first amino acid layer, capping; B) on-chip CuAAC of first sugar azide; Fmoc-deprotection, and repetition of modules A) and B) upon completion. C) Deprotection with NaOMe in MeOH and screening of the result after fluorescent staining with the corresponding fluorescently labelled lectin. Preliminary results are reported for the two positive controls containing homo-structures of GlcNAc-WGA (green) and Man-ConA (red), negative controls containing Man-WGA, GlcNAc-ConA, peptide backbone with ConA and WGA (no staining detected), and hetero-structures contain GlcNAc-Man moieties in close proximity (yellow). Cross reactivity was observed between the two lectins in the monovalent structures regardless of the corresponding binding lectin in the well bearing homo and hetero-structures.

3.3. Conclusions

A flexible, facile approach to synthesize defined multivalent glycopeptides on-chip was developed. As a proof-of-concept, seven sugar azides were tested with ConA and two sugar azides with hLangerin on the protein resistant PEPperPRINT surface. For ConA, strongest binding was detected towards α -1,2-linked di-Man **3.10**, and for hLangerin towards β -GlcNTs **3.11**. The surface dissociation constant of ConA with Man **3.4** was also evaluated to be in the low micromolar range.

To investigate the impact of surface functionalization towards lectin binding, different commercial surfaces (PEPperPRINT with spacer, PolyAn with spacer and PolyAn without spacer) were screened with nine sugar azides in respect to their specific plant and animal lectins. From this study, lectin binding showed to be spacing, density, surface and concentration dependent. For all applied lectins, PEPperPRINT slides provided generally higher signal intensities than the PolyAn slides, with the exception of DBA. For better understanding, the (water) contact angle of the surfaces was experimentally determined, showing that PEPperPRINT slides are more hydrophobic, compared to the hydrophilic PolyAn slides that maintain their character even after the spacer is attachment.

In general, most plant lectins showed a multivalent binding effect that mainly was valency dependent (with exception of the WGA). A saturation binding trend for divalent structures was detected for WGA on all microarrays, due to the chelating binding mode, leading to cross-linking. Yet, no sugar binding was observed for PNA and DBA on PEPperPRINT slides, while weak interaction was obtained on PolyAn slides with DBA. On PolyAn slides with and without spacer, most lectins showed a more linear (less multivalent) increase in the binding mode by increasing the number of the flexible azides bearing a spacer on the anomeric C-1 position. For the less flexible sugar azides, a multivalent trend was observed. The molecular spacing of the sugars on the tetrapeptides had a similar impact on the ConA, SBA, and RCA-I assay. Scaffolds with the same theoretical spacing, such as GBGB and BGBG, showed different binding strengths with the latter typically showing a stronger binding strength. Divalent structures with larger spacing (BGGB) showed stronger binding than the more adjacent scaffolds (e.g. GBBG). Lastly, binding for the mouse-derived C-type lectins was not identified, while the first attempt towards the synthesis of heteromultivalent structures on the solid support showed promising results that should be further investigated

3.4. Outlook

Future investigations will require screening of different mono- and disaccharides, such as lactose **3.18** and the T-antigen like azide **3.19** with different plant lectins such as PNA. In case of DBA, α -GalNAc **3.20** and **3.21** residues should offer a much higher binding ability than the β -GalNAc residues. Additionally, longer peptide scaffolds should be synthesized, as well as longer linkers (e.g., PEG5) should be introduced between the anomeric position and the peptide backbone, to increase the size and the flexibility of the synthesized structures (Figure 3.16).

For C-type lectins, Di Maio *et al.* recently reported a microarray assay with multivalent display of mono- and di-Man, where different C-type lectins (DC-SIGNR ECD, trivalent Langerin ECD, monomeric Dectin-2 ECD) were screened.^[168] These lectins selectively and strongly bind to the α -1,2-linked di-Man **3.10**, but almost no binding could be detected towards the α -Man **3.4** monomer. Thus, future screening should be focused on disaccharides such as α -1,6-linked di-Man **3.9** and α -1,2-linked di-Man **3.10** with higher valency. Direct fluorescent labeling of the C-type lectins might also improve the detection mode, while the replacement of mouse-derived lectins with human lectins, e.g., for Langerin, may provide more information (Figure 3.16).

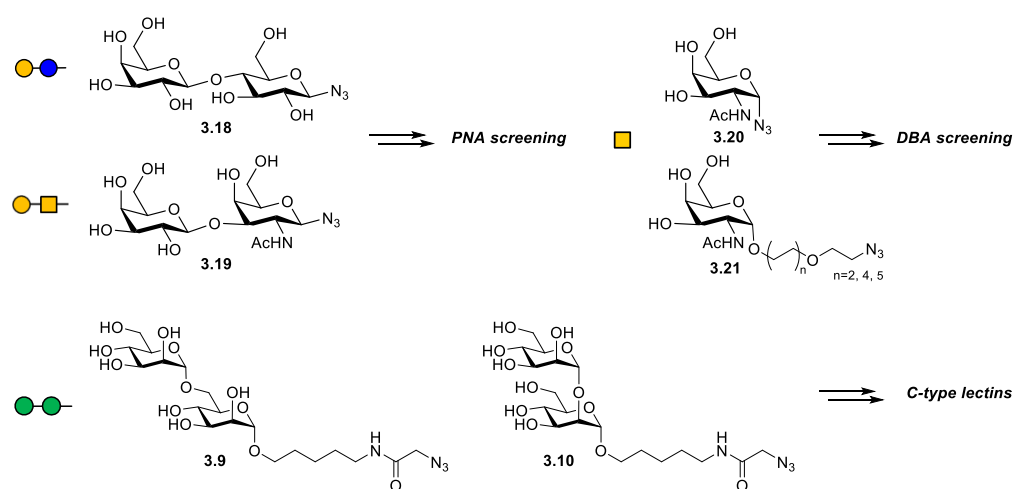


Figure 3.16: Additional sugar azides can be used for the generation of the neo-glycopeptides for plant and C-type lectin recognition.

Apart from the glass surface coating, it was observed that the molecular orientation on the scaffold also has an impact on the multivalent display: The theoretical spacing between the two scaffolds BGBG and GBGB has been considered almost identical, but yet, the observed binding strength was different, due to the opposite orientation of the scaffold on the solid support. In the future, this should be further investigated with molecular dynamics simulations. In addition, the binding strength in more flexible systems should be further investigated. Therefore, longer spacers could be installed between the anomeric positions and the sugar moiety as well as longer peptide scaffolds could be synthesized *via* replacing the used L-propargylglycine **3.2**, with L-propargyl-lysine **3.22**, propargyloxycarbonyl-L-2,3-diaminopropionic acid **3.23**, or with propargyl-L-tyrosine **3.24** allowing to study any steric effects that may occur between the sugar moieties, the formed triazole rings and the lectin (Figure 3.17). Glycine **3.1** may also be replaced in the future with β -alanine **3.25** or with

different hydrophobic (e.g., FmocHN-caprylic acid **3.26**), and hydrophilic linkers (e.g., Fmoc-8-amino-3,6-dioxaoctanoic acid **3.27**).

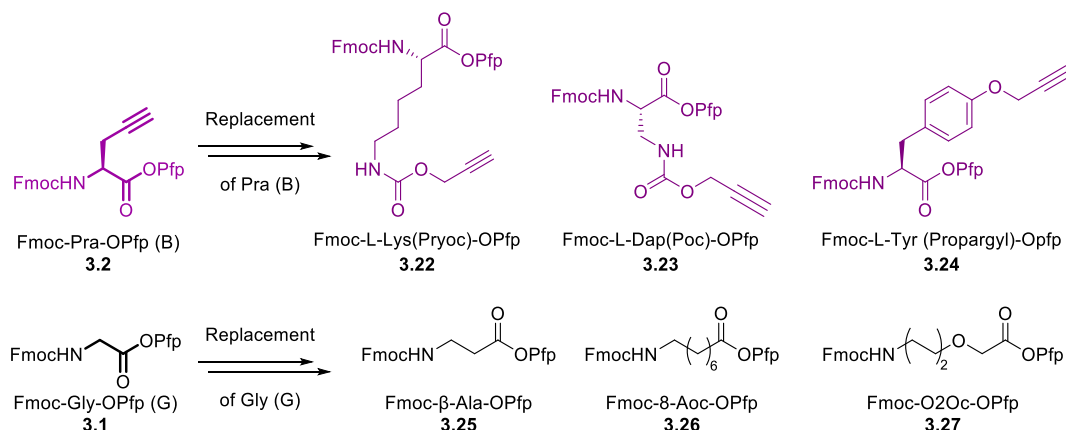


Figure 3.17: Other building blocks that can be used for on-chip generation of interesting glycomimetics.

Lastly, further investigations on the synthesis and the screening of heteromultivalent binding modes on differently functionalized surfaces with ConA and a variety of C-type animal lectins will help to understand fundamental natural binding modes and investigate nature's recognition mechanism. These investigations will give more insights regarding the binding behavior of lectins broadening the field of biomedical and immunological research.

3.5. Experimental Section

General remarks

The starting materials, applied solvents, deuterated solvents (99.5 atom% D), and chemicals were purchased from common suppliers such as *Sigma-Aldrich*, *Alfa Aesar*, *Tokio Chemical Industry (TCI)*, *Thermo Fischer Scientific*, *Acros Organics*, *Iris Biotech*, *Merck*, *BroadPharm* and used without further purification. 2-{2-[2-Azidoethoxy]ethoxy}ethyl 2-acetamido-2-deoxy-β-D-galactopyranoside (β-D-GalNAc-PEG3-azide) **3.15**, and 2-{2-[2-Azidoethoxy]ethoxy}ethyl 2-acetamido-2-deoxy-β-D-glucopyranoside (β-D-GlcNAc-PEG3-azide) **3.17** were obtained from *Conju-Probe*. Lectin Kit I, Rhodamine labeled (RLK-2200), containing: *Concanavalin A (ConA)*, *Dolichos Biflorus Agglutinin (DBA)*, *Peanut Agglutinin (PNA)*, *Ricinus Communis Agglutinin I (RCA-I/RCA-120)*, *Soybean Agglutinin (SBA)*, *Ulex Europaeus Agglutinin I (UEA I)*, and *Wheat Germ Agglutinin (WGA)* (2 mg/mL) was purchased from *Vector laboratories Burlingame, USA*, CF®633 ConA (1 mg/mL) from *Biotium, Inc., USA*. Anhydrous-solvents were dried on a Phoenix SDS-Flame-Proof Cabinet Mounted, JC-Meyer solvent purification system and stored in glass bottles over freshly

activated 3Å molecular sieves. Solids were added directly as powders and liquids by using syringes equipped with steel cannulas. Reactions were carried out at room temperature, if no other temperature is indicated. Solvents were removed at 40 °C with a rotary evaporator under reduced pressure. If not mentioned otherwise, saturated, aqueous solutions of inorganic salts were used. Thin layer chromatography (TLC) using silica gel coated aluminium plates (*MACHEREY-NAGEL*, pre-coated TLC sheets ALUGRAM® Xtra SIL G/UV₂₅₄ or *Merck*, pre-coated TLC sheets 60 F₂₅₄) was applied to monitor reactions. Detection was performed either with UV light ($\lambda = 254 \text{ nm}$) or by immersing the TLC plates in “Seebach staining solution” (mixture of phosphomolybdic acid hydrate, cerium (IV) sulfate tetrahydrate, sulfuric acid and water). Purification of the nonpolar products was done *via* flash chromatography using *MACHEREY-NAGEL* silica gel 60 (0.040 × 0.063 mm) and quartz sand and very polar compounds were purified by *MACHEREY-NAGEL* silica gel, Chromafix® C₁₈ ec cartridge. Eluents were used directly in *p.a.*, HPLC quality or distilled.

Nuclear magnetic resonance spectroscopy (NMR)

NMR spectra were measured on the following NMR devices:

- ¹H NMR 400 MHz and ¹³C NMR 101 MHz: Bruker Ascend 400
- ¹H NMR 400 MHz and ¹³C NMR 101 MHz: Varian 400 MHz
- ¹H NMR 600 MHz and ¹³C NMR 150 MHz: Varian 600 MHz

Chemical shifts δ are reported in ppm and are adjusted to internal standards of the residual proton signal of the deuterated solvent (D₂O: 4.79 ppm for ¹H, MeOD: 3.31 ppm for ¹H and 49.00 ppm for ¹³C spectra). The spectra were measured at room temperature. Having symmetrical signals, the center of the signal is given and for multiplets the area. The following characterization was used: s = singlet, d = doublet, t = triplet, q = quartet, m = multiplet or combinations like dd = doublet of doublet or dt = doublet of triplet. Coupling constants (*J*) are given in Hz. The spectra were evaluated according to 1st order. For ¹H NMR spectra, the correlation of the signals was done according to the multiplicities.

Mass spectrometry (HR-MS)

High-resolution mass spectrometry (HR-MS) was performed on a Waters Xevo G2-XS QToF device using ESI (electrospray ionization) as the ionization method. The abbreviation [M+Na]⁺ refers to the product–sodium adduct. ESI mass spectra were run on IonSpec Ultima instruments.

High-performance liquid chromatography (HPLC)

To identify the purity of the crude used products, analytical HPLC (Agilent 1200 Series spectrometer) was used:

Method A: Synergi Hydro RP18 column, 250 x 4.6 mm, flow rate of 1 mL/min with H₂O (0.1% formic acid) as eluents [isocratic (5 min), linear gradient to 35% MeCN (35 min), linear gradient to 100% MeCN (5 min)].

Method B: Synergi Hydro RP18 column, 250 x 4.6 mm, flow rate of 1 mL/min with 5% MeCN in H₂O (0.1% formic acid) as eluents [isocratic (5 min), linear gradient to 100% MeCN (35 min), linear gradient to 100% MeCN (5 min)].

Method C

Method C: Synergi Hydro RP18 column, 250 x 4.6 mm, flow rate of 1 mL/min with H₂O (0.1% formic acid) as eluents [isocratic (5 min), linear gradient to 20% MeCN (35 min), linear gradient to 100% MeCN (5 min)].

Infrared spectroscopy (IR)

IR spectra were recorded in a FT-IR Perkin-Elmer 2000 spectrometer.

Size exclusion chromatography (SEC)

Bio-Gel® P2 (Bio-Rad) was used for size exclusion chromatography for the purification of α -azido B-trisaccharide **3.14**.

Elemental analysis (EA)

Elemental analysis was carried out at the Elemental Analysis Center of the Complutense University of Madrid, using a Perkin Elmer 2400 CHN.

pH measurements

pH was determined using a FiveEasy pH/mV meter F20, equipped with a plastic pH electrode LE438 from Mettler Toledo.

Laser transfer parameters

For the array synthesis, a spot pitch of 250 μ m was used. A laser scanning system with $\lambda = 488$ nm wavelength and 120 mW maximum output power was used with a laser focus diameter of ~ 20 μ m. For **PEPperPRINT slides**, a laser power of 80 mW and a pulse duration of 6 ms per spot was applied, while for **PolyAn slides**, a laser power of 60 mW with a pulse

duration of 6 ms was applied. The final spot diameter was about 150 μm . The transfer was repeated with different donor slides until the desired amino acid pattern was completed.

Laser transfer system

Our laser system consists of a 200 mW TOPTICA iBeam smart 488-S laser with a wavelength of 488 nm (TOPTICA Photonics, AG, Gräfelfing/Bayern, Germany), which is passed through a 1:10 beam expander and a Racoon 11 laser scanning system (ARGES GmbH, Wackersdorf/Bayern, Germany), equipped with an f-Theta lens (S4LFT5110/322, Sill Optics GmbH, Wendelstein/Bayern, Germany). High quality laser transfer with reproducible results at various positions is achieved with scanning the laser beam in a 66 mm \times 66 mm plane. The acceptor slide in the lasing areas was aligned with three mechanical springs and a vacuum mechanism.^[197]

Fluorescence scan and analysis of fluorescence intensity

For each sugar azide, the reaction was performed in a separate cavity of a 16-well format incubation chamber (PEPperPRINT GmbH, Germany). Each well contained three sets of quadruplicates of the same single sugar azide and tetrapeptide, giving twelve glycopeptide replicas of each synthesized structure. The median or the mean of the fluorescence intensity of the scanned area was determined with the microarray analysis software GenePix Pro 6.0. For the analysis, the mean value of the twelve spot medians was calculated. Spots (i.e., outlier/artifacts) with more than 40% standard deviation from the mean were excluded from calculations. A Molecular Devices microarray scanner, GenePix 4000B, San Jose, USA, was used for the analysis of all arrays. The detection wavelength was $\lambda = 523$ nm (for TAMRA fluorophore and Rhodamine RCA-I, PNA, SBA, DBA, WGA), with PMT gain 400 and 500 respectively, or $\lambda = 635$ nm (for CF[®]633 ConA), with PMT gain 600. The laser power was 33% for every measurement and the pixel size was 5 μm for high-resolution scans. The fluorescence scan of the FITC-langerin labeled neo-glycopeptides was done on the high-resolution microarray scanner GenePix 4300A (MolecularDevices, Sunnyvale/California, USA) using an excitation wavelength of $\lambda = 488$ nm at 5 mm resolution.

Contact angle measurements

The contact angle measurements were performed in an in-house build setup^[240]. It consists of a macroscopic top view, which is homogeneously illuminated with a green LED, and a telecentric side view illuminated *via* a pin hole. An environmental chamber allows controlling the vapor saturation. All measurements were performed at ambient conditions.

Preparation of solutions

- **Fmoc-deprotection:** A solution of 20% piperidine in dimethylformamide (DMF) (v/v) was prepared.
- **Capping:** A solution of 10% acetic anhydride (Ac₂O) and 20% *N,N*-diisopropylethylamine (DIPEA) in anhydr. DMF (v/v) was used.
- **Washing steps:** DMF (3 × 10 mL, 3 min each), methanol (MeOH) (1 × 10 mL, 2 min), and dichloromethane (DCM) (1 × 10 mL, 1 min).

3.5.1. Synthesis of sugar azides

Section has been removed for copyright reasons in the online version. For more information about this section please check:

Mende, M.*; **Tsouka, A.***; Heidepriem, J.; Paris, G.; Mattes, D. S.; Eickelmann, S.; Bordoni, V.; Wawrzinek, R.; Fuchsberger, F. F.; Seeberger, P. H.; Rademacher C.; Delbianco M.; Mallagaray A.; Loeffler F. F.; On-Chip Neo-Glycopeptide Synthesis for Multivalent Glycan Presentation, *Chem.Eur.J.*, **2020**, 26, 9954 –9963. <https://doi.org/10.1002/chem.202001291>

Tsouka, A.; Hoetzel, K.; Mende, M.; Heidepriem, J.; Paris, G.; Eickelmann, S.; Seeberger P. H.; Lepenies, B.; and Loeffler, F. F.; Probing Multivalent Carbohydrate-Protein Interactions with On-Chip Synthesized Glycopeptides Using Different Functionalized Surfaces, *Front. Chem.*, **2021**, 9:766932. <https://doi.org/10.3389/fchem.2021.766932>

3.5.2. Donor and acceptor slide preparation

Donor slide preparation

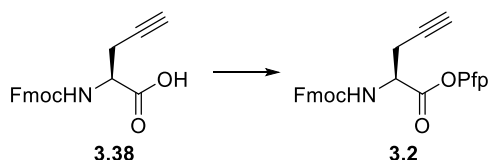
Microscope glass slides (Marienfeld Superio, Germany; size 76×26×1 mm, ground edges, pure white glass) were covered on one side with self-adhesive polyimide foil (Kapton, DuPont, USA, CMC Klebtechnik GmbH, Germany; thickness of polyimide layer approximately 25 µm, thickness of glue layer approximately 45 µm). A thin layer of the transfer material was placed on top of the polyimide foil by spin coating (80 rps, Schaefer Technologie GmbH, Germany; KLM Spin-Coater SCC-200).

Amino acid donor slide preparation

- Pre-activated amino acid (AA): Fmoc-glycine pentafluorophenyl ester, Fmoc-Gly-OPfp **3.1**, was used without prior activation, however two different spin coating solutions were prepared. Pentafluorophenyl (OPfp)-activated 9-fluorenylmethoxycarbonyl (Fmoc) protected L-glycine, (Fmoc-Gly-OPfp) **1** (3.00 mg), was pre-dissolved in dimethylformamide (DMF) (50 µL), while inert polymer matrix (27 mg) (SLEC PLT 7552,

Sekisui Chemical GmbH, Germany) was dissolved in dichloromethane (DCM) (450 μL), resulting in the final spin coating solution (500 μL).

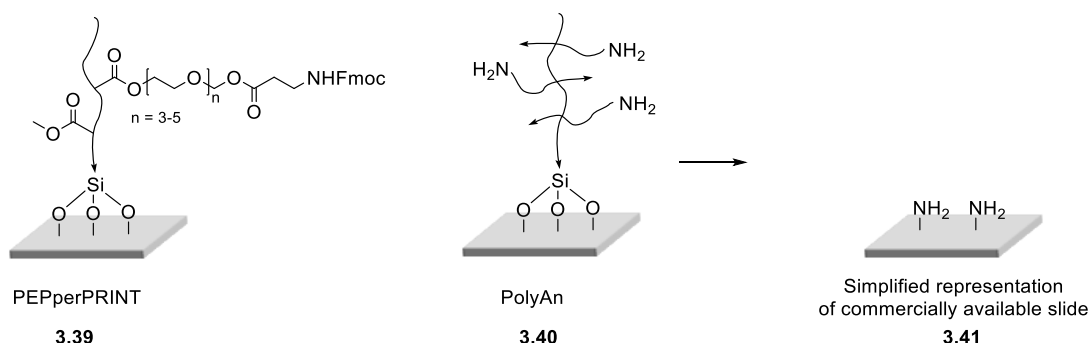
- *Non-pre-activated amino acid*: Fmoc-L-propargylglycine, Fmoc-propargyl-Gly-OH **3.38**, was prepared *in-situ* during the preparation of the spin-coating solution to form the pentafluorophenyl (OPfp)-activated amino acid **3.2**. Pentafluorophenyl (OPfp)-activated amino acid was used without isolation or further characterization.



Fmoc-propargyl-Gly-OH (**3.38**) (3.00 mg, 9.00 μmol , 1.00 equiv), *N,N'*-Diisopropylcarbodiimide (DIC) (1.40 μL , 9.00 μmol , 1.00 equiv), Pentafluorophenol (PfpOH) (1.60 mg, 9.00 μmol , 1.00 equiv) were dissolved in 50.0 μL anhydr. DMF in a vial, while 27.0 mg of inert polymer matrix (SLEC) were dissolved in 450 μL anhydr. DCM in another vial. The first solution containing the freshly activated amino acid was added into the second matrix solution. The final mixture was shaken for 2 min (vibrating orbital shaker) and afterwards the solution was spin-coated on top of the polyimide foil of the microscope glass slide, forming the thin layer of the transfer material.

Acceptor slide preparation

The commercially available 3D Fmoc-NH- β -Ala-PEGMA-co-MMA glass slide, PEPperSlide (**3.39**) from PEPperPRINT and 3D-Amino glass slides from PolyAn (**3.40**) are shown as simplified representations in the Figure below. *Fmoc-deprotection* of PEPperPRINT slides was needed to obtain the free amino groups on the glass slide functionalization.



Fmoc-deprotection of PEPperPRINT slides:

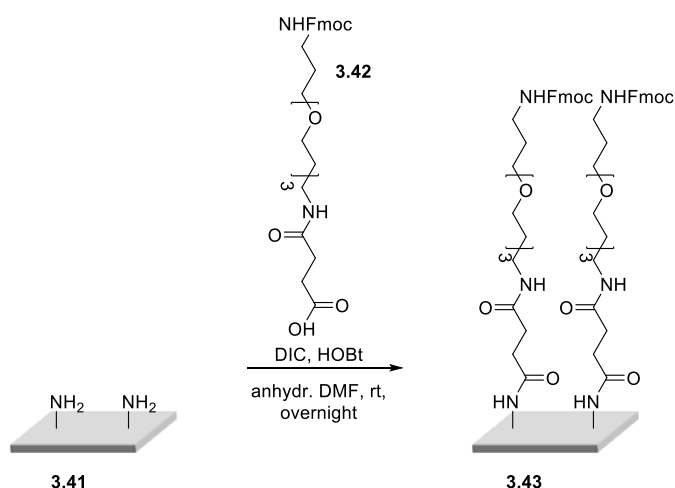
The 3D Fmoc-protected glass slide **3.39** was pre-swelled in DMF for 20 min on a shaker in a petri dish. Afterwards, the slide was immersed in 10 mL of Fmoc-deprotection solution for 20 min on a shaker. The slide was washed and dried in a jet of air to obtain the free amino groups on the glass slide **3.41**.

Acceptor slides without spacer

After pre-swelling, slides without spacer were subjected to pre-patterning. Initially, laser transfer and coupling of two layers of glycine was performed. Afterwards, the synthesis of the desired tetrapeptide scaffolds followed.

Acceptor slides with spacer

Spacer attachment:



N-Fmoc-*N*''-succinyl-4,7,10-trioxa-1,13-tridecanediamine (**3.42**) (Fmoc-TTDS-OH) (27.0 mg, 50.0 μmol, 1.00 equiv.) was dissolved in 250 μL of anhydr. DMF (peptide grade) in a vial. *N,N'*-diisopropylcarbodiimide (DIC) (23.2 μL, 18.9 mg, 150 μmol, 3.00 equiv.) and hydroxybenzotriazole (HOBT) (6.76 mg, 50.0 μmol, 1.00 equiv.) were added consecutively and the vial was shaken for a few seconds. The resulting solution was pipetted on the free amino glass slide **3.41** and another slide was placed on top of the first one (sandwich functionalization method). The slides were left overnight in a petri dish to react, and then washed and dried in a jet of air to obtain spacer-functionalized glass slide **3.43**.

Capping of unreacted amine groups:

The remaining unreacted free NH₂ groups on the acceptor slide **3.43** were subjected to acetylation for 30 min. The same process was repeated with a freshly prepared capping solution for another 30 min at room temperature (300 rpm). Then, the slide was dried in a jet of air to obtain the Fmoc-protected amine-spacer-functionalized glass slides with capped unreacted amine groups.

3.5.3. Parameter optimization for tetrapeptides synthesis

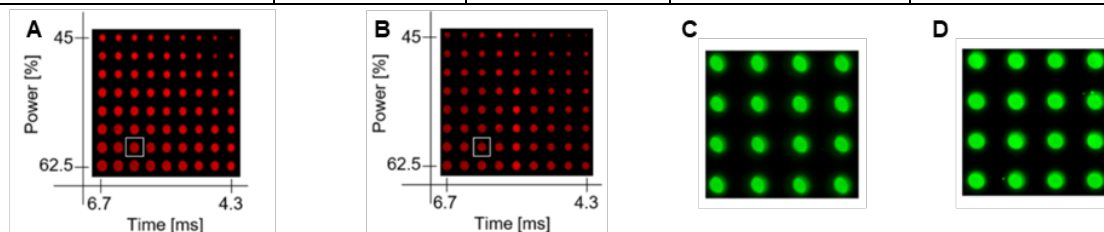
For a successful synthesis of tetrapeptides on the different solid supports, several parameters had to be tested. The key points that had to be investigated were: a) the amino acid concentration in the donor slide b); the laser power and pulse duration during the laser transfer of the material onto the solid support; c) the coupling time inside the oven to optimize the coupling efficiency.^[128]

- PEPperPRINT slide optimization

Initially for the preparation of the donor slides with already activated amino acids, e.g., Fmoc-Gly-OPfp **3.1**, 3.00 mg of the L-amino acid building block and 27.0 mg of inert polymer matrix were used, while in the case of the non-activated amino acids, Fmoc-Pra-OH **3.38**, *in-situ* activation was achieved by using 2.00 mg of L-amino acid and 18.0 mg of inert polymer matrix. During the optimization process, it was observed that the synthesis quality increased if the lasing parameters were set to 80 mW lasing power and 6 ms pulse duration, when the coupling was performed for 60 min at 95 °C. Additional experiments, shown that coupling time can be reduced from 60 min to 10 min for all amino acids.^[128] To ensure a homogeneous spot size throughout the synthesis, the coupling efficiency was compared for both amino acids for 10 min and 60 min coupling time. Single amino acid transfer of a (lasing power/pulse duration (x/y)) gradient pattern on PEPperPRINT slides, and coupling at 95 °C for 10 min and 60 min was carried out followed by staining of the transferred Gly (**3.1**) and Pra (**3.2**) with DyLight™ 633-B2 NHS ester and TAMRA azide dye **3.3** respectively. Spot size increase was detected for a coupling time of 10 min compared to the 60 min. However, screening of the stained Pra structures was challenging, since no fluorescence signal could be observed under these conditions. Self-quenching of the dye due to the energy transfer mechanism is one of the main reported challenges.^[230] To reduce the quenching effect, the PEPperPRINT slide was functionalized with a PEG-based spacer and pre-patterned with two layers of Gly prior to Pra coupling. Again, transfer of Pra **3.2** was performed using 80 mW

and 6 ms pulse duration. Staining of Pra showed that the obtained spot size of the pre-patterned glycine is larger than the size of propargylglycine spots. This can also be visually detected by the formation of a light green shade around each spot (Experimental Figure 3.1:). These shades appear to become smaller at 60 min oven coupling time compared to 10 min. To avoid visible shades around the spots for our peptide synthesis, equal amounts of Fmoc-Gly-OPfp (**3.1**) and non-activate Fmoc-Pra-OH (**3.38**) (3 mg of amino acid and 27 mg of inert matrix) were chosen and the coupling step of each layer was repeated twice to increase the synthetic yield and maintain the quality of the synthesized structures.

Entry	A	B	C	D
Amino acid	Fmoc-Gly-OPfp 3.1		Fmoc-Pra-OPfp 3.2	
Lasing parameters	Gradient pattern P: 45-77.5%, 60–100 mW ΔP : 2.5%, values: 14 Dot time: 1 ms Δt : 0.3 ms, values: 31		Power: 60%, 80 mW Pulse duration: 6 ms	
Pitch [μm]	250	250	250	250
Coupling time [min]	10	60	10	60
Surface modification	No modification		spacer-Gly-Gly	
Spot size [cm^2]	1.77×10^{-4}	1.20×10^{-4}	5.6×10^{-5}	4.3×10^{-5}



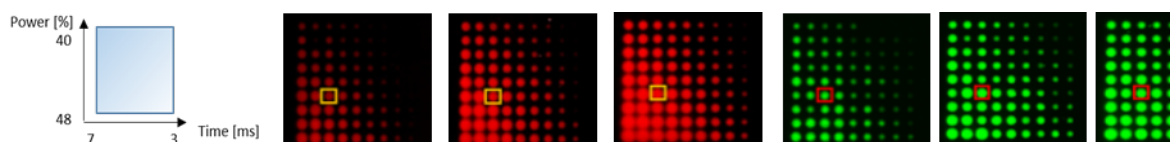
Experimental Figure 3.1: Comparison between stained glycine and propargylglycine spots on PEPperPRINT surfaces: A) Single transfer of a glycine gradient pattern and 10 min coupling (laser power/pulse duration) on a PEPperPRINT slide (6 ms and 60% power marked with a white square); B) Single transfer of a glycine gradient pattern and 60 min coupling (laser power/pulse duration) on a PEPperPRINT slide (6 ms and 60% power marked with a white square). Only an extract of the gradient pattern is shown. C) Single transfer of Fmoc-Pra-OPfp **3.2** on a pre-modified PEPperPRINT slide, and 10 min coupling time; D) single transfer of Fmoc-Pra-OPfp **3.2** on a pre-modified PEPperPRINT slide, and 60 min coupling time. Scanning parameters: Wavelengths 635/532 nm, PMT gain 400/600, power 33%, pixel size 5 μm . Distance between centers of two spots (pitch) is 250 μm .

- PolyAn slide optimization

In this case, for the preparation of the donor slides, the previously used amounts for the amino acids and inert matrix (3 mg of AA and 27 mg of inert polymer matrix) were used. Again, a gradient pattern was transferred from the AA donor slides onto unmodified and PEG-spacer modified PolyAn slides. The tested coupling time was 10 min. No quenching

effect was observed for the TAMRA azide dye labeling of Pra spots. Furthermore, no difference in spot size was recognizable, with or without spacer modification of the acceptor slide. However, the laser power, as used on PEPperPRINT surfaces (80 mW), resulted blurry and overlapping spots. Thus, an adjusted gradient transfer was performed with a subsequent coupling time of 10 min to reduce overall array manufacturing time and maintain the spot size. To investigate the number of required coupling repetitions within one amino acid layer for an optimal synthesis, transfer of the gradient pattern and coupling repeated three times (Experimental Figure 3.2). To achieve comparable spot sizes between Gly and Pra on PolyAn slides, lasing parameters of 60 mW and 6 ms were used. Three transfers seemed to be sufficient of one layer for good overall coupling quality. Moreover, the spot sizes of both amino acids after one transfer were comparable to the spot sizes of Gly on PEPperPRINT slides.

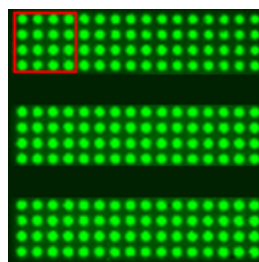
Amino acid	Fmoc-Gly-OPfp 3.1			Fmoc-Pra-OPfp 3.2		
Lasing parameters	Gradient pattern P: 40–48%, 50–62 mW ΔP : 1%, values: 9 Dot time: 1 ms Δt : 0.5 ms, values: 9					
Pitch [μm]	250			250		
Coupling time [min]	10			10		
Surface modification	Spacer			Spacer		
No. of transfers	I	II	III	I	II	I
Spot size [cm^2]	1.84×10^{-4}	2.28×10^{-4}	3.18×10^{-4}	1.17×10^{-5}	2.28×10^{-5}	2.22×10^{-5}



Experimental Figure 3.2: Comparison between glycine and propargylglycine spots on PolyAn surfaces. Up to three coupling repetitions of a gradient transfer of both amino acids is shown. Scanning parameters: Wavelengths 635/532 nm, PMT gain 400/600, power 33%, pixel size 5 μm . Distance between centers of two spots (pitch) is 250 μm for each microarray.

To determine the spot size of propargylglycine in a similar manner as on PEPperPRINT slides, a PolyAn slide was modified with a spacer and two layers of glycine. This was followed by a transfer of propargylglycine using 60 mW of laser power and a pulse duration of 6 ms. A spot size of $1.45 \times 10^{-4} \text{ cm}^2$ was calculated which is comparable in size with the results on PEPperPRINT slides (Experimental Figure 3.3).

Amino acid	Fmoc-Pra-OPfp 3.2
Laser parameters	P: 46%, 60 mW, pulse duration: 6 ms
Coupling time [min]	10
Surface modification	spacer-Gly-Gly
No. of transfers	III
Spot size [cm ²]	1.45x10 ⁻⁴



Experimental Figure 3.3: Spot size of coupled propargylglycine on PolyAn surfaces bearing the same modification as the PEPperPRINT slides (PEG-spacer-Gly-Gly). Transfer and coupling of the same pattern was repeated three times, using the respective lasing conditions. Scanning parameters: Wavelength 532 nm, PMT gain 400, laser power 33%, pixel size 5 μm . Distance between centers of two spots (pitch) is 250 μm .

3.5.4. CuAAC reaction

Quality control of synthesized tetrapeptide

CuSO_4 (530 μg , 3.36 μmol , 2.00 equiv.) and sodium ascorbate (998 μg , 5.04 μmol , 3.00 equiv.) were added to a mixture of 100 μL DMSO and 100 μL water in a vial. The vial was shaken for 5 min and, afterwards, the precipitate was centrifuged and the remaining solution was passed through a syringe filter (0.2 μm , polypropylene, and diameter 25 mm, Whatman). TAMRA azide **3.3** was dissolved in this solution (concentration of 0.1 $\mu\text{g}/\text{mL}$) and, then, applied on the acceptor surface ($c=8.4$ $\mu\text{mol}/\text{mL}$). For the incubation, a 16-well format incubation chamber (PEPperPRINT GmbH, Heidelberg/Baden-Württemberg, Germany) was used. The resulting solution (200 μL) was pipetted in one of the wells and the microarray was incubated overnight in the dark at room temperature (150 rpm). Afterwards, the slide was washed with water inside the chamber (3 \times 5 min), in a petri dish (1 \times 30 min), and dried in a jet of air. Detection was achieved using a fluorescence scanner at a wavelength of $\lambda = 523$ nm with PMT gain 400. The laser power was 33% for every measurement and the pixel size was 5 μm for high-resolution scans.

Copper-catalyzed azide-alkyne cycloaddition (CuAAC) of sugars

CuSO_4 (530 μg , 3.36 μmol , 2.00 equiv.) was dissolved in a mixture of DMSO:water (1:1, 200 μL). Sodium ascorbate (998 μg , 5.04 μmol , 3.00 equiv.) was added and the mixture was thoroughly vortexed. The precipitate was centrifuged for 1 min. The remaining solution was passed through a polypropylene syringe filter (0.2 μm polypropylene filter media with polypropylene housing, 25 mm diameter, Whatman, Global Life Sciences Solutions Operations UK). The sugar azide (1.68 μmol , 1.00 equiv.) was dissolved in this solution and then applied on the acceptor surface ($c = 8.4$ $\mu\text{mol}/\text{mL}$). For the incubation, a 16-well format incubation chamber was used. The prepared solution (200 μL) was poured in one of the

wells and then shaken overnight in the dark. The next day, the slide was washed with water three times for 5 min inside the well and one time for 30 min in a petri dish on a shaker (450 rpm). Finally, the slide was dried in a jet of air.

3.5.5. Modules of synthesis

Module A: Preparation of acceptor slide (71 min)

Acceptor glass slide **3.43** was placed inside a petri dish and swollen for 30 min in DMF on a shaker at room temperature prior to the synthesis (300 rpm). Then, the slide was washed with DMF (3×3 min), deprotected using Fmoc-deprotection solution, and washed with DMF (3×3 min), MeOH (1×2 min), and DCM (1×1 min) and then, was dried in a jet of air.

Module B: Donor slide preparation (2-5 min/slide)

The desired amino acid donor slides were prepared (3 mg BB/slide) as reported in *Section 3.5.2*.

Module C: Laser transfer (depends on the transferred pattern, ~5 min)

For the patterning process, a donor slide was placed on top of an acceptor slide, and a focused laser transferred the desired amino acid-polymer material in a defined area using a spot pattern (one pulse of 6 ms transfers one spot). Each transferred spot was of nanometer thickness and about 150 μm in diameter. The transfer was repeated with different donor slides until the desired amino acid pattern was completed.

Module D: Coupling of transferred amino acids (15 min)

For coupling reaction under heat, the patterned slide was transferred into an oven under nitrogen atmosphere at 95 °C for 10 min. Subsequently, the slides were washed with acetone twice, initially for 2 min in an ultrasonic bath, and then for another 2 min in a petri dish on a shaker (450 rpm). Then, slides were dried in a jet of air. The laser transfer of the same amino acid pattern, the coupling, and the acetone washing steps were repeated twice, to increase the coupling efficiency. Each time, a new donor slide was used for every transfer and coupling cycle.

Module E: Capping (78 min)

After completion of the coupling process, free unreacted amino groups on the slides were acetylated with a capping solution twice for 30 min. The slides were washed with DMF (3×3 min), methanol (MeOH) (1×2 min), DCM (1×1 min), and dried in a jet of air.

Module F: Fmoc-deprotection (38 min)

Deprotection of the terminal Fmoc-groups was performed for 20 min with Piperidine on a shaker (450 rpm). The slides were washed with DMF (3×3 min), MeOH (1×2 min), DCM (1×1 min), consecutively, and dried in a jet of air. The whole process was repeated, as needed, for each pattern to synthesize the desired peptides. In the case of terminal amino acids within the peptide chain, the Fmoc removal was accomplished before the acetylation step, capping the free amino groups.

Post synthesis manipulation

Module G: Quality control of synthesized microarray (overnight incubation & 50 min)

CuAAC of TAMRA azide as explained in *Section 3.5.4*.

Module H: Attachment of sugars on the peptide scaffolds (overnight incubation & 36 min)

CuAAC of sugars on the peptide scaffolds as explained in *Section 3.5.4*.

Module I: Lectin assay (57 min)

To avoid unspecific binding, the acceptor slides were incubated with a blocking buffer for 40 min (Rockland, USA; blocking buffer for fluorescent western blotting MB-070). Fluorescently labeled plant lectins, *Concanavalin A* (i.e., ConA; CF[®]633 ConA, Biotium, Inc., USA) was diluted to 100 µg/mL in lectin buffer (50 mM HEPES, 100 mM NaCl, 1 mM CaCl₂, 1 mM MnCl₂, 10% blocking buffer, 0.05% Tween-20, pH 7.5), *Human Langerin* ECD (hLangerin, FITC labeled; recombinantly expressed^[242]) was diluted to 63 µg/mL in lectin buffer, *ricinus communis* agglutinin I (RCA-I), *peanut* agglutinin (PNA), *soybean* agglutinin (SBA), *dolichos biflorus* agglutinin (DBA), and *wheat germ* agglutinin (WGA) (Rhodamine labeled, Lectin kit 1, Vector laboratories, USA) were diluted to 10 µg/mL in lectin buffer and incubated for 1h at room temperature. Subsequently, each stained well was washed with PBS-T (3×5 min). Then, the acceptor slide was rinsed with Tris buffer (1 mM Tris-HCl buffer, pH=7.4) to remove all the remaining salt residues, and dried in a jet of air. Fluorescence scanning was used to detect the lectin binding on the corresponding sugar moieties.

3.5.6. Positioning of the acceptor slide before cLIFT process

Section has been removed for copyright reasons in the online version. For more information about this section please check:

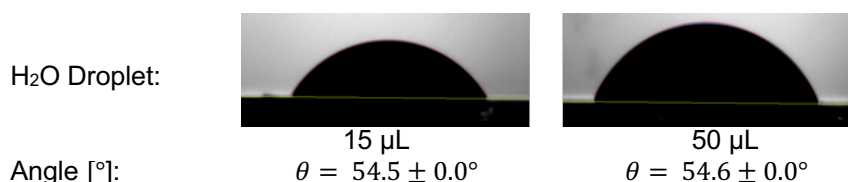
Mende, M.*; **Tsouka, A.***; Heidepriem, J.; Paris, G.; Mattes, D. S.; Eickelmann, S.; Bordoni, V.; Wawrzinek, R.; Fuchsberger, F. F.; Seeberger, P. H.; Rademacher C.; Delbianco M.; Mallagaray A.; Loeffler F. F.; On-Chip Neo-Glycopeptide Synthesis for Multivalent Glycan Presentation, *Chem.Eur.J.*, **2020**, 26, 9954 –9963. <https://doi.org/10.1002/chem.202001291>

3.5.7. Contact angle measurements

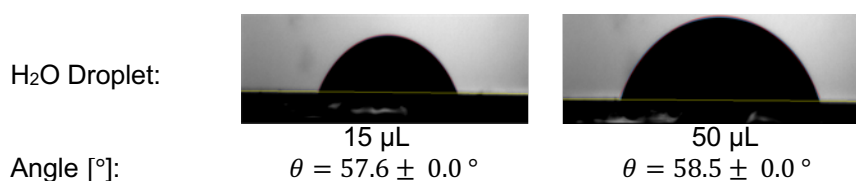
The contact angle/hydrophilicity of the used substrates, was measured as reported in the literature^[240]. Two droplets of water (15 μL and 50 μL) were deposited on each substrate, and the contact angle of the drops was derived from simultaneous imaging from the side and the top, between the sample and the drop. The top view was showing the circularity of the drop and the overall motion of the droplet during measurement. The cross section, and the distortion-free depiction of each droplet was derived from the telecentric view. The contact angle was determined and fitted with a home built spherical cap. The gravity in all these experiments was neglected, since each droplet size was smaller than the total length of the capillary used. The typical error during the measurements was estimated to $\sim 0.1^\circ$. For the entire experiment, the time between the droplet deposition and the measurement was minimized to avoid evaporation effects (< 20 s). From these experiments, it was observed that the PolyAn slides are more hydrophilic than the PEPperPRINT slides. Interestingly, between the two PolyAn slides with and without spacer, there is no significant difference on the hydrophobicity of the surface. However, the attachment of the spacer has a significant effect on the hydrophilicity of the substrate on PEPperPRINT slides, since it decreases the hydrophilicity of the surface (Experimental Figure 3.5.).

A PEPperPRINT

- without functionalization



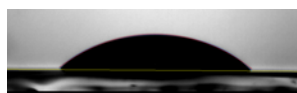
- with spacer



B PolyAn

- without functionalization

H₂O Droplet:



15 µL

Angle [°]:

$$\theta = 41.0 \pm 0.1^\circ$$

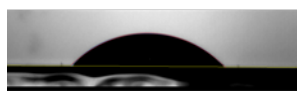


50 µL

$$\theta = 39.8 \pm 0.1^\circ$$

- with spacer

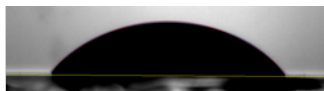
H₂O Droplet:



15 µL

Angle [°]:

$$\theta = 40.4 \pm 0.1^\circ$$



50 µL

$$\theta = 40.9 \pm 0.1^\circ$$

Experimental Figure 3.5: Side view image of water droplets on different functionalized and non-functionalized PEPperPRINT and PolyAn slides. A) PEPperPRINT slide without and with PEG-spacer functionalization, B) PolyAn slide without and with PEG-spacer functionalization.

3.5.8. Calculation of the spatial distances of sugar moieties

Section has been removed for copyright reasons in the online version. For more information about this section please check:

Mende, M.*; **Tsouka, A.***; Heidepriem, J.; Paris, G.; Mattes, D. S.; Eickelmann, S.; Bordoni, V.; Wawrzinek, R.; Fuchsberger, F. F.; Seeberger, P. H.; Rademacher C.; Delbianco M.; Mallagaray A.; Loeffler F. F.; On-Chip Neo-Glycopeptide Synthesis for Multivalent Glycan Presentation, *Chem.Eur.J.*, **2020**, 26, 9954 –9963. <https://doi.org/10.1002/chem.202001291>

4. VaporSPOT: Parallel Synthesis of Oligosaccharides on Membranes

This chapter has been modified in part from the following article:

Tsouka, A.*; Dallabernardina, P.*; Mende, M.; Sletten E. T.; Lechnitz, S.; Bienert, K.; Le Mai Hoang, K.; Seeberger, P. H.; and Loeffler, F. F.; VaporSPOT: Parallel Synthesis of Oligosaccharides on Membranes; *J. Am. Chem. Soc.* **2022**, *144*, 19832–19837.

DOI: 10.1021/jacs.2c07285.

*These authors contributed equally.

Specific contribution

I performed the synthesis, characterization and purification of all synthesized building blocks (unless otherwise stated within the chapter), as well as all final oligosaccharide structures. I synthesized the used photocleavable linker with input from Dr. Kim Le Mai Hoang. Dr. Sabrina Lechnitz synthesized and provided the differently protected mannopyranosyl phosphate building block, while Dr. Eric Sletten assisted with the analytical data required for the characterization of the final structures. Dr. Pietro Dallabernardina synthesized the base-labile linker. I developed the methodology with the assistance of Dr. Marco Mende and Dr. Pietro Dallabernardina. The reported home-built machine/setup used for this methodology was constructed by Klaus Bienert.

4.1. Introduction

Oligosaccharides are the most abundant biopolymers in nature and play a fundamental role in many biological functions. Despite their relevance in many processes of life, their role is still not sufficiently understood.^[2] Their structural heterogeneity, complexity, and diversity, often make their isolation from natural sources laborious and their synthesis a cumbersome process. Different automated platforms for enzymatic,^[74,75,77] chemoenzymatic,^[75] and chemical oligosaccharide^[101–103,105,106] synthesis have been developed, giving access to complex and biologically valuable structures.^[7,69,100] In the last two decades, the development of automated glycan assembly (AGA) has enabled the successful synthesis of defined and complex synthetic oligosaccharide libraries of biological and medical interest,^[7,106,107,110,113,116–118] as well as very long polysaccharides including complex branching, up to 100-mers.^[111,112] Currently, AGA is used to prepare one single oligosaccharide at a time. Parallel oligosaccharide synthesis would be more cost- and time-efficient. Compared to the well-established parallel peptide and oligonucleotide synthesis methods,^[61,128] the parallel synthesis of oligosaccharides remains a major challenge. Different chemical and enzymatic approaches for on-chip synthesis have been reported the last decades and none of these methods were advanced beyond the proof-of-principle stage.^[54,60,62]

In this work, VaporSPOT method for parallel oligosaccharide synthesis was developed, that overcomes these limitations. SPOT synthesis, initially developed by Frank *et al.*,^[180] can be performed manually or in an automated fashion^[183,185,186,188] and is commonly used to simultaneously generate peptide, small-molecule, or glycopeptide libraries.^[188–191] The original SPOT method follows the 9-fluorenylmethoxycarbonyl (Fmoc)-based solid phase synthesis protocol under ambient conditions (*Section 1.5.1*), using cellulose membranes as solid support. Cleavage of the products can be achieved after treatment with strong bases or acids, giving access to a library of soluble and/or cellulose tethered peptides. However, the SPOT synthesis is incompatible with chemical carbohydrate synthesis, since the conditions are neither inert nor temperature-controlled. To solve this problem, a novel method was devised, and a setup was designed to ensure controlled conditions suitable for glycosylation reactions. In the first part of this chapter (*Section 4.2.1*), the new VaporSPOT method was developed, based on the SPOT synthesis approach. Then, a collection of glycosyl donors was synthesized, bearing different protecting groups (*Section 4.2.2*), to study the glycosylation outcome of each building block under the same conditions. Simultaneously, screening of possible candidates for chain elongation was performed, which led to the

synthesis of oligosaccharides with up to four residues in length. Additionally, the role of the temperature and the amount of activating catalyst were investigated and optimized for the successful activation of the synthesized glycosyl donors. All synthesized structures could be characterized and purified using common analytical methods. Finally, the method was employed for the parallel synthesis of oligosaccharides (*Section 4.2.3*). No diffusion or contamination between structures on different membrane pieces or on a functionalized glass slide were observed, under the same vapor conditions.

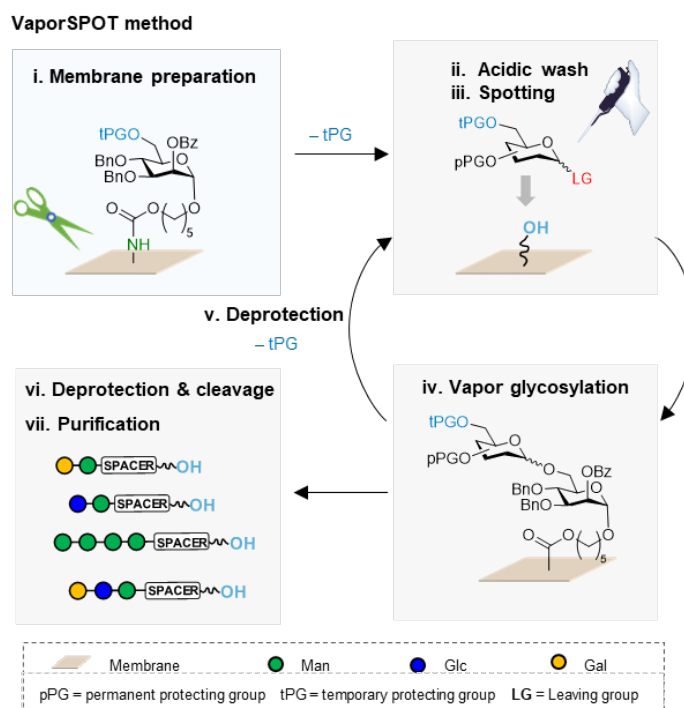


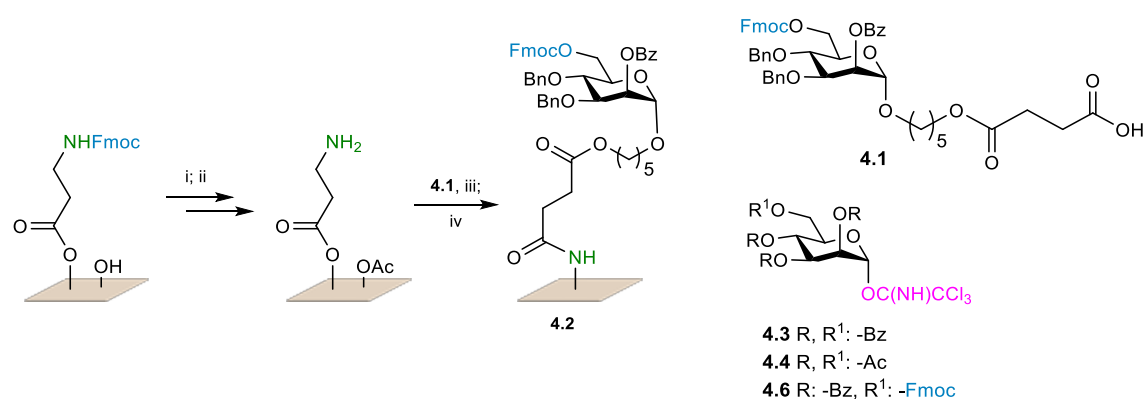
Figure 4.1: Overview on the research aims described for the development of the VaporSPOT method. Modules of VaporSPOT process: A) preparation of the membrane; B) acidic wash of membrane; C) spotting of the building block; D) chemical vapor glycosylation; E) removal of tPG; F) deprotection of pPGs and release of oligosaccharides from the solid support; and G) purification and characterization of synthesized structures (modified^[252]).

4.2. Results and Discussion

4.2.1. Development of VaporSPOT method and initial screening

The VaporSPOT method under inert conditions was designed for building block delivery at room temperature and subsequent chemical vapor glycosylation at low temperature. The process (Figure 4.1) begins with the functionalization and preparation of cellulose membrane which was preloaded with the base-labile mannopyranoside linker **4.1**¹. Linker **4.1** bears an

Fmoc group on the C-6 position, serving as the nucleophile for the first glycosylation after deprotection. Therefore, the commercially available Fmoc- β -alanine esterified cellulose membrane (Scheme 4.1) was acetylated to minimize unspecific glycosylation reactions. After Fmoc-deprotection, mannopyranoside linker **4.1** was attached, and the unreacted free amino groups of the β -alanine were acetylated. The functionalized membrane **4.2** was deprotected, followed by an acidic wash to remove any residual base and dried under high vacuum. The perbenzoylated and peracetylated mannose imidates **4.3** and **4.4**^[214,232] were synthesized as reference building blocks^{II} to establish the VaporSPOT process.



Scheme 4.1: Reagents and conditions for membrane functionalization, and building block synthesized for method development: i) capping 10% Ac₂O and 2% MsOH in DCM (v/v), rt, 30 min; ii) 20% Piperidine in DMF (v/v), rt, 20 min; iii) attachment of linker, rt, overnight; iv) capping 10% Ac₂O and 20% DIPEA in DMF (v/v), rt, 30 min.

The membrane was cut into pieces and each membrane piece (~2 cm²) was spotted with a building block, and dried under high vacuum. Each membrane was transferred separately to the bottom of the custom-built instrument (Figure 4.2) and cooled to -15 °C. Activation of the glycosyl donors, similar to batch or solid phase syntheses, was achieved by delivery and condensation of 8% TMSOTf in dichloromethane (DCM) vapor inside the glycosylation chamber (2 min). Then, the temperature was slowly increased to room temperature and maintained for 30 min^{III}. After completion, the remaining condensate was removed from the glycosylation chamber under high vacuum. Subsequently, the membrane(s) were transferred to a petri dish and washed with DCM, and DMF to remove the residuals. Simultaneous deprotection of the ester protecting groups and release of the product(s) from the surface was achieved by treatment with NaOMe in MeOH, followed by purification and characterization. After cleavage, the delivered disaccharide **4.5** was obtained in 26% yield from Man BB **4.3** and in 21% yield from Man BB **4.4** (Scheme 4.2). Afterwards, BB **4.6**^{IV}

^I Synthesized and provided by Dr. Pietro Dallabernardina

^{II} Building block **4.3** is mentioned as building block **2.6** in *Chapter 2*. The analytical data of the building block is reported in the *Experimental Section 2.5.1*, and building block **4.4** was synthesized as reported in literature.

^{III} The vapor glycosylation conditions were chosen based on the optimized conditions of *Chapter 2*.

(Scheme 4.1) was synthesized bearing an Fmoc-protecting group on the C-6 position, which can be removed with piperidine, unmasking the nucleophile for the next synthesis cycle.

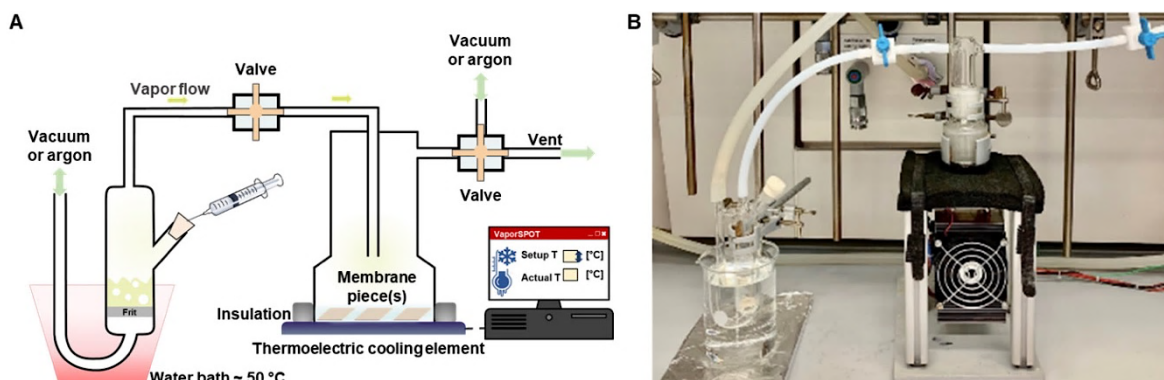
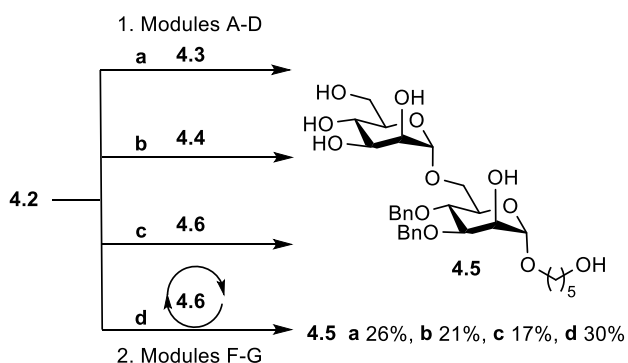


Figure 4.2: VaporSPOT setup: A) Schematic representation, and B) experimental setup of the custom-built apparatus for parallel and temperature-controlled oligosaccharide synthesis on membranes.

Prior to synthesizing longer structures, the coupling efficiency of Man BB **4.6** was investigated. Single glycosylation of **4.6** under the aforementioned glycosylation conditions (modules A, B, C, D, F and G) delivered only 17% of the desired dimer **4.4**, while repetition of the glycosylation cycle (modules C and D) afforded dimer **4.4** in 30% yield (Scheme 2.4, Figure 4.3). Therefore, for higher coupling efficiencies with poorly reactive and/or sterically hindered building blocks (BBs) (e.g., Man BB **4.6**), the coupling cycle should be repeated.



Scheme 4.2: Screening of mannopyranosides **4.3**, **4.4** and **4.6** under the same vapor glycosylation conditions for the synthesis of dimer **4.5**. Reagents and conditions for each coupling step following VaporSPOT modules: 1) A) Fmoc-deprotection, 20% piperidine in DMF (v/v), rt, 20 min; B) acidic wash of membrane, 0.5% TMSOTf in DCM (v/v); C) spotting of 6.00 equiv/per cycle of building block; D) chemical vapor glycosylation using 8% TMSOTf in DCM (v/v); -15 °C to rt, 30 min; 2) deprotection of pPGs and release of oligosaccharides from the solid support; and G) purification and characterization of synthesized structures. Isolated yields are based on membrane loading. For building block **4.6** the coupling cycle was repeated.

^{IV} Building block **4.6** is mentioned as building block **2.18** in *Chapter 2*. The synthesis of the building block is reported in the *Experimental Section 2.5.1*.

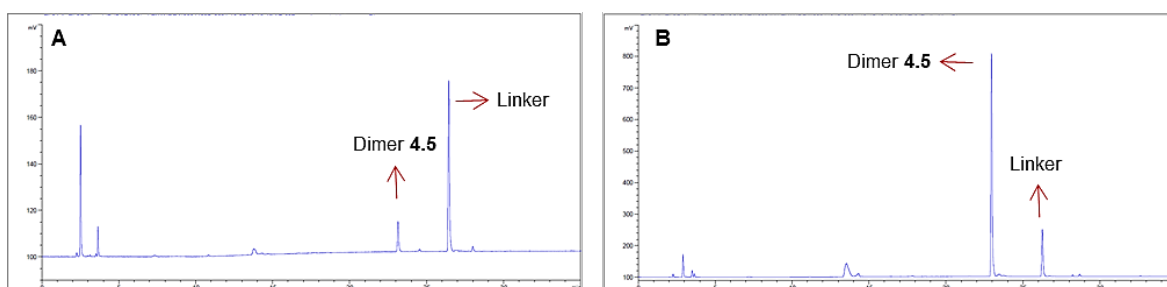


Figure 4.3: Analytical RP-HPLC chromatograms of crude reaction mixture after base-labile cleavage for VaporSPOT of building block **4.6**: A) single chemical vapor glycosylation cycle of building block, and B) double glycosylation of building block. Detection: ELSD

4.2.2. Oligosaccharide synthesis

Two main parameters needed to be further investigated for the validation of the vapor glycosylation conditions: the temperature inside the glycosylation chamber and the concentration of the activator solution delivered into the glycosylation chamber. Both parameters affect the reactivity of the glycosyl donors and the glycosylation efficiency.^[84,85,87,253] Thus, 11 additional BBs were synthesized (Figure 4.4), either following established protocols (**4.7**, **4.10**, **4.12**, **4.14-4.17**),^[69,109,204,214,216-218,232,254] or prepared from commercially available precursors (trichloroacetimidates **4.6**, **4.8**, **4.13** and phosphates **4.9** and **4.11**).^v

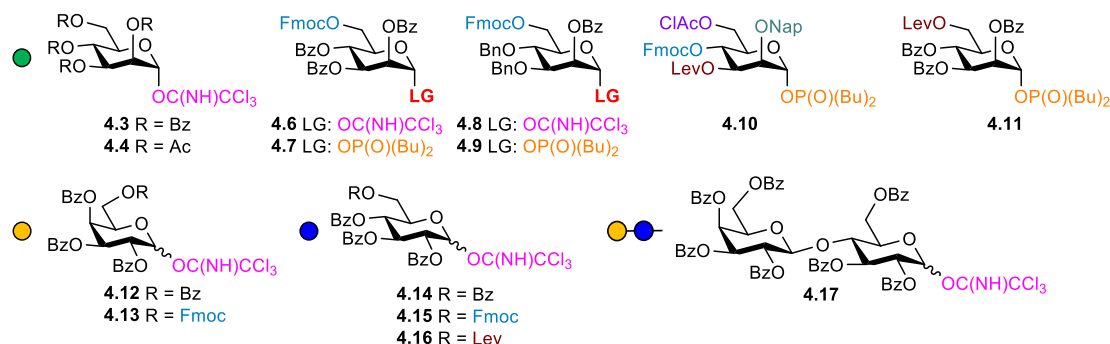


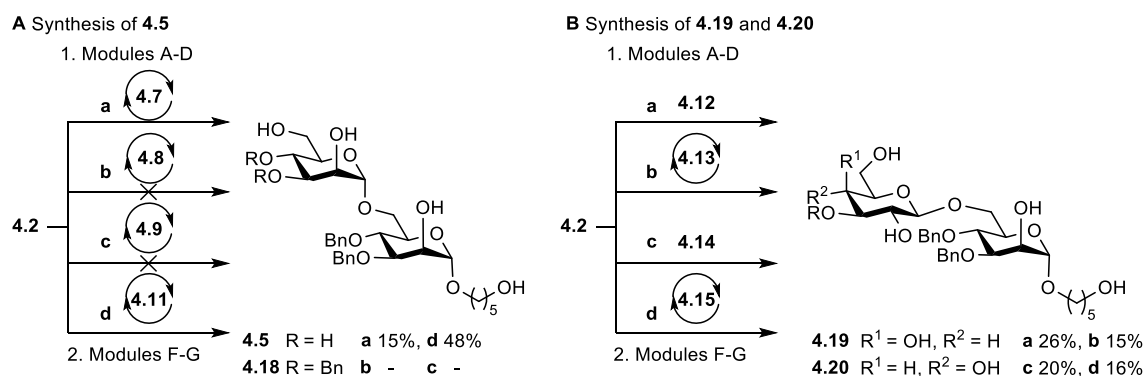
Figure 4.4: Synthesized building blocks for VaporSPOT synthesis

Glycosyl donors **4.7-4.9**, and **4.11-4.15** were screened, using the already developed protocol (8% TMSOTf in DCM activator solution, -15 °C to room temperature), to furnish the corresponding dimers **4.5**, **4.18** (Scheme 4.3A), **4.19** and **4.20** (Scheme 4.3B), in different

^v Building blocks **4.8**, **4.11-4.15**, and **4.17** are mentioned as building block **2.19**, **2.21**, **2.24**, **2.25**, **2.22**, **2.23** and **2.26** respectively, in *Chapter 2*. The synthesis of the building blocks is reported in the *Experimental Section 2.5.1*. Building block **4.9** provided by Dr. Pietro Dallabernardina.

yields. While perbenzoylated BBs (**4.3**, **4.12**, **4.14**) show relatively similar results, mannoside **4.3** (Scheme 4.2), bearing an Fmoc temporary protecting group on the C-6 position, gave the best glycosylation outcome in comparison to galactoside **4.12** and glucoside **4.14**, due to its higher reactivity (armed/disarmed effect)^[84,93] in this temperature range. Moreover, no formation of disaccharide **4.18** was observed with the more reactive BBs **4.8** and **4.9** bearing two electron-donating groups on the C-3 and C-4 positions. This is likely due to the currently limited minimum temperature (-15 °C) achievable by the setup.

However, a significantly higher yield was obtained using the Man phosphate **4.11**. Double glycosylation with the phosphate BB **4.7** bearing an Fmoc group on the C-6 position, yielded 15% of the desired dimer **4.5**, while phosphate **4.11**, where the Fmoc was replaced with the more electron-withdrawing Lev group, resulted in 48% of the targeted dimer under the exact same conditions (Scheme 4.3, Figure 4.5.). Although BB **4.11** resulted in a higher yield, the Lev deprotection would require extensive optimization on the cellulose membrane. Thus, the already established Fmoc deprotection strategy was chosen for longer oligosaccharide synthesis.



Scheme 4.3: Screening of building blocks **4.7-4.9**, and **4.11-4.15** under the same VaporSPOT glycosylation conditions for the synthesis of dimer A) **4.5**, and B) **4.19-4.20**. Obtained yields after cleavage and characterization of the target dimers. Reagents and conditions for each coupling step following VaporSPOT modules: 1) A) Fmoc-deprotection, 20% piperidine in DMF (v/v), rt, 20 min; B) acidic wash of membrane, 0.5% TMSOTf in DCM (v/v); C) spotting of 6.00 equiv./per cycle of building block; D) chemical vapor glycosylation using 8% TMSOTf in DCM (v/v); -15 °C to rt, 30 min; 2) deprotection of pPGs and release of oligosaccharides from the solid support; and G) purification and characterization of synthesized structures. Isolated yields are based on membrane loading. For building blocks **4.7-4.11**, **4.13** and **4.15** the coupling cycle was repeated.

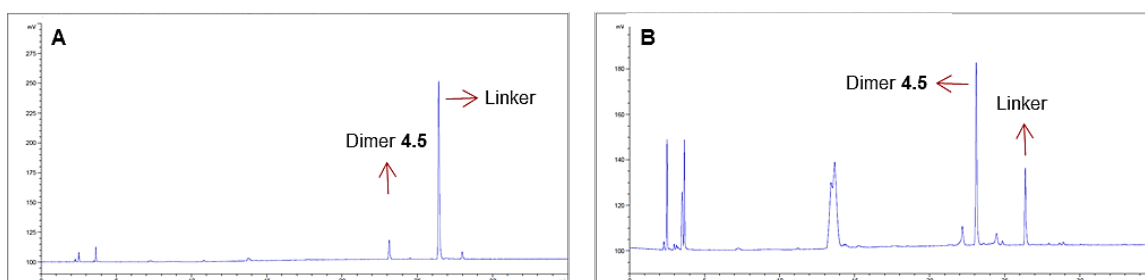
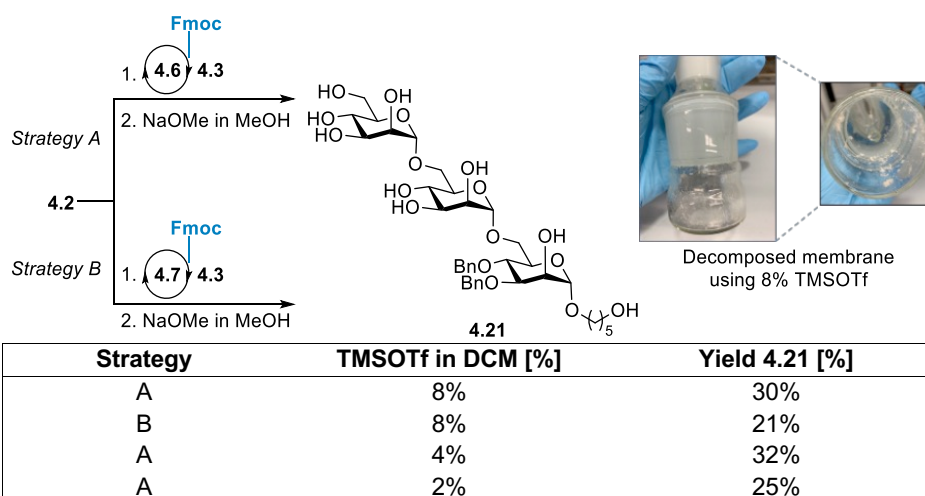


Figure 4.5: Analytical RP-HPLC chromatograms of crude reaction mixtures after double glycosylation and base-labile cleavage for the VaporSPOT of: A) glycosyl donor **4.7**, and B) glycosyl donor **4.11**. Detection: ELSD

After the VaporSPOT conditions were successfully optimized, next goal was the synthesis of longer oligosaccharides. For the synthesis of tri-Man **4.21**, two major routes, involving glycosyl imidates **4.6** and **4.3** as well as phosphate **4.7** and **4.3** were considered. Synthesis of the trisaccharide following strategy A resulted in 30% yield of trimer **4.21**, while synthesis *via* strategy B, afforded 21% yield of the targeted structure (Scheme 4.4). For both synthetic routes, six equivalents of donor/glycosylation cycle were used. However, during synthesis, partial decomposition of the membrane and reproducibility issues were observed. Specifically, using 8% TMSOTf in DCM resulted in reduced flexibility of the cellulose membrane or in decomposition after the second or third glycosylation cycle. Therefore, different concentrations of activator for trisaccharide synthesis were investigated using glycosyl trichloroacetimidates **4.6** and **4.3** (Scheme 4.4). A reduced concentration of activator solution improved both membrane stability and glycosylation yield. A 4% activator solution afforded trisaccharide **4.21** in 32% yield, while retaining the integrity of the membrane, and a 2% solution resulted in 25% yield of the targeted trisaccharide **4.20**. Thus, for further syntheses, the 4% activator solution was selected.



Scheme 4.4: VaporSPOT synthesis of trisaccharide **4.21**. VaporSPOT conditions: Reagents and conditions for each coupling step following VaporSPOT modules: 1) A) Fmoc-deprotection, 20% piperidine in DMF, rt, 20 min;

B) acidic wash of membrane, 0.5% TMSOTf in DCM (v/v); C) spotting of 6.00 equiv./per cycle of building block; D) chemical vapor glycosylation using different activator solutions, -15 °C to rt, 30 min; E) removal of Fmoc using 20% piperidine in DMF (v/v), rt, 20 min; 2) deprotection of pPGs and release of oligosaccharides from the solid support; and G) purification and characterization of synthesized structures. Isolated yields are based on membrane loading.

Since the amount of the activator solution was reassessed, also the concentration/equivalents of glycosyl donor required per glycosylation were investigated in respect to the loading of the membrane **4.2** (1.00 equiv.). Single VaporSPOT glycosylation of **4.3** onto membrane **4.2** was performed, using four different concentrations. Then, each membrane was individually subjected to deprotection and cleavage. For these investigations, only qualitative data were obtained from the crude reaction mixture as detected from the ELSD, calculating the ratio of the integral peaks of dimer **4.5** vs. linker conversion were assessed (Figure 4.6). Minor differences were observed in the dimer/linker ratio between four, six, and eight equivalents (Figure 4.6) of donor, while the peak intensity of the synthesized dimer **4.5** increased with more equivalents of the donor. The intensity of the synthesized dimer between six and eight equivalents was relatively similar and since a cost-efficient methodology needed to be established, six equivalents were chosen as the optimum amount of donor per glycosylation cycle.

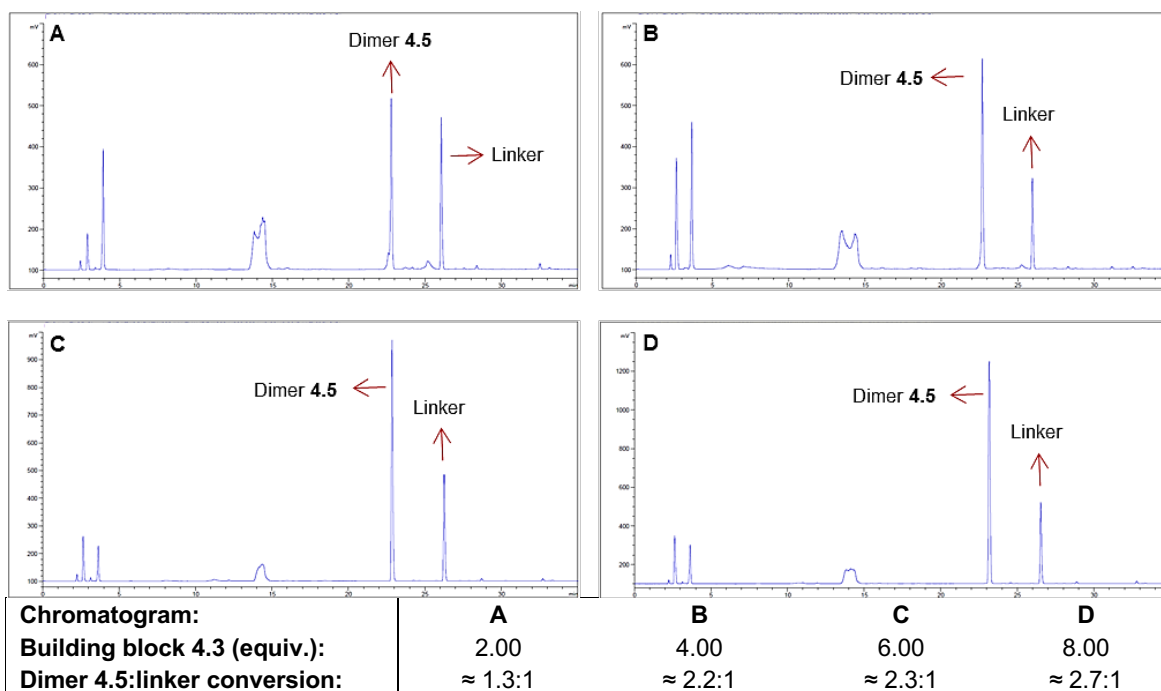
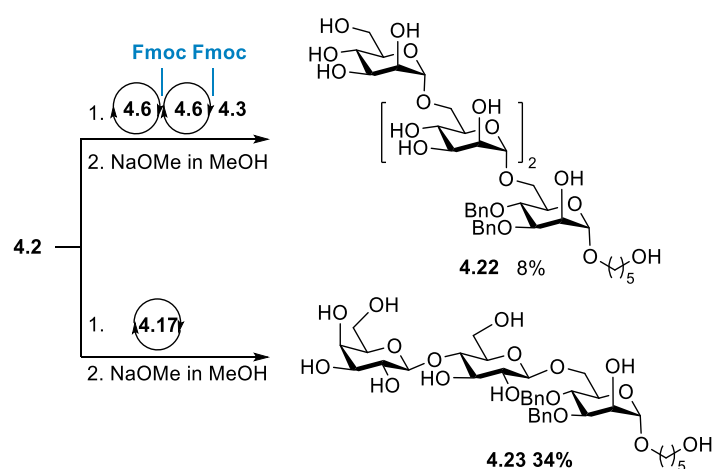


Figure 4.6: Analytical RP-HPLC chromatograms for VaporSPOT of **4.5** (crude reaction mixture after base-labile cleavage) using different equivalents of building block **4.3** per glycosylation cycle. Mannosylation with A) two equiv., B) four equiv., C) six equiv., and D) eight equiv. of building block. Reagents and conditions for each coupling step following VaporSPOT modules: 1) B) acidic wash of membrane, 0.5% TMSOTf in DCM (v/v); C) spotting of building block; D) chemical vapor glycosylation using 4% TMSOTf in DCM (v/v); -15 °C to rt, 30 min; 2) deprotection of pPGs and release of oligosaccharides from the solid support. Detection with ELSD.

Using the optimized VaporSPOT conditions, tetrasaccharide **4.22** was successfully synthesized in eight steps, in an overall yield of 8%, while trisaccharide **4.23** was obtained in 34% yield with β -(1-6) and β -(1-4) linkage, starting from the disaccharide **4.17** (Scheme 4.5). All final structures **4.5**, and **4.19-4.23** were characterized using mass spectrometry (MS), and nuclear magnetic resonance spectroscopy (NMR). Both, purity and anomeric purity of the final structures were determined by high performance liquid chromatography (HPLC) and decoupled ^1H - ^{13}C heteronuclear single quantum coherence spectroscopy (HSQC NMR).



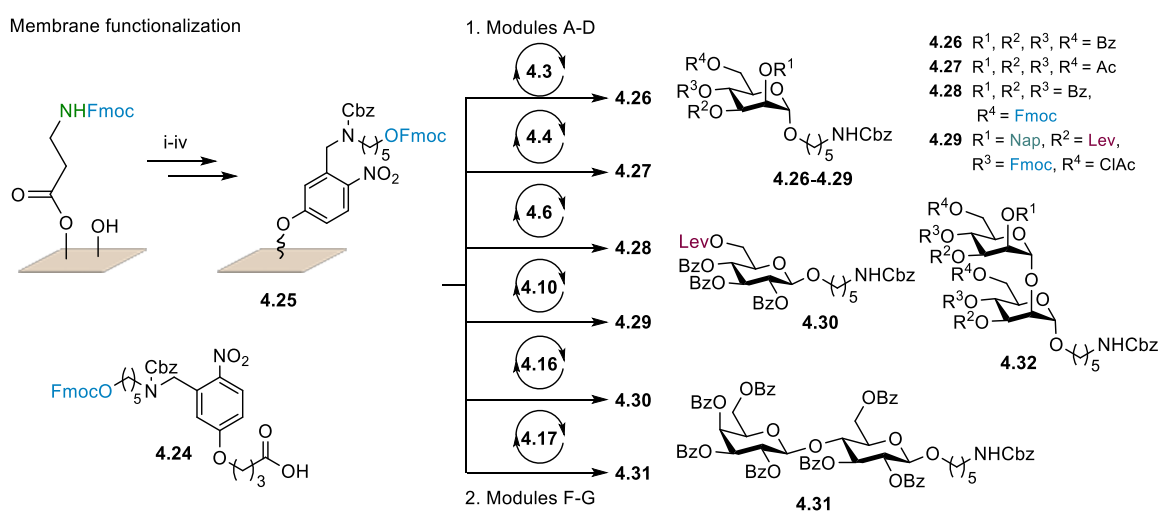
Scheme 4.5: VaporSPOT synthesis of tetrasaccharide **4.22** and trisaccharide **4.23**. VaporSPOT reagents and conditions for each coupling step following VaporSPOT modules: 1) A) Fmoc-deprotection, 20% piperidine in DMF (v/v), rt, 20 min; B) acidic wash of membrane, 0.5% TMSOTf in DCM (v/v); C) spotting of 6.00 equiv/per cycle of building block; D) chemical vapor glycosylation, 4% TMSOTf in DCM (v/v); -15 °C to rt, 30 min; E) removal of Fmoc using 20% piperidine in DMF (v/v), rt, 20 min; 2) deprotection of pPGs and release of oligosaccharides from the solid support; and G) purification and characterization of synthesized structures. Isolated yields are based on membrane loading.

4.2.3. Parallel synthesis

Encouraged by the successful vaporSPOT synthesis of six different oligosaccharides individually, the parallel synthesis of oligosaccharides was investigated (Scheme 4.6). To assess, whether diffusion or contamination can occur between different membrane pieces placed in close proximity inside the setup, the photocleavable linker **4.24** was designed and synthesized^{vi}. With the current set of BBs, mainly bearing ether and carbonyl protecting groups, the base-labile linker **4.1** would deliver partially deprotected compounds of mostly indistinguishable molecular weight, since cleavage from the solid support and deprotection would occur simultaneously. In contrast, with the photocleavable linker **4.24**, only protected

^{vi} Photocleavable linker **4.24** is mentioned as photocleavable linker **2.12**, in *Chapter 2*. The synthesis is reported in the *Experimental Section 2.5.1*.

compounds with distinguishable molecular weight can be obtained. Using the same experimental setup, reaction time, and the 4% activator solution, six different glycosyl donors **4.3**, **4.4**, **4.6**, **4.10**, **4.16**, and **4.17**, bearing different protecting groups, were coupled onto six individual functionalized cellulose membrane pieces in parallel. Functionalization of the cellulose membrane with the photocleavable linker was achieved in four steps as reported for the base-labile membrane **4.2**, affording membrane **4.25**. The VaporSPOT glycosylation was performed twice on the membranes, while the positions of the membranes were shuffled between the glycosylations to detect any possible diffusion or contamination. The desired products **4.26-4.31** were obtained after parallel cleavage under UV-light irradiation (365 nm) and detected based on their molecular weight using MALDI-ToF mass spectrometry (Figure 4.7). During the parallel synthesis, no diffusion/contamination between the different membranes was observed. Nevertheless, in the case of the peracetylated Man trichloroacetimidate **4.4**, the targeted monomer but also a dimer was detected (e.g., **4.32**). Further characterization of the formed structures was not possible due to inefficient photo cleavage.



Scheme 4.6: VaporSPOT parallel synthesis of **4.26-4.31** using the glycosyl donors **4.3**, **4.4**, **4.6**, **4.10**, **4.16**, and **4.17** respectively. Reagents and conditions of entire VaporSPOT synthesis: Functionalization of photocleavable membrane **4.25** in four steps with photocleavable linker **4.24**, i) capping 10% Ac_2O , 2% MsOH in DCM (v/v), rt, 30 min; ii) 20% Piperidine in DMF (v/v), rt, 20 min; iii) attachment of linker **4.24**, rt, overnight; iv) capping 10% Ac_2O , 20% DIPEA in DMF (v/v), rt, 30 min. Modules A) Fmoc-deprotection, 20% piperidine in DMF (v/v), rt, 20 min; B) acidic wash of membrane, 0.5% TMSOTf in DCM (v/v); C) spotting of each membrane with 6.00 equiv/per cycle of building block; D) chemical vapor glycosylation, 4% TMSOTf in DCM (v/v); -15°C to rt, 30 min; 2) F) release of oligosaccharides from the solid support under UV; and G) characterization of synthesized structures by MALDI (modified^[252]).

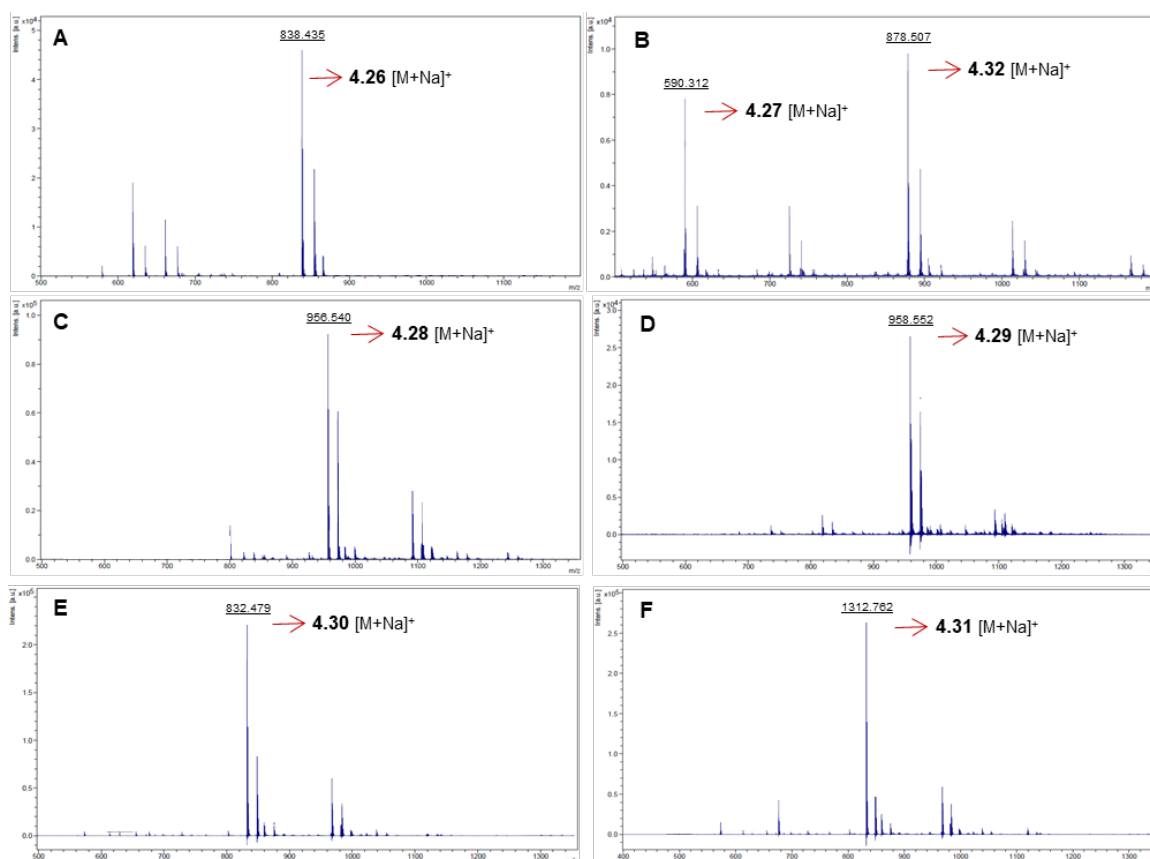


Figure 4.7: MALDI detection of the structures A) **4.26**; B) **4.27**; C) **4.28**; D) **4.29**; E) **4.30**; and F) **4.31** synthesized in parallel from building blocks **4.3**, **4.4**, **4.6**, **4.10**, **4.16**, and **4.17** respectively via VaporSPOT after UV cleavage.

Finally, to display the flexibility and usefulness of this approach, the vaporSPOT approach was employed on a functionalized glass slide **4.33**^{VII} for *in-situ* synthesis of an array (Figure 4.8). Man BBs **4.3**, **4.4**, **4.6**, and Glc BBs **4.15**, **4.16** and **4.34**^[255] were spotted on defined areas on the solid support and then glycosylated under vapor. Cleavage of the ester and carbonate groups was performed using NaOMe in MeOH, while the synthesized dimers **4.35** and **4.36** remained attached to the solid support. Subsequently, the compounds were stained using ConA (as previously reported in *Chapter 2*) and the result was screened after fluorescence scanning. This approach shows the future potential of this method to be used with different printing technologies for combinatorial synthesis on a variety of solid supports.

^{VII} Functionalized glass slide **4.33** is mentioned as functionalized-acceptor glass slide **2.5**, in *Chapter 2*. The functionalization of the used glass slide is reported in the *Experimental Section 2.5.2*.

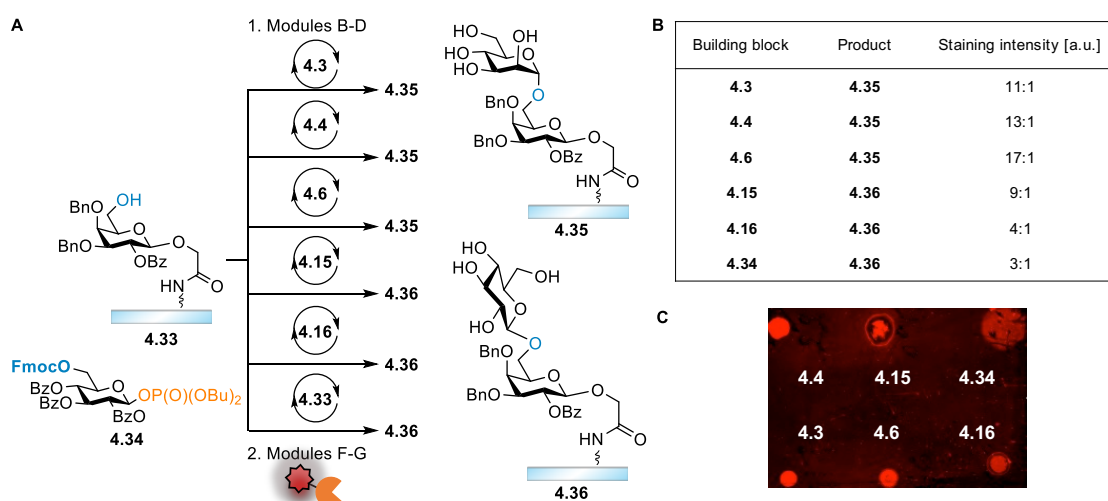


Figure 4.8: *In-situ* glycosylation onto the functionalized-acceptor glass slides **4.33** using VaporSPOT: A) Building blocks **4.3**, **4.4**, **4.6**, **4.15**, **4.16** and **4.33** spotted onto the glass slide to form structures **4.35** and **4.36**. B) Signal to noise ratio of stained structures with ConA. C) Fluorescence scan obtained after staining with ConA. VaporSPOT reagents and conditions in modules: B) acidic wash of membrane **4.33**, 0.5% TMSOTf in DCM (v/v); C) spotting of each membrane with 2 mg of building block /20 μ L of DCM; D) chemical vapor glycosylation; 2) F) deprotection of the pPGs of oligosaccharides from the solid support with NaOMe in MeOH; and G) screening of synthesized structures with fluorescently labelled ConA. ConA (CF@633 labelled) at a concentration of 100 μ g/mL.

4.3. Conclusions

SPOT-synthesis is the well-established gold standard for the parallel synthesis of peptides. Here, VaporSPOT synthesis was developed for the parallel synthesis of oligosaccharides on cellulose membranes. Inert and temperature controlled chemical vapor conditions were achieved by a custom-built setup. The conditions were meticulously optimized prior to successful synthesis. VaporSPOT is a flexible and cost-efficient way to rapidly screen the glycosylation outcome of different glycosyl donors. It enables the synthesis of different oligosaccharides in good purity on micromolar scale with currently up to four units. In the parallel synthesis approach, diffusion or contamination between the different spotted glycosyl donors was not detected. All synthesized structures **4.5**, and **4.19-4.23** using the base-labile functionalized membrane **4.2** were partially deprotected, purified and characterized by MS, and NMR. Both, purity and anomeric excess of these structures were analyzed by HPLC and HSQC NMR. For structures **4.26-4.31**, synthesized in parallel using the functionalized photocleavable membrane **4.25**, only MALDI detection was applied due to inefficient photocleavage from the solid support. Finally, the same VaporSPOT method was applied on a functionalized glass slide for *in-situ* microarray generation (as described in *Chapter 2*).

4.4. Outlook

Since the VaporSPOT approach enables the rapid synthesis of a glycan collection, it is ideal for the production of microarrays. Thus, the covalent site-specific immobilization of the herein synthesized oligosaccharides on commercially available glass slides (e.g., hydrazide, aminoxy-, and epoxy- coated) should be further investigated.

In the future, chemical optimization of the methodology by screening of mono and/or oligosaccharides with different protecting groups and linkers will allow for more complex structures in higher yields. For example, replacing the Fmoc protecting group with the more electron-withdrawing Lev group on the C-6 position should lead to higher glycosylation yields as shown with building block **4.11**. The phosphate leaving group can be substituted with a trichloroacetimidate, forming building block **4.37** that might lead to even higher coupling yields due to its high reactivity under milder activating conditions. Furthermore, cleavage of benzyl ether groups (-Bn) on the synthesized oligosaccharides obtained by VaporSPOT should be investigated to obtain fully deprotected oligosaccharides. Different conditions that should be applied are catalytic hydrogenolysis, Birch reduction or even milder conditions using 2,3-dichloro-5,6-dicyano-1,4-benzoquinone (DDQ) under visible-light irradiation.^[219] In addition, the use of the differently protected mannose building block **4.10**, bearing multiple orthogonal protecting groups (Fmoc, Lev, Nap, and ClAc) will increase the flexibility of the method giving access to more complex and branched structures. Besides, technical improvements (e.g., minimum achievable temperature) may enable more flexible chemical strategies (Figure 4.9).

Furthermore, other solid supports, such as cross-linked cellulose,^[256] polypropylene, or Teflon patterned membranes,^[188] may further improve the spot density, substrate stability, and synthesis yield. The same VaporSPOT approach may be further expanded to high-throughput glycan array synthesis on functionalized glass slides (*Chapter 2*) or even beyond glycochemistry, for precisely controlled polymerization or cross-coupling reactions. Together with automated spotting of building blocks, this should enable even higher parallelization. Such oligosaccharide collections are ideal for microarray production, to drastically accelerate the screening of glycan-glycan binding protein interactions.

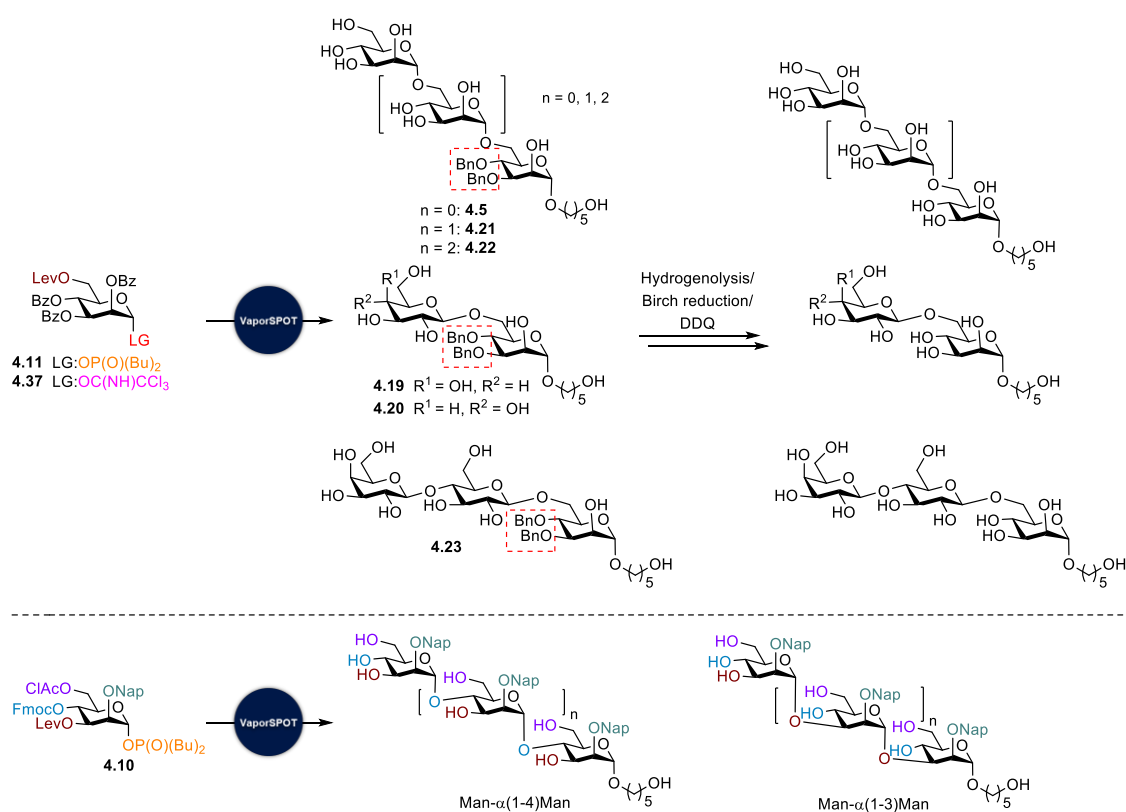


Figure 4.9: Deprotection of Bn groups on the micromolar scale and additional building blocks that may be used for oligosaccharide synthesis.

4.5. Experimental Section

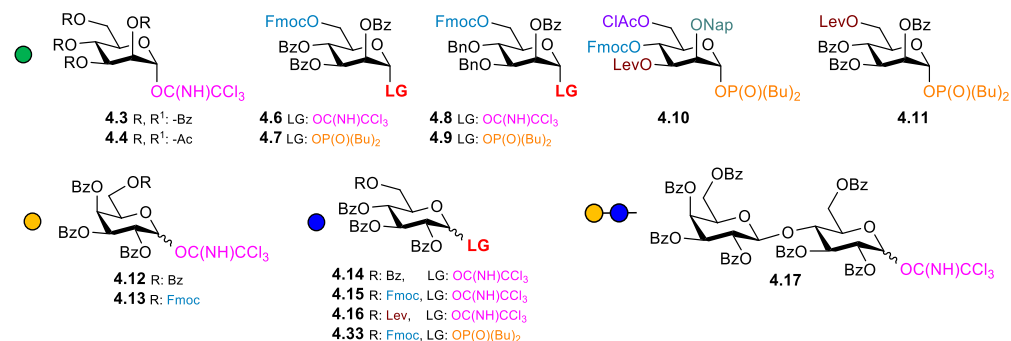
General remarks

All applied solvents, deuterated solvents (99.5 atom% D), and chemicals were purchased from common suppliers such as Sigma-Aldrich, Alfa Aesar, Tokio Chemical Industry (TCI), Thermo Fischer Scientific, Acros Organics, Iris Biotech, Merck, and used without further purification. For High-Performance Liquid Chromatography (HPLC) solvents with corresponding quality were used. All starting materials and all starting glycopyranoside building blocks used for the synthesis of the targeted compounds were purchased from GlycoUniverse GmbH & Co KGaA, apart from the lactose starting material purchased from Tokio Chemical Industry (TCI). The cellulose membrane used was acquired from AIMS Scientific Products GmbH. If not mentioned otherwise, saturated aqueous solutions of inorganic salts were used. Thin layer chromatography (TLC) using silica gel coated aluminium plates (MACHEREY-NAGEL, pre-coated TLC sheets ALUGRAM® Xtra SIL G/UV254 or Merck, pre-coated TLC sheets 60 F254) was applied to monitor reactions until completion. Compounds were visualized by UV light ($\lambda = 254$ nm) or stained either with

Seebach (phosphomolybdic acid hydrate, cerium(IV) sulfate tetrahydrate, sulfuric acid and water), *p*-anisaldehyde (*p*-anisaldehyde, acetic acid, sulfuric acid and ethanol) or with potassium permanganate solution (potassium permanganate, potassium carbonate, sodium hydroxide and water). Flash column chromatography was carried out by using MACHEREY-NAGEL silica gel 60 (0.040 × 0.063 mm) and quartz sand. Final deprotected oligosaccharides were lyophilized using a Christ Alpha 2–4 LD plus freeze dryer. The spectra were recorded on Varian 400-MR (400 MHz), Bruker Ascend 400 (400 MHz), Varian 600-MR (600 MHz), or Bruker Biospin AVANCE700 (700 MHz) spectrometer. Chemical shifts δ are reported in ppm and are adjusted to internal standards of the residual proton signal of the deuterated solvent (CDCl₃: 7.26 ppm for ¹H and 77.0 ppm for ¹³C, D₂O: 4.79 ppm for ¹H). The spectra were measured at room temperature. Having symmetrical signals, the center of the signal is given and for multiplets the area. The following characterization was used: s: singlet, sbr: singlet broad, d: doublet, t: triplet, q: quartet, m: multiplet or combinations like dd: doublet of doublet or dt: doublet of triplet and m: multiplet. Coupling constants (*J*) are given in Hz. The spectra were evaluated according to 1st order. For ¹H NMR spectra, the correlation of the signals was done according to the multiplicities. IR spectra were recorded on a FT-IR spectrometer from Perkin-Elmer. High-resolution mass spectrometry (HRMS) was conducted on a Waters Xevo G2-XS QToF device using ESI (electrospray ionization). Low-resolution mass spectrometry (LRMS) were obtained using an HPLC-System Serie 1100 coupled with ESI-single quadrupole from Agilent. The abbreviation [M+Na]⁺ refers to the product–sodium adduct. ESI mass spectra were run on IonSpec Ultima instruments and MALDI-ToF autoflexTM (Bruker) instrument. Analytical reverse phase HPLC was performed on an HPLC-System Serie 1200 from Agilent using Synergi 4 μ m Hydro-RP 80 Å column (250 × 4.6 mm) and preparative reverse phase HPLC was performed on an Agilent 1200 using a preparative Synergi 4 μ m Hydro-RP 80 Å column (250 × 10 mm). UV-cleavage of the photo-labile linker was performed in a Vilber Lourmat black light ((VL.208.BL) lamp emitting 365 nm UV light with fractions of visible light (wavelength [nm]: 365, filter size [mm]: 230 × 60, power [W]: 2 × 8).

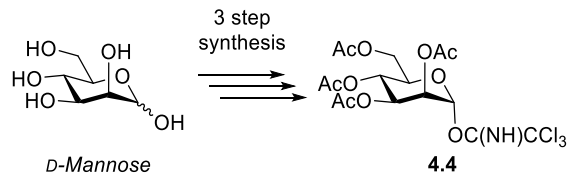
4.5.1. Syntheses of linkers and building blocks

Building block synthesis

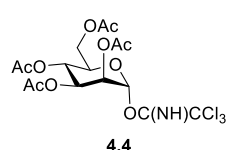


Building blocks **4.3**, **4.4**, **4.7**, **4.10**, **4.12**, **4.14-4.17**,^[69,109,204,214,216-218,232,254] were synthesized as reported, and their analytical data agree with the literature. Building blocks **4.3**, **4.6**, **4.8**, **4.11-4.15**, and **4.17** are mentioned as building block **2.18**, **2.19**, **2.21**, **2.24**, **2.25**, **2.22**, **2.23** and **2.26** respectively, in *Chapter 2*. The synthesis of the building blocks is reported in the *Experimental Section 2.5.1*.

Synthesis of 2,3,4,6-tetra-*O*-acetyl- α -D-mannopyranosyl trichloroacetimidate (**4.4**)



4.4 was prepared according to previously established procedures.

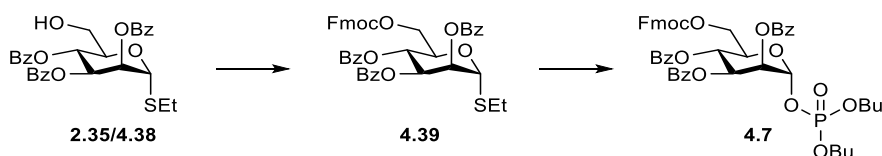


1,2,3,4,6-penta-*O*-acetyl-*D*-mannopyrane (4.33 g, 11.1 mmol, 1.00 equiv.) was dissolved in anhydr. dimethylformamide (52 mL) under argon atmosphere and hydrazine acetate (1.13 g, 12.2 mmol, 1.10 equiv.) was added. The solution was stirred for 1 h at room temperature, after which the solution was diluted with DCM and then washed with aqueous NaHCO₃ solution (100 mL). The aqueous phase was extracted with DCM (2 × 80 mL). The organic phases were combined, dried over MgSO₄ and the solvent was removed under reduced pressure. The crude product (yellow oil) was re-dissolved in anhydr. dichloromethane (80 mL) under argon atmosphere and trichloroacetonitrile (12.0 mL, 11.1 mmol, 10.0 equiv.) and DBU (410 μL, 2.78 mmol, 0.25 equiv.) were added consecutively. The solution was stirred for 2 h at room temperature. The solvent was removed under reduced pressure. The crude product was purified by flash chromatography using a mixture of hexane/ethyl acetate (3:1) as eluent.

The product was obtained as yellow solid in 60% yield (3.30 g, 6.69 mmol). ^1H NMR (400 MHz, CDCl_3): δ = 8.79 (s, 1H, C(NH)CCl₃), 6.28 (d, J = 1.9 Hz, 1H, H -1), 5.47 (dd, J = 2.9, 1.9 Hz, 1H, H -2), 5.43 – 5.37 (m, 2H, H -3, H -4), 4.28 (dd, J = 12.1, 4.7 Hz, 1H, H -6a), 4.22 – 4.18 (m, 1H, H -6b, H -5), 2.20 (s, 3H, $-\text{CH}_3$), 2.08 (s, 3H, $-\text{CH}_3$), 2.07 (s, 3H, $-\text{CH}_3$), 2.01 (s, 3H, $-\text{CH}_3$) ppm; ^{13}C NMR (101 MHz, CDCl_3): δ = 170.7, 169.9, 169.9, 169.7, 159.8, 94.5, 90.5, 71.4, 68.8, 67.9, 65.4, 62.1, 20.9, 20.8, 20.8, 20.7 ppm.

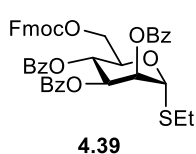
* The analytical data agree with the literature.^[232]

Synthesis of dibutoxyphosphoryloxy 2,3,4-*O*-tri-benzoyl-6-*O*-(9-fluorenylmethoxy-carbonyl)- α -D-mannopyranosyl phosphate (4.7)



Ethyl 2,3,4-tri-*O*-benzoyl-1-thio- α -D-mannosylpyranoside **2.35/4.38** was synthesized as reported in the literature^[204]

Ethyl 2,3,4-tri-*O*-benzoyl-6-*O*-(9-fluorenylmethoxycarbonyl)- α -D-thio- α -D-mannosylpyranoside (4.39)

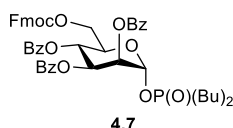


Ethyl 2,3,4-tri-*O*-benzoyl-1-thio- α -D-mannosylpyranoside **2.35/4.38** (300 mg, 0.56 mmol, 1.00 equiv.) was dissolved in anhydr. dichloromethane (6 mL) and fluorenylmethoxycarbonyl chloride (FmocCl) (217 mg, 0.84 mmol, 1.50 equiv.) and pyridine (0.23 mL, 2.80 mmol, 5.00 equiv.) were added. The reaction was stirred at room temperature overnight and after complete conversion of the starting material (TLC: hexane/ethyl acetate, 2:1), the solution was diluted with dichloromethane, extracted with 1 M aqueous HCl and aqueous NaHCO_3 solution. The organic phase was dried over MgSO_4 , filtrated and the solvent was removed under reduced pressure. The crude product was purified by flash column chromatography using a mixture of hexane/ethyl acetate (2:1). The product was obtained as a white foam in 66% yield (281 mg, 0.37 mmol). ^1H NMR (400 MHz, CDCl_3): δ = 8.12 – 7.28 (m, 23H, $-\text{Ar}$), 6.00 (d, J = 3.4 Hz, 1H, H -2), 5.81 (t, J = 10.0 Hz, 1H, H -4), 5.65 (dd, J = 10.0, 3.5 Hz, 1H, H -3), 5.08 (dd, J = 3.4, 1.7 Hz, 1H, H -1), 4.52 (dd, J = 11.8, 6.7 Hz, 1H, H -6a), 4.46 – 4.28 (m, 4H, H -6b, $-\text{CH}_2\text{-CH- Fmoc}$), 4.21 (t, J = 7.5 Hz, 1H, $-\text{CH}_2\text{-CH- Fmoc}$), 4.17 – 4.03 (m, 1H, H -5), 2.82 (m, 2H, $-\text{CH}_2\text{-CH}_3$ SEt), 1.34 (t, J = 7.4 Hz, 3H, $-\text{CH}_2\text{-CH}_3$ SEt) ppm; ^{13}C NMR (101 MHz, CDCl_3): δ = 165.7, 165.5, 165.5, 154.9, 143.4, 143.4, 141.4, 141.4, 133.7, 133.6, 133.4,

130.2 (2C), 129.9 (2C), 129.8, 129.2, 128.9 (2C), 128.7(2C), 128.6(2C), 128.4, 128.0, 127.3, 127.3, 125.4, 125.3, 120.2, 120.1, 83.1, 72.7, 71.4, 70.2, 67.1, 67.0, 66.8, 46.8, 26.1, 15.1 ppm.

* The analytical data agree with the literature.^[204]

Bibutoxyphosphoryloxy 2,3,4-O-tri-benzoyl-6-O-(9-fluorenylmethoxycarbonyl)- α -D-mannopyranosyl phosphate (4.7)

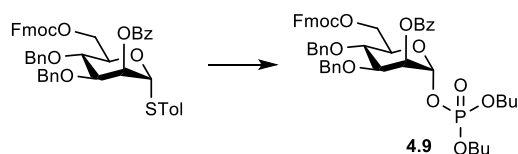


Ethyl 2,3,4-tri-O-benzoyl-6-O-(9-fluorenylmethoxycarbonyl)- 1-thio- α -D-mannosylpyranoside **4.39** (228 mg, 0.30 mmol, 1.00 equiv.) was co-evaporated twice with toluene. Freshly activated molecular sieves 4Å

and NIS (83.0 mg, 0.37 mmol, 1.23 equiv.) were suspended in DCM (3.50 mL) under argon atmosphere and the solution was cooled 0 °C. Dibutyl phosphate (0.12 mL, 0.60 mmol, 2.00 equiv.) and triflic acid (10.0 μ L, 0.09 mmol, 0.30 equiv.) were added and the reaction was stirred at 0 °C for 1 h. After complete conversion of the starting material (tlc: hexanes/ethyl acetate, 2.5:1) the reaction was quenched with aqueous NaHCO₃ solution(1.00 mL). The organic layer was washed with Na₂S₂O₃ (5.00 mL) and water (5.00 mL), dried with Na₂SO₄, filtered and the solvent was removed under reduced pressure. The crude product was purified by flash column chromatography using a mixture of hexane/ethyl acetate (2.5:1). The product was obtained as a yellow oil in 91% yield (247 mg, 0.27 mmol). ¹H NMR (400 MHz, CDCl₃): δ = 8.15 – 7.28 (m, 23H, -Ar), 6.02 (t, *J* = 10.1 Hz, 1H, *H*-4), 5.96 – 5.90 (m, 2H, *H*-1, *H*-2), 5.78 (t, *J* = 2.6 Hz, 1H, *H*-3), 4.62 – 4.56 (m, 1H, *H*-5), 4.50 – 4.43 (m, 2H, -CH₂- Fmoc), 4.43 – 4.39 (m, 1H, *H*-6a), 4.32 (dd, *J* = 10.4, 7.6 Hz, 1H, *H*-6b), 4.21 (m, 5H, 2 -OCH₂-, -CH- Fmoc), 1.77 – 1.69 (m, 4H, 2 -OCH₂-CH₂-), 1.46 (m, 4H, 2-CH₂-CH₃), 0.96 (m, 6H, 2 -CH₂-CH₃) ppm;¹³C NMR (101 MHz, CDCl₃): δ = 165.5, 165.4, 165.2, 155.0, 143.5, 143.3, 141.4, 141.3, 133.9, 133.7, 133.4, 130.1 (3C), 130.0 (2C), 129.8 (2C), 129.0, 129.0, 128.9, 128.8 (3C), 128.6 (2C), 128.5 (2C), 128.0, 128.0, 127.3, 127.3, 125.4, 125.3, 120.1, 120.1, 94.9, 70.4, 70.3, 69.7, 69.2, 68.5, 68.5, 68.4, 68.4, 66.36, 66.09, 46.8, 32.4, 32.4, 18.8, 13.7 ppm.

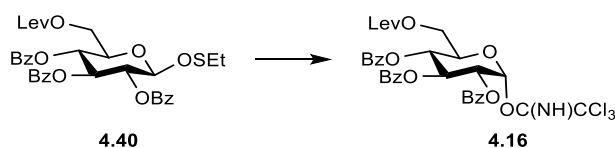
* The analytical data agree with the literature.^[204]

Synthesis of dibutoxyphosphoryloxy 2-O-benzoyl-3,4-di-O-benzyl-6-O-(9-fluorenylmethoxy-carbonyl)- α -D-mannopyranosyl phosphate (4.9)



A solution of dibutyl phosphate (2.50 mL, 12.6 mmol, 16.80 equiv.) in DCM (5 mL) was dried over molecular sieves. After 1 h the supernatant (0.90 mL) was added to a solution of 2-O-benzoyl-3,4-di-O-benzyl-6-O-(9-fluorenylmethoxycarbonyl)- α -D-mannopyranosyl thioglycoside (598 mg, 0.75 mmol, 1.00 equiv.) in DCM (5 mL) and cooled to 0 °C. Then, *N*-iodosuccinimide (NIS) (204 mg, 0.91 mmol, 1.20 equiv.) and triflic acid (TfOH) (20 μ L, 0.23 mmol, 0.30 equiv.) were added. The reaction was stirred for 2h, and quenched with an aqueous Na₂S₂O₃/NaHCO₃ solution (1:1, 100 mL), and extracted with DCM (100 mL). The organic layer was dried over Na₂SO₄ and the crude product was purified by flash column chromatography using a mixture of hexane/ethyl acetate (3:1) as eluent. The product was obtained as a yellow oil in 82% yield (544 mg, 0.62 mmol). ¹H NMR (400 MHz, CDCl₃): δ = 8.15 – 7.21 (m, 23H -Ar), 5.78 (dd, *J* = 6.5, 2.1 Hz, 1H, *H*-1), 5.71 (t, *J* = 2.6 Hz, 1H, *H*-2), 4.93 (d, *J* = 10.8 Hz, 1H, -CHH- Bn), 4.83 (d, *J* = 11.2 Hz, 1H, -CHH- Bn), 4.61 (dd, *J* = 11.1, 8.5 Hz, 2H, 2 -CHH-, Bn), 4.43 – 4.34 (m, 2H, *H*-6a, *H*-6b), 4.43 – 4.36 (m, 2H, -CH₂-CH-Fmoc), 4.26 (t, *J* = 7.4 Hz, 1H, -CH-, Fmoc), 4.20 – 3.99 (m, 6H, *H*-3, *H*-4, 2-OCH₂-CH₂-, Bu), 1.84 – 1.58 (m, 4H, 2-CH₂-CH₃, Bu), 1.49 – 1.33 (m, 1H, 4H, 2-CH₂-CH₃, Bu), 0.93 (q, *J* = 7.3 Hz, 6H, 2-CH₃ Bu) ppm; ¹³C NMR (101 MHz, CDCl₃): δ = 165.1, 155.0, 143.3, 143.1, 141.2, 137.6, 137.4, 133.4, 130.0, 129.9, 129.3, 128.5, 128.4, 128.3, 128.2, 128.1, 128.0, 127.9, 127.8, 127.1, 125.1, 120.0, 95.3, 75.3, 73.0, 71.7, 71.4, 70.0, 68.2, 68.0, 66.3, 46.7, 32.2 18.6, 13.5 ppm; IR (neat) ν_{max} : 1750, 1452, 1268, 1099, 1027 cm⁻¹; ESI-HRMS: *m/z* [M+Na]⁺ calcd. for C₅₀H₅₅O₁₂PNa: 901.3323 found 901.3353.

Synthesis of 2,3,4-tri-O-benzoyl-6-O-levulinoyl- α -glucopyranosyl trichloroacetyl imidate (4.16)

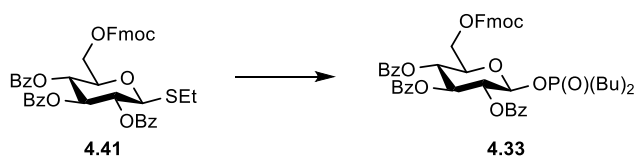


Compound 4.40 was synthesized according to literature.^[255]

Thioglycoside **4.40** (542 mg, 0.85 mmol, 1.00 equiv.) was dissolved in DCM/H₂O (21.4 mL, 10:1, v/v) and *N*-bromosuccinimide (NBS) (304 mg, 1.71 mmol, 2.00 equiv.) was added to the solution. The resulting mixture was stirred at room temperature overnight. Then, the reaction mixture was diluted with DCM (50 mL) and washed with aqueous NaHCO₃ solution (50 mL), Na₂S₂O₃ solution (50 mL), NaCl solution (50 mL), dried over Na₂SO₄, and the solvent was removed under reduced pressure. The crude product was purified by flash column chromatography using a mixture of hexane/ethyl acetate (1:1) as eluent and the obtained compound (401 mg) was used without further characterization. To a stirred solution of the pure hydrolyzed product (401 mg, 0.68 mmol, 1.00 equiv.) in anhydr. DCM (20 mL), trichloroacetonitrile (0.68 mL, 6.79 mmol, 10.0 equiv.) and 1,8-dizaabicyclo [5.4.0] undec-7-ene (DBU) (40 μ L, 0.27 mmol, 0.4 equiv.) were added consecutively, and the solution was stirred for 2 h at room temperature. The solvent was removed under reduced pressure, and the crude product was purified by flash column chromatography using a mixture of hexane/ethyl acetate (1:1) as eluent. The product was obtained as a white foam in 58% yield over 2 steps (287 mg, 0.40 mmol). ¹H NMR (400 MHz, CDCl₃): δ = 8.65 (s, 1H, C(NH)CCl₃), 7.98 – 7.83 (m, 6H, -Ar), 7.56 – 7.27 (m, 9H, -Ar), 6.82 (d, *J* = 3.6 Hz, 1H, *H*-1), 6.24 (t, *J* = 10.0 Hz, 1H, *H*-3), 5.74 – 5.67 (m, 1H, *H*-4), 5.59 (dd, *J* = 10.2, 3.6 Hz, 1H, *H*-2), 4.50 (dt, *J* = 10.3, 3.6 Hz, 1H, *H*-5), 4.32 (d, *J* = 3.8 Hz, 2H, *H*-6a, *H*-6b), 2.79 – 2.72 (m, 2H, -CH₂-Lev), 2.66 – 2.60 (m, 2H, -CH₂-Lev), 2.20 (s, 3H, -CH₃ Lev) ppm; ¹³C NMR (101 MHz, CDCl₃): δ = 206.4, 172.3, 165.6, 165.4, 165.2, 160.5, 133.6, 133.6, 133.3, 129.9, 129.8, 128.8, 128.5, 128.5, 128.5, 128.4, 128.3, 93.1, 90.7, 70.6, 70.5, 70.0, 68.3, 62.1, 37.8, 29.8, 27.8 ppm; ESI-LRMS: *m/z* [M+Na]⁺ calcd. for C₃₄H₃₀Cl₃NO₁₁Na: 756.0 found 756.0.

*The analytical data agree with the literature.^[254]

Synthesis of dibutoxyphosphoryloxy 2,3,4-tri-*O*-benzoyl-6-*O*-(9-fluorenylmethoxycarbonyl)- β -D-glucopyranosyl phosphate (**4.33**)



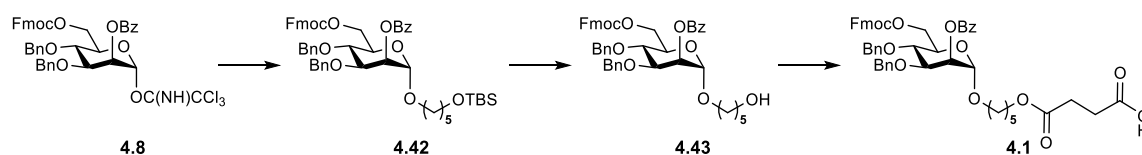
2,3,4-Tri-*O*-benzoyl-6-*O*-(9-fluorenylmethoxycarbonyl)-1-thio- β -D-glucopyranoside **4.41** was synthesized as reported in the literature.^[255]

Dibutyl hydrogen phosphate (0.16 mL, 0.79 mmol, 3.00 equiv.) was added to a round-bottom flask containing activated 4Å molecular sieves anhydr. DCM (3.00 mL) and left to stir for

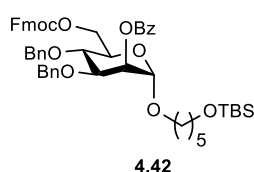
1.5 h. The molecular sieves were allowed to settle, and the supernatant (3.00 mL) was added to a solution of donor **4.41** (200 mg, 0.26 mmol, 1.00 equiv.) in anhydr. DCM (3.00 mL). The mixture was cooled down to 0 °C and NIS (72.9 mg, 0.32 mmol, 1.23 equiv.) and triflic acid (6.0 μ L, 0.79 mmol, 0.30 equiv.) were added. The reaction was stirred for 1 h and then quenched with NaHCO₃ solution (1.00 mL). The organic layer was washed with Na₂S₂O₃ (5.00 mL) and water (5.00 mL), dried with Na₂SO₄, filtered and the solvent was removed under reduced pressure. The crude product was purified by flash column chromatography using a mixture of hexane/ethyl acetate (2:1.5). The product was obtained as a white solid in 79% yield (210 mg, 0.23 mmol, 88%). ¹H NMR (400 MHz, CDCl₃): δ = 8.02 – 7.91 (m, 4H, -Ar), 7.87 – 7.81 (m, 2H, -Ar), 7.77 (d, J = 7.0 Hz, 2H, -Ar), 7.61 (m, 2H, -Ar), 7.57 – 7.48 (m, 2H, -Ar), 7.47 – 7.27 (m, 11H, -Ar), 5.94 – 5.81 (m, 1H, H-2), 5.70 – 5.59 (m, 3H, H-1, H-3, H-4), 4.51 – 4.28 (m, 4H, 2-OCH₂-, Bu), 4.27 – 4.16 (m, 2H, H-5, -CH- Fmoc), 4.11 – 3.99 (m, 2H, -CH₂- Fmoc), 3.85 – 3.67 (m, 2H, H-6a, H-6b), 1.68 – 1.57 (m, 2H, -CH₂-, Bu), 1.39 – 1.17 (m, 4H, -CH₂-, Bu), 1.13 – 1.00 (m, 2H, -CH₂-, Bu), 0.88 (t, J = 7.4 Hz, 3H, -CH₃, Bu), 0.70 (t, J = 7.4 Hz, 3H, -CH₃, Bu) ppm; ¹³C NMR (101 MHz, CDCl₃) δ 206.3, 172.3, 165.3, 165.0, 133.8, 133.6, 133.3, 129.9, 129.8, 129.7, 128.9, 128.8, 128.7, 128.5, 128.3, 94.8, 70.3, 69.7, 69.6, 69.1, 68.4, 68.4, 68.3, 68.3, 66.0, 62.4, 37.8, 32.3, 32.3, 32.2, 32.2, 29.8, 27.7, 18.6, 13.6 ppm; IR (neat) ν_{max} : 1736, 1452, 1262, 1258, 1092, 1026 cm⁻¹; ESI-HRMS: m/z [M+Na]⁺ calcd. for C₅₀H₅₁O₁₄PNa: 929.2909 found 929.2792.

Synthesis of linkers

Synthesis base-labile linker (4.1)



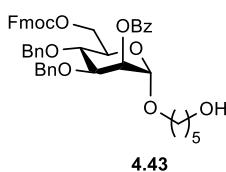
4-tert-butyltrimethylsilyloxy-pent-1-yl-2-O-benzoyl-3,4-di-O-benzyl-6-O-(9-fluorenylmethoxycarbonyl)- α -D-mannopyranoside (4.42)



2-O-Benzoyl-3,4-di-O-benzyl-6-O-(9-fluorenylmethoxycarbonyl)- α -D-mannopyranosyl trichloroacetimidate (**4.8**) (2.33 g, 2.80 mmol, 1.16 equiv.) was dissolved in anhydr. DCM (20 mL) under argon atmosphere in the presence of 4 Å molecular sieves (powder) and 5-(tert-butyl-dimethylsilyloxy)-1-pentanol (0.83 mL, 3.38 mmol, 1.40 equiv.) was added. The mixture was cooled down to -78 °C and stirred for 15 min. TMSOTf (0.04 mL, 0.24 mmol,

0.10 equiv.) was added and stirring was continued for further 10 min at $-78\text{ }^{\circ}\text{C}$. After that the mixture was allowed to warm over 1 h to $0\text{ }^{\circ}\text{C}$. The molecular sieves were filtered off and the reaction was quenched by adding NaHCO_3 solution and the organic layer was washed with NaCl solution (80 mL). The organic layer was dried over MgSO_4 and the solvent was removed under reduced pressure. The crude product was purified by flash column chromatography using a mixture of hexane/ethyl acetate (3:1) as eluent. The product was obtained as a white foam in 56% yield (1200 mg, 1.35 mmol). ^1H NMR (400 MHz, CDCl_3): δ = 8.10 – 7.17 (m, 23H, -Ar), 5.59 (dd, J = 4.2, 2.1 Hz, 1H, *H*-2), 4.91 (d, J = 1.9 Hz, 1H, *H*-1), 4.89 (d, J = 10.8 Hz, 1H, -CHH- Bn), 4.78 (d, J = 11.2 Hz, 1H, -CHH- Bn), 4.56 (m, 2H, -CHH- Bn, -CHH- Bn), 4.45 (d, J = 2.8 Hz, 2H, *H*-6 α , *H*-6 β), 4.36 (d, J = 7.6 Hz, 2H, -CH₂-CH- Fmoc), 4.23 (t, J = 7.6 Hz, 1H, -CH- Fmoc), 4.11 (dd, J = 8.6, 3.1 Hz, 1H, *H*-3), 3.97 – 3.86 (m, 2H, *H*-4, *H*-5), 3.68 (dt, J = 9.4, 6.6 Hz, 1H, -CHH-OSi), 3.57 (t, J = 6.4 Hz, 2H, -O-CH₂-), 3.42 (dt, J = 9.5, 6.5 Hz, 1H, -CHH-OSi), 1.62 – 1.46 (m, 4H; -CH₂-CH₂-CH₂-), 1.35 (ddt, J = 14.9, 8.3, 4.8 Hz, 2H; -CH₂-), 0.85 (s, 9H; -C(CH₃)₃,TBS), 0.01 (s, 6H, -Si(CH₃)₂,TBS) ppm; ^{13}C NMR (101 MHz, CDCl_3): δ = 165.7, 155.2, 143.4, 143.3, 141.2, 137.9, 137.8, 133.3, 129.9, 129.8, 128.5, 128.4, 128.3, 128.3, 128.1, 128.1, 127.9, 127.9, 127.7, 127.2, 125.2, 125.2, 120.1, 97.7, 78.4, 75.3, 73.8, 73.8, 71.5, 71.5, 70.0, 69.7, 68.8, 68.2, 66.8, 63.0, 46.7, 32.6, 29.2, 22.5, 18.4 ppm; IR (neat) ν_{max} : 2931, 2355, 1730, 1452, 1259, 1098 cm^{-1} ; ESI-HRMS: m/z $[\text{M}+\text{Na}]^+$ calcd. for $\text{C}_{53}\text{H}_{62}\text{O}_{10}\text{SiNa}$: 909.4004 found 909.4043.

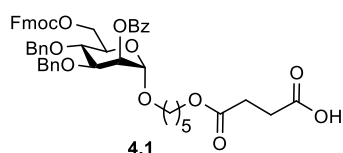
Synthesis of 5-hydroxypent-1-yl-2-O-benzoyl-3,4-di-O-benzyl-6-O-(9-fluorenylmethoxy-carbonyl)- α -D-mannopyranoside (4.43)



To a stirred solution of **4.42** (1.16 g, 1.31 mmol, 1.00 equiv.) in anhydr. MeOH (20 mL) acetyl chloride (AcCl) (0.20 mL, 0.28 mmol, 0.22 equiv.) was added, and the reaction mixture was stirred for 1 h at room temperature. Then, DCM was added (50 mL), and the reaction was neutralized with NaHCO_3 solution (50 mL). The aqueous phase was extracted with DCM (50 mL) and washed with water (70 mL). The combined organic layer was dried over Na_2SO_4 and the solvent was removed under reduced pressure. The crude product was purified by flash column chromatography using a mixture of hexane/ethyl acetate (3:1) as eluent. The product was obtained as a white foam in 98% of yield (989 mg, 1.28 mmol). ^1H NMR (400 MHz, CDCl_3): δ = 8.14 – 7.25 (m, 23H, -Ar), 5.62 (dd, J = 3.2, 1.9 Hz, 1H, *H*-2), 4.97 – 4.91 (m, 2H, *H*-1, -CHH- Bn), 4.82 (d, J = 11.2 Hz, 1H, -CHH- Bn), 4.60 (t, J = 10.8 Hz, 2H, -CHH- Bn, -CHH- Bn), 4.52 – 4.45 (m, 2H, *H*-6 α , *H*-6 β), 4.40 (d, J = 7.5 Hz, 2H, -CH₂-CH- Fmoc), 4.27 (t, J = 7.5 Hz, 1H, -CH- Fmoc), 4.14 (m, 1H, *H*-3), 3.99 – 3.92 (m, 2H, *H*-4, *H*-

5), 3.73 (dt, $J = 9.7, 6.5$ Hz, 1H, -CHH-OH), 3.64 (t, $J = 6.5$ Hz, 2H, -O-CH₂-), 3.47 (dt, $J = 9.7, 6.3$ Hz, 1H, -CHH-OH), 1.66 – 1.52 (m, 4H, -CH₂-CH₂-CH₂-), 1.43 (qd, $J = 7.7, 5.5$ Hz, 2H, -CH₂-), ppm; ¹³C NMR (101 MHz, CDCl₃): $\delta = 165.7, 155.2, 143.4, 143.3, 141.2, 137.9, 137.8, 133.3, 129.9, 129.8, 128.5, 128.4, 128.3, 128.3, 128.1, 128.1, 127.9, 127.9, 127.7, 127.2, 125.2, 125.2, 120.1, 97.7, 78.4, 75.3, 73.8, 73.8, 71.5, 71.5, 70.0, 69.7, 68.8, 68.2, 66.8, 63.0, 46.7, 32.6, 29.2, 22.5, 18.4$ ppm; IR (neat) ν_{\max} : 2982, 1723, 1452, 1263, 1073 cm⁻¹; ESI-HRMS: m/z [M+Na]⁺ calcd. for C₄₇H₄₈O₁₀Na: 795.3140 found 795.3163.

Synthesis of 4-succinoyloxypent-1-yl-2-O-benzoyl-3,4-di-O-benzyl-6-O-(9-fluorenylmethoxy-carbonyl)- α -D-mannopyranoside (4.1)



To a stirred solution of **4.43** (989 mg, 1.28 mmol, 1.00 equiv.) in pyridine (4 mL) were added succinic anhydride (384 mg, 3.84 mmol, 3.00 equiv.) and stirred at 65 °C overnight under argon atmosphere. After conversion, solvents were removed under reduced pressure, and the residue was co-evaporated with toluene (3 × 10 mL). The crude product was purified by flash column chromatography using a mixture of hexane/ethyl acetate (1:1, with 0.5% of acetic acid) as eluent. The product was obtained as a white foam in 79% yield (885 mg, 1.02 mmol, 79%). ¹H NMR (400 MHz, CDCl₃): $\delta = 8.14 - 7.20$ (m, 23H, -Ar), 5.68 (dd, $J = 3.2, 1.9$ Hz, 1H, H-2), 4.96 – 4.90 (m, 3H, H-1, -CHH- Bn), 4.82 (d, $J = 11.1$ Hz, 1H, -CHH- Bn), 4.64 (d, $J = 10.9$ Hz, 1H, -CHH- Bn), 4.60 (d, $J = 11.1$ Hz, 1H, -CHH- Bn), 4.47 (m, 2H, H-6 α , H-6 β), 4.40 (d, $J = 1.5$ Hz, 2H, -CH₂-CH- Fmoc), 4.27 (d, $J = 7.5$ Hz, 1H, -CH- Fmoc), 4.23 – 4.18 (m, 1H, H-3), 4.18 – 4.09 (m, 2H, -CH₂-O-CO), 4.03 – 3.96 (m, 2H, H-4, H-5), 3.72 (ddd, $J = 9.6, 7.1, 5.3$ Hz, 1H, -O-CH₂-CH₂-), 3.47 (dt, $J = 9.6, 5.7$ Hz, 1H, -O-CH₂-CH₂-), 2.66 – 2.55 (m, 4H, -CO-CH₂-CH₂-COOH), 1.64 (tp, $J = 17.7, 5.9$ Hz, 4H, -CH₂-CH₂-CH₂-), 1.45 (ddt, $J = 15.4, 13.5, 7.7$ Hz, 2H, -CH₂-CH₂-CH₂-) ppm; ¹³C NMR (101 MHz, CDCl₃): $\delta = 174.8, 172.4, 166.0, 155.3, 143.5, 143.4, 141.4, 137.9, 137.5, 133.5, 130.1, 129.8, 129.1, 128.7, 128.6, 128.6, 128.4, 128.3, 128.2, 128.2, 128.0, 127.8, 127.3, 125.3, 125.3, 120.2, 97.9, 78.2, 75.5, 73.9, 71.6, 70.1, 69.6, 69.1, 68.2, 66.8, 64.7, 46.8, 29.2, 28.6, 23.1$ ppm; IR (neat) ν_{\max} : 2982, 1724, 1386, 1255, 1154 cm⁻¹; ESI-HRMS: m/z [M+Na]⁺ calcd. for C₅₁H₅₂O₁₃Na: 895.3300 found 895.3337.

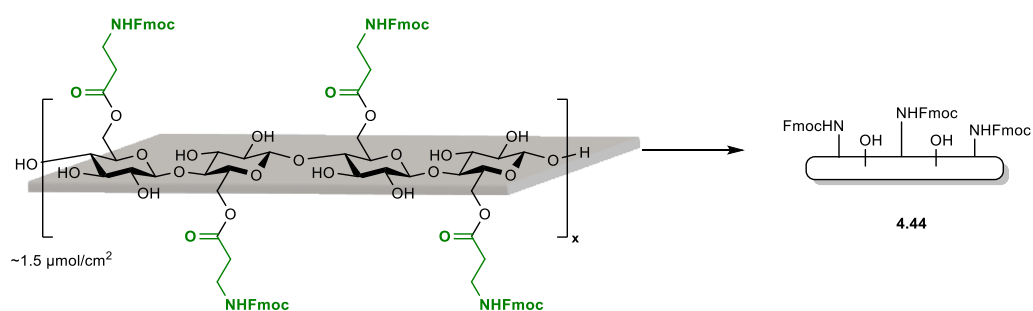
Synthesis of photocleavable linker (4.23)

Photocleavable linker **4.23** is mentioned as photocleavable linker **2.12**, in *Chapter 2*. The synthesis is reported in the *Experimental Section 2.5.1*.

4.5.2. Functionalization of cellulose membrane

Pretreatment of cellulose membrane

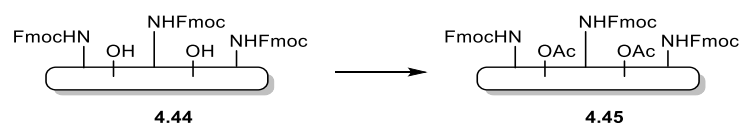
Commercially available Fmoc- β -alanine functionalized membrane is shown as a simplified representation **4.44** (Experimental Figure 4.1). The membrane was immersed in DMF for swelling in a petri dish. After 15 min of shaking (300 rpm) at ambient temperature, DMF was removed. The membrane was washed consecutively with DMF (3 \times 3 min each), MeOH (1 \times 2 min), DCM (1 \times 1 min) and dried in a jet of air.



Experimental Figure 4.1: Simplified representation of cellulose membrane used for our experiments

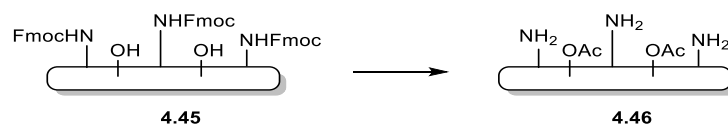
Capping of β -alanine-cellulose membrane

The free hydroxyl groups on the membrane **4.44** were capped, with the acidic capping mixture (see Preparation of stock solutions) for 30 min. The same process repeated for another 30 min at room temperature (300 rpm). Then, the membrane washed consecutively with DMF (3 \times 10 mL for 3 min each), MeOH (1 \times 10 mL for 2 min), DCM (1 \times 10 mL for 1 min) and dried in a jet of air.



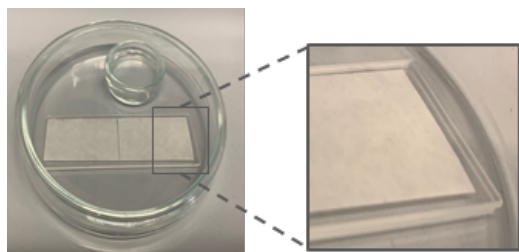
Fmoc-deprotection of β -alanine on cellulose membrane

The Fmoc-protected β -alanine-cellulose membrane **4.45** was immersed in Fmoc-deprotection solution (2 mL/cm² of membrane, see Preparation of solutions) for 20 min on a shaker. The membrane was washed and dried by a jet of air to obtain the free amino groups on the membrane **4.46**.



Functionalization with base-labile linker

Base-labile linker attachment



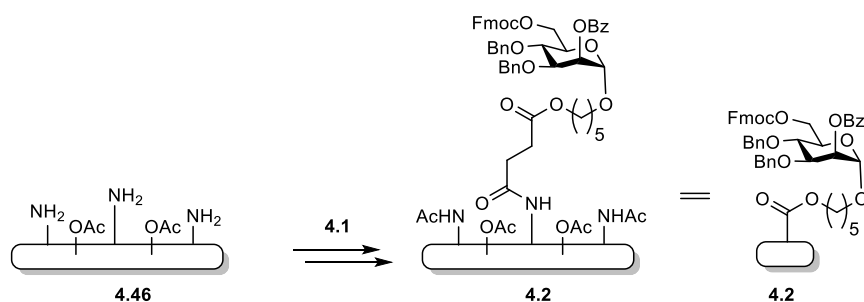
Experimental Figure 4.2: Attachment of linker on cellulose membrane (sandwich method).

Base-labile linker **4.1** (2.00 equiv) was dissolved in DMF (peptide grade) (0.05 mL/cm²) in a vial, DIC (2.00 equiv.) and hydroxybenzotriazole (HOBt) (2.00 equiv.) were added consecutively, and the vial was shaken for 5 min. The resulting solution was pipetted on the free amino membrane **4.46** between two microscope glass slides in a sandwich approach (Experimental Figure 4.2), and

was left overnight in a Petri dish to react under humid DMF conditions. Then, the membrane was washed consecutively with DMF (3 × 10 mL for 3 min each), MeOH (1 × 10 mL for 2 min), and DCM (1 × 10 mL for 1 min) and dried by a jet of air.

Capping of unreacted amine groups

The remaining unreacted free NH₂ groups on the membrane were subjected to basic acetylation (see Preparation of solutions) for 30 min. The same process was repeated with a freshly prepared capping solution for another 30 min at room temperature (300 rpm). Then, the membrane was dried in a jet of air to obtain the Fmoc-protected amine base-labile functionalized membrane **4.2** with capped unreacted amine groups.



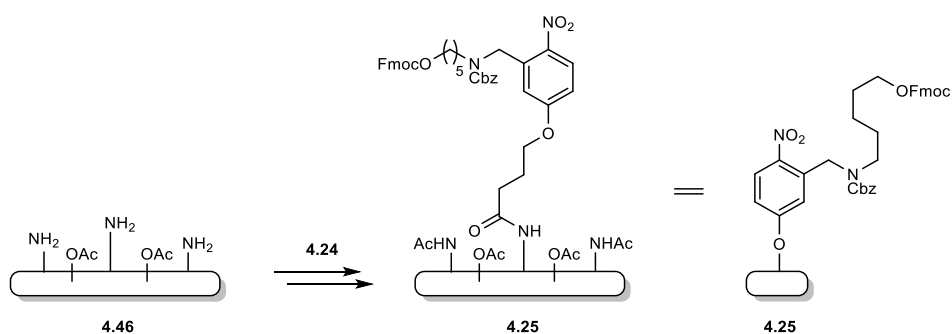
Functionalization with photocleavable linker

Photocleavable linker attachment

Photocleavable linker **4.24** (2.00 equiv.) was dissolved in DMF (peptide grade) (0.05 mL/cm²) in a vial, DIC (2.00 equiv.) and HOBt (2.00 equiv.) were added consecutively and the vial was shaken for 5 min. The resulting solution was pipetted on the free amino membrane **4.46**, between two microscope glass slides, in a sandwich approach (Experimental Figure 4.2), and was left overnight in a petri dish to react under humid DMF conditions. Then, the membrane was washed consecutively with DMF (3 × 10 mL for 3 min each), MeOH (1 × 10 mL for 2 min), DCM (1 × 10 mL for 1 min) and dried by a jet of air.

Capping of unreacted amine groups

The remaining unreacted free NH₂ groups on the membrane were subjected to basic acetylation (see Preparation of solutions) for 30 min. The same process was repeated with a freshly prepared capping solution for another 30 min at room temperature (300 rpm). Then, the membrane was dried in a jet of air to obtain the Fmoc-protected amine-base-labile-functionalized membrane **4.25** with capped unreacted amine groups.



Quantification/loading determination of functionalized membrane

Dry functionalized **4.2/4.25** membrane (2 cm², suppliers loading: 1.55-1.33 μmol/cm²), was immersed in DMF for swelling in a vial. After 15 min of shaking (300 rpm) at rt, DMF was removed and Fmoc-deprotection solution was added. The membrane was shaken for 20 min at room temperature (300 rpm). From this vial, containing the membrane, 100 μL of the Fmoc deprotection solution were diluted in 900 μL of the stock deprotection solution reaching 1.00 mL of total volume and the UV absorption of this solution was measured at 290 nm. Calibration of the absorbance of the spectrophotometer was performed at 290 nm using 1.00 mL of the stock Fmoc-deprotection solution. The absorbance was measured three times

for each solution and the average value was obtained for the determination of the Fmoc loading of the functionalized membrane using the following equation:

$$\text{Loading } \left(\frac{\mu\text{mol}}{\text{cm}^2} \right) = (E \times V \times DF) / (d \times \epsilon \times A)$$

E: Average of absorbance of the sample solution at 290 nm

V: Volume of deprotection solution used (4.00 mL)

DF: Dilution factor (10)

d: Path length of cuvette (1 cm)

ϵ : Molar absorption coefficient at 290 nm (5253 M⁻¹ cm⁻¹)

A: Size of membrane (2 cm²)

Loading of used membrane: $(0.20 \times 4 \text{ mL} \times 10) / (1 \text{ cm} \times 5253 \times 10^3 \text{ mL} \times 10^{-6} \mu\text{mol}^{-1} \text{ cm}^{-1} \times 2 \text{ cm}^2) \approx 0.76 \mu\text{mol}/\text{cm}^2$

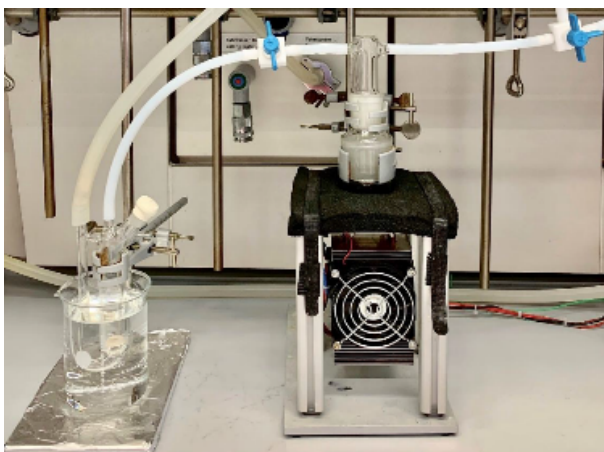
4.5.3. VaporSPOT glycosylation

Preparation of stock solutions

- **Building block solution:** BB (6.00 equiv./cycle) was dissolved in 50 μL of anhydr. DCM.
- **Fmoc-deprotection:** A solution of 20% piperidine in DMF (v/v) was prepared.
- **Acidic capping:** A solution of 10% Ac₂O and 2% MsOH in DCM (v/v) was used.
- **Basic capping:** A solution containing 10% Ac₂O and 20% DIPEA in DMF (v/v) was prepared.
- **Acidic wash:** A solution containing 0.5% TMSOTf in anhydr. DCM was prepared.
- **Activator solution A:** A solution of 8% TMSOTf in anhydr. DCM was prepared.
- **Activator solution B:** A solution of 4% TMSOTf in anhydr. DCM was prepared.
- **Activator solution C:** A solution of 2% TMSOTf in anhydr. DCM was prepared.
- **Methanolysis solution:** Solution for deprotection of the ester protecting groups & cleavage from the membrane prepared dissolving 0.5 mL of sodium methoxide (NaOMe, 0.5 M) solution in 5 mL of methanol (MeOH).

Homebuilt setup

The glycosylation setup (Experimental Figure 4.3: Experimental setup used for VaporSPOT glycosylation.) consists of five components: a vapor generator; a syringe; a glycosylation



Experimental Figure 4.3: Experimental setup used for VaporSPOT glycosylation.

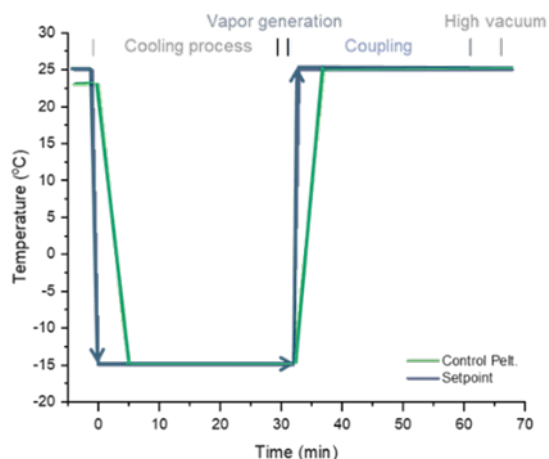
chamber; two valves controlling the flow and the amount of the deposited solution, and a computer system for temperature control inside the glycosylation chamber. The temperature is controlled by a thermoelectric cooling element, which is located at the bottom of the glycosylation chamber, connected to a computer for automated software control of the temperature during the synthesis. The thermoelectric cooling element PE-127-14-11 (15.7 V, 8.5 A, 82 W, Laird

Connectivity, UK) for temperature control of the chamber was connected to a power supply unit Manson HCS - 3402 (0 – 32 V, 0 – 20 A, Manson Engineering Industrial Ltd, Hong Kong). To ensure temperature stability of the system, the back of the thermoelectric element is connected to a CPU heat sink with a fan, whereas the top is covered with a thin copper plate and an insulating foam with a cutaway for the glycosylation chamber. A custom-developed software (LabView) is used to control the temperature of the thermoelectric cooling element, which is monitored by a temperature sensor at the copper plate. The two valves provide control over the atmosphere inside the setup (air, vacuum, and argon). The right valve provides atmospheric air, as well as high vacuum or argon (connection with the Schlenk line), while the left valve is connected with the vapor generator vessel. The vapor generation vessel is a fritted U-shaped glass tube connected with the Schlenk line for argon flow, which results in vapor generation of the activator solution and transfer into the glycosylation chamber. The activator solution is injected into the vapor generator with a 1 mL syringe. All tubing and valves are PTFE-based.

Temperature profile and regulation system

The thermoelectric cooling element, which is located at the bottom of the glycosylation chamber is connected to a computer. The temperature range per glycosylation cycle is from -15 °C to room temperature (25 °C), set temperature (set point, **Error! Reference source not found.**, blue). The cooling process, before initiating the glycosylation, lasts 30 min, while the cooling rate is 8 °C/min. After the cooling process, the reaction starts by transferring the total amount of the activator solution into the glycosylation chamber using argon flow (2 min) at -15 °C. Then, the temperature is increased from -15 °C to room temperature (25 °C), and

the reaction continues for 30 min under these conditions. The heating and cooling rate are both 8 °C/min. After 30 min, the setup was subjected to high vacuum for 5 min at 25 °C, to remove the remaining solvent and activator from the glycosylation chamber. Experimental Figure 4.4. depicts the temperature profile of every step inside the glycosylation chamber, with the green line representing the actual (measured) temperature profile and in blue the set points.



Experimental Figure 4.4: Temperature profile inside the reaction vessel during one coupling cycle (cooling and heating rate: 8 °C/min).

Modules of VaporSPOT

Module A: Membrane preparation for synthesis (39 min)

All syntheses were performed on 2 cm² cellulose membrane pieces (unless otherwise stated). The membrane **4.2/4.25** was initially placed into a vial, and swollen for 15 min in DMF on a shaker (300 rpm) at room temperature prior to synthesis. Then, the membrane was washed with DMF (3 × 3 min), deprotected using the Fmoc-deprotection solution, and washed with DMF (3 × 3 min), MeOH (1 × 3 min), and DCM (1 × 3 min) consecutively. The membrane was placed in a Schlenk flask and dried overnight under high vacuum (16 h).

Module B: Acidic wash prior to glycosylation (58 min)

The membrane was swollen again for 15 min in anhyd. DCM under inert conditions, and washed with anhydr. DCM (3 mL, 3 × 1 min). The acidic wash solution was added to the flask under inert conditions and stirred for 1 min. The acidic solution was removed, the membrane washed with anhydr. DCM (3 mL, 1 × 3 min), DMF (3 mL, 1 × 3 min), DCM (3 mL, 1 × 3 min) and dried under high vacuum for 30 min.

Module C: Spotting of BB (31 min)

The building block solution (6.00 equiv./glycosylation cycle in 100 μ L of anhydr. DCM, with respect to the loading of the used functionalized membrane) was spotted onto the membrane carefully under high argon flow inside the flask, 1 min, and dried for 30 min under high vacuum.



Experimental Figure 4.5: Spotting of a glycosyl donor onto a functionalized membrane, bearing a glycosyl acceptor, inside a Schlenk flask under argon counter flow.

Module D: Vapor glycosylation (106 min)

The membrane, carrying an unreacted glycosyl donor (and the acceptor) was placed inside the glycosylation chamber and the temperature adjusted to $-15\text{ }^{\circ}\text{C}$. For the next 30 min, the glycosylation chamber was kept under constant argon flow, and after the set temperature was reached, the reaction started by transferring the activator solution into the glycosylation chamber using argon flow. After complete deposition of solvent and activator inside the chamber (2 min), the two valves of the system were closed. Then, the temperature was increased to room temperature ($8\text{ }^{\circ}\text{C}/\text{min}$ to $25\text{ }^{\circ}\text{C}$). After 30 min, the setup was subjected to high vacuum for 5 min to remove the remaining solvent and activator from the glycosylation chamber. Finally, the membrane was washed with DCM ($1 \times 3\text{ min}$), DMF ($1 \times 3\text{ min}$), DCM ($1 \times 3\text{ min}$), dried in a jet of air, and stored under high vacuum for 30 min. Modules C and D were repeated one more time to ensure high/quantitative conversion.

Module E: Fmoc-deprotection (35 min)

The membrane was deprotected using the Fmoc-deprotection solution for 20 min, and washed with DMF ($3 \times 3\text{ min}$), MeOH ($1 \times 3\text{ min}$), and DCM ($1 \times 3\text{ min}$). Then, the membrane was placed in a Schlenk flask, and dried overnight under high vacuum (16 h). All modules were repeated for the synthesis of longer structures.

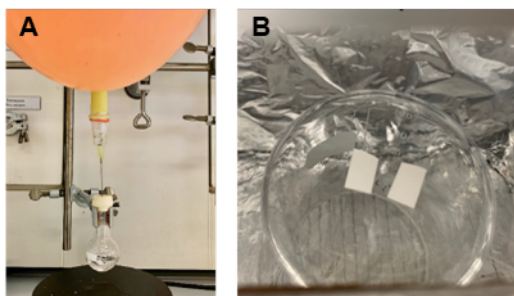
Post-Synthesis manipulation

Module F1: Base-labile linker

After completion of the synthesis, the oligosaccharides were deprotected and simultaneously cleaved from the solid support/ membrane using Zemplén deprotection conditions. The membranes were placed separately in 5 mL flasks, containing a stirring bar and 2 mL of the deprotection solution was added. The mixtures were left to react overnight at room temperature (Experimental Figure 4.6A). Then, the solution was neutralized by Amberlite IR-120 H⁺. Finally, the solution was filtered off, washed with acetonitrile (MeCN) and water *via* a hydrophobic syringe filter, and concentrated under reduced pressure.

Module F2: Photocleavable linker

After completion of the synthesis, the oligosaccharides bound to the photo-labile linker were subjected to cleavage under a UV-lamp (365 nm, 2 × 8 W). The distance between the lamp and the membranes was approximately 4 cm, and the membranes were irradiated for 15 min on both sides (Experimental Figure 4.6B). Then, each membrane was cut into small pieces and placed inside a vial. The pieces were washed with MeOH (2 mL × 5 min) and DCM (2 mL × 5 min). The solutions were concentrated under reduced pressure.



Experimental Figure 4.6: Post synthesis manipulation of synthesized structures: A). Deprotection and cleavage of the synthesized structure using NaOMe in MeOH solution, and B) Parallel UV-cleavage of synthesized structures on two different membrane pieces under UV-light.

Purification & Characterization

Module G: Reverse-phase purification

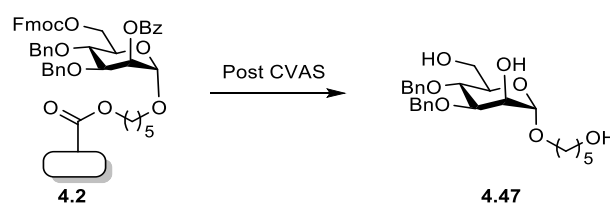
To identify and characterize the final oligosaccharides, the crude products were dissolved in water and purified in a preparative reverse phase HPLC (Agilent 1200 Series, Method A), and the pure compounds were analyzed using an analytical HPLC (Agilent 1200 Series, Method B).

- Method A: Synergi Hydro RP18 column, 250 × 10 mm, flow rate of 4 mL/min with 5% MeCN in H₂O (0.1% formic acid) as eluents [isocratic (5 min), linear gradient to 5% MeCN (35 min), linear gradient to 100% MeCN (5 min)].
- Method B: Synergi Hydro RP18 column, 250 × 4.6 mm, flow rate of 1 mL/min with 5% MeCN in H₂O (0.1% formic acid) as eluents [isocratic (5 min), linear gradient to 5% MeCN (35 min), linear gradient to 100% MeCN (5 min)].

Finally, all deprotected products were lyophilized prior to characterization.

4.5.4. Oligosaccharide syntheses

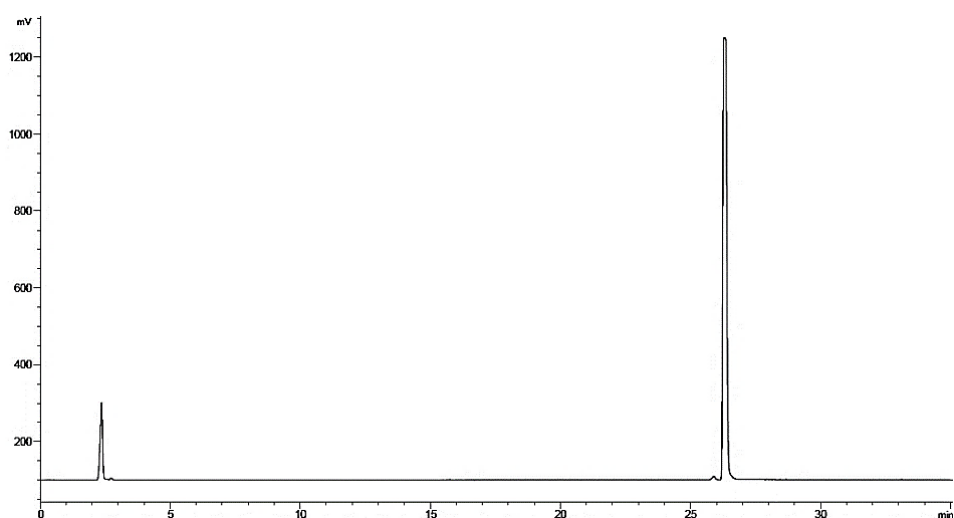
5-Hydroxypentyl 3,4-di-O-benzy- α -D-mannopyranoside (4.47)



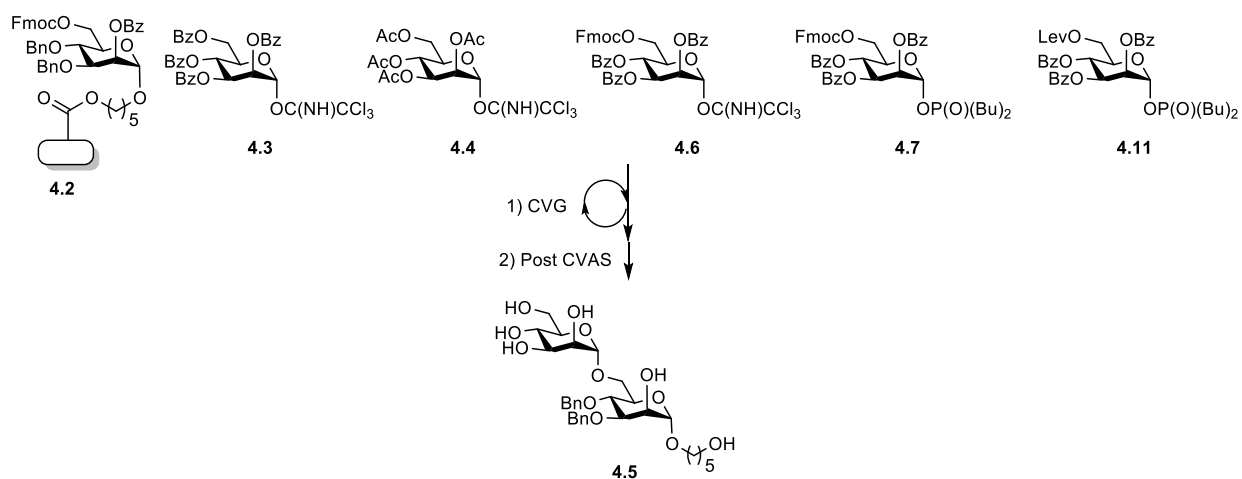
Action	BB	Modules	Notes	Result (mg, μ mol, yield)
CVG	-	A	4.2 swell	0.45 mg, 1.00 μ mol, 40%
Post CVG	-	F1	-	

¹H NMR (400 MHz, D₂O): δ = 7.51 – 7.17 (m, 10H, -Ar), 4.81 (d, J = 1.9 Hz, 1H, H -1), 4.71y (dd, J = 11.0, 1.9 Hz, 2H; -CH₂-Ar), 4.70 (d, J = 1.3 Hz, 2H; -CH₂-Ar); 4.09 (dd, J = 3.1, 1.9 Hz, 1H; H -2), 3.81 – 3.75 (m, 2H, H -3; H -6 α), 3.71 (d, J = 9.8 Hz, 1H; H -4), 3.69 – 3.66 (m, 1H; H -6 β), 3.66 – 3.60 (m, 1H; -O-CHH-CH₂-), 3.57 (ddd, J = 9.8, 5.5, 2.1 Hz, 1H; H -5), 3.51 (t, J = 6.6 Hz, 2H, -CH₂-OH), 3.45 (dd, J = 9.9, 6.0 Hz, 1H, -O-CHH-CH₂-), 3.57 (ddd, J = 9.8, 5.5, 2.1 Hz, 4H, -CH₂-CH₂-), 1.28 – 1.11 (m, 2H, -O-CH₂-CH₂-) ppm; ¹³C NMR (101 MHz, CDCl₃): δ = 171.9, 138.2, 138.0, 129.7, 129.6, 129.4, 129.3, 100.5, 79.4, 76.0, 75.0, 72.8, 72.2, 68.6, 67.9, 62.6, 61.6, 31.9, 29.1, 22.7 ppm; ESI-HRMS: m/z [M+Na]⁺ calcd. for C₂₅H₃₄O₇Na: 469.2196 found 469.2203.

RP-HPLC (ELSD trace, Method B, t_R = 26.2 min)



5-Hydroxypentyl α -D-mannopyranosyl-(1 \rightarrow 6)-3,4-di-O-benzyl- α -D-mannopyranoside (4.5)



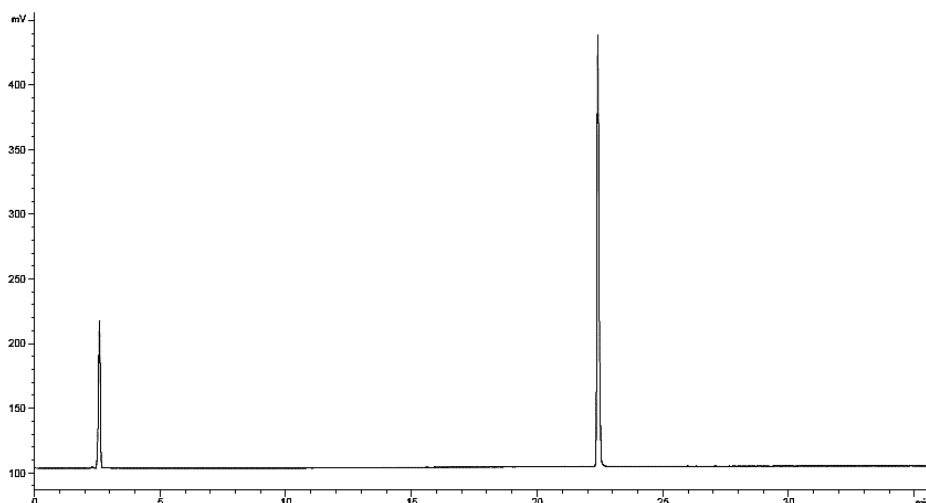
Action	BB	Modules	Notes	Result (mg, μ mol, yield)
Method A				
CVG	4.3	A	4.2 swell; Fmoc-deprotection	
Post CVG		B; C; D	Activator solution A, 1.00 mL	0.35 mg, 0.58 μ mol, 26%
		F1		
Method B				
CVG	4.3	A	4.2 swell; Fmoc-deprotection (1 cm ²)	
Post CVG		B; C; D	Activator solution B, 1.00 mL	0.1 mg, 0.16 μ mol, 21%
		F1		

Method C			
		A	4.2 swell; Fmoc-deprotection
CVG	4.4	B; C; D	Activator solution A, 1.00 mL
			0.29 mg, 0.48 μ mol, 21%
Post CVG		F1	
Method D			
		A	4.2 swell; Fmoc-deprotection
CVG	4.6	B; C; D; C; D ^[*]	Activator solution A, 1.00 mL
			0.41 mg, 0.67 μ mol, 30%
Post CVG		F1	
Method E			
		A	4.2 swell; Fmoc-deprotection
CVG	4.7	B; C; D; C; D	Activator solution A, 1.00 mL
			0.21 mg, 0.35 μ mol, 15%
Post CVG		F1	
Method F			
		A	4.2 swell; Fmoc-deprotection (1 cm ²)
CVG	4.11	B; C; D; C; D	Activator solution A, 1.00 mL
			0.23 mg, 0.38 μ mol, 48%
Post CVG		F1	

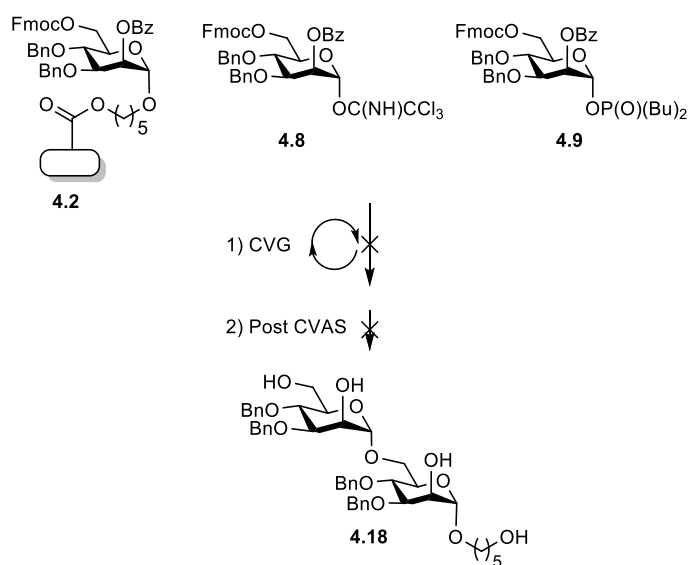
[*] Single glycosylation of building block **4.6** under the same glycosylation conditions (modules A, B, C, D, and Post CVG) delivered only 0.24 mg, 17% of the desired dimer **4.5**. Thus, repetition of modules C and D was required to increase the coupling yield. According to this result, Modules C and D were repeated for all building blocks bearing electron-donating groups (EDG) as well temporary protecting groups for chain elongation.

¹H NMR (700 MHz, D₂O): δ = 7.37 – 7.25 (m, 8H), 7.22 – 7.18 (m, 2H), 4.65 (s, 2H), 4.63 (s, 1H), 4.48 (dd, *J* = 11.2, 5.0 Hz, 2H), 4.03 (t, *J* = 2.4 Hz, 1H), 3.85 – 3.79 (m, 1H), 3.78 – 3.34 (m, 13H), 1.43 (dd, *J* = 21.1, 7.2 Hz, 4H), 1.28 – 1.11 (m, 2H) ppm; ¹³C NMR (176 MHz, D₂O): δ = 128.7, 128.4, 128.4, 99.5, 78.2, 74.7, 73.7, 72.6, 71.3, 70.1, 69.8, 67.9, 66.6, 66.1, 65.9, 61.1, 60.5, 30.7, 27.6, 22.0 ppm (in respect to the coupled ¹H–¹³C HSQC NMR); ESI-HRMS: *m/z* [M+Na]⁺ calcd. for C₃₁H₄₄O₁₂Na: 631.2724 found 631.2745.

RP-HPLC (ELSD trace, Method B, *t_R* = 22.4 min)



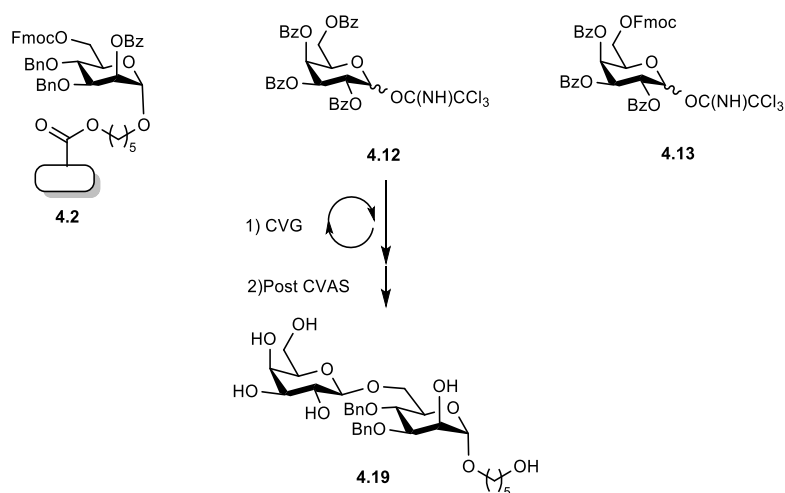
5-Hydroxypentyl 3,4-di-O-benzyl- α -D-mannopyranosyl-(1 \rightarrow 6)-3,4-di-O-benzyl- α -D-manno-pyranoside (4.18)



Action	BB	Modules	Notes	Result (mg, mmol, yield)
Method A				
CVG	4.8	A	4.2 swell; Fmoc-deprotection	--
Post CVG		B; C; D; C; D	Activator solution A, 1.00 mL	
		F1		
Method B				
CVG	4.9	A	2 swell; Fmoc-deprotection	--
Post CVG		B; C; D; C; D	Activator solution A, 1.00 mL	
		F1		

The desired disaccharide **4.18** was not obtained. The glycosylation reaction for BBs **4.8** and **4.9** were performed using 8% TMSOTf activator solution and 6.00 equiv. of BB/glycosylation.

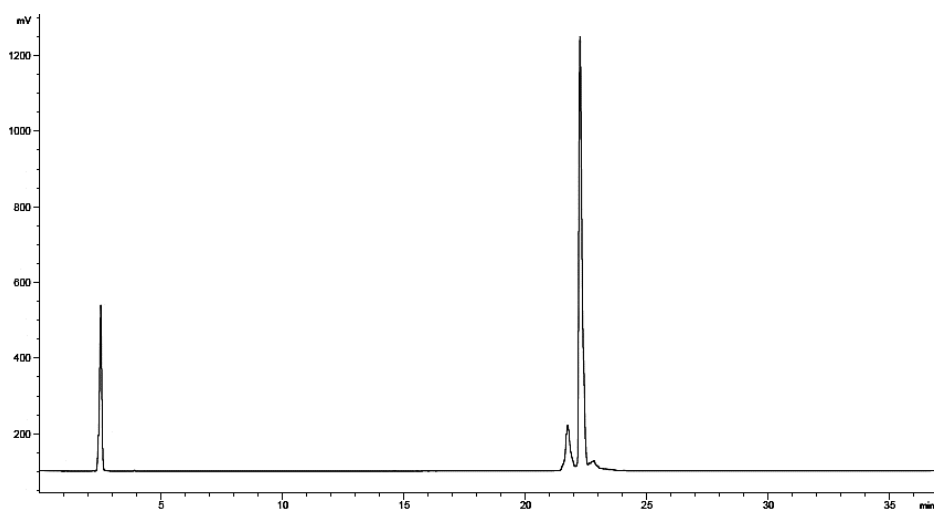
5-Hydroxypentyl β -D-galactopyranosyl-(1 \rightarrow 6)-3,4-di-O-benzyl- α -D-mannopyranoside (4.19)



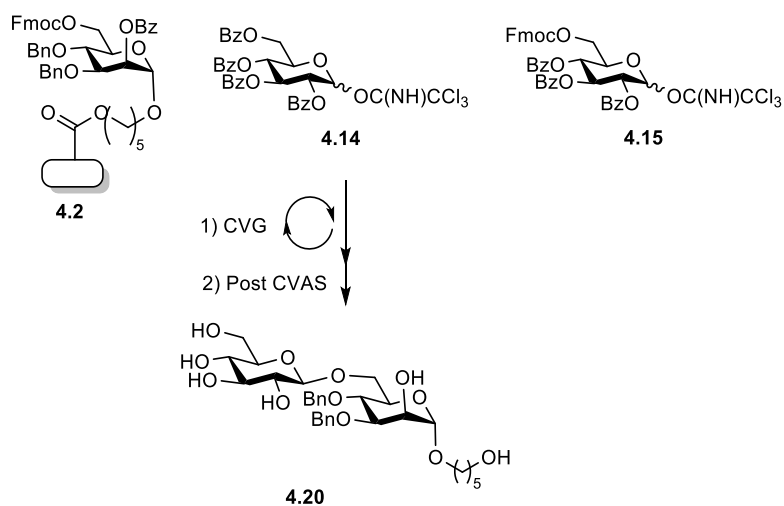
Action	BB	Modules	Notes	Result (mg, μ mol, yield)
Method A				
CVG	4.12	A	4.2 swell; Fmoc-deprotection	0.35 mg, 0.58 μ mol, 26%
Post CVG		B; C; D	Activator solution A, 1.00 mL	
		F1		
Method B				
CVG	4.13	A	4.2 swell; Fmoc-deprotection	0.17 mg, 0.28 μ mol, 15%
Post CVG		B; C; D; C; D	Activator solution A, 1.00 mL	
		F1		

^1H NMR (600 MHz, D_2O): δ = 7.37 – 7.27 (m, 10H), 4.78 (m, 3H), 4.57 – 4.50 (m, 2H), 4.22 (d, J = 7.8 Hz, 1H), 4.07 – 3.97 (m, 3H), 3.83 – 3.43 (m, 14H), 2.67 (d, J = 11.0 Hz, 1H), 1.54 – 1.42 (m, 4H), 1.35 – 1.24 (m, 2H) ppm; ^{13}C NMR (176 MHz, D_2O): δ = 128.5, 128.4, 127.1, 103.0, 99.4, 78.5, 75.1, 74.9, 73.3, 72.6, 70.8, 70.5, 70.0, 67.7, 67.6, 66.4, 60.8, 30.7, 27.0, 21.7 ppm (in respect to the HSQC); ESI-HRMS: m/z $[\text{M}+\text{Na}]^+$ calcd. for $\text{C}_{31}\text{H}_{44}\text{O}_{12}\text{Na}$: 631.2724 found 631.2754.

RP-HPLC (ELSD trace, Method B, t_R = 22.2 min)



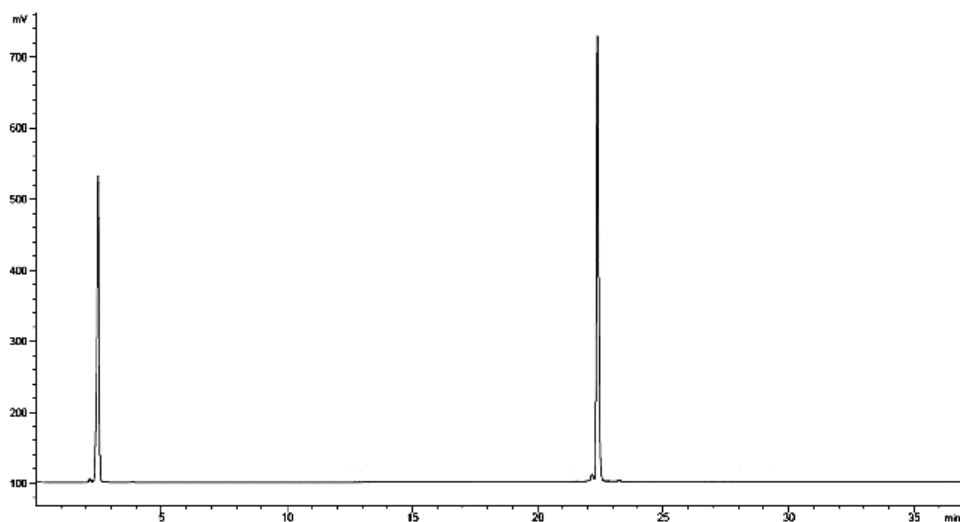
5-Hydroxypentyl β -D-glucopyranosyl-(1 \rightarrow 6)-3,4-di-O-benzyl- α -D-mannopyranoside (4.20)



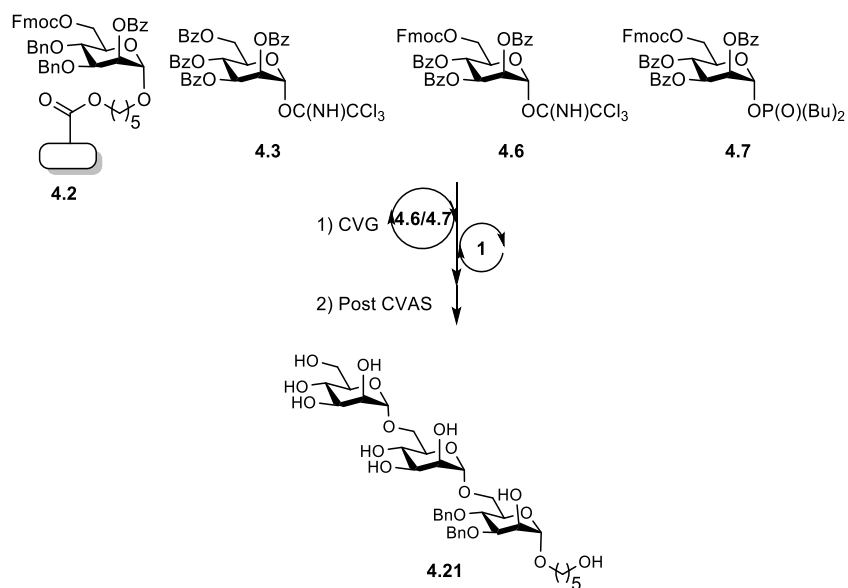
Action	BB	Modules	Notes	Result (mg, mmol, yield)
Method A				
CVG	4.14	A	4.2 swell; Fmoc-deprotection	
		B; C; D	Activator solution A, 1.00 mL	0.29 mg, 0.48 μ mol, 20%
Post CVG		F1		
Method B				
CVG	4.15	A	4.2 swell; Fmoc-deprotection	
		B; C; D; C; D	Activator solution A, 1.00 mL	0.08 mg, 0.13 mmol, 16%
Post CVG		F1		

^1H NMR (600 MHz, D_2O): $\delta = 7.38 - 7.24$ (m, 10H), 4.78 (m, 3H), 4.55 (t, $J = 11.3$ Hz, 2H), 4.27 (d, $J = 7.9$ Hz, 1H), 4.09 – 3.96 (m, 2H), 3.83 – 3.18 (m, 14H), 1.59 – 1.45 (m, 4H), 1.28 – 1.11 (m, 2H ppm); ^{13}C NMR (176 MHz, D_2O , D_2O): $\delta = 128.8, 128.6, 128.5, 102.6, 99.6, 78.2, 75.3, 75.3, 75.1, 73.3, 72.6, 70.9, 70.4, 66.7, 69.4, 69.2, 61.5, 30.6, 27.7, 21.7$ ppm (in respect to the coupled ^1H - ^{13}C HSQC NMR); ESI-HRMS: m/z $[\text{M}+\text{Na}]^+$ calcd. for $\text{C}_{31}\text{H}_{44}\text{O}_{12}\text{Na}$: 631.2724 found 631.2756.

RP-HPLC (ELSD trace, Method B, $t_R = 22.3$ min)



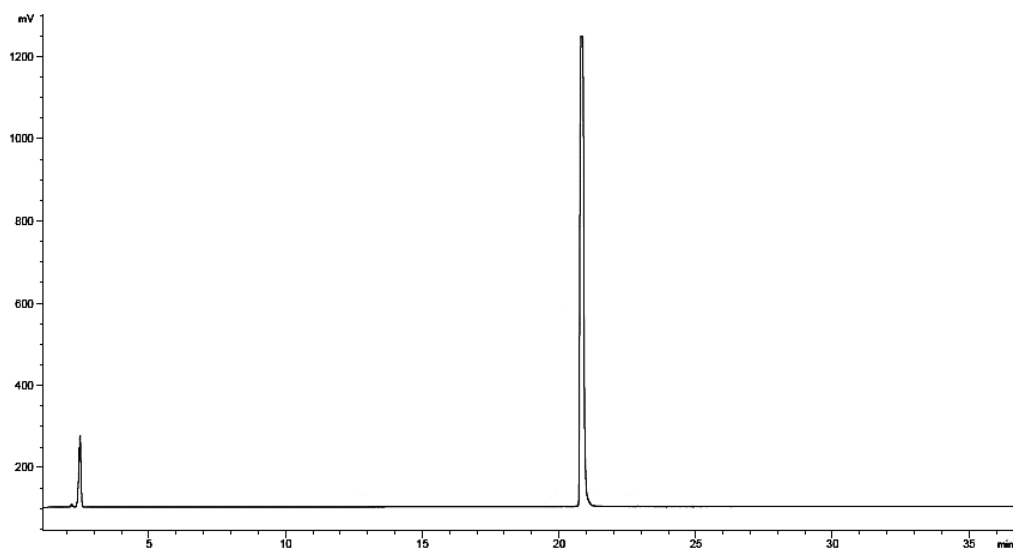
5-Hydroxypentyl α -D-mannopyranosyl (1 \rightarrow 6)- α -D-mannopyranosyl-(1 \rightarrow 6)-3,4-di-O-benzyl- α -D-mannopyranoside (4.21)



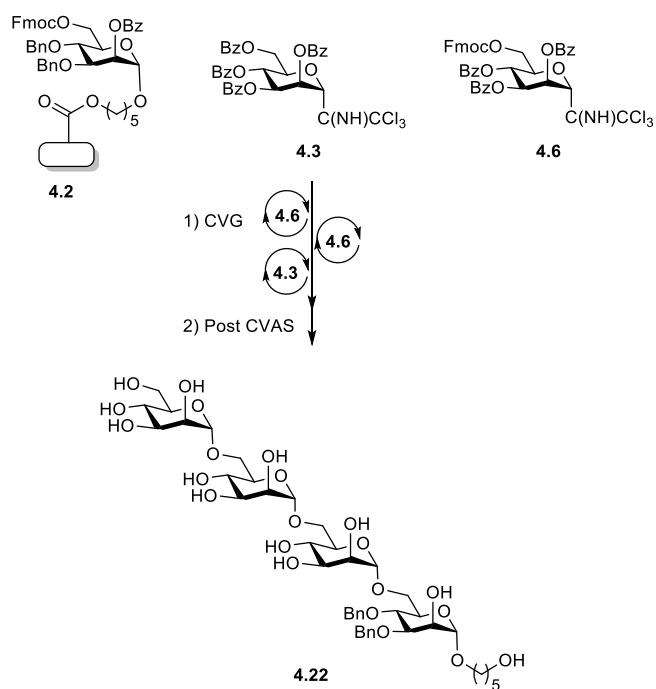
Action	BB	Modules	Notes	Result (mg, μmol , yield)
Method A				
		A	4.2 swell; Fmoc-deprotection	
CVG	4.6	B; C; D; C; D, E,	Activator solution A, 1.00 mL	0.49 mg, 0.64 μmol , 30%
	4.3	B; C; D	Activator solution A, 1.00 mL	
Post CVG		F1		
Method B				
		A	4.2 swell; Fmoc-deprotection	
CVG	4.7	B; C; D; C; D, E,	Activator solution A, 1.00 mL	0.4 mg, 0.52 μmol , 21%
	4.3	B; C; D	Activator solution A, 1.00 mL	
Post CVG		F1		
Method C				
		A	4.2 swell; Fmoc-deprotection	
CVG	4.6	B; C; D; C; D, E,	Activator solution B, 1.00 mL	0.49 mg, 0.64 μmol , 32%
	4.3	B; C; D	Activator solution B, 1.00 mL	
Post CVG		F1		
Method D				
		A	4.2 swell; Fmoc-deprotection	
CVG	4.6	B; C; D; C; D, E,	Activator solution C, 1.00 mL	0.34 mg, 0.44 μmol , 25%
	4.3	B; C; D	Activator solution C, 1.00 mL	
Post CVG		F1		

^1H NMR (600 MHz, D_2O): δ = 7.49 – 7.32 (m, 10H), 4.85 (d, J = 11.2 Hz, 4H), 4.61 (dd, J = 23.0, 11.2 Hz, 2H), 4.17 (s, 1H), 3.97 (d, J = 2.7 Hz, 1H), 3.91 – 3.53 (m, 21H), 1.65 – 1.57 (m, 2H), 1.55 (q, J = 7.2 Hz, 2H), 1.43 – 1.31 (m, 2H), 1.16 (d, J = 6.4 Hz, 1H) ppm; ^{13}C NMR (151 MHz, D_2O) δ = 170.9, 137.1, 137.0, 131.1, 128.7, 128.6, 128.6, 128.3, 128.3, 128.2, 99.99, 99.6, 99.3, 78.3, 74.7, 73.7, 72.5, 71.1, 70.9, 70.7, 70.4, 69.9, 69.8, 69.7, 67.7, 66.8, 66.6, 66.3, 65.9, 65.9, 65.3, 61.5, 60.8, 30.9, 28.1, 21.7 ppm; ESI-HRMS: m/z $[\text{M}+\text{Na}]^+$ calcd. for $\text{C}_{37}\text{H}_{54}\text{O}_{17}\text{Na}$: 793.325318 found 793.3313.

RP-HPLC (ELSD trace, Method B, t_R = 20.8 min)



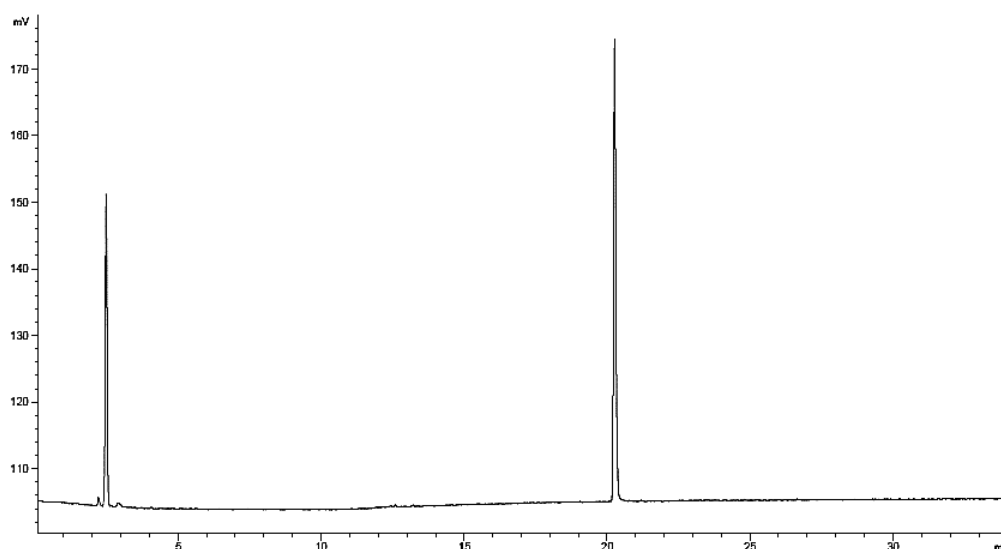
5-Hydroxypentyl α -D-mannopyranosyl (1 \rightarrow 6)- α -D-mannopyranosyl-(1 \rightarrow 6)- α -D-mannopyranosyl-(1 \rightarrow 6)-3,4-di-O-benzyl- α -D-mannopyranoside (4.22)



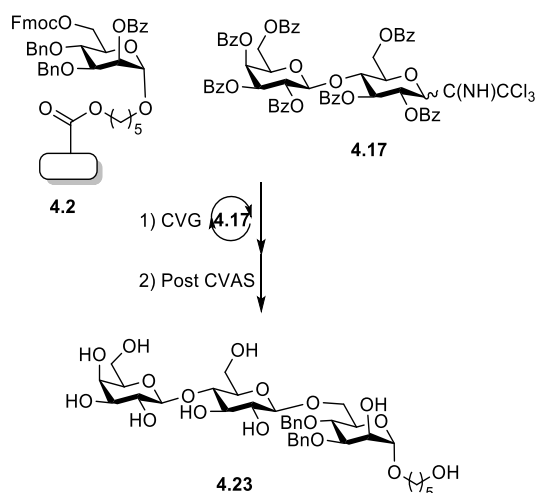
Action	BB	Modules	Notes	Result (mg, μ mol, yield)
		A	4.2 swell; Fmoc-deprotection (4 cm ²)	
CVG	4.6	B; C; D; C; D, E,	Activator solution B, 1.00 mL	0.22 mg, 0.24 μ mol, 8% overall yield
	4.6	B; C; D; C; D, E,	Activator solution B, 1.00 mL	
	4.3	B; C; D	Activator solution B, 1.00 mL	
Post CVG		F1		

^1H NMR (700 MHz, D_2O): δ = 7.45 – 7.25 (m, 10H), 4.87 – 4.82 (m, 4H), 4.74 (m, 2H), 4.57 (dd, J = 24.6, 11.2 Hz, 2H), 4.14 (t, J = 2.1 Hz, 1H), 3.92 (d, J = 14.0 Hz, 2H), 3.88 – 3.46 (m, 26H), 1.62 – 1.47 (m, 4H), 1.40 – 1.14 (m, 3H) ppm; ^{13}C NMR (176, D_2O): δ = 128.7, 128.3, 128.1, 99.8, 99.2, 99.2, 78.2, 74.2, 73.6, 72.3, 70.6, 70.1, 69.9, 69.7, 67.8, 66.7, 66.6, 65.4, 65.1, 61.2, 60.7, 30.6, 28.1, 21.80 ppm (in respect to the coupled ^1H - ^{13}C HSQC NMR); ESI-HRMS: m/z $[\text{M}+\text{Na}]^+$ calcd. for $\text{C}_{43}\text{H}_{64}\text{O}_{22}\text{Na}$: 955.3781 found 955.3873.

RP-HPLC (ELSD trace, Method B, t_{R} = 20.2 min)



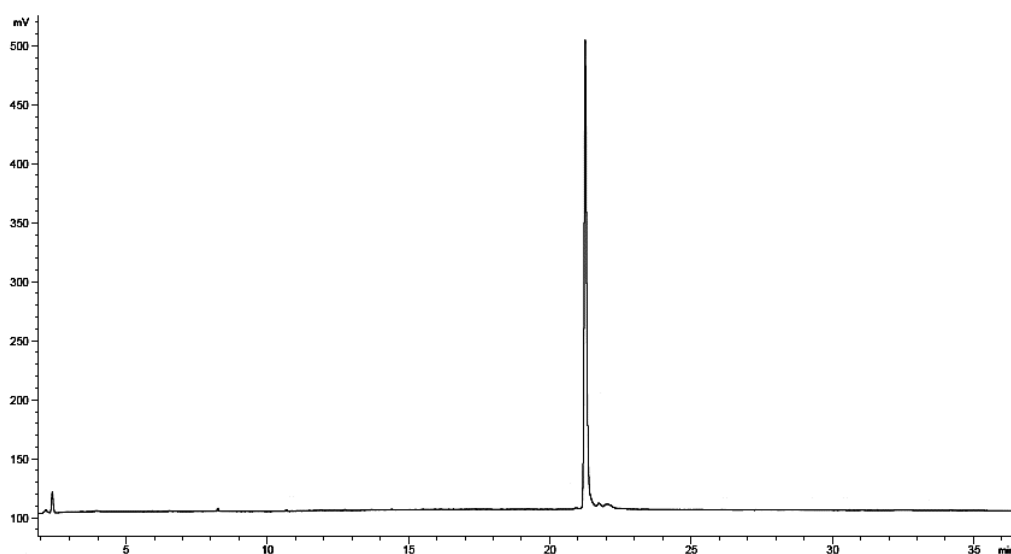
5-Hydroxypentyl β -D-galactopyranosyl (1 \rightarrow 4)- β -D-glucopyranosyl-(1 \rightarrow 6)-3,4-di-O-benzyl- α -D-mannopyranoside (4.23)



Action	BB	Modules	Notes	Result (mg, μ mol, yield)
Method A				
		A	4.2 swell; Fmoc-deprotection	
CVG	4.17	B; C; D; C; D	Activator solution B, 1.00 mL	0.37 mg, 0.48 μ mol, 34%
Post CVG		F1		

^1H NMR (600 MHz, D_2O): δ = 7.42 (tt, J = 33.7, 7.0 Hz, 10H), 4.86 (s, 1H), 4.76 – 4.70 (m, 2H), 4.66 – 4.61 (m, 2H), 4.43 (d, J = 7.9 Hz, 1H), 4.39 (d, J = 7.9 Hz, 1H), 4.15 (d, J = 4.9 Hz, 1H), 4.08 (d, J = 11.2 Hz, 1H), 3.97 – 3.90 (m, 2H), 3.88 – 3.79 (m, 4H), 3.79 – 3.73 (m, 3H), 3.73 – 3.68 (m, 2H), 3.67 – 3.60 (m, 3H), 3.57 (t, J = 6.6 Hz, 2H), 3.52 (dt, J = 15.0, 7.5 Hz, 3H), 3.34 (t, J = 8.3 Hz, 1H), 1.61 (m, 2H), 1.53 (m, 2H), 1.36 (m, 2H) ppm; ^{13}C NMR (176 MHz, D_2O) δ = 170.9, 137.1, 136.9, 128.7, 128.7, 128.6, 128.4, 128.3, 102.8, 102.4, 99.6, 78.2, 75.2, 75.1, 74.6, 74.1, 73.8, 72.6, 72.42, 71.27, 70.8, 70.5, 68.4, 68.1, 67.8, 61.5, 60.9, 59.9, 30.9, 28.0, 21.7 ppm; ESI-HRMS: m/z $[\text{M}+\text{Na}]^+$ calcd. for $\text{C}_{37}\text{H}_{54}\text{O}_{17}\text{Na}$: 793.3253 found 793.3307.

RP-HPLC (ELSD trace, Method B, t_{R} = 22.3 min)

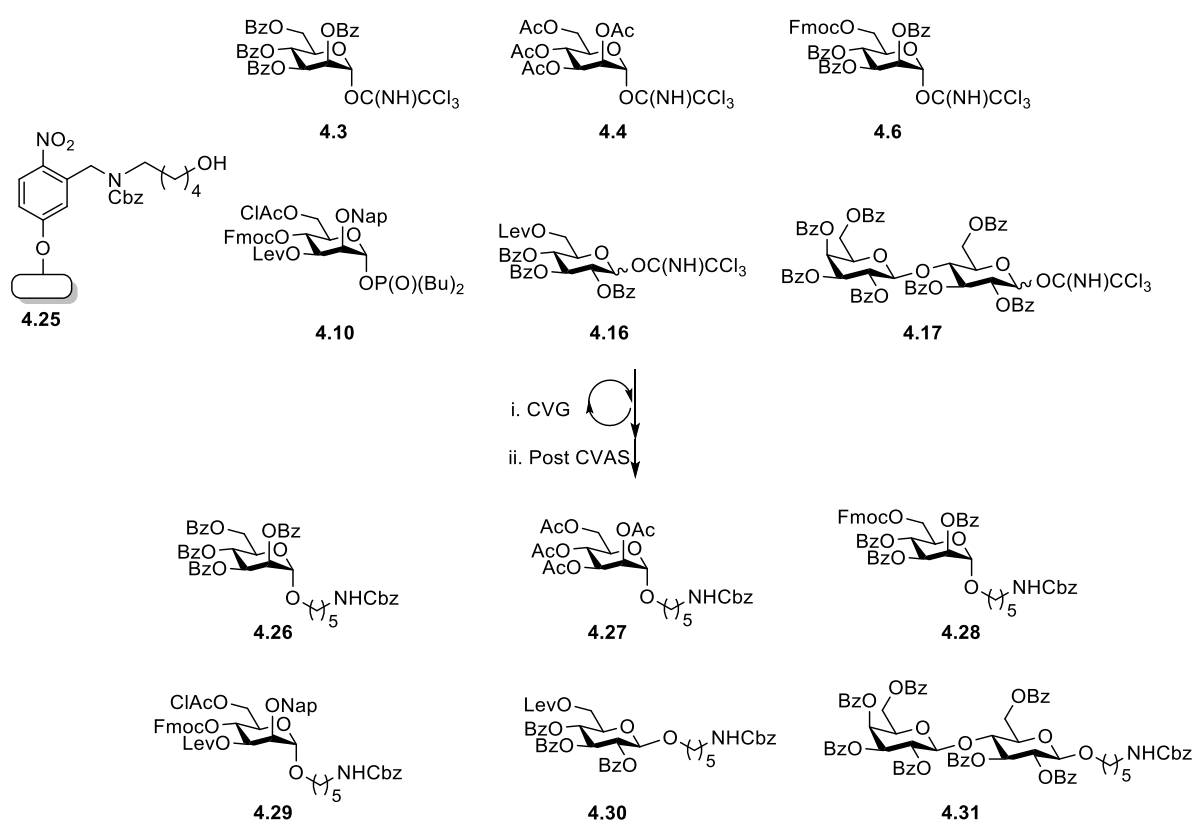


4.5.5. Parallel synthesis

On cellulose membrane

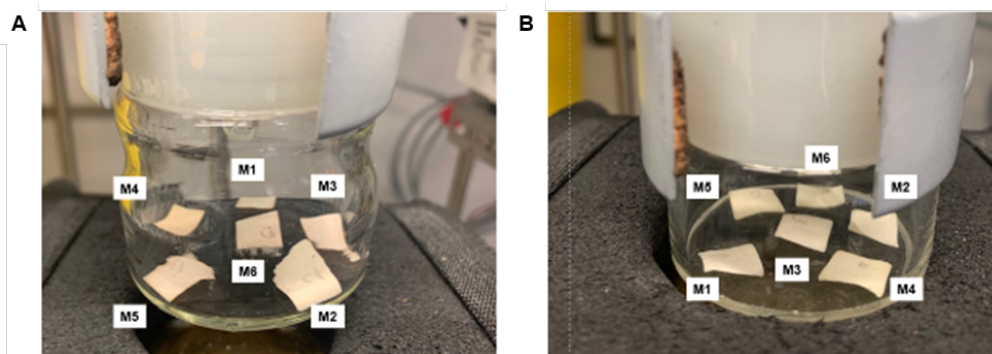
To perform this high-throughput experiment six different BBs (**4.3**, **4.4**, **4.6**, **4.10**, **4.16**, **4.17**) were used with different molecular weight, and the traceless photocleavable linker **4.24** was synthesized. For this specific experiment, six different membrane pieces of **4.25** (1 cm^2 each) with the exact same functionalization bearing the photocleavable linker **4.24**, were placed in

six different Schlenk flasks. The chosen building blocks were spotted in the corresponding membranes in separate flasks while for glycosylation all membranes were placed inside the glycosylation chamber having equal distances ($\approx 1-1.5$ cm) (Experimental Figure 4.7). Between the first and the second glycosylation, the membranes were placed in different positions with different neighboring membranes to detect any possible diffusion between the spotted glycosyl donors. After UV-cleavage and MALDI-detection of the synthesized residues, no diffusion during the two glycosylation steps was observed and successful synthesis of the desired structures was detected. Further purification and characterization was not performed.



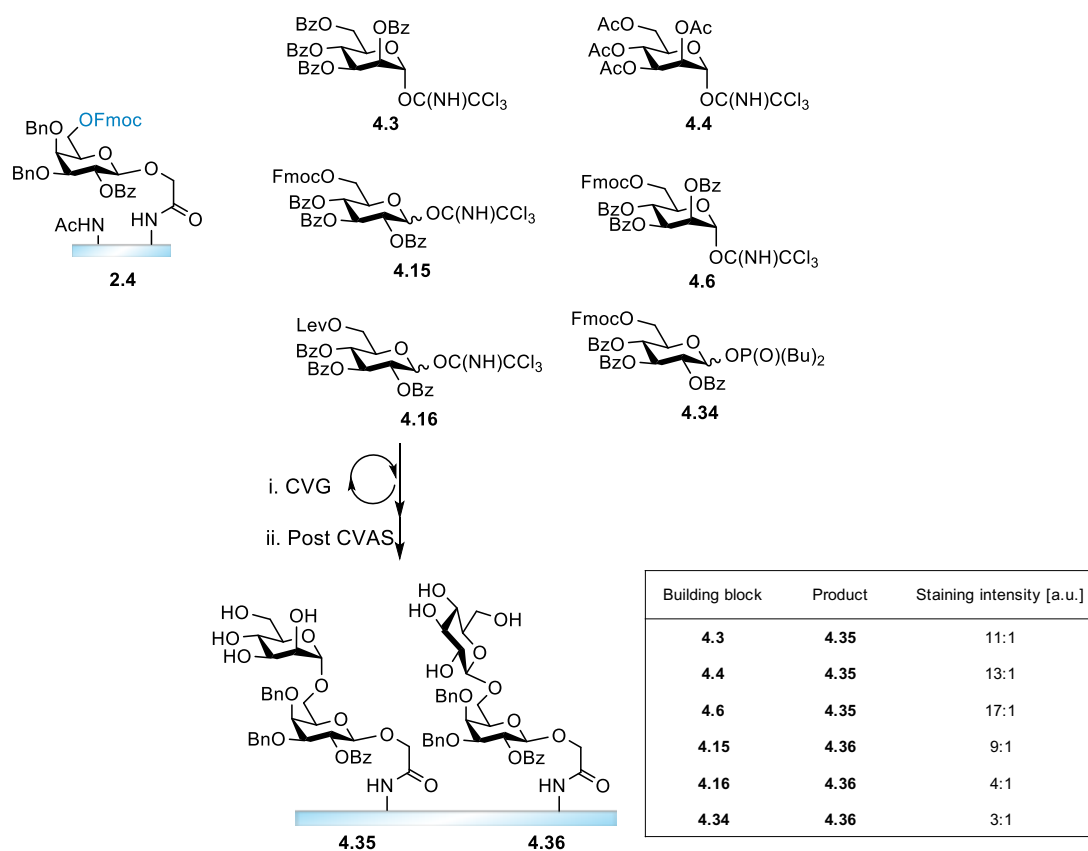
Action	BB	Modules	Notes	Result
		A, B	4.25 swell, 6 pieces in 50 mL Schlenk flask	
		Each membrane transferred in a different flask for spotting		
CVG	4.3	C; D; C; D	Activator solution B, 0.60 mL	4.26
	4.4	C; D; C; D	Activator solution B, 0.60 mL	4.27
	4.6	C; D; C; D	Activator solution B, 0.60 mL	4.28
	4.10	C; D; C; D	Activator solution B, 0.60 mL	4.29

	4.16	C; D; C; D	Activator solution B, 0.60 mL	4.30
	4.17	C; D; C; D	Activator solution B, 0.60 mL	4.31
Post CVG		F2	in parallel	



Experimental Figure 4.7: Position of spotted membranes bearing their corresponding building blocks during the A) first glycosylation and, B) second glycosylation.

On glass slide



Action	BB (2 mg/20 μ L of DCM)	Modules	Notes	Result
		A, B	2.4 glass slide	
			-5 °C to rt	
	4.3	C; D	Activator solution A, 0.70 mL	4.35
	4.4	C; D	Activator solution A, 0.70 mL	4.35
CVG	4.6	C; D	Activator solution A, 0.70 mL	4.35
	4.15	C; D	Activator solution A, 0.70 mL	4.36
	4.16	C; D	Activator solution A, 0.70 mL	4.36
	4.34	C; D	Activator solution A, 0.70 mL	4.36
Post CVG		F2	in parallel	
		Staining	ConA 100 μ g/mL	

Lectin staining: Before lectin staining, acceptor slides were incubated with a blocking buffer for 30 min (Rockland, USA; blocking buffer for fluorescent western blotting MB-070). Fluorescently labeled plant lectins, concanavalin A (ConA; CF®633 ConA, Biotium, Inc., USA) was diluted to 100 μ g/mL in lectin buffer (50 mM HEPES, 100 mM NaCl, 1 mM CaCl₂, 1 mM MnCl₂, 10% blocking buffer, 0.05% Tween 20, pH 7.5), and incubated for 30 min at room temperature. Subsequently, the slide was washed with PBS-T (3 \times 3 min). Then, the acceptor slide was rinsed with Tris buffer (1 mM Tris-HCl buffer, pH=7.4) to remove all the remaining salt residues, and dried in a jet of air. Fluorescence scanning was performed in a Molecular Devices microarray scanner, GenePix 4000B, San Jose, USA. The detection wavelength was $\lambda = 635$ nm with PMT gain 600. The laser power was 33% for every measurement and the pixel size was 5 μ m for high-resolution scans.

5. Conclusion and Perspectives

Aim of this work was to develop new methodologies, based on solid phase synthesis, for the generation of oligosaccharide and glycomimetic libraries for biological interaction studies. These methodologies were designed to leverage the synthetic flexibility of chemical building blocks and be cost- and time-efficient. Two novel methodologies, based on the principles derived from automated peptide synthesis, were modified and adapted to obey the rules of carbohydrate chemistry.

In the first part (*Chapter 2*), a new sugarLIFT method was developed for *in-situ* chemical synthesis of oligosaccharides on functionalized-glass slides, based on the cLIFT approach^[126,128]. A home-built setup was designed for chemical vapor glycosylation reactions under inert and temperature-controlled conditions. A reference glycosyl donor building block, bearing ester protecting groups (-Bz), was synthesized and used for the optimization of the entire process. Two different linkers were designed and incorporated for the functionalization of the solid support for lectin and mass detection. After the successful optimization of the sugarLIFT process, a glycosyl donor library was synthesized, offering different protecting and leaving groups. Parallel screening of the synthesized library with sugarLIFT led to the formation of different saccharides with up to three units. Detection of the synthesized structures was achieved by staining with fluorescently labelled lectins, while promising candidates for chain elongation were identified for the synthesis of longer structures.

So far, sugarLIFT is the first parallelized method for on-chip chemical synthesis of oligosaccharides under stereochemical control (α - and β -linkage between the sugar moieties). Detection of the synthesized moieties can be performed by mass spectrometry and lectin binding. Despite the large potentials, currently reported chemical on-chip methodologies showed stereochemical limitations, delivering only β -linkages, while detection was only achieved by mass spectrometry.^[60] Despite the enzymatic^[62,210] and chemoenzymatic^[211] technologies reported to circumvent these limitations, by using glycosyltransferases for regio- and stereo-specificity, the number of commercially available glycosyl transferases is still limited. This emphasizes the importance of this chemical approach. Currently, the sugarLIFT building block library is expanding to glycosyl donors containing more than one orthogonal protecting group, to synthesize more complex and branched structures (e.g., series of Globo H oligosaccharides, and Lewis antigens).^[62] After investigating selective deprotection conditions of different protecting groups on the glass-solid support, the method might be further expanded to *O*- and *N*-glycopeptide synthesis, by

combining sugarLIFT with the standard cLIFT approach (coupling of amino acids under heat) and enzymatic sialylation and fucosylation, to ensure higher glycosylation efficiency of demanding building blocks. However, preliminary results showed that coupling of amino acids can also be performed under solvent (dichloromethane and toluene) vapor conditions at low temperatures. The use of low temperatures for amino acid coupling can enable racemization control of temperature sensitive and demanding building blocks. Validation of this approach would first require the synthesis of known peptide sequences (e.g., HA, FLAG and Myc tags) that can be selectively recognized by commercially available antibodies. Then, this could be further expanded to combinatorial synthesis of thousands of peptides and glycopeptides for infectious disease research as well as glycomimetics for multivalency studies.

In the second part of this work (*Chapter 3*), multivalent glycomimetics were synthesized on chip *via* cLIFT for lectin interaction studies. Chemical synthesis of peptide scaffolds directly on functionalized glass slides was achieved bearing alkyne-functionalities, followed by copper-catalyzed azide-alkyne cycloaddition (CuAAC) of sugar azides. The applied sugar azides, with lengths of up to three sugar units, were equipped with and without a spacer to restrict or increase their flexibility for binding. The method was optimized and implemented for different surfaces to evaluate their impact on the lectin binding mode. Studying their interaction with several different lectins showed that not only the spatially defined sugar presentation, but also the surface functionalization and wettability, as well as accessibility and flexibility, play an essential role in such interactions. A variety of fluorescently labeled lectins were probed, indicating that different lectin-glycan pairs require different surface functionalizations and spacers for enhanced binding. This approach allows for rapid screening and evaluation of spacing-, density-, ligand and surface-dependent parameters, to find optimal lectin binders.

This is the first method so far allowing the flexible and cost-efficient *in-situ* synthesis of defined multivalent glycopeptides in terms of valency, length and spacing, directly on-chip. A low-budget system, using this technology is also available, giving the ability to almost everyone in the scientific community to construct such arrays.^[127] The lasing system has already been optimized and is automated for high-density peptide array synthesis with high precision, reaching a spot-to-spot distance of down to 100 μm (10000 peptides/ cm^2).^[128] Currently, the automated lasing system is being applied for glycomimetic synthesis with 150 μm spot-to-spot distance, highlighting the importance of density for the glycan-lectin screening, as reported in literature.^[160,168,257] In the future, longer and more diverse

glycomimetics with higher yields should be synthesized to study the influence of functional groups of the peptide backbone, as well as how hydrophilic/-phobic spacers between the sugar moieties on the peptide backbone could affect the lectin recognition. Additionally, with this approach, different multivalent glycopeptides, containing natural, unnatural, and glycosylated amino acids may be used for the generation of the peptide backbone, to compare how simple changes may affect the lectin binding in known systems. Finally, the focus of interest should also cover the synthesis of heteromultivalent structures. Highly complex heteromultivalent structures could be synthesized, for example, by alternating amide bond formation and CuAAC or other chemoselective ligation approaches^[258] for conjugation on the microarray surface.

In the last part of this work (*Chapter 4*), VaporSPOT was developed for the parallel synthesis of oligosaccharides on cellulose membranes. A custom-built vapor setup was employed to ensure inert and temperature-controlled conditions during glycosylation reactions. A base labile linker was synthesized for straightforward cleavage, purification, and characterization of partially deprotected oligosaccharides, while a photocleavable linker was used for parallel synthesis of protected oligosaccharides. Different parameters were optimized, allowing the synthesis of different oligosaccharides with up to four residues in the micromolar scale (~1 μmol). The attained derivatives were fully characterized and analyzed in respect to purity and anomeric purity.

In contrast to other solid phase approaches, this method uses a simple setup that saves time and reagents by parallelization. To my knowledge, this is the first method, for parallel chemical synthesis of oligosaccharides on cellulose membranes. Although glycopeptide libraries have been already synthesized on membranes,^[191] they were restricted to amide bond formation only. Here, vaporSPOT may be further expanded and optimized to potentially replace the existing methodologies. Glycosylated amino acids may soon no longer be required for simple parallel glycopeptide synthesis, since glycosylations on a peptide backbone may be performed with stereochemical control. The peptide backbone can be synthesized using the classical SPOT approach,^[180] or amino acid coupling may also be performed under vapor conditions, as previously mentioned. In the future, different spotting techniques and membranes should be tested to generate high-density glycan arrays. This may lead to fully automated glycan and array synthesis platforms for lectin screening and multivalency studies. Finally, another possible path, beyond carbohydrate chemistry could be the use of the vaporSPOT principle in polymerization and cross-coupling reactions, as a miniaturized and cost-efficient screening platform for multiple reactions in parallel.

Concluding, the presented approaches in this work, may solve the current problems in the generation of well-defined glycans, glycomimetics and glycopeptides, by offering a simple, time- and cost-efficient route to parallel synthesis. However, the extensive building block manipulation to synthesize the suitable glycosyl donors remains a challenge. The amount of the used BBs/ coupling cycle should also be reduced, since this is currently the most cost-demanding factor (hundreds to thousands of €/g of BB depending on the complexity and the rareness). The vaporSPOT requires only 6.00 equiv of BB (~10 mg) /coupling cycle for one compound, while the sugarLIFT approach requires a similar amount (5 mg/coupling cycle) for potentially hundreds or thousands of oligosaccharide spots in the array format. Further cost reduction may be achieved by the preparation of custom-made solid supports (commercial membranes cost ~1 €/1 cm², glass slide ~20 €/slide) with enhanced chemical stability and flexibility. The construction of automated devices for laser-based transfer or spotting with cheaper and recyclable materials could open the path for the commercialization of these technologies for many biomedical and immunological screening applications.

6. References

- [1] M. M. Fuster, J. D. Esko, *Nat. Rev. Cancer* **2005**, *5*, 526–542.
- [2] A. Varki, R. D. Cummings, J. D. Esko, P. Stanley, G. W. Hart, M. Aebi, D. Mohnen, T. Kinoshita, N. H. Packer, J. H. Prestegard, et al., *Essentials of Glycobiology, 4th Edition*, Cold Spring Harbor Laboratory Press, **2022**.
- [3] J. Y. Zhou, B. A. Cobb, *Annu. Rev. Immunol.* **2021**, *39*, 511–536.
- [4] S. M. Muthana, C. T. Campbell, J. C. Gildersleeve, *ACS Chem. Biol.* **2012**, *7*, 31–43.
- [5] D. B. Werz, R. Ranzinger, S. Herget, A. Adibekian, C.-W. von der Lieth, P. H. Seeberger, *ACS Chem. Biol.* **2007**, *2*, 685–691.
- [6] C. D. Rillahan, J. C. Paulson, *Annu. Rev. Biochem.* **2011**, *80*, 797–823.
- [7] M. Guberman, P. H. Seeberger, *J. Am. Chem. Soc.* **2019**, *141*, 5581–5592.
- [8] H. Lis, N. Sharon, *Chem. Rev.* **1998**, *98*, 637–674.
- [9] P. Valverde, J. D. Martínez, F. J. Cañada, A. Ardá, J. Jiménez-Barbero, *ChemBioChem* **2020**, *21*, 2999–3025.
- [10] S. Tommasone, F. Allabush, Y. K. Tagger, J. Norman, M. Köpf, J. H. R. Tucker, P. M. Mendes, *Chem. Soc. Rev.* **2019**, *48*, 5488–5505.
- [11] C. Fasting, C. A. Schalley, M. Weber, O. Seitz, S. Hecht, B. Kokschi, J. Dervede, C. Graf, E.-W. Knapp, R. Haag, *Angew. Chem. Int. Ed.* **2012**, *51*, 10472–10498.
- [12] D. Kilpatrick, *Biochim. Biophys. Acta - Gen. Subj.* **2002**, *1572*, 187–197.
- [13] R. Loris, T. Hamelryck, J. Bouckaert, L. Wyns, *Biochim. Biophys. Acta - Protein Struct. Mol. Enzymol.* **1998**, *1383*, 9–36.
- [14] J. H. Naismith, C. Emmerich, J. Habash, S. J. Harrop, J. R. Helliwell, W. N. Hunter, J. Raftery, A. J. Kalb (Gilboa), J. Yariv, *Acta Crystallogr. Sect. D Biol. Crystallogr.* **1994**, *50*, 847–858.
- [15] V. Wittmann, R. J. Pieters, *Chem. Soc. Rev.* **2013**, *42*, 4492.
- [16] S. K. Natchiar, K. Suguna, A. Surolia, M. Vijayan, *Crystallogr. Rev.* **2007**, *13*, 3–28.
- [17] R. Ravishankar, M. Ravindran, K. Suguna, A. Surolia, M. Vijayan, *Curr. Sci.* **1997**, *72*, 855–861.
- [18] T. W. Hamelryck, R. Loris, J. Bouckaert, M.-H. Dao-Thi, G. Strecker, A. Imberty, E. Fernandez, L. Wyns, M. E. Etzler, *J. Mol. Biol.* **1999**, *286*, 1161–1177.

- [19] S. Sinha, N. Mitra, G. Kumar, K. Bajaj, A. Surolia, *Biophys. J.* **2005**, *88*, 1300–1310.
- [20] M. E. A. Pereira, E. A. Kabat, N. Sharon, *Carbohydr. Res.* **1974**, *37*, 89–102.
- [21] A. Dessen, D. Gupta, S. Sabesan, C. F. Brewer, J. C. Sacchettini, *Biochemistry* **1995**, *34*, 4933–4942.
- [22] C. Schubert, W. And, G. E. Kellogg, *Differences in Hydropathic Properties of Ligand Binding at Four Independent Sites in Wheat Germ Agglutinin-Oligosaccharide Crystal Complexes*, Cambridge University Press, **1996**.
- [23] M. E. Taylor, K. Drickamer, in *Glycosci. Biol. Med.*, Springer Japan, Tokyo, **2015**, pp. 1015–1020.
- [24] H. Feinberg, T. J. W. Rowntree, S. L. W. Tan, K. Drickamer, W. I. Weis, M. E. Taylor, *J. Biol. Chem.* **2013**, *288*, 36762–36771.
- [25] H. Feinberg, M. E. Taylor, N. Razi, R. McBride, Y. A. Knirel, S. A. Graham, K. Drickamer, W. I. Weis, *J. Mol. Biol.* **2011**, *405*, 1027–1039.
- [26] E.-C. Wamhoff, J. Schulze, L. Bellmann, M. Rentzsch, G. Bachem, F. F. Fuchsberger, J. Rademacher, M. Hermann, B. Del Frari, R. van Dalen, et al., *ACS Cent. Sci.* **2019**, *5*, 808–820.
- [27] H. Feinberg, A. S. Powlesland, M. E. Taylor, W. I. Weis, *J. Biol. Chem.* **2010**, *285*, 13285–13293.
- [28] M. E. Mnich, R. van Dalen, N. M. van Sorge, *Front. Cell. Infect. Microbiol.* **2020**, *10*, 309.
- [29] G. Artigas, J. T. Monteiro, H. Hinou, S.-I. Nishimura, B. Lepenies, F. Garcia-Martin, *J. Med. Chem.* **2017**, *60*, 9012–9021.
- [30] S. Mayer, M.-K. Raulf, B. Lepenies, *Histochem. Cell Biol.* **2017**, *147*, 223–237.
- [31] L. Bhattacharyya, C. F. Brewer, *Eur. J. Biochem.* **1988**, *176*, 207–212.
- [32] A. Gabba, A. Bogucka, J. G. Luz, A. Diniz, H. Coelho, F. Corzana, F. J. Cañada, F. Marcelo, P. V Murphy, G. Birrane, *Biochemistry* **2021**, *60*, 1327–1336.
- [33] G. D. Brown, J. A. Willment, L. Whitehead, *Nat. Rev. Immunol.* **2018**, *18*, 374–389.
- [34] F. S. Coulibaly, B.-B. C. Youan, *Biosens. Bioelectron.* **2014**, *59*, 404–411.
- [35] N. Green, *Biochem. J.* **1963**, *89*, 599–609.
- [36] D. C. Ranawakage, T. Takada, Y. Kamachi, *Sci. Rep.* **2019**, *9*, 6895.
- [37] S.-J. Richards, M. I. Gibson, *JACS Au* **2021**, *1*, 2089–2099.

- [38] R. Haag, *Beilstein J. Org. Chem.* **2015**, *11*, 848–9.
- [39] R. J. Pieters, *Org. Biomol. Chem.* **2009**, *7*, 2013.
- [40] A. Camaleño de la Calle, C. Gerke, X. J. Chang, A. Grafmüller, L. Hartmann, S. Schmidt, *Macromol. Biosci.* **2019**, *19*, 1900033.
- [41] C. Müller, G. Despras, T. K. Lindhorst, *Chem. Soc. Rev.* **2016**, *45*, 3275–3302.
- [42] P. Rohse, S. Weickert, M. Drescher, V. Wittmann, *Chem. Sci.* **2020**, *11*, 5227–5237.
- [43] J. E. Gestwicki, C. W. Cairo, L. E. Strong, K. A. Oetjen, L. L. Kiessling, *J. Am. Chem. Soc.* **2002**, *124*, 14922–14933.
- [44] G. B. Sigal, M. Mammen, G. Dahmann, G. M. Whitesides, *J. Am. Chem. Soc.* **1996**, *118*, 3789–3800.
- [45] M. Delbianco, P. Bharate, S. Varela-Aramburu, P. H. Seeberger, *Chem. Rev.* **2016**, *116*, 1693–1752.
- [46] R. Loris, D. Maes, F. Poortmans, L. Wyns, J. Bouckaert, *J. Biol. Chem.* **1996**, *271*, 30614–30618.
- [47] C.-S. Chen, H. Zhu, *Biotechniques* **2006**, *40*, 423–429.
- [48] J. M. Rosenberg, P. J. Utz, *Front. Immunol.* **2015**, *6*, 1–8.
- [49] S. Fodor, J. Read, M. Pirrung, L. Stryer, A. Lu, D. Solas, *Science.* **1991**, *251*, 767–773.
- [50] A. C. Pease, D. Solas, E. J. Sullivan, M. T. Cronin, C. P. Holmes, S. P. Fodor, *Proc. Natl. Acad. Sci. U. S. A.* **1994**, *91*, 5022–6.
- [51] J. Ziauddin, D. M. Sabatini, *Nature* **2001**, *411*, 107–110.
- [52] D. Wang, S. Liu, B. J. Trummer, C. Deng, A. Wang, *Nat. Biotechnol.* **2002**, *20*, 275–281.
- [53] S. Fukui, T. Feizi, C. Galustian, A. M. Lawson, W. Chai, *Nat. Biotechnol.* **2002**, *20*, 1011–1017.
- [54] R. Liang, L. Yan, J. Loebach, M. Ge, Y. Uozumi, K. Sekanina, N. Horan, J. Gildersleeve, C. Thompson, A. Smith, et al., *Science.* **1996**, *274*, 1520–1522.
- [55] S. Purohit, T. Li, W. Guan, X. Song, J. Song, Y. Tian, L. Li, A. Sharma, B. Dun, D. Mysona, et al., *Nat. Commun.* **2018**, *9*, 258.
- [56] R. Roy, *Curr. Opin. Struct. Biol.* **1996**, *6*, 692–702.
- [57] J. G. Briard, H. Jiang, K. W. Moremen, M. S. Macauley, P. Wu, *Nat. Commun.* **2018**, *9*, 880.
- [58] M. Sojitra, S. Sarkar, J. Maghera, E. Rodrigues, E. J. Carpenter, S. Seth, D. Ferrer Vinals, N.

- J. Bennett, R. Reddy, A. Khalil, et al., *Nat. Chem. Biol.* **2021**, *17*, 806–816.
- [59] M. Yan, Y. Zhu, X. Liu, Y. Lasanajak, J. Xiong, J. Lu, X. Lin, D. Ashline, V. Reinhold, D. F. Smith, et al., *Anal. Chem.* **2019**, *91*, 9221–9228.
- [60] L. Ban, M. Mrksich, *Angew. Chem. Int. Ed.* **2008**, *47*, 3396–3399.
- [61] D. S. Mattes, N. Jung, L. K. Weber, S. Bräse, F. Breitling, *Adv. Mater.* **2019**, *31*, 1806656.
- [62] H. R. Heo, K. Il Joo, J. H. Seo, C. S. Kim, H. J. Cha, *Nat. Commun.* **2021**, *12*, 1395.
- [63] S. Park, J. C. Gildersleeve, O. Blixt, I. Shin, *Chem. Soc. Rev.* **2013**, *42*, 4310–4326.
- [64] Y. Kim, J. Y. Hyun, I. Shin, *Chem. Soc. Rev.* **2022**, *51*, 8276–8299.
- [65] D. N. Karunaratne, *The Complex World of Polysaccharides*, InTech, **2012**.
- [66] Q. Zhang, Z. Li, X. Song, *Front. Chem.* **2020**, *8*, 508.
- [67] D. F. Smith, R. D. Cummings, X. Song, *Biochem. Soc. Trans.* **2019**, *47*, 1–11.
- [68] K. M. Koeller, C.-H. Wong, *Nature* **2001**, *409*, 232–240.
- [69] M. Liu, X. Qin, X.-S. Ye, *Chem. Rec.* **2021**, *21*, 3256–3277.
- [70] J.-I. Kadokawa, *Chem. Rev.* **2011**, *111*, 4308–4345.
- [71] K. W. Moremen, A. Ramiah, M. Stuart, J. Steel, L. Meng, F. Forouhar, H. A. Moniz, G. Gahlay, Z. Gao, D. Chapla, et al., *Nat. Chem. Biol.* **2018**, *14*, 156–162.
- [72] H. Yu, X. Chen, *Org. Biomol. Chem.* **2016**, *14*, 2809–2818.
- [73] P. Sears, C. H. Wong, *Science*. **2001**, *291*, 2344–2350.
- [74] J. Zhang, C. Chen, M. R. Gadi, C. Gibbons, Y. Guo, X. Cao, G. Edmunds, S. Wang, D. Liu, J. Yu, et al., *Angew. Chem. Int. Ed.* **2018**, *57*, 16638–16642.
- [75] T. Li, L. Liu, N. Wei, J.-Y. Yang, D. G. Chapla, K. W. Moremen, G.-J. Boons, *Nat. Chem.* **2019**, *11*, 229–236.
- [76] C. Zhao, Y. Wu, H. Yu, I. M. Shah, Y. Li, J. Zeng, B. Liu, D. A. Mills, X. Chen, *Chem. Commun.* **2016**, *52*, 3899–3902.
- [77] T. Matsushita, I. Nagashima, M. Fumoto, T. Ohta, K. Yamada, H. Shimizu, H. Hinou, K. Naruchi, T. Ito, H. Kondo, et al., *J. Am. Chem. Soc.* **2010**, *132*, 16651–16656.
- [78] D. Crich, *Cite This J. Am. Chem. Soc.* **2021**, *143*, 34.
- [79] D. Crich, *Acc. Chem. Res.* **2010**, *43*, 1144–1153.

- [80] J. Hofmann, H. S. Hahm, P. H. Seeberger, K. Pagel, *Nature* **2015**, *526*, 241–244.
- [81] S. van der Vorm, T. Hansen, J. M. A. van Hengst, H. S. Overkleeft, G. A. van der Marel, J. D. C. Codée, *Chem. Soc. Rev.* **2019**, *48*, 4688–4706.
- [82] C. Chang, M. Lin, C. Chan, K. Su, C. Wu, W. Lo, S. Lam, Y. Cheng, P. Liao, C. Wong, et al., *Angew. Chem. Int. Ed.* **2021**, *60*, 12413–12423.
- [83] C. C. Wang, C. W. Chang, M. H. Lin, C. H. Wu, T. Y. Chiang, *J. Org. Chem.* **2020**, *85*, 15945–15963.
- [84] O. T. Tuck, E. T. Sletten, J. Danglad-Flores, P. H. Seeberger, *Angew. Chem. Int. Ed.* **2022**, *61*, e202115433.
- [85] S. Chatterjee, S. Moon, F. Hentschel, K. Gilmore, P. H. Seeberger, *J. Am. Chem. Soc.* **2018**, *140*, 11942–11953.
- [86] A. Kafle, J. Liu, L. Cui, *Can. J. Chem.* **2016**, *94*, 894–901.
- [87] P. R. Andreana, D. Crich, *ACS Cent. Sci.* **2021**, *7*, 1454–1462.
- [88] G. M. N. Bashandy, *J. Anesth.* **2015**, *29*, 269–278.
- [89] I. V Alabugin, L. Kuhn, N. V Krivoshchapov, P. Mehaffy, M. G. Medvedev, *Chem. Soc. Rev.* **2021**, *50*, 10212–10252.
- [90] A. Imamura, H. Ando, S. Korogi, G. Tanabe, O. Muraoka, H. Ishida, M. Kiso, *Tetrahedron Lett.* **2003**, *44*, 6725–6728.
- [91] S. S. Nigudkar, A. V Demchenko, *Chem. Sci.* **2015**, *6*, 2687–2704.
- [92] B. S. Komarova, Y. E. Tsvetkov, N. E. Nifantiev, *Chem. Rec.* **2016**, *16*, 488–506.
- [93] D. R. Mootoo, P. Konradsson, U. Udodong, B. Fraser-Reid, *J. Am. Chem. Soc.* **1988**, *110*, 5583–5584.
- [94] S. S. Kulkarni, C.-C. Wang, N. M. Sabbavarapu, A. R. Podilapu, P.-H. Liao, S.-C. Hung, *Chem. Rev.* **2018**, *118*, 8025–8104.
- [95] Y. Wu, D.-C. Xiong, S.-C. Chen, Y.-S. Wang, X.-S. Ye, *Nat. Commun.* **2017**, *8*, 14851.
- [96] Z. Zhang, I. R. Ollmann, X.-S. Ye, R. Wischnat, T. Baasov, C.-H. Wong, *J. Am. Chem. Soc.* **1999**, *121*, 734–753.
- [97] C. W. Cheng, Y. Zhou, W. H. Pan, S. Dey, C. Y. Wu, W. L. Hsu, C. H. Wong, *Nat. Commun.* **2018**, *9*, 1–9.
- [98] W. Yao, D.-C. Xiong, Y. Yang, C. Geng, Z. Cong, F. Li, B.-H. Li, X. Qin, L.-N. Wang, W.-Y.

- Xue, et al., *Nat. Synth.* **2022**, *1*, 854–863.
- [99] C. Schuerch, J. M. Frechet, *J. Am. Chem. Soc.* **1971**, *93*, 492–496.
- [100] M. Panza, S. G. Pistorio, K. J. Stine, A. V. Demchenko, *Chem. Rev.* **2018**, *118*, 8105–8150.
- [101] T. Nokami, R. Hayashi, Y. Saigusa, A. Shimizu, C.-Y. Liu, K.-K. T. Mong, J. Yoshida, *Org. Lett.* **2013**, *15*, 4520–4523.
- [102] F. A. Jaipuri, N. L. Pohl, *Org. Biomol. Chem.* **2008**, *6*, 2686–2691.
- [103] N. V. Ganesh, K. Fujikawa, Y. H. Tan, K. J. Stine, A. V. Demchenko, *Org. Lett.* **2012**, *14*, 3036–3039.
- [104] S. Escopy, Y. Singh, K. J. Stine, A. V. Demchenko, *Chem. – A Eur. J.* **2022**, *28*, e20220118.
- [105] K. Machida, Y. Hirose, S. Fuse, T. Sugawara, T. Takahashi, *Chem. Pharm. Bull.* **2010**, *58*, 87–93.
- [106] O. J. Plante, E. R. Palmacci, P. H. Seeberger, *Science.* **2001**, *291*, 1523–1527.
- [107] H. S. Hahm, M. K. Schlegel, M. Hurevich, S. Eller, F. Schuhmacher, J. Hofmann, K. Pagel, P. H. Seeberger, *Proc. Natl. Acad. Sci.* **2017**, *114*, E3385–E3389.
- [108] Y. Yu, A. Kononov, M. Delbianco, P. H. Seeberger, *Chem. - A Eur. J.* **2018**, *24*, 6075–6078.
- [109] J. Danglad-Flores, S. Lechnitz, E. T. Sletten, A. Abragam Joseph, K. Bienert, K. Le Mai Hoang, P. H. Seeberger, *J. Am. Chem. Soc.* **2021**, *143*, 8893–8901.
- [110] P. H. Seeberger, *Acc. Chem. Res.* **2015**, *48*, 1450–1463.
- [111] A. A. Joseph, A. Pardo-Vargas, P. H. Seeberger, *J. Am. Chem. Soc.* **2020**, *142*, 8561–8564.
- [112] Y. Zhu, M. Delbianco, P. H. Seeberger, *J. Am. Chem. Soc.* **2021**, *143*, 9758–9768.
- [113] T. Tyrikos-Ergas, E. T. Sletten, J.-Y. Huang, P. H. Seeberger, M. Delbianco, *Chem. Sci.* **2022**, *13*, 2115–2120.
- [114] M. Guberman, M. Bräutigam, P. H. Seeberger, *Chem. Sci.* **2019**, *10*, 5634–5640.
- [115] M. G. Ricardo, E. E. Reuber, L. Yao, J. Danglad-Flores, M. Delbianco, P. H. Seeberger, *J. Am. Chem. Soc.* **2022**, *144*, 18429–18434.
- [116] P. Dallabernardina, V. Benazzi, J. D. Laman, P. H. Seeberger, F. F. Loeffler, *Org. Biomol. Chem.* **2021**, *19*, 9829–9832.
- [117] H. S. Hahm, F. Broecker, F. Kawasaki, M. Mietzsch, R. Heilbronn, M. Fukuda, P. H. Seeberger, *Chem* **2017**, *2*, 114–124.

- [118] H. S. Hahm, M. Hurevich, P. H. Seeberger, *Nat. Commun.* **2016**, *7*, 12482.
- [119] G. Fittolani, D. Vargová, P. H. Seeberger, Y. Ogawa, M. Delbianco, *J. Am. Chem. Soc.* **2022**, *144*, 12469–12475.
- [120] C. Ghosh, P. Priegue, H. Leelayuwapan, F. F. Fuchsberger, C. Rademacher, P. H. Seeberger, *ACS Appl. Bio Mater.* **2022**, *5*, 2185–2192.
- [121] S. K. Khilji, F. Goerdeler, K. Frensemeier, D. Warschkau, J. Lühle, Z. Fandi, F. Schirmeister, Z. A. Chen, O. Turak, A. Mallagaray, et al., *Cell Chem. Biol.* **2022**, *29*, 1353-1361.e6.
- [122] K. Anggara, Y. Zhu, G. Fittolani, Y. Yu, T. Tyrikos-Ergas, M. Delbianco, S. Rauschenbach, S. Abb, P. H. Seeberger, K. Kern, *Proc. Natl. Acad. Sci.* **2021**, *118*, e2102168118.
- [123] T. Tyrikos-Ergas, S. Gim, J.-Y. Huang, S. Pinzón Martín, D. Varón Silva, P. H. Seeberger, M. Delbianco, *Nat. Commun.* **2022**, *13*, 3954.
- [124] V. Romanov, S. N. Davidoff, A. R. Miles, D. W. Grainger, B. K. Gale, B. D. Brooks, *Analyst* **2014**, *139*, 1303–1326.
- [125] M. Mende, V. Bordoni, A. Tsouka, F. F. Loeffler, M. Delbianco, P. H. Seeberger, *Faraday Discuss.* **2019**, *219*, 9–32.
- [126] F. F. Loeffler, T. C. Foertsch, R. Popov, D. S. Mattes, M. Schlageter, M. Sedlmayr, B. Ridder, F. X. Dang, C. Von Bojničić-Kninski, L. K. Weber, et al., *Nat. Commun.* **2016**, *7*, 1–9.
- [127] S. Eickelmann, A. Tsouka, J. Heidepriem, G. Paris, J. Zhang, V. Molinari, M. Mende, F. F. Loeffler, *Adv. Mater. Technol.* **2019**, *4*, 1900503.
- [128] G. Paris, J. Heidepriem, A. Tsouka, Y. Liu, D. S. Mattes, S. Pinzón Martín, P. Dallabernardina, M. Mende, C. Lindner, R. Wawrzinek, et al., *Adv. Mater.* **2022**, *34*, 2200359.
- [129] R. D. Piner, J. Zhu, F. Xu, S. Hong, C. A. Mirkin, *Science.* **1999**, *283*, 661–663.
- [130] D. J. Valles, Y. S. Zholdassov, A. B. Braunschweig, *Polym. Chem.* **2021**, *12*, 5724–5746.
- [131] E. L. Shipp, L. C. Hsieh-Wilson, *Chem. Biol.* **2007**, *14*, 195–208.
- [132] K.-S. Ko, F. A. Jaipuri, N. L. Pohl, *J. Am. Chem. Soc.* **2005**, *127*, 13162–13163.
- [133] S.-H. Chang, J.-L. Han, S. Y. Tseng, H.-Y. Lee, C.-W. Lin, Y.-C. Lin, W.-Y. Jeng, A. H.-J. Wang, C.-Y. Wu, C.-H. Wong, *J. Am. Chem. Soc.* **2010**, *132*, 13371–13380.
- [134] Y. Li, E. Arigi, H. Eichert, S. B. Levery, *J. Mass Spectrom.* **2010**, *45*, 504–519.
- [135] O. E. Galanina, M. Mecklenburg, N. E. Nifantiev, G. V. Pazynina, N. V. Bovin, *Lab Chip* **2003**, *3*, 260.

- [136] D. Wang, G. T. Carroll, N. J. Turro, J. T. Koberstein, P. Kováč, R. Saksena, R. Adamo, L. A. Herzenberg, L. A. Herzenberg, L. Steinman, *Proteomics* **2007**, *7*, 180–184.
- [137] G. T. Carroll, N. J. Turro, A. Mammana, J. T. Koberstein, *Photochem. Photobiol.* **2017**, *93*, 1165–1169.
- [138] H.-Y. Hsiao, M.-L. Chen, H.-T. Wu, L.-D. Huang, W.-T. Chien, C.-C. Yu, F.-D. Jan, S. Sahabuddin, T.-C. Chang, C.-C. Lin, *Chem. Commun.* **2011**, *47*, 1187–1189.
- [139] S. Park, I. Shin, *Angew. Chemie Int. Ed.* **2002**, *41*, 3180–3182.
- [140] S. Park, M. R. Lee, S. J. Pyo, I. Shin, *J. Am. Chem. Soc.* **2004**, *126*, 4812–4819.
- [141] D. M. Ratner, E. W. Adams, M. D. Disney, P. H. Seeberger, *ChemBioChem* **2004**, *5*, 1375–1383.
- [142] C. Liu, C. Li, Q. Niu, C. Cai, G. Li, G. Yu, *New J. Chem.* **2019**, *43*, 9145–9151.
- [143] M. D. Disney, P. H. Seeberger, *Chem. Biol.* **2004**, *11*, 1701–1707.
- [144] C. L. Pereira, A. Geissner, C. Anish, P. H. Seeberger, *Angew. Chem. Int. Ed.* **2015**, *127*, 10154–10157.
- [145] M. Lee, I. Shin, *Org. Lett.* **2005**, *7*, 4269–4272.
- [146] J. L. de Paz, D. Spillmann, P. H. Seeberger, *Chem. Commun.* **2006**, 3116.
- [147] B. T. Houseman, M. Mrksich, *Chem. Biol.* **2002**, *9*, 443–454.
- [148] H. S. G. Beckmann, A. Niederwieser, M. Wiessler, V. Wittmann, *Chem. - A Eur. J.* **2012**, *18*, 6548–6554.
- [149] K. Godula, D. Rabuka, K. T. Nam, C. R. Bertozzi, *Angew. Chem. Int. Ed.* **2009**, *121*, 5073–5076.
- [150] M. Köhn, R. Wacker, C. Peters, H. Schröder, L. Soulère, R. Breinbauer, C. M. Niemeyer, H. Waldmann, *Angew. Chem. Int. Ed.* **2003**, *42*, 5830–5834.
- [151] P.-H. Liang, S.-K. Wang, C.-H. Wong, *J. Am. Chem. Soc.* **2007**, *129*, 11177–11184.
- [152] S. Cecioni, A. Imberty, S. Vidal, *Chem. Rev.* **2015**, *115*, 525–561.
- [153] R. L. Redman, I. J. Krauss, *J. Am. Chem. Soc.* **2021**, *143*, 8565–8571.
- [154] M. Kilcoyne, J. Q. Gerlach, R. Gough, M. E. Gallagher, M. Kane, S. D. Carrington, L. Joshi, *Anal. Chem.* **2012**, *84*, 3330–3338.
- [155] E. Laigre, C. Tiertant, D. Goyard, O. Renaudet, *ACS Omega* **2018**, *3*, 14013–14020.

- [156] W. Hawkes, D. Huang, P. Reynolds, L. Hammond, M. Ward, N. Gadegaard, J. F. Marshall, T. Iskratsch, M. Palma, *Faraday Discuss.* **2019**, *219*, 203–219.
- [157] L. Moni, G. Pourceau, J. Zhang, A. Meyer, S. Vidal, E. Souteyrand, A. Dondoni, F. Morvan, Y. Chevolut, J.-J. Vasseur, et al., *ChemBioChem* **2009**, *10*, 1369–1378.
- [158] K. Godula, C. R. Bertozzi, *J. Am. Chem. Soc.* **2010**, *132*, 9963–9965.
- [159] C. Zilio, A. Bernardi, A. Palmioli, M. Salina, G. Tagliabue, M. Buscaglia, R. Consonni, M. Chiari, *Sensors Actuators B Chem.* **2015**, *215*, 412–420.
- [160] D. J. Valles, Y. Naeem, A. Y. Rozenfeld, R. W. Aldasooky, A. M. Wong, C. Carbonell, D. R. Mootoo, A. B. Braunschweig, *Faraday Discuss.* **2019**, *219*, 77–89.
- [161] O. Oyelaran, Q. Li, D. Farnsworth, J. C. Gildersleeve, *J. Proteome Res.* **2009**, *8*, 3529–3538.
- [162] Y. Zhang, Q. Li, L. G. Rodriguez, J. C. Gildersleeve, *J. Am. Chem. Soc.* **2010**, *132*, 9653–9662.
- [163] H. S. Kim, J. Y. Hyun, S. H. Park, I. Shin, *RSC Adv.* **2018**, *8*, 14898–14905.
- [164] H. M. Branderhorst, R. Ruijtenbeek, R. M. J. Liskamp, R. J. Pieters, *ChemBioChem* **2008**, *9*, 1836–1844.
- [165] N. Parera Pera, H. M. Branderhorst, R. Kooij, C. Maierhofer, M. van der Kaaden, R. M. J. Liskamp, V. Wittmann, R. Ruijtenbeek, R. J. Pieters, *ChemBioChem* **2010**, *11*, 1896–1904.
- [166] X. Zhou, C. Turchi, D. Wang, *J. Proteome Res.* **2009**, *8*, 5031–5040.
- [167] T. Fukuda, S. Onogi, Y. Miura, *Thin Solid Films* **2009**, *518*, 880–888.
- [168] A. Di Maio, A. Cioce, S. Achilli, M. Thépaut, C. Vivès, F. Fieschi, J. Rojo, N.-C. Reichardt, *Org. Biomol. Chem.* **2021**, *19*, 7357–7362.
- [169] J. S. Temme, C. T. Campbell, J. C. Gildersleeve, *Faraday Discuss.* **2019**, *219*, 90–111.
- [170] C. Ruprecht, A. Geissner, P. H. Seeberger, F. Pfrengle, *Carbohydr. Res.* **2019**, *481*, 31–35.
- [171] Y. Fei, Y.-S. Sun, Y. Li, K. Lau, H. Yu, H. A. Chokhawala, S. Huang, J. P. Landry, X. Chen, X. Zhu, *Mol. Biosyst.* **2011**, *7*, 3343.
- [172] R. B. Merrifield, *J. Am. Chem. Soc.* **1963**, *85*, 2149–2154.
- [173] E. Atherton, H. Fox, D. Harkiss, C. J. Logan, R. C. Sheppard, B. J. Williams, *J. Chem. Soc. Chem. Commun.* **1978**, 537.
- [174] B. Merrifield, *Science.* **1986**, *232*, 341–347.
- [175] P. H. Seeberger, W.-C. Haase, *Chem. Rev.* **2000**, *100*, 4349–4394.

- [176] J. M. Palomo, *RSC Adv.* **2014**, *4*, 32658–32672.
- [177] S. Y. Han, Y. A. Kim, *Tetrahedron* **2004**, *60*, 2447–2467.
- [178] A. El-Faham, F. Albericio, *Chem. Rev.* **2011**, *111*, 6557–6602.
- [179] S. B. Daniels, M. S. Bernatowicz, J. M. Coull, H. Köster, *Tetrahedron Lett.* **1989**, *30*, 4345–4348.
- [180] R. Frank, *Tetrahedron* **1992**, *48*, 9217–9232.
- [181] L. C. Szymczak, H. Y. Kuo, M. Mrksich, *Anal. Chem.* **2018**, *90*, 266–282.
- [182] F. Deiss, W. L. Matochko, N. Govindasamy, E. Y. Lin, R. Derda, *Angew. Chemie - Int. Ed.* **2014**, *53*, 6374–6377.
- [183] F. Deiss, Y. Yang, W. L. Matochko, R. Derda, *Org. Biomol. Chem.* **2016**, *14*, 5148–5156.
- [184] R. Frank, *J. Immunol. Methods* **2002**, *267*, 13–26.
- [185] B. Ay, R. Volkmer, P. Boisguerin, *Tetrahedron Lett.* **2007**, *48*, 361–364.
- [186] D. F. H. Winkler, K. Hilpert, O. Brandt, R. E. W. Hancock, *Synthesis of Peptide Arrays Using SPOT-Technology and the CelluSpots-Method*, **2009**.
- [187] P. M. López-Pérez, E. Grimsey, L. Bourne, R. Mikut, K. Hilpert, *Front. Chem.* **2017**, *5*, 25.
- [188] K. Hilpert, D. F. H. Winkler, R. E. W. Hancock, *Nat. Protoc.* **2007**, *2*, 1333–1349.
- [189] H. Blackwell, *Curr. Opin. Chem. Biol.* **2006**, *10*, 203–212.
- [190] D. F. H. Winkler, W. D. Campbell, in *Methods Mol. Biol.*, Humana Press, **2008**, pp. 47–70.
- [191] A. Y. Mehta, R. K. H. Veeraiyah, S. Dutta, C. K. Goth, M. S. Hanes, C. Gao, K. Stavenhagen, R. Kardish, Y. Matsumoto, J. Heimbürg-Molinario, et al., *Cell Chem. Biol.* **2020**, *27*, 1207–1219.
- [192] R. S. Braudy, *Proc. IEEE* **1969**, *57*, 1771–1772.
- [193] J. Bohandy, B. F. Kim, F. J. Adrian, *J. Appl. Phys.* **1986**, *60*, 1538–1539.
- [194] P. Serra, A. Piqué, *Adv. Mater. Technol.* **2019**, *4*, 1800099.
- [195] G. Paris, A. Klinkusch, J. Heidepriem, A. Tsouka, J. Zhang, M. Mende, D. S. Mattes, D. Mager, H. Riegler, S. Eickelmann, et al., *Appl. Surf. Sci.* **2020**, *508*, 144973.
- [196] G. Paris, D. Bierbaum, M. Paris, D. Mager, F. F. Loeffler, *Appl. Sci.* **2022**, *12*, 1361.
- [197] M. Mende, A. Tsouka, J. Heidepriem, G. Paris, D. S. Mattes, S. Eickelmann, V. Bordoni, R. Wawrzinek, F. F. Fuchsberger, P. H. Seeberger, et al., *Chem. – A Eur. J.* **2020**, *26*, 9954–9963.

- [198] D. S. Mattes, B. Streit, D. R. Bhandari, J. Greifenstein, T. C. Foertsch, S. W. Münch, B. Ridder, C. v. Bojničić-Kninski, A. Nesterov-Mueller, B. Spengler, et al., *Macromol. Rapid Commun.* **2019**, *40*, 1800533.
- [199] J. Zhang, Y. Zou, S. Eickelmann, C. Njel, T. Heil, S. Ronneberger, V. Strauss, P. H. Seeberger, A. Savateev, F. F. Loeffler, *Nat. Commun.* **2021**, *12*, 3224.
- [200] Y. Liu, P. H. Seeberger, N. Merbouh, F. F. Loeffler, *Chem. - A Eur. J.* **2021**, *27*, 16098–16102.
- [201] S. Eickelmann, S. Moon, Y. Liu, B. Bitterer, S. Ronneberger, D. Bierbaum, F. Breitling, F. F. Loeffler, *Langmuir* **2022**, *38*, 2220–2226.
- [202] K. Le Mai Hoang, A. Pardo-Vargas, Y. Zhu, Y. Yu, M. Loria, M. Delbianco, P. H. Seeberger, *J. Am. Chem. Soc.* **2019**, *141*, 9079–9086.
- [203] E. T. Sletten, J. Danglad-Flores, S. Lechnitz, A. Abragam Joseph, P. H. Seeberger, *Carbohydr. Res.* **2022**, *511*, 108489.
- [204] O. Calin, S. Eller, P. H. Seeberger, *Angew. Chem. Int. Ed.* **2013**, *52*, 5862–5865.
- [205] EP18213784.4, *Method and Device for Producing Saccharides and Saccharide Arrays*, **n.d.**
- [206] P. H. Seeberger, D. B. Werz, *Nature* **2007**, *446*, 1046–1051.
- [207] A. Geissner, A. Reinhardt, C. Rademacher, T. Johannssen, J. Monteiro, B. Lepenies, M. Thépaut, F. Fieschi, J. Mrázková, M. Wimmerova, et al., *Proc. Natl. Acad. Sci.* **2019**, *116*, 1958–1967.
- [208] P. H. Seeberger, *Perspect. Sci.* **2017**, *11*, 11–17.
- [209] N. Murthy Sabbavarapu, P. H. Seeberger, *J. Org. Chem.* **2021**, *86*, 7280–7287.
- [210] C. S. Kim, H. R. Heo, J. H. Seo, H. J. Cha, *Chem. Commun* **2019**, *55*, 71.
- [211] S. Serna, J. Etxebarria, N. Ruiz, M. Martin-Lomas, N.-C. Reichardt, *Chem. - A Eur. J.* **2010**, *16*, 13163–13175.
- [212] A. Wissner, C. V. Grudzinskas, *J. Org. Chem.* **1978**, *43*, 3972–3974.
- [213] C. D. Spicer, M. Pujari-Palmer, H. Autefage, G. Insley, P. Procter, H. Engqvist, M. M. Stevens, *ACS Cent. Sci.* **2020**, *6*, 226–231.
- [214] F. Bien, T. Ziegler, *Tetrahedron: Asymmetry* **1998**, *9*, 781–790.
- [215] G. Gellerman, A. Elgavi, Y. Salitra, M. Kramer, *J. Pept. Res.* **2001**, *57*, 277–291.
- [216] M. S. Sandbhor, N. Soya, A. Albohy, R. B. Zheng, J. Cartmell, D. R. Bundle, J. S. Klassen, C. W. Cairo, *Biochemistry* **2011**, *50*, 6753–6762.

- [217] S. Rio, J.-M. Beau, J.-C. Jacquinet, *Carbohydr. Res.* **1991**, *219*, 71–90.
- [218] T. Zhang, X. Li, H. Song, S. Yao, *New J. Chem.* **2019**, *43*, 16881–16888.
- [219] C. Cavedon, E. T. Sletten, A. Madani, O. Niemeyer, P. H. Seeberger, B. Pieber, *Org. Lett.* **2021**, *23*, 514–518.
- [220] J. Zhang, Y. Liu, S. Ronneberger, N. V Tarakina, N. Merbouh, F. F. Loeffler, *Adv. Mater.* **2022**, *34*, 2108493.
- [221] A. Tsouka, K. Hoetzel, M. Mende, J. Heidepriem, G. Paris, S. Eickelmann, P. H. Seeberger, B. Lepenies, F. F. Loeffler, *Front. Chem.* **2021**, *9*, 931.
- [222] G. Wei, L. Zhang, C. Cai, S. Cheng, Y. Du, *Tetrahedron Lett.* **2008**, *49*, 5488–5491.
- [223] A. Geissner, C. Anish, P. H. Seeberger, *Curr. Opin. Chem. Biol.* **2014**, *18*, 38–45.
- [224] C. L. O’Neil, K. J. Stine, A. V. Demchenko, *J. Carbohydr. Chem.* **2018**, *37*, 225–249.
- [225] C. Gao, M. Wei, T. R. McKittrick, A. M. McQuillan, J. Heimbürg-Molinario, R. D. Cummings, *Front. Chem.* **2019**, *7*, 833.
- [226] G. Y. Wiederschain, *Biochem.* **2009**, *74*, 1056–1056.
- [227] A. Geissner, P. H. Seeberger, *Annu. Rev. Anal. Chem.* **2016**, *9*, 223–247.
- [228] A. Tikhonov, O. Smoldovskaya, G. Feyzkhanova, N. Kushlinskii, A. Rubina, *Clin. Chem. Lab. Med.* **2020**, *58*, 1611–1622.
- [229] V. Stadler, R. Kirmse, M. Beyer, F. Breitling, T. Ludwig, F. R. Bischoff, *Langmuir* **2008**, *24*, 8151–8157.
- [230] A. Shiba, E. Kinoshita-Kikuta, E. Kinoshita, T. Koike, *Sensors* **2017**, *17*, 1877.
- [231] B. Kang, P. Okwieka, S. Schöttler, S. Winzen, J. Langhanki, K. Mohr, T. Opatz, V. Mailänder, K. Landfester, F. R. Wurm, *Angew. Chem. Int. Ed.* **2015**, *54*, 7436–7440.
- [232] M. K. Patel, B. Vijaykrishnan, J. R. Koeppe, J. M. Chalker, K. J. Doores, B. G. Davis, *Chem. Commun.* **2010**, *46*, 9119–9121.
- [233] E. D. Soli, A. S. Manoso, M. C. Patterson, P. DeShong, D. A. Favor, R. Hirschmann, A. B. Smith, *J. Org. Chem.* **1999**, *64*, 3171–3177.
- [234] V. Tsoulougian, E. E. Psykarakis, T. Gimisis, *Org. Biomol. Chem.* **2019**, *17*, 973–981.
- [235] G. Pastuch-Gawolek, K. Malarz, A. Mrozek-Wilczkiewicz, M. Musioł, M. Serda, B. Czaplinska, R. Musiol, *Eur. J. Med. Chem.* **2016**, *112*, 130–144.
- [236] E. A. Smith, W. D. Thomas, L. L. Kiessling, R. M. Corn, *J. Am. Chem. Soc.* **2003**, *125*, 6140–

6148.

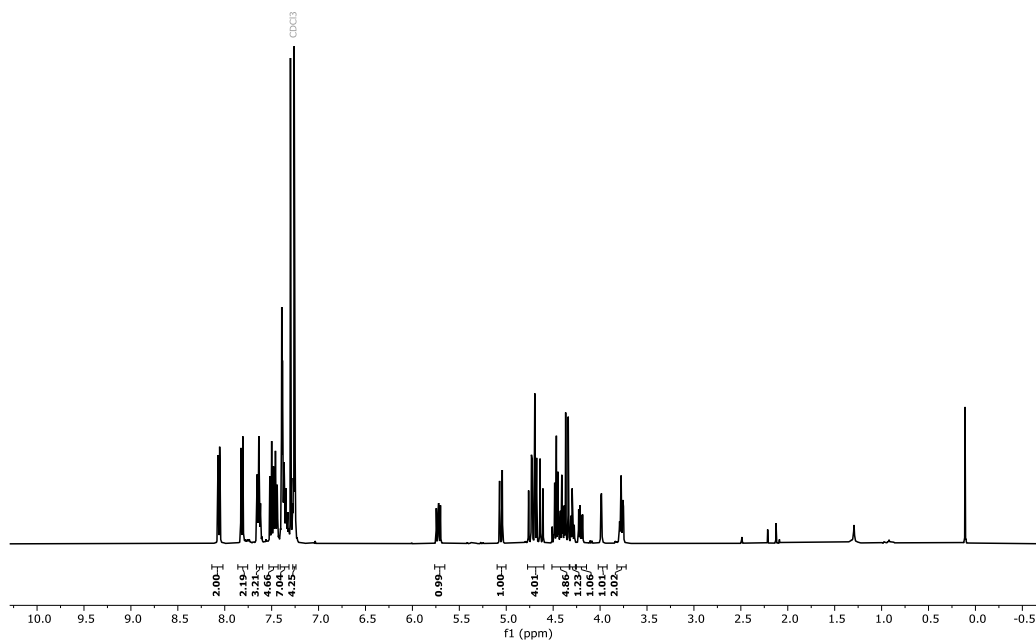
- [237] B. Pandey, Y. H. Tan, K. Fujikawa, A. V. Demchenko, K. J. Stine, *J. Carbohydr. Chem.* **2012**, *31*, 466–503.
- [238] M. Maglinao, M. Eriksson, M. K. Schlegel, S. Zimmermann, T. Johannssen, S. Götze, P. H. Seeberger, B. Lepenies, *J. Control. Release* **2014**, *175*, 36–42.
- [239] D. Ponader, P. Maffre, J. Aretz, D. Pussak, N. M. Ninnemann, S. Schmidt, P. H. Seeberger, C. Rademacher, G. U. Nienhaus, L. Hartmann, *J. Am. Chem. Soc.* **2014**, *136*, 2008–2016.
- [240] S. Karpitschka, F. Liebig, H. Riegler, *Langmuir* **2017**, *33*, 4682–4687.
- [241] M. Ghirardello, D. Perrone, N. Chinaglia, D. Sádaba, I. Delso, T. Tejero, E. Marchesi, M. Fogagnolo, K. Rafie, D. M. F. van Aalten, et al., *Chem. - A Eur. J.* **2018**, *24*, 7264–7272.
- [242] J. Hanske, J. Schulze, J. Aretz, R. McBride, B. Loll, H. Schmidt, Y. Knirel, W. Rabsch, M. C. Wahl, J. C. Paulson, et al., *J. Biol. Chem.* **2017**, *292*, 862–871.
- [243] L. S. Z. Györgydeák, *Liebigs Ann. Chem.* **1987**, *1987*, 235–241.
- [244] K. Asano, S. Matsubara, *Org. Lett.* **2010**, *12*, 4988–4991.
- [245] G. Pastuch-Gawolek, K. Malarz, A. Mrozek-Wilczkiewicz, M. Musioł, M. Serda, B. Czaplinska, R. Musiol, *Eur. J. Med. Chem.* **2016**, *112*, 130–144.
- [246] N. O. L. Seto, C. A. Compston, A. Szpacenko, M. M. Palcic, *Carbohydr. Res.* **2000**, *324*, 161–169.
- [247] N. Sindhuwinata, E. Munoz, F. J. Munoz, M. M. Palcic, H. Peters, T. Peters, *Glycobiology* **2010**, *20*, 718–723.
- [248] N. Kong, M. R. Shimpi, J. H. Park, O. Ramström, M. Yan, *Carbohydr. Res.* **2015**, *405*, 33–38.
- [249] Y. Terada, Y. Hoshino, Y. Miura, *Chem. – An Asian J.* **2019**, *14*, 1021–1027.
- [250] N. V. Bhagavan, C.-E. Ha, *Essentials of Medical Biochemistry: With Clinical Cases*, Elsevier/Academic Press, **2015**.
- [251] H., Wamhoff, *Comprehensive Heterocyclic Chemistry: The Structure, Reactions, Synthesis and Uses of Heterocyclic Compounds*, Pergamon Press, Oxford, **1984**.
- [252] A. Tsouka, P. Dallabernardina, M. Mende, E. T. Sletten, S. Lechnitz, K. Bienert, K. Le Mai Hoang, P. H. Seeberger, F. F. Loeffler, *J. Am. Chem. Soc.* **2022**, *144*, 19832–19837.
- [253] S. Moon, S. Chatterjee, P. H. Seeberger, K. Gilmore, *Chem. Sci.* **2021**, *12*, 2931–2939.
- [254] B. Liu, F. Zhang, Y. Zhang, G. Liu, *Org. Biomol. Chem.* **2014**, *12*, 1892–1896.

- [255] D. Majumdar, T. Zhu, G. J. Boons, *Org. Lett.* **2003**, *5*, 3591–3594.
- [256] S. Shi, K. Zhu, X. Chen, J. Hu, L. Zhang, *ACS Sustain. Chem. Eng.* **2019**, *7*, 19799–19806.
- [257] T. K. Dam, C. F. Brewer, *Glycobiology* **2010**, *20*, 270–279.
- [258] V. Agouridas, O. El Mahdi, V. Diemer, M. Cargoët, J.-C. M. Monbaliu, O. Melnyk, *Chem. Rev.* **2019**, *119*, 7328–7443.

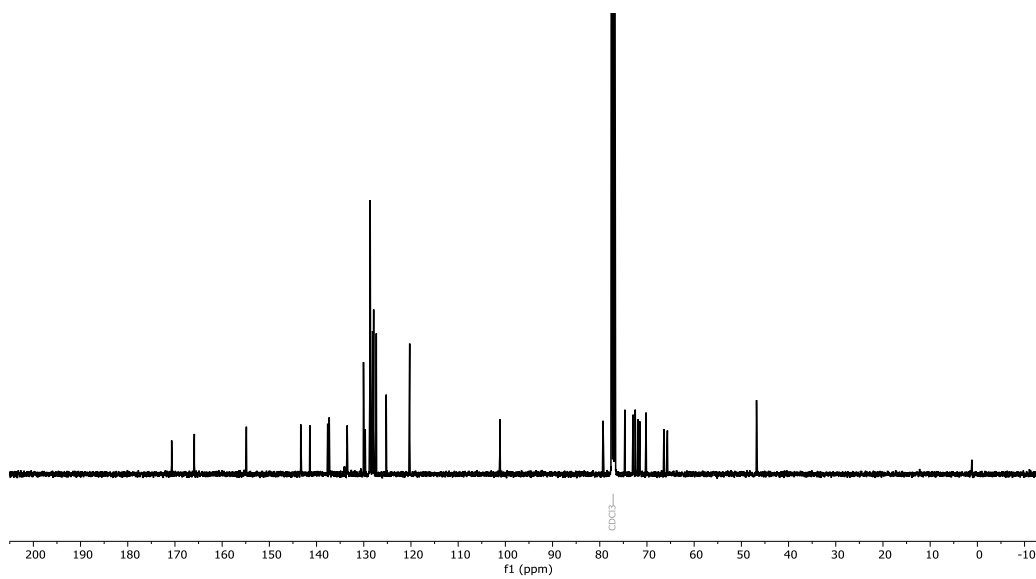
7. Appendix

NMR Spectra of New Compounds

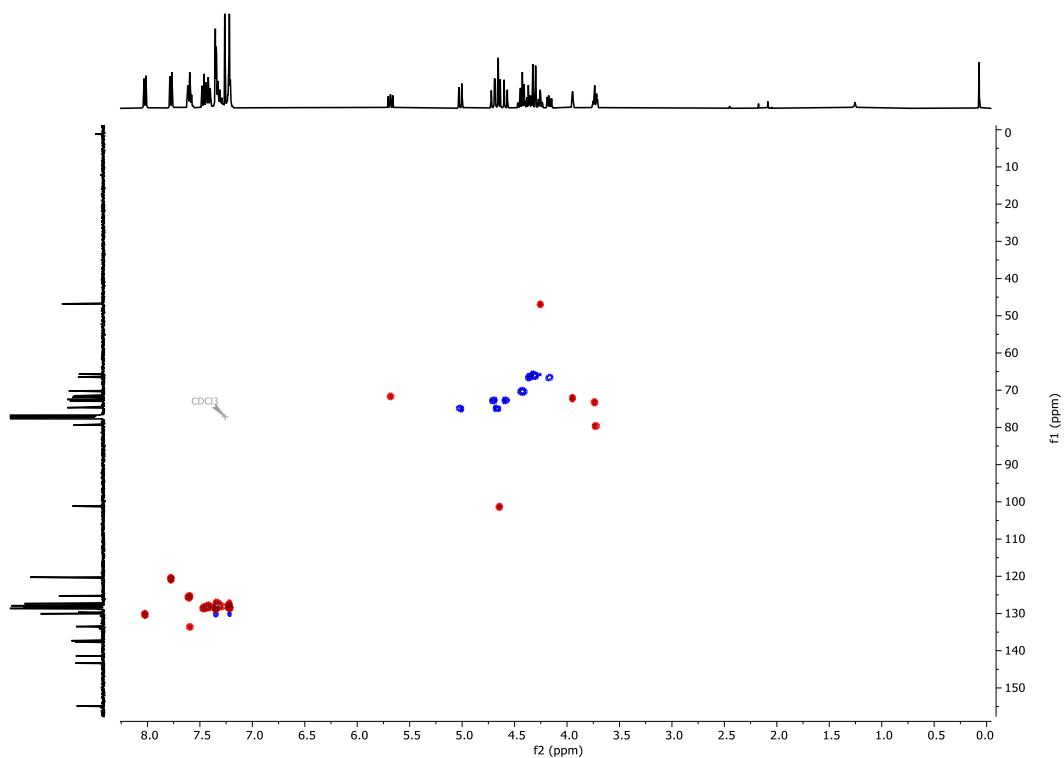
^1H NMR (CDCl_3): 2.1



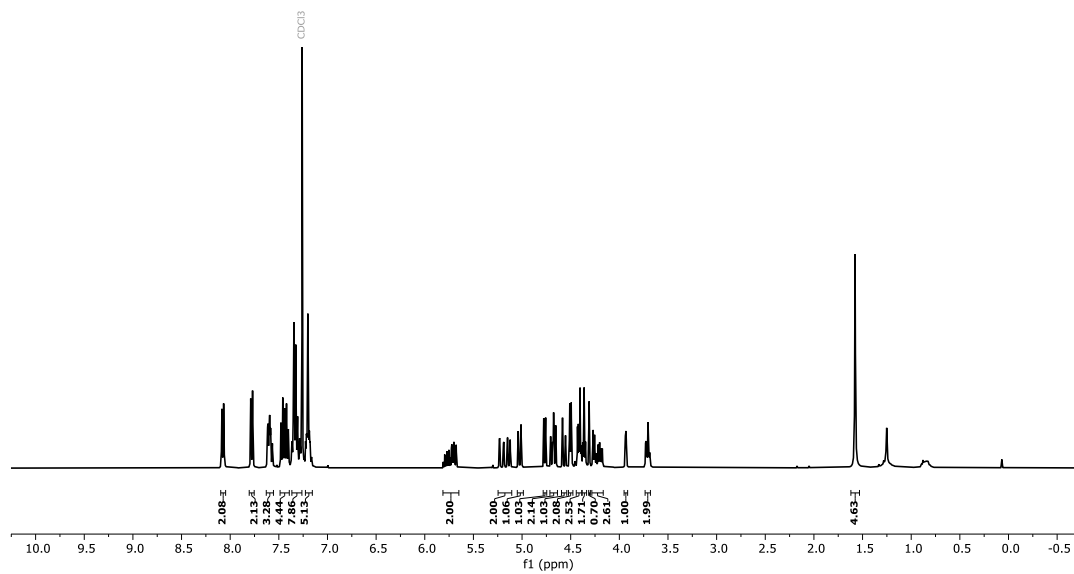
^{13}C NMR (CDCl_3): 2.1



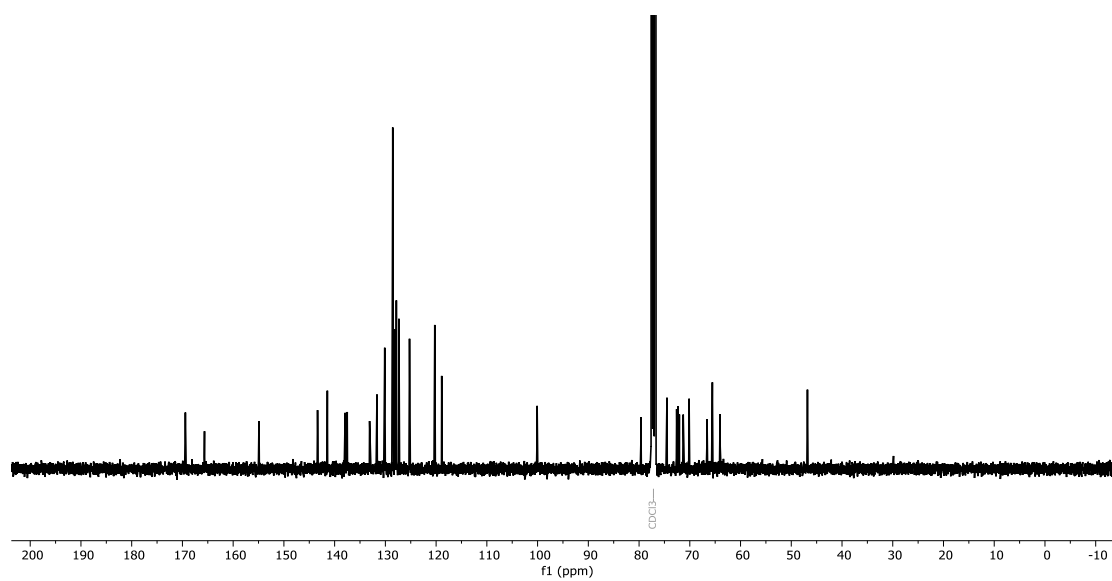
HSQC NMR (CDCl₃): 2.1



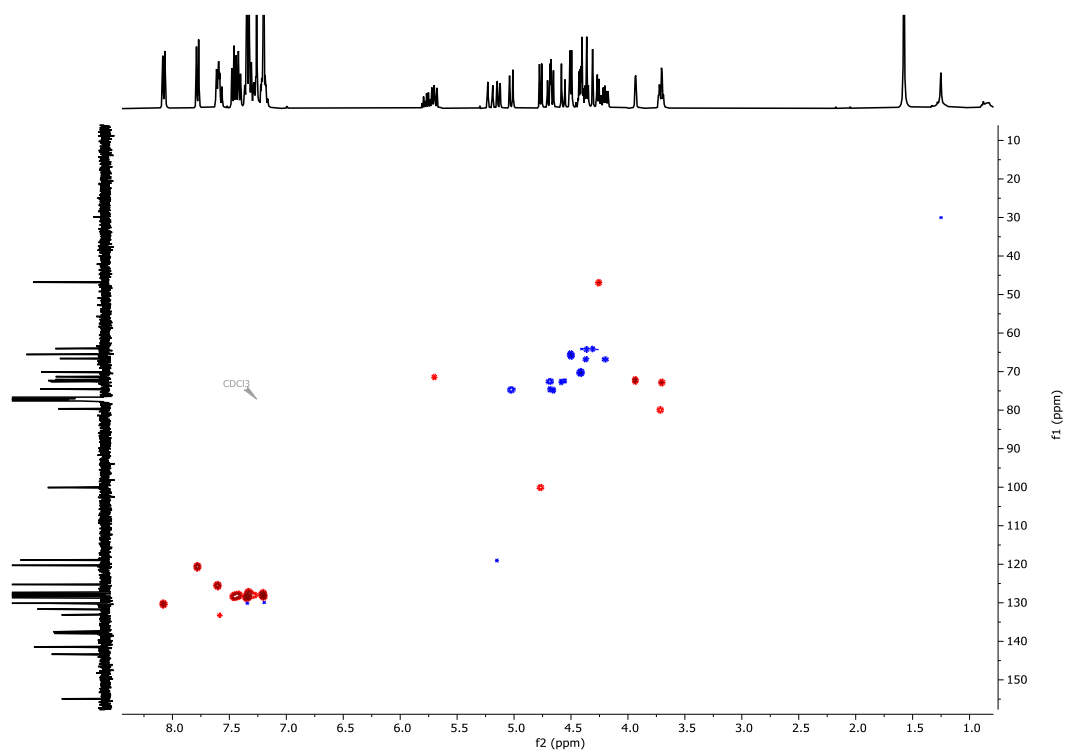
¹H NMR (CDCl₃): 2.3



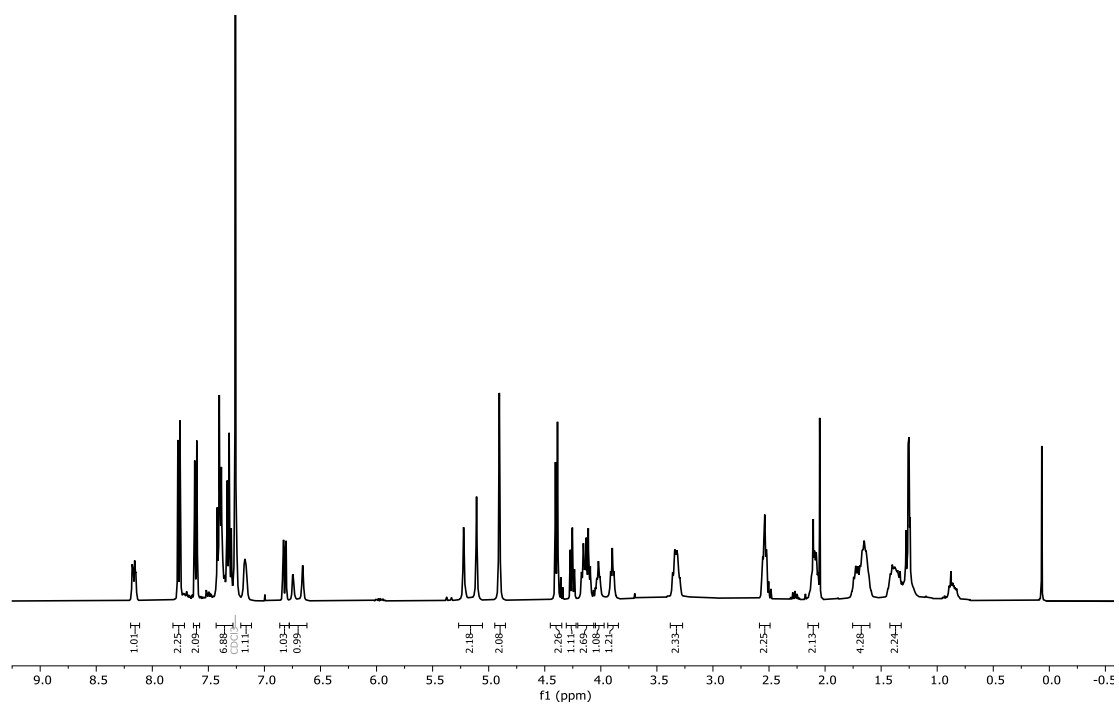
^{13}C NMR (CDCl_3): 2.3



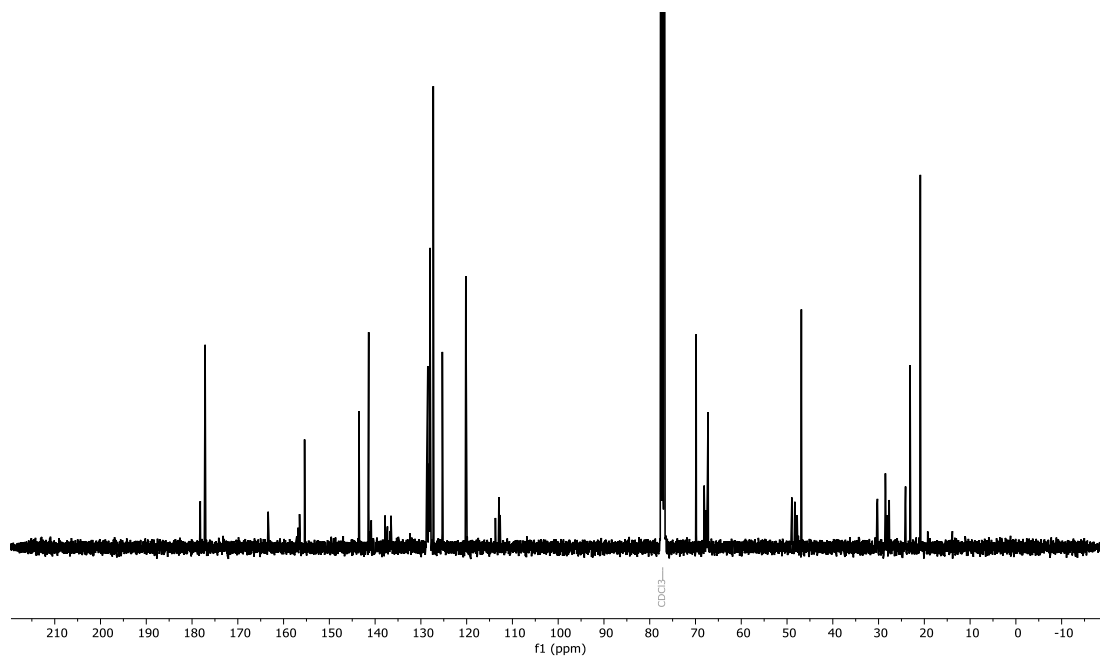
HSQC NMR (CDCl_3): 2.3



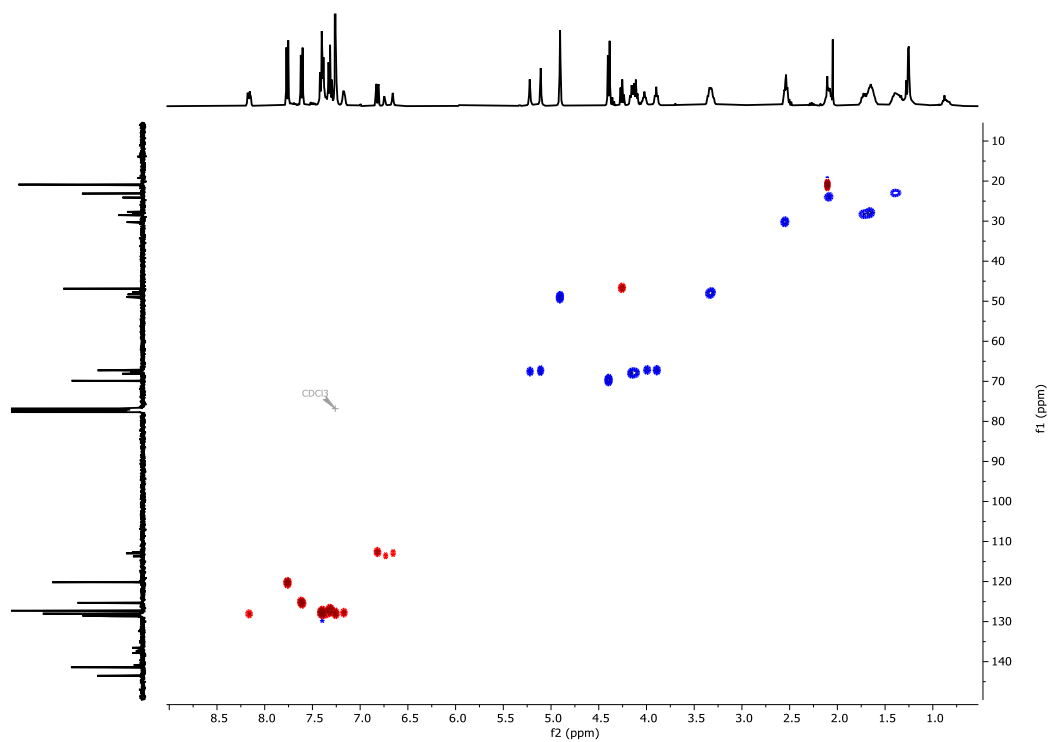
^1H NMR (CDCl_3): 2.12/4.24



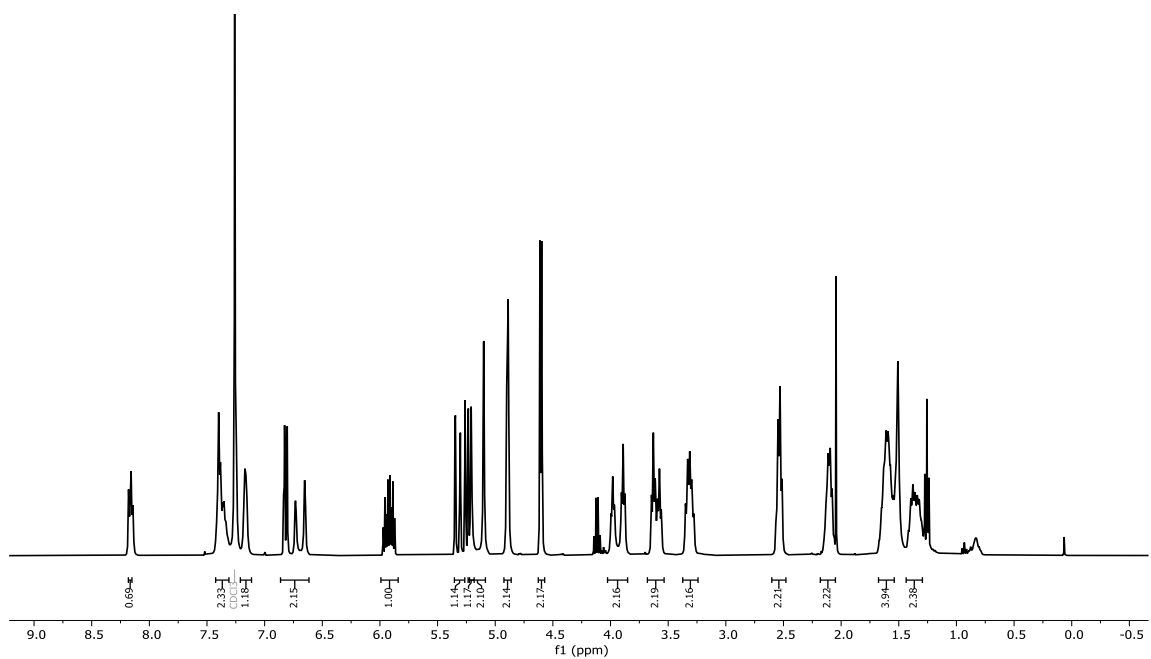
^{13}C NMR (CDCl_3): 2.12/4.24



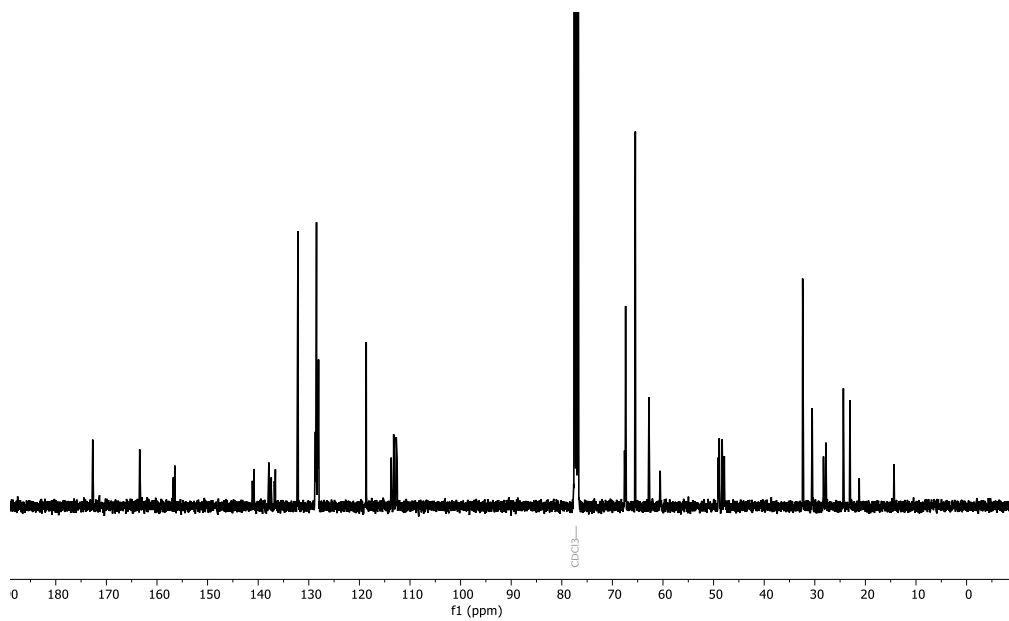
HSQC NMR (CDCl₃): 2.12/4.24



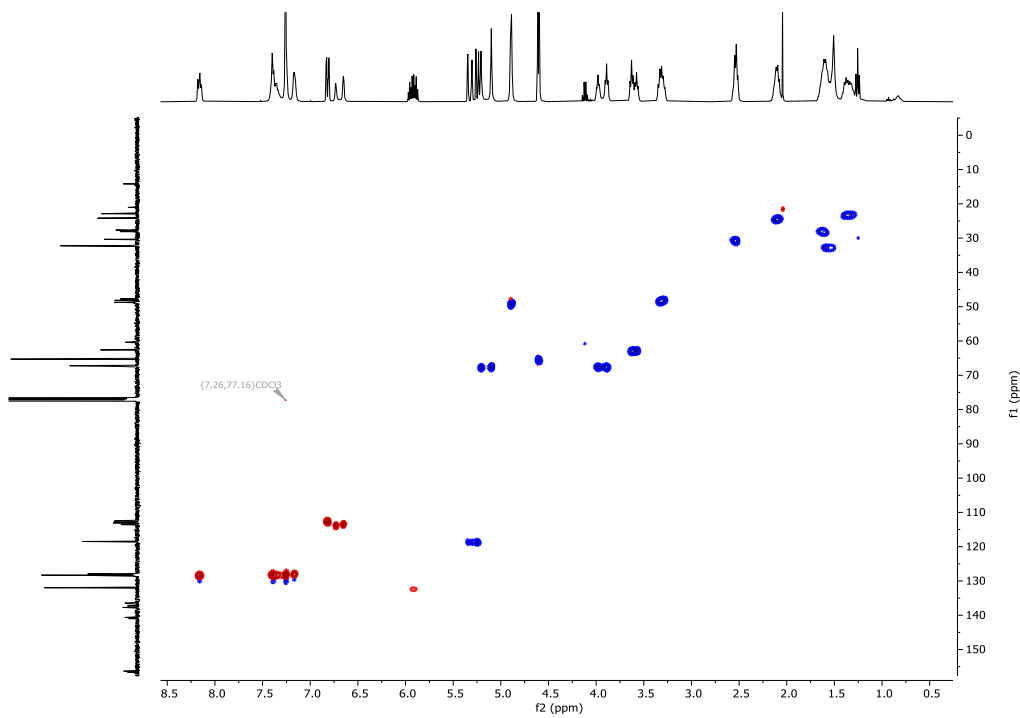
¹H NMR (CDCl₃): 2.14



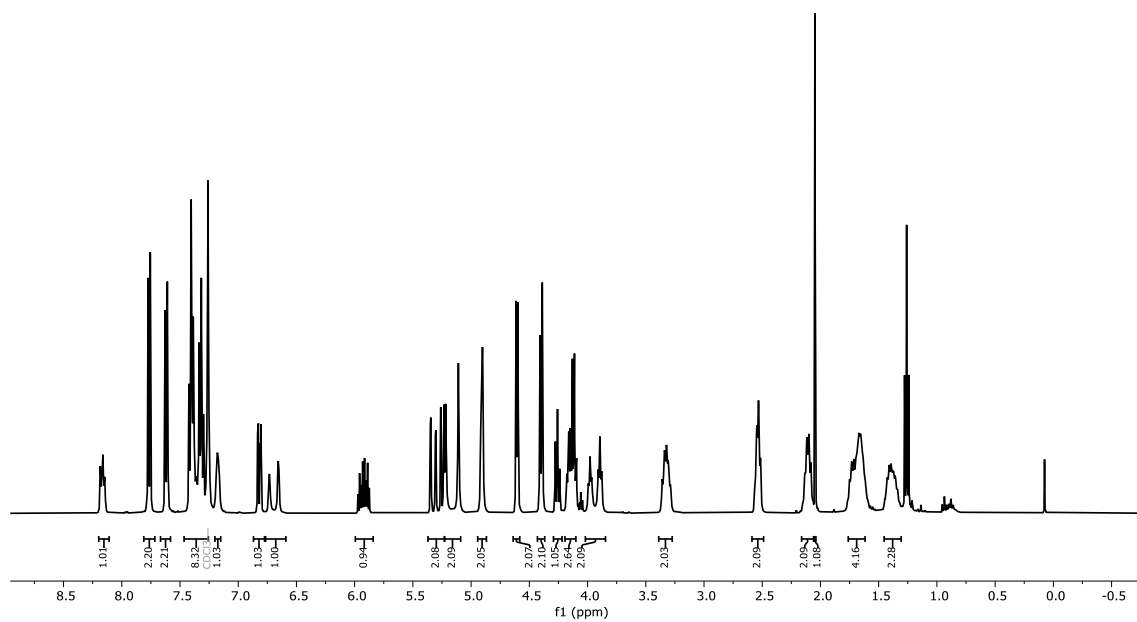
^{13}C NMR (CDCl_3): 2.14



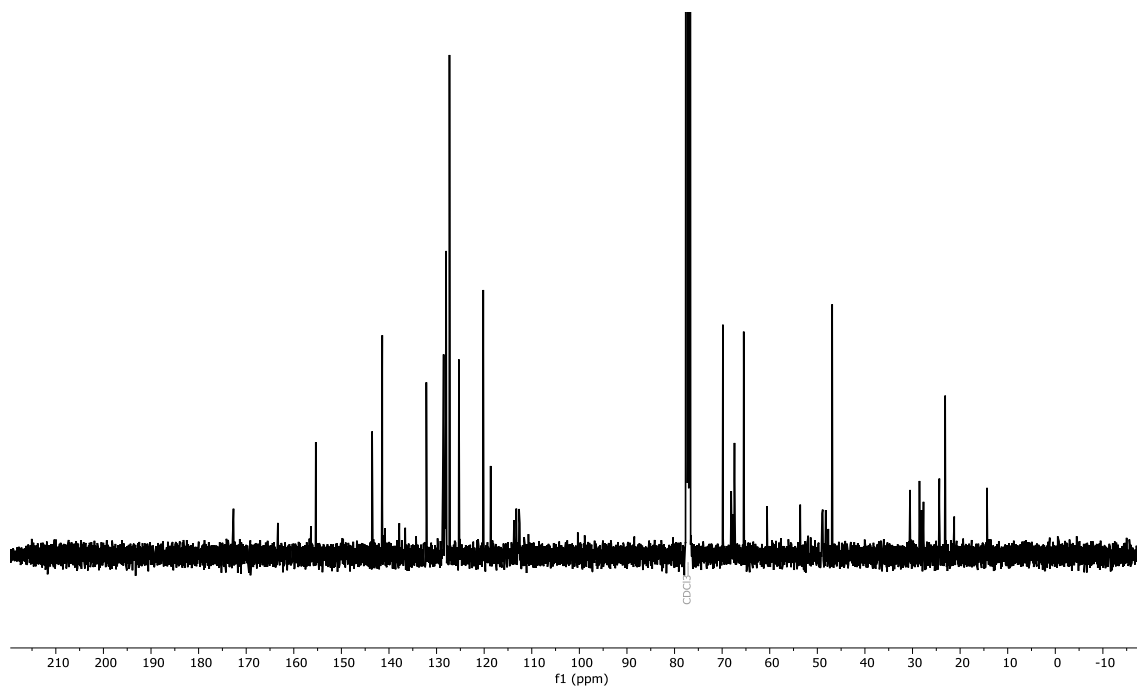
HSQC NMR (CDCl_3): 2.14



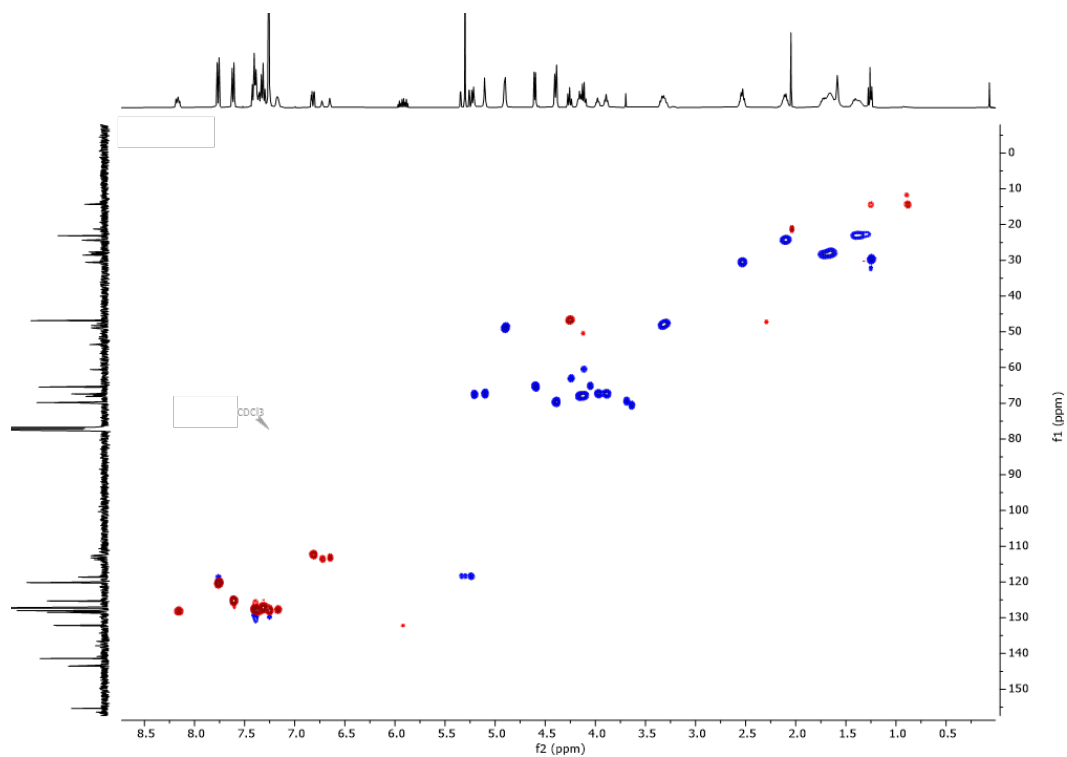
^1H NMR (CDCl_3): 2.15



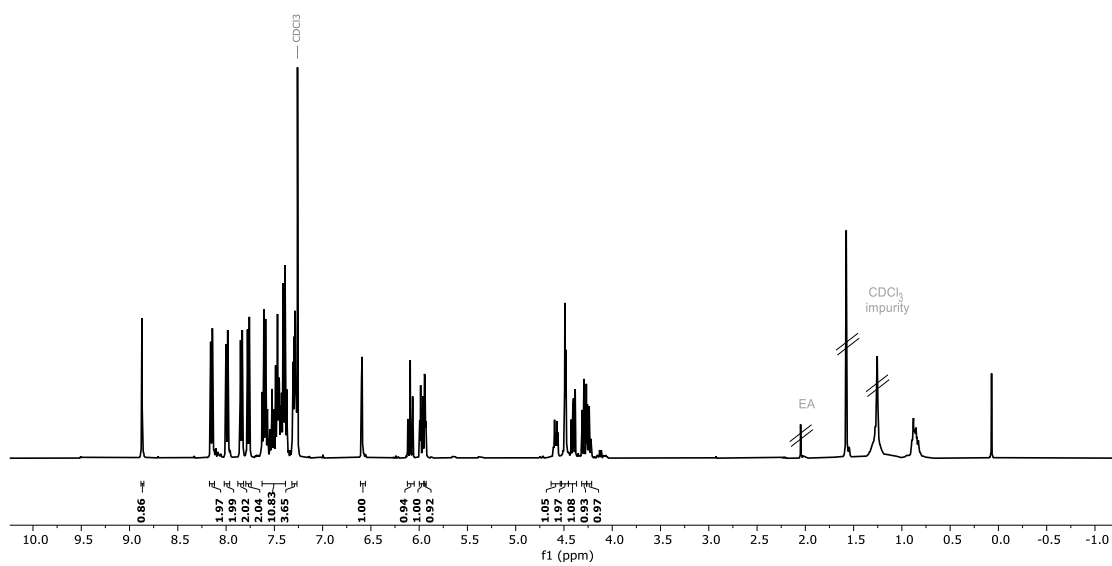
^{13}C NMR (CDCl_3): 2.15



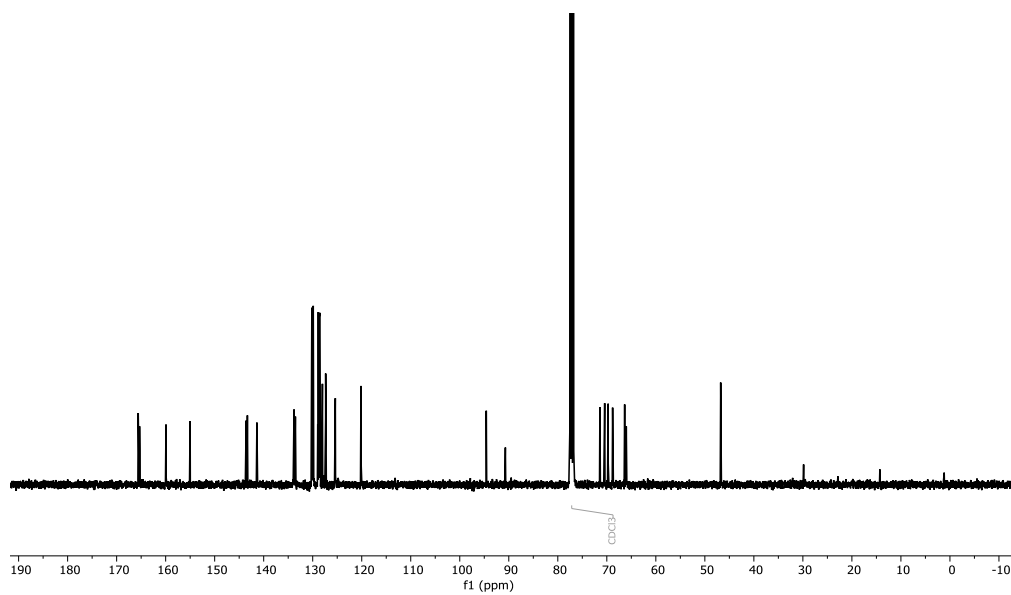
HSQC NMR (CDCl₃): 2.15



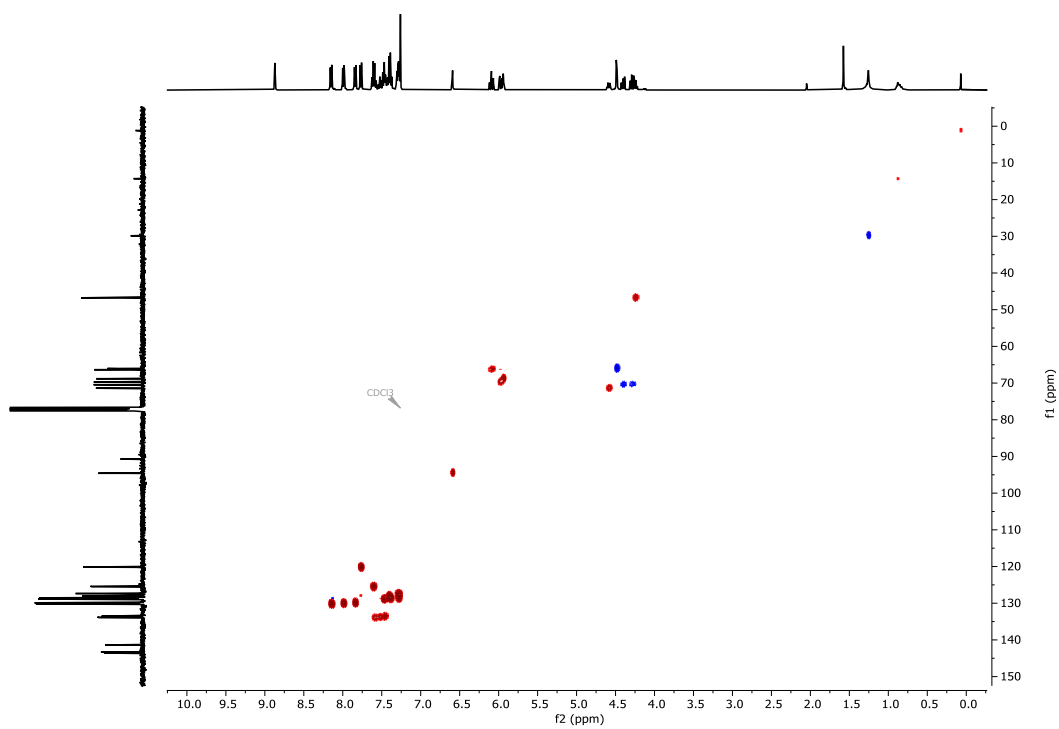
¹H NMR (CDCl₃): 2.18/4.6



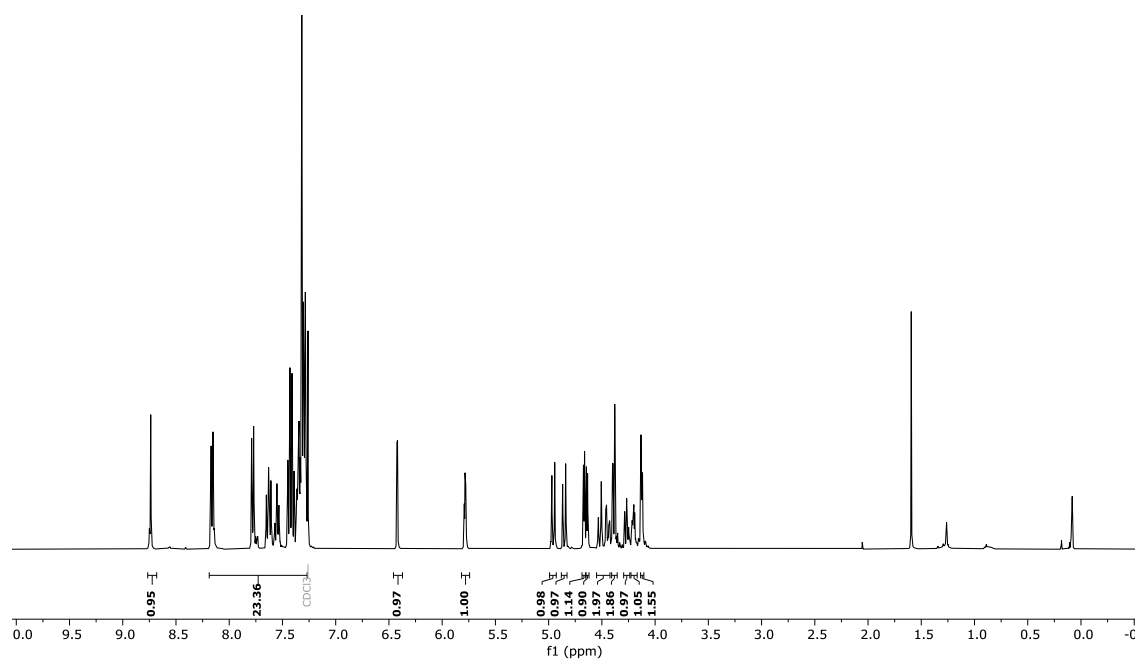
^{13}C NMR (CDCl_3): 2.18/4.6



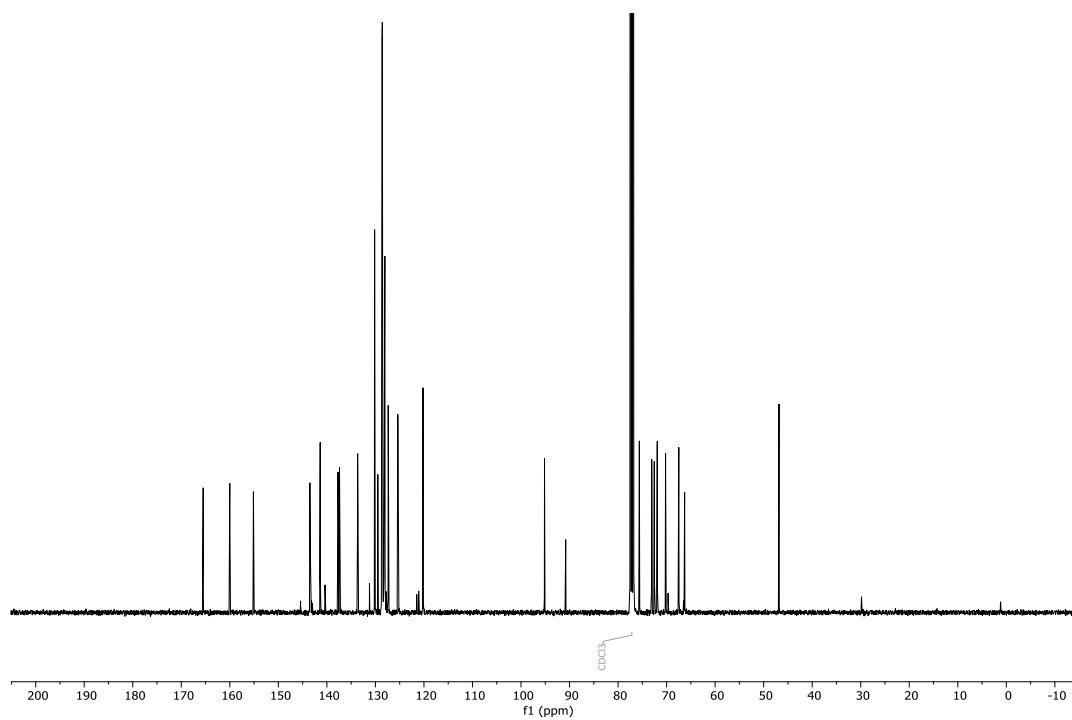
HSQC NMR (CDCl_3): 2.18/4.6



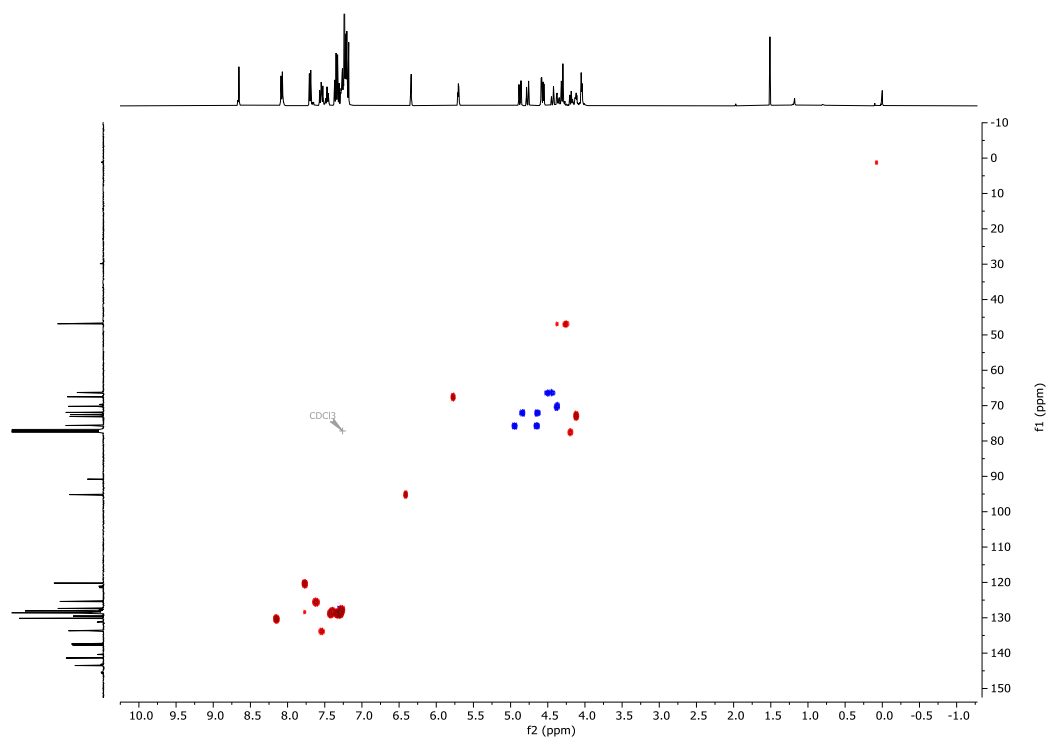
^1H NMR (CDCl_3): 2.19/4.8



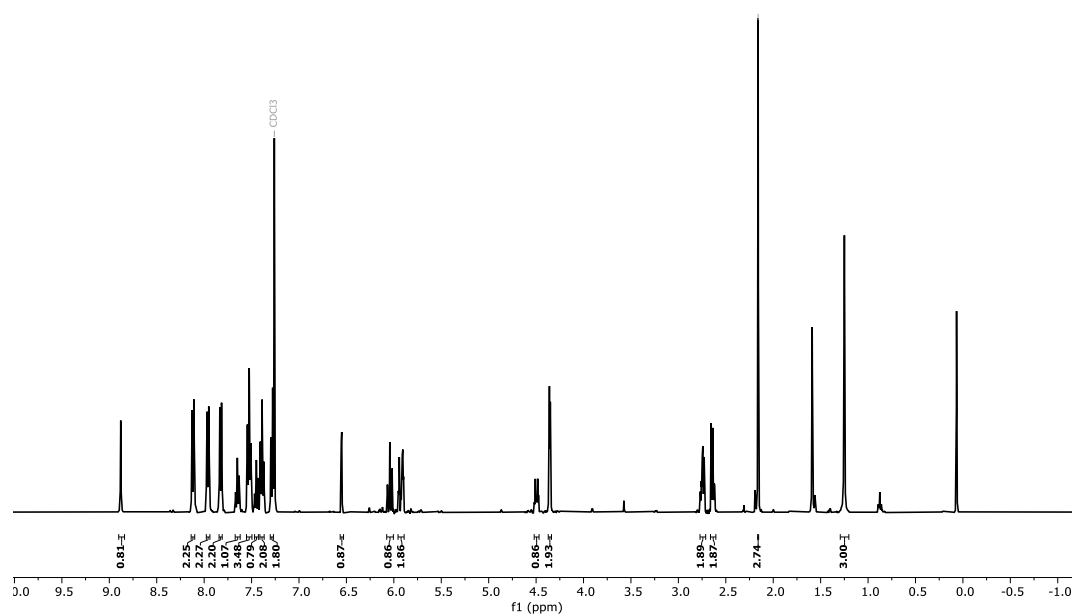
^{13}C NMR (CDCl_3): 2.19/4.8



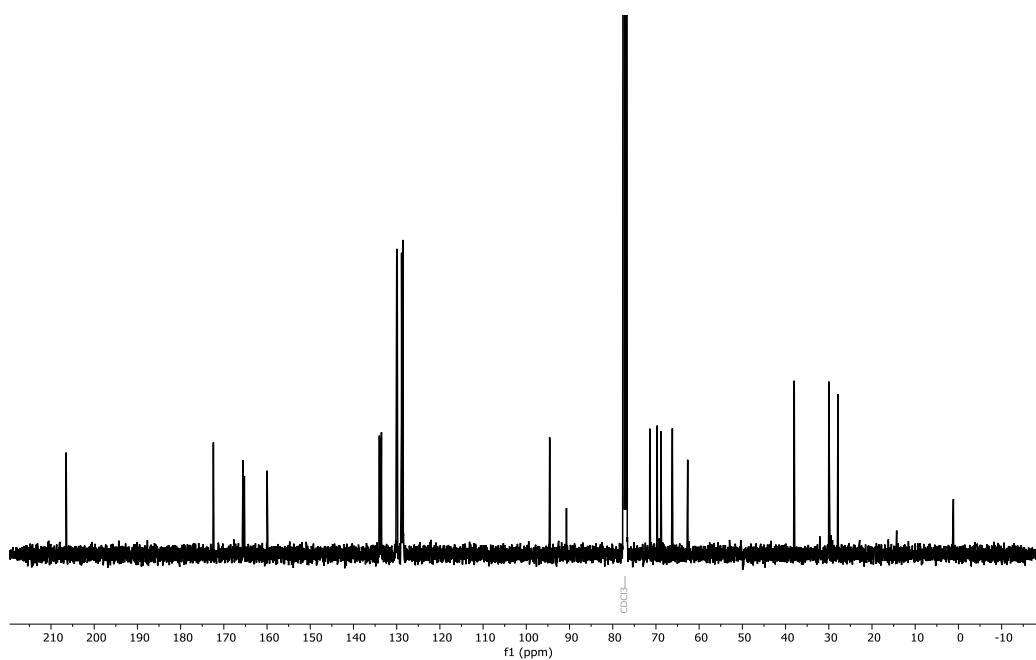
HSQC (CDCl₃): 2.19/4.8



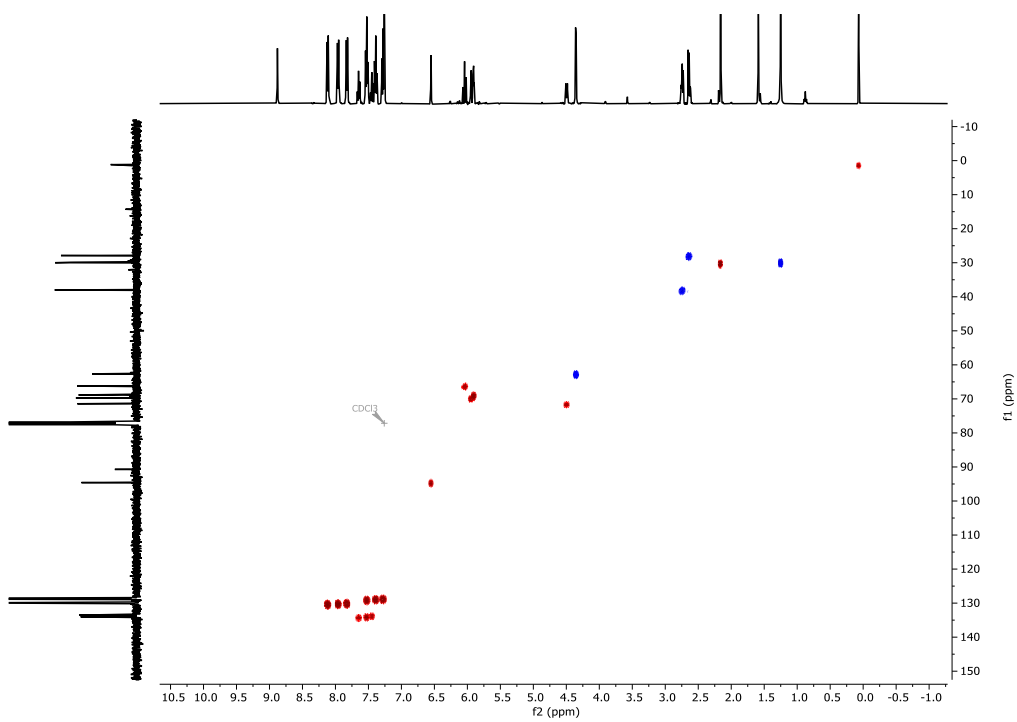
¹H NMR (CDCl₃): 2.20



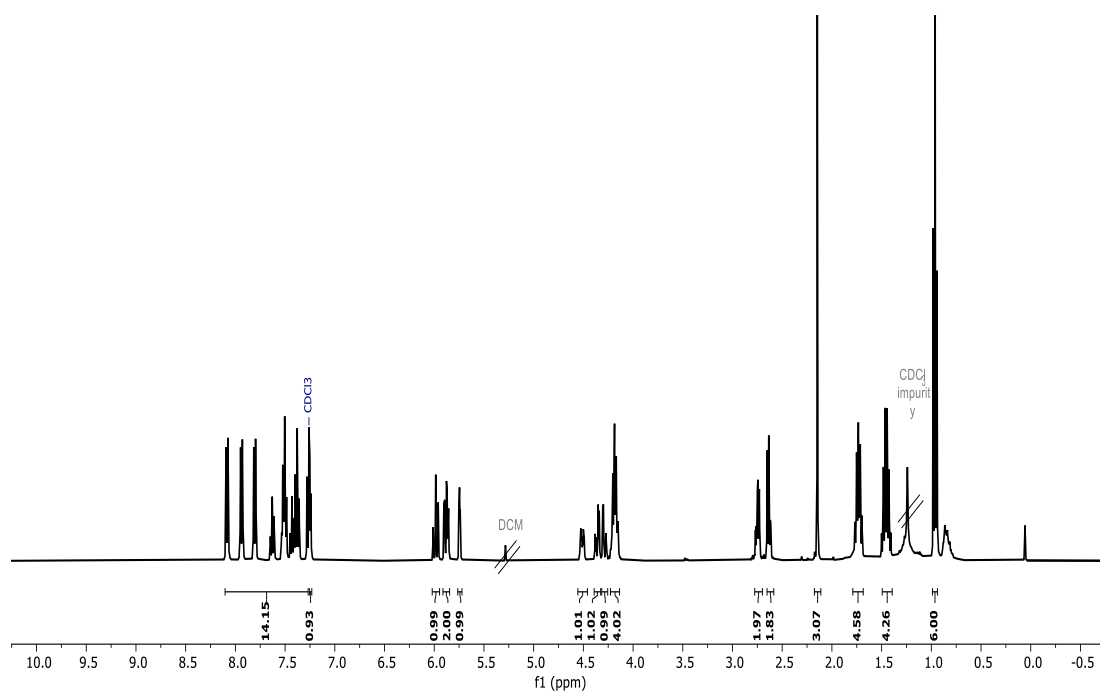
^{13}C NMR (CDCl_3): **2.20**



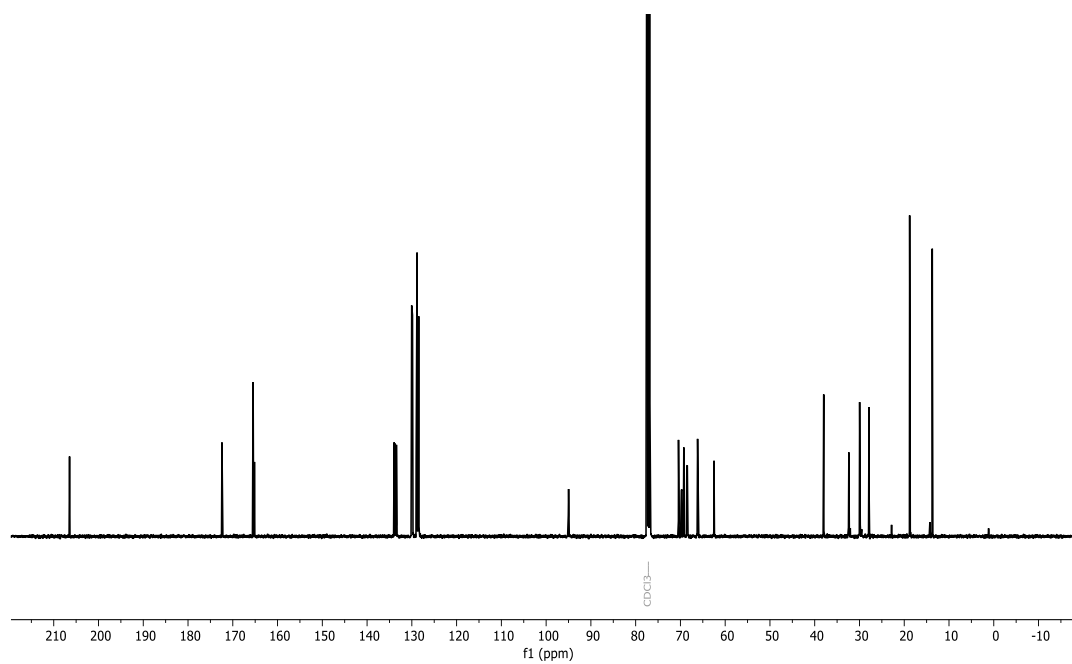
HSQC NMR (CDCl_3): **2.20**



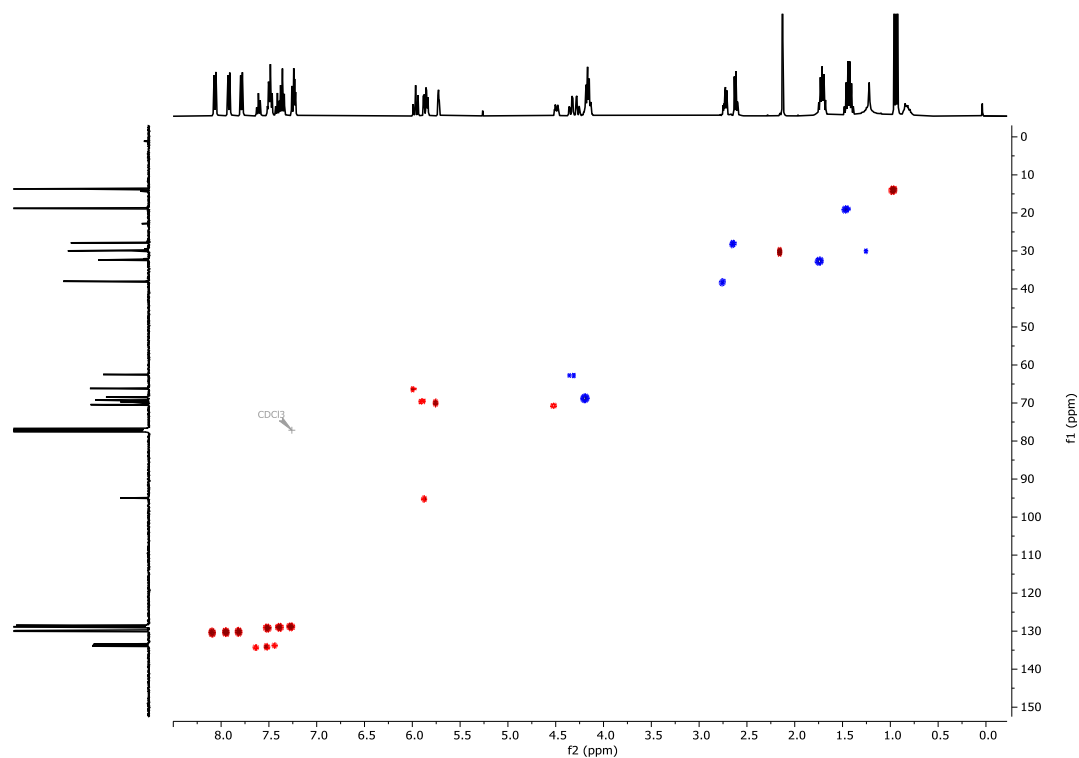
^1H NMR (CDCl_3): 2.21/4.11



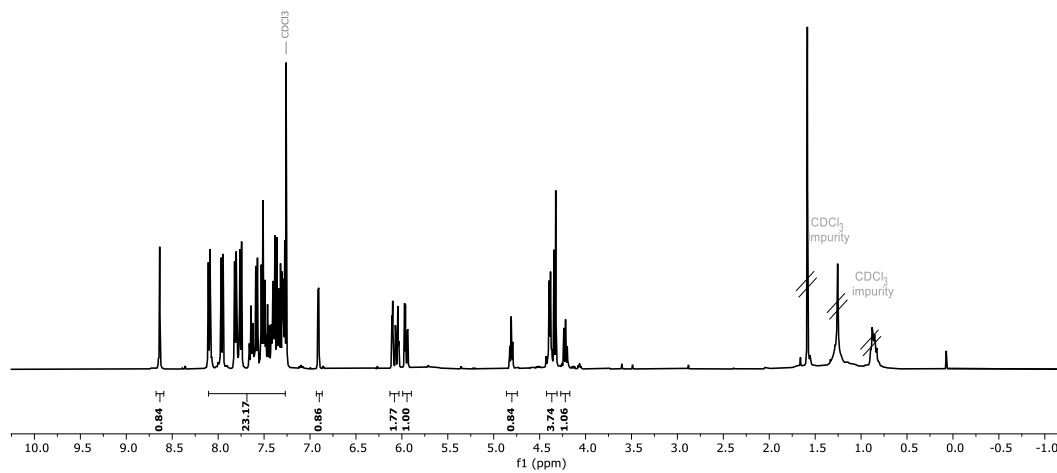
^{13}C NMR (CDCl_3) 2.21/4.11



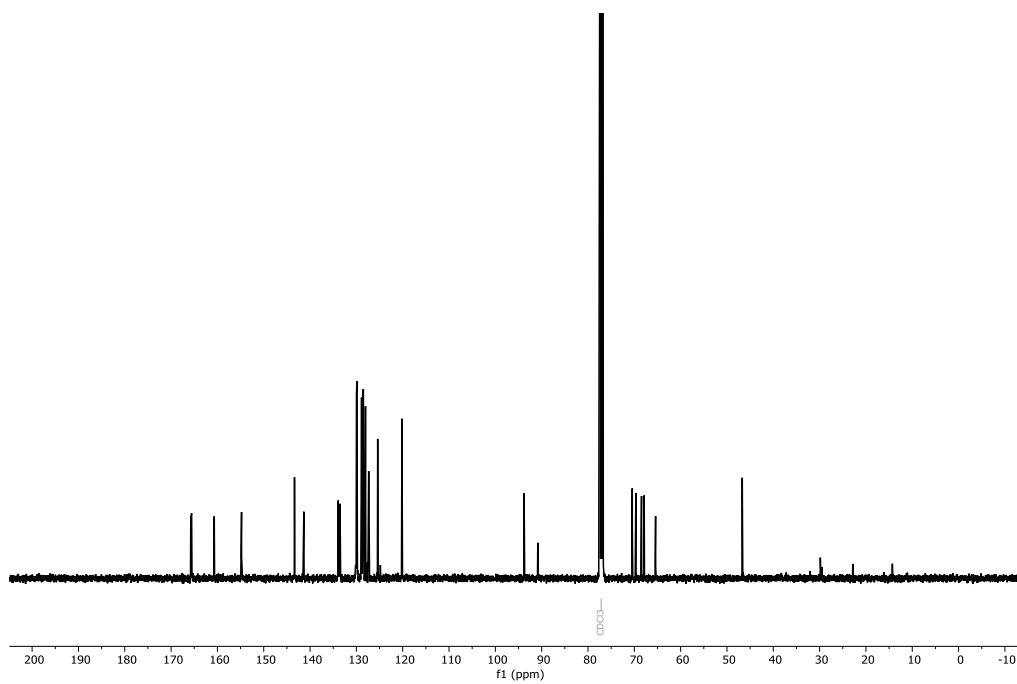
HSQC NMR (CDCl₃): 2.21/4.11



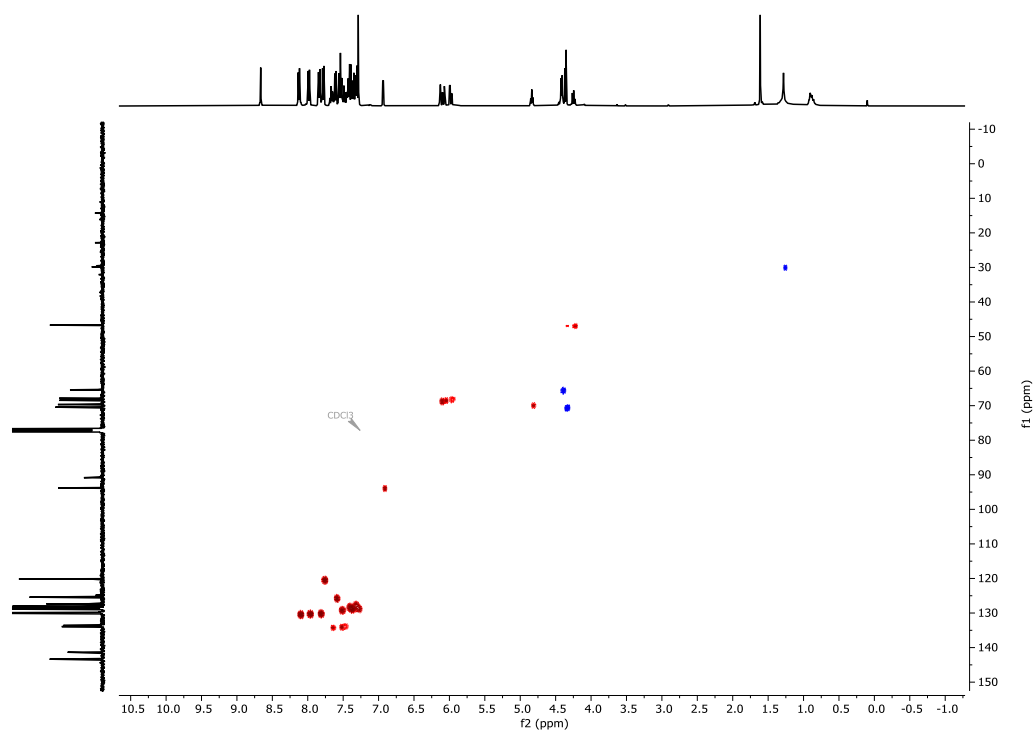
¹H NMR (CDCl₃): 2.25/4.13



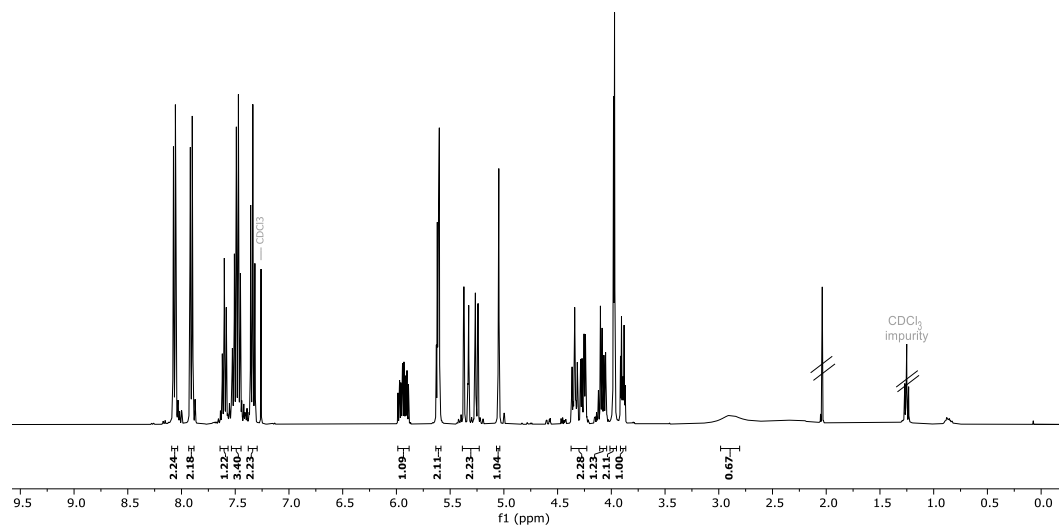
^{13}C NMR (CDCl_3): 2.25/4.13



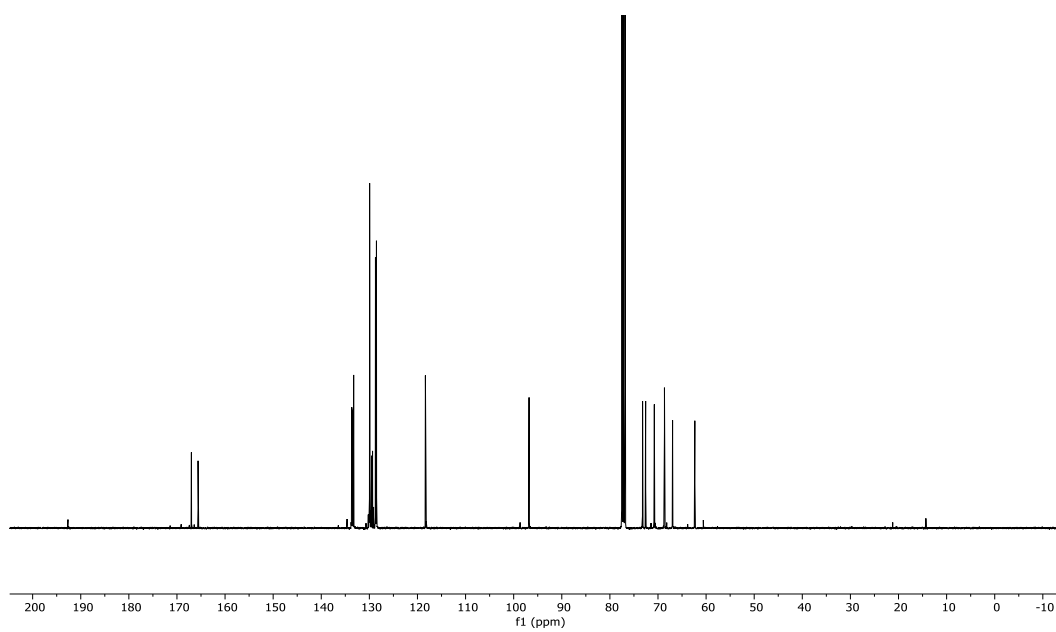
HSQC NMR (CDCl_3): 2.25/4.13



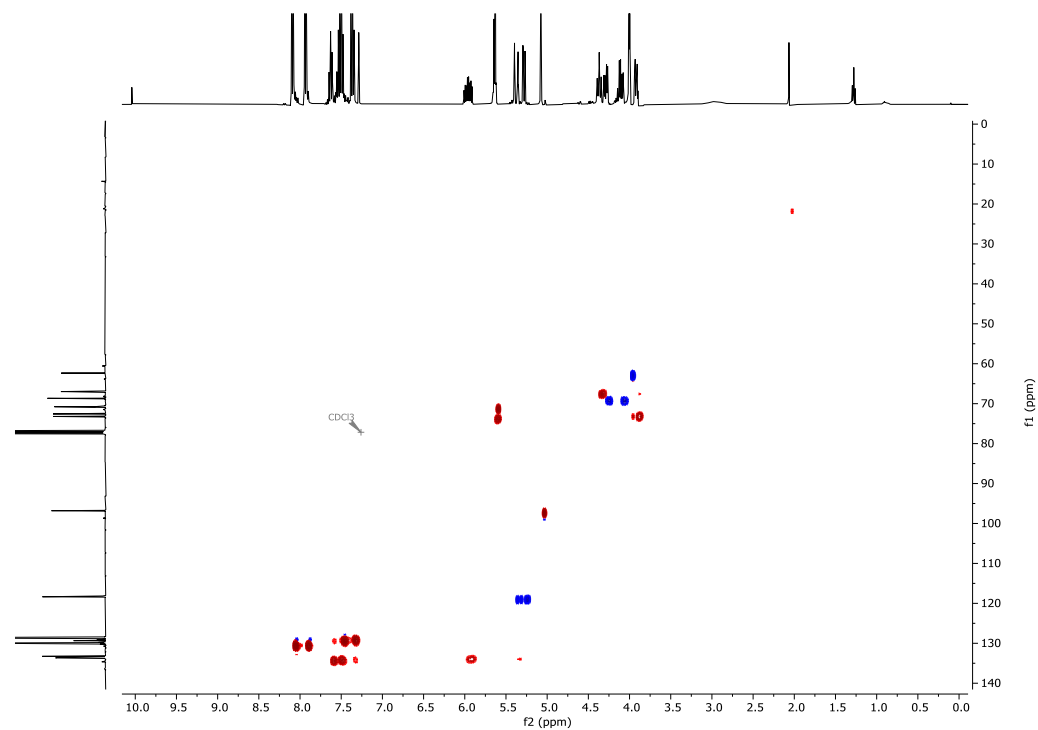
^1H NMR (CDCl_3): **2.27**



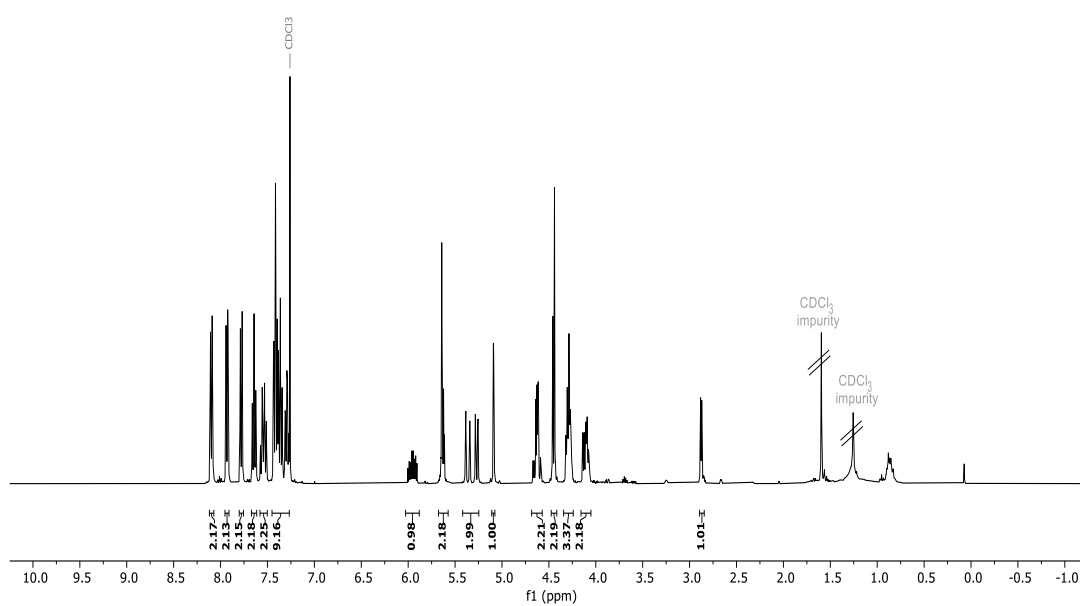
^{13}C NMR (CDCl_3): **2.27**



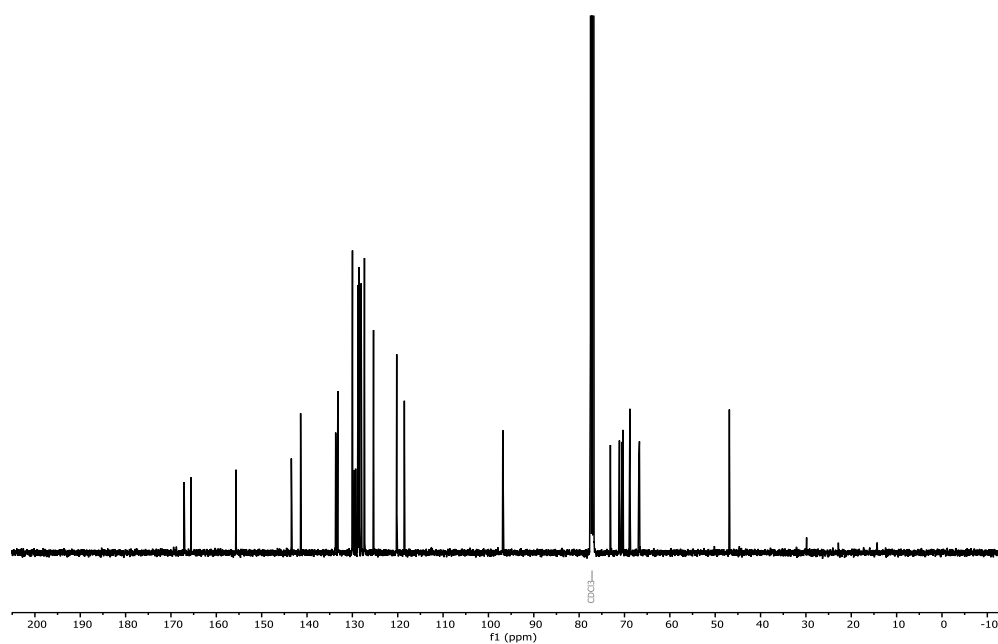
HSQC NMR (CDCl₃): 2.27



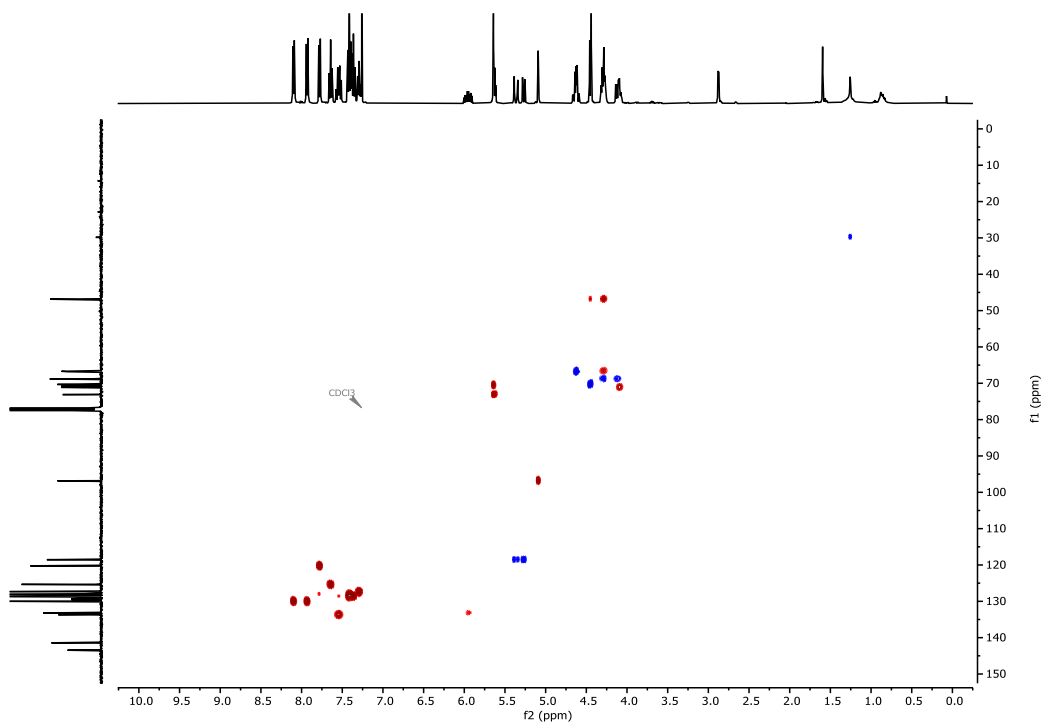
¹H NMR (CDCl₃): 2.28



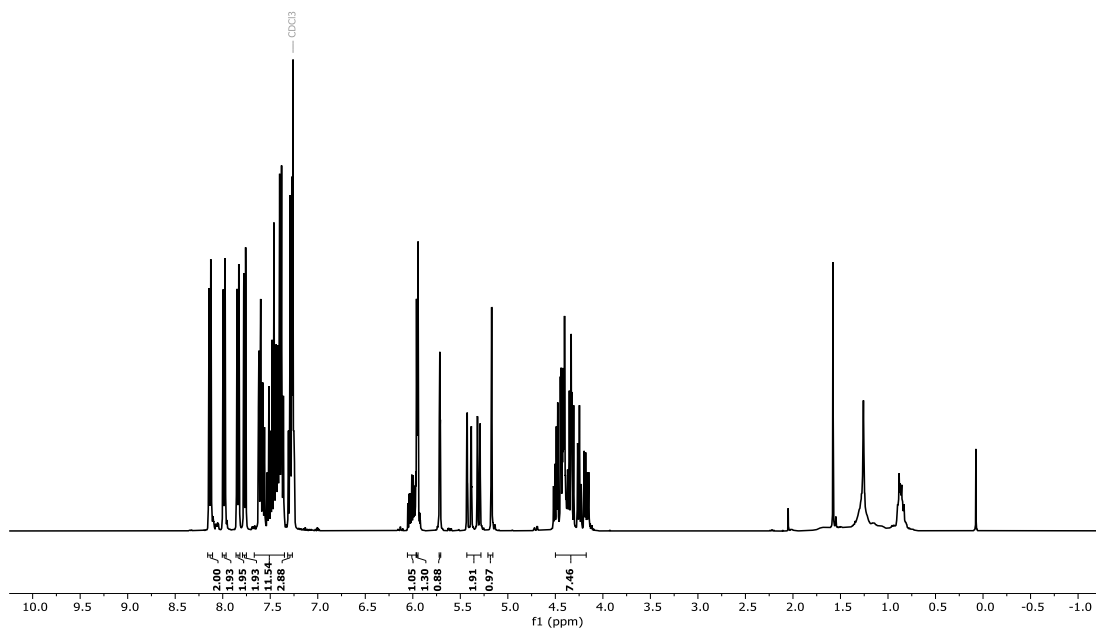
^{13}C NMR (CDCl_3): **2.28**



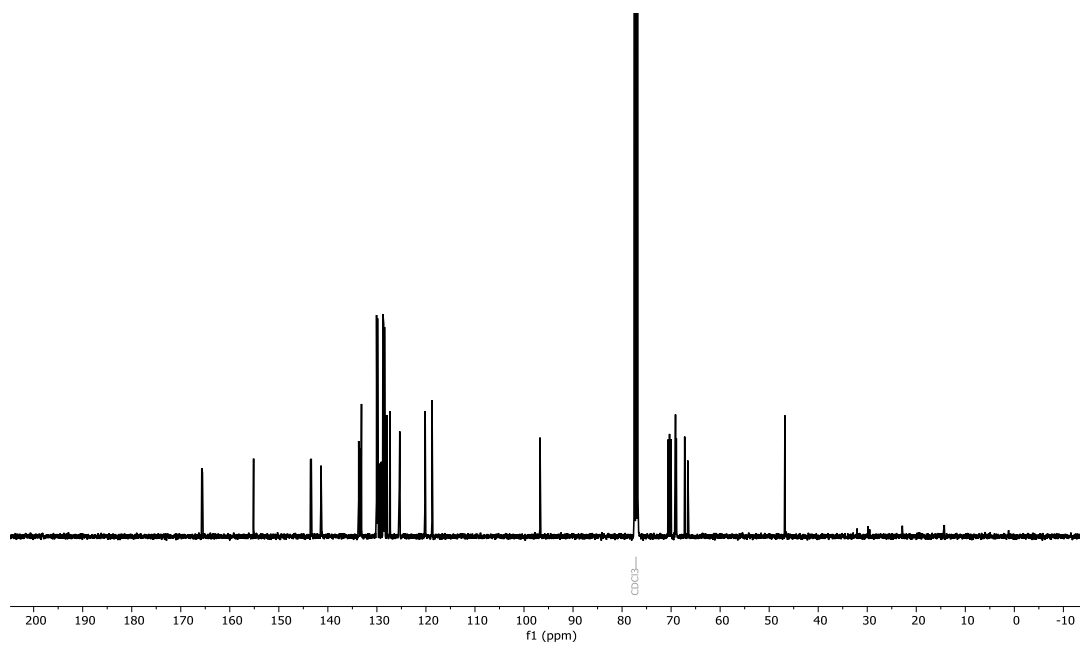
HSQC NMR (CDCl_3): **2.28**



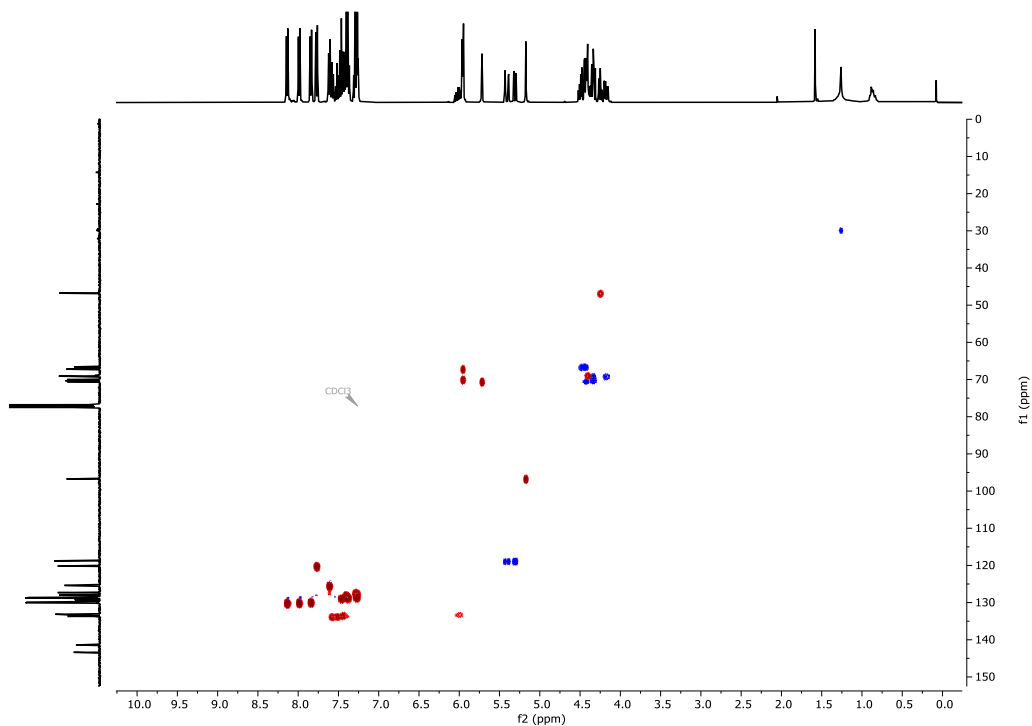
^1H NMR (CDCl_3): 2.29



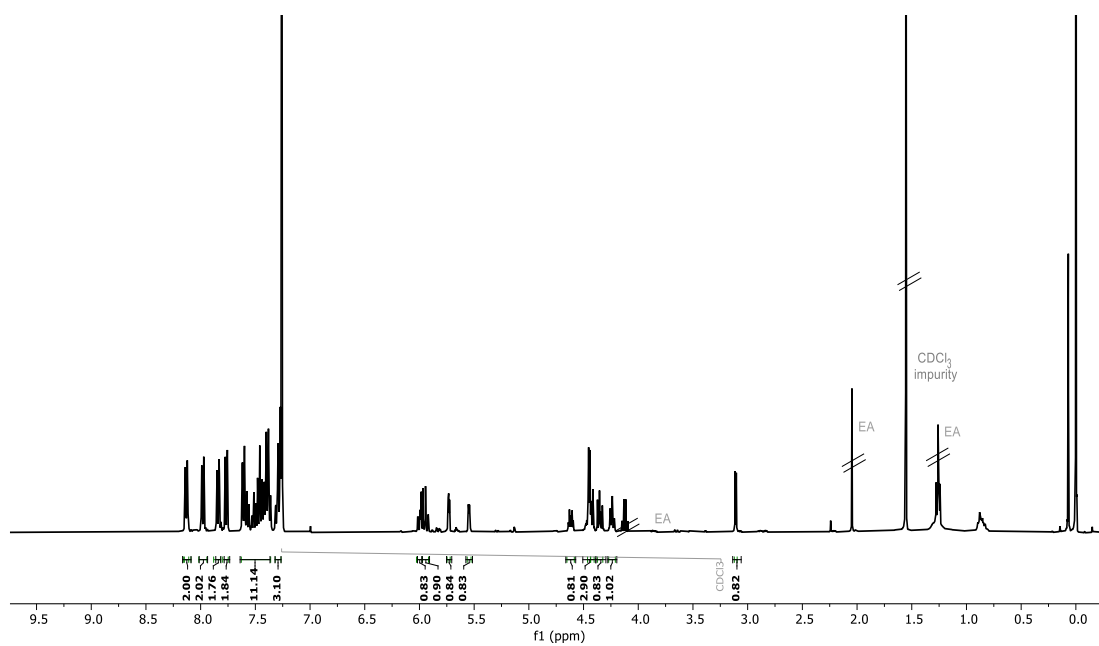
^{13}C NMR (CDCl_3): 2.29



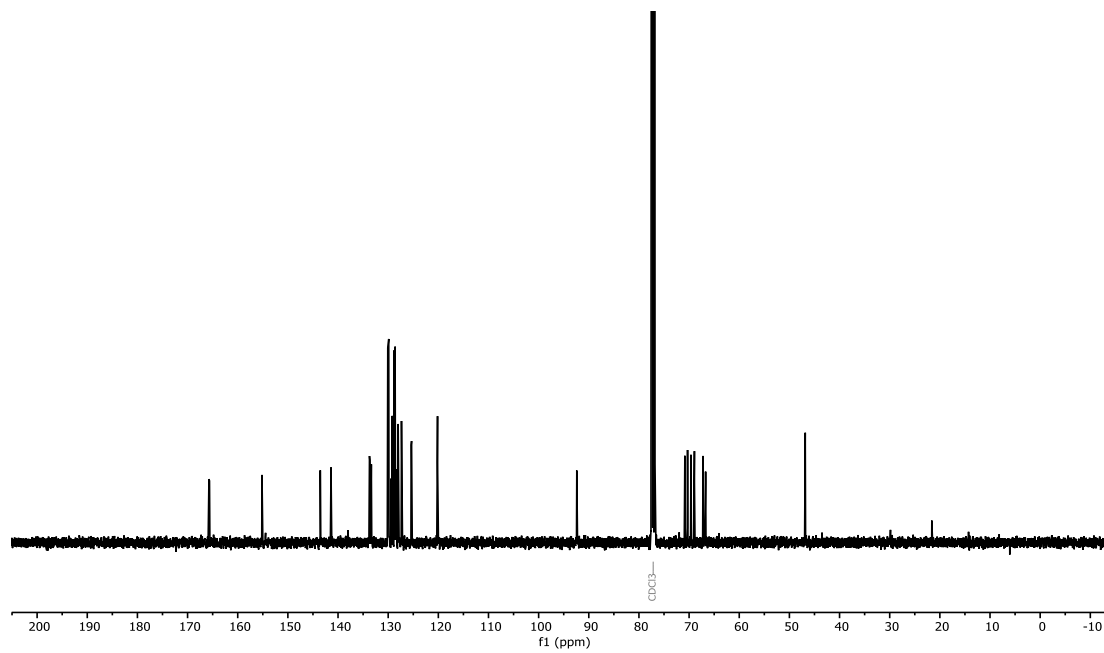
HSQC (CDCl₃): 2.29



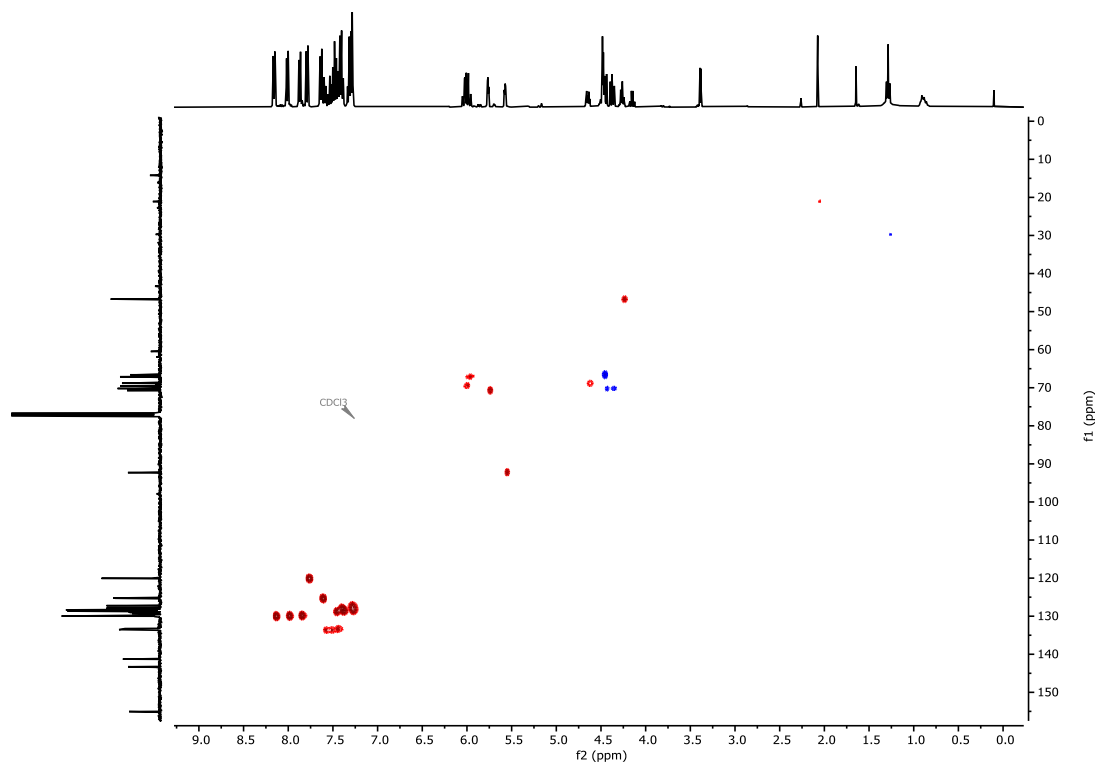
¹H NMR (CDCl₃): 2.30



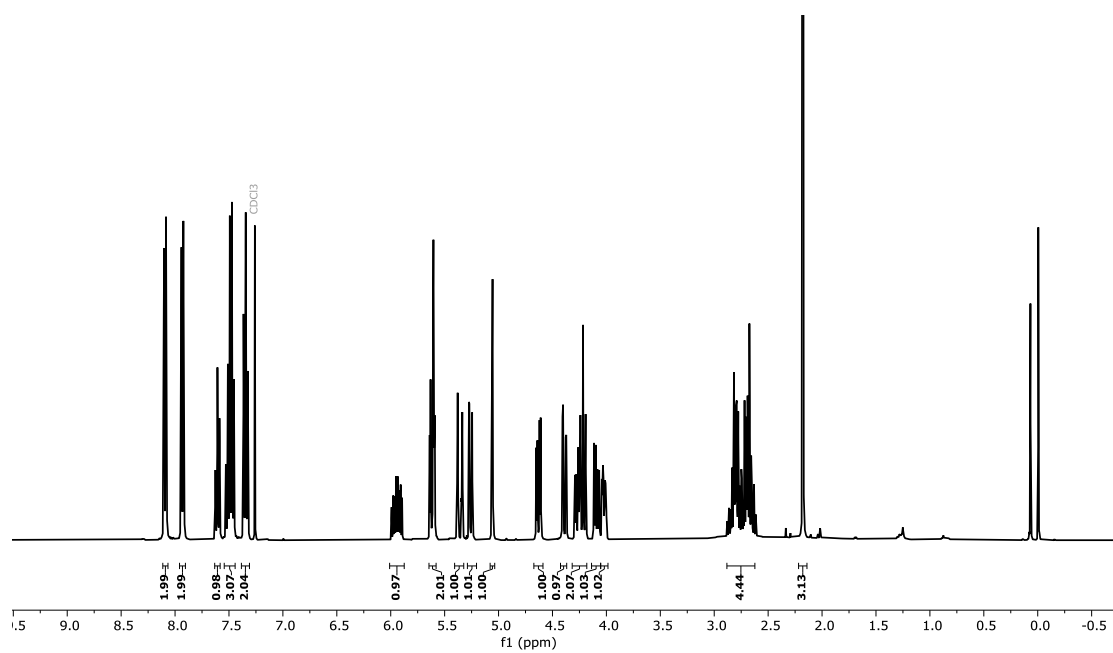
^{13}C NMR (CDCl_3): 2.30



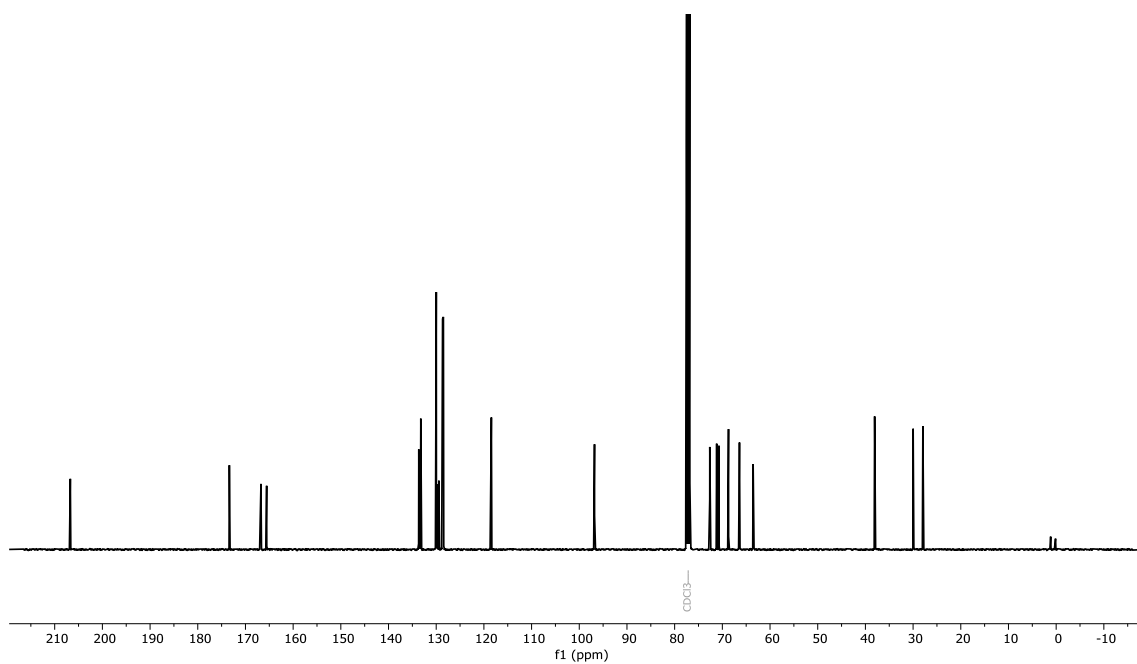
HSQC (CDCl_3): 2.30



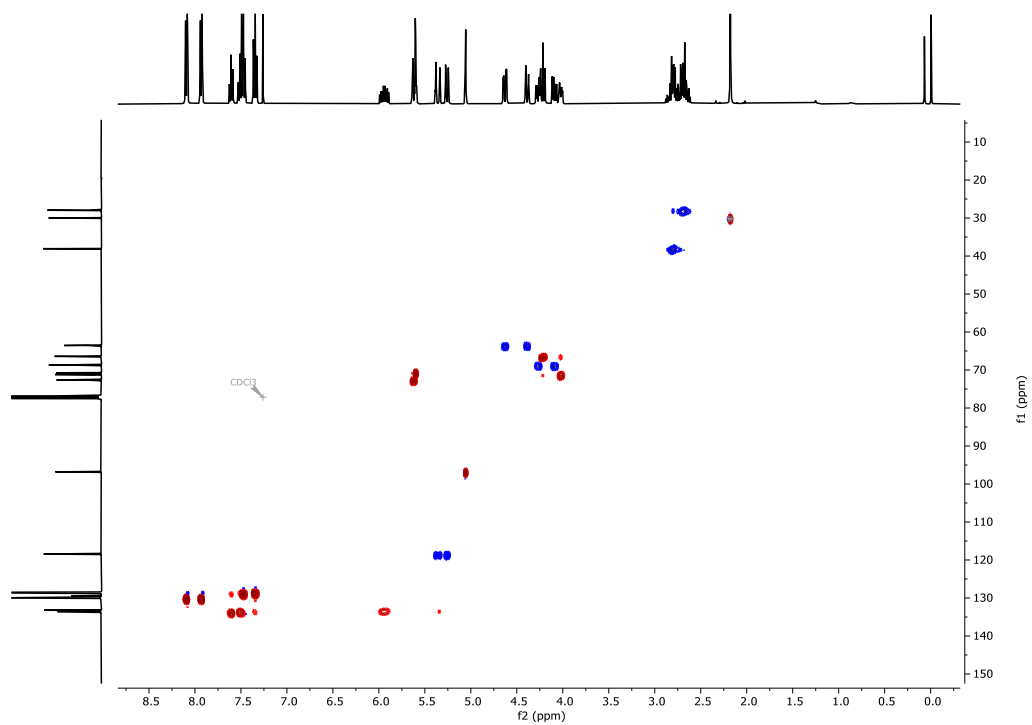
^1H NMR (CDCl_3): 2.31



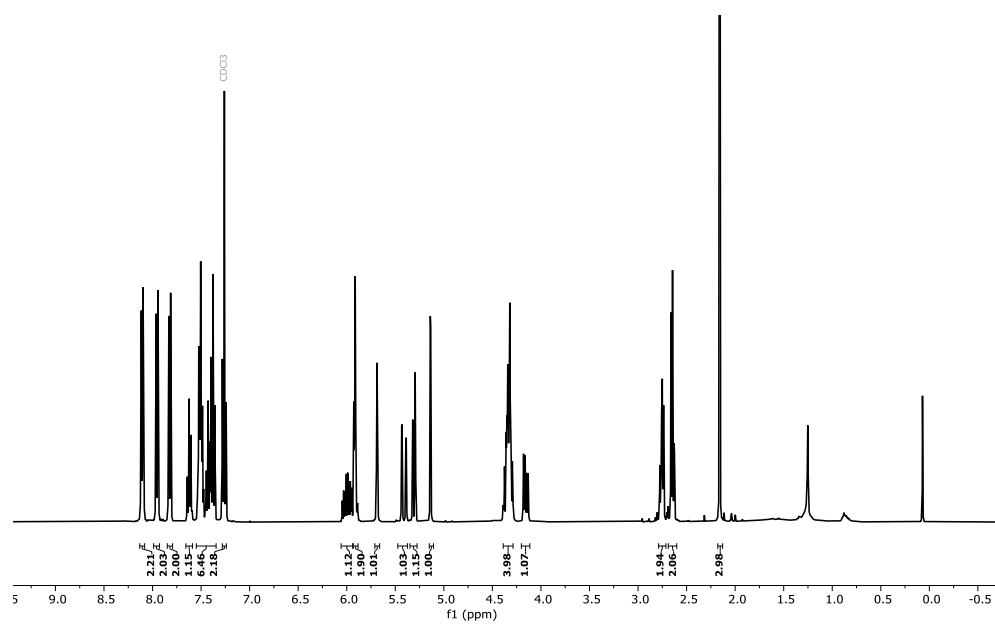
^{13}C NMR (CDCl_3): 2.31



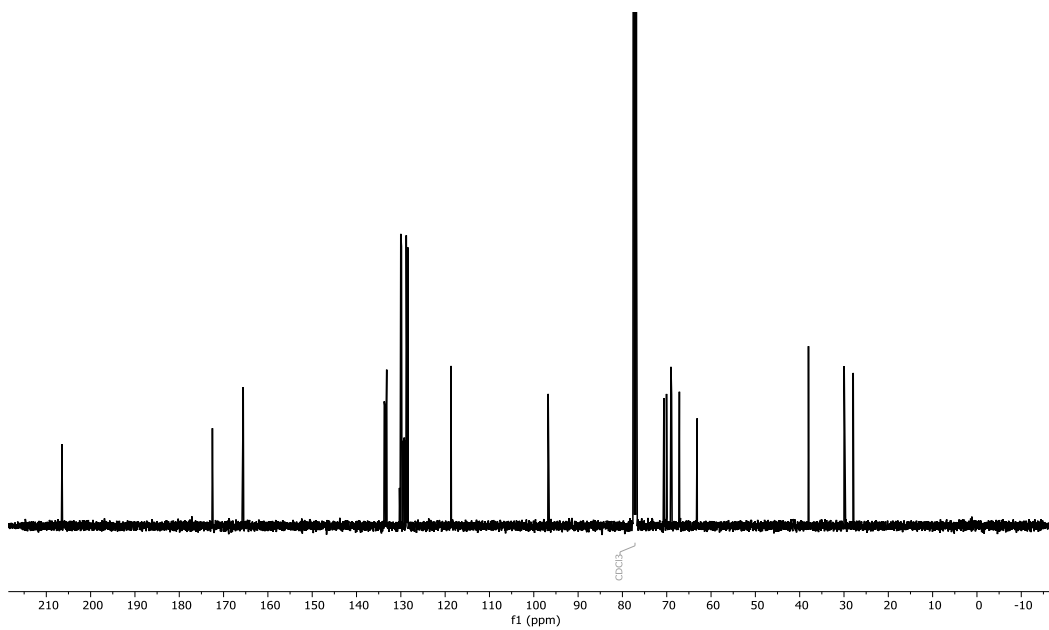
HSQC NMR (CDCl₃): 2.31



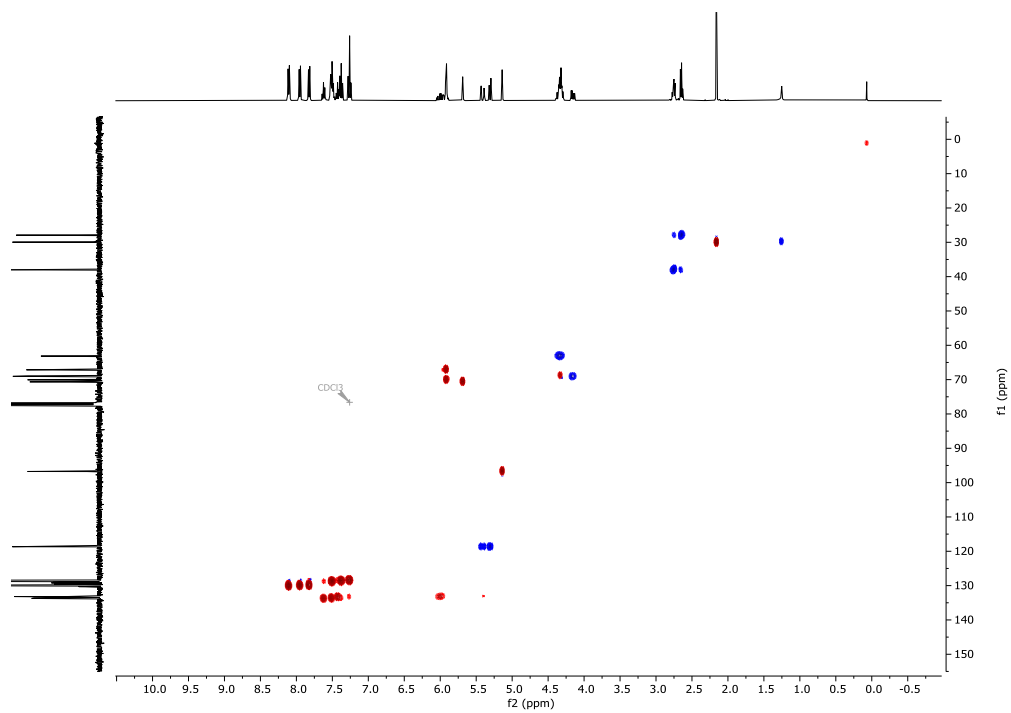
¹H NMR (CDCl₃): 2.32



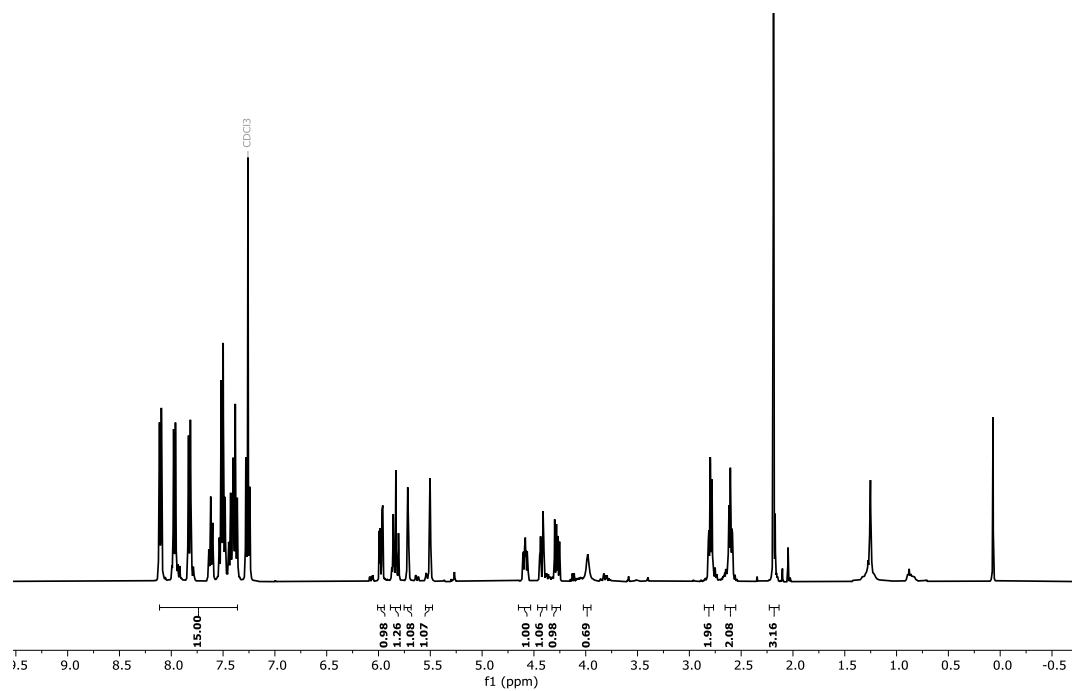
^{13}C NMR (CDCl_3): 2.32



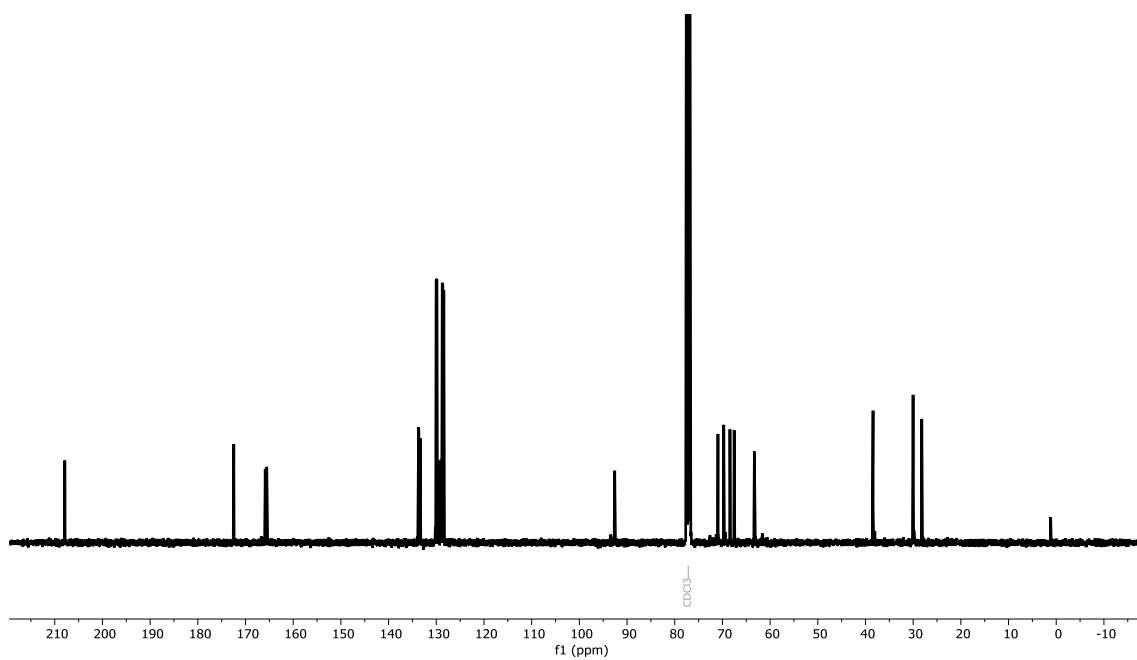
HSQC NMR (CDCl_3): 2.32



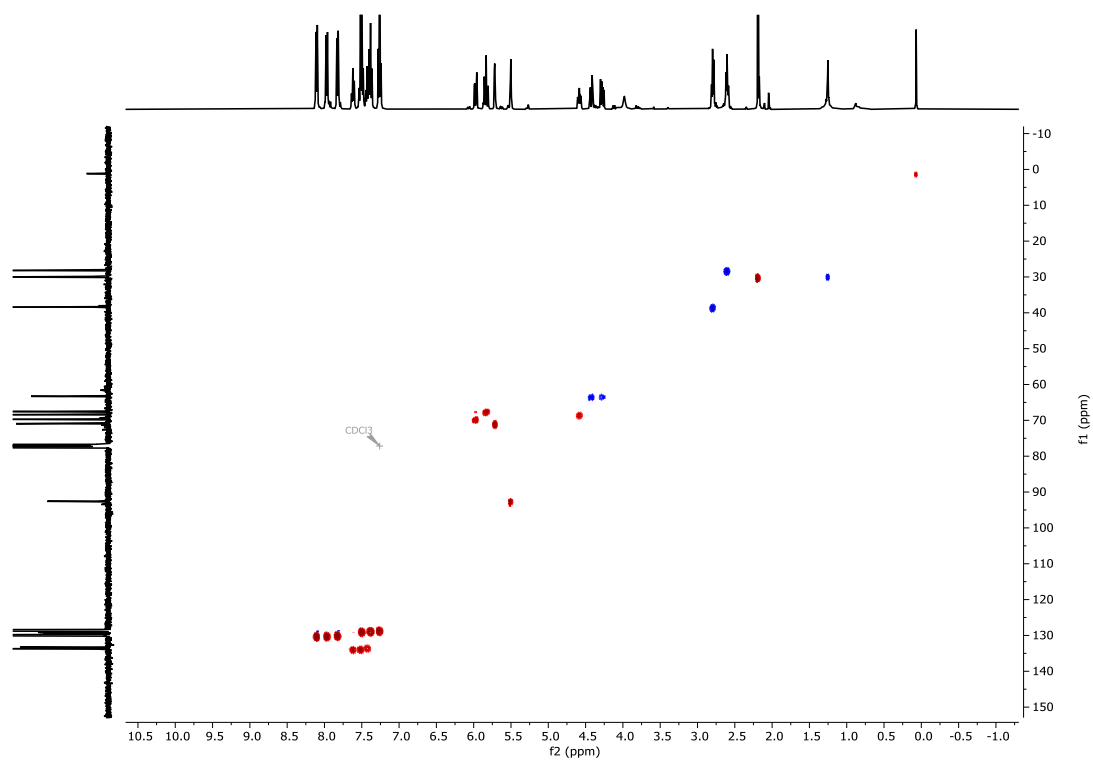
¹H NMR (CDCl₃): 2.33



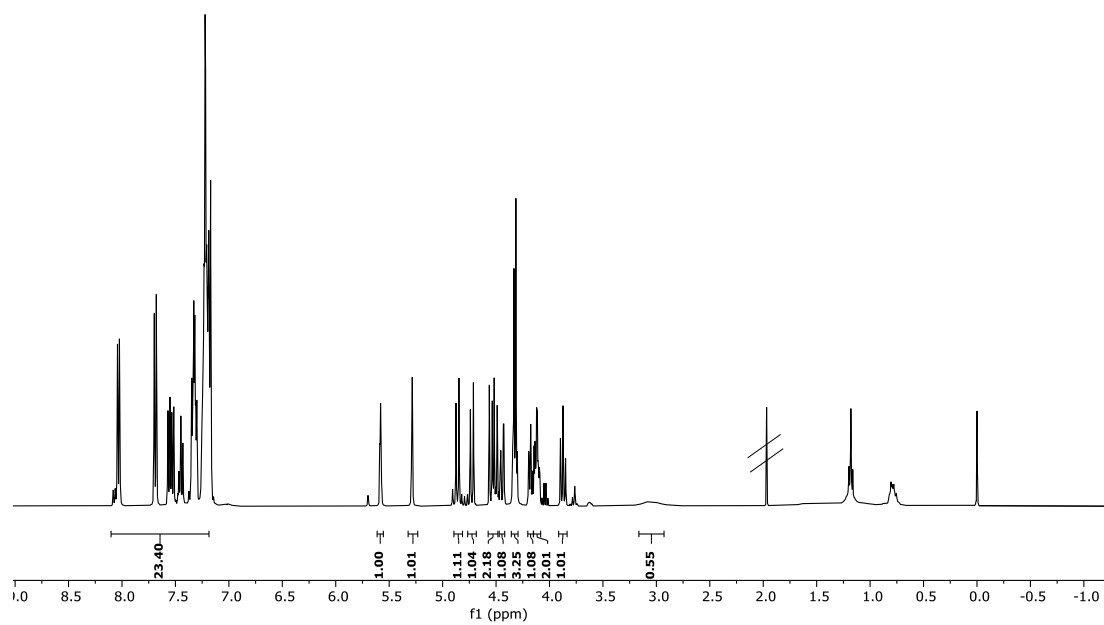
¹³C NMR (CDCl₃): 2.33



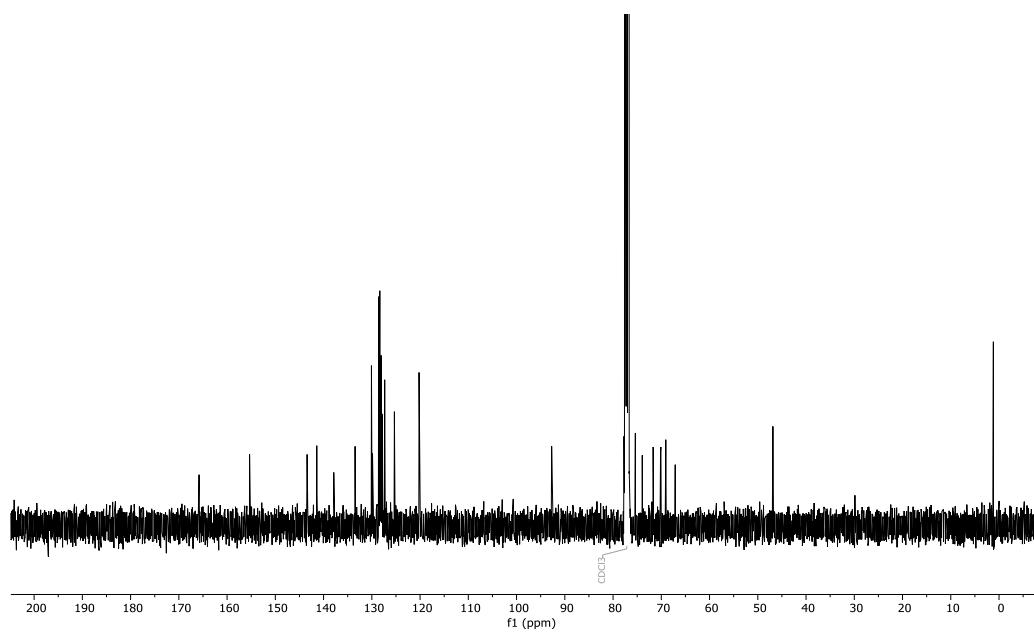
HSQC NMR (CDCl₃): 2.33



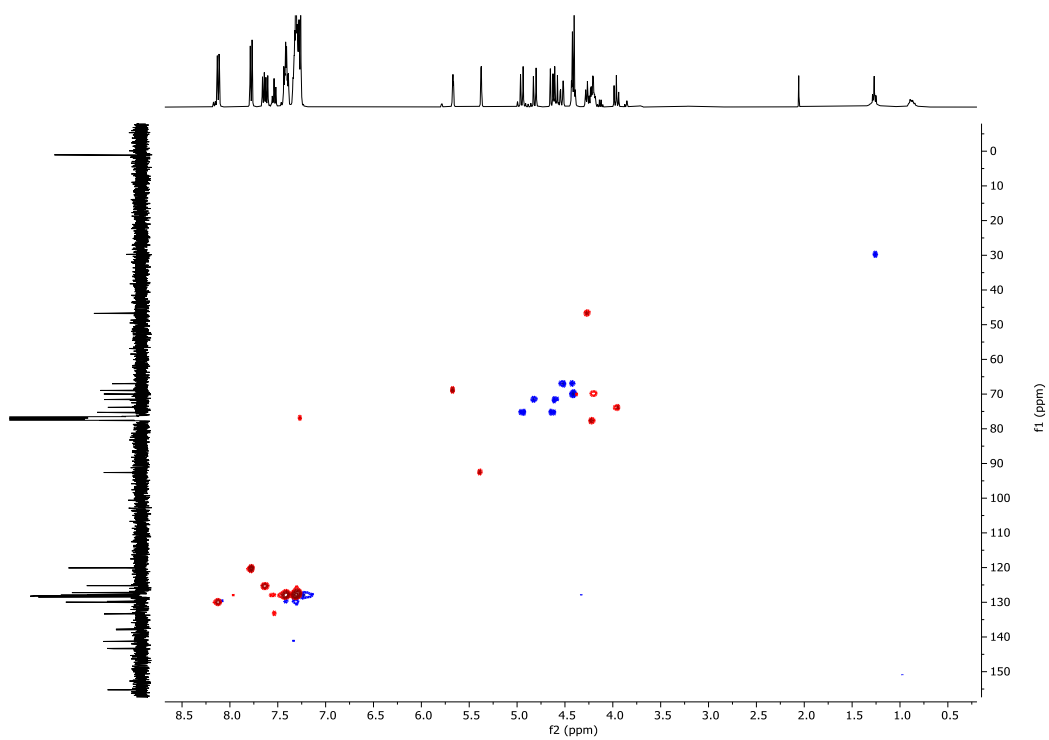
¹H NMR (CDCl₃): 2.34



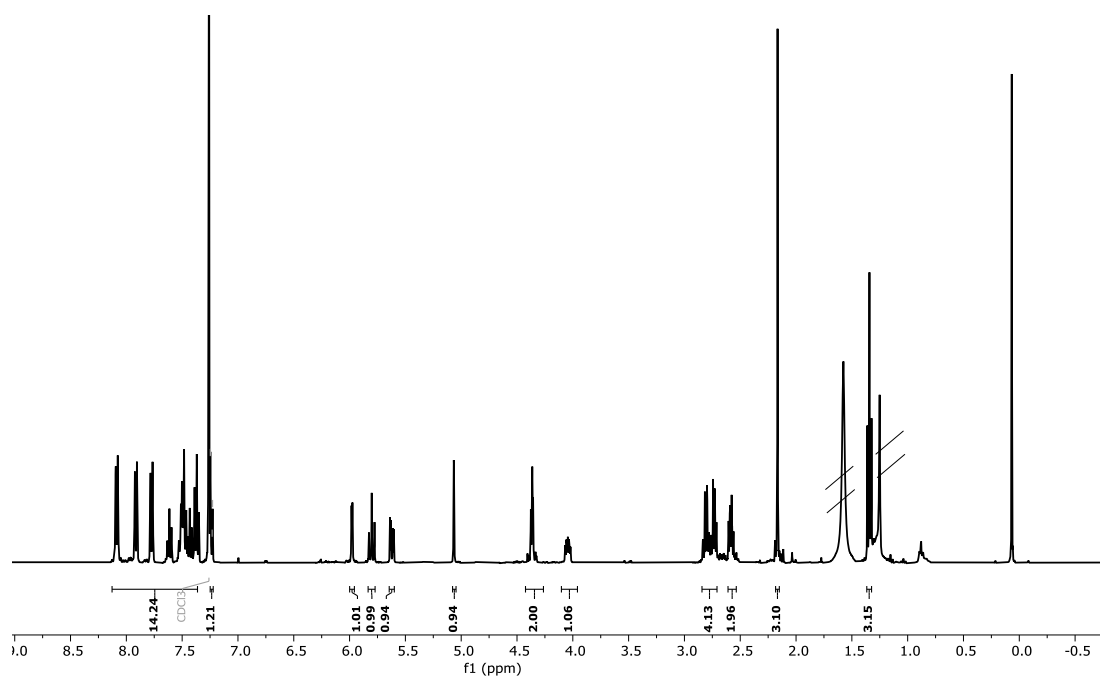
^{13}C NMR (CDCl_3): 2.34



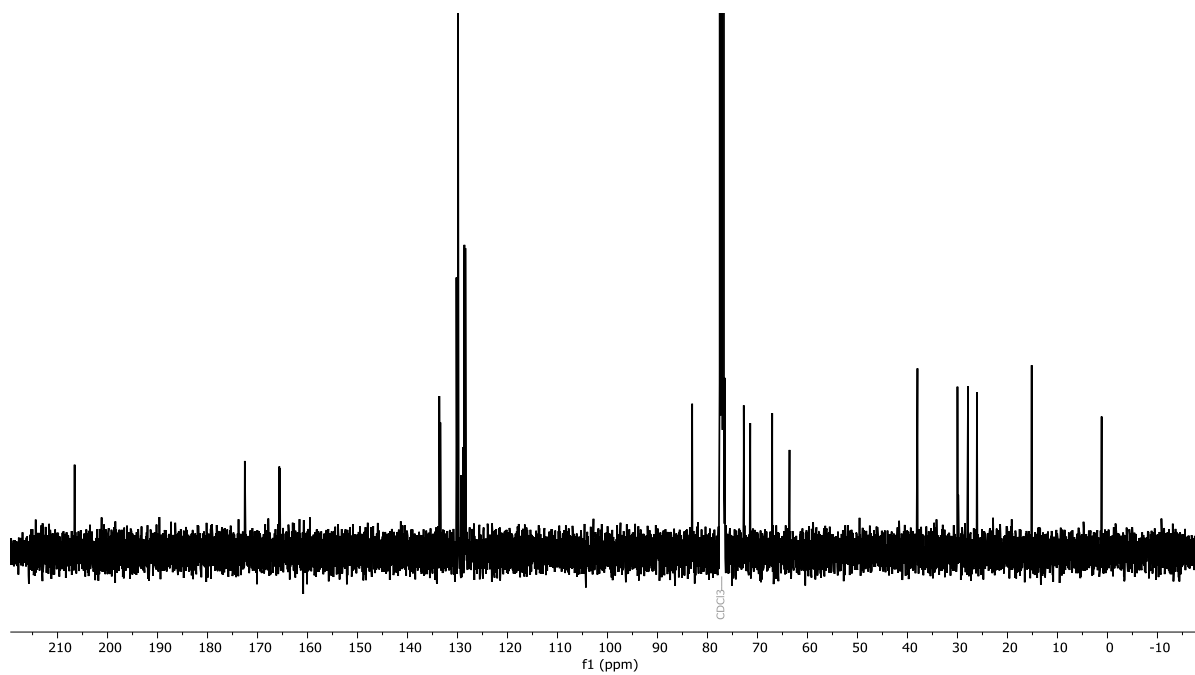
HSQC NMR (CDCl_3): 2.34



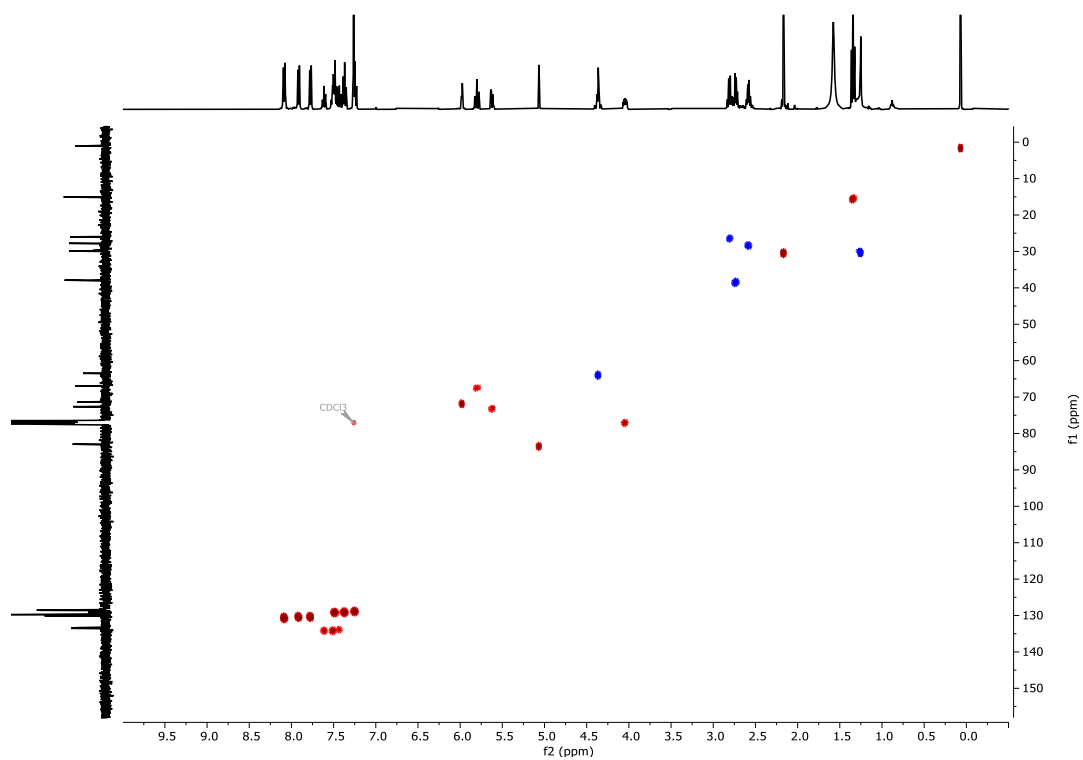
^1H NMR (CDCl_3): 2.36



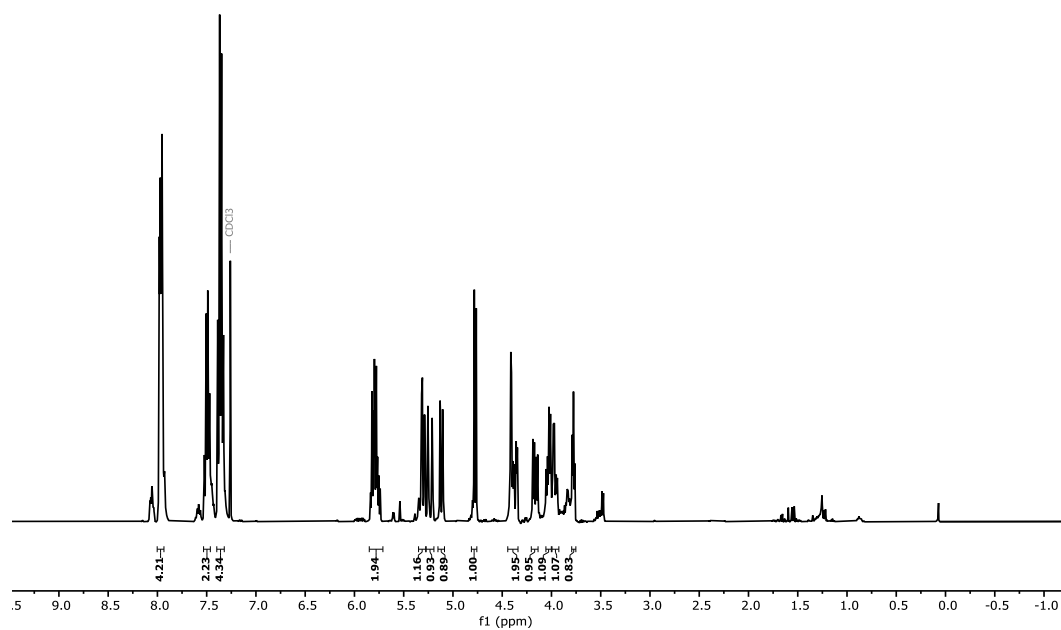
^{13}C NMR (CDCl_3): 2.36



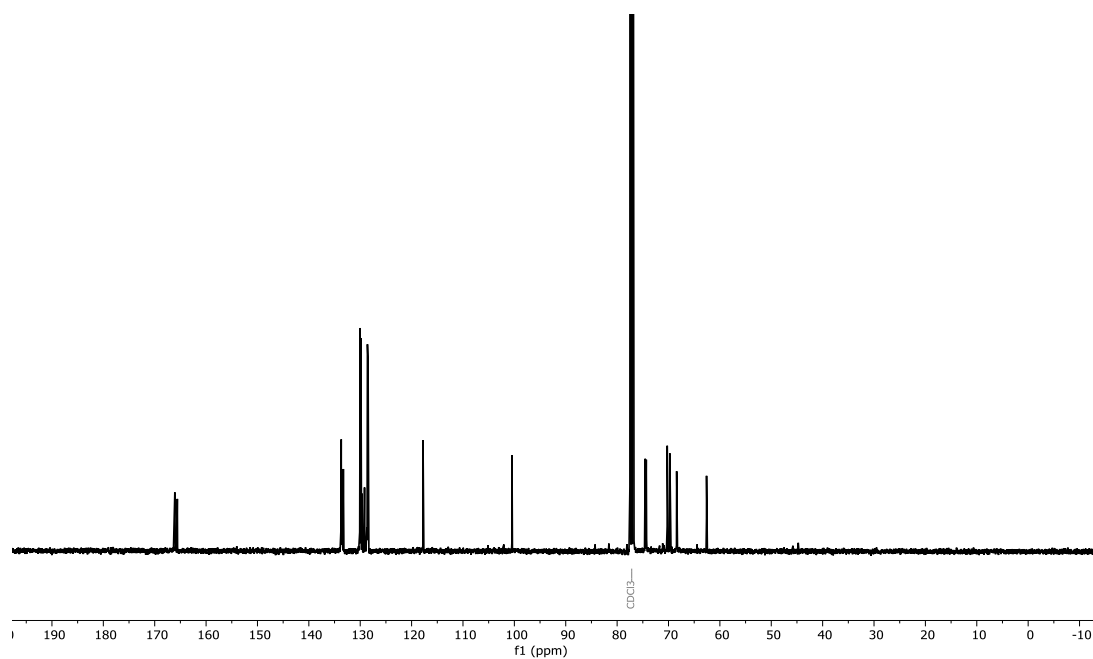
HSQC NMR (CDCl₃): 2.36



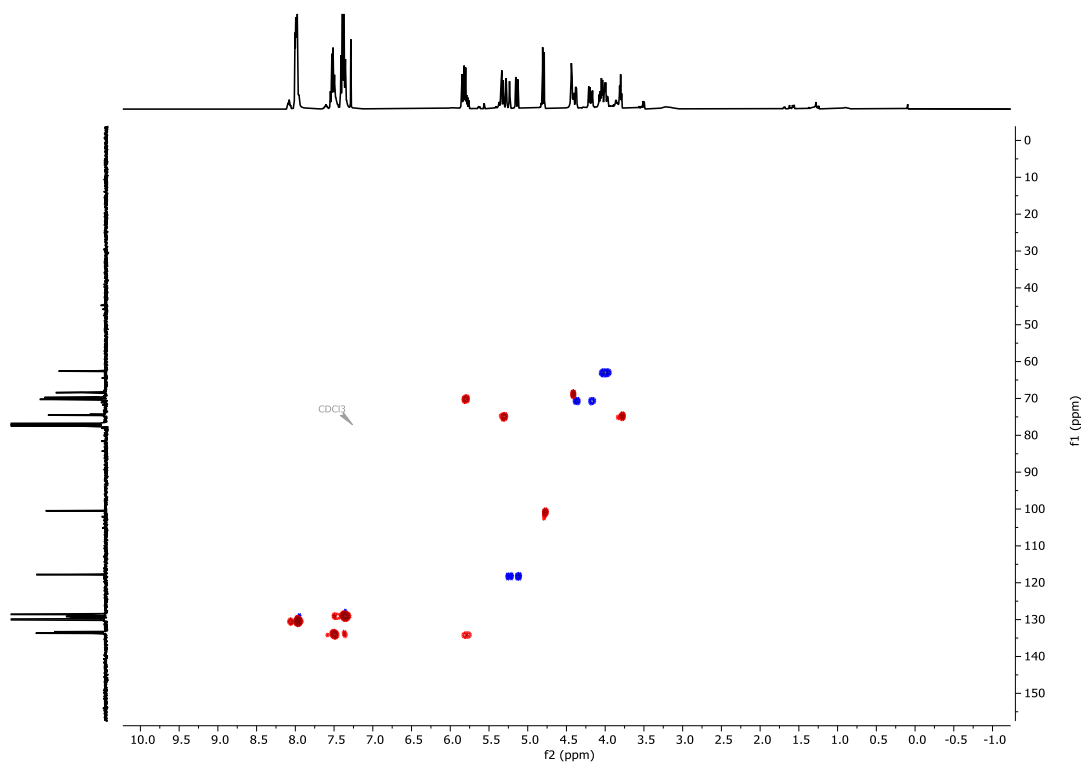
¹H NMR (CDCl₃): 2.37



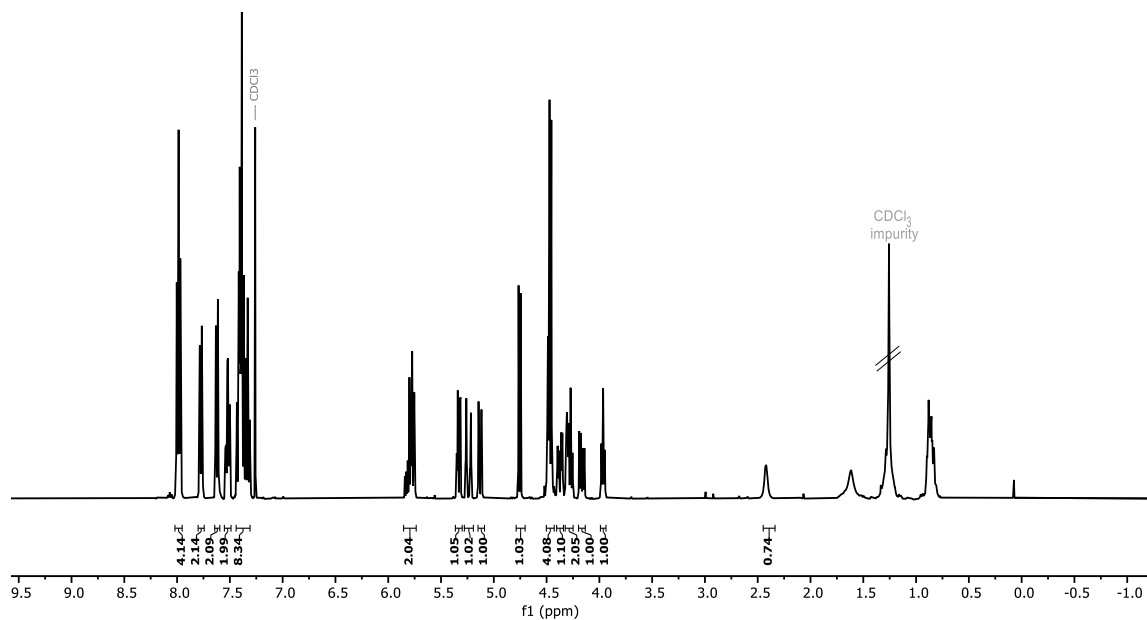
^{13}C NMR (CDCl_3): **2.37**



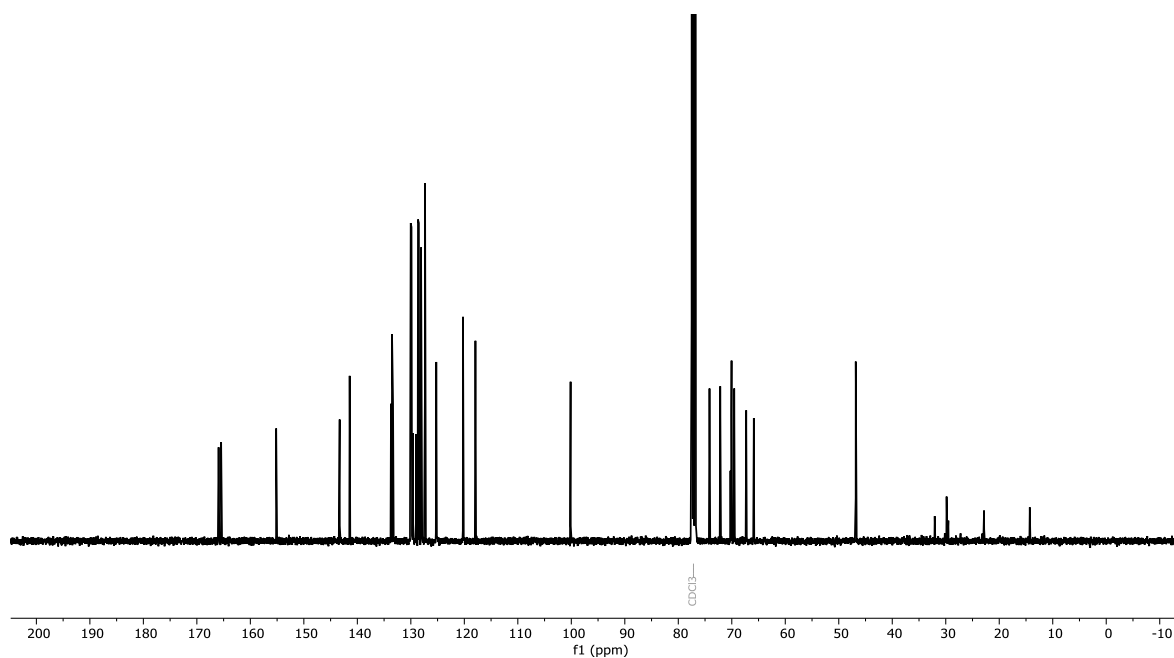
HSQC NMR (CDCl_3): **2.37**



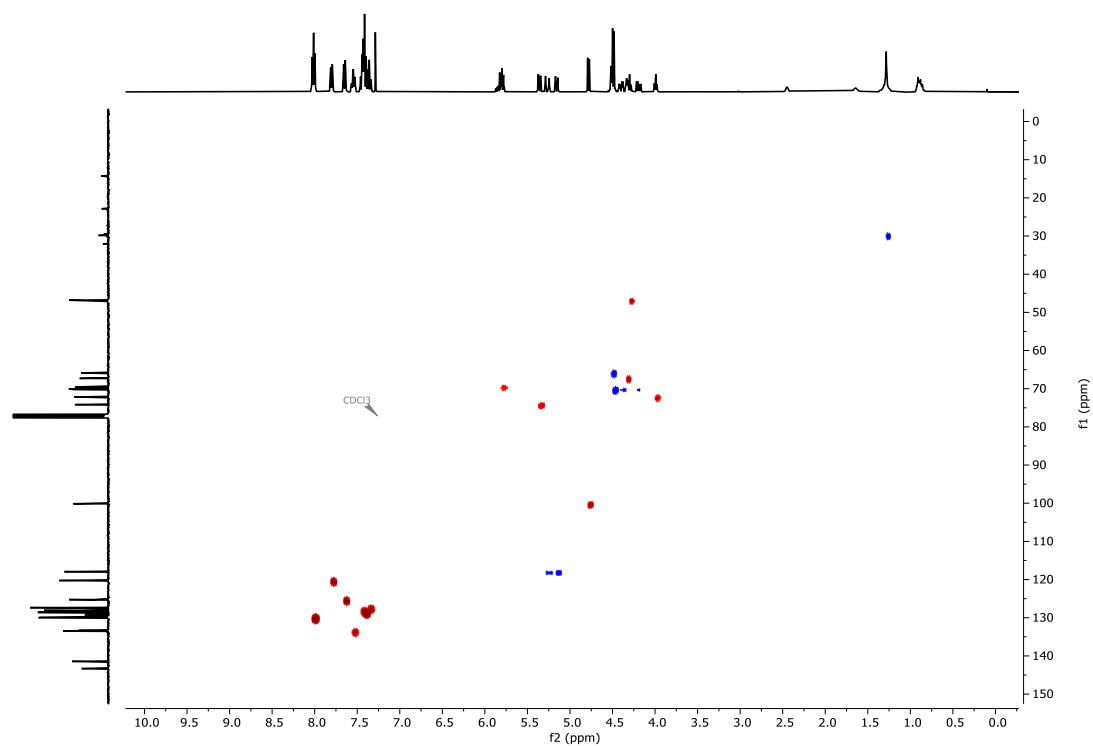
^1H NMR (CDCl_3): **2.38**



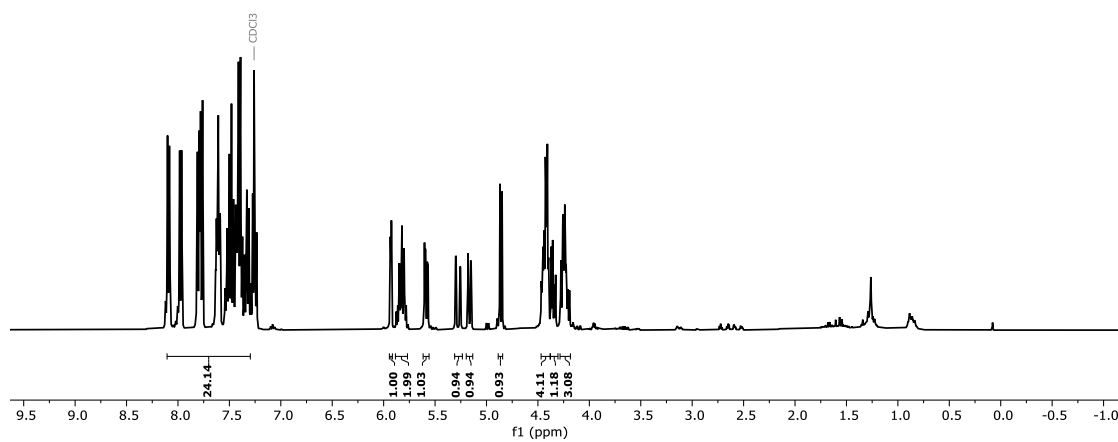
^{13}C NMR (CDCl_3): **2.38**



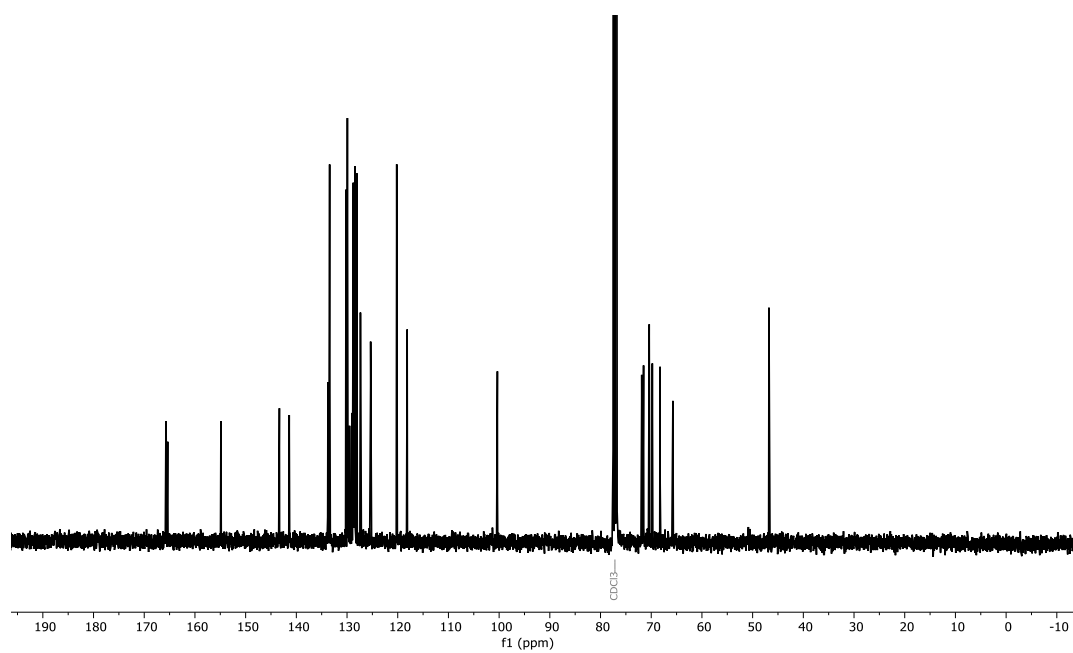
HSQC NMR (CDCl₃): 2.38



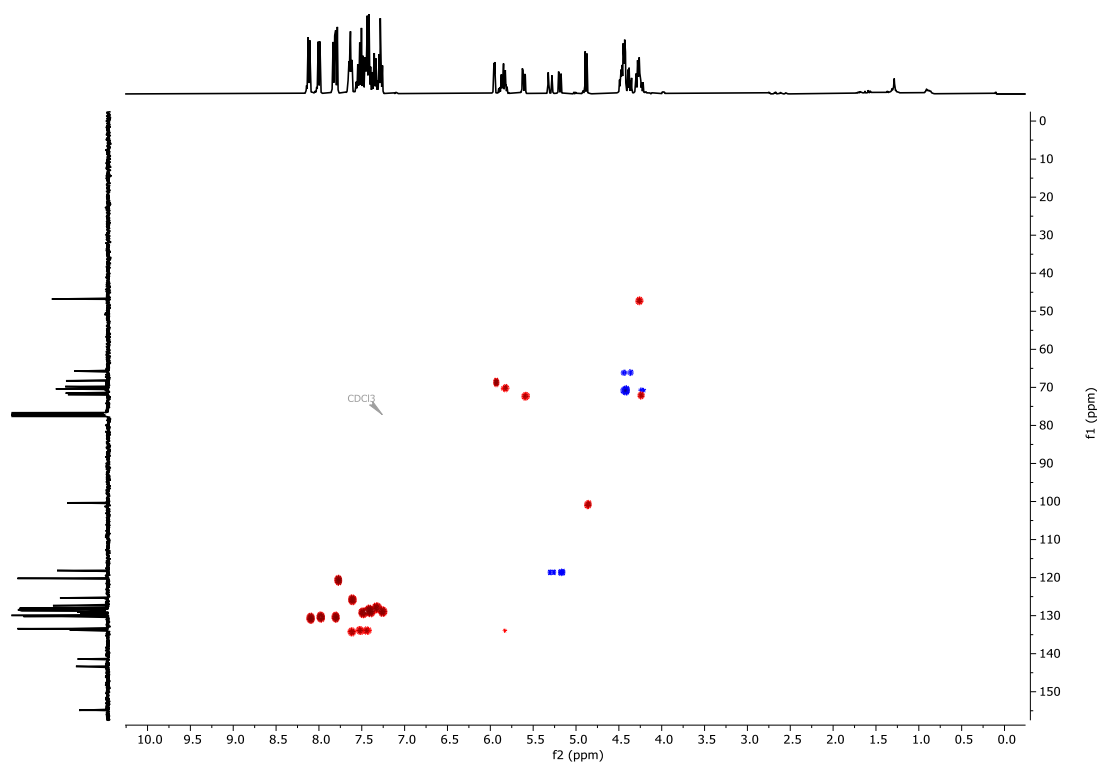
¹H NMR (CDCl₃): 2.39



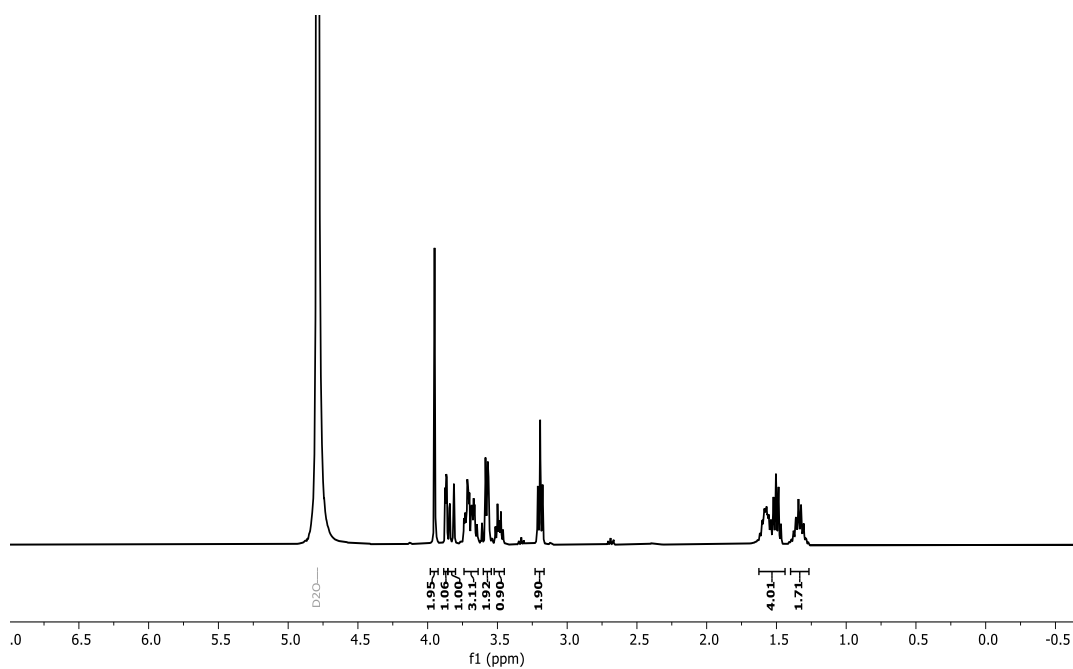
^{13}C NMR (CDCl_3): **2.39**



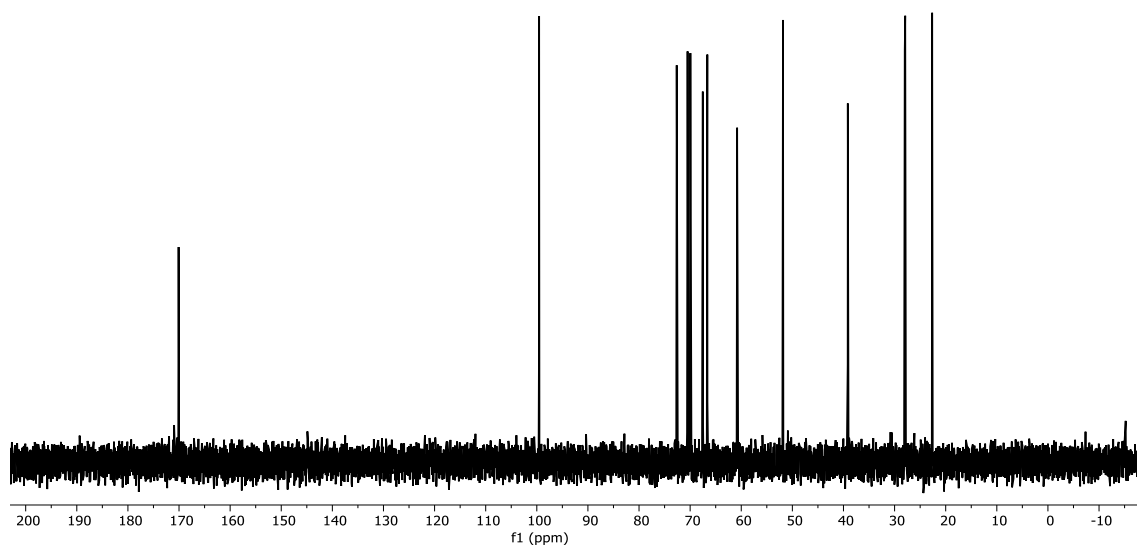
HSQC NMR (CDCl_3): **2.39**



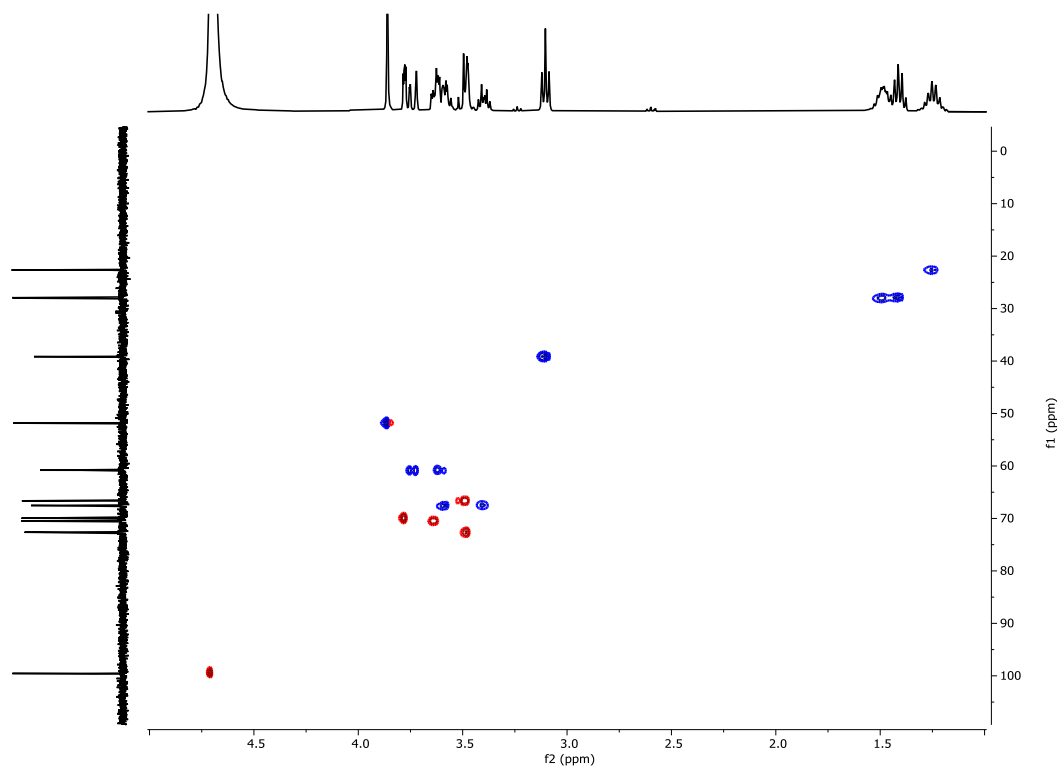
^1H NMR (D_2O): 3.10



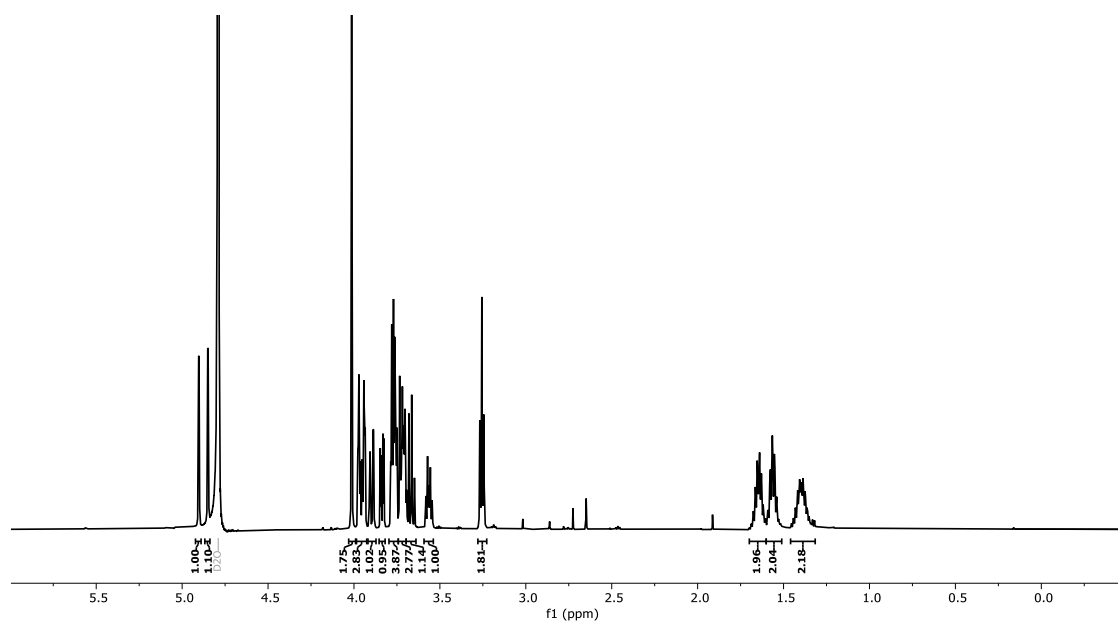
^{13}C NMR (D_2O): 3.10



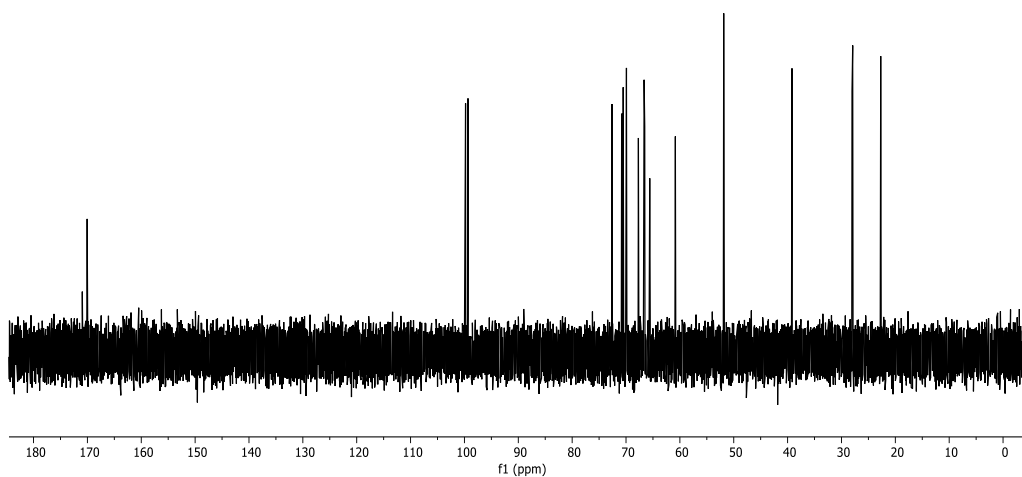
HSQC NMR (D₂O): 3.10



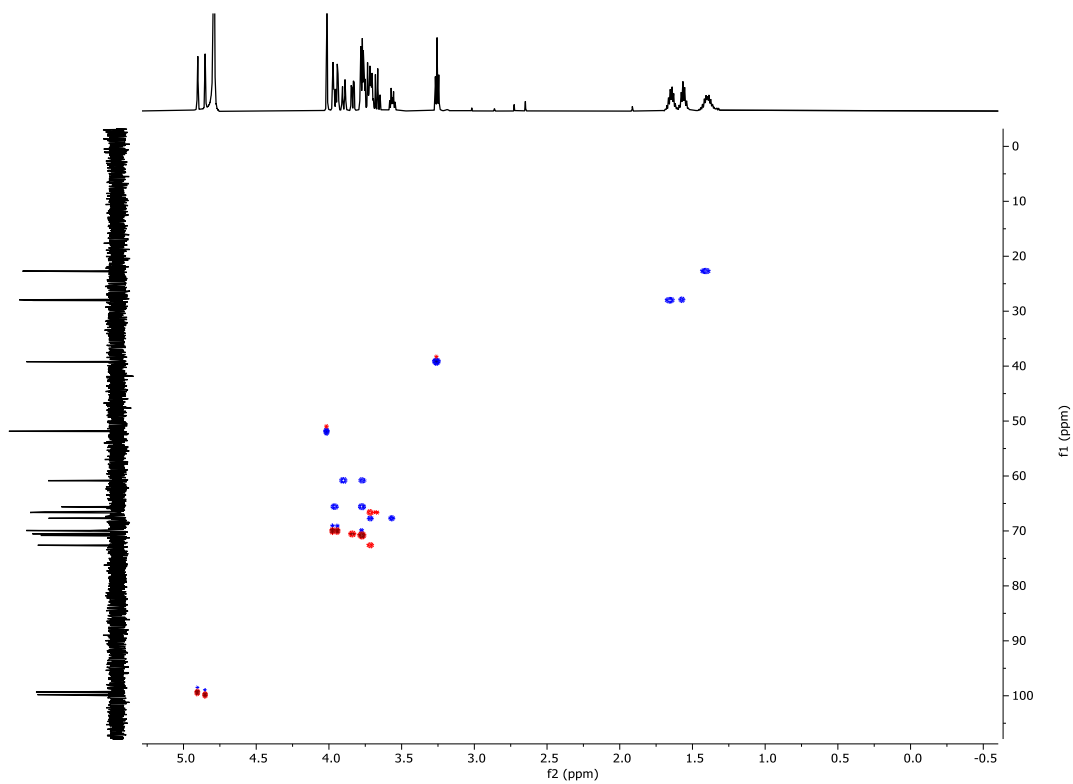
¹H NMR (D₂O): 3.11



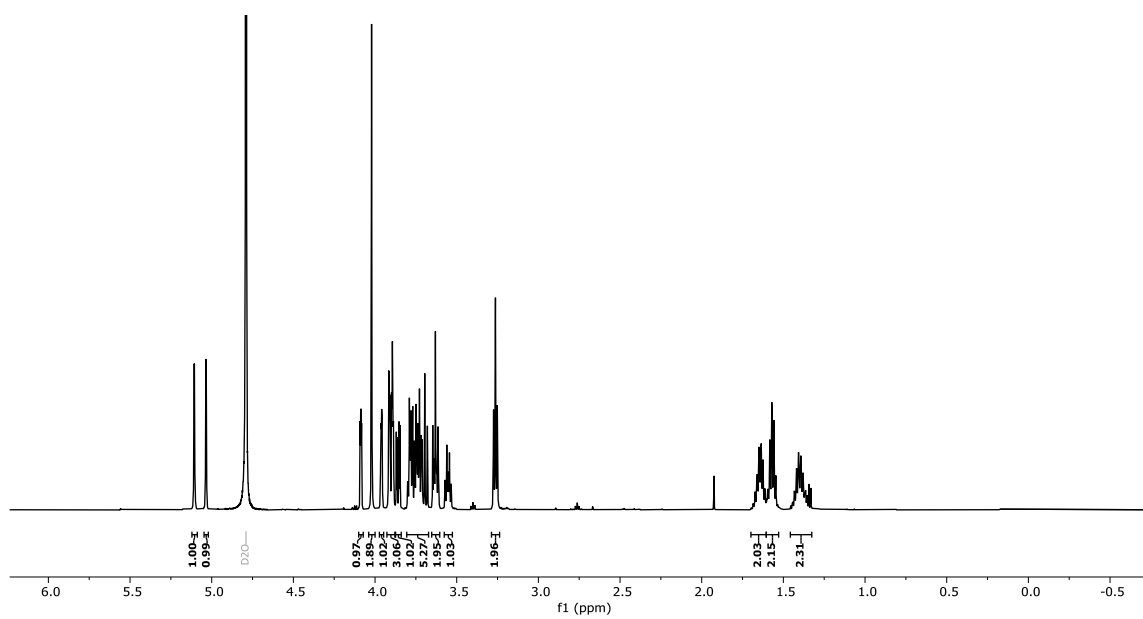
^{13}C NMR (D_2O): 3.11



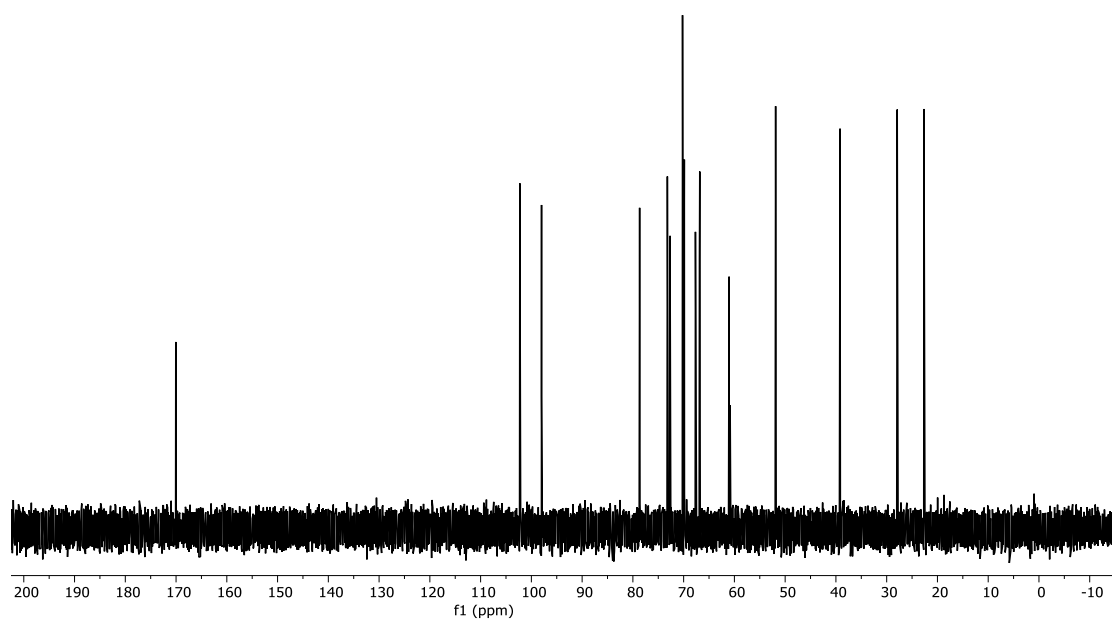
HSQC NMR (D_2O): 3.11



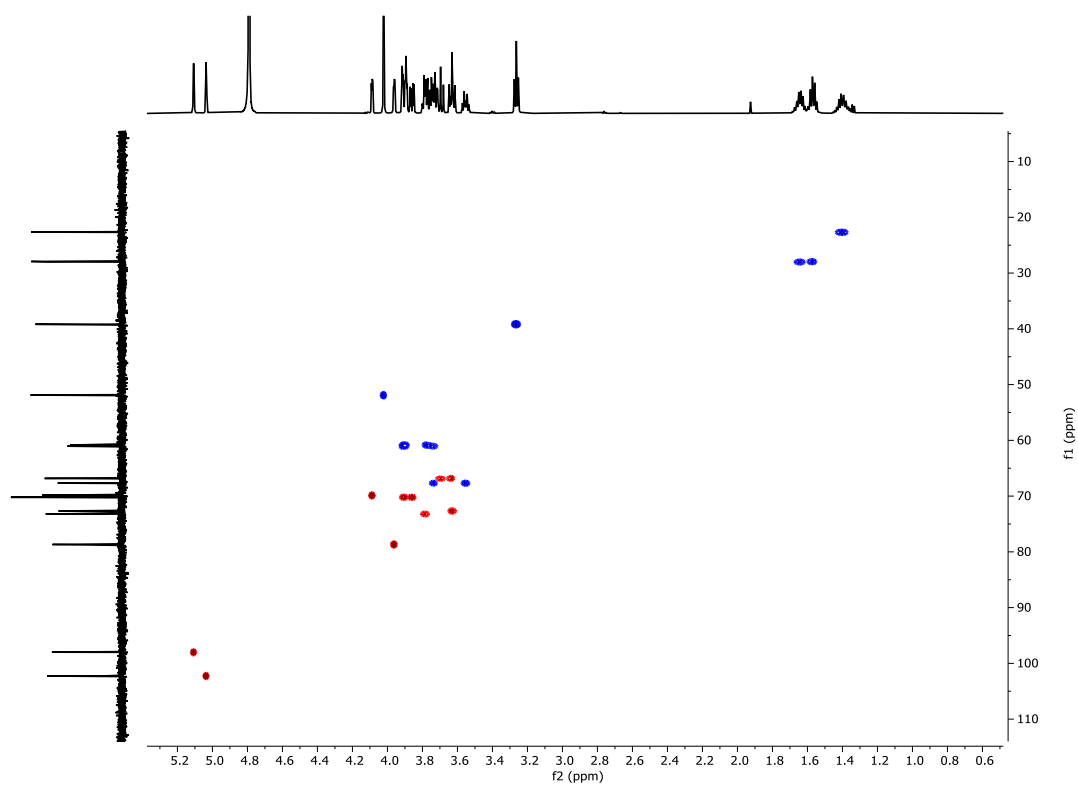
¹H NMR (D₂O): 3.12



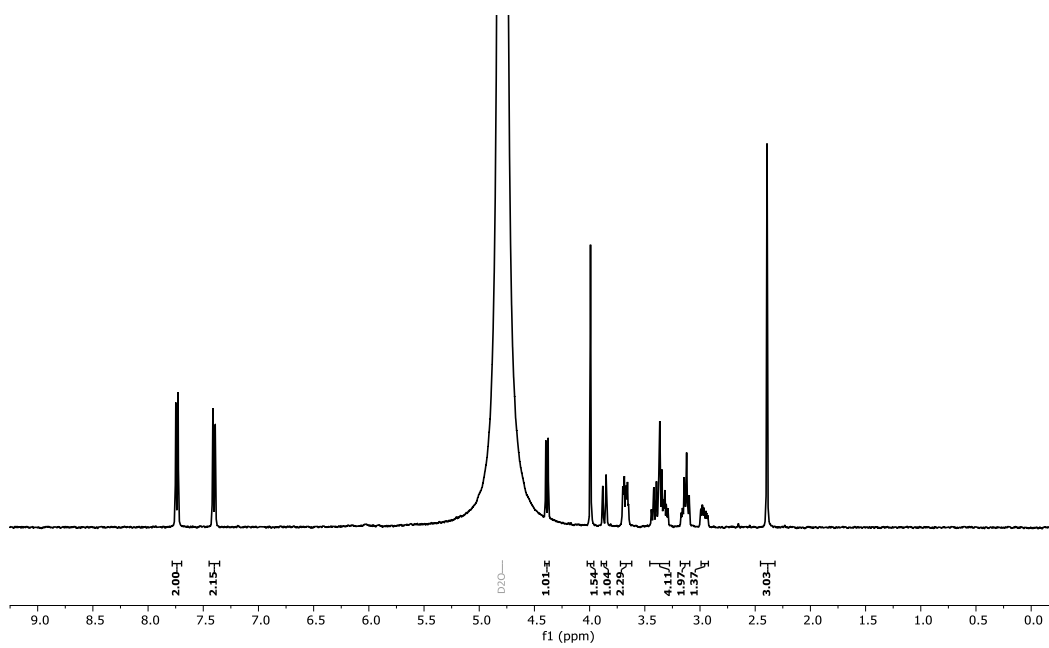
¹³C NMR (D₂O): 3.12



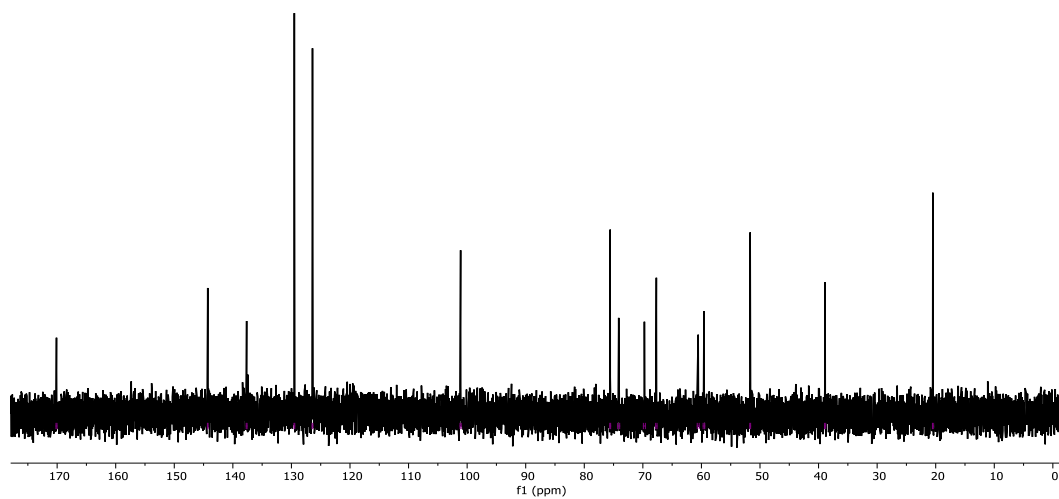
HSQC NMR (D₂O): 3.12



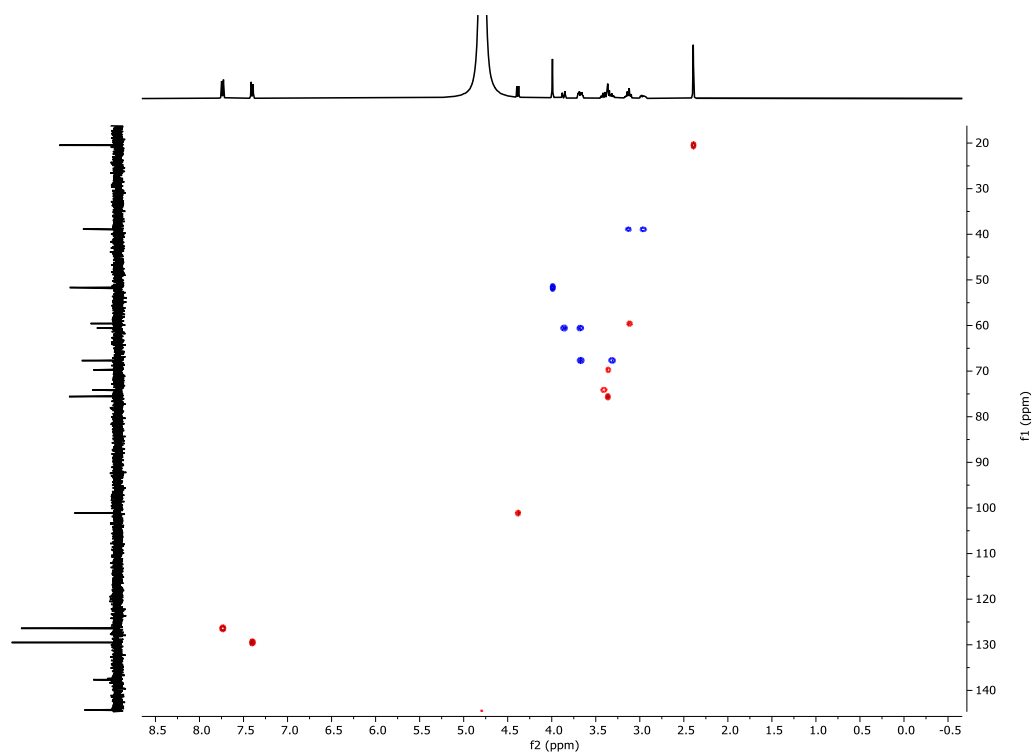
¹H NMR (D₂O): 3.13



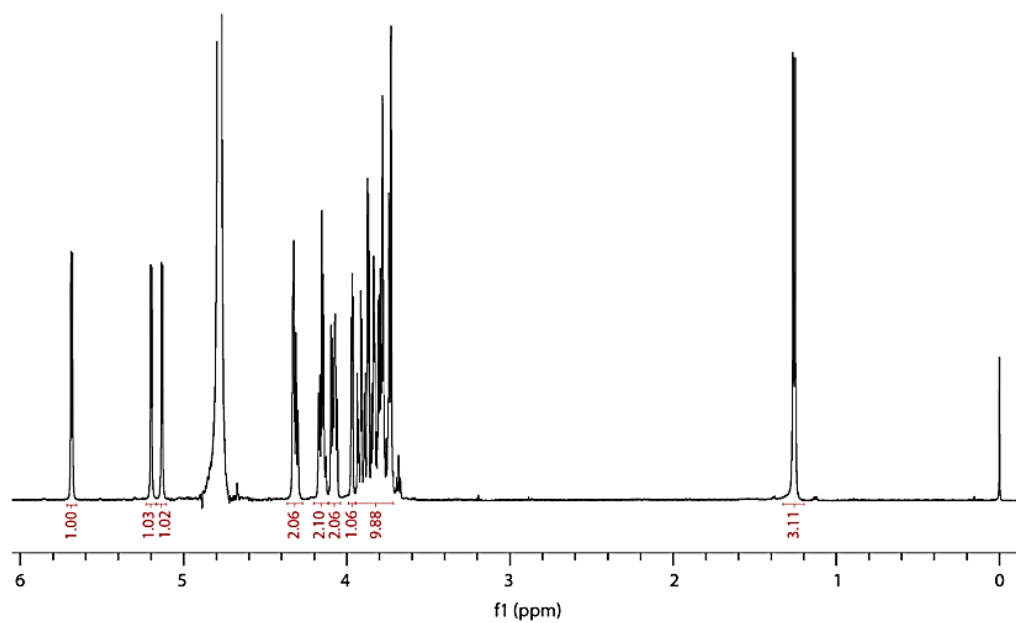
^{13}C NMR (D_2O): 3.13



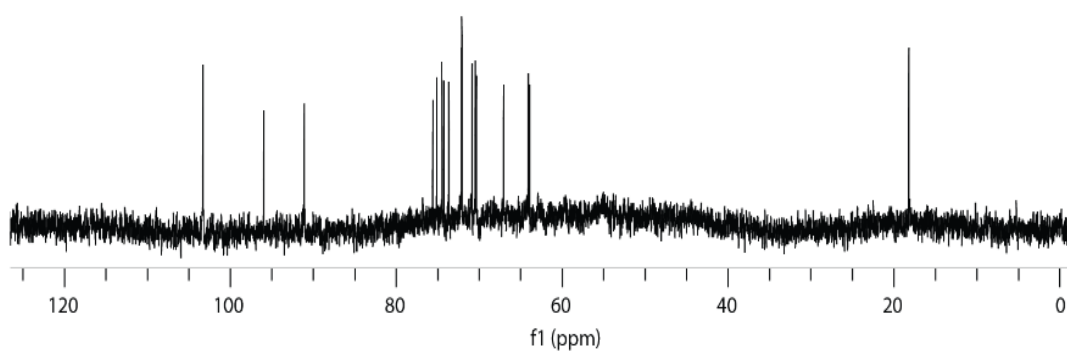
HSQC NMR (D_2O): 3.13



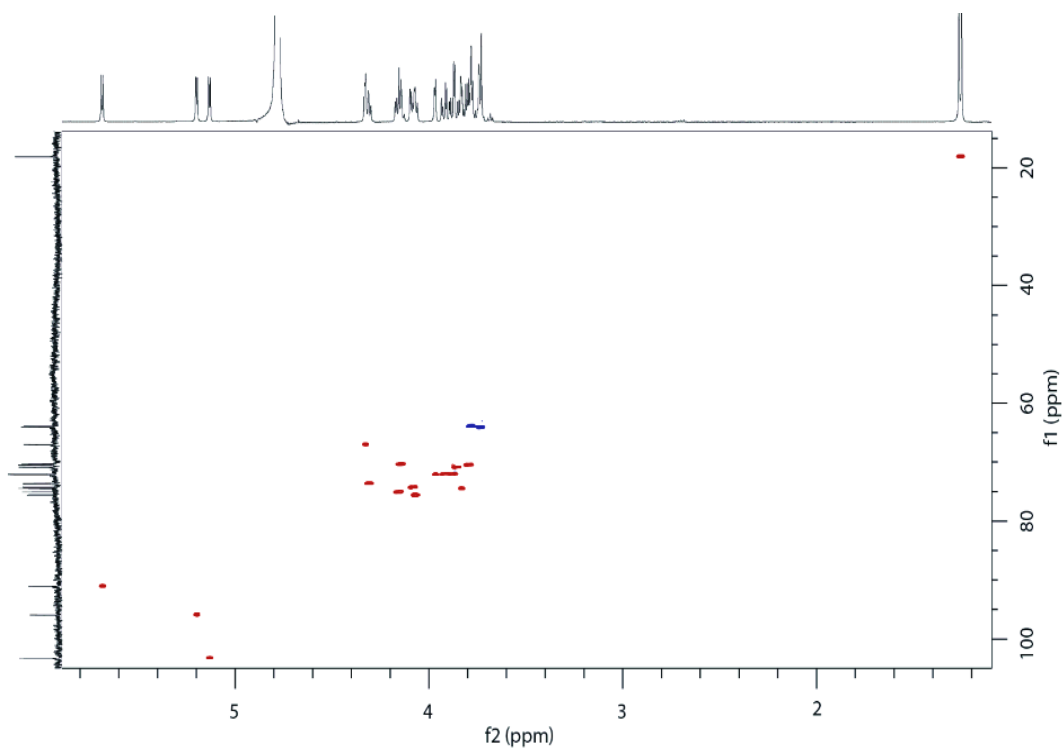
^1H NMR (D_2O): 3.14



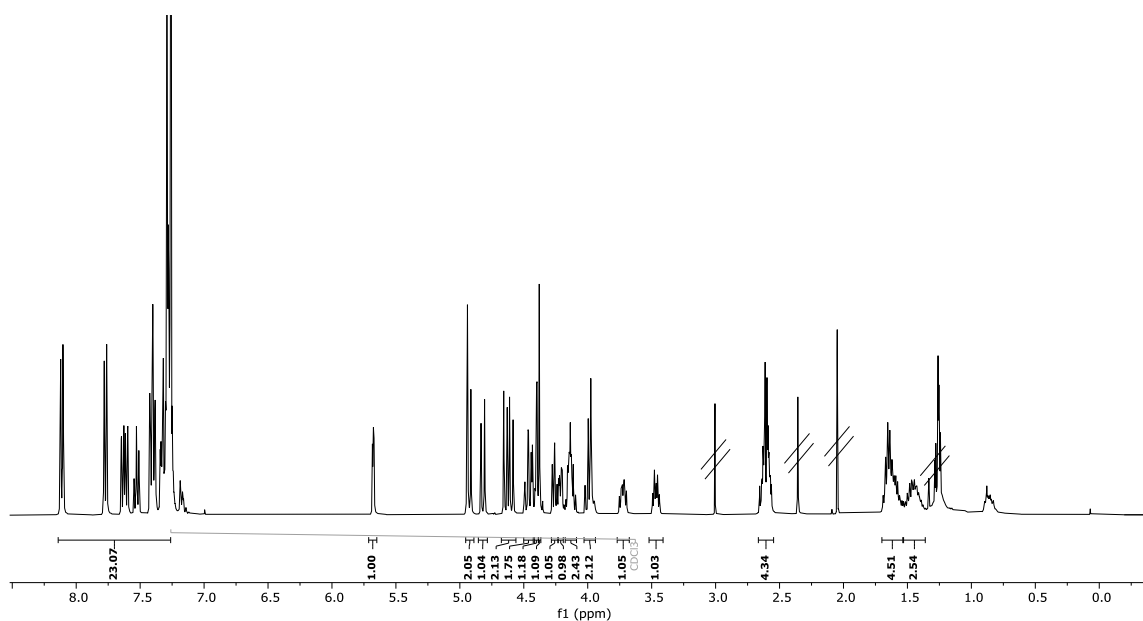
^{13}C NMR (D_2O): 3.14



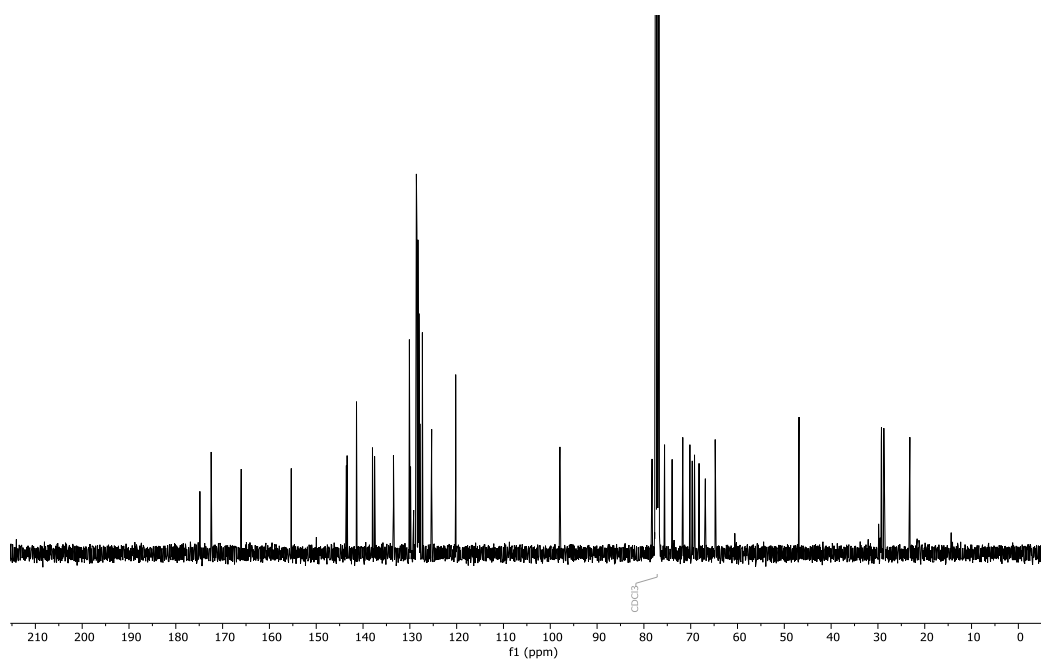
HSQC NMR (D₂O): 3.14



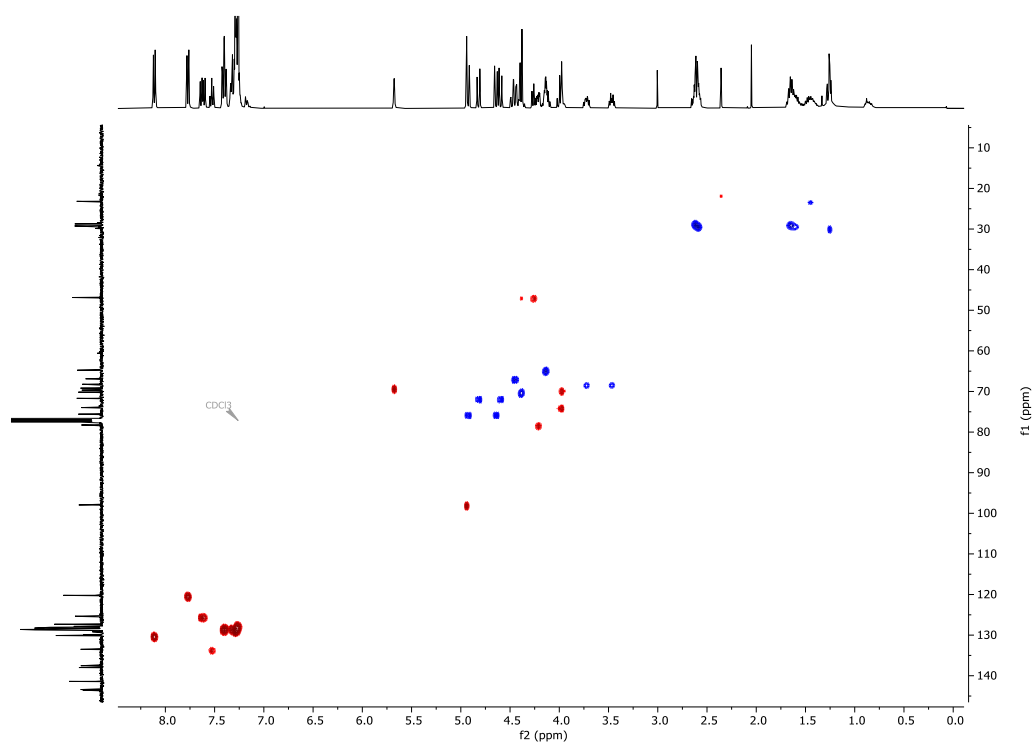
¹H NMR (CDCl₃): 4.1



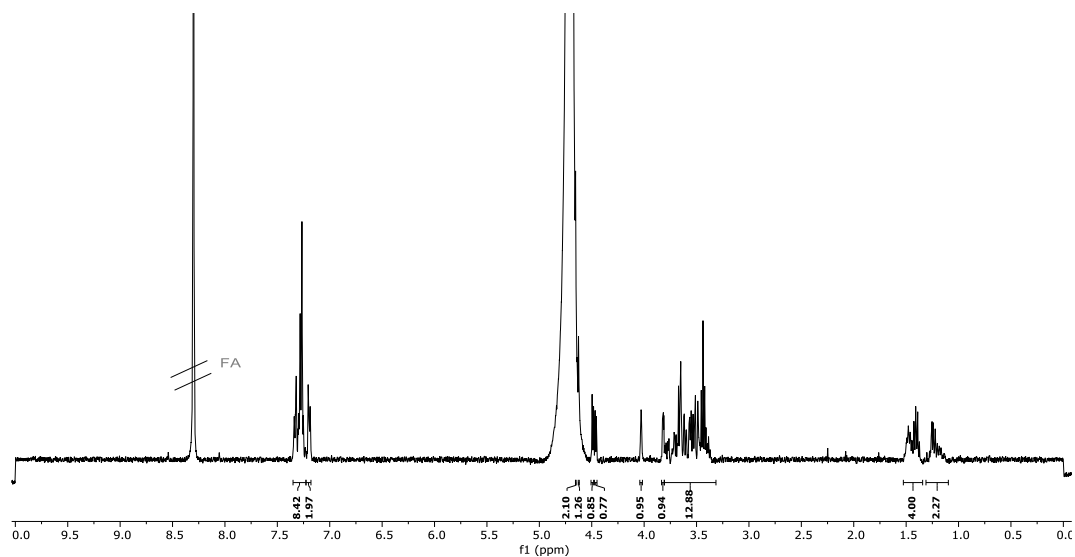
^{13}C NMR (CDCl_3): 4.1



HSQC NMR (CDCl_3): 4.1

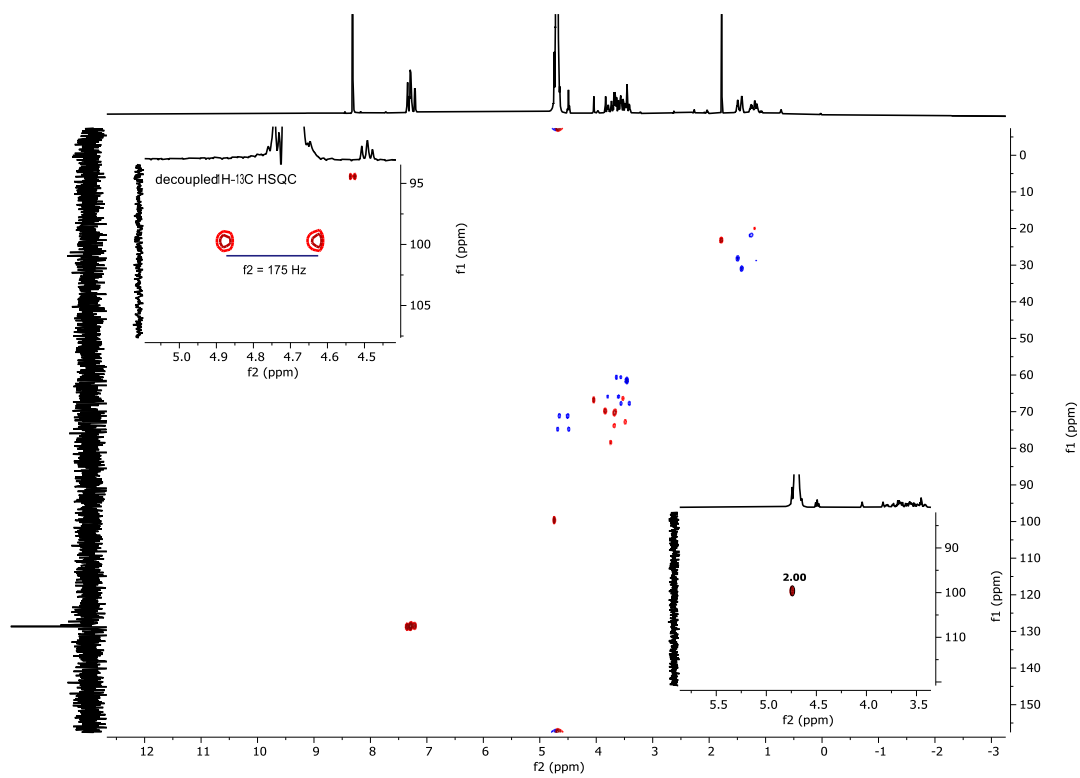


^1H NMR (D_2O): 4.5

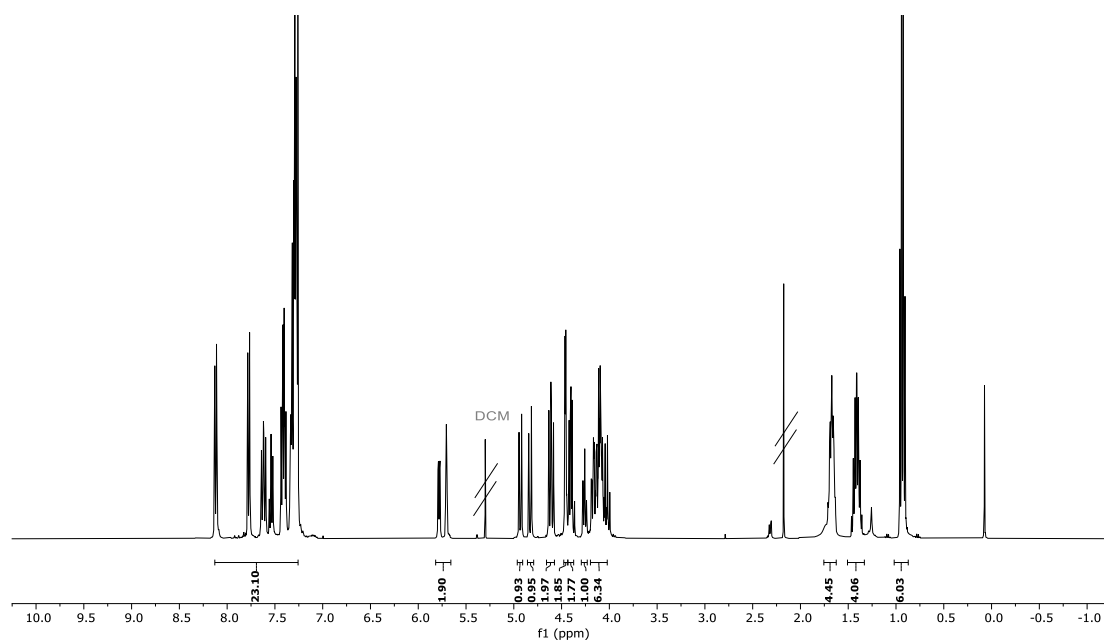


^{13}C NMR (D_2O): 4.5 could not be obtained due to low amount of material.

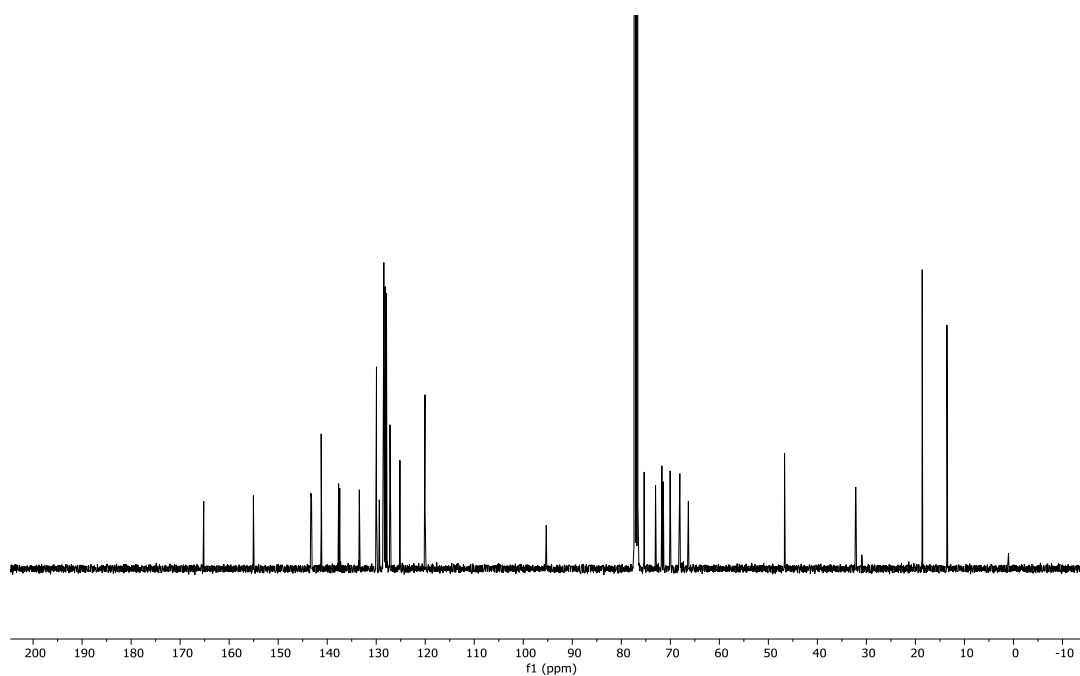
HSQC NMR (D_2O): 4.5



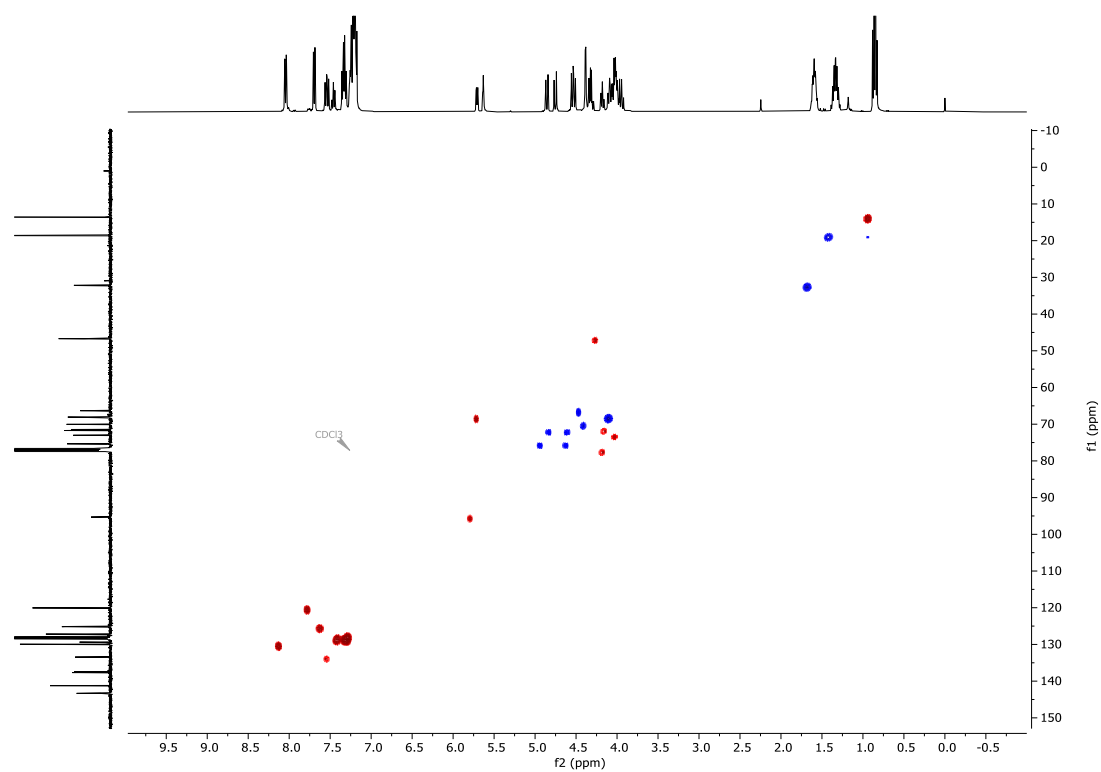
^1H NMR (CDCl_3): 4.9



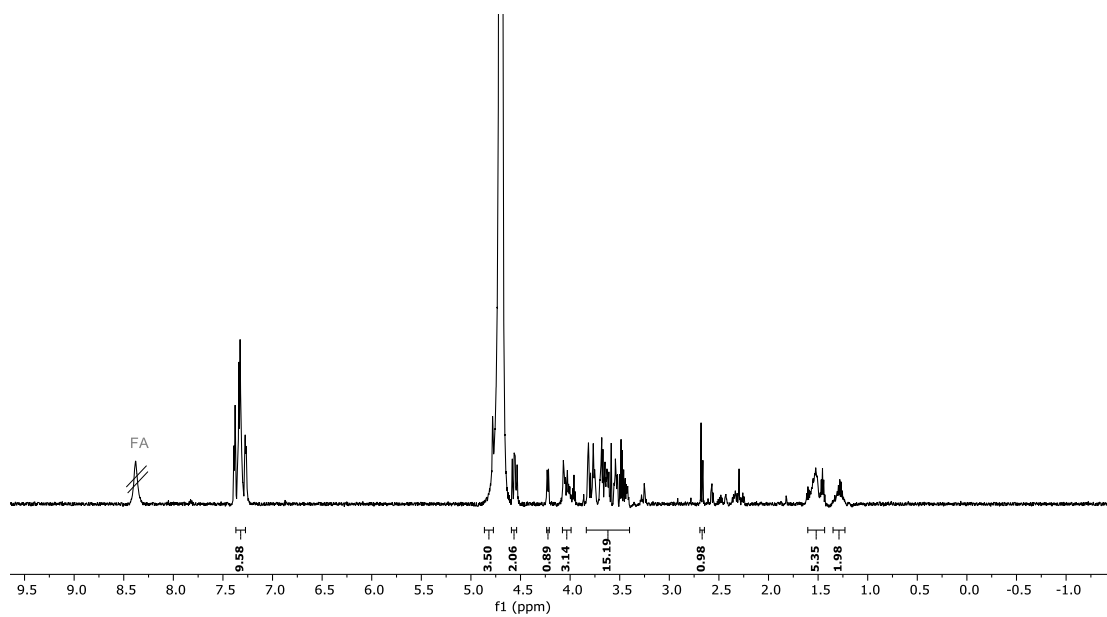
^{13}C NMR (CDCl_3): 4.9



HSQC NMR (CDCl₃): 4.9

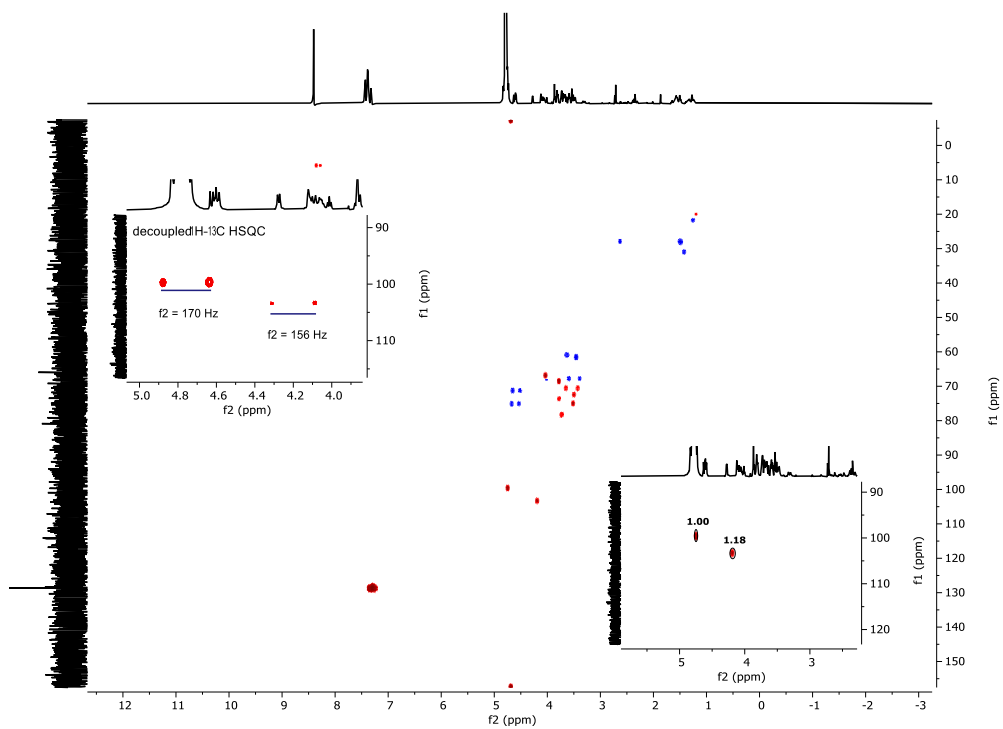


¹H NMR (D₂O): 4.19

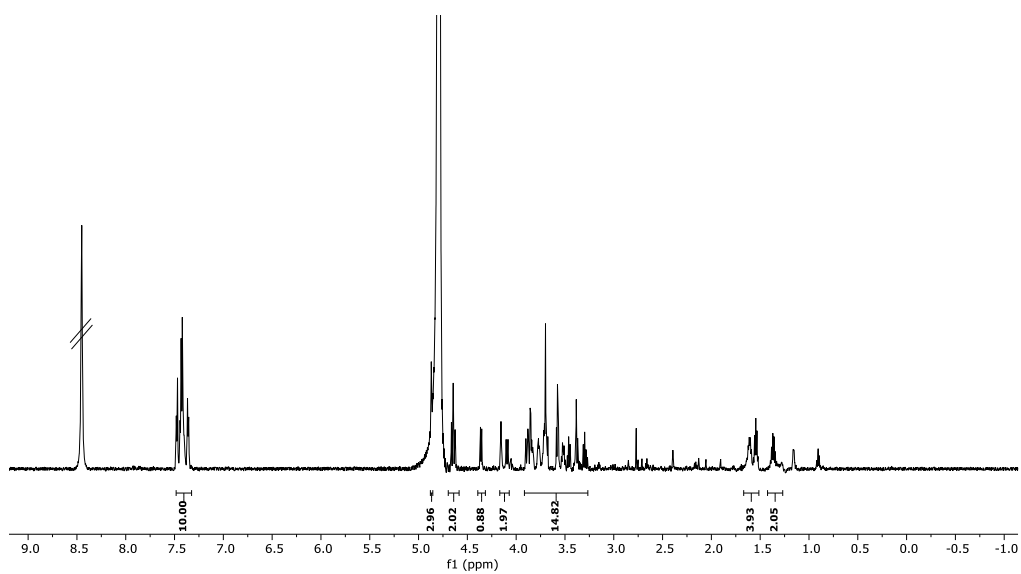


^{13}C NMR (D_2O): **4.19** could not be obtained due to low amount of material.

HSQC NMR (D_2O): **4.19**

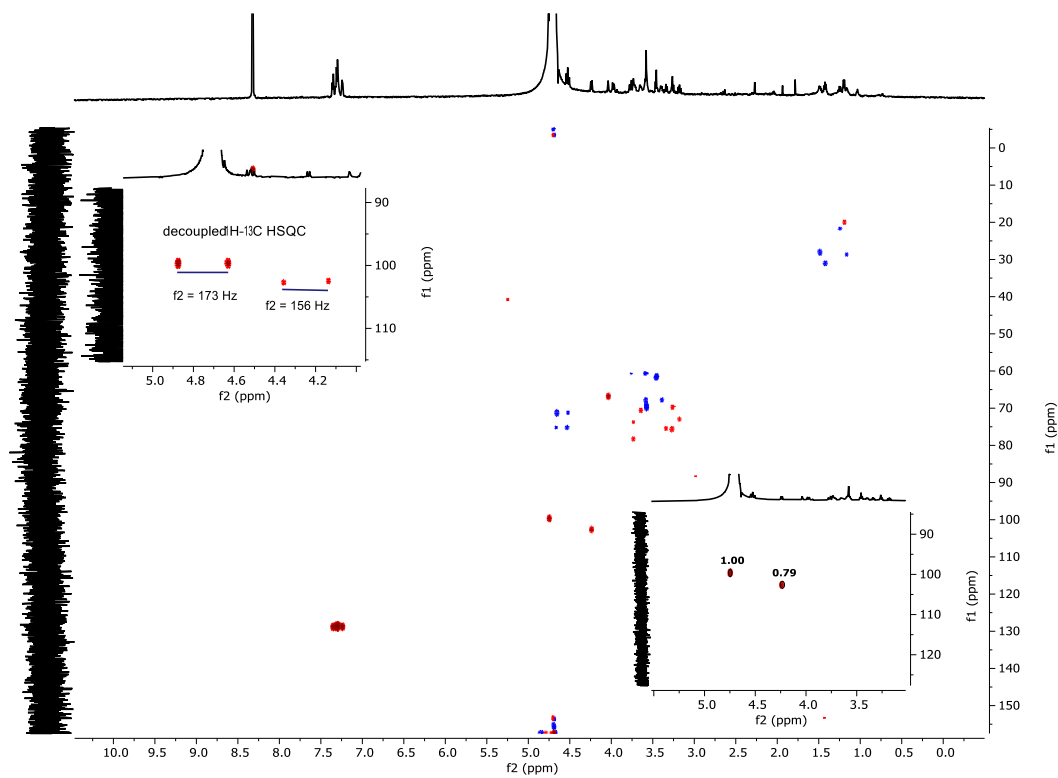


^1H NMR (D_2O): **4.20**

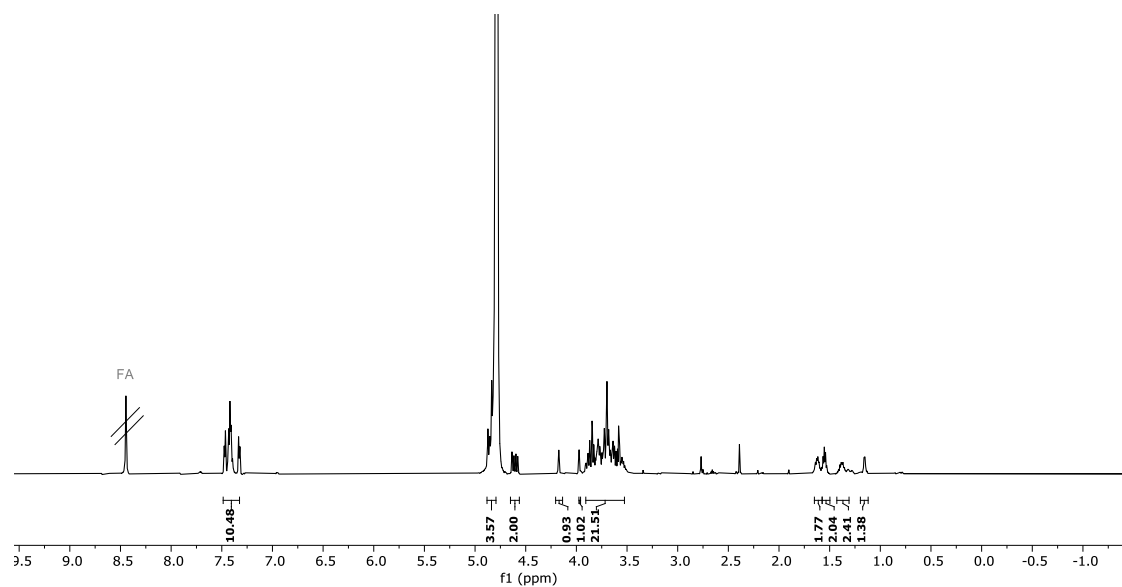


^{13}C NMR (D_2O): **4.20** could not be obtained due to low amount of material.

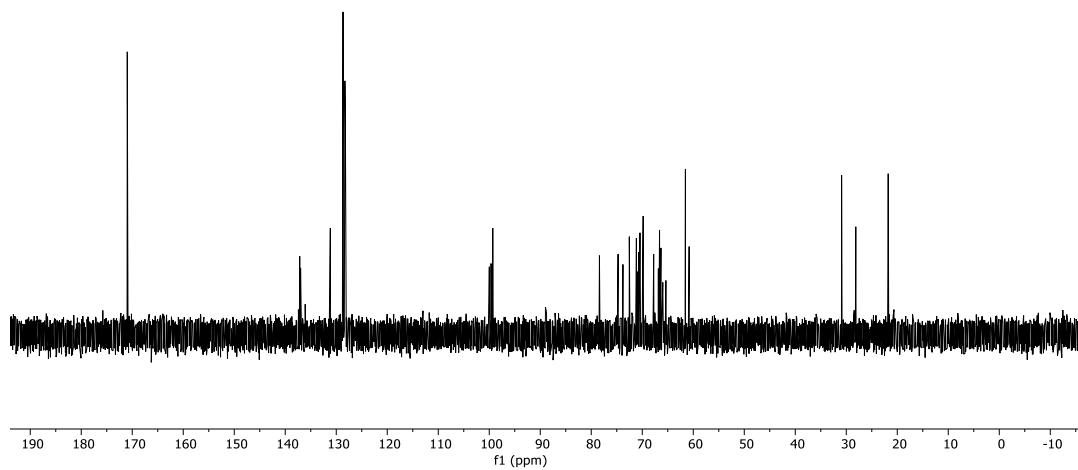
HSQC NMR (D_2O): **4.20**



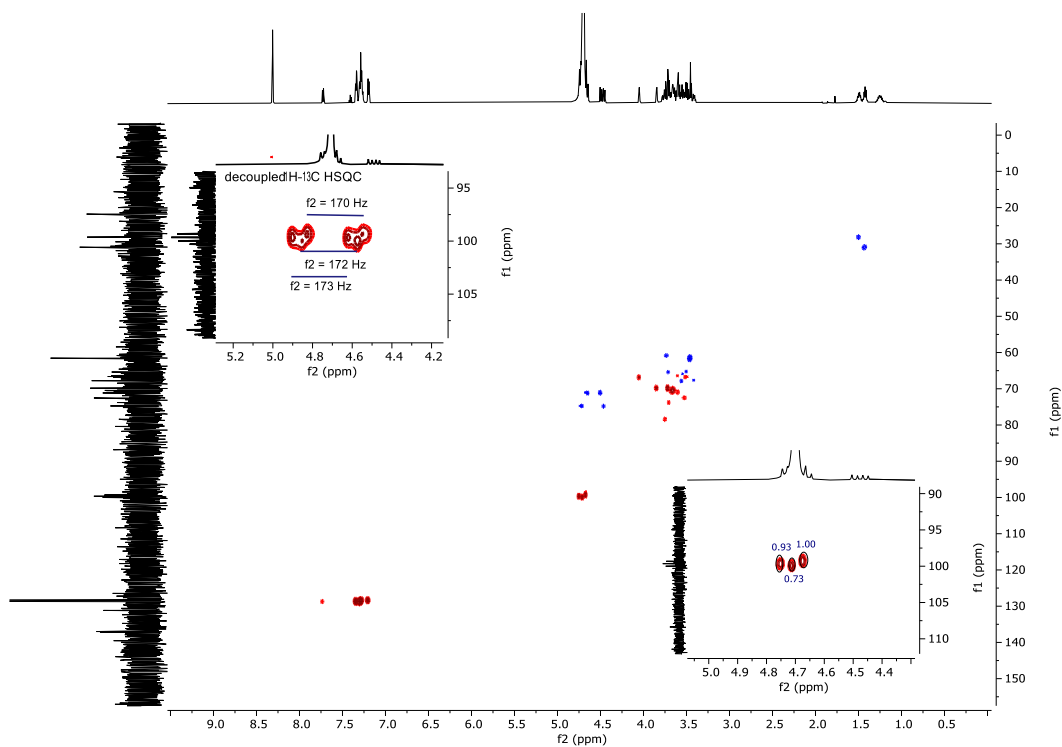
^1H NMR (D_2O): **4.21**



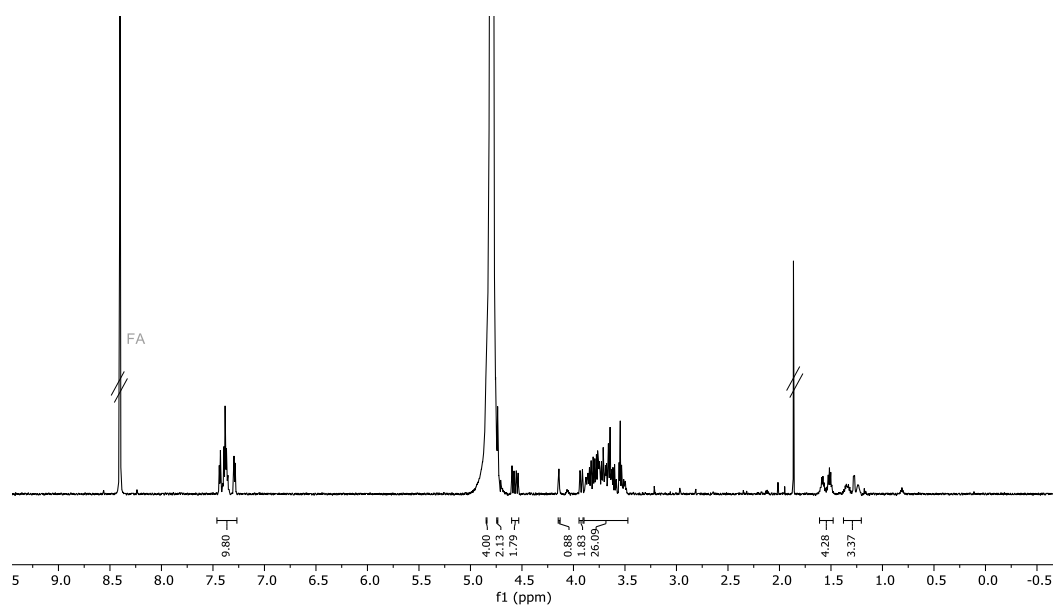
^{13}C NMR (D_2O): 4.21



HSQC NMR (D_2O): 4.21

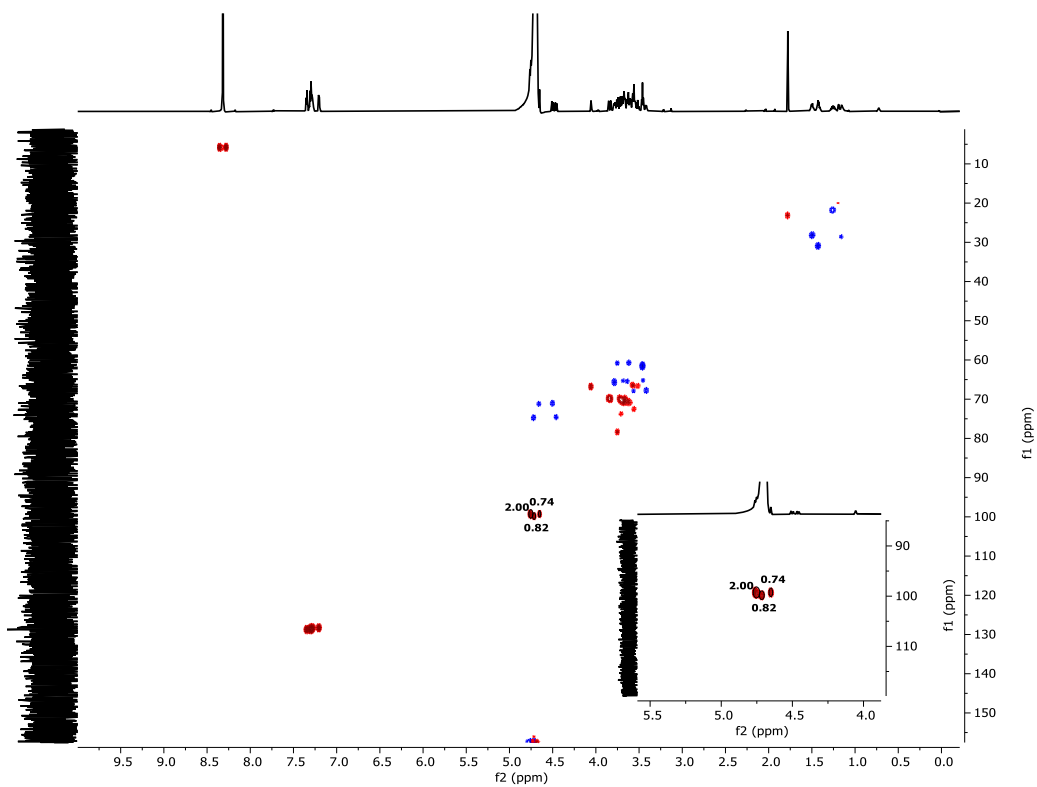


^1H NMR (D_2O): **4.22**

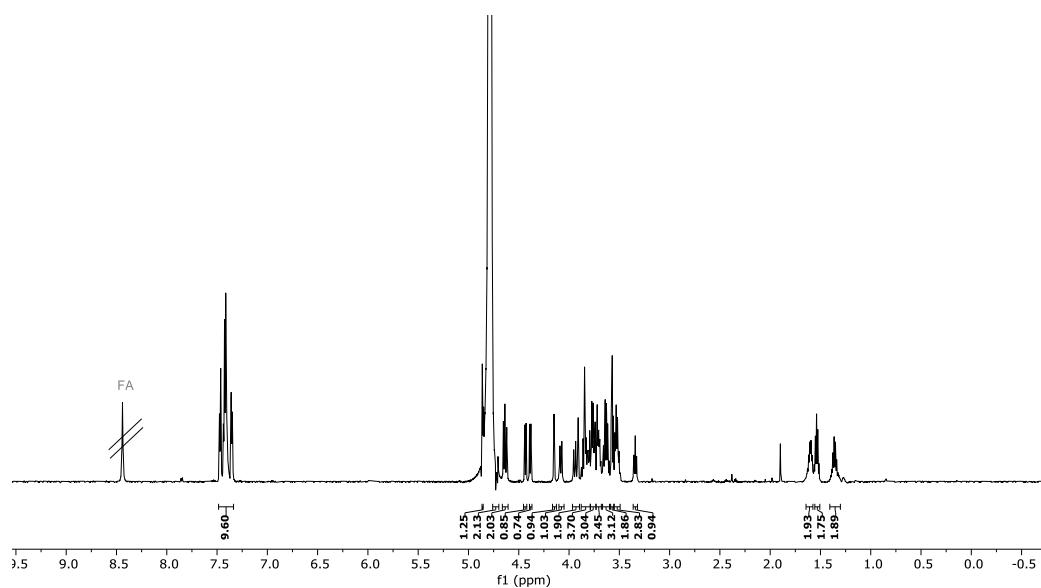


^{13}C NMR (D_2O): **4.22** could not be obtained due to low amount of material.

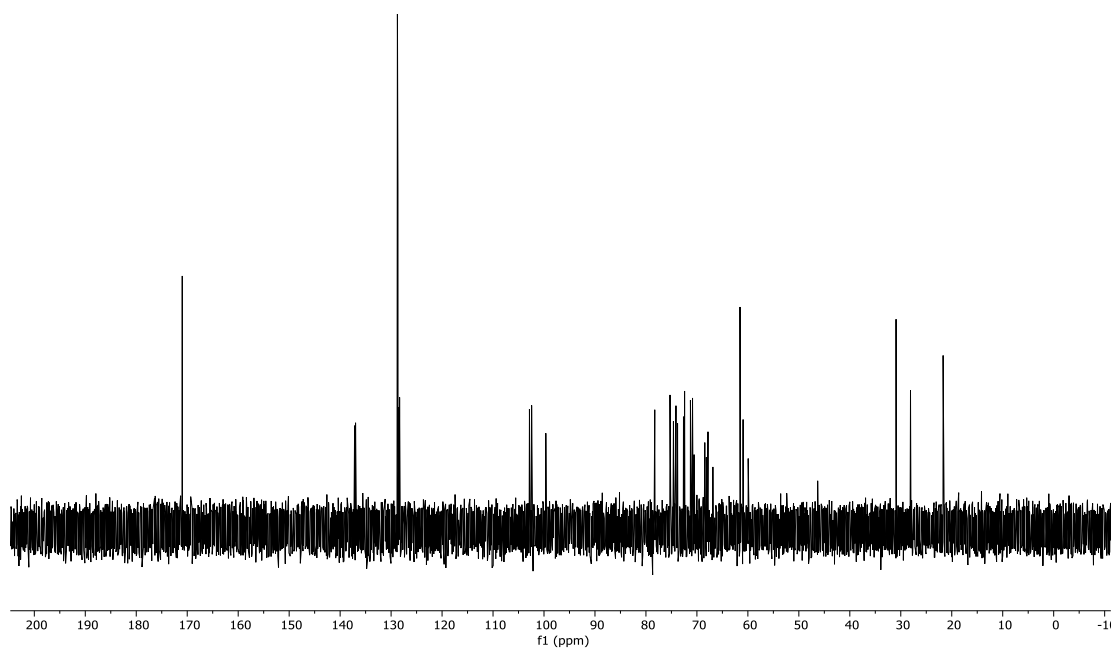
HSQC NMR (D_2O): **4.22**



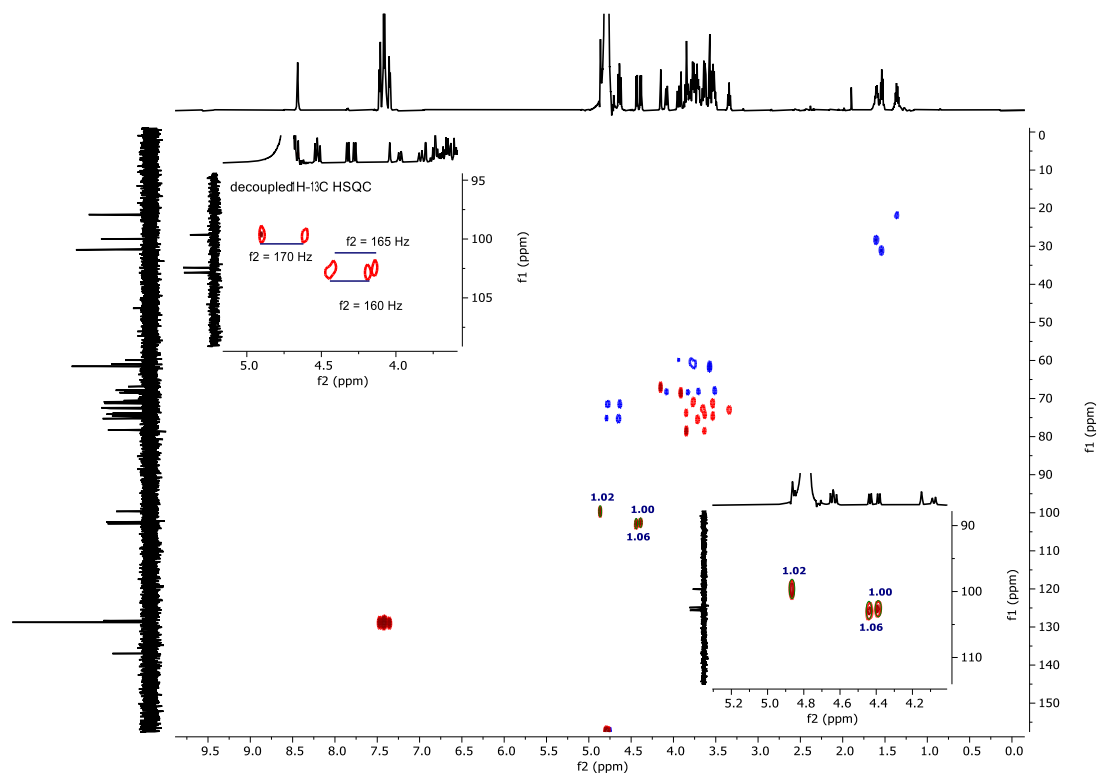
¹H NMR (D₂O): 4.23



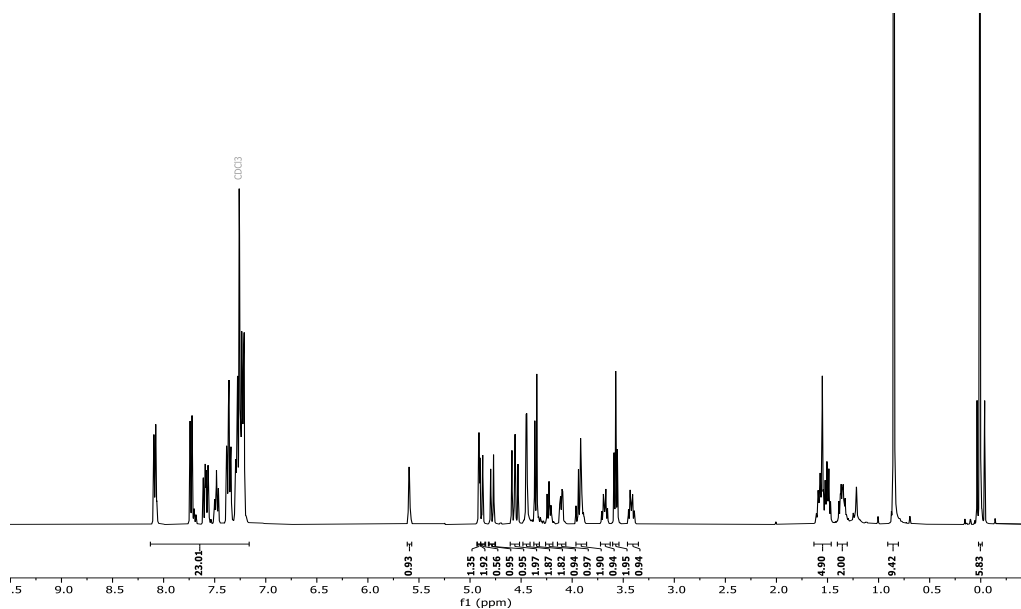
¹³C NMR (D₂O): 4.23



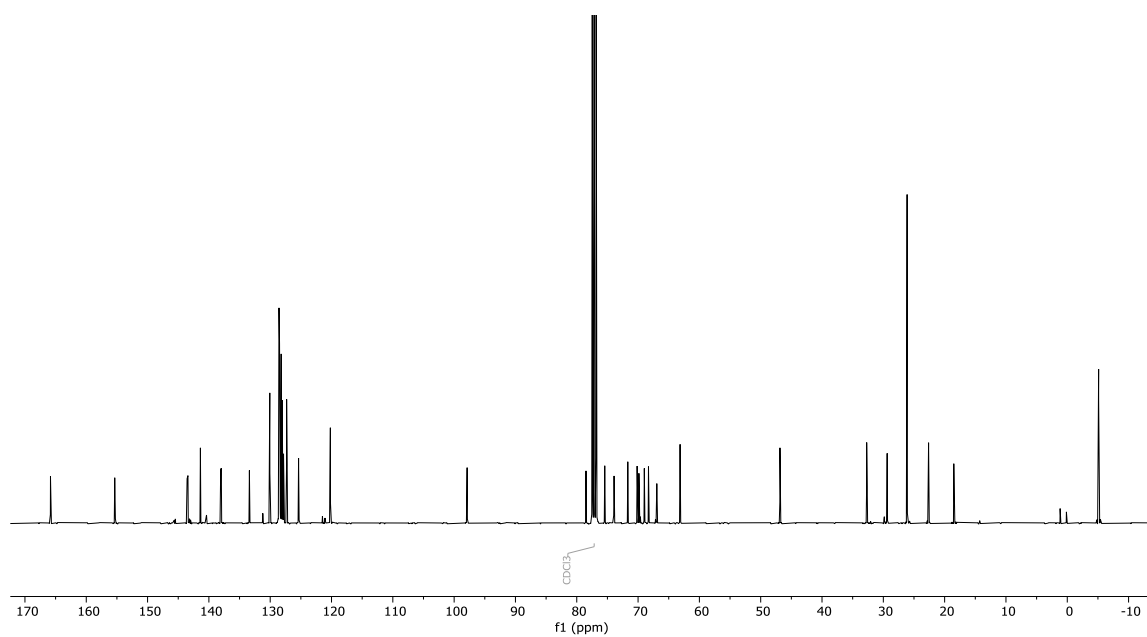
HSQC NMR (D₂O): 4.23



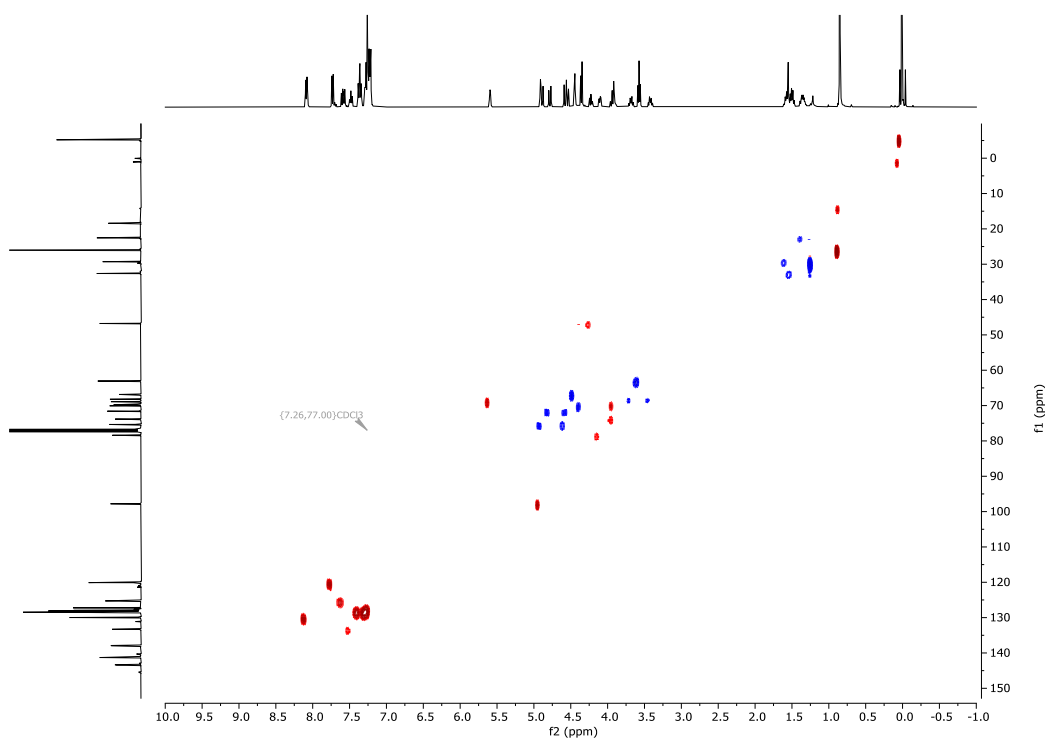
¹H NMR (CDCl₃): 4.42



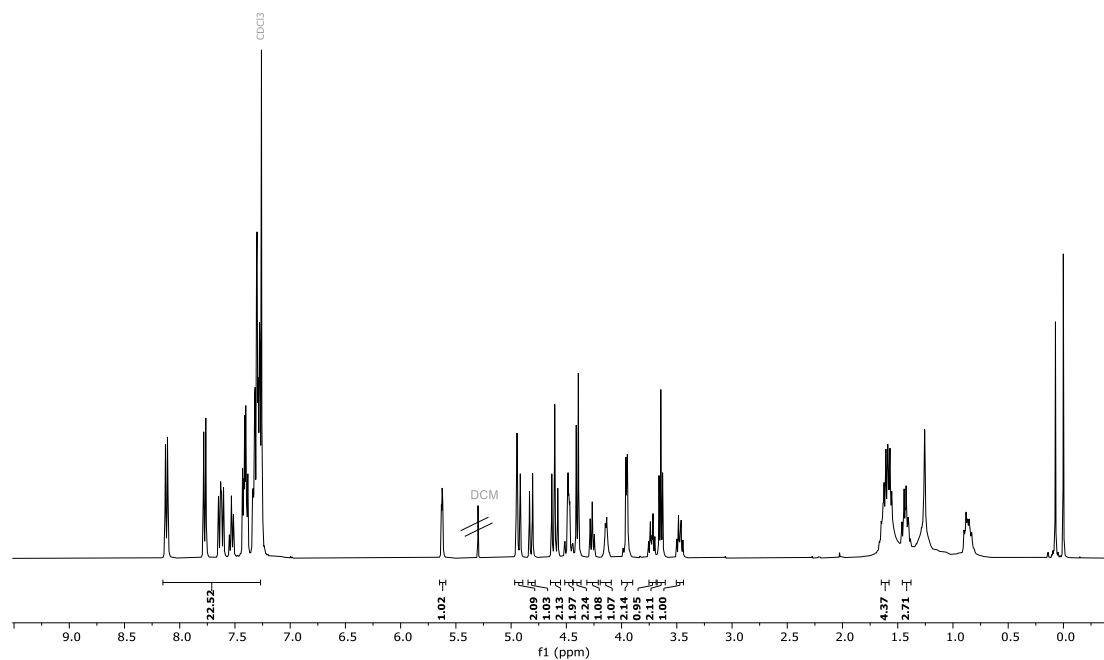
^{13}C NMR (CDCl_3): 4.42



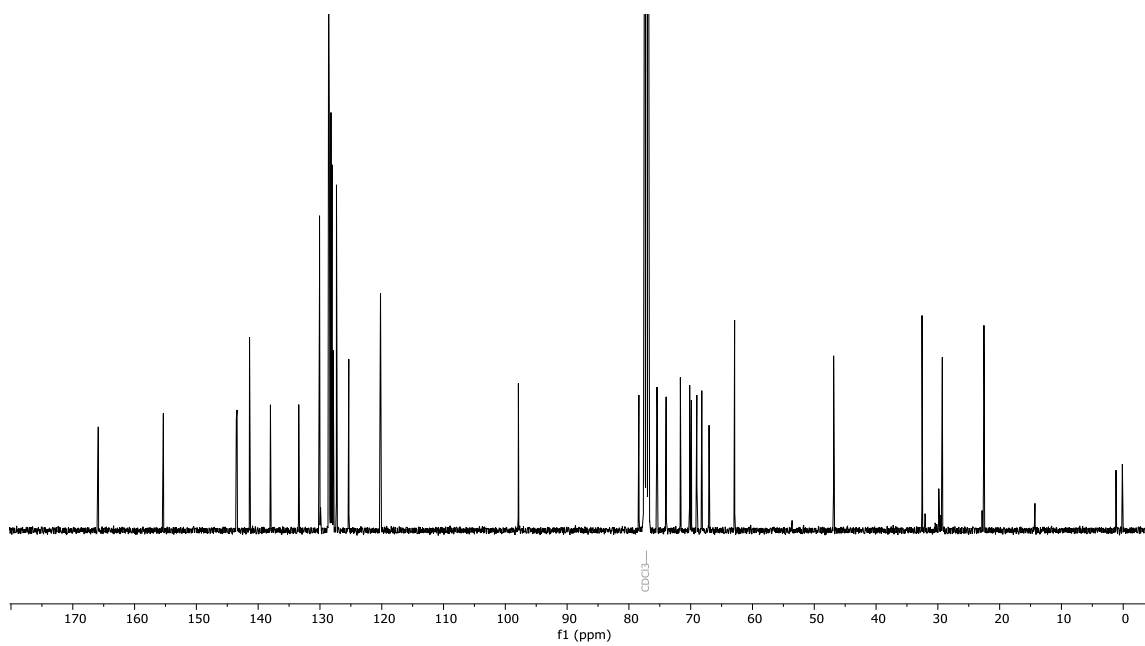
HSQC NMR (CDCl_3): 4.42



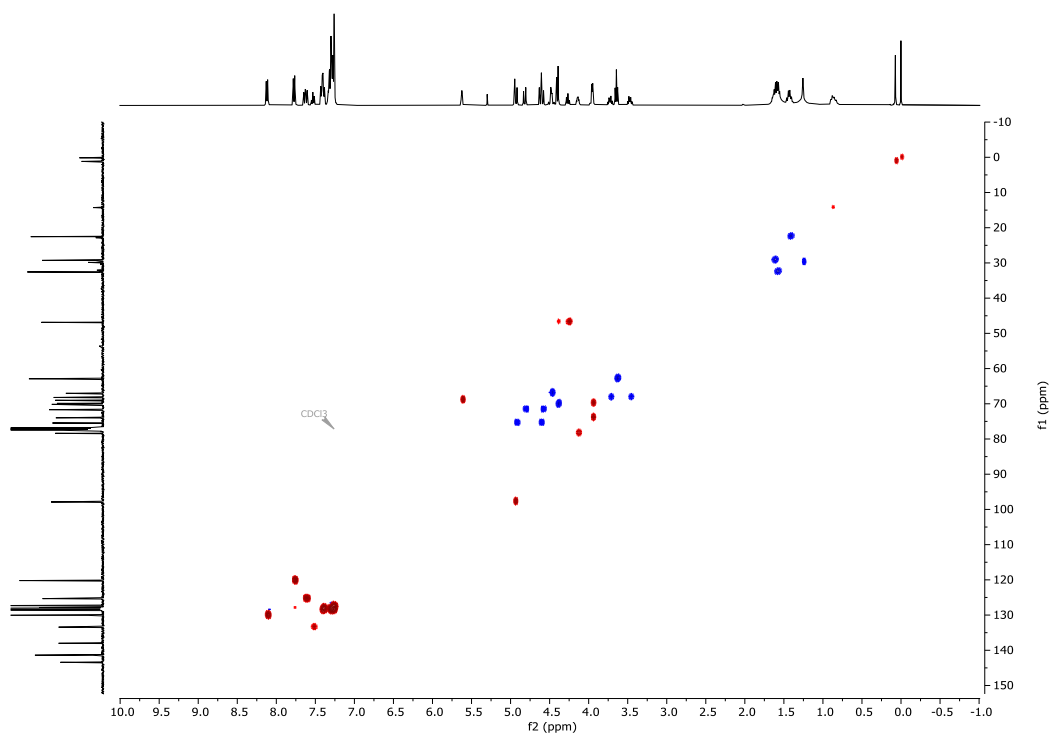
¹H NMR (CDCl₃): 4.43



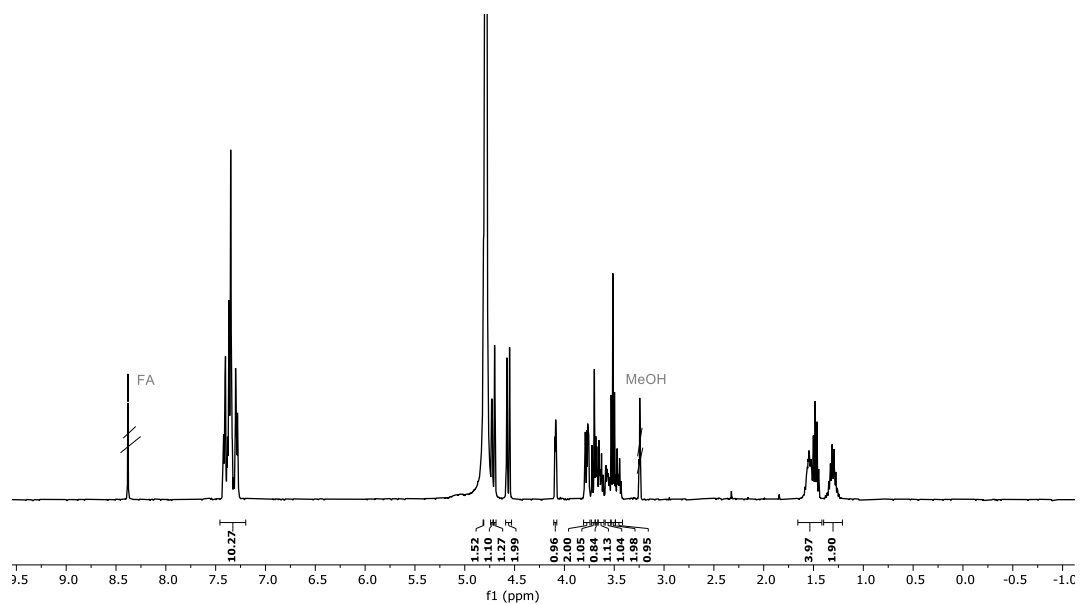
¹³C NMR (CDCl₃): 4.43



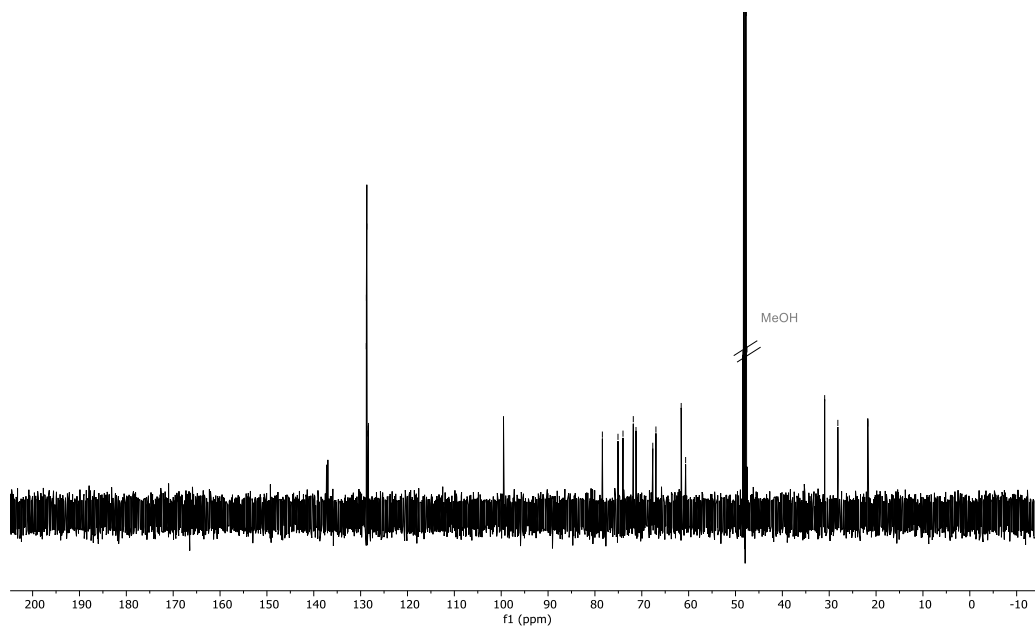
HSQC NMR (CDCl₃): 4.43



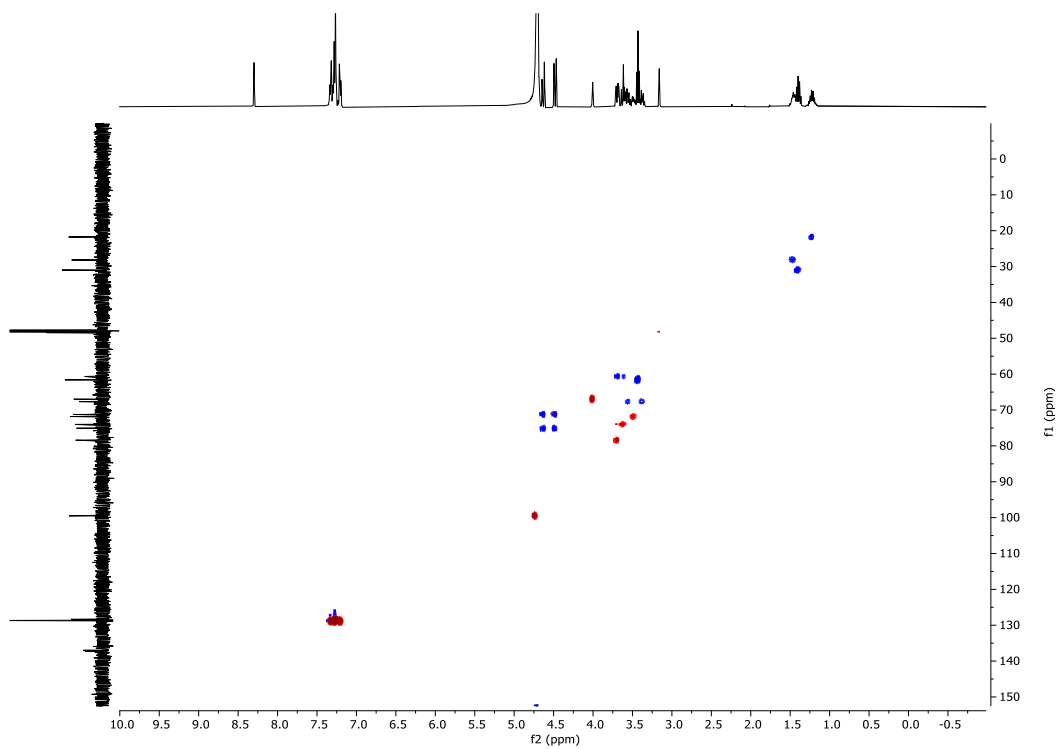
¹H NMR (D₂O): 4.47



^{13}C NMR (D_2O): 4.47



HSQC NMR (D_2O): 4.47

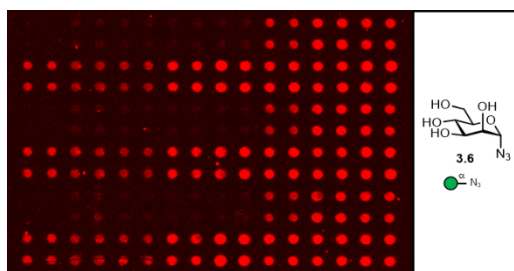


Fluorescence scan images of the neo-glycopeptides

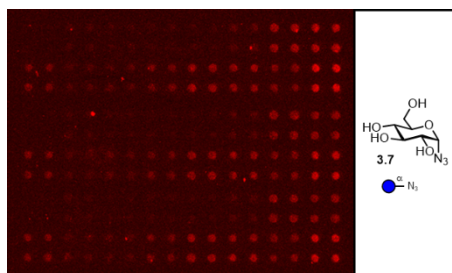
In the following figures the fluorescence scanning images of the three sets of quadruplicates for each neo-glycopeptide and the plain peptides (consisting only of propargylglycine/glycine) with the sugar azides **3.6-3.14** of *Section 3.2.2*. Whenever a spot from a neo-glycopeptide is overlapping with impurities on the microarray, which distort the original fluorescence intensity, the spots were omitted from the calculations.



Appendix Figure 1: Fluorescence scan image of the plain peptides after incubation with CF@633 ConA. Incubation was performed in HEPES-buffer (50 mM HEPES, 100 mM NaCl, pH 7.5) containing 1 mM CaCl₂, 1 mM MnCl₂, 10% blocking buffer and 0.05% Tween-20 at a ConA concentration of 100 µg/mL. Scanning parameters: Wavelengths 635 nm, PMT gain 600, power 33%, pixel size 5 µm. Distance between the centres of two spots (pitch) is 250 µm for each microarray. This experiment was used as a negative control.

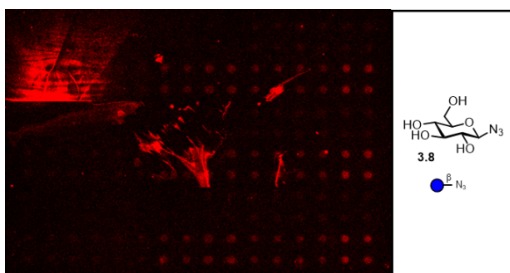


Appendix Figure 2: Fluorescence scan image of neo-glycopeptides containing mannose **3.6** after incubation with CF@633 ConA. Labelling was performed in HEPES-buffer (50 mM HEPES, 100 mM NaCl, pH 7.5) containing 1 mM CaCl₂, 1 mM MnCl₂, 10% blocking buffer and 0.05% Tween-20 at a ConA concentration of 100 µg/mL. Scanning parameters: Wavelengths 635 nm, PMT gain 600, power 33%, pixel size 5 µm. Distance between the centres of two spots (pitch) is 250 µm for each microarray.

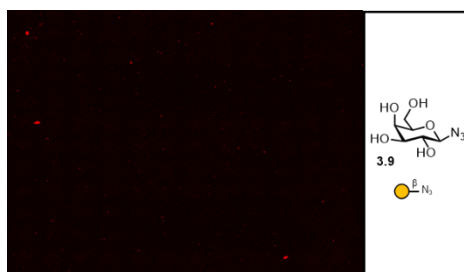


Appendix Figure 3: Fluorescence scan image of neo-glycopeptides containing glucose **3.7** after incubation with CF@633 ConA. Labelling was performed in HEPES-buffer (50 mM HEPES, 100 mM NaCl, pH 7.5) containing 1 mM CaCl₂, 1 mM MnCl₂, 10% blocking buffer and 0.05% Tween-20 at a ConA concentration of 100 µg/mL.

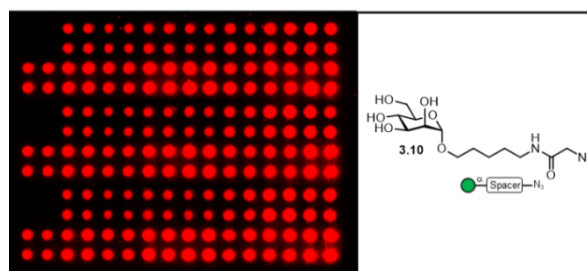
Scanning parameters: Wavelengths 635 nm, PMT gain 600, power 33%, pixel size 5 μm . Distance between the centres of two spots (pitch) is 250 μm for each microarray.



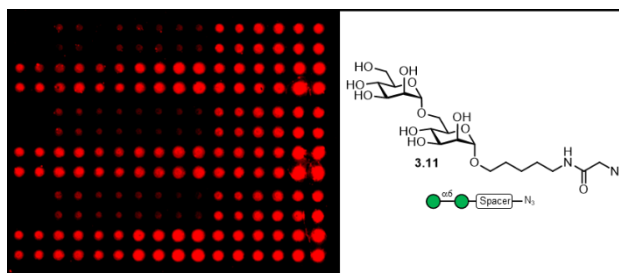
Appendix Figure 4: Fluorescence scan image of neo-glycopeptides containing glucose **3.8** after incubation with CF@633 ConA. Labelling was performed in HEPES-buffer (50 mM HEPES, 100 mM NaCl, pH 7.5) containing 1 mM CaCl₂, 1 mM MnCl₂, 10% blocking buffer and 0.05% Tween-20 at a ConA concentration of 100 $\mu\text{g}/\text{mL}$. Scanning parameters: Wavelengths 635 nm, PMT gain 600, power 33%, pixel size 5 μm . Distance between the centres of two spots (pitch) is 250 μm for each microarray.



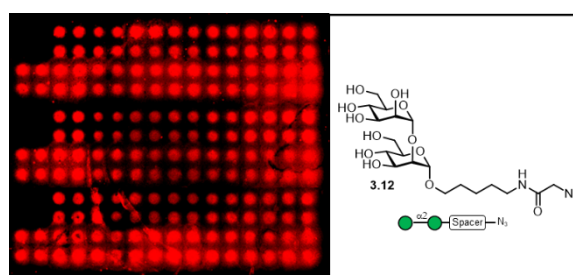
Appendix Figure 5: Fluorescence scan image of neo-glycopeptides containing galactose **3.9** after incubation with CF@633 ConA. Labelling was performed in HEPES-buffer (50 mM HEPES, 100 mM NaCl, pH 7.5) containing 1 mM CaCl₂, 1 mM MnCl₂, 10% blocking buffer and 0.05% Tween-20 at a ConA concentration of 100 $\mu\text{g}/\text{mL}$. Scanning parameters: Wavelengths 635 nm, PMT gain 600, power 33%, pixel size 5 μm . Distance between the centres of two spots (pitch) is 250 μm for each microarray. This experiment was used as a negative control.



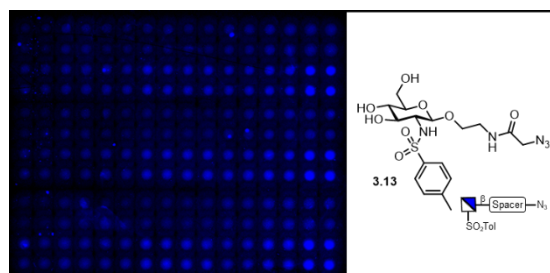
Appendix Figure 6: Fluorescence scan image of neo-glycopeptides containing spacer modified mannose **3.10** after incubation with CF@633 ConA. Labelling was performed in HEPES-buffer (50 mM HEPES, 100 mM NaCl, pH 7.5) containing 1 mM CaCl₂, 1 mM MnCl₂, 10% blocking buffer and 0.05% Tween-20 at a ConA concentration of 100 $\mu\text{g}/\text{mL}$. Scanning parameters: Wavelengths 635 nm, PMT gain 600, power 33%, pixel size 5 μm . Distance between the centres of two spots (pitch) is 250 μm for each microarray.



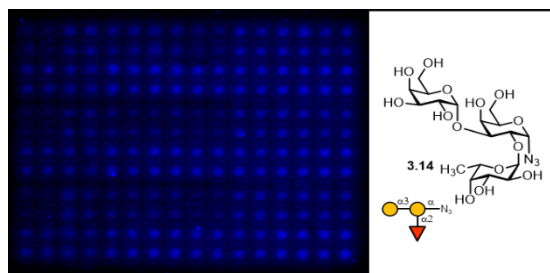
Appendix Figure 7: Fluorescence scan image of neo-glycopeptides containing spacer modified 1,6-di-mannose **3.11** after incubation with CF@633 ConA. Labelling was performed in HEPES-buffer (50 mM HEPES, 100 mM NaCl, pH 7.5) containing 1 mM CaCl₂, 1 mM MnCl₂, 10% blocking buffer and 0.05% Tween-20 at a ConA concentration of 100 µg/mL. Scanning parameters: Wavelengths 635 nm, PMT gain 600, power 33%, pixel size 5 µm. Distance between the centres of two spots (pitch) is 250 µm for each microarray.



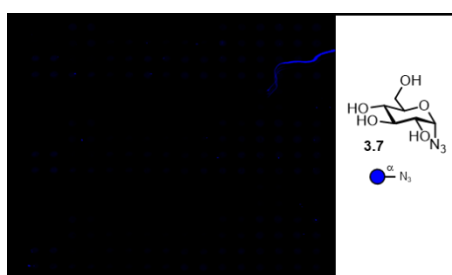
Appendix Figure 8: Fluorescence scan image of neo-glycopeptides containing spacer modified 1,2-di-mannose **3.12** after incubation with CF@633 ConA. Labelling was performed in HEPES-buffer (50 mM HEPES, 100 mM NaCl, pH 7.5) containing 1 mM CaCl₂, 1 mM MnCl₂, 10% blocking buffer and 0.05% Tween-20 at a ConA concentration of 100 µg/mL. Scanning parameters: Wavelengths 635 nm, PMT gain 600, power 33%, pixel size 5 µm. Distance between the centres of two spots (pitch) is 250 µm for each microarray.



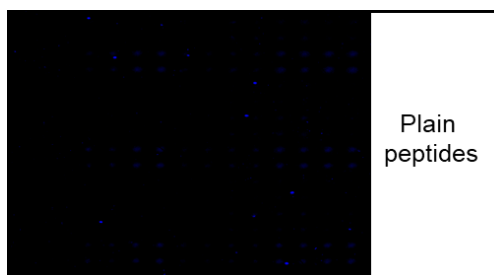
Appendix Figure 9: Fluorescence scan image of neo-glycopeptides containing glucosamine **3.13** after incubation with FITC-labelled human langerin ECD. Labelling was performed in HEPES-buffer (50 mM HEPES, 100 mM NaCl, pH 7.5) containing 10 mM CaCl₂, 1 mM MnCl₂, 10% blocking buffer and 0.05% Tween-20 at a langerin concentration of 100 µg/mL. Scanning parameters: Wavelengths 488 nm, PMT gain 600, power 33%, pixel size 5 µm. Distance between the centres of two spots (pitch) is 250 µm for each microarray.



Appendix Figure 10: Fluorescence scan image of neo-glycopeptides containing human blood group antigen B **3.14** after incubation with FITC-labelled human langerin ECD. Labelling was performed in HEPES-buffer (50 mM HEPES, 100 mM NaCl, pH 7.5) containing 10 mM CaCl₂, 1 mM MnCl₂, 10% blocking buffer and 0.05% Tween-20 at a langerin concentration of 100 µg/mL. Scanning parameters: Wavelengths 488 nm, PMT gain 600, power 33%, pixel size 5 µm. Distance between the centres of two spots (pitch) is 250 µm for each microarray.



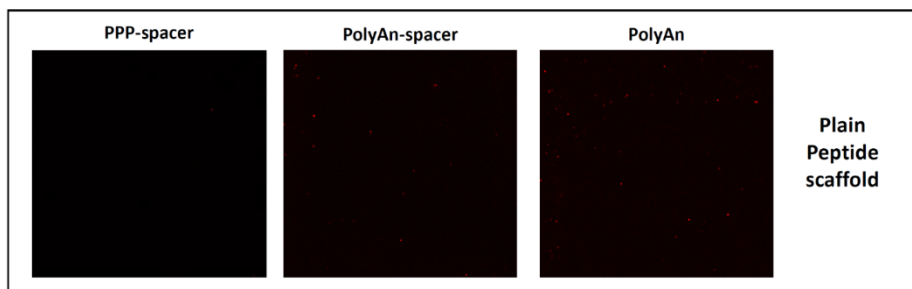
Appendix Figure 11: Fluorescence scan image of neo-glycopeptides containing glucose **7** after incubation with FITC-labelled human langerin ECD. Incubation was performed in HEPES-buffer (50 mM HEPES, 100 mM NaCl, pH 7.5) containing 10 mM CaCl₂, 1 mM MnCl₂, 10% blocking buffer and 0.05% Tween-20 at a langerin concentration of 100 µg/mL. Scanning parameters: Wavelengths 488 nm, PMT gain 600, power 33%, pixel size 5 µm. Distance between the centres of two spots (pitch) is 250 µm for each microarray. This experiment was used as a negative control.



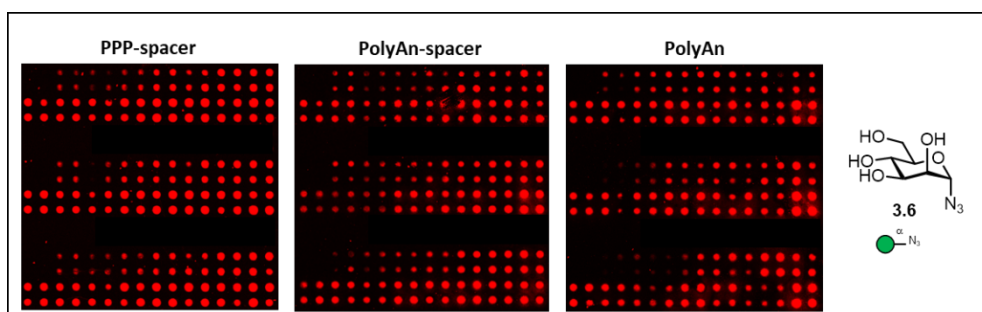
Appendix Figure 12: Fluorescence scan image of the plain peptides after incubation with FITC-labelled human langerin ECD. Incubation was performed in HEPES-buffer (50 mM HEPES, 100 mM NaCl, pH 7.5) containing 10 mM CaCl₂, 1 mM MnCl₂, 10% blocking buffer and 0.05% Tween-20 at a langerin concentration of 100 µg/mL. Scanning parameters: Wavelengths 488 nm, PMT gain 600, power 33%, pixel size 5 µm. Distance between the centres of two spots (pitch) is 250 µm for each microarray. This experiment was used as a negative control.

In the following figures the fluorescence scan images of all synthesized and screened glycopeptides with sugar azides **3.6**, **3.9**, and **3.15-3.19** of *Section 3.2.4*. are shown after incubation of each structure with the corresponding fluorescently labeled lectin (ConA, RCA-I, PNA, SBA, DBA, and WGA). The plain peptides were used as negative controls.

Concanavalin A (ConA)

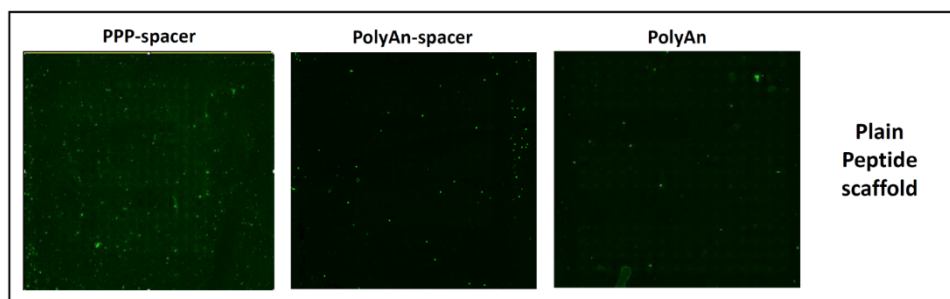


Appendix Figure 13: Fluorescence scan image of the plain peptides (negative control) after incubation with CF@633 ConA. Incubation was performed in HEPES-buffer (50 mM HEPES, 100 mM NaCl, 1 mM CaCl₂, 1 mM MnCl₂, 10% blocking buffer and 0.05% Tween-20, pH 7.5) at 100 µg/mL ConA concentration. Scanning parameters: Wavelength 635 nm, PMT gain 600, laser power 33%, pixel size 5 µm. Spot pitch is 250 µm.

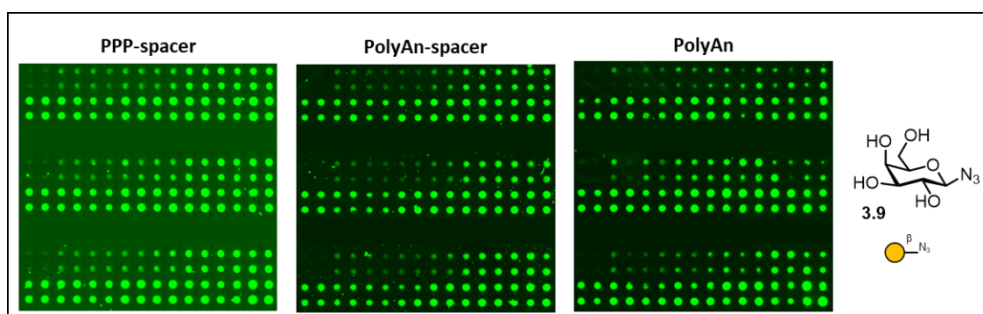


Appendix Figure 14: Fluorescence scan image of glycopeptides containing Man azide **3.6** after incubation with CF@633 ConA. Staining was performed in HEPES-buffer (50 mM HEPES, 100 mM NaCl, 1 mM CaCl₂, 1 mM MnCl₂, 10% blocking buffer and 0.05% Tween-20, pH 7.5) at 100 µg/mL ConA concentration. Scanning parameters: Wavelength 635 nm, PMT gain 600, laser power 33%, pixel size 5 µm. Spot pitch is 250 µm.

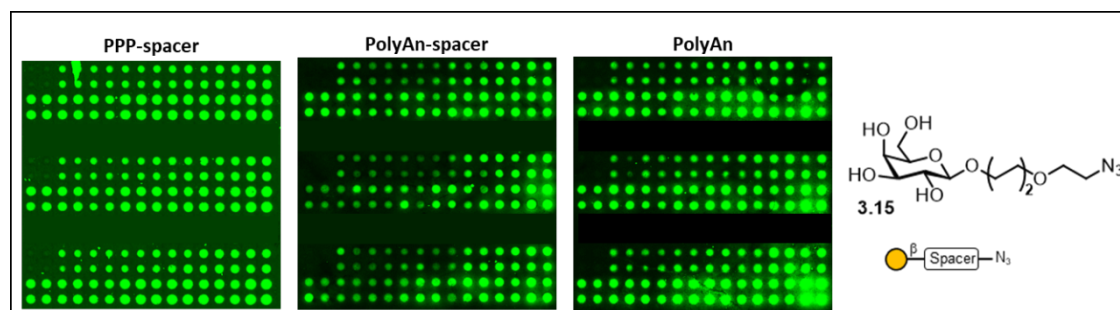
Ricinus Communis Agglutinin I (RCA-I)



Appendix Figure 15: Fluorescence scan image of the plain peptides (negative control) after incubation with Rhodamine-labelled RCA-I. Incubation was performed in HEPES-buffer (50 mM HEPES, 100 mM NaCl, 1 mM CaCl₂, 1 mM MnCl₂, 10% blocking buffer and 0.05% Tween-20, pH=7.5) at 10 µg/mL lectin concentration. Scanning parameters: Wavelength 532 nm, PMT gain 500, laser power 33%, pixel size 5 µm. Spot pitch is 250 µm.

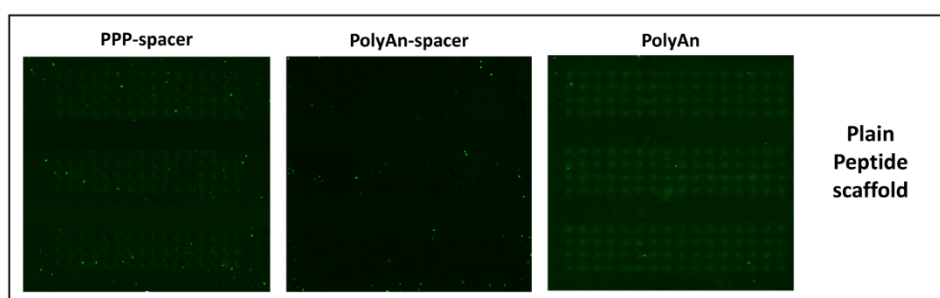


Appendix Figure 16: Fluorescence scan image of glycopeptides containing β -Gal azide **3.9** after incubation with Rhodamine-labelled RCA-I. Staining was performed in HEPES-buffer (50 mM HEPES, 100 mM NaCl, 1 mM CaCl_2 , 1 mM MnCl_2 , 10% blocking buffer and 0.05% Tween-20, pH 7.5) at 10 $\mu\text{g}/\text{mL}$ RCA-I concentration. Scanning parameters: Wavelength 532 nm, PMT gain 500, laser power 33%, pixel size 5 μm . Spot pitch is 250 μm .

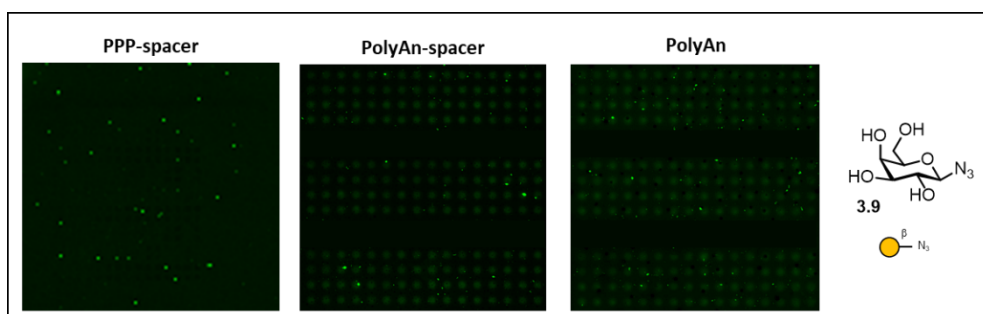


Appendix Figure 17: Fluorescence scan image of glycopeptides containing β -Gal-PEG3 azide **3.15** after incubation with Rhodamine-labelled RCA-I. Staining was performed in HEPES-buffer (50 mM HEPES, 100 mM NaCl, 1 mM CaCl_2 , 1 mM MnCl_2 , 10% blocking buffer and 0.05% Tween-20, pH 7.5) at 10 $\mu\text{g}/\text{mL}$ RCA-I concentration. Scanning parameters: Wavelength 532 nm, PMT gain 500, laser power 33%, pixel size 5 μm . Spot pitch is 250 μm .

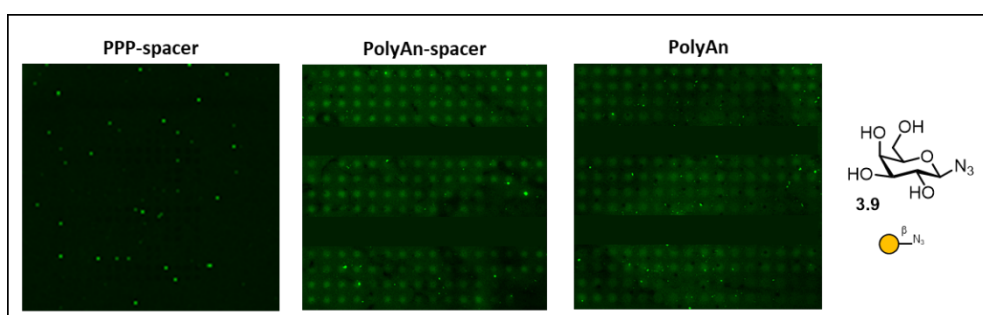
Peanut Agglutinin (PNA)



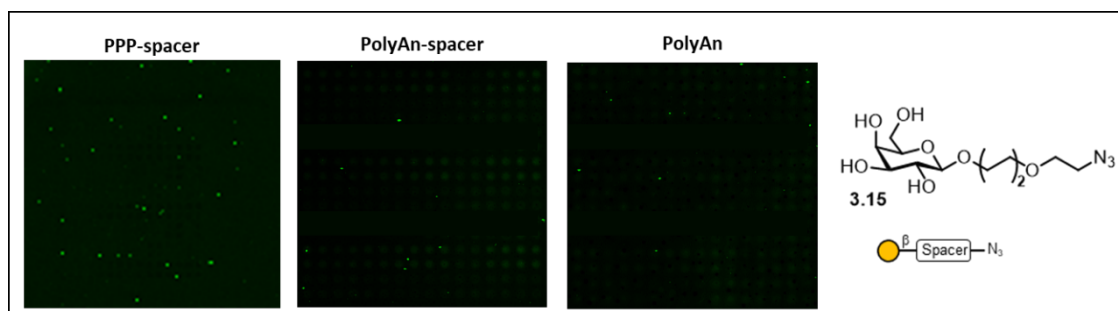
Appendix Figure 18: Fluorescence scan image of the plain peptides (negative control) after incubation with Rhodamine-labelled PNA. Incubation was performed in HEPES-buffer (50 mM HEPES, 100 mM NaCl, 1 mM CaCl_2 , 1 mM MnCl_2 , 10% blocking buffer and 0.05% Tween-20, pH 7.5) at 10 $\mu\text{g}/\text{mL}$ lectin concentration. Scanning parameters: Wavelength 532 nm, PMT gain 500, laser power 33%, pixel size 5 μm . Spot pitch is 250 μm .



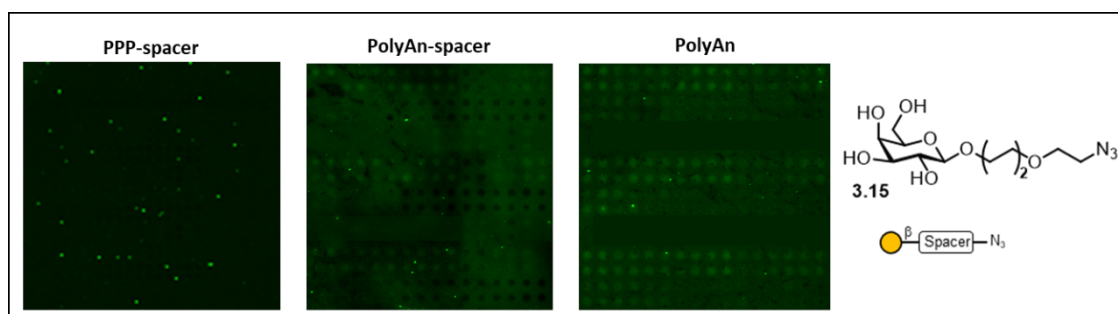
Appendix Figure 19: Fluorescence scan image of glycopeptides containing β -Gal azide **3.9** after incubation with Rhodamine-labelled PNA. Staining was performed in HEPES-buffer (50 mM HEPES, 100 mM NaCl, 1 mM CaCl_2 , 1 mM MnCl_2 , 10% blocking buffer and 0.05% Tween-20, pH 7.5) at 100 $\mu\text{g}/\text{mL}$ lectin concentration. Scanning parameters: Wavelength 532 nm, PMT gain 500, laser power 33%, pixel size 5 μm . Spot pitch is 250 μm .



Appendix Figure 20: Fluorescence scan image of glycopeptides containing galactose **3.9** after incubation with Rhodamine-labelled PNA. Staining was performed in HEPES-buffer (50 mM HEPES, 100 mM NaCl, 1 mM CaCl_2 , 1 mM MnCl_2 , 10% blocking buffer and 0.05% Tween-20, pH 7.5) at 10 $\mu\text{g}/\text{mL}$ lectin concentration. Scanning parameters: Wavelength 532 nm, PMT gain 500, laser power 33%, pixel size 5 μm . Spot pitch is 250 μm .

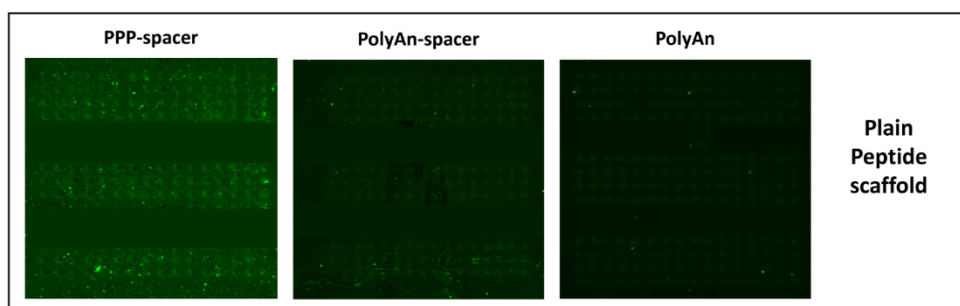


Appendix Figure 21: Fluorescence scan image of glycopeptides containing β -Gal-PEG3 azide **3.15** after incubation with Rhodamine-labelled PNA. Staining was performed in HEPES-buffer (50 mM HEPES, 100 mM NaCl, 1 mM CaCl_2 , 1 mM MnCl_2 , 10% blocking buffer and 0.05% Tween-20, pH 7.5) at 100 $\mu\text{g}/\text{mL}$ lectin concentration. Scanning parameters: Wavelength 532 nm, PMT gain 500, laser power 33%, pixel size 5 μm . Spot pitch is 250 μm .

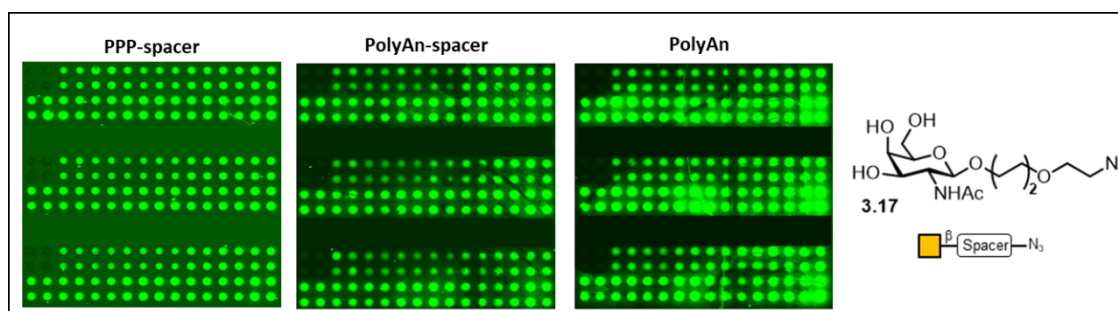


Appendix Figure 22: Fluorescence scan image of glycopeptides containing β -Gal-PEG3 azide **3.15** after incubation with Rhodamine-labelled PNA. Staining was performed in HEPES-buffer (50 mM HEPES, 100 mM NaCl, 1 mM CaCl₂, 1 mM MnCl₂, 10% blocking buffer and 0.05% Tween-20, pH 7.5) at 10 μ g/mL lectin concentration. Scanning parameters: Wavelength 532 nm, PMT gain 500, laser power 33%, pixel size 5 μ m. Spot pitch is 250 μ m.

Soybean Agglutinin (SBA)

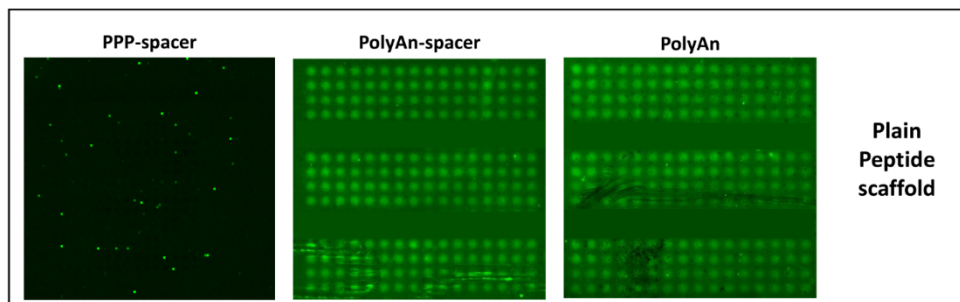


Appendix Figure 23: Fluorescence scan image of the plain peptides (negative control) after incubation with Rhodamine-labelled SBA. Incubation was performed in HEPES-buffer (50 mM HEPES, 100 mM NaCl, 1 mM CaCl₂, 1 mM MnCl₂, 10% blocking buffer and 0.05% Tween-20, pH 7.5) at 10 μ g/mL lectin concentration. Scanning parameters: Wavelength 532 nm, PMT gain 500, laser power 33%, pixel size 5 μ m. Spot pitch is 250 μ m.

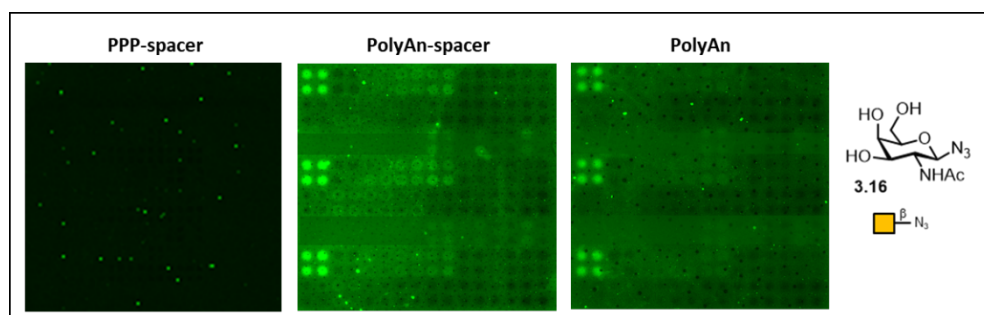


Appendix Figure 24: Fluorescence scan image of glycopeptides containing β -GalNAc-PEG3 azide **3.17** after incubation with Rhodamine-labelled SBA. Staining was performed in HEPES-buffer (50 mM HEPES, 100 mM NaCl, 1 mM CaCl₂, 1 mM MnCl₂, 10% blocking buffer and 0.05% Tween-20, pH 7.5) at 10 μ g/mL lectin concentration. Scanning parameters: Wavelength 532 nm, PMT gain 500, laser power 33%, pixel size 5 μ m. Spot pitch is 250 μ m.

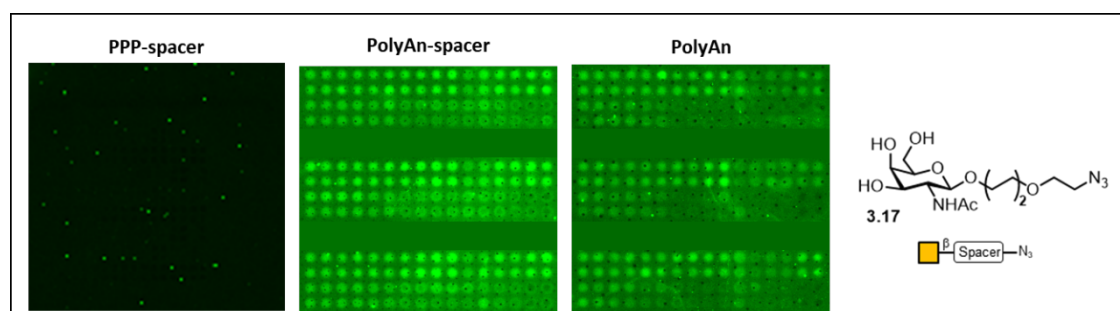
Dolichos Biflorus Agglutinin (DBA)



Appendix Figure 25: Fluorescence scan image of the plain peptides (negative control) after incubation with Rhodamine-labelled DBA. Incubation was performed in HEPES-buffer (50 mM HEPES, 100 mM NaCl, 1 mM CaCl₂, 1 mM MnCl₂, 10% blocking buffer and 0.05% Tween-20, pH 7.5) at 10 µg/mL lectin concentration. Scanning parameters: Wavelength 532 nm, PMT gain 500, laser power 33%, pixel size 5 µm. Spot pitch is 250 µm.

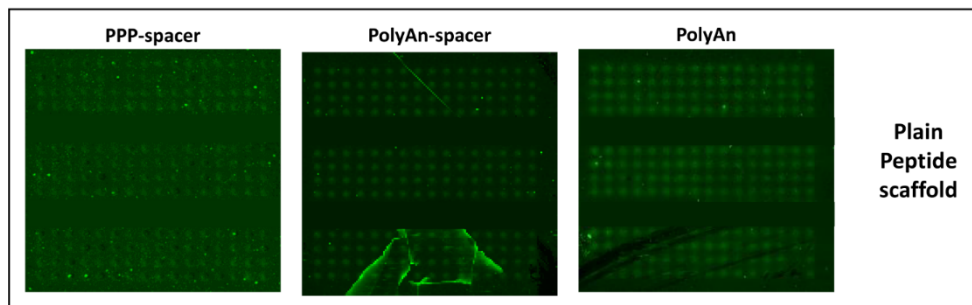


Appendix Figure 26: Fluorescence scan image of glycopeptides containing β -GalNAc azide **3.16** after incubation with Rhodamine-labelled DBA. Staining was performed in HEPES-buffer (50 mM HEPES, 100 mM NaCl, 1 mM CaCl₂, 1 mM MnCl₂, 10% blocking buffer and 0.05% Tween-20, pH 7.5) at 10 µg/mL lectin concentration. Scanning parameters: Wavelength 532 nm, PMT gain 500, laser power 33%, pixel size 5 µm. Spot pitch is 250 µm.

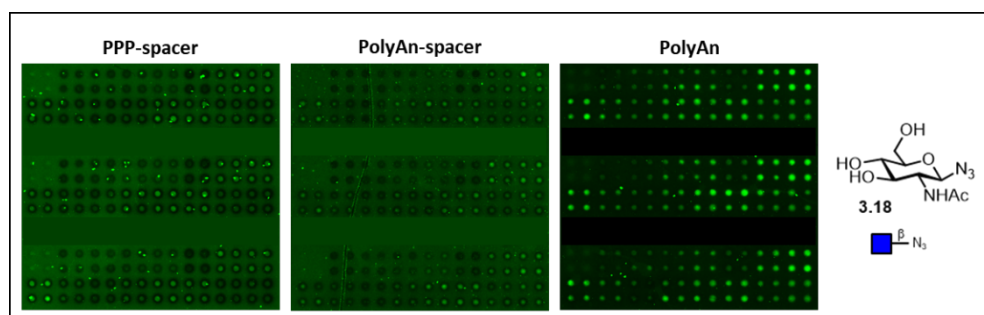


Appendix Figure 27: Fluorescence scan image of glycopeptides containing β -GalNAc-PEG3 azide **3.17** after incubation with Rhodamine-labelled DBA. Staining was performed in HEPES-buffer (50 mM HEPES, 100 mM NaCl, 1 mM CaCl₂, 1 mM MnCl₂, 10% blocking buffer and 0.05% Tween-20, pH 7.5) at 10 µg/mL lectin concentration. Scanning parameters: Wavelength 532 nm, PMT gain 500, laser power 33%, pixel size 5 µm. Spot pitch is 250 µm.

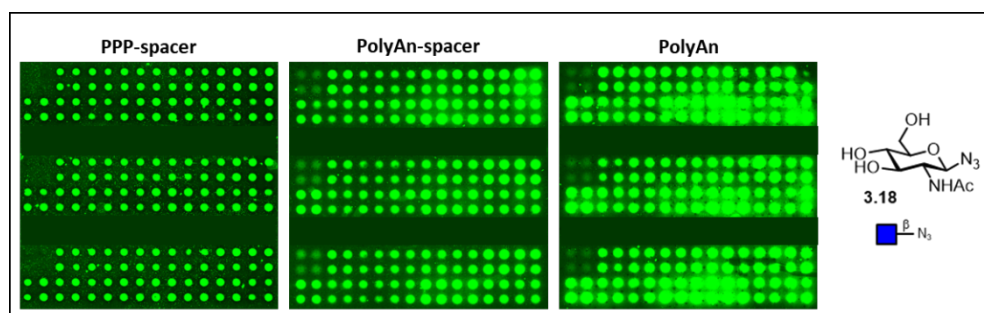
Wheat Germ Agglutinin (WGA)



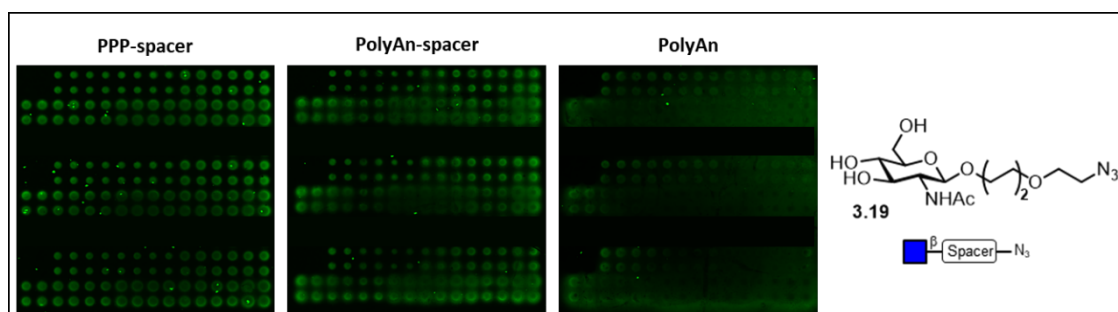
Appendix Figure 28: Fluorescence scan image of the plain peptides (negative control) after incubation with Rhodamine-labelled WGA. Incubation was performed in HEPES-buffer (50 mM HEPES, 100 mM NaCl, 1 mM CaCl₂, 1 mM MnCl₂, 10% blocking buffer and 0.05% Tween-20, pH 7.5) at 10 µg/mL lectin concentration. Scanning parameters: Wavelength 532 nm, PMT gain 500, laser power 33%, pixel size 5 µm. Spot pitch is 250 µm.



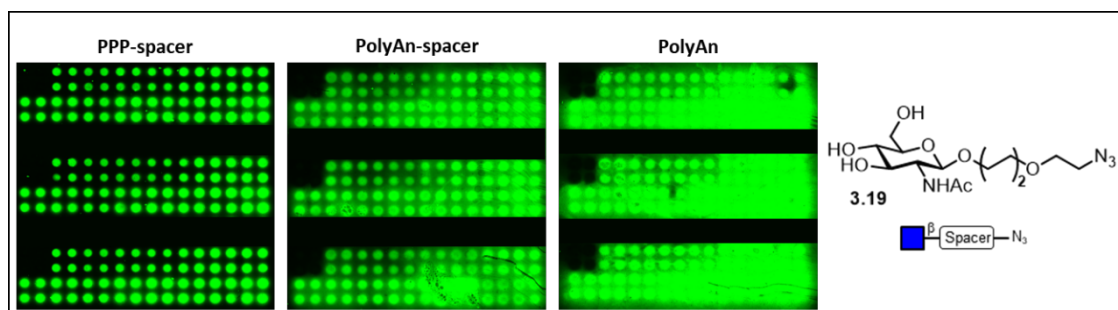
Appendix Figure 29: Fluorescence scan image of glycopeptides containing β -GlcNAc azide **3.18** after incubation with Rhodamine-labelled WGA. Staining was performed in HEPES-buffer (50 mM HEPES, 100 mM NaCl, 1 mM CaCl₂, 1 mM MnCl₂, 10% blocking buffer and 0.05% Tween-20, pH 7.5) at 0.2 µg/mL lectin concentration. Scanning parameters: Wavelength 532 nm, PMT gain 500, laser power 33%, pixel size 5 µm. Spot pitch is 250 µm.



Appendix Figure 30: Fluorescence scan image of glycopeptides containing β -GlcNAc azide **3.18** after incubation with Rhodamine-labelled WGA. Staining was performed in HEPES-buffer (50 mM HEPES, 100 mM NaCl, 1 mM CaCl₂, 1 mM MnCl₂, 10% blocking buffer and 0.05% Tween-20, pH 7.5) at 10 µg/mL lectin concentration. Scanning parameters: Wavelength 532 nm, PMT gain 500, laser power 33%, pixel size 5 µm. Spot pitch is 250 µm.



Appendix Figure 31: Fluorescence scan image of glycopeptides containing β -GlcNAc-PEG3 azide **3.19** after incubation with Rhodamine-labelled WGA. Staining was performed in HEPES-buffer (50 mM HEPES, 100 mM NaCl, 1 mM CaCl_2 , 1 mM MnCl_2 , 10% blocking buffer and 0.05% Tween-20, pH 7.5) at 0.2 $\mu\text{g}/\text{mL}$ lectin concentration. Scanning parameters: Wavelength 532 nm, PMT gain 500, laser power 33%, pixel size 5 μm . Spot pitch is 250 μm .



Appendix Figure 32: Fluorescence scan image of glycopeptides containing β -GlcNAc-PEG3 azide **3.19** after incubation with Rhodamine-labelled WGA. Staining was performed in HEPES-buffer (50 mM HEPES, 100 mM NaCl, 1 mM CaCl_2 , 1 mM MnCl_2 , 10% blocking buffer and 0.05% Tween-20, pH 7.5) at 10 $\mu\text{g}/\text{mL}$ lectin concentration. Scanning parameters: Wavelength 532 nm, PMT gain 500, laser power 33%, pixel size 5 μm . Spot pitch is 250 μm .

Fluorescence intensities of TAMRA azide dye 3.5

Appendix Table 1: Fluorescence intensities of the TAMRA labelled peptides shown in **Figure 3.4** (Section 3.2)

Entry	Peptide sequence	Number of TAMRA molecules	Fluorescence intensity [a. u.]	Standard deviation
1	GGGG	0	249.6	176.1
2	GGGB	1	8715.2	502.5
3	GGBG	1	8426.0	295.6
4	GBGG	1	9578.8	886.7
5	BGGG	1	8717.8	350.4
6	GGBB	2	7025.2	200.3
7	GBGB	2	7149.9	117.8
8	BGGB	2	7778.7	167.1
9	BGBG	2	7530.7	207.6
10	BBGG	2	9262.3	180.4
11	GBBG	2	8162.5	216.6

12	BBBG	3	6661.4	154.2
13	BBGB	3	6988.1	150.7
14	BGBB	3	6812.2	216.5
15	GBBB	3	7033.3	209.9
16	BBBB	4	6265.0	159.3

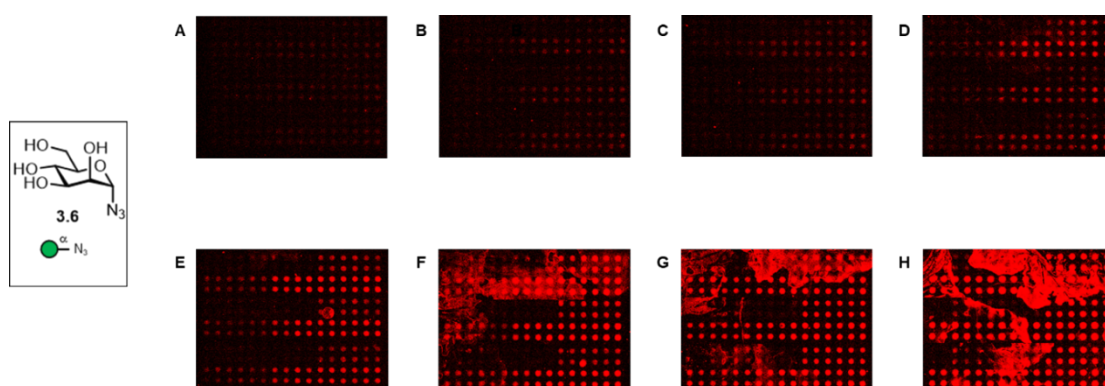
Appendix Table 2: Fluorescence intensities of the TAMRA labelled peptides shown in **Figure 3.9** (*Section 0*)

Entry	Peptide sequence	Number of TAMRA molecules	Fluorescence intensity [a. u.]			Standard deviation		
			PEPPERPRIN T	PolyAn-spacer	PolyAn	PEPPERPRIN T	PolyAn-spacer	PolyAn
1	GGGG	0	221.75	645.33	699.00	56.01	162.71	262.27
2	GGGB	1	3715.58	5223.33	3944.17	321.71	489.40	513.30
3	GGBG	1	3421.92	4887.08	4202.67	660.54	251.25	217.27
4	GBGG	1	3686.92	4796.42	4296.50	307.76	423.16	199.17
5	BGGG	1	4310.08	4566.75	4452.67	363.35	471.95	164.52
6	GGBB	2	3451.92	4841.75	4025.75	661.82	283.69	333.20
7	GBGB	2	3269.58	4601.75	4130.83	355.77	359.92	294.13
8	BGBB	2	4097.17	4648.42	4387.00	515.06	197.66	502.16
9	BGBG	2	3567.25	4815.33	4079.58	357.48	231.85	108.53
10	BBGG	2	4065.08	4708.33	4228.08	332.11	339.34	259.25
11	GBBG	2	3436.58	4858.58	4080.92	668.75	198.01	109.42
12	BBBG	3	4071.17	4428.75	4110.92	486.43	140.10	100.51
13	BBGB	3	3404.42	4584.08	3879.25	354.44	458.38	192.26
14	BGBB	3	3545.58	4602.92	3834.08	440.49	181.04	259.31
15	GBBB	3	3621.50	4569.83	4006.00	523.28	322.87	214.79
16	BBBB	4	3627.00	4250.83	3885.42	348.57	368.14	243.36

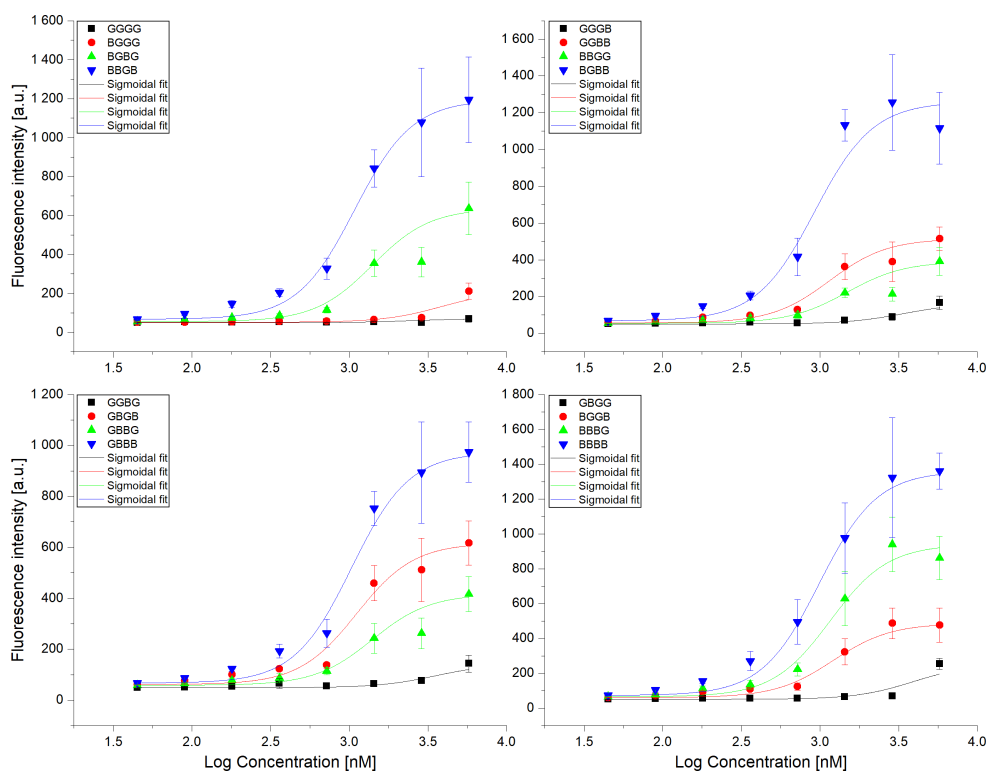
ConA dilution series for $K_{D,surf}$ determination

Fluorescence scanning images of the three sets of quadruplicates for the neo-glycopeptides (consisting only of propargylglycine/glycine) were applied only mannose azide **3.6** (*Section 3.2.2*). For the labeling of the molecules eight different ConA concentrations were used. Each picture represents another concentration of ConA lectin for the determination of the $K_{D,surf}$ values for each of the sixteen neo-glycopeptides. Wherever a spot from a neo-glycopeptide was overlapping with impurities on the microarray, distorting the original fluorescence intensity, the spots were omitted from the calculations. The mean values were used for the plotting of each peptide sequence against the applied ConA concentration on a

logarithmic scale for the determination of the $K_{D,surf}$ (Appendix Figure 34). A nonlinear curve (Category: Growth/Sigmoidal; Function: DoseResp; Iteration Algorithm: Levenberg, (except BGGB, using Orthogonal Distance Regression (Pro), showing higher standard deviation)) was fitted to the data points and the $K_{D,surf}$ values were calculated using the software Origin 2019 (OriginLab, Northhampton/Massachusetts, USA).



Appendix Figure 33: Fluorescence scan images of neo-glycopeptides containing mannose **3.6** after incubation with CF[®]633 ConA. Labelling was performed in HEPES-buffer (50 mM HEPES, 100 mM NaCl, pH 7.5) containing 1 mM CaCl₂, 1 mM MnCl₂, 10% blocking buffer and 0.05% Tween-20 at different ConA concentration. A) c(ConA) = 45 nM; B) c(ConA) = 90 nM; C) c(ConA) = 180 nM; D) c(ConA) = 360 nM; E) c(ConA) = 720 nM; F) c(ConA) = 1440 nM; G) c(ConA) = 2880 nM; H) c(ConA) = 5760 nM. Scanning parameters: Wavelength 635 nm, PMT gain 600, power 33%, pixel size 5 μ m. Distance between the centers of two spots, pitch 250 μ m for each microarray.



Appendix Figure 34: Nonlinear curve fit to the data received from the ConA dilution series experiments on a logarithmic scale.

